Epigenetic regulation of Ewing's sarcoma stem cells

Ghadeer Mohsen Albadrani

Submitted in accordance with the requirements for the degree of
Doctor of Philosophy

The University of Leeds
Leeds Institute of Cancer and Pathology
Molecular Oncology
School of Medicine

October, 2017

I, Ghadeer Albadrani, confirm that the work submitted is my own and that appropriate credit has been given where reference has been made to the work of others.

Acknowledgements

First of all, thankfulness to God, who gave me the strength to complete my PhD journey. I would like also to thank my mother and father for being in my life and for their support and encouragement.

I would like to thank my supervisors, Professor Susan Burchill and Ms Samantha Brownhill for their consistent support, encouragement and guidance. Thanks for my postgraduate tutor, Professor Valerie Speirs for assistance and support during this project.

I would also like to thank the following people for their continued help and valuable suggestions throughout this project:

Mrs Andrea Berry for flow cytometry and western blot of SOX-17, Dr Elizabeth Roundhill for ABCG1 overexpressing construct, and Ms Kimberly Cass for tissue culture and mycoplasma test. Also, I would like to thank Mr Michael Shires and Dr Filomena Esteves for tissue/cells processing and histological support. Thank to Dr Jo-an Roulson for analysing and describing CIZ1 tissues.

Special thanks to my previous supervisors: Dr Justin Ainscough, Dr David Miller and Professor Trevor Batten. I would also like to thank Dr Karen Hemmings and Dr Sumia Bageghni for their assistance and valuable support throughout my PhD journey.

Last but not least I would like to thank my husband Ismail Abualsundos, for his patience, love, understanding and consistent support from start to finish, to my Son ‘Husam’ for his love and smile that gave me encouragement.

Abstract

Emerging evidence suggests that cancer stem-like (CS-like) cells are responsible for cancer progression and relapse. The identification and characterisation of CS-like cells is therefore important to reveal potential targets that could be used to design more effective personalised treatment to improve outcomes. The cell surface marker prominin-1 (CD133) has been used to identify Ewing sarcoma (ES) CS-like cells (ES-CS-like), however some primary ES cells are devoid of CD133 and may be down-regulated by the microenvironment in cell culture. Therefore, alternative approaches are required to identify ES-CS-like cells. Two approaches were compared to enrich for putative ES-CSCs from ES cell lines; isolation of ES-CS-like cells by CD133 expression and using a functional single cell self-renewal assay. The second approach was more reliable for studying the miRNA and mRNA expression profiles in ES-CS-like spheroids compared to ES cells grown as monolayers. In ES-CS-like spheroids, the expression of the stem cell marker EBAF ($q<0.03$), miR-210-3p ($q<0.12$) and the ABC transporter protein ABCG1 ($q<0.14$) were all significantly increased. The phenotypic significance of ABCG1 was investigated using knock-in and knock-out experiments. Overexpressing ABCG1 protein using a lentiviral vector was unachievable as a result of the increased expression of the E3 ligase; NEDD4-1. This ligase prevented the post translational overexpression of ABCG1 mRNA. Interestingly, knock-down of ABCG1 mRNA appeared to stabilise ABCG1 protein and decrease viable number of ES cell line (SK-N-MC), suggesting ABCG1 may have a cell cycle or survival function.

In conclusion, growth of ES spheroids from single cells enriches for cells which express stem cell markers, suggesting that the single cell self-renewal assay can be used to enrich for ES-CS-like cells. Furthermore, ABCG1 and miR-210-3p may be drivers of the ES-CS-like phenotype and might be used to select patients at greatest risk and inform design of targeted treatments. These observations require validation using functional assays and confirmation in patient derived cells and tumours. Whether CDKN1A-interacting zinc finger protein 1 (CIZ1) plays a role in the ES-CS-like phenotype is yet to be investigated.

Table of Contents

List of Tables

List of Figures

List of Abbreviations

2D	Two-Dimensional
3D	Three Dimension
3-W-Spheroids	Three Week Spheroids
ABCA1	ATP Binding Cassette Subfamily A Member 1
ABCG1	ATP Binding Cassette Subfamily G Member 1
ABCG2	ATP Binding Cassette Subfamily G Member 2
ActR-II	Activin Receptor Type-I
ActR-II	Activin Receptor Type-II
ACVR1b	Activin Receptor Type-1B
AGO	Argonaute
BC	Breast Carcinoma
Bcl-2	B-Cell Lymphoma 2
Bcl-Xl	B-Cell Lymphoma-Extra-Large
bFGF	Basic Fibroblast Growth Factor
Brdu	Bromodeoxyuridine
BSA	Bovine Serum Albumin
C. Elegans	Caenorhabditis Elegans
CASP8AP2	Caspase-8 Associated Protein-2
Cdk	Cyclin-Dependent Kinase
CFTR	Cystic Fibrosis Transmembrane Conductance Regulator
CIZKO	CIZ1 Knockout
CRC	Colorectal Carcinoma
DAX1	DSS-AHC critical region on the X chromosome protein 1
DED	Death-Effector Domain
DGCR8	Digeorge Syndrome Critical Region Gene 8
dH2O	Distilled Water
Dicer	Ribomuclease Dicer 1
Drosha	Ribonuclease enzyme Dorsha
EBAF	Endometrial Bleeding Associated Factor
EEC	Euro-Ewing Consortium
EGF	Epidermal Growth Factor

EGFP-Ciz1	Mouse CIZ1 Tagged with EGFP
ER	Endoplasmic Reticulum
Exportin-5	Nuclear transporter receptor protein
EZH2	Enhancer of zeste homolog 2
FACS	Fluorescence Activated Cell Sorter
FCS	Foetal Calf Serum
FGF5	Fibroblast Growth Factor 5
FGFRL1	Fibroblast Growth Factor Receptor-Like 1
FLASH	FLICE-Associated Protein
FLT1	Fms-Like Tyrosine Kinase 1
GATA6	GATA-Binding Factor 6
GBC	Gall Bladder Carcinoma
GLI1	Glioma-associated oncogene
Glut-1	Glucose transporter 1
GPD1L	Glycerol-3-Phosphate Dehydrogenase 1-Like
h	Hours
HAF	Hypoxia-associated factor
HBZ	Haemoglobin Subunit Zeta
HD	Hanging Drop Method
HDCT/Auto-SCT	High-Dose Chemotherapy and Autologous Stem Cell Transplantation
HDL	High-Density Lipoprotein
hES	Human Embryonic Stem
HIF-1α	Hypoxia Inducible Factor 1-Alpha
HOXA3	Homeobox Protein Hox-A3
IC	Immunocytochemistry
ID2	DNA-binding protein inhibitor
IFU	Infectious Units of Virus
IGF1	Insulin-Like Growth Factor 1
IGF1	Insulin-like growth factor 1
IGF1R	IGF1 Receptor
IGFBP3	Insulin-like growth factor-binding protein 3
IHC	Immunohistochemistry
IMP2	Septation Protein Imp2

ISCU1/2	Iron-Sulfur Cluster Proteins 1 And 2
LacZ	Reporter Gene
LAMC1	Laminin Subunit Gamma 1
LB	Luria Bertani
LDL	Low-Density Lipoprotein
LEFTA	Left-Right Determination Factor A
LEFTB	Left-Right Determination Factor B
LEFTY-1	Left-Right Determination Factor 1
LEFTY-2	Left-Right Determination Factor 2
LEFTYA	Left-Right Determination Factor A
LEFTYB	Left-Right Determination Factor B
LICAP	Leeds Institute of Cancer and Pathology
LIMMA	Linear Models for Microarray
LIN28	Lin-28 Homolog A
Lin-4	Lineage-4
M	Mitosis
Mdm2	Mouse Double Minute 2 Protein
MgCl2	Magnesium Chloride
MI	Migration Indexes
min	Minutes
miRNA	Microrna
MK-STYX	Serine/threonine/tyrosine-interacting-like protein 1
mRNA	Messenger RNA
MSC	Mesenchymal Stem Cells
MYC-C	Myc proto-oncogene protein
N2102EP	Human Embryonal Carcinoma
NCBI	National Centre for Biotechnology Information
NKX2.2	Homeobox protein Nkx-2.2
nt	Nucleotides
Oct-4	Octamer-Binding Transcription Factor 4
ORF	Open read frame
OS or OST	Osteosarcoma
P2	Dissociated Spheroids at Passage Two
p21	Cyclin-dependent kinase inhibitor 1

p57kip	Cyclin-dependent kinase inhibitor 1C
PBS	Phosphate Buffered Saline
P-CMV	Minimal Cytomegalovirus Promoter
PFA	Paraformaldehyde
PHD	Prolyl Hydroxylase
PI3KR1	Phosphoinositide-3-Kinase, Regulatory Subunit 1 (Alpha)
PLD2	Phospholipase D2
PMSF	Phenylmethylsulfonyl Fluoride
PODXL	Podocalyxin Like
POU5F1	POU Domain, Class 5, Transcription Factor 1
pPNET	Peripheral Primitive Neuroectodermal Tumour
PR	Partial Remission
Prb	Retinoblastoma Protein
Pre-miRNA	Precursor Mirna
Pre-RC	Pre-Replication Complex
Pri-miRNA	Primary Transcript Mirna
PTEN	Phosphatase and Tensin Homolog
Ran-GTP	Cofactor of exportin-5
RC	Renal Carcinoma
Reecur	Recurrent ES
RIN	RNA Integrity Number
RISC	RNA-Induced Silencing Complex
ROS	Reactive Oxygen Species
RS	Rhabdomyosarcoma
RT	Reverse Transcribed
RTqPCR	Quantitative Real-Time Polymerase Chain Reaction
SC	Stem Cells
SCID	Severe Combined Immune Deficient Mice
SDS	Sodium Dodecyl Sulphate
sec	Seconds
SERP2	Sentrin-Specific Protease 2
shRNA	Short Hairpin RNA
siRNA	Small Interfering RNA

SOX17	Transcription Factor SOX-17
SOX2	Transcription factor SOX-2
SP	Side Population
SR-B1	Scavenger receptor B1
STAG2	Stromal Antigen 2
TARBP2	Trans-activation-responsive RNA-binding protein
TBE	Tris-Borate-EDTA
TBP	TATA-Box-Binding Protein
TDGF1	Teratocarcinoma-Derived Growth Factor 1
Tet-Violet	2(4-Lodophenyl)-3 –(4-Nitrophenyl)-5 – Phenyltetrazolium Violet
TGFB2	Transforming growth factor beta-2
TGF-β	Transforming Growth Factor Beta
TICs	Tumour Initiating Cells
TLB	Tail Lysis Buffer
TLDA	Taqman® Low-Density Array
TNF	Tumour Necrosis Factor
TOPK	T-cell-originated protein kinase
TP53	Tumour Protein P53
TPBS	PBS, 0.1% Tween-20
TRE	Tetracycline Response Element
TSG	Tumour Suppressor Genes
tTA	Tetracycline Transactivator
UV	Ultra-Violet
VDC-IE	Vincristine, Doxorubicin and Cyclophosphamide Altered with Ifosfamide and Etoposide
VIDE	Vincristine, Ifosfamide, Doxorubicin and Etoposide
WB	Western Blot
WSI	Whole Slide Imaging
Xist	X-Inactive Specific Transcript
ZMYM3	Zinc Finger MYM-Type Containing 3

Chapter 1
Main introduction

1.1 Ewing's sarcoma (ES) family of tumours

1.1.1 ES biology and diagnosis

Ewing's sarcoma (ES) family tumours (ESFT) is a group of cancers defined by the presence of non-random chromosomal translocation between chromosome 22q12 (the 5'-end of the *EWS* gene) with 3'-end of a member of transcription factors known as *ETS* gene family, consequently EWS-ETS fusion proteins are considered as the main genetic signature for ES family tumours (Burchill, 2003; Burchill, 2008). This family has been renamed by the World Health Organisation (WHO) and the new terminology is 'Ewing Sarcoma' (ES), which doesn't reflect the variety of tumours within the family but refers to James Ewing who first described this type of tumour (Ewing, 1921; Francis et al., 2013). The ES family include tumours that arise outside of the bone and they can frequently invade into the bones of the patient and are named Ewing sarcoma (Ewing, 1921), whereas if the initiation of tumour was in the soft tissue surrounding bones they're known as extraosseous Ewing tumour (EOE) (Angervall and Enzinger, 1975). The third type of tumour that is included in the ES family is the peripheral primitive neuroectodermal tumour (pPNET), which can occur in bone or soft tissue (Stout, 1918). Where tumours arise in the chest wall they are also known as Askin tumour (Askin et al., 1979). Also, pPNET arise in soft tissue or bone (Armbruster et al., 2008). In the United Kingdom (UK), approximately 13 per million cases of ES arise between the ages of 10 to 24 years old per year (Cotterill et al., 2000). ES can also occur in adults although this is rare (McNally et al., 2012). ES commonly arise in specific bony sites (Table 1.1) and are marginally, more common in males than females (McNally et al., 2012). *EWS-FLI1* fusion is the most frequently described translocation and has been found in 85% of ES family tumours, 60% of these cases have a translocation between exon 7 of *EWS* and exon 6 of *FLI1* known as *EWS*-

FLI1 type I. The remaining cases (25%) have translocation between exon 7 of *EWS* and exon 5 of *FLI1* known as *EWS-FLI1* type II (van Doorninck et al., 2010). The remaining 15% of ES cases have a translocation between *EWS* with the *ERG* gene (10%; chromosome 21q22), or with *ETV1* (<1%; chromosome 7p22), or *E1AF* (<1%; chromosome 17q12) or *FEV* (<1%; chromosome 2q33) (Delattre et al., 1992; Burchill, 2008).

Location of tumour		Reference	Frequently
Bone	Pelvis	Bernstein, m. et al. (2006)	26%
	Femur		20%
	Chest wall		16%
Extraosseous sites	Small intestine	Shek et al. (2001)	Grier (1997) 15%
	Stomach	Kim, H.S. et al. (2012)	
	Kidney	Maeda et al. (2008), Chu, W.C. et al. (2008)	
	Uterus	Park et al. (2007)	
	Liver	Huang, S. et al. (2011)	
	Other rare sites	Tanida et al. (2000), Colovic et al. (2009) Shibuya et al. (2015), Peng, L. et al. (2015)	

Table 1.1 Organs and tissues in which ESs can arise

The ES cells are small round, poorly differentiated cells. They have large nuclei and scant cytoplasm and 90% of ES cells express the cell surface membrane protein known as MIC-2 which is a single-chain type-1 glycoprotein also known as Cluster of differentiation 99 (CD99) (Ambros et al., 1991). Membrane expression of CD99 is used as a marker to diagnose and distinguish ES from other small round cell tumours (Weidner and Tjoe, 1994) (Figure 1.1).

In over 80% of ES cases, secondary genetic abnormalities such as gain or loss of chromosomes occur in addition to the EWS-ETS fusion (Burchill, 2008). The gain of chromosomes is the most frequent event after EWS-ETS fusion, particularly chromosome 8, 12 and 1q comparing with loss of 1p (Maurici et al., 1998; Hattinger et al., 2002; Roberts et al., 2008). Interestingly, a low rate of somatic mutation has been identified consistent

with the hypothesis that tumours in children and young people arise through different mechanism. For example, cyclin-dependent kinase Inhibitor 2A (CDKN2A) deletions (12%) and Stromal Antigen 2 (STAG2) mutations (17%) (Tirode et al., 2014). Other mutations that have been described at lower frequency include the tumour protein p53 (TP53), Enhancer of zeste homolog 2 (EZH2), BCL-6 corepressor (BCOR), and Zinc Finger MYM-Type Containing 3 (ZMYM3) (Tirode et al., 2014).

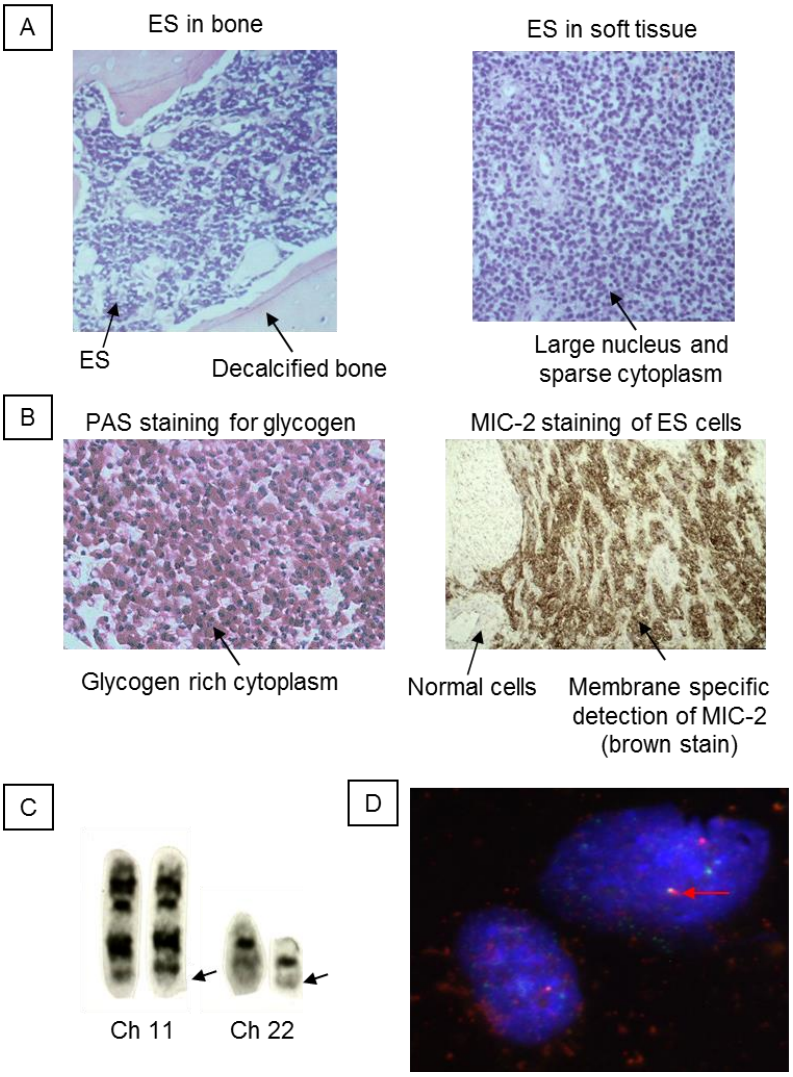

Figure 1.1 Diagnostic features of ES. A) Haematoxylin and eosin stained sections of ES located in the bone and in the soft tissue show the small round cells with sparse cytoplasm characteristic of ES. B) Glycogen is identified in the cytoplasm of ES cells by PAS staining (pink cytoplasmic staining). ES cells express MIC-2 protein, detected by immunohistochemistry (membrane specific brown stain). C) G-banding of metaphase chromosomes identifies exchange of material between chromosome 11 (Ch 11) and chromosome 22 (Ch 22), arrows denote exchange of chromosomal material. D) Fluorescence in situ hybridisation (FISH) identifies the EWS-FLI1 fusion transcript using a probe on chromosome 11q23 (green) and a probe on chromosome 22q12 (red). The arrow indicates an EWS-FLI1 gene rearrangement.

1.1.2 Prognostic factors and outcome of patients with ES

Poor prognosis and outcome is mainly associated with patient age (≥ 20 years), the location of the primary tumour within the pelvic region, size of primary tumour (>10 cm), the presence of metastatic disease (to the lung, bone or bone marrow) at diagnosis and poor response to treatment (i.e.>90% necrosis after treatment of tumour) (Duchman et al., 2015). The survivors of ES are at increased risk of developing second cancer including thyroid (Navid et al., 2008), breast (van den Berg et al., 2009) and sarcoma (Fuchs et al., 2003; Goldsby et al., 2008; Wasilewski-Masker et al., 2009; Sultan et al., 2010). Also, it has been reported that the metastasis was not associated with the time of diagnosing ES (Brasme et al., 2014). Therefore understanding the biology of ES, especially the cells responsible for initiation and progression is essential in order to develop more selective, effective agents to improve outcome.

1.1.3 Treatment type depends on whether patients have localized or disseminated disease

Treatment for patients with disseminated diseases includes surgery, radiotherapy and chemotherapy. Systemic therapy (chemotherapy), is almost always the first step of the treatment. This is usually followed by localised therapy (surgery and/or radiotherapy) used as the second stage of treatment followed by an additional dose of chemotherapy. Randomized trials are ongoing for localized ES and are assessing the current chemodrugs combination with respect to the toxicity before and after the localised therapy (Gaspar et al., 2015). In the Euro-Ewing 2012 trial, in Europe, a combination of vincristine, ifosfamide, doxorubicin and etoposide (VIDE) is used at the first stage of treatment (induction), whereas vincristine, doxorubicin and cyclophosphamide altered with ifosfamide and etoposide (VDC-IE) is used in North America (Gaspar et al., 2015). Also, the North America trial (COG AEWS1031) evaluated the addition of cyclophosphamide and topotecan to VDC-IE combination, whereas the first Euro-Ewing Consortium (EEC) study for recurrent ES (rEECur) is focusing on identifying the best regimen out of the four regimens that have shown promising

responses: topotecan plus cyclophosphamide (Hunold et al., 2006), temozolomide plus irinotecan (Casey et al., 2009), gemcitabine plus docetaxel (Fox et al., 2012) and high-dose ifosfamide (Ferrari et al., 2009).

The third treatment offered is high-dose chemotherapy and autologous stem cell transplantation (HDCT/auto-SCT) (Choi et al., 2016). Chemotherapy normally damages the cells of the bone marrow, increasing the drug-dose leading to a shortage of white blood cells (so causes neutropenia). Therefore, stem cell transplant is needed for these patients to replace the cells destroyed by chemotherapy. It has been hypothesised that HDCT/auto-SCT might benefit patients that retune ES after the standard treatment or patients with metastatic disease. This is feasible for patients in complete remission (CR) or partial remission (PR) prior to HDCT/auto-SCT. Also, HDCT/auto-SCT required maximal effort to reduce tumour burden prior to the treatment to improve the outcomes (Choi et al., 2016). Despite these trials and intensive treatment, the survival rate for patients with ES has remained the same for the last 30 years. Therefore, biomarkers that can predict and classify ES patients' risk to relapse at the time of diagnosis are needed.

1.1.4 ES expression profile

Gene expression profile can be used to classify patient risk and it has been evaluated and validated in several human cancers (Erho et al., 2013; Trinquand et al., 2013), including neuroblastoma (Stricker et al., 2014), rhabdomyosarcoma (Missiaglia et al., 2012; Wilson et al., 2013), and leukaemia (Cleaver et al., 2010; Kang et al., 2010). In ES, several profiling studies have been reported, and biomarkers were identified (Ohali et al., 2004; Schaefer et al., 2008; Scotlandi et al., 2009; Bennani-Baiti et al., 2010; Volchenboum et al., 2015; Huertas-Martínez et al., 2017). Furthermore, EWS-FLI1 protein is expressed in the majority of ES cases (Section 1.1.1). This protein has been reported to be transcriptional activator or repressor for important target genes (Table **1.2**) and also considered to be a biomarker. Alongside EWS-FLI1 protein, multiple mutations are required to cooperate in the development of ES (Funes et al., 2007; Lin, P. et al., 2011). Mutated p53

is unlikely to be essential in ES, since p53 mutations are found only in about 10% of ES patients (Huang, H. et al., 2005). Even though several prognostic gene signatures and TP53 mutational studies have shown promise as prognostic biomarkers, none have yet been successfully validated in independent cohorts of equivalently treated patients (Shukla et al., 2013; Volchenboum et al., 2015).

Role of EWS-FLI1	Gene symbol	Full name	reference
Promote cell survival and proliferation genes	IGF1	Insulin-like growth factor 1	Cironi et al. (2008)
	MYC-C	Myc proto-oncogene protein	Sollazzo, M. et al. (1998)
	TOPK	T-cell-originated protein kinase	Herrero-Martin et al. (2009)
	NKX2.2	Homeobox protein Nkx-2.2	Smith et al. (2006)
	ID2	DNA-binding protein inhibitor	Fukuma et al. (2003)
	DAX1	DSS-AHC critical region on the X chromosome protein 1	Garcia-Aragoncillo et al. (2008)
	GLI1	Glioma-associated oncogene	Zwerner et al. (2008)
	EZH2	Enhancer of zeste homolog 2	(Richter et al., 2009)
	MK-STYX	Serine/threonine/tyrosine-interacting-like protein 1	(Siligan et al., 2005)
	PLD2	Phospholipase D2	(Kikuchi et al., 2007)
Represses cell cycle arrest and apoptosis genes	TGFB2	Transforming growth factor beta-2	(Hahm et al., 1999)
	p21	Cyclin-dependent kinase inhibitor 1	(Nakatani et al., 2003)
	p57kip	Cyclin-dependent kinase inhibitor 1C	(Dauphinot et al., 2001)
	IGFBP3	Insulin-like growth factor-binding protein 3	(Prieur et al., 2004)
Upregulates genes that are involved in cell differentiation	SOX2	Transcription factor SOX-2	(Riggi et al., 2010)
	EZH2	Enhancer of zeste homolog 2	(Richter et al., 2009)

Table 1.2 Summary of genes that regulated by EWS-FLI1 protein.

1.2 Putative cancer stem-like cells (CS-like cells)

The terminology CS-like cells represents cancer cells that display some of normal stem cell features such as self-renewal ability, differentiation into the cell types observed in tumors and also might acquire additional features such as migration and drug resistance.

The vast majority of cells in tumours are non-tumorigenic, tumour growth and progression resulting from a small population of cells. These cells have intrinsic resistance to treatment, metastasis and self-renewal ability (Hanahan and Coussens, 2012; Visvader and Lindeman, 2012). This rare population is referred to as cancer initiating cells (CICs), or tumour initiating cells (TICs) also known as cancer stem cells (CSCs) or cancer stem-like (CS-like) cells. The term "TIC" and "CIC" reflect functional definitions that represent cancer cells with capability to form tumour in xenotransplantation studies. However, the term "CSC" is widely used by many researchers and it reflects a characteristic term as it represents the existence of a subset of poorly differentiated cell with stem cell feature within tumours. CSCs are not true stem cells because they are only able to contribute to tumour initiation.

Furthermore, it was hypothesized that the currently available cancer treatments are not completely effective, as CSCs might be resistant to therapy (Koren and Fuchs, 2016). After treatment, CSCs might regenerate CSCs, initiate tumour growth and/or differentiate to produce tumours. So, CSCs-targeted therapy is needed alongside the currently available cancer treatments to ensure cure (Figure 1.2).

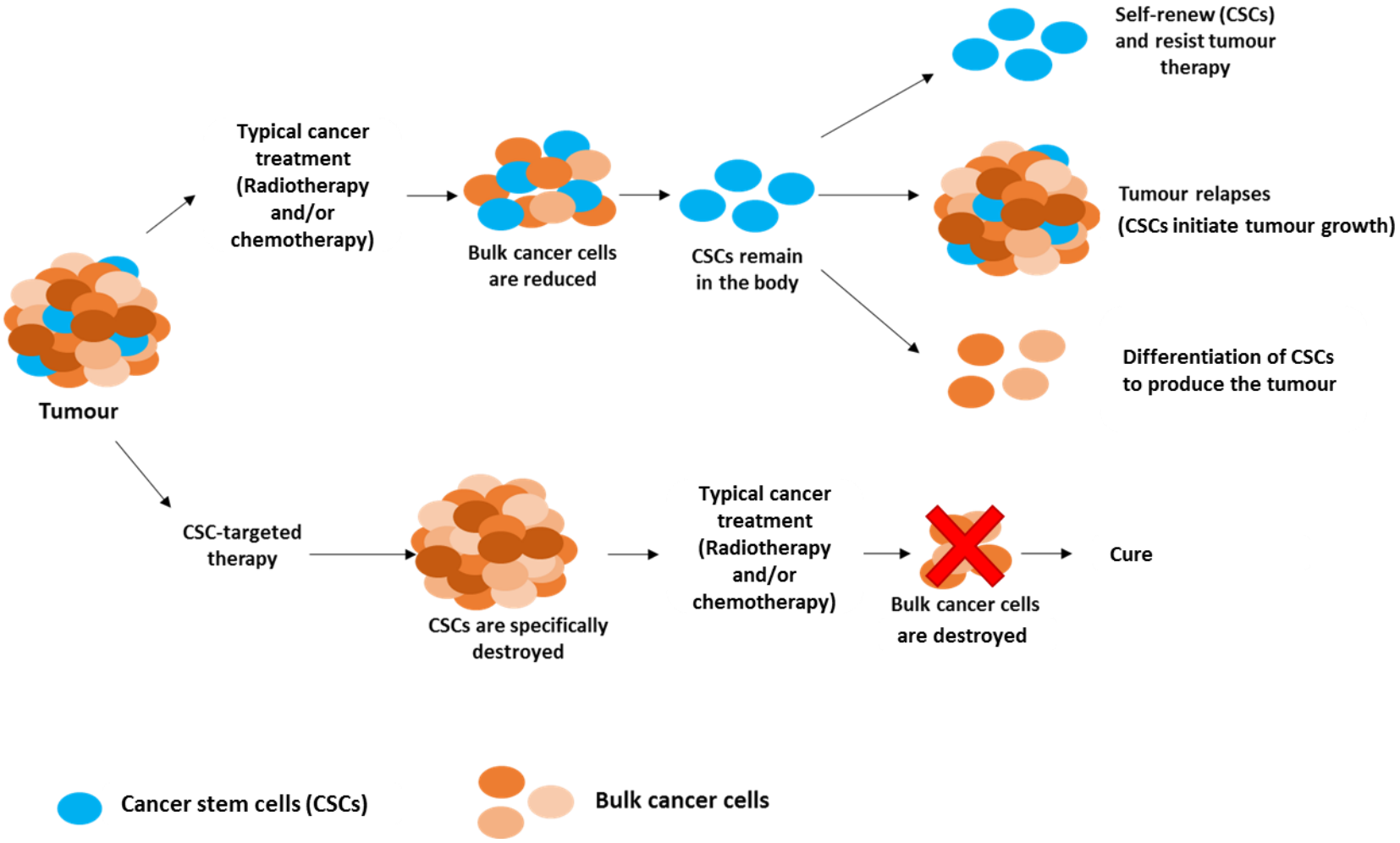

Figure 1.2 The potential of targeted CSCs therapy to improve outcome

In my opinion the majority, if not all tumours contain a heterogeneous subset of cells that contribute to tumour initiation. Tumour cells need to be supported by stromal cells, tumour bulk and CSCs (Hanahan and Coussens, 2012). There are three classes of stromal cells; endothelial cells, infiltrating immune cells and pericytes that are organized within the vasculature of primary tumours (Calabrese et al., 2007) and metastatic tumours (Psaila and Lyden, 2009). The cancer-associated fibroblasts (CAFs) cells, which are characterized as mesenchymal stem cells (MSC) differentiated into myofibroblasts, as well as similar stem cell niche-forming cells (Kidd et al., 2009; Liu, S. et al., 2011; Hanahan and Coussens, 2012). Even with the current advance studies in CSC biology, the optimal method for isolation and identification of CSCs still remains incompletely established.

1.2.1 Putative CSCs in ES

Prominin-1 (CD133) has been used as a putative CSCs marker (See section 1.3.1). Based on the expression of CD133, Suvàs group identify CSCs in ES (Suvà et al., 2009). Like MSC, these CSCs express stem cell markers and have the ability to differentiate to adipogenic, osteogenic and chondrogenic lineages (Suvà et al., 2009). However, it has been reported that the expression of CD133 was very heterogeneous in ES family and also the drug resistant feature was not consistently in CD133+ cells (Jiang et al., 2010). Even with this confirmation, there is still controversy as to the perfect marker of CSCs of ES family tumours. Moreover, effluxion of Hoechst dye that is described in (Section 1.3.3.1) has been used as method to isolate putative CSCs known as side population (SP). In SK-ES-1 which is an ES cell line, the SP cells were 1.2% of the total cell population. These cells can regenerate both SP and non-SP cells suggesting they are capable of differentiating into the non-SP tumour cells that make up most of the tumour (Yang, M. et al., 2010). Identifying the ES-CSC is essential to prevent disease relapse and improve the outcome.

1.3 Methods for the identification and /or enrichment of CSC

1.3.1 Antigenic method

A number of cell surface markers have been described and used to isolate and identify CSCs from non-CSC cells within tumour and the normal surrounding tissues. These markers have been used to identify CSCs using immunohistochemistry (IHC), immunocytochemistry (IC) or flow cytometry. The first identified CSCs were in leukaemia using surface markers ($CD34^+$ $CD38^-$) (Lapidot et al., 1994). The identification of cell surface markers to detect CSCs in different solid tumours has been more controversial. Such markers include, CD20, CD34, CD44, CD90, CD117 and CD133 were used as individual marker or combination of markers to identify CSCs in solid tumours including brain (Singh et al., 2004), breast (Al-Hajj et al., 2003), colon (Ricci-Vitiani et al., 2007), liver (Yin, S. et al., 2007), lung (Eramo et al., 2007), melanoma (Fang et al., 2005), prostate (Collins et al., 2005) and sarcomas (Tirino et al., 2008).

The microenvironment such as, cellular stress and hypoxia were reported to induce changes in CD133 expression in glioblastoma cells (Platet et al., 2007). Also, in melanoma, down-regulating CD133 expression in terms of treatment applications affects cell proliferation and metastasis (Rappa et al., 2008). Moreover, CD133 has been reported as a unique surface marker on CD34+ progenitor hematopoietic stem cells (Yin, A.H. et al., 1997). The capability of CD133+ cells to develop tumours in immune compromised mice has been confirmed in brain (Singh et al., 2004), liver (Suetsugu et al., 2006) pancreatic cancer (Hermann et al., 2007), melanoma (Klein et al., 2006), and lung tumours (Eramo et al., 2007). These findings suggest that CD133 could be a suitable cell surface marker for the identification of sarcoma and ES CSCs as previously in (Section 1.2.1). However, other investigators have confirmed the expression of CD133 in several normal cells and tissues such as salivary glands, brain, kidney, bone marrow, liver, colon and mammary glands (Mizrak et al., 2008; Wu, Y. and Wu, 2009). Also, it has been revealed that colon and brain tumours can be produced following injection of CD133− cells into immune compromised mice (Ogden et al., 2008; Shmelkov et al., 2008; Wang, J. et al., 2008). Therefore, the use of a single

antigenic method (E.g. CD133, or indeed potentially any cell surface protein markers) to identify and isolate CSCs is not recommended because the expression is not stable and perhaps at present a combination of assays for the identification and isolation of putative CS-like cells would be more powerful.

1.3.2 Transplant method (animal models)

The consistent ability of a subpopulation of cancer cells to produce tumours when injected into immune compromised mice, especially after serial transplantation, continues to be the “gold standard” for detecting CICs (Clarke et al., 2006). Multiple factors control the expansion and reversion of CIC to original bulk tumour cells such as intrinsic alterations or micro-environmental influences (hypoxia/reoxygenation, secretion of growth factors and inflammatory cytokines) may cause CIC to expand or revert to original bulk tumour cells (Chang, J.C., 2016).

It has been reported that cells with self-renewal capacity *in vitro* are able to initiate tumour growth in immunodeficient mice (Li, C. et al., 2007; Quintana et al., 2008; O'Brien, C. A. et al., 2012). In leukaemia, cells with a $CD34^+$ $CD38^-$ profile were believed to be the only subpopulation that could develop leukaemia in severe combined immune deficient (SCID) mice (Lapidot et al., 1994; Civin et al., 1996; Bhatia et al., 1997). However, other studies have indicated that cells enriched in $CD34^+$ $CD38^+$ also have the capacity to produce tumours in SCID mice (Hogan et al., 2002; Taussig et al., 2008). Similarly, regardless of the expression of cell surface markers, serial transplantation of tumour cells from patients in SCID mice lead to an expression of CICs with 28% of cells obtained directly from patients capable of initiating tumours in melanoma (Quintana et al., 2010).

Therefore, unlike hematologic cancers, the experimental procedures that are used for isolation of CSCs from solid tumours based on antigenic markers require numerous processes that probably has an effect on cell viability or behaviour (Rosen and Jordan, 2009). Furthermore, the micro/macro-environment of CSCs that are isolated from human tissues is different to the xenograft environment even if orthotopic transplantation was used. For

example, tumour necrosis factor (TNF) is not cross-species reactive in mice (Bossen et al., 2006; Rongvaux et al., 2013). These variations between mice and human should be taken in consideration when using murine models to study human diseases as they could impart selective forces on tumour cells (Mestas and Hughes, 2004; Magee et al., 2012; Kreso and Dick, 2014). So far, it remains unclear whether the enriched population truly represents CSCs, or illustrates an ability to exploit the microenvironment of the mice to allow tumour growth.

1.3.3 Functional methods

1.3.3.1 Side-population that efflux Hoechst dye

One of the frequently described functional characteristic of CSCs is the low level of Hoechst staining when identified by flow cytometry. The low level of Hoechst resulted from increased expression of the ATP binding cassette (ABC) family proteins, which are membrane proteins that have the ability to efflux various molecules such as cytotoxic drugs and dyes from the cells (Scharenberg et al., 2002). This subset of cells, known as the side population (SP) have been identified in a range of cancer cell lines and primary tumours including neuroblastoma (Hirschmann-Jax et al., 2004), leukaemia, breast, brain tumours (Patrawala et al., 2005), hepatocellular carcinoma (Chiba et al., 2006), ovarian (Szotek et al., 2006), lung (Ho et al., 2007), mesenchymal neoplasms (Wu, C. et al., 2007) and Ewing's sarcoma (Yang, M. et al., 2010). SP cells have been linked with enriched CSC properties such as clonogenicity and multipotent differentiation in cancers of the gastrointestinal system, Ewing's sarcoma and colorectal cancer (Haraguchi et al., 2006; Yang, M. et al., 2010; Xu, X.T. et al., 2012), whereas others could not prove that SP cells contain an increased CSC fraction in gastrointestinal cancers (Burkert et al., 2008). It has been reported that ABC transporters are able to efflux a wide range of drugs for instance, doxorubicin, etoposide and vinblastine (Dean, 2009). Mainly, ABC transporters protect cells from toxic insults, whereas ATP binding cassette subfamily G member 2 (ABCG2), also known as BCRP or MXR, could be a driver for a part of the stem cell phenotype of SP cells in glioma (Wee et al.,

2016). In human hematopoietic progenitors, in addition to drug efflux, the involvement of ABCG2 in maintaining pluripotent stem cells state has been described (Zhou et al., 2001; Scharenberg et al., 2002).

Recommendation for the identification of CSCs using the SP have been developed and standardize reporting (Golebiewska et al., 2011). Several differentiated cells in adult tissue were observed to have the SP phenotype (Mayer et al., 1996; Smit et al., 1998; Schinkel, 1999). Consequently, in tumours and stromal cells, caution is essential whilst applying the SP assay for CSC identification since flow cytometry analysis varies from research group to another (Golebiewska et al., 2011).

1.3.3.2 Treatment resistance capacity

The CSCs are predicted to be resistant to apoptosis and escape chemotherapy induced DNA damage by decreasing the production of reactive oxygen species (ROS) and enhancing DNA checkpoint activity (Bao et al., 2006; Diehn et al., 2009). Furthermore, CSCs seem to maintain high expression of the ABC transporter that can excrete anticancer drugs and contribute to the development of treatment resistance (Ho et al., 2007; Matsui et al., 2008; Collura et al., 2013; Hashimoto et al., 2014). Resistance to treatment by effluxing chemotherapy from within the cells is the basic principle of the SP assay that has been described in (Section 1.3.3.1). However, it is difficult to distinguish between the expression of ABC transporter proteins that have a role in the intrinsic phenotype of CSCs or those cells that have acquired drug resistance during tumorigenesis. Thus, focusing on the functional drug resistance capacity in isolation might not be a good method for the identification of CSCs.

1.3.3.3 Population that hold the fluorescent lipophilic dyes

The first fluorescent lipophilic dye, PKH3, was reported for the first time in 1989 (Slezak and Horan, 1989). Other lipophilic dyes such as PKH2 (Zeine and Owens, 1992), PKH26 (Lansdorp, 1993), and PKH67 (Boutonnat et al., 2000) were subsequently designed to increase stable labelling and decrease

cell-to-cell transfer. These dyes were used as cell tracers and also for cell localization application (Avnet et al., 2013). However, the retention characteristic of these dyes are the same as PKH3 (Li, P. et al., 2013). Furthermore, these dyes were used in proliferation analysis and identification of quiescent or slowly dividing cells of mammary stem cells (Cicalese et al., 2009). The label retention approach is used to identify CSCs based on the assumption that CSCs are quite quiescent, proliferate slowly and use asymmetric division (Dick, 2008). As result of CSC quiescent traits and slow division, CSCs can retain the dyes such as lipophilic dyes or bromodeoxyuridine (BrdU) for longer periods than differentiated cells (Pece et al., 2010). So far, this methodology has been used to identify CSC in the human colon (Chu, P. et al., 2009; Pastò et al., 2012), breast cancer (Fillmore and Kuperwasser, 2008), colorectal cancers and intestinal inflammation (Buczacki et al., 2013) and prostate (Ceder et al., 2017).

1.3.3.4 Autofluorescence

In 2014, a novel strategy to isolate and identify CSC from different types of human epithelial cancers including colorectal carcinoma (CRC) was described (Miranda-Lorenzo et al., 2014). This approach focused on the autofluorescent cells which showed critical properties such as self-renewal capacity, and ability to form tumours in immune compromised mice consistent with the CSCs phenotype. These cells autofluoresce because they concentrate riboflavin, which is a fluorescent vitamin. The accumulation of riboflavin was in intracellular vesicles which are covered with an ATP-dependent transporter known as ABCG2 (Miranda-Lorenzo et al., 2014). The accumulation of riboflavin in autofluorescent vesicles could help to identify CSCs (Sainz et al., 2015). However, this needs to be confirmed in other studies. It has been reported previously that riboflavin-derived molecules are also the likely cause of autofluorescence within macrophages (Aubin, 1979; Thorell, 1983; Njoroge et al., 2001), which may limit the use of this approach for identifying or isolating CSC.

1.3.3.5 Three dimension (3D) spheroids assays

In various cancer types, CSCs have been identified by exploiting their self-renewal capacity and ability to form spheroids in anchorage independent culture (Hermann et al., 2007; Ricci-Vitiani et al., 2007; Chung et al., 2015). Spheroid formation can be used to enrich for CSCs whereas differentiated cells such as non-malignant cells and fibroblasts undergo anoikis as result of the lack of adherence (Weiswald et al., 2015; Qureshi-Baig et al., 2016; Dubash et al., 2016). The spheroids grown in anchorage independent culture retain the key characteristics of the original tumour such as relevant mutations and might be helpful tools to identify a gene expression signature leading to the identification of targets for the development of more effective therapeutic strategies (Lee, J. et al., 2006; Mori et al., 2009; Lee, S. et al., 2015). As to whether the applied growth conditions select for CSCs or drive cancer cells to adopt a CSCs phenotype, some studies have used growth media to select cells that are capable of producing spheroids in the 3D assay (Dontu et al., 2003; Ponti et al., 2005). However, in the 3D assay, there are some factors that need to be taken into consideration such as the use of specific culture media and where multiple cell populations are combined to generate spheroids, which may lead to molecular heterogeneity, including inter- and intra-variability in marker expression (Vermeulen, L. et al., 2008; Pastrana et al., 2011; Smart et al., 2013).

1.4 Gene signalling pathways

There are several signalling pathways play essential roles in gene regulation capacity such as Wnt, Notch, phosphatidylinositol 3-kinase/phosphatase and tensin homolog, (PI3K/PTEN) and nuclear factor-κB (NF- κB) signalling pathways. As yet the precise functional CSC signalling pathways have not been clarified.

1.4.1 miRNA biogenesis

MiRNAs are small (19-23 nucleotides) non-protein-coding RNA (Lagos-Quintana et al., 2001). The first miRNA known as Lineage-4 (lin-4) was

discovered in Caenorhabditis elegans (C. elegans) over two decades ago (Lee, C. et al., 1993). By 2016, more than 2578 mature miRNA sequences had been reported in miRNA data base (http://www.mirbase.org). However, the functions of many miRNAs remain to be elucidated (Peng, Y. and Croce, 2016).

Usually, miRNAs are transcribed by RNA polymerase II into primary transcripts (pri-miRNA). These primary transcripts are several kilobases long and contain a region in which the sequences are imperfectly complementary forming a hairpin. (Lee, Y. et al., 2004; Borchert et al., 2006). In the nucleus, the hairpin structure is recognised by the ribonuclease enzyme Drosha and its partner DiGeorge syndrome critical region gene 8 (DGCR8) protein. Together Drosha and DGCR8 form a large complex (around 650kDa) known as the microprocessor complex that mediates cleavage of the pri-miRNA at the stem of the hairpin structure, releasing a small hairpin termed the precursor miRNA (pre-miRNA). Pre-miRNA is then transferred out the nucleus to the cytoplasm by the nuclear transporter receptor protein exportin-5 (Lee, Y. et al., 2003; Bohnsack et al., 2004) (Figure **1.3**).

Following nuclear export, the pre-miRNA is further cleaved by the ribonuclease Dicer 1 in conjunction with its interacting partner Trans-activation-responsive RNA-binding protein (TARBP2) to form a double-stranded miRNA of approximately 22 nucleotides which consists of a passenger strand and a guide strand (Bernstein, E. et al., 2001; Knight and Bass, 2001). When this duplex is unwound, the guide strand is loaded onto an argonaute (AGO) protein and incorporated into the RNA-induced silencing complex (RISC). Upon incorporation into the RISC complex the miRNA can now target mRNA sequences and modulate gene expression (Mourelatos et al., 2002; Valencia-Sanchez et al., 2006; Vasudevan et al., 2007; Vasudevan, 2012). Although the exact mechanism of miRNAs in the regulation of the human transcriptome is not fully understood, increasing studies support the association of miRNAs in the regulation of gene expression.

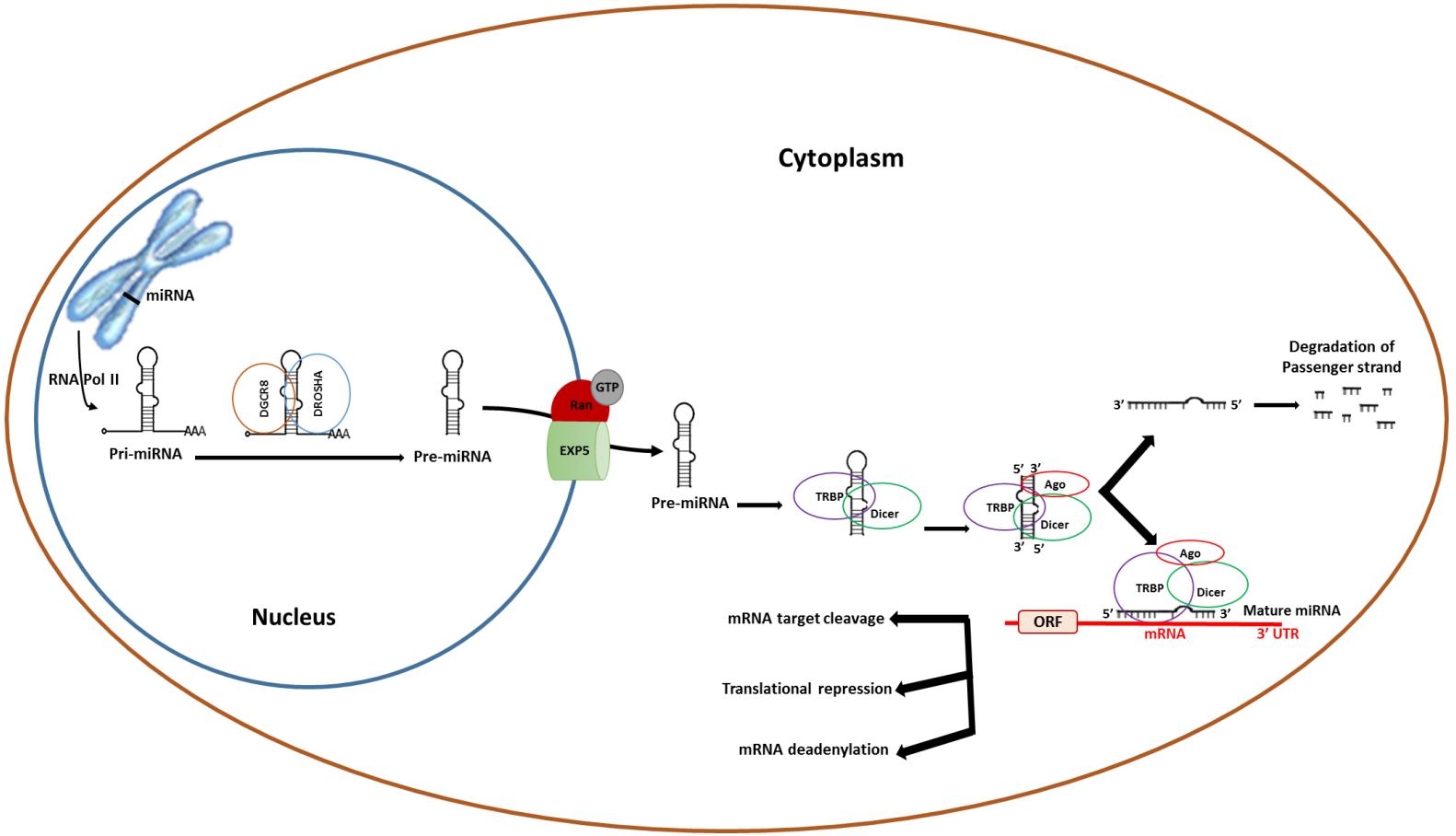

Figure 1.3 **miRNA biogenesis in human cells**. primary transcripts (pri-miRNA), ribonuclease enzyme Drosha (Drosha), DiGeorge syndrome critical region gene 8 (DGCR8), precursor miRNA (pre-miRNA), nuclear transporter receptor protein (exportin-5), cofactor of exportin-5 (Ran-GTP), Trans-activation-responsive RNA-binding protein (TARBP2), ribonuclease Dicer 1 (Dicer), argonaute (AGO), massengar RNA (mRNA), open read frame (ORF)

- 17 -

1.4.2 Impact of the altered miRNA expression in cancer

Large-scale dysregulation of miRNAs plays a critical role in cancer development and progression. Some miRNAs function as oncogene or tumour suppressor under certain conditions. The abnormal expression of miRNA has been found to be the responsible for the uncontrolled growth and division in cancer cells by targeting cell cycle components as well as signalling pathways. For example, deletion of *Dicer-1* in *Drosophila* germline stem cells leads to block the cells in the G1/S transition and also increased expression of one of the p21/p27 family of cyclin-dependent kinase (Cdk) inhibitors known as Dacapo (Hatfield et al., 2005). In non-small-cell lung cancer it has been reported that the downregulation of miRNA, which target insulin-like growth factor 1 (IGF1), IGF1 receptor (IGF1R), and phosphoinositide-3-kinase, regulatory subunit 1 (alpha) (PI3KR1, or p85a), increases the PI3K signalling pathways (Peng, Y. et al., 2013).

Furthermore, circumvention of apoptosis is believed to be regulated by miRNAs which have the ability to protect p53 from degradation by directly supressing the expression of mouse double minute 2 protein (Mdm2) (Pichiorri et al., 2010). Overexpression of p53 target miRNA leads to escape from cell death (Yan et al., 2009). Moreover, there are some miRNAs which target anti-apoptotic regulators such as B-cell lymphoma 2 (Bcl-2) and B-cell lymphoma-extra-large (Bcl-xL) as well as proapoptotic factors Bax, Bim and Puma which have essential role in cell death (Zhang, H. et al., 2011; Nie et al., 2012; Denoyelle et al., 2014). MiRNAs can also regulate mechanisms of the extrinsic (death receptor mediated) apoptotic pathway, included the Fas ligand/receptor, which play an essential role in the cancer progression and of the immune system regulation (Shaffiey et al., 2013; Wang, P. et al., 2013). Growing evidence has confirmed the involvement of miRNAs in activating invasion and metastasis as well as inducing angiogenesis (Kong et al., 2008; Ghosh, G. et al., 2010; Liu, L. et al., 2011; Lou et al., 2012).

According to the genome-wide profiling, the association of the expression signatures of miRNA with tumour type, grade and clinical outcomes has been proven (Vychytilova-Faltejskova et al., 2016). Therefore, miRNAs could be potential diagnostic and prognostic biomarkers and also might be reveal

targets and pathways for the development of more effective treatments. However, more studies are required to screen and validate the miRNA candidates in more patient samples.

1.4.2.1 miRNA in Ewing's sarcoma

Downregulation of miR-193b leads to inhibition of anchorage-independent growth in soft agar and metastasis, negatively regulating the expression of ErbB4 (Moore et al., 2017), which is reported to promote metastasis (Mendoza-Naranjo et al., 2013). Furthermore, miR-199b-5p, which is downregulated in ES cell lines, is suggested to be a tumour suppressor and also directly targets cyclin-L1 (CCNL1) (Li, W. et al., 2015). The expression and amplification of CCNL1 in head and neck squamous cell carcinoma is associated with the survival rate of these patients. It is also reported as cell cycle regulatory protein and suggested to be a potential oncogene (Redon et al., 2002; Sticht et al., 2005). An increase of miR-301a expression in ES compared with MSC has been reported, miR-301a has a direct inhibitory effect on phosphatase and tensin homolog (PTEN) mRNA translation in ES (Kawano et al., 2016) and breast cancer (Ma, F. et al., 2014). PTEN is a tumour suppressor often mutated in human cancers and leads to increased survival and oncogenesis by activation of the phosphoinositide 3-kinase (PI3K)/ protein kinase B (Akt) pathway (Podsypanina et al., 1999; Di Cristofano et al., 2001). TAp73β, which is a p53-family protein, is inhibited by miR-193a-5p and implicated in Cisplatin chemoresistance of osteosarcoma and ES (Jacques et al., 2016). The miR-17-92 cluster is associated with the TGFB/BMP pathway (Schwentner et al., 2017). The increased expression of miR-34a at diagnosis was associated with better outcome in ES (Nakatani et al., 2012) and the correlation of miR-34a with cyclin D1 and Ki-67 was also reported in ES (Marino et al., 2014). In EWS knockout mice, the upregulation of DROSHA was reported and that led to increased miR-125a and miR-351, which decreased UV radiation resistance-associated gene protein (UVRAG) mRNA. As result, the UVRAG-dependent autophagy pathway was deregulated (Kim, Y. et al., 2015).

1.4.3 miRNA regulation of CSC

The expression of miRNA has an effect on multiple genes (targets) and their involvement in tumorigenesis might result from their regulation of some specific targets. Identifying these specific targets is a critical step to clarify the role of miRNAs in cancer development. While the self-renewal mechanism and differentiation remain unclear in normal stem cells (SC) as well as CSCs, it has been proven in *Dicer1* and *DGCR8* null mouse models that changing the expression of miRNA leads to abnormalities in murine embryonic SC differentiation (Kanellopoulou et al., 2005; Wang, Y. et al., 2007). It is believed that miRNA can regulate a panel of transcription factors (Table 1.3) that modulate the self-renewal and differentiation processes.

Classification	miRNAs	Target genes		References
		Full name	Symbol	
Pluripotent	miR-137	Mind bomb 1	*Mib1*	(Smrt et al., 2010) (Mahmoudi and Cairns, 2017)
	miR-184	Numblike	*Numbl*	(Liu, C. et al., 2010)
	miR-200	Zinc finger E-box binding homeobox	*ZEB1; ZEB2*	(Wang, G. et al., 2013)
	miR-290	Cyclin-dependent kinase inhibitor 1a	*CDKN1a*	(Wang, Y. et al., 2008) (Wang, G. et al., 2013)
	miR-302		*Cyclin D1*	(Greer Card et al., 2008)
		Lysine-specific demethylase 1B	*AOF1*	
		Lysine-specific demethylase 1A	*AOF2*	
		Methyl CpG binding protein 1-p66 beta component	*MECP1-p66*	
		Methyl CpG binding protein 2	*MECP2*	
	miR-9	Leukemia-associated phosphoprotein p18	*Stathmin*	(Zheng et al., 2013) (Fenger et al., 2016)
Pro-differentiation	let-7	lin-28 homolog A	*Lin28*	(Peter, 2009) (Li, X. et al., 2012) (Yu et al., 2007) (Shimono et al., 2009)
		lin-28 homolog B	*Lin28B*	
		Insulin-like growth factor 2 mRNA binding protein 1	*IMP-1*	
		v-Ha-*ras* Harvey rat sarcoma viral oncogene homolog	*HRAS*	
		High mobility group AT-hook 2	*HMGA2*	
	miR-122		ND	(Deng et al., 2014)
	miR-134	Homeobox protein NANOG	*Nanog*	(Tay et al., 2008)
		Nuclear receptor subfamily 5, group A, member 2	*LRH1*	
		Sex determining region Y-box 2	*Sox2*	
	miR-145	Octamer-binding transcription factor 4	*Oct4*	(Xu, N. et al., 2009)
			Sox2	
		Kruppel-like factor 4	*KLF4*	
	miR-181		*Lin28*	(Li, X. et al., 2012) (Ji et al., 2009)
	miR-296		*Nanog*	(Tay et al., 2008)
	miR-470		*Nanog and Oct4*	(Tay et al., 2008)

Table 1.3 **Summary of miRNAs that regulate specific genes in CSCs.** List of miRNAs that are drivers of genes that regulate self-renewal and differentiation of CSCs. *ND (Not determined)* adopted from (Wang, Z.M. et al., 2013).

Furthermore, some transcription factors such as Myc-c can regulate the expression of miRNA that can affect the signalling pathways linked to self-renewal and differentiation (Greer Card et al., 2008; Lin, C. et al., 2009; Wang, G. et al., 2013). Also, MYC-C can be considered as regulator for many processes such as cell cycle progression, metabolism, epithelial–mesenchymal transition (EMT), metastasis, stemness, angiogenesis and assisting tumour initiation and progression (Jackstadt and Hermeking, 2015).The expression and activity of MYC-C are under the control of miRNAs and MYC-C itself directly regulate expression of some miRNA. These miRNAs are listed in the following Table 1.4.

The role of MYC-C					
MYC-induced miRNAs		MYC-repressed miRNAs		miRNAs targeting MYC-C	
miRNA	References	miRNA	References	miRNA	References
miR-9	(Ma, L. et al., 2010)	Lin28/let-7	(Friedman et al., 2009), (Schulte et al., 2008)	let-7	(Liao and Lu, 2011)
miR-17	(O'donnell et al., 2005), (He et al., 2005)	miR-15a/ 16-1	(Schulte et al., 2008), (Zhang, X. et al., 2012)	miR-24	(Kress et al., 2011), (Lal et al., 2009)
miR-18a	(Tanzer and Stadler, 2004), (Ventura et al., 2008)	miR-23a	(Lee, Y.S. and Dutta, 2007)	miR-34b/c	(Yamamura et al., 2012)
miR-19a	(O'donnell et al., 2005), (He et al., 2005)	miR-23b	(Lee, Y.S. and Dutta, 2007)	miR-145	(Sachdeva et al., 2009)
miR-19b-1	(O'donnell et al., 2005), (He et al., 2005)	miR-26a	(Hermeking, 2012), (Suzuki et al., 2009)	miR-148a	(Yang, J.D. and Roberts, 2010)
miR-20a	(O'donnell et al., 2005), (He	miR-29a/b	(Hermeking, 2012), (Mott	miR-184	(Liao and Lu, 2011)

	et al., 2005)		et al., 2010)		
miR-22	(Hermeking, 2012)	miR-34a	(Hermeking, 2012)	miR-185	(Han et al., 2013)
miR-25	(Kumar et al., 2013)	miR-148a	(Yang, J.D. and Roberts, 2010)	miR-196b	(Sampson et al., 2007)
miR-92a-1	(O'donnell et al., 2005), (He et al., 2005)	miR-185	(Han et al., 2013)	miR-449c	(Zhen et al., 2013)
miR-93	(Kumar et al., 2013)	miR-363	(Yang, J.D. and Roberts, 2010)	miR-494	(Sander et al., 2008)
miR-106b	(Kumar et al., 2013)				
miR-130a	(Mestdagh et al., 2010)				
miR-214	(Mestdagh et al., 2010)				
miR-378	(Feng et al., 2011)				

Table 1.4 List of miRNAs induced/repressed by MYC or targeting c-MYC

1.5 Cancer development and cell cycle regulation

It is now accepted that most cancers arise following accumulation of mutations in deoxyribonucleic acid (DNA), which can be inherited through cancer progeny and/or acquired with progression. The most commonly observed mutations found in cancer cells occur in tumour suppressor genes (TSG) and oncogenes. Loss of TSG expression such as p53, retinoblastoma protein (pRB) and phosphatase and tensin homolog (PTEN) frequently lead to cancer development (Friend et al., 1987; Lane and Crawford, 1979; Li, J. et al., 1997). Additionally, mutations in oncogenes or overexpression of proto-oncogenes result in increased proliferation and/or prevention of apoptosis contributing to cancer development and progression (Chang, E.H. et al., 1982; Payne et al., 1982). Initially, it was proposed that cancer

development required at least two genetic mutations (Knudson, 1971), more recently it has been estimated that 10 or more mutations are necessary for cancers to occur (Tomlinson, I.P. and Bodmer, 1995; Stoler et al., 1999; Tomlinson, I.P. et al., 2002) although this is likely cancer type dependent. Paediatric cancers have lower rates of mutations due to the developmental origins of these cancers, which differs from the accumulation of abnormalities with time in adult cancers (Vogelstein et al., 2013).

Alternatively, translocations between chromosomes, known as gene fusions, can drive cancer development and were reported for the first time in leukaemia (Rowley, 1973). Currently, high-resolution sequencing technologies such as next generation sequencing have enabled exploration of more fusion genes in tumours (Fonseca et al., 2017) revealing *BRAF, NTRK3*, and *RET* gene fusions in colorectal cancer (Kloosterman et al., 2017).

These mutations and fusions lead cancer cells to obtain more capabilities defined as the hallmarks of cancer. The development of cancer is extremely complex and has been considered a heterogeneous disease (Hanahan and Weinberg, 2000). Early research has focused on the development and cause of drug resistance in cancer, and studying the genetic and biochemical mechanisms that drive this phenomena to identify potential strategies to improve outcome (Hanahan and Weinberg, 2000). More recently, the intra-tumoral heterogeneity and microenvironment have been taken into consideration (Hanahan and Weinberg, 2011) and the mechanisms driving heterogeneity in cellular function remain uncertain. Non-genetic factors are also responsible for the maintenance of cancer stem cells (CSCs) hierarchies and also the development of neoplasm. Although the hierarchical organisation of tumours and how best to identify and isolate CSCs are not clear. The CSCs seem to have properties that make them clinically relevant (Kreso and Dick, 2014). Strong evidence suggests that a number of non-genetic factors essential in developmental pathways and epigenetic modifications, including DNA methylation, histone modification, chromatin openness, microRNA (miRNA), and expression of noncoding RNA are also essential in cancer development (Dick, 2008; Meacham and Morrison, 2013). Also, abnormal cell cycle activity is common in cancer as a

result of mutations or genetic lesions in genes encoding cell cycle proteins (Esteller, 2000).

1.6 The role of cell cycle proteins

The cell cycle is regulated by numerous cellular proteins known as cyclin-dependent kinases (CDKs) and their partner cyclins, and cell cycle inhibitors such as CDK inhibitors (CDKI) and CDK4 inhibitor (INK) (White and Dalton, 2005). These act together at different stages of the cell cycle to promote and/or restrain proliferation dependent on external cues.

During G1 phase, CDK4 and CDK6 work with cyclin D to promote entry into the cell cycle, while CDK2 acts with cyclin E to control progression from G1 to S phase (Sherr, 1994). CDK2 then complexes with cyclin A throughout S phase. Cyclin A also acts with CDK1 in late G2 and early mitosis to promote mitosis (M). CDK1-Cyclin B complex regulates M phase. Throughout the cell cycle, the levels of CDK proteins remain steady but the cyclin levels fluctuate to activate CDKs (Peng, J. et al., 1998).

1.6.1 Cell cycle factors in cancer

The accumulation of abnormalities in proto-oncogenes and tumour suppressor genes (TSGs) (E.g.; p53, p16, pRB, topoisomerase II, Chk1, MAD2, Cdc20 and breast cancer 1 (BRCA1) proteins) led to loss of cell cycle maintenance. In addition, overexpression of oncogenes (E.g. *RAS* family that involved in cell cycle maintenance), are common in cancer cells. These abnormalities result in cells pushed into a highly proliferative state with uncontrolled cell cycle (Hanahan and Weinberg, 2000). Moreover, the upregulation of selected anti-apoptotic proteins, for instance, B-cell lymphoma protein 2 (BCL-2), BCL-2 antagonist of cell death (BCL-xl) and BCL-2 like protein (BCL-w) and also downregulation of the pro-apoptotic proteins such as Bcl-2-associated X protein (BAX), BCL-2 homologous antagonist killer (BAK), BD3-interacting domain death agonist (BID) and

BCL-2 like protein 11 (BIM) increased the ability of cancer cells to evade apoptosis (Hanahan and Weinberg, 2000).

1.6.2 Involvement of CDKN1A-interacting zinc finger protein 1 (CIZ1) in cell cycle regulation

It has been shown that CIZ1 plays a central role in coordinating at least some of the key cell cycle transitions, CIZ1 interacting directly with the CDK inhibitor p21 (Mitsui et al., 1999), CDK2 (den Hollander et al., 2006), cyclin E and cyclin A (Copeland et al., 2010) (Figure 1.4).

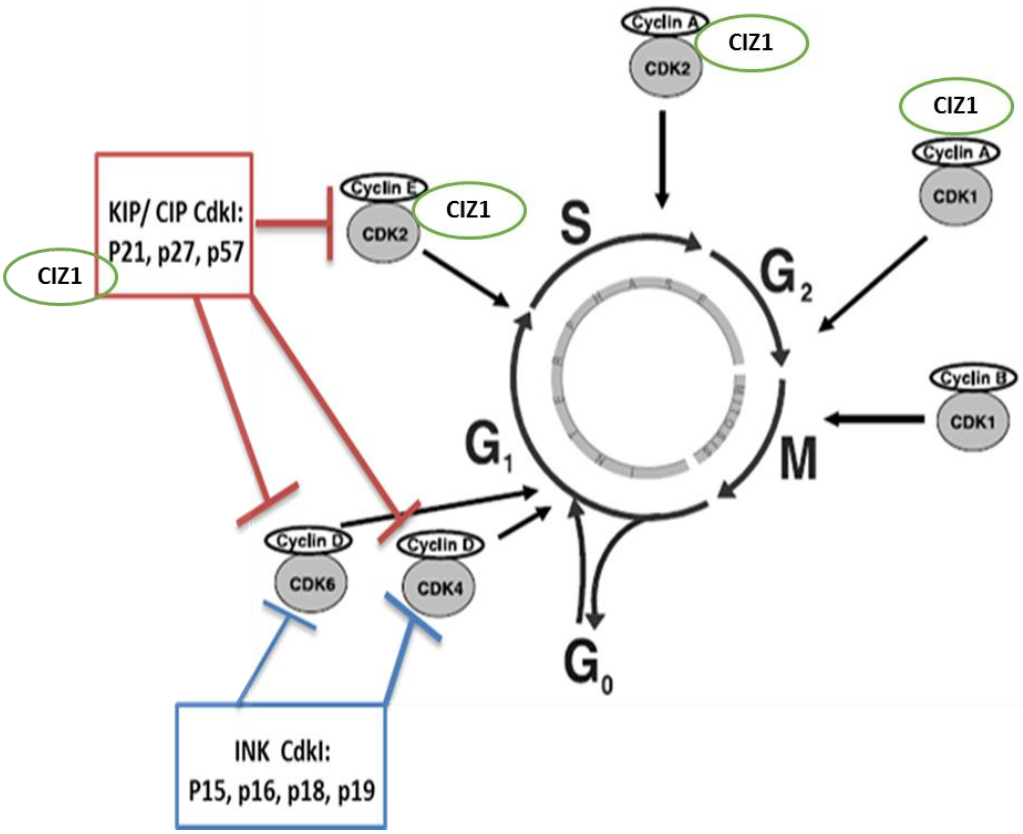

Figure 1.4 **Cell cycle regulators and inhibitors.** Cell cycle regulation by Cdk-Cyclin complexes and cell cycle inhibitors (Adapted from (Vermeulen, K. et al., 2003)). Kinase inhibitor protein (KIP), CDK inhibitors (CdkIs) and CDK interacting protein (CIP).

CIZ1 occupies sub-nuclear foci coincident with DNA replication foci in early S-phase, and was found to promote initiation of S-phase in a p21

independent manner (Coverley et al., 2005; Ainscough et al., 2007). These studies also determined that DNA replication activity is driven through *N*-terminal regions of the protein, while interaction with the dynamic sub-nuclear scaffold (nuclear matrix) is encoded within the *C*-terminus (Ainscough et al., 2007). Also, the existence of binding sites for the pre-replication complex (pre-RC) protein cell division cycle 6 (Cdc6) and cyclin A-CDK2 in the *N*-terminus has been confirmed (Copeland et al., 2015). Importantly, the CIZ1-matrix interaction is strong in differentiated cells, but relatively weak in stem cells, providing a means for alteration in nuclear activities, including transcription and DNA replication, as the cell undergoes the process of changing identity (Ainscough and Coverley, unpublished observations). More likely that the matrix itself is more dynamic (less fixed) in stem cells. CIZ1 is most likely part of the matrix.

1.6.3 CIZ1 in development and disease including cancer

CIZ1 has been associated with a growing number of disorders in which cell identity is deregulated (den Hollander et al., 2006; Rahman et al., 2007; Higgins et al., 2012) or involves altered control of proliferation (Judex et al., 2003; Dahmcke et al., 2008). Also, loss of CIZ1 associated with leukemia (Nishibe et al., 2013) and lymphoma (Ridings-Figueroa et al., 2017) (Table 1.5).

Cancer type	Role of CIZ1	References
Lung cancer	Knocking down of b-variant of CIZ1 lead to reduced tumour growth	Higgins et al. (2012)
Colorectal carcinoma (CRC)	Silencing of CIZ1 lead to reduced proliferation, and colony formation	Yin, J. et al. (2013)
Gall bladder carcinoma (GBC)	Knocking down of CIZ1 lead to reduced tumour growth and cell migration	Zhang, D. et al. (2015)
Prostate cancer	Silencing of CIZ1 lead to reduced tumour growth, reduced cell proliferation and affect G1 checkpoint activation	Liu, T. et al. (2015)

Cancer type	Role of CIZ1	References
Breast cancer	Knocking down of CIZ1 lead to reduced proliferation and anchorage dependence Overexpressing CIZ1 lead to increased oestrogen sensitivity and tumour size	den Hollander and Kumar (2006) (den Hollander et al., 2006)
Hepatocellular carcinoma	The present of CIZ1 increased proliferation and migration Knocking down of CIZ1 lead to reduced growth and metastasis	Lei et al. (2016) Wu, J. et al. (2016)
Leukaemia	The present of CIZ1 has anti-tumorigenesis effects	Nishibe et al. (2013)
Ewing's sarcoma family tumours	The role of overexpression of variant CIZ1ΔE8-12 and CIZ1ΔE4 remain unclear	Rahman et al. (2007) Rahman et al. (2010)
Lymphoma	The present of CIZ1 has anti-tumorigenesis effects	Ridings-Figueroa et al. (2017)

Table 1.5 **Summary of the confirmed association of CIZ1 in several types of cancers** Adapted from (Wu, J. et al., 2016; Pauzaite et al., 2017)

Different disorders appear to be associated with specific splice variants of the protein, some of which are expressed during normal mammalian development (Greaves et al., 2012) and in cultured stem cells (Greaves et al., 2012). Like cells and the embryonic or germ cell lineages, Ewing sarcoma (ES) family tumours lack exon 4 which affects the formation of CIZ1 foci as well as DNA replication (Rahman et al., 2007).

Full length CIZ1 is the most predominant form expressed in somatic adult tissues, including heart and lung, whereas CIZ1 splice variants are highly represented in differentiating male germ cells, with at least 7 variants found in the testis (Greaves et al., 2012). Also, a novel cancer-associated variant (CIZ1 delta 8-12) has been identified and validated in a range of cancer cell lines such as ES and primary lung tumours (Rahman et al., 2010).

While the relative roles of the individual splice forms still remains to be elucidated, it was recently demonstrated that overexpression of full length CIZ1 exclusively in cardiomyocytes of transgenic mice causes enlargement of the heart due to hyperplasia, without affecting cardiac function (Bageghni et al., 2017). The differences in CIZ1 variant expression and behavior in stem and differentiated cells, and observations of the loss of identity with

inappropriate variant expression, are consistent with a role in modulating the differentiation or malignancy process.

1.7 Thesis hypothesis and objectives

1.7.1 CIZ1 hypothesis

CIZ1 might plays a role in cancer development and regulation of pluripotency and differentiation and the loss of CIZ1 being sufficient to give rise to high frequency malignancy without introduction of additional oncogenic stimuli. Towards answering this hypothesis, I generated and characterized a CIZ1 null mouse. This work has been published (Ridings-Figueroa et al., 2017).

1.7.2 ES-CS-like hypothesis

Three-dimensional (3D) spheroids arising from a single cell will enrich for cells that have cancer stem-like properties and may be a useful *in vitro* tool to identify factors that contribute to tumour initiation and development. This may identify targets for the development of novel therapeutics.

The objectives of this part of my thesis have therefore been to;

1.7.2.1 Enrichment for ES-CS-like

Three methods (antigen expression, spheroid formation and selected growth in stem cell media) were investigated as methods to identify and enrich putative CS-like from ES cell lines.

1.7.2.2 Profiling the mRNA and miRNA signature in putative ES-CS-like

The spheroids produced from single cells (putative CS-like) were profiled using Taqman low density arrays for drug resistance and stem- and differentiation mRNAs, and selected miRNAs to identify the molecular drivers of putative CS-like in ES.

Chapter 2
Identification of the ES Family Tumours Cancer Stem-like Cells (CS-like)

2.1 Introduction

In 1976, Peter Nowell proposed the clonal evolution model of cancer development whereby cancer cells developed from normal cells which had accumulated a series of mutations, which result in proliferative advantage and tumour growth initiation at primary and secondary (metastatic) sites (Nowell, 1976). Furthermore, the hierarchical or cancer stem cells (CSC) model was developed in 1977 (Hamburger and Salmon, 1977). The CSC model, which showed that a small subpopulation of cells within the tumour, acquired a tumour initiating mutation which leads to increased capability for self-renewal and clonal expansion (Hamburger and Salmon, 1977). According to the CSC model, cancer cells derived from a mutated stem cell inherited self-renewal features from the stem cells, differentiation ability, clonal expansion and the expression of surface markers such as prominin-1 (CD133) (Zhu et al., 2009). Therefore, it is more accurate to term them cancer stem-like cells (CSCs) or cancer initiating cells (CIC), as they do not represent true stem cells since they are specialised; and they can give rise to various tumour populations similar to primary tumours.

In 1997, the presence of CSCs have been confirmed for the first time by transplantation assays using acute myeloid leukaemia cells (Bonnet and Dick, 1997). Also, CSCs have been verified in solid tumours in the breast (Al-Hajj et al., 2003), brain (Singh et al., 2003), prostate, pancreas (Li, C. et al., 2007) and colon (O'Brien, C. A. et al., 2007) . In 2009, CSCs were identified in the Ewing's sarcoma (ES) family of tumours (ESFT), by sorting cells for expression of the cell surface marker human prominin-1 (CD133) (Suvà et al., 2009). Some ES tumours are devoid of CD133 expressing cells (Jiang et al., 2010), consistent with the hypothesis that CD133 fails to identify all ES CSCs. Furthermore, CD133 expression may be down-regulated by the cellular microenvironment, such that the ES CSC becomes elusive.

Furthermore, Nestin protein has been proposed to represent a powerful prognostic marker and its expression has been evaluated in osteosarcoma (Zambo et al., 2012), whereas it remains uncertain in ES (Evola et al., 2017). Nestin-positive cells were detected in all of the examined high-grade osteosarcomas and it has been proposed that the high expression of nestin was associated with poorer clinical outcomes. However, their conclusion was that nestin is not an ideal marker to be used in conventional methods (Zambo et al., 2012). It would be interesting to check the expression of nestin in ES CD133 +ve/-ve population and the specify for CSC.

MYC-C, a proto-oncogene, is often upregulated in cancer, and it is highly expressed in ES cell lines (Sollazzo, M.R. et al., 1998). It has been suggested that the activation of the MYC-C promoter occurs through an indirect mechanism by the EWS-FLI1 gene (Bailly et al., 1994). MYC-C plays an important role in stem cell maintenance and nuclear reprogramming and also promotes stem cell properties. Moreover, it can regulate the expression of miRNA that can affect the signalling pathways linked to self-renewal and differentiation. Thus, it would be useful to evaluate the expression of MYC-C in ES cell lines as well as the putative ES-CS-like cells.

In the early 70s, the spherical cancer model had been developed (Inch et al., 1970; Sutherland et al., 1971). This three-dimensional (3D) model has been used at present under different terminologies and various preparation protocols. Due to the rapid development in CSC studies and the lack of exclusivity of CSC surface markers, CSCs have been identified and studied on the basis of functional criteria such as self-renewal capacity as well as migration ability. In human sarcoma cell lines, the 3D spheroids model enriches for key markers of normal stem cells more than cells in two-dimensional (2D) monolayer culture (Fujii et al., 2009). This has also been supported in lung cancer (Chung et al., 2015). Moreover, the morphology, as well as the proliferative index of spheroids generated from ES cell lines, have been confirmed to be more closely related to primary cells and to cell–cell junctions, and kinase activation (Lawlor et al., 2002).

The spheroid formation feature is specific for CSCs (Pastrana et al., 2011; Tirino et al., 2013; Martínez-Serrano et al., 2015). Several scientific groups have used serum-free medium containing one or both of the exogenous mitogens epidermal growth factor (EGF) and basic fibroblast growth factor (bFGF) to culture CSCs as spheroids (Fujii et al., 2009; Pastrana et al., 2011; Tirino et al., 2013; Chung et al., 2015). On the other hand, bFGF induces cell death in ES cell lines (Sturla et al., 2000). In glioma as well as lung cancer, the CSCs have the ability to form spheroids in the absence of exogenous mitogenic stimulation (Rafiee et al., 2015; Kelly, J.J.P. et al., 2009; Yakisich et al., 2016). In several murine and human cancer cell lines, the 3D culture can induce an enrichment in CSCs but only in a cell line manner, and spheroids occasionally show lower tumorigenic potential than 2D cells (Calvet et al., 2014). However, primary ES cells that cultured in serum-free medium showed no differences in the phenotype of the 2D cells and 3D spheroids, stating that the 3D culture does not enhance the self-renewal ability to generate secondary spheroids and the *in-vivo* tumorigenicity of primary ES cells (Leuchte et al., 2014).

I have sought to confirm that functional assay would be better approach than use cell surface markers (i.e. CD133) or stem cells media to enrich for ES-CS-like. The functional assay expected to enrich cells with self-renewal capacity with reduce migration that might be responsible for tumour relapse or progression. To help us test this hypothesis we need to:

1- Characterise the ES cell line capacity for migration, self-renewal and check the expression of CD133 and MYC-C.
2- Isolate/enriching the putative CS-like cells from ES cell lines using two different approaches: sorting cells for the putative CSC marker CD133 and identifying ES-CS-like cells exploiting self-renewing capacity in 3D cultures
3- Test the effect of two different stem cell media on the growth of ES cell lines and putative CSCs.
4- Characterise the putative ES CSCs capacity for migration, self-renewal and check the expression of CD133 and MYC-C. Also, check the morphology using immunohistochemistry.

2.2 Methodology

All reagents in this chapter were purchased from Sigma-Aldrich Ltd and all plastic ware from Corning® unless otherwise stated.

2.2.1 ES family tumours cell lines

There are six substrate adherent ES family tumours cell lines available in Professor S. Burchill group. Each cell line was cultured in a specific medium (Table 2.1) supplemented with 10% foetal calf serum (v/v; FCS, BioSera, Labtech International Ltd, East Sussex, UK) and 2mM L-glutamine (w/v). Cells were screened for mycoplasma contamination every four months by Ms Kimberley Cass (Leeds institute of Cancer and Pathology (LICAP); Clinical Trials Assistant, The University of Leeds) using the EZ-PCR mycoplasma test (Geneflow Ltd, Fradley, UK).

Cell Line		Medium	Origin	Fusion type	P53	Tumour source	Cell line source
ES family tumours	SK-N-MC	DMEM + F12 HAM + 10% FCS+ 2mM Glutamine	pPNET	EWS-FLI1 Type 1	Del*	14yr female	ATCC
	TC-32	RPMI 1640 + 10% FCS + 2mM Glutamine	pPNET	EWS-FLI1 Type 1	WT	17yr female	Gift from Dr Toretsky
	TTC-466	10% Conditioned RPMI 1640 + 10% FCS + 2mM Glutamine	Ewing's Sarcoma (extra osseous)	EWS-ERG	MS	Female Metastatic	Gift from Dr Paul Sorenson
	A673	DMEM+ 10% FCS + 2mM Glutamine	pPNET	EWS-FLI1 Type I	FS*	15yr female	ATCC
	RD-ES	RPMI + 10% FCS + 2mM Glutamine	Ewing's sarcoma	EWS-FLI1 Type II	MS	19yr male	ATCC
	SKES-1	McCoy's 5a + 15% FCS + 2mM Glutamine	Ewing's sarcoma	EWS-FLI1 Type II	MS	18yr male	ATCC
Colon cancer	Caco-2	RPMI 1640 + 10% FCS + 2mM Glutamine	N/A	N/A	N/A	N/A	Gift from Dr Sandra Bell

Table 2.1 **Characteristics and growth conditions of ES family tumours cell lines and other cell lines used as control**. All cell lines are human origin unless otherwise stated. All media was purchased from Invitrogen™ unless otherwise stated. Details of the origin of the ES cell line as well as EWS-ETS fusion type are given. DMEM = Dulbecco's Modified Eagle's Medium, pPNET = peripheral primitive neuroectodermal tumour, WT = wild type, FS = frameshift mutation, MS = missense mutation, * = mutation has caused loss of protein expression, ATCC = American Type Culture Collection, yr = years old, N/A= not applicable and Colon cancer = colorectal adenocarcinoma

2.2.2 Cell culture

All procedures were carried out in a class II microbiological safety cabinet (Envair Ltd, Lancashire, UK). All cell lines were cultured on Primaria™ 75 cm^2 plastic tissue culture flasks (BD Biosciences, Oxford, UK) at 37°C in 5% CO_2 in air (CO_2 incubator, SANYO Gallenkamp PLC, Leicestershire, UK). Cells were checked using a light microscope (Olympus CKX41 microscope, Southend-on-Sea, UK) and passaged when they were approximately 80% confluent. Phosphate buffered saline (PBS; w/v), 1xTrypsin (v/v) (10x Trypsin diluted in PBS), 0.1% (w/v) ethylenediaminetetraacetic acid (EDTA) and medium were pre-warmed to 37°C in a water bath prior to use.

To passage the cells, the medium was removed and cells washed with 5mL of pre-warmed PBS and then incubated with 0.1% EDTA (5mL) for 2 min. The EDTA was removed and cells were then incubated in 5mL of trypsin for 2 min at room temperature; the flask was tapped gently to and checked using a light microscope to ensure the majority of cells had detached. Cells were harvested into 5mL of medium and then pelleted in a tube by centrifugation for 5 min at 402*g*. The cell pellet was gently re-suspended in the splitting-ratio-growth medium for each cell line, using a fine tip strippette (StarLab Ltd, Milton Keynes, UK).

2.2.3 Determination of viable cell number

Viable cell number was determined using the trypan blue exclusion assay. Briefly, 10 µL of the cell suspension was mixed with an equal volume of trypan blue (0.4%; v/v); the cells were gently mixed and loaded into the chamber of a Neubauer haemocytometer (Hawksley, Sussex, UK). The total number of clear viable cells in the 16-box-grid was counted. Cells which take up the dye and appear blue are dead and were therefore excluded from the counts. The obtained value was multiplied by 104 to give the number of cells per mL. Alternatively, the Vi-CELL™ XR Cell Counter (Beckman Coulter, High Wycombe, UK) was used to determine cell viability. This instrument automates the manual trypan blue exclusion assay. Cell suspension (1mL)

was transferred to a sample cup and placed on the Vi-CELL™ XR Cell Counter. The cell suspension is taken up by the instrument, trypan blue dye added, and the number of viable cells is counted automatically. The calculated value of the viable cell number x 10^6/mL is provided. All viable cell numbers were performed in triplicate.

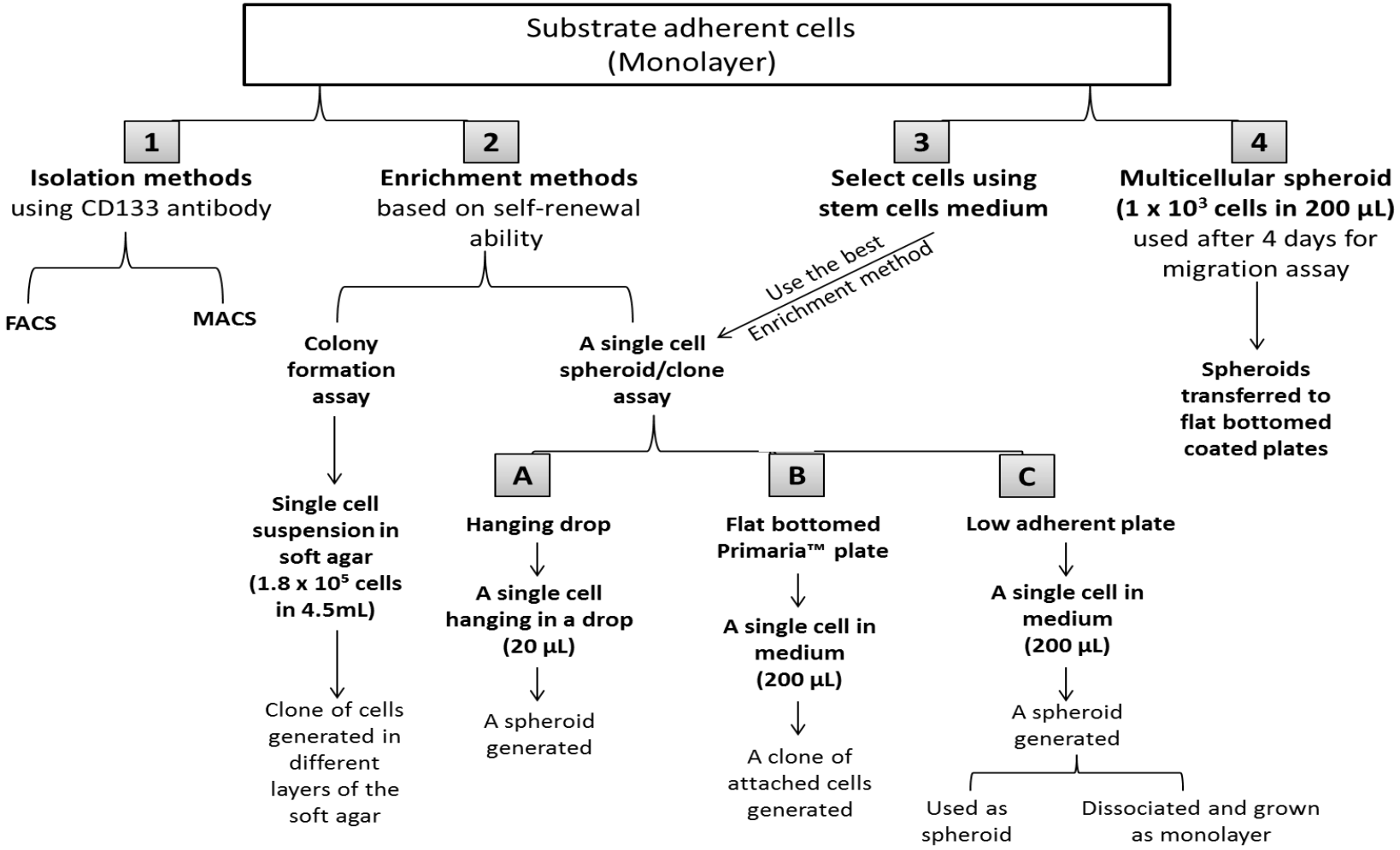

Figure 2.1 Different culture system that used to setup experiments in this chapter.

2.2.4 Isolation and enrichment methods for putative CS-like cells

2.2.4.1 **Selection of ES family tumours cells in stem cell medium**

ES family tumours cell lines (SK-N-MC, TTC-466 and TC-32) were seeded in either standard ES family tumours medium (Table 2.1), AggreWell™ medium or mTeSR™1 basal medium (STEMCELL Technologies Inc. Manchester, UK), supplemented with 100 mL of mTeSR™1 5X supplement, in non-coated or matrigel™ hESC-qualified matrix (BD Biosciences, supplied by VWR) pre-coated wells. The matrigel™ hESC-qualified matrix was aliquoted in cryovials according to the manufacturer's protocols (standard volume range = 270-350µl in each cryovial) as a single use. All aliquots were stored at -20°C and thawed on ice at 4°C overnight prior to use. To coat the wells of a 24 well flat-bottomed plate with matrigel™ solution, an aliquot of the thawed matrigel™ was added to a pre-chilled 50mL tube containing 25mL of cold DMEM/F12 medium. The mixture was mixed very well by pipetting up and down, and used immediately to coat the wells (200µL per well). Plates were incubated for 1 h at room temperature to allow the matrigel™ to solidify. Medium (1mL) was added to each well prior to use.

Cell suspensions (5 x10^4 cells /mL) were prepared in the three different types of medium. Cell suspension (1 mL/well) was seeded into three wells of a 24 for each condition; 1 mL of PBS was added into empty wells to maintain humidity. The plate was incubated at 37°C in 5% CO_2 in air for 24h, 48h or 72h. Each day, cells were harvested and the viable cell number was counted using Vi-CELL™ XR (Section 2.2.3).

2.2.4.2 **Single cell (Self-renewing) assays**

2.2.4.2.1 Hanging drops assay

Self-renewal ability was determined using the hanging drop method. A single cell suspension of 5 x 10^3 cells/mL was prepared (Section 2.2.3). This suspension was serially diluted in medium to achieve a dilution of one cell per 20 µL. The lid of a 100x20 mm tissue culture dish (BD Biosciences) was removed and 10mL of PBS was placed in the bottom of the dish to humidify

the dish. The lid was inverted and 20µl drops (each containing a single cell) were pipetted onto the bottom of the lid. In each dish, 40 drops of 20 µL were placed sufficiently apart so as to not touch. The lid was carefully inverted onto the PBS-containing bottom (Figure 2.2). The dish was carefully replaced into the incubator at 37°C, 5% CO_2 in air. The drops were monitored weekly using a light microscope for up to six weeks

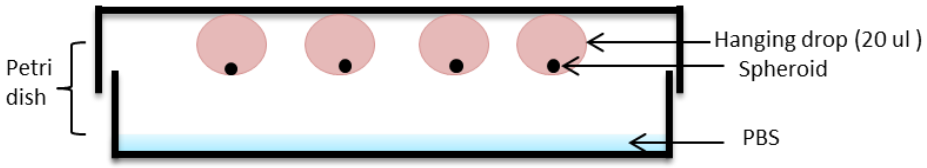

Figure 2.2 Schematic diagram of the layout of the hanging drop assay.

2.2.4.2.2 A single cell in low-adherent or flat Primaria™ plate

Cells were harvested (See section 2.2.3) and serially diluted to produce a single cell suspension in 200µL; initially, cells were diluted to 10^4 cells/mL. From this, a cell suspension (100µL) was added to 900µL of medium (1:10 dilution) to produce a 10^3 cells/mL cell suspension. Then 100µL of this suspension was added to 20mL of medium to get one cell per well (200µL). A single cell suspension (200µL) was added to all wells of a 96-well (Costar® Ultra- Low attachment multiwall or flat Primaria™ plates (Corning, supplied by SLS)). The plate was placed in an incubator at 37°C, 5% CO_2 in air for three to six weeks. Each week, spheroids were assessed and imaged by using a light microscope.

2.2.4.2.3 Colony formation assay

Two concentrations of noble agar solution in distilled water (3% and 5%; w/v) were prepared by dissolving agar powder 3mg and 5mg, respectively, in 100mL distilled water. These agar solutions were autoclaved and stored at room temperature prior to use. Cell line specific medium was pre-warmed to 37°C. Then medium (4.5 mL) was aliquoted into 15mL falcon tubes. The 5%

stock agar was heated in a microwave to melt the sterile-solid-agar and then placed in a water bath at 40°C. In the hood, 0.5mL of 5% agar was mixed with 4.5mL of medium and agitated quickly to ensure a uniform solution (without lumps of agar). The mixture (5mL of 0.5% agar) was poured into a 60mm tissue culture dish (Falcon, BD Biosciences, Oxford, UK) and allowed to set within the hood for 1h. This first layer of agar was used to prevent cells from attaching to the plastic. To set up the second layer of agar, the 3% agar was liquefied in the microwave and cooled in the water bath (40°C). While the 3% agar was cooling to 40°C, cells were harvested (Section 2.2.2), counted (Section 2.2.3) and re-suspended at a concentration of 1.8×10^5 cells in 4.5mL medium. The cell suspension was mixed with 0.5mL of 3% agar. Then the uniform mixture (0.3% agar) was poured over the 0.5% agar layer and the petri dishes were left in the hood at room temperature until the agar solidified. Agar dishes were then placed into a square dish (120x120mm) (Gosselin) containing an open dish (size of the dish= 60x15 mm; Falcon) containing 2mL of PBS to maintain humidity in the larger dish. The dishes were incubated at 37°C, in 5% CO_2 in air for nine days. After nine days, 0.2% (w/v) 2(4-Iodophenyl)-3 –(4-nitrophenyl)-5 – phenyltetrazolium violet (Tet-violet) was prepared by dissolving Tet-violet powder (100 mg) in distilled water (dH_2O;50 mL) and then filtering the dye into a sterile bottle. Tet-violet (500 µL) was layered onto the surface of the agar plate, and then the plates were returned to the incubator, 37°C, in 5% CO_2 in air for 24 h. The excess of Tet-violet dye was aspirated and the surface of the agar plate was washed with PBS (500 µL). The plate was examined using a light microscope at 10x magnification. The Tet-violet dye was used to distinguish between viable (dark pink or violet) and non-viable (clear) cells and colonies. Colony formation was calculated by counting the mean number of viable colonies in 16 fields of view (Figure 2.3). The resulting value was divided by the number of cells seeded in one field of view, and then multiplied by 100. To calculate the number of cells seeded into a field of view, the volume of a field of view (mm^3) was divided by the volume of the plate (mm^3), multiplied by the number of cells seeded; volume is equal to Pie multiplied by the depth of the agar, multiplied by the radius squared ($v = \pi r^2 h$).

$$\text{Colony forming efficiency (\%)} = \frac{\text{Number of colonies formed in field of view}}{\text{Number of cells seeded in field of view}} \times 100$$

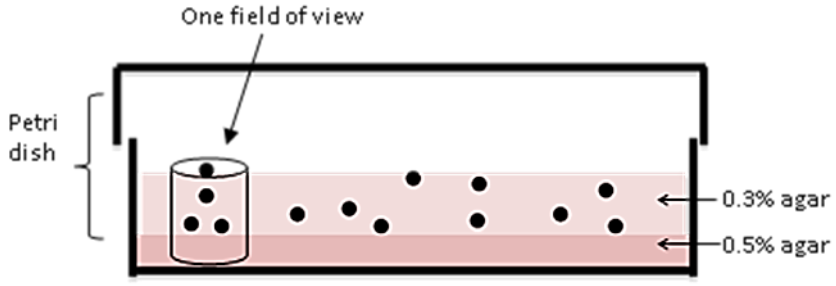

Figure 2.3 Schematic diagram of colony formation assay

2.2.4.3 **Antigenic isolation methods**

2.2.4.3.1 Cell separation using Magnetic MACS® Separator

Unless stated all reagents were purchased from Miltenyi Bio Ltd (Surrey, UK) and catalogue numbers in Appendix B.1. The cells were harvested and the total cell number was counted, as described previously (section 2.2.3 and section 2.2.3). Direct magnetic labelling was used; cells were centrifuged at 402*g* for 5 min, supernatant aspirated and cell pellets were re-suspended with a labelling mixture, which is enough to label up to 10^8 cells, consisting of 200 µL MACS buffer (0.5% BSA + 2mM EDTA in PBS), 100 µL FcR blocking buffer and 200 µL CD133 microbeads. If the total cell number exceeded 10^8 the volume of reagents was adjusted accordingly. The re-suspended cells were incubated at 4 °C for 30 min. Cells were then washed with 2mL of MACS buffer, centrifuged for 5 min at 402*g* and supernatant aspirated. The resulting cell pellet was re-suspended in 500 µL of MACS buffer. Three MACS columns were placed into a magnetic MACS® Separator, as illustrated in Figure 2.4 and washed with 3mL of MACS buffer.

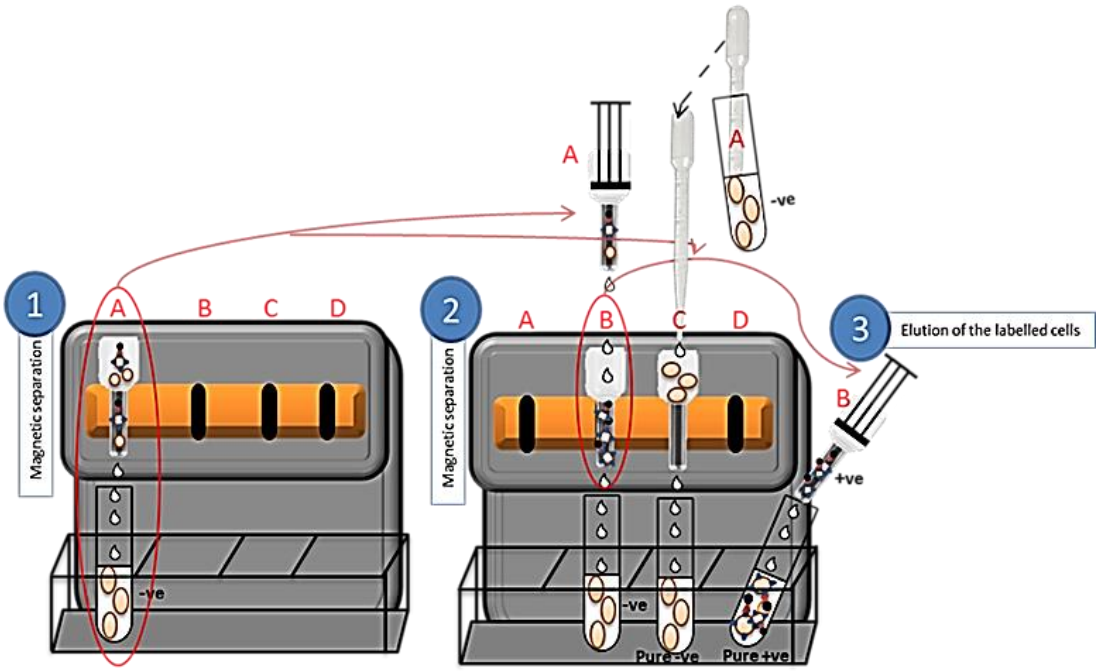

Figure 2.4 **Magnetic MACS® Separator that used to enrich for CD133 positive cell population**. Cells were labelled with CD133 micro-magnetic-beads. LS columns were used in columns A & B to enrich for CD133 positive cells. The CD133 negative fraction was collected from column C using an LD column that is specially designed for the stringent depletion of unlabelled cells (negative fraction).

The single cell suspension was loaded onto the first LS MACS column (LS column A) and washed three times with 3mL of MACS buffer. Cell flow through (negative fraction) was collected, centrifuged for 5 min at 402*g* and supernatant aspirated. The cell pellet was resuspended in 500 µL of MACS buffer and loaded onto LD column C. The LD column C was washed with 2 x 1mL MACS buffer, and the cells in the flow through were collected; these are the CD133 negative cells. To elute the positive fraction, LS column A was placed in the upper chamber of a second LS column B. 5mL of MACS buffer was added to LS column A and a plunger used to elute the positive cells from column A to column B. LS column B was washed three times with 3mL MACS buffer and the washes were discarded. LS column B was taken off the magnetic stand and the positive cell fraction was eluted in 5mL MACS buffer using the plunger. The positive and negative cells were centrifuged for 5 min at 402*g* and the total viable cell number was determined (see section 2.2.3).

Cells were processed, as illustrated in Figure 2.5, and incubated at 37°C, 5% CO_2 in the air. The flat bottom Primaria™ flasks were used to expand the sorted cells to be used for future downstream experiments. The purity of cells sort was checked by flow cytometry.

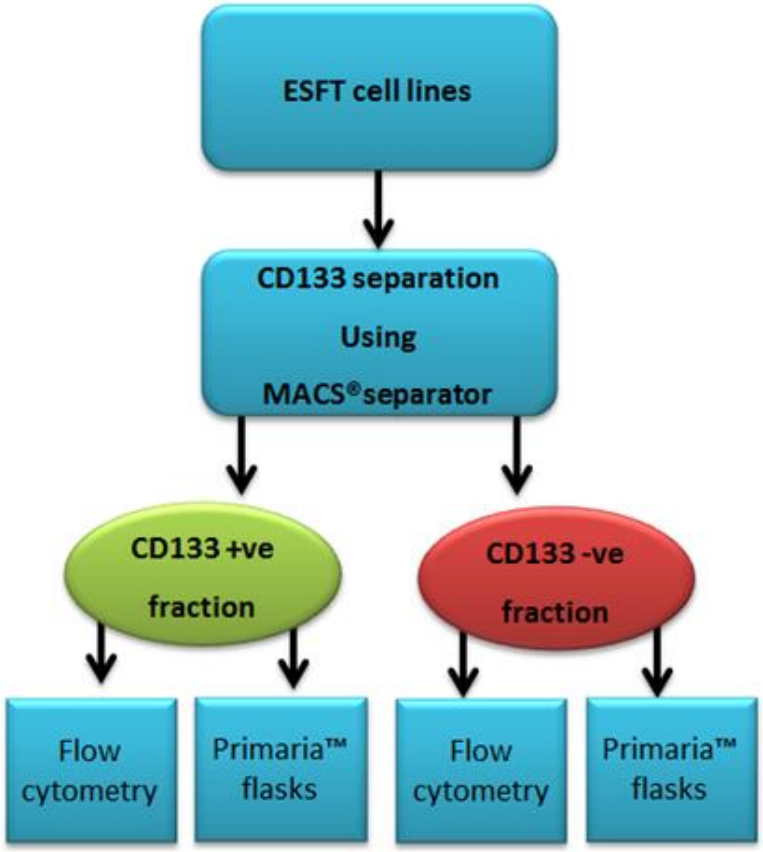

Figure 2.5 ES family tumours culture pathway after MACS® separation

2.2.4.3.2 Fluorescence Activated Cell Sorter (FACS)

All reagents were purchased from Miltenyi Bio Ltd (Surrey, UK) and catalogue numbers in Appendix B.2. A serial cell sort was performed by Dr. Adam Davison and/or Mrs Liz Straszynski (LICAP, St. James's University Hospital, Leeds) on three different ES family tumours cell lines (SK-N-MC, TTC-466 and TC-32). The cells were harvested and counted, as previously described in section 2.2.2 and section 2.2.3. The cells were stained in three different batches to keep the majority of cells alive during the long period of

sorting. To label up to 10^7 cells/100ul, an FcR blocking buffer (1:10) was mixed with an isotype or CD133 antibody (1:11) in MACS buffer (0.5%BSA +2mM EDTA in PBS) and incubated for 10 min at 4°C. The cells were centrifuged and the supernatant aspirated. The cells were washed with MACS buffer and centrifuged, and the supernatant aspirated. The resulting pellet was resuspended in 1mL MACS buffer and sorted by the FACS (BD Influx 6 Way Cell Sorter; BD Bioscience, UK). A single cell from the parental cell line was sorted into each well of a total of 30 plated of 96-well plates from each cell line. Similarly, the CD133+ve population and the CD133–ve population were sorted into wells from a total of 30 plated on 96-well plates. The rest of the stained cells were separated into sterile tubes for downstream experiments, as illustrated in Figure 2.16. All plates and flasks were incubated at 37°C, 5% CO_2 in the air.

2.2.5 Analytical methods

2.2.5.1 **Migration assay**

The migration assay was adapted from a previously published method (Vinci et al., 2013). The cell number was counted (Section 2.2.3) and the cells were diluted to 5 x 10^3 cells/mL in medium. Cell suspension (1 x 10^3 cells in 200 µL) was added to each well of a 96 well round bottomed Costar® Ultra- Low attachment multiwall plate (Corning,); 200µL of PBS was added into empty wells to prevent evaporation. The plate was incubated at 37°C, 5% CO_2 in air for four days. On the fifth day, a 24 well, flat-bottomed plate (BD Biosciences) was coated with 200 µL of 0.1% gelatin (in sterile distilled water). The gelatin was allowed to set for 1 h in an incubator at 37°C, 5% CO_2 in air. Growth medium (500 µL) was added to each well of the coated plate. Medium (100 µL) was removed and discarded from wells containing spheroids, taking care not to disrupt or move the spheroid. The remaining 100 µL of medium containing the spheroids was transferred into the gelatine coated plate using a sterile tip which was then removed; one spheroid was placed into each well. The cell spheroids were allowed to adhere to the gelatine and imaged using a light microscope at 4x magnification on the

same day (0h) and after 24, 48 and 72 h. Images were analysed using Volocity software 6.3 (PerKin Elmer, Cambridge, UK). Spheroid core and migration zone were outlined using the freehand tool of Volocity (Figure 2.6). At each time point, the calculated pixel count was noted for each of these zones. The migration value for each time point was calculated by using the following formula:

$$\text{Migration index (MI)} = \frac{(\text{migration zone - core at time point})}{\text{core at 0 hour}}$$

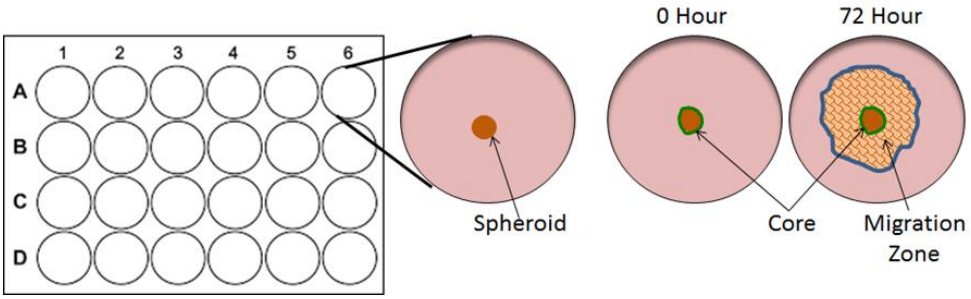

Figure 2.6 **Schematic diagram of migration assay**. Green = the edge of spheroid core and Blue = the edge of migration zone.

2.2.5.2 **Protein analysis**

Frozen cells pellets from human embryonic stem (hES) cells known as SHEF4 were used as control. These cells was gifted from Professor Peter Andrews (Department of Biomedical Science, The University of Sheffield) and cultured by Mrs Andrea Berry (Senior research technician, LICAP, The University of Leeds) using feeder-free culture conditions using Matrigel™ coated plastic and mTesR™1 medium. Additionally, frozen cell pellets from previously sorted cells based on their expression of CD133 by Mrs Berry as well as substrate adherent cells and a pool of three week spheroids (3-w-spheroids) were used. The 3-w-SK-N-MC spheroids were resuspended and cultured as substrate adherent cells and passaged 3 times. At each time point, cells were pelleted and frozen for future use.

2.2.5.2.1 Protein extraction

Medium was aspirated from ES family tumours cell lines and the cells were washed with PBS (5mL). The cells were scraped into 0.5mL PBS using a scraper (IWAKI, ASAHI Techna Glass, 9000-220, Japan) and then transferred to a 1.5mL centrifuge tube. Cells were pelleted at 1000 rpm for 5 min and the excess PBS was aspirated. The cells were re-suspended in RIPA buffer (1% Nonidet P-40, 0.5% Sodium Deoxycholate and 0.1% Sodium dodecyl sulphate (SDS) in PBS) containing inhibitors (100 µL/mL phenylmethylsulfonyl fluoride (PMSF; 1mg/mL in isopropanol), 10 µL/mL Sodium Orthovanadate (100nM Stock), 30 µL/mL Leupeptin (10µg/mL stock), and 30 µL/mL Aprotinin) to lyse the cells. The lysate was incubated on ice for 30 min with vigorous mixing and then centrifuged at 1300 rpm for 10 min at 4°C. Supernatants were used for the protein assay and western blotting, whereas the pellets were discarded.

2.2.5.2.2 Bradford Protein-assay

The concentration of the extracted protein was measured using Bio-Rad protein assay following the recommended protocol (Bio-Rad Laboratories Ltd., Hertfordshire, UK). Briefly, seven standard dilution series (0.1 to 2 µg/µl) of Bovine Serum Albumin (BSA; 2mg/mL in 10% RIPA buffer) were prepared (Appendix A.1.2). Proteins were diluted with dH_2O (5µl of protein into 45µl of dH_2O). Each dilution out of the seven dilution series (5µl) was loaded into a row of a 96 well flat-bottomed plate (Corning) in triplicate. The test proteins were loaded in triplicate into remaining wells. SA reagent (25µl), which contained 20µl and 1mL of reagent S and A respectively, was added to each well. Then 200µl of reagent B was added to each well and mixed gently. The plate was incubated at room temperature for 15 min and then protein absorbance was measured at a wavelength of 690nm on a multi-scan microplate reader connected with ascent software (Titertek®, Titertek Instruments Ltd, Lancashire, UK). To calculate the protein concentration, the average absorbance value of the BSA standard triplicates was calculated, and the average protein concentration triplicates was also calculated.

Concentrations were plotted versus absorbance using a scatter plot with a trend-line, using Microsoft Excel to calculate the equation: y=mx + c.

2.2.5.2.3 Western blot

Proteins were mixed with an equal volume of 2x SDS-loading buffer containing 20% DTT, heated to 95°C for 5 min before cooling immediately on ice. To analyse the extracted proteins, a mini-protein® TGX Gel (4-20%) plate (Bio-Rad Laboratories, Inc., Hertfordshire, UK) was placed into a gel tank filled with 2x SDS running buffer (0.1% SDS (w/v), 25mM Tris-HCl pH8.3 (ICN Biomedicals Inc. Hampshire, UK) and 250mM Glycine). The samples (50µg) were loaded into each lane, and a Tris-Glycine molecular weight marker (3µl; Geneflow Ltd, Staffordshire, UK) was also loaded. Gel was run at 150 volts at room temperature to separate protein bands until the dye ran off the gel (≈ one h).

Protein bands were transferred to a nitrocellulose membrane (Hybond™-C membrane; Amersham, Little Chalfont, Buckinghamshire, UK) by electroblotting. The gel was removed from the mini-protein® TGX Gel (4-20%) plate and integrated into a sandwich with a filling of foam; a 7.5 x 10 cm filter paper (Bio-Rad); a single sheet of nitrocellulose membrane; the gel; a 7.5 x 10 cm filter paper, and another foam. All sandwich components were pre-soaked in a cold transfer buffer (0.01% SDS (w/v), 25mM Tris-HCl pH8.3, 192mM Glycine and 20% methanol). The sandwich was placed into a western blotting tank (Bio-Rad) and run at 300 mA for 90 min at room temperature, with an ice pack and magnetic stirrer used to maintain a stable temperature.

The membrane was then incubated in a Li-cor blocking buffer (5 mL; Li-cor Biosciences) and placed on a rotating platform at room temperature for 30 min. Next, the blocking buffer was replaced with a 1° antibody at working strength (Appendix A.1.1) in 50:50 Blocking buffer: PBS, 0.1% Tween-20 (TPBS) and incubated overnight at 4°C on a shaking platform (Heidolph Unimux 1010). The following day, the membrane was washed three times with TPBS (10 mL) over a period of 5 min to remove any unbound 1°

antibody. Next, the membrane was incubated for 1 hr with 50: 50 mixture supplemented with an HRP conjugated 2° antibody (1:5000) on a rotating platform at room temperature. Again, the membrane was washed with three changes of 10mL TPBS spanning a 5 min period, followed by two washes with PBS 5 min each. Finally, the membrane was scanned using Li-cor Odyssey infrared imaging system software (Li-cor Biosciences) in order to visualise the immunoreactive bands. To check the protein loading, Ponceau S Stain (Amresco, USA) was applied to the membrane and washed with tap water after 15 min incubation. The membrane was left to dry at room temperature and then imaged.

2.2.5.3 **Molecular analysis**

2.2.5.3.1 Total RNA extraction

ES family tumours cell lines were pelleted and lysed in a 1.5mL tube using miRNeasy Micro Kit (Qiagen, Manchester, UK) by adding 700 µL of QIAzol Lysis Reagent and pipetting or vortexing. Homogenates were incubated at room temperature for 5 min to dissociate nucleoprotein complexes. Then chloroform (140µL) was added and the samples were shaken vigorously for 15 s before being incubated at room temperature for 2-3 min. The samples were centrifuged at 4°C for 15 min at 12,000*g*. The upper aqueous RNA containing phase was transferred to a 1.5mL microfuge tube. Following the addition of 100% ethanol (525 µl) and thoroughly mixing, the solution was transferred into an RNeasy MinElute spin column in a 1.5 mL collection tube. RNA was separated by centrifugation for 15 s at 8000*g* at room temperature. The spin column containing total RNA was washed with 700 µl of RWT buffer (prepared with ethanol) and centrifuged for 15 s at 8000*g*. Then the spin column membrane was washed with 500 µl of RPE buffer (Salt prepared with 100% ethanol) and centrifuged for 15 s at 8000*g*. The final wash was with 80% ethanol and centrifuged for 2 min at 8000*g*. Then the collection tube was changed and the spin column was centrifuged with the lid open for 5 min at 8000*g*. Total RNA, including miRNA and other small RNA molecules, was

eluted in a new collection tube by adding 10-14 µL RNase-free water to the centre of the spin column membrane and centrifuge with the lid closed for 1 min.

2.2.5.3.2 NanoDrop® spectrophotometer

The concentration of RNA samples was measured using a NanoDrop® spectrophotometer (NanoDrop 1000; labtech International Ltd, East Sussex, UK). The protein content was calculated at a wavelength of 280nm. The absorbance ratio at A260nm/A280nm was calculated to measure the amount of protein content in relation to RNA. Then total RNA was incubated for 5 min at 95°C, and then stored at -80°C until required.

2.2.5.3.3 Preparation of complementary DNA (cDNA)

Total RNA was reverse transcribed (RT) into first-strand cDNA using SuperScript™ III. RNA made up (120ng) in 15µl of RNase-free H_2O and denatured by heating to 95°C for 5 min, cooled on ice for 5 min and then added to the RT reaction (5µl for each reaction). A total of 20 µl reaction was prepared for each target including RT positive (RT+ve; target gene and housekeeping gene) and an RT negative (RT-ve; housekeeping gene) to ensure that no genomic DNA contamination and the amplification detected is from the synthesised cDNA only. RT was prepared containing the following reagents in (Table **2.2**). The reaction was heated to 25°C for 5 min, and then incubated at 50°C for 60 min and deactivated at 70°C for 15 min using the TC-500 (Techne, supplied by SLS). The cDNA was stored at -80°C until required.

		RT+ve per sample		RT-ve per sample	
Reagent	Suppliers	Volume (µl)	Final concentration	Volume (µl)	Final concentration
RNase-free H_20		7.8		4.9	
1 x First-Strand Buffer	Invitrogen™	8	1X	4	1X
deoxyribonucleotide triphosphate (dNTPs)	Amersham Biosciences	4	1mM	2	1mM
Magnesium chloride ($MgCl_2$)	Invitrogen™	3.2	8mM	1.6	8mM
Random Hexamer Primers	Invitrogen™	2	0.3µg	1	0.3µg
RNasin® Plus RNase Inhibitor	Promega	1	16 units	0.5	16 units
Dithiothreitol (DTT)	Invitrogen™	2	0.1M	1	0.1M
Superscript™ III Reverse Transcripase	Invitrogen™	2	200 units	N/A	N/A
Total mix per sample		30		15	

Table 2.2 Reagents in RT+ve and RT-ve reactions

2.2.5.3.4 Quantitative real-time polymerase chain reaction (RTqPCR)

To determine gene expression levels relative to the housekeeping gene (PPIA), TaqMan® Gene Expression Assays (Life technologies) were used. The assay reaction contained cDNA (20µl) that was prepared as described previously (Section 2.2.5.3.3) and a mixture of reagents (Table 2.3). Samples (25µl/well) were loaded in triplicate in 96 well plates (Applied Biosystems). The plates were covered with MicroAmp Optical Adhesive Film (Applied Biosystems) and centrifuged for 1-2 min, before being analysed using a ABI PRISM™ 7500 Sequence detector under the following conditions: 50°C for 2 min, 95°C for 10 min and then 40 cycles of 95°C for 15 s and 60°C for 1 min. The results were analysed using 7500 System SDS software version 1.2.3. The fold change in the target gene expression was normalised to the expression of an endogenous control (PPIA) and relative to a reference sample and calculated by the formula:

$$\textbf{\% Relative to PPIA} = 2^{-\Delta\Delta Ct} \times 100.$$

Where; ΔCt for gene = Ct gene – Ct housekeeping gene

ΔΔCt = ΔCt test sample - ΔCt reference sample

	Reagents	Volume (µl, per sample)	Final concentration
Target Mix	TaqMan Universal PCR Master Mix	50	1X
	20X Assay-on-Demand™ primer/probe mix (Applied Biosystems; Appendix D.1.1)	5	1X
	RNase free H2O	25	
PPIA Mix	TaqMan Universal PCR Master Mix	50	1X
	PPIA forward primer (10µM) 5'-GGACCCAACACAAATGGTTCC-3'	2	200 nM
	PPIA reverse primer (10µM) 5'-CTTTCACTTTGCCAAACACCA-3'	2	200 nM
	PPIA probe (20µM) 5'-ATGCTTGCCATCCAACCACTCAGTCTTG-3'	0.5	100 nM
	RNase free H2O	22.5	

Table 2.3 **RTqPCR reagents using Assay-on-Demand™ and PPIA as housekeeping gene**

2.2.5.4 **Flow cytometry**

All catalogue numbers of antibodies and isotypes can be found in Appendix B.2. Cells were seeded at a concentration of 5 x 10^5 cells/well into Primaria™ 6-well plates and incubated at 37°C, 5% CO_2 in air for 24 h to allow the cells to adhere. Cells were then harvested and counted (as described previously in section 2.2.2 and 2.2.3), stained, and fixed for flow cytometric analysis. Two different procedures were used depending on the cellular localisation of the target protein and the epitopes to which the antibodies were bound. For extracellular epitopes, all centrifugation steps were carried out at 402*g* for 5 min. When labelling intracellular epitopes, all centrifugation steps were carried out at 200*g* for 5 min. All data analyses were performed in triplicate and analysed on an Attune®cytometer (ThermoFisher Scientific, UK).

2.2.5.4.1 Labelling extracellular epitopes

Cell pellets were re-suspended in 50 µL a primary antibody (CD133-PE) at the dilution of 1:10 (Personal communication) with an FcR blocking buffer (1:10; Miltenyi Biotec Ltd.) in MACS buffer (0.5%BSA +2mM EDTA in PBS) and incubated for 10 min at 4°C. The cells were centrifuged and the supernatant aspirated, and then they were washed with 0.5mL MACS buffer before being centrifuged and the supernatant aspirated. The cells were fixed with freshly prepared 1% paraformaldehyde (PFA) in PBS for 15 min at room temperature. The resulting pellet was resuspended in 1mL MACS buffer and analysed. An isotype matched (IgG2b-PE) control was used to assess the non-specific binding of the secondary antibody. A total of 10,000 events for each sample were analysed and all experiments performed in triplicate. The fold change in expression was calculated as the fluorescence of the target stained cells divided by the fluorescence of cells stained with the isotype matched control antibody.

2.2.5.4.2 Labelling the intracellular epitopes

The harvested cells were permeabilised on ice with 500µl 0.1% Triton X-100 (Amersham, GE Healthcare; in 5% FCS/PBS) for 30 min followed by a wash in 0.5mL FACS buffer (10%FCS in 1x PBS), then centrifuged and the supernatant aspirated. Cell pellets were suspended in 50 µL conjugated antibody (c-Myc or Isotype Control) at a serial dilution of 1:25 -1:400 in FACS buffer and incubated for 30 min at 4°C in the dark. The cells were washed with FACS buffer, centrifuged at 200*g* for 5 min and the supernatant aspirated. The resulting cell pellets were fixed with freshly prepared 1% PFA in PBS for 15 min at room temperature, washed and then analysed as described above (section 2.2.5.4.1). The optimal concentration of 1:25 was used to stain ES family tumours cell lines as three replicates per experiment, and three biological repeats were performed.

2.2.5.4.3 Double staining

Cells have been stained with CD133 antibody as described in Section 2.2.5.4.1. After fixation cells were permeabilised then stained with MYC-C antibody as described in Section 2.2.5.4.2. ES family tumours cell lines stained as three replicates per experiment and three biological repeats were performed.

2.2.5.5 **Histology**

2.2.5.5.1 Cells and spheroids processing and sectioning

Cells were harvested as described previously (Section 2.2.2). Blunted 1mL pipette tips were used to protect the spheroids' shape when they were collected. Cell pellets and spheroids were fixed with 10% neutral buffered formalin (CellPath Ltd, UK) overnight. The fixative was aspirated and replaced with 70% ethanol before embedding. The spheroids were embedded in 2% agar (2g of agar in 100 mL PBS); the mixture was heated in the microwave until it became homogenous, and then cooled prior to use. Solidified cell pellets and spheroids-in-agar were placed in histological cassettes and kept in 70% ethanol before processing.

Cassettes were processed on a Leica ASP200 tissue processor (Leica Microsystems (UK) Ltd, UK) using a routine protocol. Briefly, cassettes were dehydrated in a series of ethanol solutions, starting with 70% and completing with 100%. Cassettes were cleared from ethanol by using multiple changes of xylene, and finally infused with paraffin wax (The protocol details; Appendix C.1.1). Then agar embedded cells pellet and spheroids were embedded in paraffin wax (CellPath Ltd, UK) and the paraffin blocks were stored at 4˚C until sectioning.

The paraffin blocks were sectioned at 4µm using a rotatory microtome (AS325 retraction Thermo Shandon; Thermo Scientific, UK). Sections were placed in a water bath (Leica HI1210; Leica Microsystems (UK) Ltd, UK) at 45˚C and, carefully, one section was placed onto superfrost® plus glass slides (Thermo Scientific, UK). The slides were dried overnight in an oven

(Galaxy B; Scientific Laboratory Supplies Ltd (SLS), UK) at 37˚C. Prior to staining, the slides were heated for 20 min at 60˚C on a hot plate (SH3, Stuart Scientific, Bibby Scientific Limited (Group HQ), UK).

2.2.5.5.2 Haematoxylin and Eosin (H&E) Staining

The slides were dewaxed in two changes of xylene for 5 min each and rehydrated in three changes of graded ethanol (100%, 90% and 70%) for 2 min each. The slides were washed with running tap water for 5 min. Cell nuclei were stained with Meyer's haematoxylin (Appendix C.1.2) for 15sec. The slides were rinsed in running tap water for 1 min. Sections were immersed in Scott's solution (sodium hydrogen carbonate (0.35%; w/v), magnesium sulphate (2%; w/v) in dH2O) for 1 min and then rinsed in tap water for 1 min. The cells were stained with eosin (Eosin Y-solution 0.5% aqueous) for 2 min and then rinsed in tap water for 1 min.

The slides were dehydrated for 1 min in two changes of graded ethanol (70% and 90%) and 2 min in 100% ethanol. The slides were transferred in two changes of xylene for 2 min each, and then permanently mounted in DPX (Distrene, Plasticizer, Xylene or Dibutyl, Phthalate, Xylene) mounting medium. The slides were imaged using the Axioplan two light microscope (Zeiss, Cambridge, UK).

2.2.5.5.3 Detection of antigens using three-stage peroxidase method

The slides were dewaxed and rehydrated, as described in Section 2.2.5.5.2. Antigen retrieval was performed submerging the slides in a citric acid buffer (10mM Citric acid, pH6, Sigma) and heating in a microwave for 12 min. The slides were transferred onto ice for cooling. Sections were rinsed in running tap water for 5 min. To reduce endogenous peroxidase activity, the sections were incubated in 3% hydrogen peroxide in PBS for 5 min; this was followed by submersion for 5 min in two changes of PBS. To block biotin-binding proteins or endogenous biotin, the Avidin/Biotin blocking kit (Invitrogen, UK) was used. The sections were incubated with Avidin (2 drops; 50 µL/drop from

the stock) for 10 min then washed twice in TPBS (0.1% Tween in PBS). Then the sections were incubated with Biotin (2 drops; 50 µL/drop from the stock) for 10 min before being washed twice in TPBS. To block non-specific secondary antibody binding sites, the sections were incubated for 1 h with a diluted normal serum (1:10; in TPBS) enriched from the same species as the secondary antibody (Dako, Cambridgeshire, UK). The sections were incubated with 100 µL of a diluted primary antibody (Appendix C.1.3) in antibody diluent for 1 h then washed twice in TPBS. An optimised concentration (1:200; diluted in antibody diluent) of secondary antibody (100 µL; Dako) was applied to sections and incubated for 30 min then washed twice in TPBS. Sections were incubated with 100 µL Streptavidin-Peroxidase (Abcam) for 10 min then washed twice in TPBS. Sections were covered with 3, 3'diaminobenzidine (DAB) substrate (one drop of DAB chromogen per mL of the substrate buffer; Dako) and incubated for 5-15 min, allowing a brown precipitate to develop. The sections were rinsed in running tap water for 5 min then counterstained with Haematoxylin for 15 s and sections were then washed in running tap water for 1 min. Then the sections were submersed in Scott's solution for 1 min and rinsed in tap water for 1 min. The sections were dehydrated and mounted as described previously (Section 2.2.5.5.2). The slides were imaged using a Zeiss Axioplan light microscope.

2.2.5.5.4 Cytospin

Cells were harvested and counted as described in Section 2.2.2 and 2.2.3. Superfrost® plus glass slides were placed in the bottom of a cytospin-carrier. A filter card was added on top of the slides, and a funnel chamber was secured with the fastening ring. Cell suspension (500 µL) was loaded into the cytospin funnel, and the top covering was secured to the cytospin chamber and placed in a Hettich Rotorfix 32A centrifuge. The slides were centrifuged for 3 min at 1000 rpm. The supernatant, and then the funnel were removed. The slides were centrifuged for a further minute at 3000 rpm before being air-dried overnight at room temperature. The slides were wrapped in aluminium foil and stored at -80˚C in the freezer until they were stained.

2.2.5.5.5 Immunofluorescence staining

Cytospin slides were defrosted at room temperature for 20 min. Once the slides were dried, two fixatives were investigated: slides were immersed in 4% PFA in PBS or fresh 0.3% w/v 1,4-benzoquinone in 1X DPBS for 10 min. The slides were rinsed with PBS for 1 min, and then the slides with a Shandon Coverplate™ were placed on a Shandon Sequenza™ Slide Rack (Thermo scientific, UK). Blocking buffer (100µL; 10%; v/v goat serum in Tween-PBS) was applied and slides incubated at room temperature for 30 min. In CD133/2 (293C3) pure optimisation, 100 µl of a diluted primary antibody (Appendix C.1.4) in the blocking buffer was applied and allowed to sit for 10 min at 4°C. Whereas, for Nestin optimisation, the slides were incubated for 30 min at 4°C with a primary antibody (Appendix C.1.4) in the blocking buffer. Then the slides were rinsed four times with TPBS for 1 min each. The secondary antibody was added (100 µl; 1:500 in blocking buffer) and incubated for 30 min at room temperature. The negative control slide for each antibody was stained with the secondary antibody alone. Then the slides were rinsed four times with TPBS for 1 min each, then once in PBS for 1 min before being mounted permanently onto superfrost microscope slides (Thermo Scientific) using a drop of Dako Faramount Aqueous Mounting Medium Ready-to-use (Dako). The mounting medium was allowed to set overnight in the dark at room temperature before imaging using a Nikon Eclipse Ti-E Inverted Microscope System (Nikon Instruments, Nikon UK Limited UK).

In a separate experiment, slides were stained with the CD133/2 (293C3) pure antibody in the optimised concentration (1:10) for 10 min at 4°C. Then the slides were rinsed. Next, the secondary antibody was added and washed as described above. Following the washing step, Nestin antibody was added to the slides at a 1:200 dilution and slides were rinsed, mounted and imaged as described above (Section 2.2.5.5.5).

2.2.6 Statistical methods

Analyses were undertaken using GraphPad prism 7 software. When comparing more than 3 cell lines, data were analysed by ANOVA with Tukey's multiple comparisons test as post-hoc test. The difference between cell lines was assessed using a two-tailed unpaired t test with Welch’s correction. The differences were considered significant when $p<0.05$.

2.3 Results

2.3.1 Characterization of ES cell lines

In this section, three cell lines from the original panel of six were selected based on the expression of p53 that remains a promising prognostic biomarker (Section 1.1.4, for more details). TC-32 expresses wild-type p53, whereas TTC-466 expresses mutated p53 (missence mutation) and deletion of p53 occurs in SK-N-MC. Like TTC-466, RD-ES and SKES-1 express mutated p53. Thus, they were excluded from the study. On other hand, frameshift mutation is occurring in A673 and caused loss of protein expression (Brownhill et al., 2007). In addition, the karyotyping result showed multiple-copies of chromosomes in A673 (Brownhill, personal communication), thus it was excluded from the study.

2.3.1.1 Migration capability of ES

Migration indexes (MI), which is the area covered by at least 70% of cells 'migration zone' minus the area of the core, of ES cell lines were determined as described (Section 2.2.5.1). SK-N-MC and TTC-466 showed no difference (29.3 ± 1.4 and 29.5 ± 1.3, respectively), whereas TC-32 cells migrated less than SK-N-MC and TTC-466 cells at 72 h (MI = 19.5 ± 1.6). The difference between SK-N-MC and TC-32 was significant (ANOVA, Tukey's multiple comparisons tests; p = 0.0016); and there was also a significant difference between TTC-466 and TC-32 (p = 0.0003; Figure 2.7).

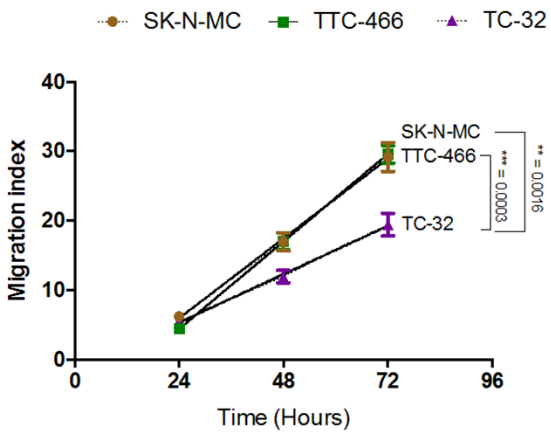

Figure 2.7 **Summary of migration results of ES cell lines.** Migration of ES cell lines (SK-N-MC, TTC-466, and TC-32). Independent experiments (n = 3 experiments, with 3 replicates in each experiment) were combined and grouped into three different time points.

Although there was no significant difference in the maximum migration of SK-N-MC and TTC-466 cells, there were substantial differences in the migration phenotypes. The cores of TTC-466 cells disappeared after 24 h, and the majority of cells migrated as a sheet with a defined edge. This was in contrast to the migration of the TC-32 cells in which case individual cells seemed to migrate from the spheroid core, which increased in size over 72 h (fold change: 6.2 ± 0.6). The SK-N-MC cells, however, maintained a distinct spheroid core (fold change: 2.2 ± 0.2), while most of the cells had migrated as a sheet with a defined edge (Figure 2.8).

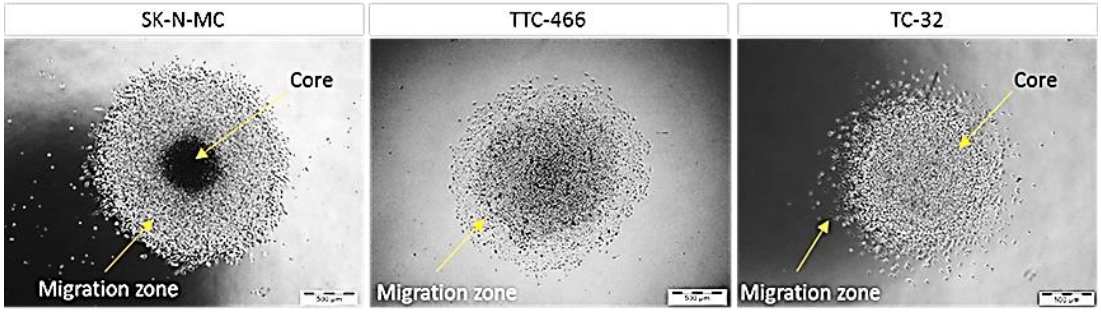

Figure 2.8 Phenotype of ES cell spheroid migration. ES cell lines grown as spheroids for four days then plated onto gelatine (0.1%)-coated plastic and imaged at 72 h.

2.3.1.2 Self-renewing capacity of ES in soft agar

ES cell lines formed colonies of different sizes (five to 50+ cells) in soft agar. SK-N-MC cells formed the largest colonies, and there was a trend for the largest colonies to sit in the top layer, whereas the smaller colonies were in the lower layer of the agar. However, there was no difference between the colony size of TTC-466 and TC-32 cells (Figure 2.9). The colony formation assay was repeated three times. The cells had the ability to form colonies in soft agar in all the three cell lines. SK-N-MC cells had the highest capability to form colonies (8.3% ± 0.15) in soft agar. TTC-466 cells had a colony-forming efficiency of 6.8% ± 0.05; TC-32 cells had the lowest colony-forming efficiency (4.1% ± 1.15; Figure 2.10). The majority of TC-32 cells were single cells; therefore, TC-32 cells have the lowest number of colonies compared to SK-N-MC and TTC-466 cells. The colony-forming efficiency was significantly

higher in SK-N-MC and TTC-466 cells than in TC-32 cells (p<0.0001). SK-N-MC and TTC-466 cells also showed a significant difference between them (p=0.0003; Figure 2.10).

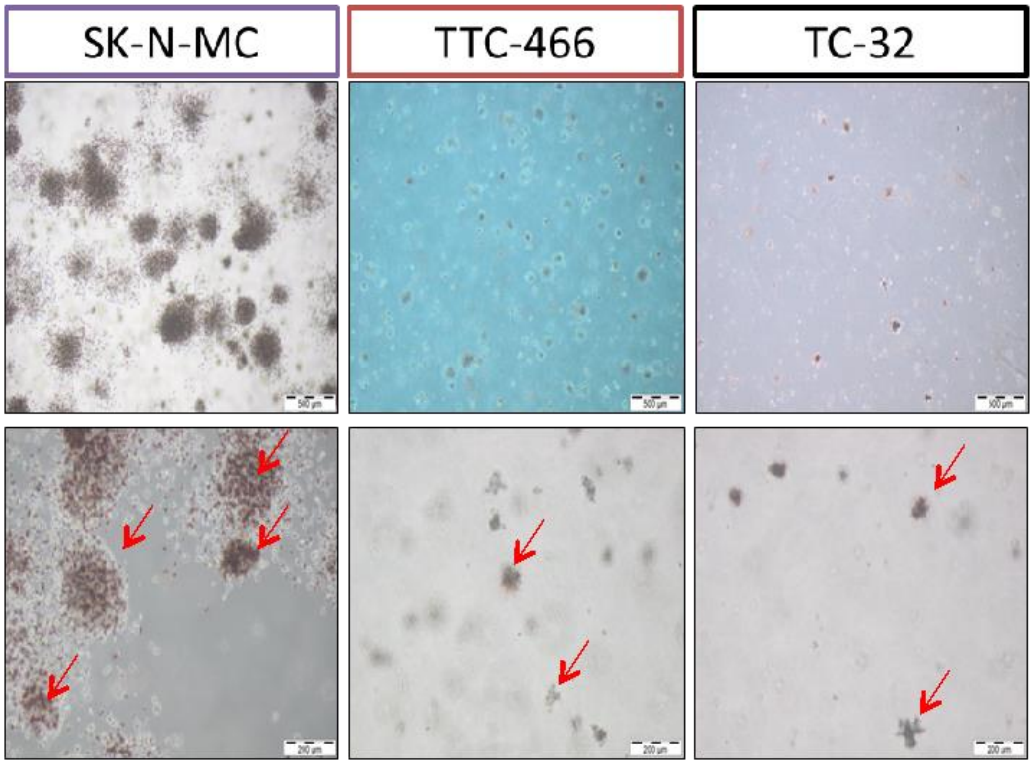

Figure 2.9 **Phenotype of clonogenic assay results of ES cell lines.** Clonogenic assay shows the ability of ES cell lines (SK-N-MC, TTC-466, and TC-32) to form colonies from single cells in soft agar. Dark pink/violet colonies are viable (see arrows), whereas clear cells are non-viable.

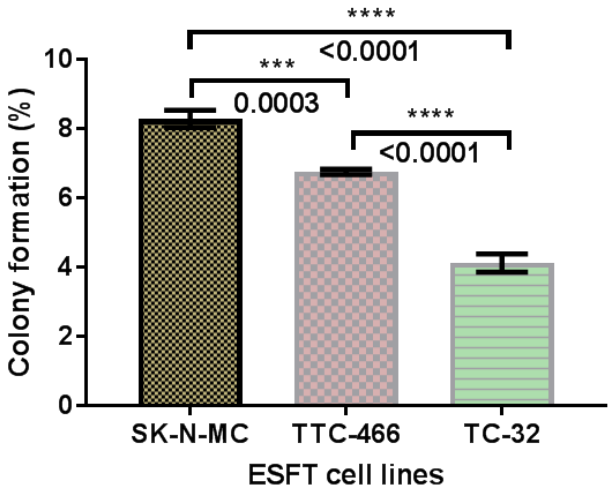

Figure 2.10 **Summary of clonogenic assay results of ES cell lines**. Colony-formation efficiency in ES cell lines (SK-N-MC, TTC-466, and TC-32). Summary of three independent experiments, two repeats in each experiment.

2.3.1.3 Expression of a putative stem cell marker, prominin-1 (CD133)

In ES cell lines, the percentages of CD133+ve populations in 10,000 events were 1.7%±0.6, 14.5%±0.7, and 4.9%±1.9 in SK-N-MC, TTC-466, and TC-32 cells, respectively (Figure 2.11 B).

2.3.1.4 The expression level of MYC-C

MYC-C, a proto-oncogene, is often upregulated in cancer, and it also promotes stem cell properties. MYC-C is expressed intracellularly, thus cells required permeabilisation step before staining. The dilution of the MYC-C antibody was optimized using serial dilutions ranging from 1:25 to 1:400, and the optimization was performed in triplicate (Figure 2.12). The optimal dilution (1:25) was used to investigate the expression of MYC-C in ES cell lines. For the double staining experiment, an additional control (strongly positive for CD133) are required. CaCo-2 is an ideal positive control for CD133, but it was available toward the end of my project.

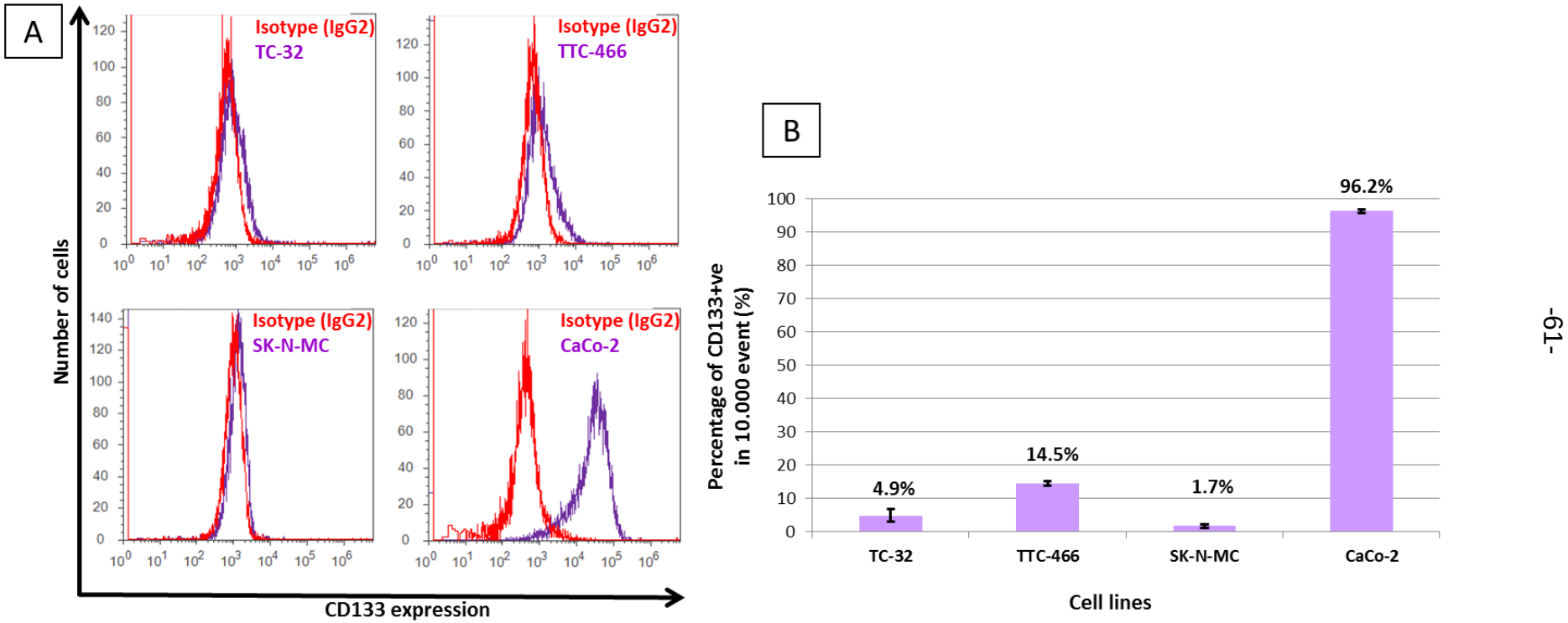

Figure 2.11 Protein expression of CD133 in ES cell lines and CaCo-2 determined by flow cytometry. A) Representative fluorescence plots of cell lines stained with an isotype control (Red) and a CD133 antibody (Purple). B) Shows the calculated percentage of CD133 expression relative to the isotype control. Results are presented as the mean of three independent replicates.

-61-

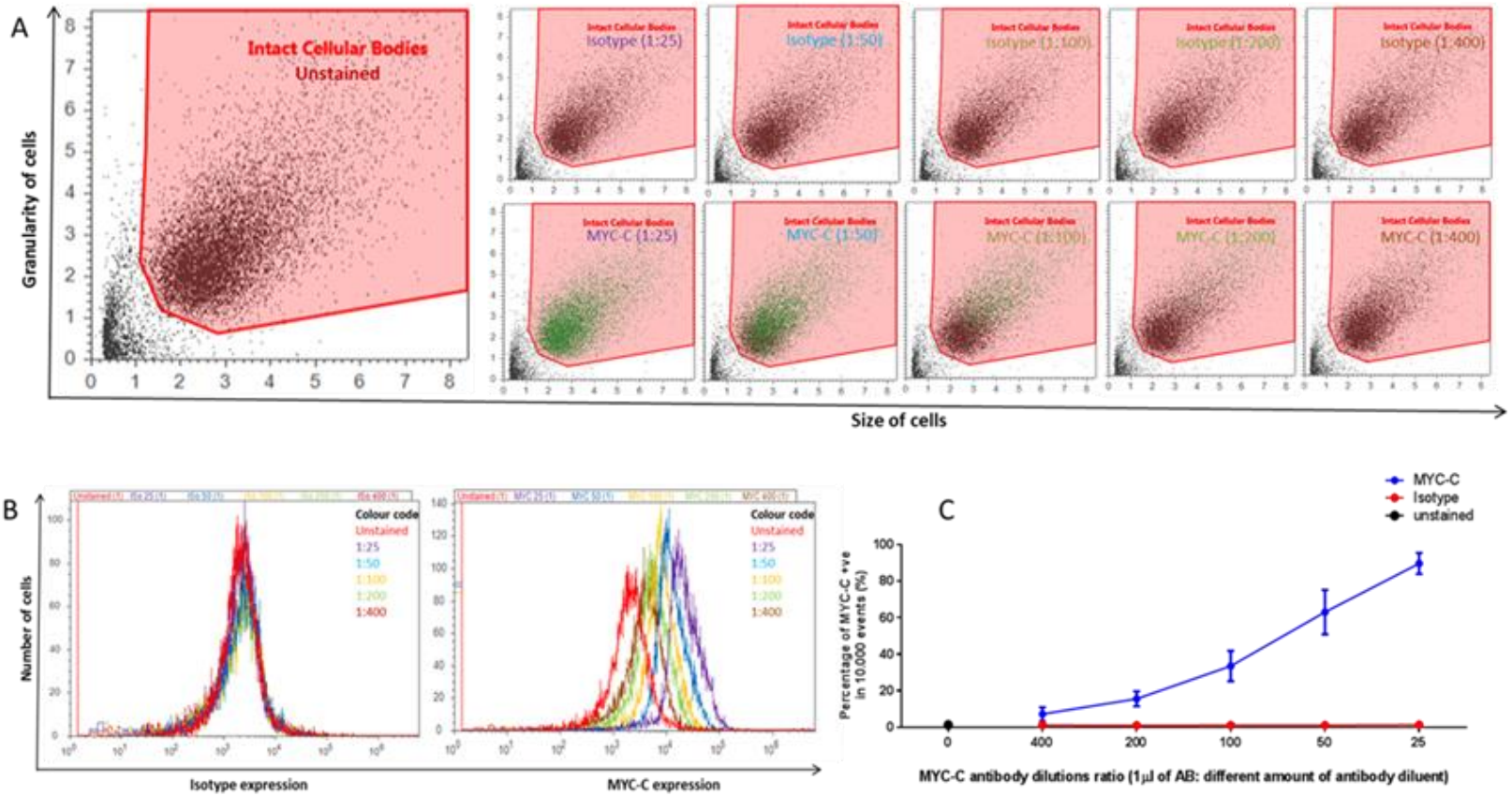

Figure 2.12 Titration of MYC-C antibody in TC-32 cell lines determined by flow cytometry. A) Representative cell scatters show gated, intact cellular bodies by using the back-gating tool for each concentration. This tool was used to determine which cells would fall into the analysis: isotype or negative cells (Black) and positive cells (Green). B) Representative fluorescence plots of cells stained with serial dilutions of isotype control and MYC-C antibody (Red [unstained], purple [1:25], blue [1:50], yellow [1:100], green [1:200], and brown [1:400]). C) Displays the percentage of the positive population that was stained with the isotype control and MYC-C. Results are presented as the mean of three independent replicates.

-62-

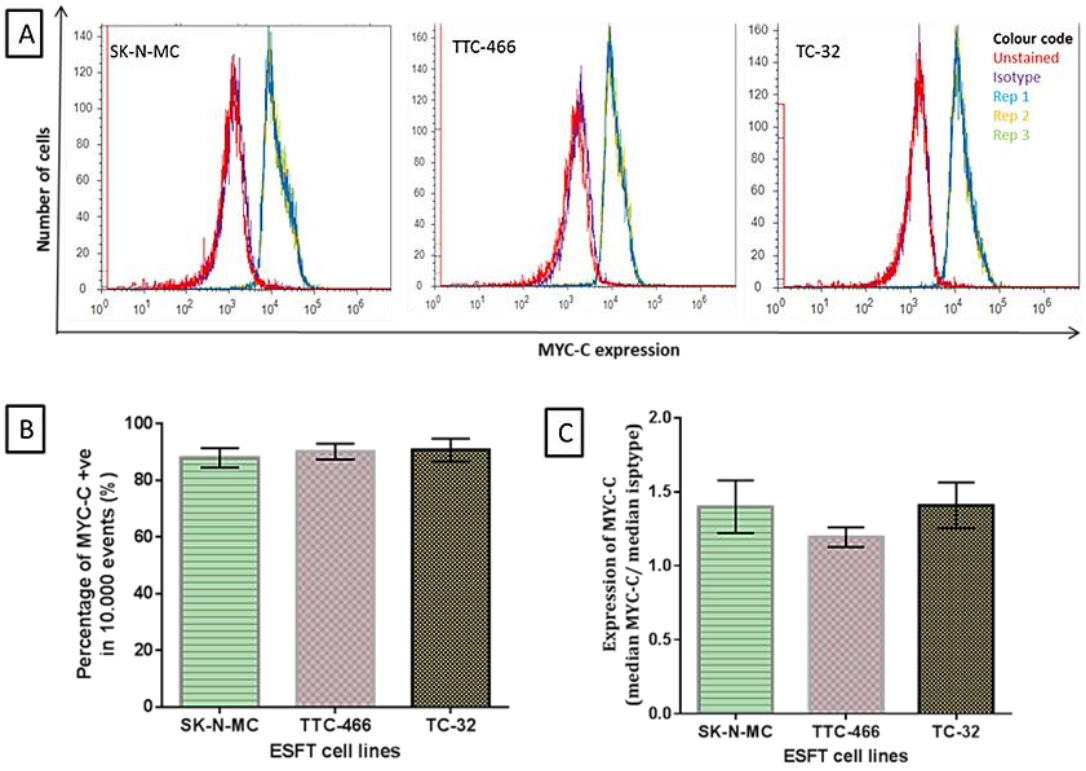

Figure 2.13 **MYC-C expression in ES cell lines determined by flow cytometry**. A) Representative fluorescence plots of cells stained with 1:25 dilutions of the isotype control (Purple) and the MYC-C antibody (three repeats: blue, yellow and green). The unstained cells used to confirm the negativity (Red). B) Displays the percentage of the positive population that normalized using an isotype control. C) The expression level of MYC-C in ES cell lines. Results are presented as the mean of three independent replicates.

ES cell lines highly express MYC-C (Figure 2.13 A). The percentage of MYC-C in SK-N-MC, TTC-466, and TC-32 cells analysed by FACS was 87.96%±3.4, 90.17% ± 2.8, and 90.96% ± 4.0, respectively (Figure 2.13 B, left). There was no significant difference in the level of MYC-C expression across all three ES cell lines: SK-N-MC, TTC-466, and TC-32 (median fluorescence: 1.4 ± 0.18, 1.19 ± 0.07, and 1.4 ± 0.15, respectively; Figure 2.13 C). In ES cell lines, the majority of CD133-ve cells are strongly positive for MYC-C. In CD133+ve cells, 35.4% of SK-N-MC, 27.3% of TC-32 and 34.6% of TTC-466 were expressing CD133 only, whereas, 64.6%, 72.7% and 65.4% were co-expressing CD133 and MYC-C in SK-N-MC, TC-32 and TTC-466 respectively (Figure 2.14).

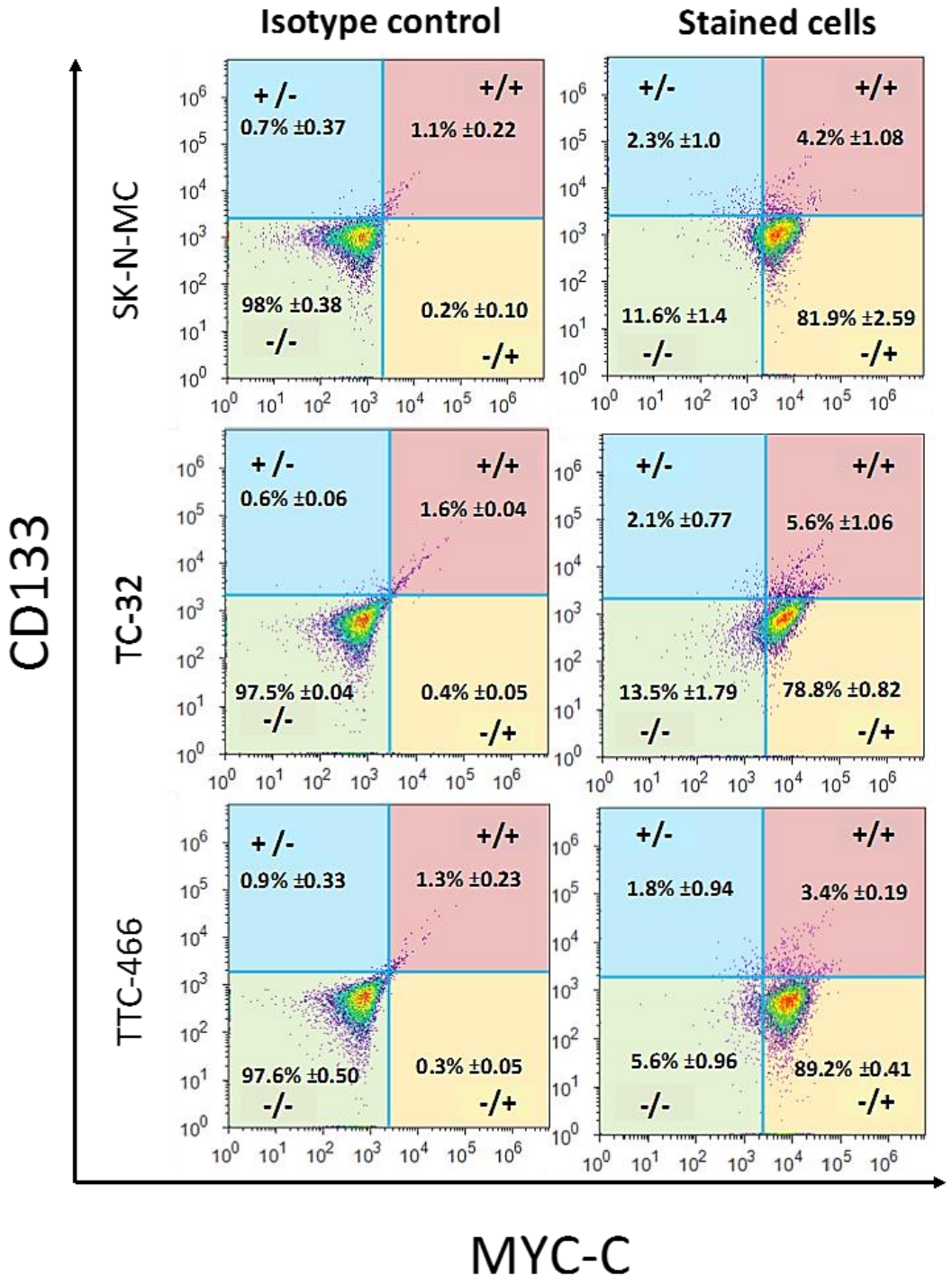

Figure 2.14 Expression of CD133 and MYC-C analysis by flow cytometry. Results demonstrate the percentages of CD133 MYC-C +ve/-ve cells in ES cell lines. Averages of cells are normalised to the matched isotype. This figure is representative of three experiments with a total of three repeats in each cell line.

MYC-C expression was also checked by western blot in all the ES cell lines. The expression of MYC-C was homogeneous in ES cell lines. MYC-C expression was slightly lower in A-673 and very low in SHEF-4 compared to the other ES cell lines (Figure 2.15). The antibody detects a band between 57 and 65 kDa that may include several isoforms of MYC-C. This may be a possible reason for seeing additional bands for MYC-C.

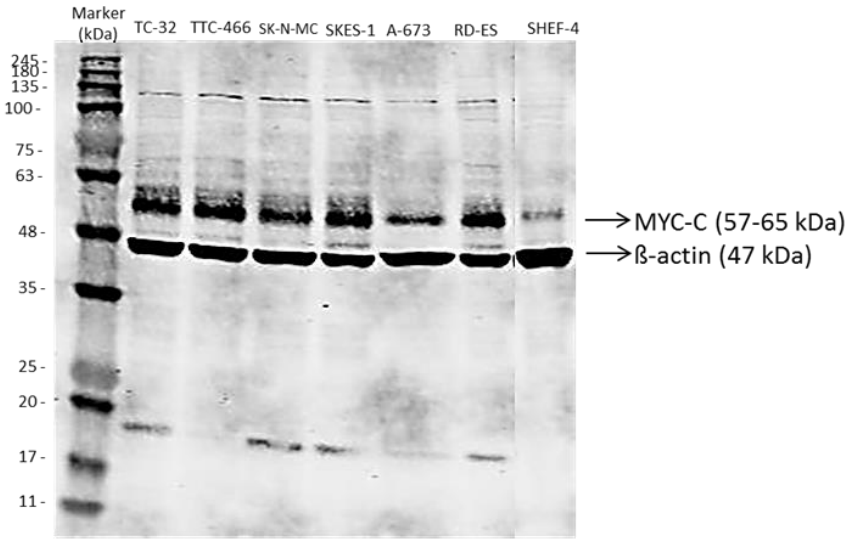

Figure 2.15 Protein expression of MYC-C. ES cell lines (TC-32, TTC-466, SK-N-MC, SKES-1, A-673, and RD-ES) and embryonic stem cells (SHEF-4) expressed MYC-C normally (upper band), as well as Beta-actin (loading control; lower band).

2.3.2 Isolation of putative ES-CSCs

2.3.2.1 Antigenic method using prominin-1 (CD133)

Two different methods were used to enrich and to isolate CD133+ve population. The first method used was magnetic cell separation via manual MACS® cell separation. The percentages of CD133+ve viable cells after sorting the ES cell line were 0.8% ± 0.5, 1.5% ± 0.8 and 2.9% ± 2.5 in SK-N-MC, TTC-466 and TC-32, respectively. Some of CD133-ve population were used as a negative control. The purities of the separated population were

60% for CD133+ve cells and 12% for CD133-ve cells. The optimised antibody concentration was increased to improve the separation efficiency; however, the number of cells, recovered from the separation, was very small and we could not run a purity check on flow cytometry or immunofluorescence.

The second technique used for positive and negative selection was a FACS; BD Influx 6-Way Cell Sorter (BD Biosciences). To sort the CD133 populations the CD133+ve cells region is designated the positive events, and the CD133-ve region is designated the negative events (Figure **2.17** A). After sorting the cells an aliquot from the positive and negative populations was analysed by FACS to check the purity of the two populations then culture as illustrated in Figure 2.16. Some of the CD133+ve/-ve fractions were cultured in flat bottom Primaria™ flasks for future downstream experiments, whereas cytospin used to confirm the purity of the sorted cells using IF technique. Also, to check the ability of CD133+ve and –ve cells to self-renewal and to generate spheroids/clones, cells were sorted as single cell in each well of 96-well plates.

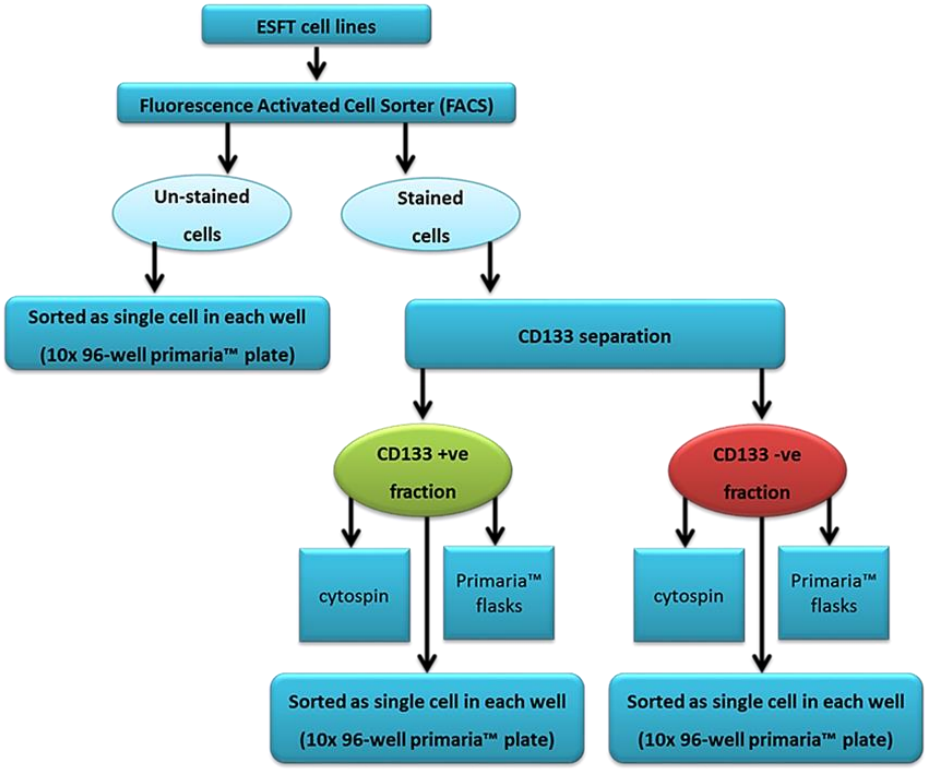

Figure 2.16 ES family tumours culture pathway after the FACS sort

The FACS showed that all sorted ES cell lines were highly pure (Figure **2.17** B). In TC-32, the purity for the CD133+ve population was 99.07%, whereas CD133-ve was 98.63% pure. The sorted TTC-466 cells were 98.67% CD133-ve and 96.91% CD133+ve. In SK-N-MC cells, the purity of the CD133+ve cells was not checked due to the small number of sorted SK-N-MC-positive cells; however, the CD133-ve was 99.37% pure.

To confirm the purity of the sorted cells the cells were stained by immunofluorescence (Figure 2.18). Two fixatives, 0.3% 1,4-benzoquinone and 4% PFA, were used to identify the ideal fixative and then CD133 antibody was optimized using dilutions at 1:5 and 1:10 as described (Section 2.2.5.4.1, Figure 2.18, the dilution of CD133 was 1:5 and 1:10; other dilutions data not shown). Some staining was identified in the 4% PFA-fixed cells at all concentrations, whereas the 0.3% 1,4-benzoquinone fixative resulted in reproducible staining for CD133 (Figure 2.18). Like CD133, Nestin antibody was optimized using the ideal fixative for CD133 (method described in Section 2.2.5.4.3, data not shown). The positive population of sorted ES cell lines showed a high positivity for CD133, whereas the negative population was completely negative. All ES cell lines expressed Nestin protein, whether CD133+ve or CD133-ve. In ES cells, the positive population showed a co-localization between CD133 and Nestin (Figure 2.19).

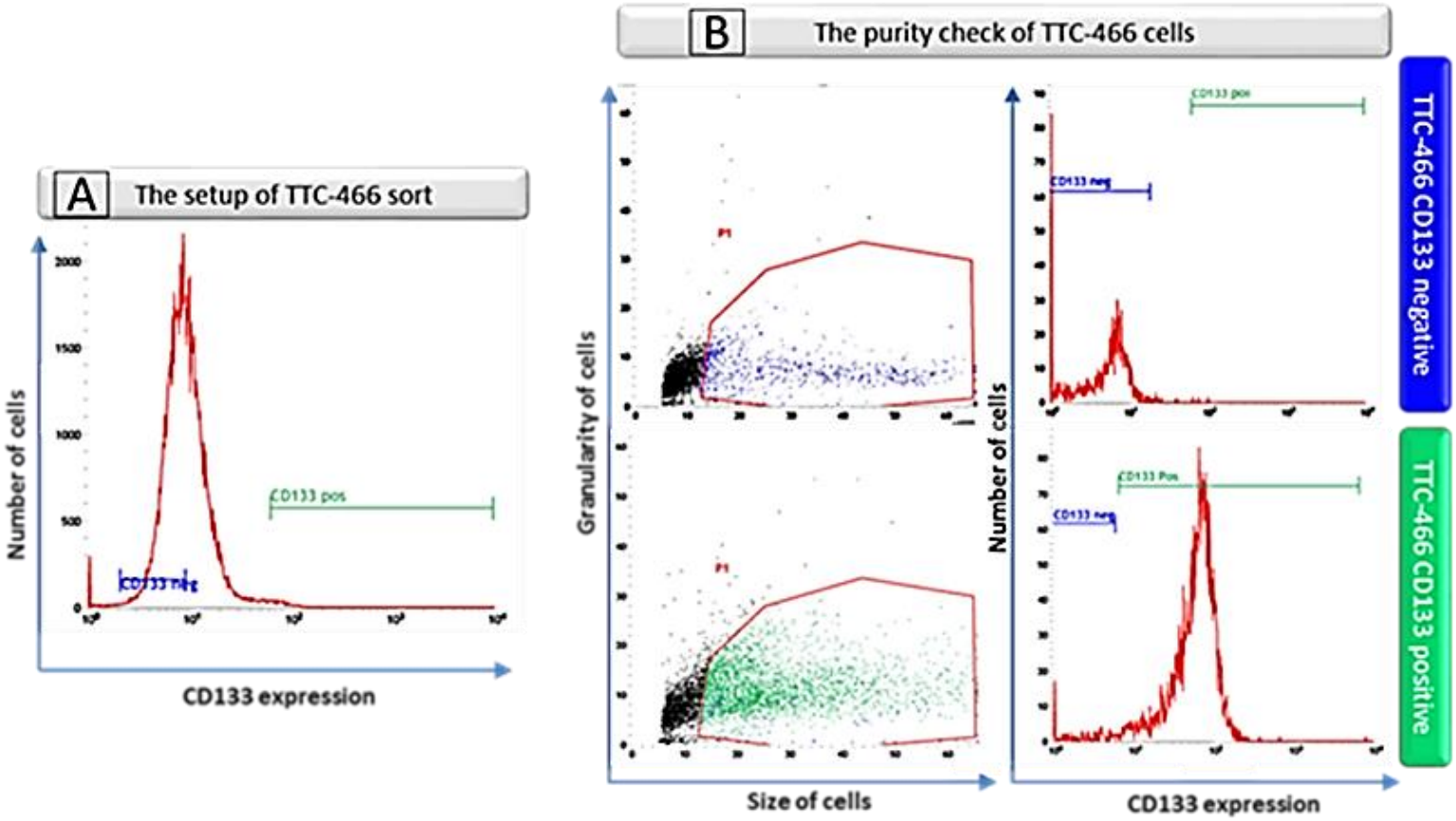

Figure 2.17 **The setup of the cell sort and purity check of ES cell lines that labelled with CD133 antibody.** A) Illustrative TTC-466 cell line fluorescence plots show the collection regions of the negative (Blue) and positive (Green) cells of CD133 primary antibody. B) Representative cell scatter and fluorescence plots show the purity of the sorted cells. The majority of TTC-466 CD133-ve cells were in the CD133-ve region (Blue), whereas the majority of TTC-466 CD133+ve cells were in the CD133+ve region (Green).

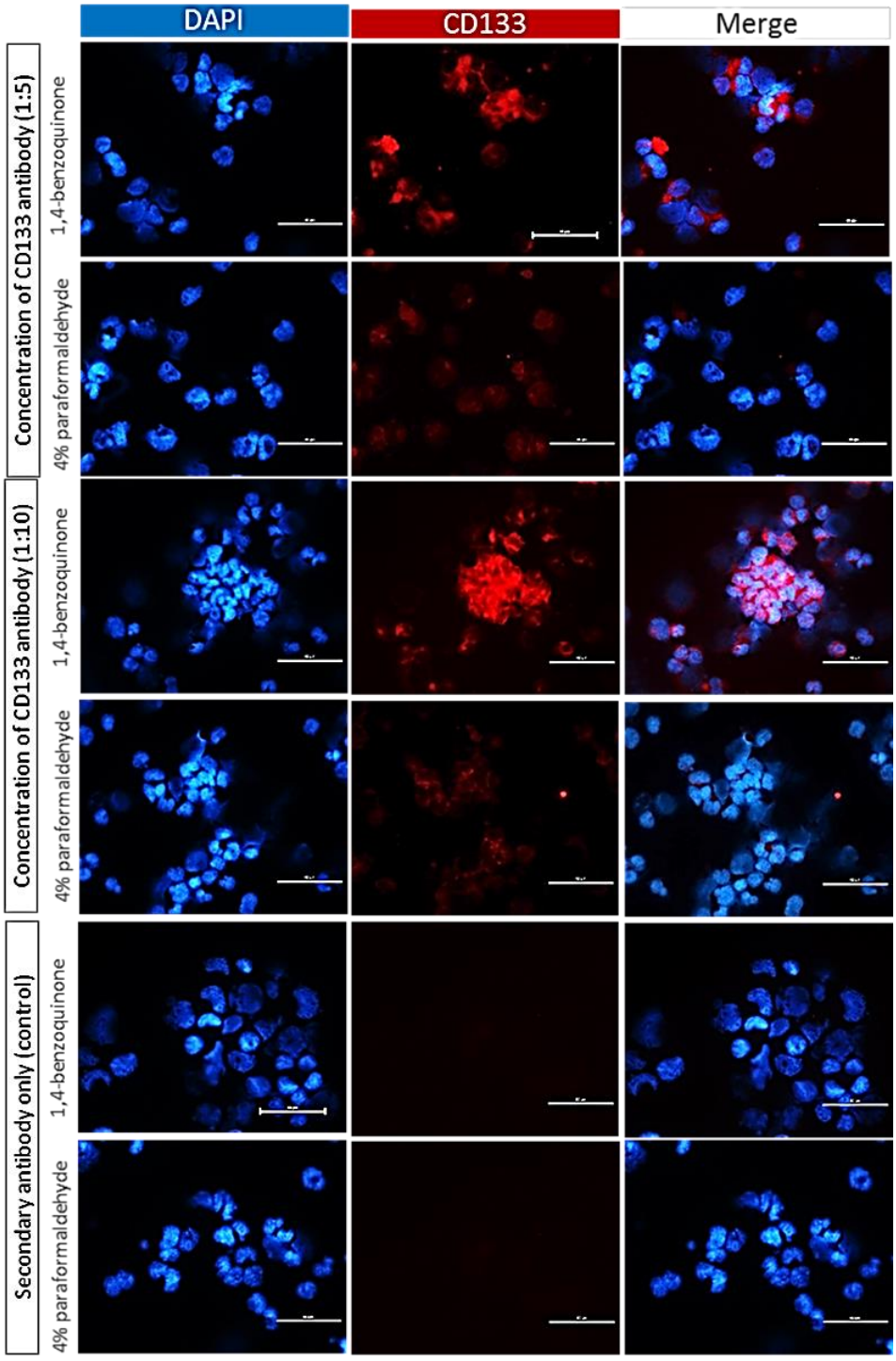

Figure 2.18 Optimization of CD133 and identifying the best fixative to be used for immunofluorescence staining. CD133 used to stain TC-32 CD133+ve cells, sorted previously by Ms Andrea Bury. Two fixatives (1,4-benzoquinone and 4% PFA) and two concentrations of CD133 antibody (1:5 and 1:10) were tested. CD133 antigen is in red, and the cell nucleus is in blue. The negative control was stained with the secondary antibody only. Scale bar = 50µm.

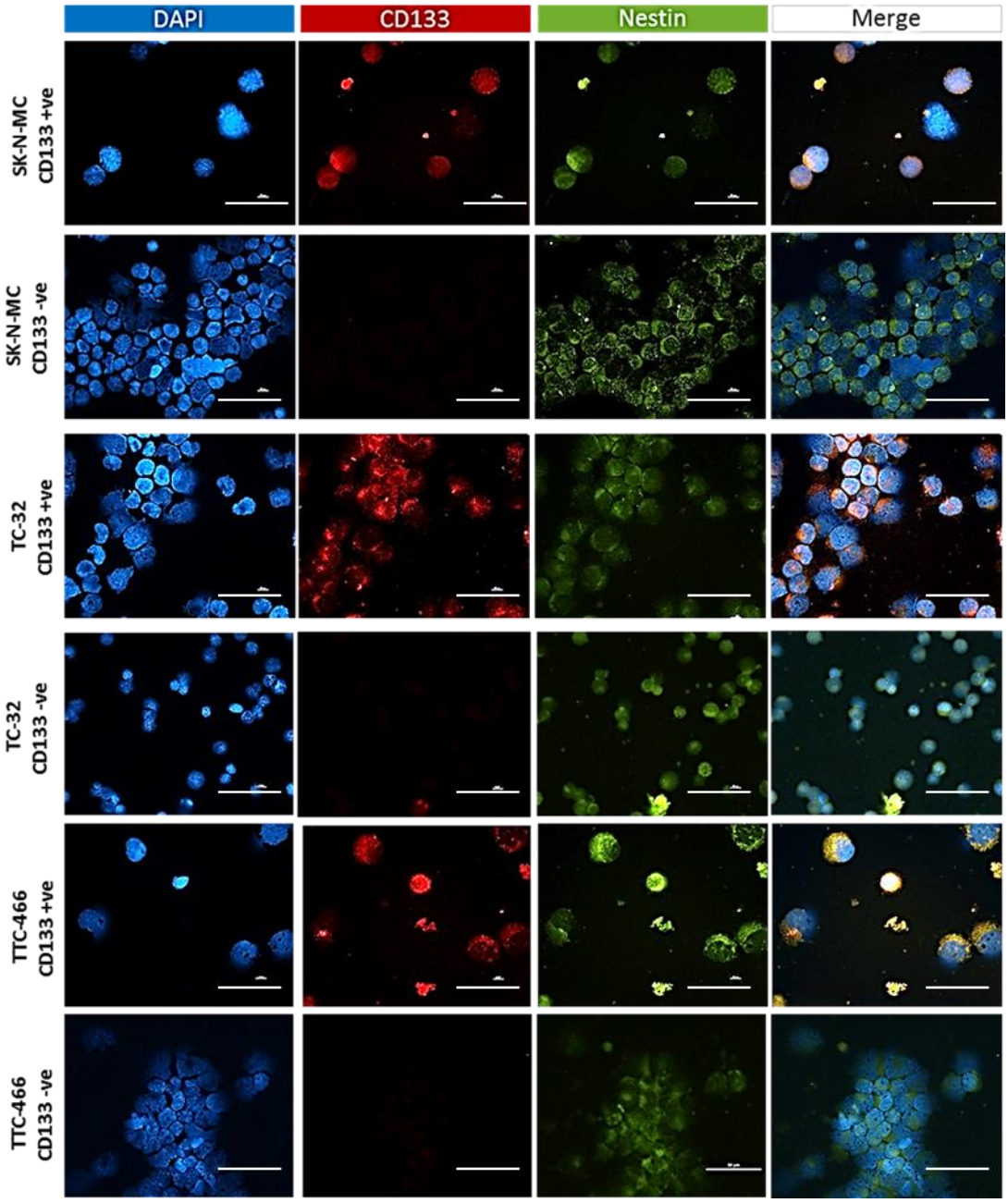

Figure 2.19 Expression of CD133 and Nestin in sorted ES CD133+ve and CD133-ve cells using immunofluorescence staining. ES CD133+ve and CD133-ve cells, sorted previously by Dr Adam Davison, were fixed using 1,4-benzoquinone and then stained with CD133 antibody (1:10) and Nestin (1:100). CD133 antigen is in red, Nestin is in green, and the cell nucleus is in blue. Scale bar for all images (50µm).

To examine the self-renewal capability of CD133+ve and CD133-ve cells, a single cell was seeded into each well of a flat Primaria™ plate using FACS sorter. The CD133+ve and CD133-ve populations grown in medium supplemented with antibiotic to reduce the risk of contamination. Cells grown as extraordinary shapes in flat bottom plates, as well as in the parental cell line, at three weeks (

Figure 2.20: SK-N-MC cell line; other cell lines' images not shown). As previously mentioned (Section 1.1.1), ES is characterized by a gene fusion that involves the Fli-1 gene, specifically expressed by endothelial cells. As result of that, ES cells gain characteristics normally restricted to endothelial cells such as formation of a circulatory system (vasculogenic mimicry) that is stimulated by hypoxia (Schaft et al., 2006). This explanation clarifies the reason behind the interesting structures generated from the spheroids.

The sorted cells were scored at three weeks and when the well was confluent they were split into 24 well plates and then split into T25 flasks. The percentages of successfully expanded colonies were 10.2% for SK-N-MC CD133+ve cells and 17.1% for CD133-ve. In TTC-466, 0.7% for CD133+ve and 4.6% for CD133-ve survived. TC-32 has the lowest percentage of clone formation. There was no statically difference between CD133+ve and CD133-ve (0.3% and 1.1% respectably) (Figure 2.21).

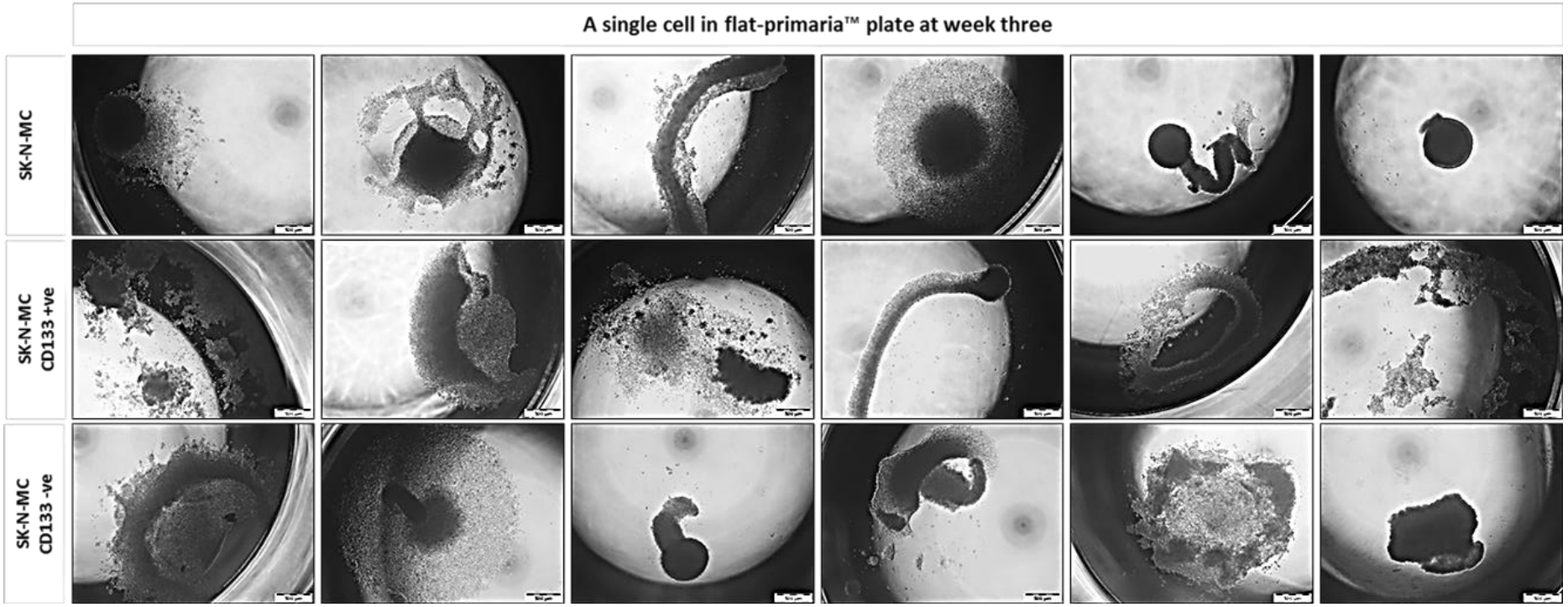

Figure 2.20 Morphological variances within the same population of the sorted ES cell lines. The first row represents the sorted unstained SK-N-MC cell line. The second and third rows illustrate cells stained with CD133 antibody and then sorted into positive and negative populations using FACS. The generated clones from a single cell in a flat Primaria™ plate were imaged at week three.

-72-

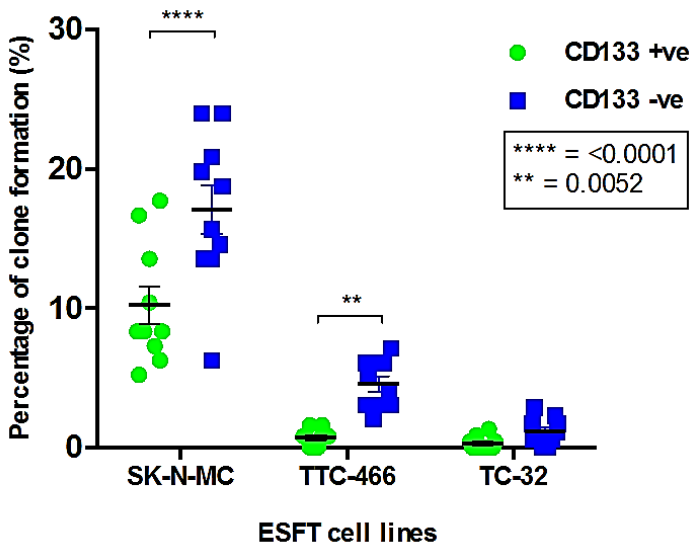

Figure 2.21 The percentage of clone formation using ES CD133 populations. ES cell lines were labelled with CD133 antibody then a single cell was sorted into each well in Primaria plates.

2.3.2.2 Functional method using a 3D or 2D culture

The experiment, which proved the accuracy of single cell assay, was performed by Mariona Chicón Bosch (PhD student, LICAP, University of Leeds) and the resulted data was analysed by Dr. Alastair Droop (Visiting Research Fellow, School of Molecular and Cellular Biology, University of Leeds). The summary of the performed experiment is single cell assay was setup as described in (Section 2.2.4.2.2). Wells were fixed the following day and stained with DAPI. The resulted data from scanning wells was analysed using Poisson distribution (Data not shown). The realistic possibilities for occurrence per well was no higher than one cell (Mariona Chicón Bosch, personal communication).

2.3.2.2.1 Optimisation of method to enrich self-renewing ES-CS-like cells from a single cell

ES cell lines (SK-N-MC, TTC-466, and TC-32) were capable of generating colonies from a single cell using two different 3D cultures (Figure 2.22) and a

2D culture (Figure 2.23). Unlike hanging drop, in low-adherent plates, the morphology of ES spheroids changed over time, with the spheroids being observed between one and six weeks. In 2D culture using flat bottom plates, the single cell of SK-N-MC grew as a spheroid and these spheroids either maintained their shape or started to generate tails or cells migrated from the edge of spheroid at week three. TTC-466 cells also showed different morphology; the cells grew as a group of individual cells in one zone or as spheroids or as cells migrated from a sphere as sheet of cells. Furthermore, TC-32 cells appear as a distinct core of cells surrounded with some individual cells or with a small colony of cells. Also, some TC-32 cells grew as an expanded sphere and as a sheet without a distinct core (Figure 2.23).

The spheroids of ES cell lines, generated from single cells using the hanging drop assay, appeared as small cellular clumps after one week and then grew into spherical and healthy colonies in weeks two and three. They then started to disaggregate in week four, and they exploded and lost their shape completely and became cell debris by week six (Figure 2.24).

In low-adherent plates, the spheroid started to become detected at week three. The spheroids looked healthy with a spherical shape in week two, by week three, the spheroids could be seen by the naked eye, and some spheroids started to develop a small tail of non-viable cells possibly. Three-week-old spheroids could easily be pipetted for transportation into a collection tube. The four-week-old spheroids generated multiple large tails. When spheroids reached weeks five and six, their shapes became irregular, and they disaggregated easily; therefore, they were not easily pipetted into a collection tube (Figure 2.25).

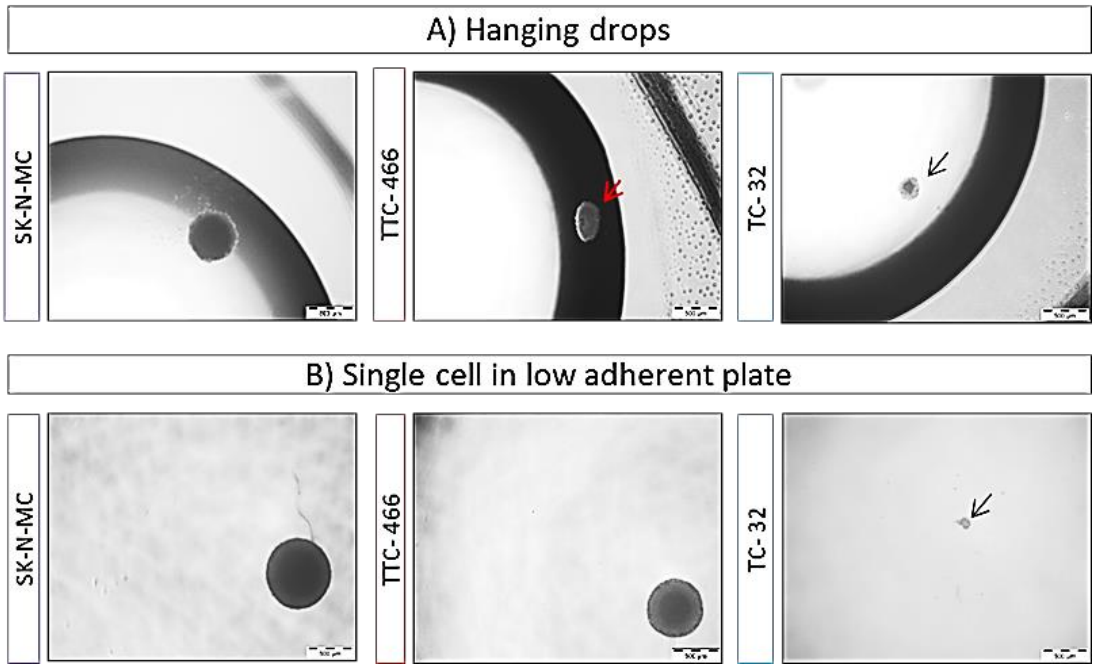

Figure 2.22 Compare the morphological differences in spheroid formation from a single cell using two techniques. SK-N-MC, TTC-466, and TC-32 cells were used in this assay A) the hanging drop method (HD) and B) low-adherent plates. Spheroids were imaged at week three.

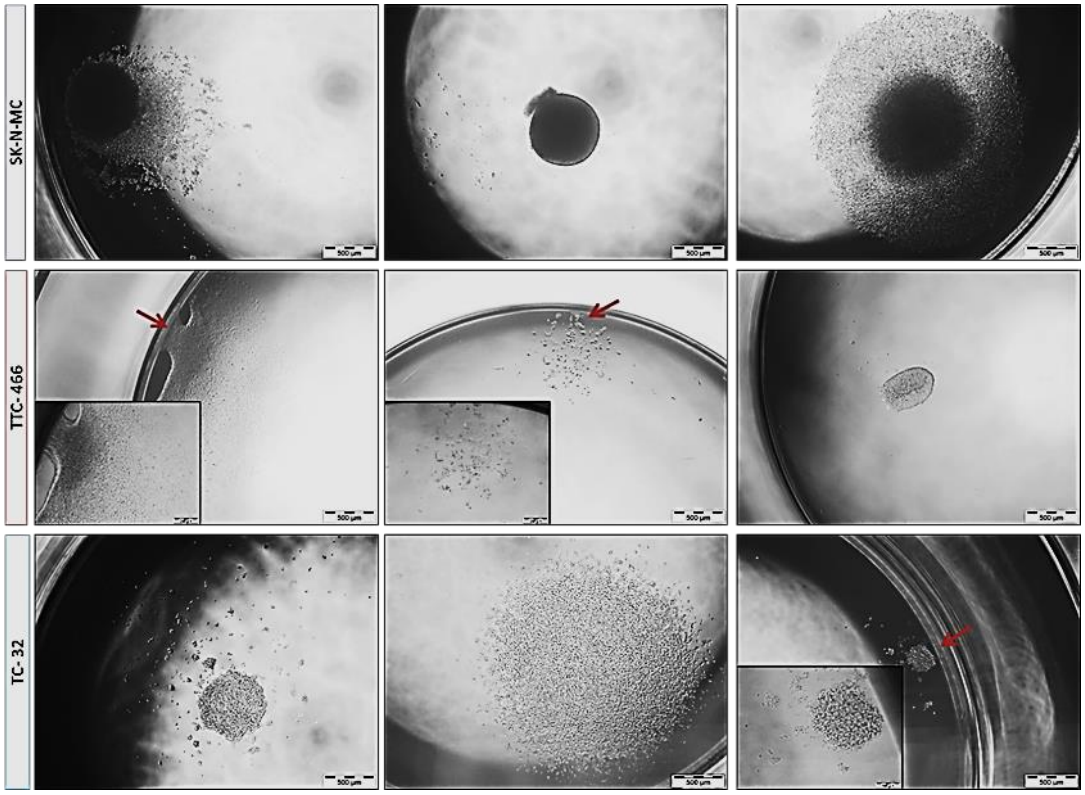

Figure 2.23 Morphological differences in ES cell lines' clones within the third technique of spheroid formation from a single cell. Clones generated from a single cell in a flat Primaria™ plate and imaged at week three.

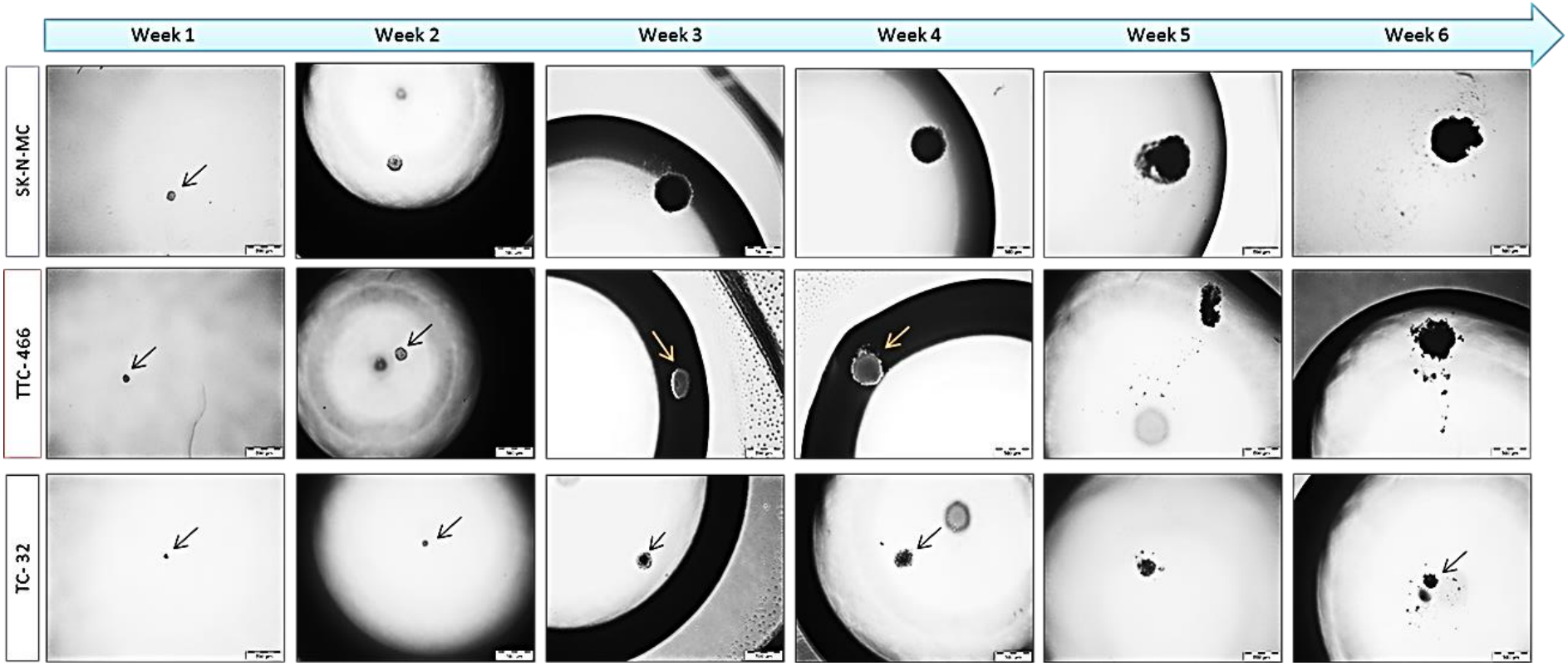

Figure 2.24 Comparison of spheroid formation in ES cell using the hanging drop assay (HD). ES cell lines' (SK-N-MC, TTC-466, and TC-32) spheroid formation from a single cell using the hanging drop assay (HD). Spheroids were imaged at different times (from one to six weeks).

-76-

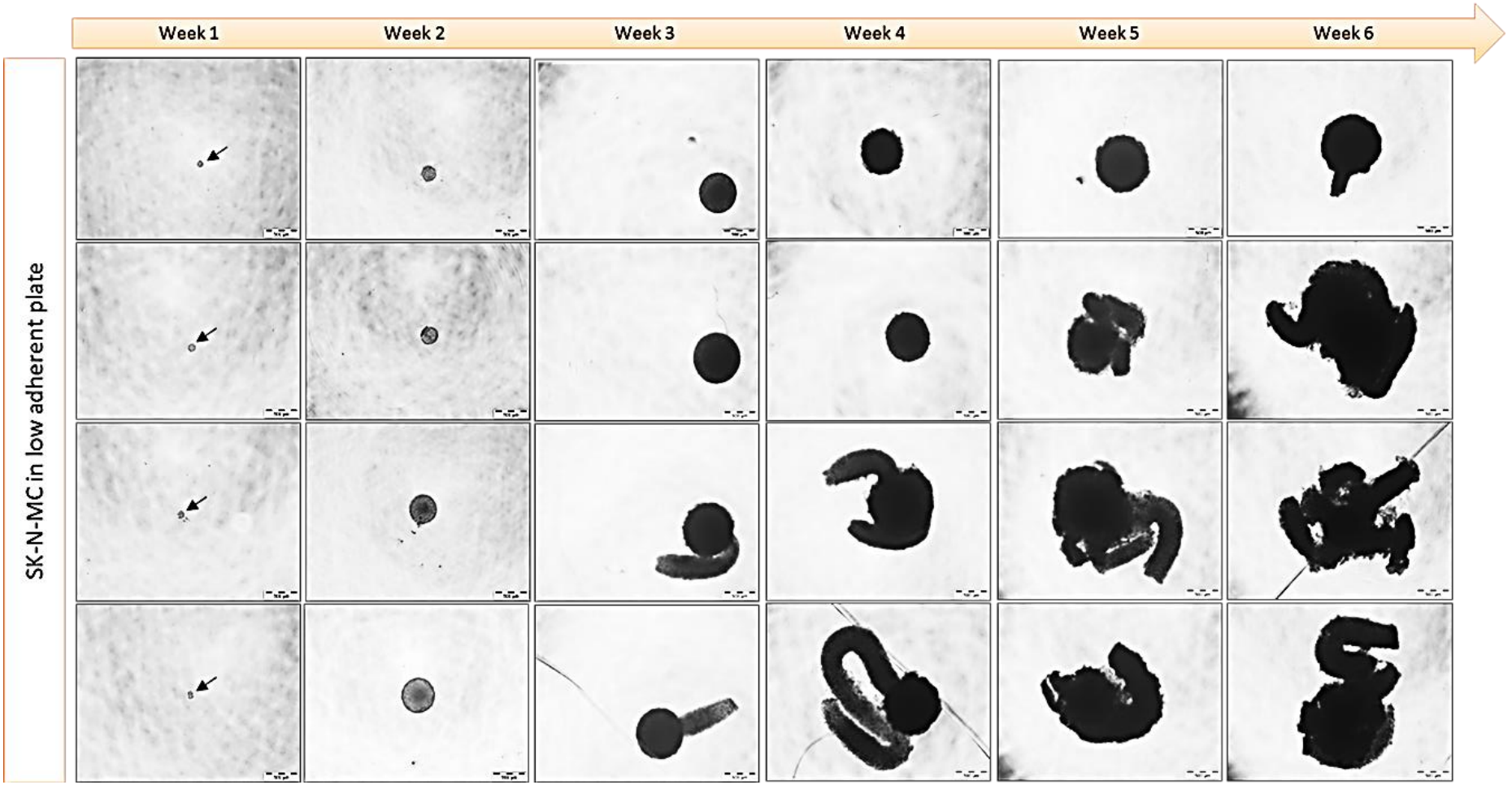

Figure 2.25 Morphological changes in SK-N-MC spheroids' low-adherent plate from one to six weeks.

The percentage of spheroid formation per experiment at week three was calculated in five biological repeats, and 80 drops or wells were carried out per experiment. In the hanging drop assays, the percentage of spheroid formation was 6.75 (± 4.30, n = 5) in the SK-N-MC cell line, while TTC-466 and TC-32 cells formed 0.75 (± 0.75, n = 5) and 1.00 (± 1.00, n = 5), respectively. Furthermore, this assay was repeated five times and it was not reproducible (Figure 3.26 B). In contrast, the frequency of spheroid formation following the seeding of a single cell into a low-adherence plate was 48.5 (± 2.10, n = 5) for SK-N-MC cells, while TTC-466 and TC-32 cells formed 12.25 (± 2.30, n = 5) and 0.25 (± 0.25, n = 5), respectively (Figure 2.26 A).

Furthermore, ES cell lines were sorted as a single cell into one well of a 96-well flat Primaria™ plate by FACS. This assay was done in 10 plates per cell line. The percentage of cellular growth was 41.25% (± 2.07, n = 10) in the SK-N-MC cell line, while TTC-466 and TC-32 cells formed 3.13% (± 0.88, n = 10) and 3.13% (± 0.64, n = 10), respectively (Figure 2.26 C).

The SK-N-MC cell line showed the highest percentage of spheroid formation from a single cell in both assays, using hanging drop (HD) and low-adherent plates. In the HD assay, there were no significant differences between the self-renewing capacities of the three ES cell lines ($p = 0.3 – 0.9$). However, in the low-adherence plate assay, there was a statistically significant difference between the number of spheroids formed from SK-N-MC, TTC-466, and TC-32 cells. SK-N-MC compared to TTC-466 ($p = < 0.0001$), and SK-N-MC compared to TC-32 ($p = < 0.0001$). Furthermore, TTC-466 and TC-32 showed a significant difference between them ($p = 0.0013$). TC-32 does not produce spheroids from a single cell (Figure 2.26).

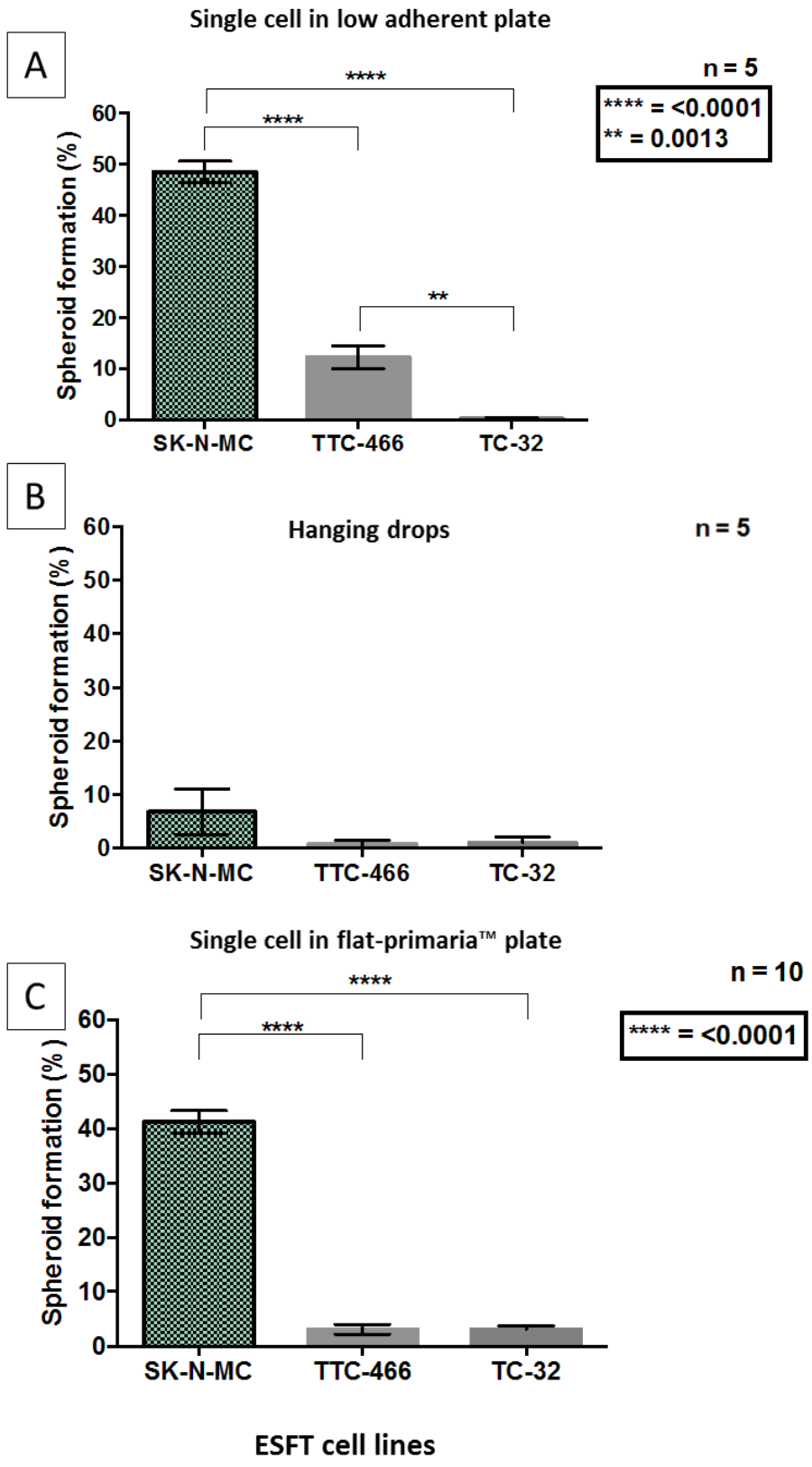

Figure 2.26 Comparison of the three techniques that used for spheroid formations from a single ES cell. Spheroid formations from a single ES cell (SK-N-MC, TTC-466, and TC-32) in A) low-adherent plates, B) the hanging drops, and C) the flat Primaria™ plate assays. The difference between cell lines within each assay was assessed using one-way ANOVA, and the post-hoc was Tukey's multiple comparisons test.

Because the hanging drop assays could not be reproduced, the focus was on comparing the low-adherent plates with the flat Primaria™ plate. The 95% confidence interval for the difference in the mean percentage of spheroid/cellular formation between the low-adherent plates and the flat Primaria™ plate was 1.167 to 13.33 in SK-N-MC and 3.042 to 15.21 in TTC-466. The flat Primaria™ plate has a lower mean percentage of spheroid/cellular formation than the low-adherent plates. The difference between the two different plates was statistically significant ($p = 0.0159$ in SK-N-MC and $p = 0.0019$ in TTC-466). Using a flat Primaria™ plate slightly improved the self-renewal ability in TC-32. That improvement by using the 2D culture was not statistically significant compared with the 3D culture (Table 2.4). Consequently, the low-adherence plates were the best plates to enrich self-renewing ES-CS-like from a single cell.

		Tukey's multiple comparisons test			
	Methods comparisons	Mean of difference	95% CI of difference	Adjusted P Value	Summary
SK-N-MC	Low-adherent plate vs. Hanging drop	41.75	34.73 to 48.77	< 0.0001	****
	Low-adherent plate vs. Flat Primaria™ plate	7.25	1.167 to 13.33	0.0159	*
	Hanging drop vs. Flat Primaria™ plate	-34.5	-40.58 to -28.42	< 0.0001	****
TTC-466	Low-adherent plate vs. Hanging drop	11.5	4.476 to 18.52	0.0007	***
	Low-adherent plate vs. Flat Primaria™ plate	9.125	3.042 to 15.21	0.0019	**
	Hanging drop vs. Flat Primaria™ plate	-2.375	-8.458 to 3.708	0.6162	Ns
TC-32	Low-adherent plate vs. Hanging drop	-0.8	-7.824 to 6.224	0.9592	Ns
	Low-adherent plate vs. Flat Primaria™ plate	-2.925	-9.008 to 3.158	0.4818	Ns
	Hanging drop vs. Flat Primaria™ plate	-2.125	-8.208 to 3.958	0.6781	ns

Table 2.4 **Comparison of 3D- and 2D-culturing methods using ES cell lines**. Results were from the two-way ANOVA test, and the post-hoc test was a Tukey's multiple comparisons test. CI = Confidence Interval; ns = not significant

2.3.3 Enhance the growth of CSCs by using different formulations of stem cell medium

The experiment was done in two different stages (Figure 2.27). The first stage (ended by yellow box in Figure 2.27) was growing ES cells in stem cell medium then calculating the viable cells number and percentage to know the effect of the medium on ES cells. The second stage (ended by blue box in Figure 2.27) was repeating the first stage then setup of single cell assay based on the viable cell number to check the self-renewal ability of viable cells in stem cells medium.

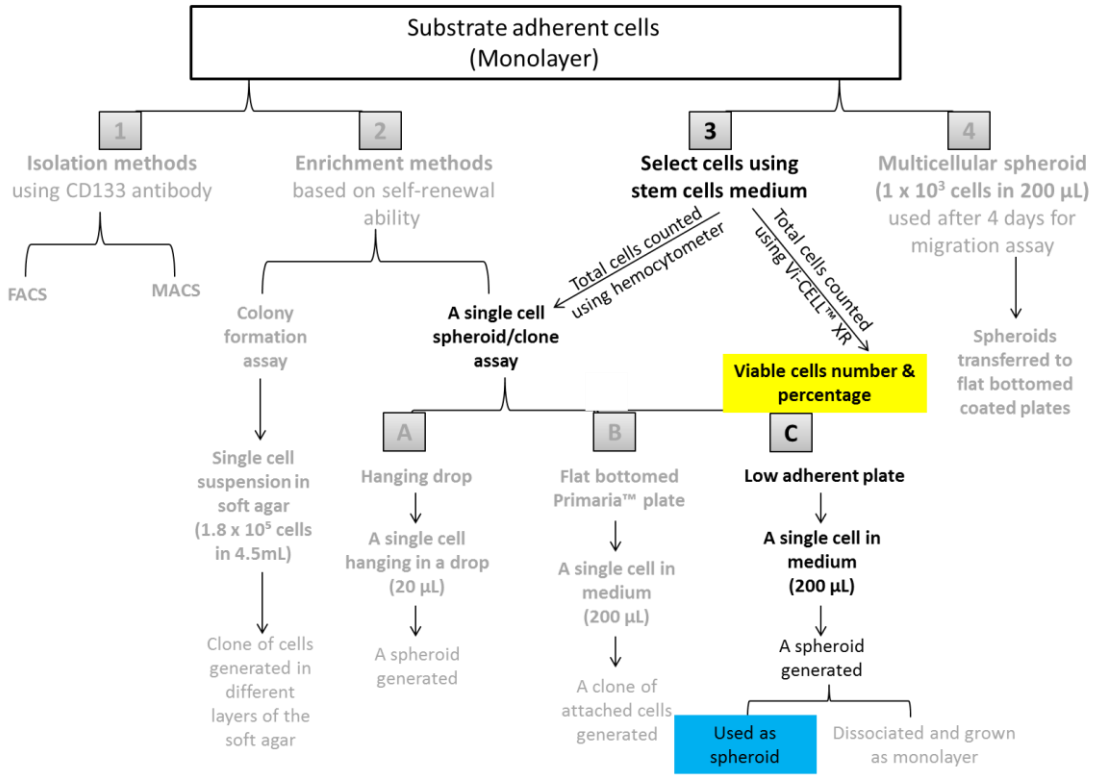

Figure 2.27 The flow diagram illustrates the experimental design of using stem cell medium

ES cell lines (SK-N-MC, TTC-466, and TC-32) were cultured in three different types of culture medium (ES medium, mTeSR™1 and AggreWell™ medium). SK-N-MC, TTC-466, and TC-32 cultured in ES medium attached to the bottom of the tissue culture plates, while in stem cell medium

(mTeSR™1 with or without Matrigel™ and AggreWell™ medium), the cells were clumped together and detached from the dish (Figure 2.28). Furthermore, the number of viable cells in the ES cell lines almost remained stable over time in the three conditions (Figure 2.28, right).

The percentages of viable cells after 72 h of incubation in ES medium were 93.9% ± 0.3, 94.4% ± 0.4, and 97.2% ± 0.4 in SK-N-MC, TTC-466, and TC-32, respectively (Figure 2.29). In SK-N-MC, 34.4% ± 0.7 of the cells remained viable after 72 h of incubation in mTeSR™1 medium, and coating tissue culture plates with Matrigel™ did not increase the percentage of viable cells (33.4% ± 2.5). A slightly higher percentage of TTC-466 and TC-32 cells managed to stay alive in mTeSR™1 medium with Matrigel™ (51% ± 3.6 and 58% ± 6.3, respectively) and without (49% ± 5.5 and 57.2% ± 5.1, respectively). At 72h, there was no change in the percentage of viable cell cultured in mTeSR™1, with or without Matrigel™, in any of the three ES cell lines (Figure 2.29). Furthermore, 35% ± 1.6, 48.6% ± 2.6, and 62.9% ± 2.7 of SK-N-MC, TTC-466, and TC-32 cells, respectively, were viable after 72 h of incubation in AggreWell™ medium, which is normally used to differentiate stem cells and to generate embryoid bodies (Figure 2.29).

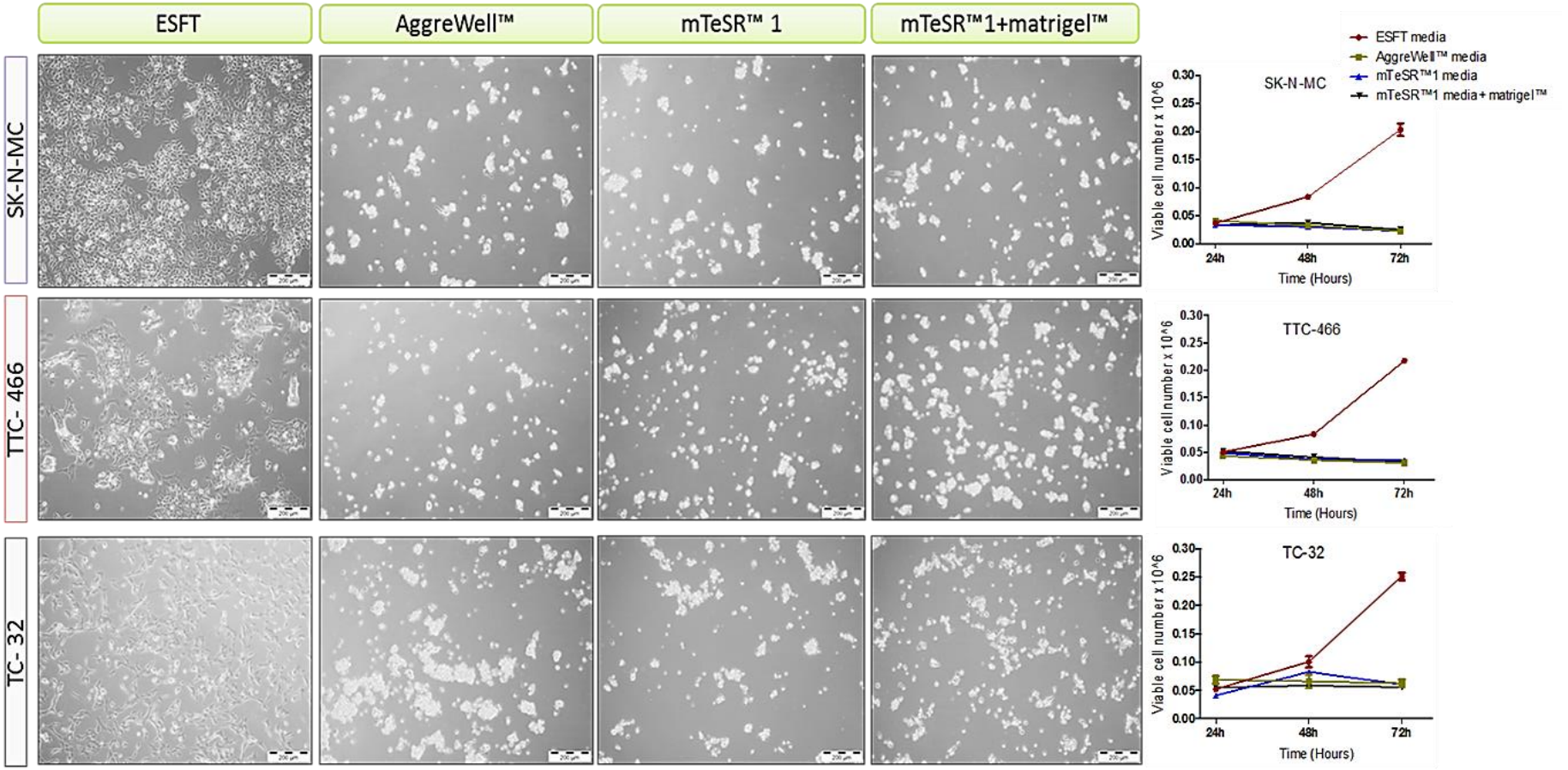

Figure 2.28 The affect of three different types of media on viability of ES cell lines. Cells were seeded in three different types of media and imaged before harvesting at 72 h. The viable cells were counted at each time point using the trypan blue exclusive assay (Vi-CELL™ XR)

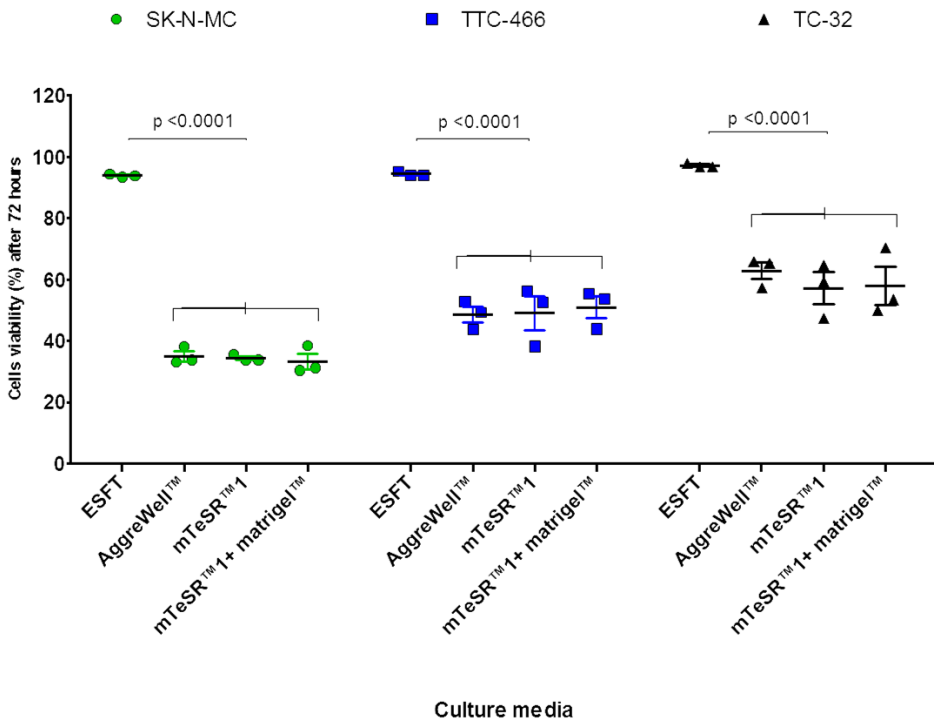

Figure 2.29 The percentage of viable cells of ES cell lines seeded in three different types of media. Cells were harvested and counted at 72 h using Vi-CELL™ XR. The percentages were calculated using the following formula (%) = (viable cell number/total cell number)x100

Since only a small population of viable cells remained after 72 h, it was decided to repeat the selection of SK-N-MC cells in AggreWell™ and mTeSR™ 1 media to harvest cells after 48 h and to investigate whether these cells are ES CSCs, using a single-cell self-renewal assay in low-adherent 96-well plates. Unlike ES media, the majority of cells that seeded into mTeSR™ 1 media and AggreWell™ media were non-viable. There was no difference between the number of viable cells seeded into mTeSR™ 1 media and AggreWell™ media. The number of viable cell at 48h was very high in ES media comparing with mTeSR™ 1 media ($p = 0.0001$) and AggreWell™ media ($p<0.0001$; Figure 2.30). These experiments clearly demonstrate that using different media results in a different number of viable cells. However, the viable cells that survived in the stem cell media were not able to self-renew or generate a spheroid from a single cell, whereas cells that had been grown in their specific ES media generated spheroids from a single cell (Figure **2.31**).

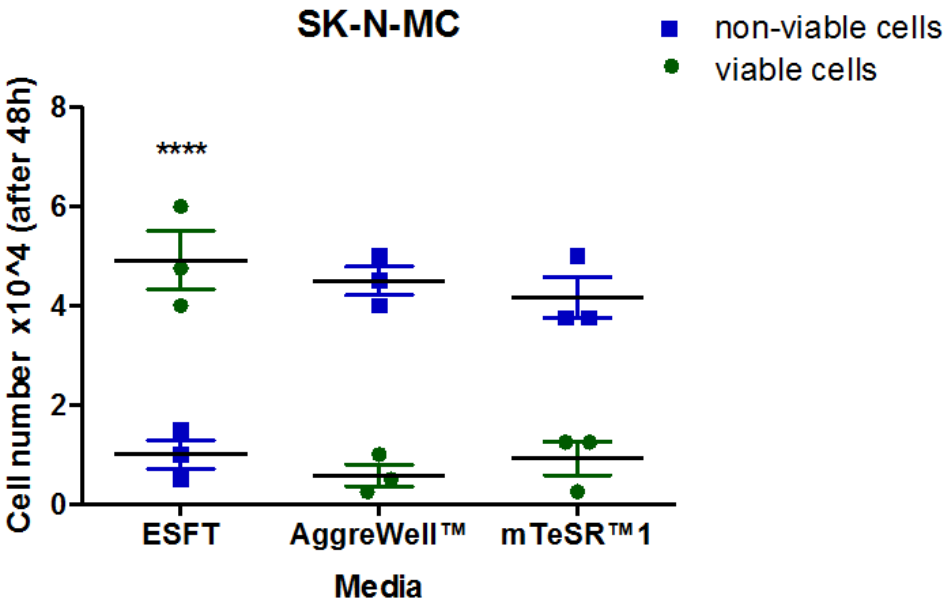

Figure 2.30 Selection of a cell population using stem cell media. SK-N-MC cells were seeded into stem cell media and into its normal medium. Cells were harvested after 48 h, and the viable cells were counted using the trypan blue exclusive assay. Since the anticipated number of cells was small in these experiments, viable cells were counted using a haemocytometer to achieve accurate cell numbers.

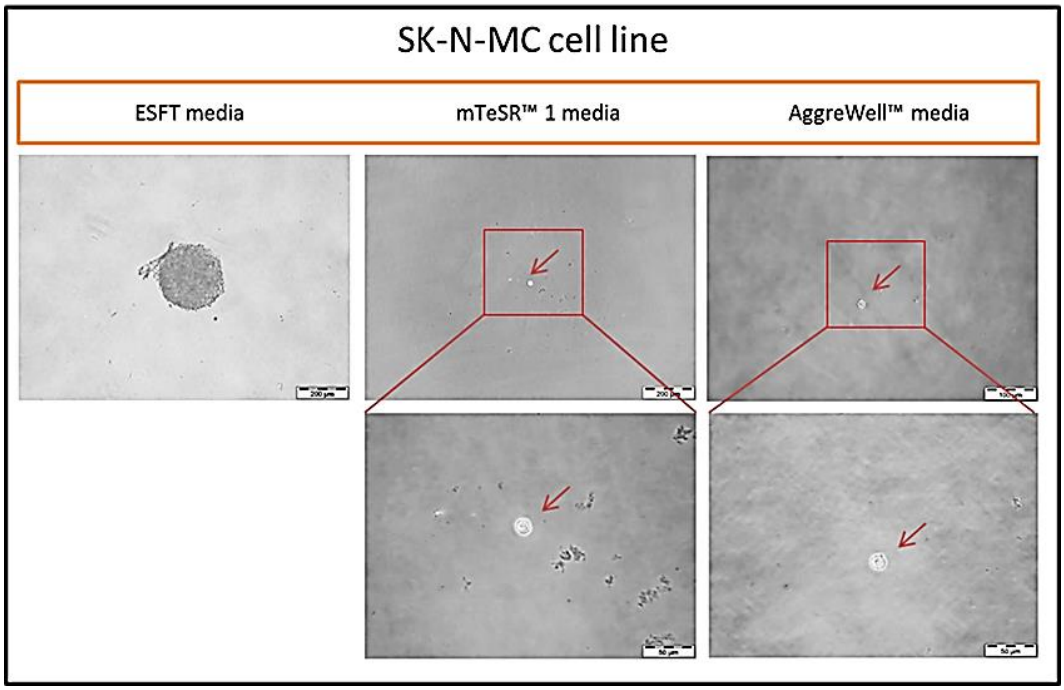

Figure 2.31 Spheroid formation in three different media using the selected population from stem cell media. ES media is the most suitable medium that allows ES cells to generate spheroids from a single cell, whereas stem cell medium killed the cells..

2.3.4 Characterisation of ES spheroids enriched using low-adherent plates

2.3.4.1 Spheroids' size and viable cell number with time

According to the spheroid morphology described in Section 2.3.2.2;

Figure 2.25, spheroids from week four and above have been excluded from the study. To determine the appropriate incubation time at which to collect ES spheroids, spheroid sizes were measured at one, two and three weeks using light microscopy. ES spheroids from a single cell start to become visible after a week of culture. The sizes of TTC-466 spheroids were 74.52 µm (± 5.30, n=8) and 229.1 µm (± 27.88, n=8) at weeks one and two, respectively. SK-N-MC spheroids were 107.2 µm (± 5.96, n = 8) at week one and 358.0 µm (± 34.22, n = 8) at week two. These spheroids were very small in size and were not be used for any downstream experiments. SK-N-MC spheroids were twofold larger than TTC-466 spheroids. The diameter of three-week-old spheroids for SK-N-MC and TTC-466 were 779.6 µm (± 28.0, n = 8) and 457.5 µm (± 51.6, n = 8), respectively. However, there was no significant difference between the growth rate of SK-N-MC and TTC-466. On average, SK-N-MC grew by 95.03% ± 4.9(n=8) each week, whereas TTC-466 grew by 81.87%± 4.8(n=8) per week.

At three weeks, a number of SK-N-MC spheroids were transferred as a whole spheroid to a well in 24-well plates or dissociated physically by pipetting cells up and down and then seeding them into wells as a single clone per well. Since the predicted number of cells was small in this experiment, the viable cells were counted at different time points (0 -168 h) using a haemocytometer to obtain accurate cell numbers. The ratio of viable to non-viable cells was 0.94:1 at 0 h. In the transferred whole spheroid, this ratio was increased slightly from 0.98:1 to 1.32:1 at 24 to 72 h, respectively. Afterwards, the ratio decreased to 0.62:1 at 120 h. At 168 h, the whole spheroid contained extensive cell debris, and the ratio become 1.05:1. However, the dissociated spheroids showed an increase in the ratio of viable to non-viable cells by time. At 24h, the ratios of viable to nonviable cells was 2.12:1 and 2.90:1 at 72h. After that the ratio increased to 5:1 at 120h and 22.8:1 at 168 h (Figure **2.32**).

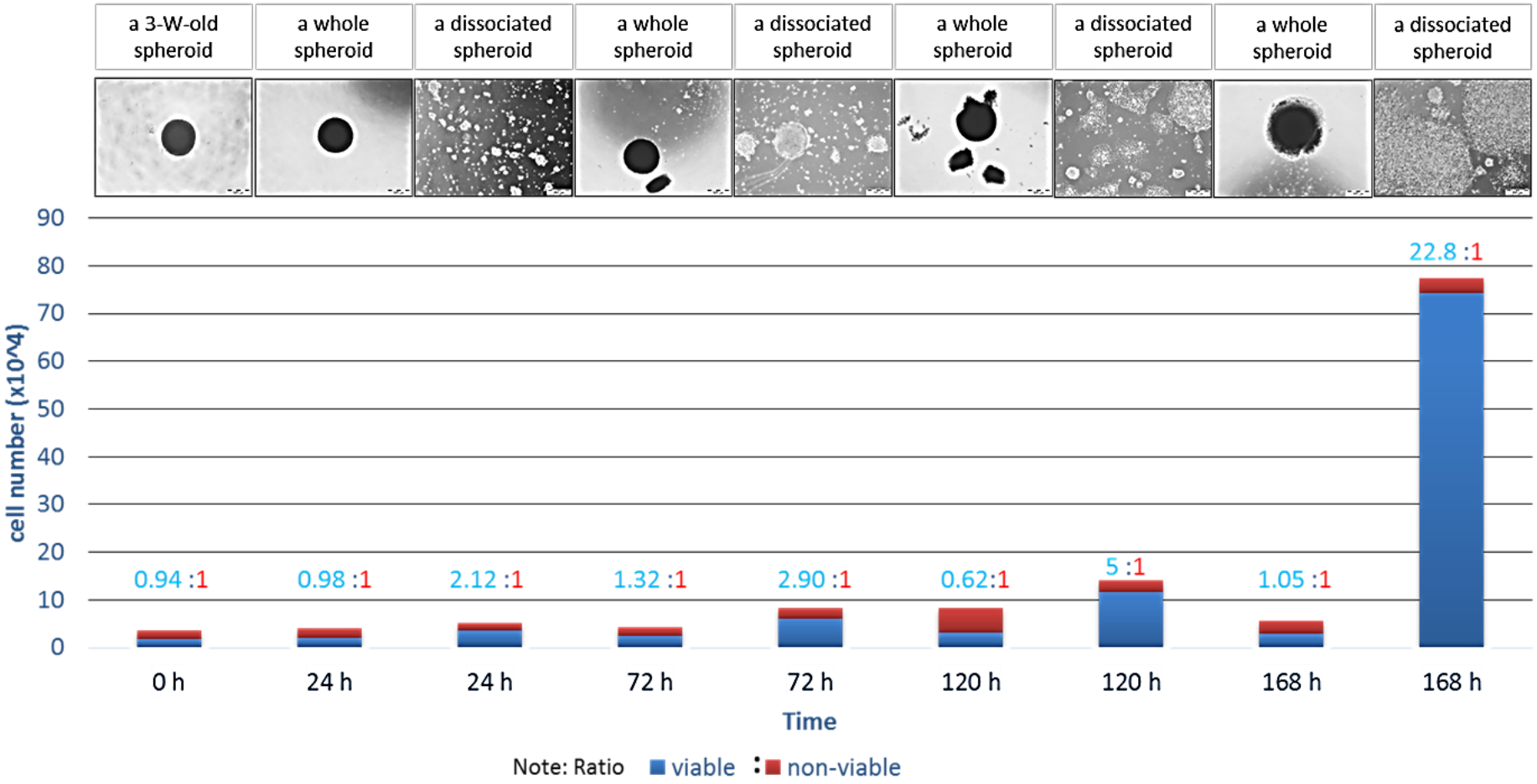

Figure 2.32 The total cell number and ratio for spheroids with time

2.3.4.2 Histology of spheroids with time

2.3.4.2.1 Optimization of Glut-1, a marker of hypoxia, and Ki67, a proliferation marker in ES

SK-N-MC spheroids grown under hypoxic conditions were used as a positive control. The spheroid cells were quiescent and characterised by hypoxia in their cores. A gradient of hypoxic rim extended to the outer layer, which consisted of proliferating cells. The primary antibodies were diluted from 1:50 to 1:200. Glut-1 antibody dilutions of 1:50 and 1:100 showed strong positivity in the hypoxic areas of spheroid sections. The dilution 1:200 showed a clear outer rim with a small number of positive cells (Figure 2.33, right). However, the first two dilutions of Ki-67, 1:50 and 1:100, showed some non-specific staining, whereas the dilution 1:200 showed specific staining only (Figure 2.33, left).

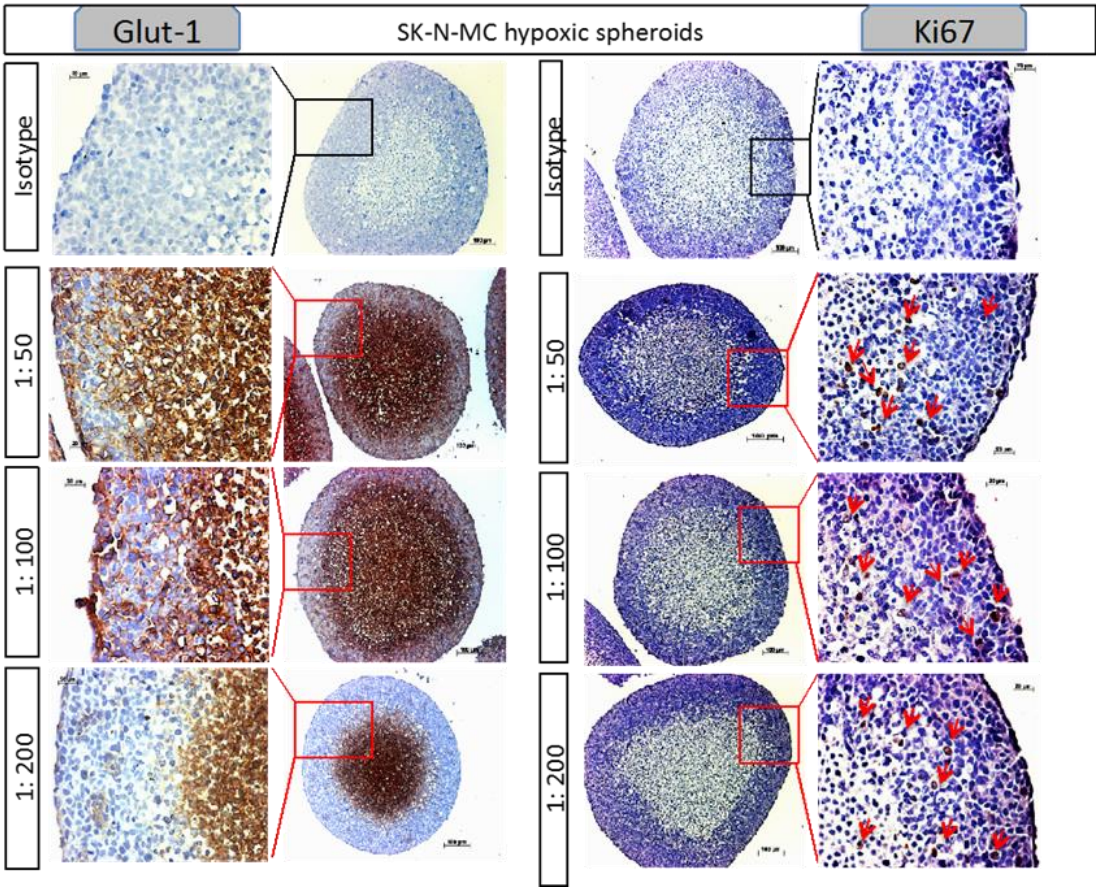

Figure 2.33 Optimization of the hypoxic marker (Glut-1) and proliferation marker (Ki67) in SK-N-MC hypoxia-spheroids. Three antibody dilution were used (1:50 – 1:200). Red arrows represent positive cells

The SK-N-MC spheroid sections at a different time point were stained with H&E, Glut-1, and Ki-67 at a 1:200 concentration to assess the proportion of proliferating cells over time (Figure 2.34). SK-N-MC spheroids at three weeks developed intense Glut-1 staining and a number of proliferations, as measured by Ki-67 staining. Over time, the number of proliferating cells decreased, and those spheroids developed a more concentrated Glut-1 staining that correlates with hypoxia.

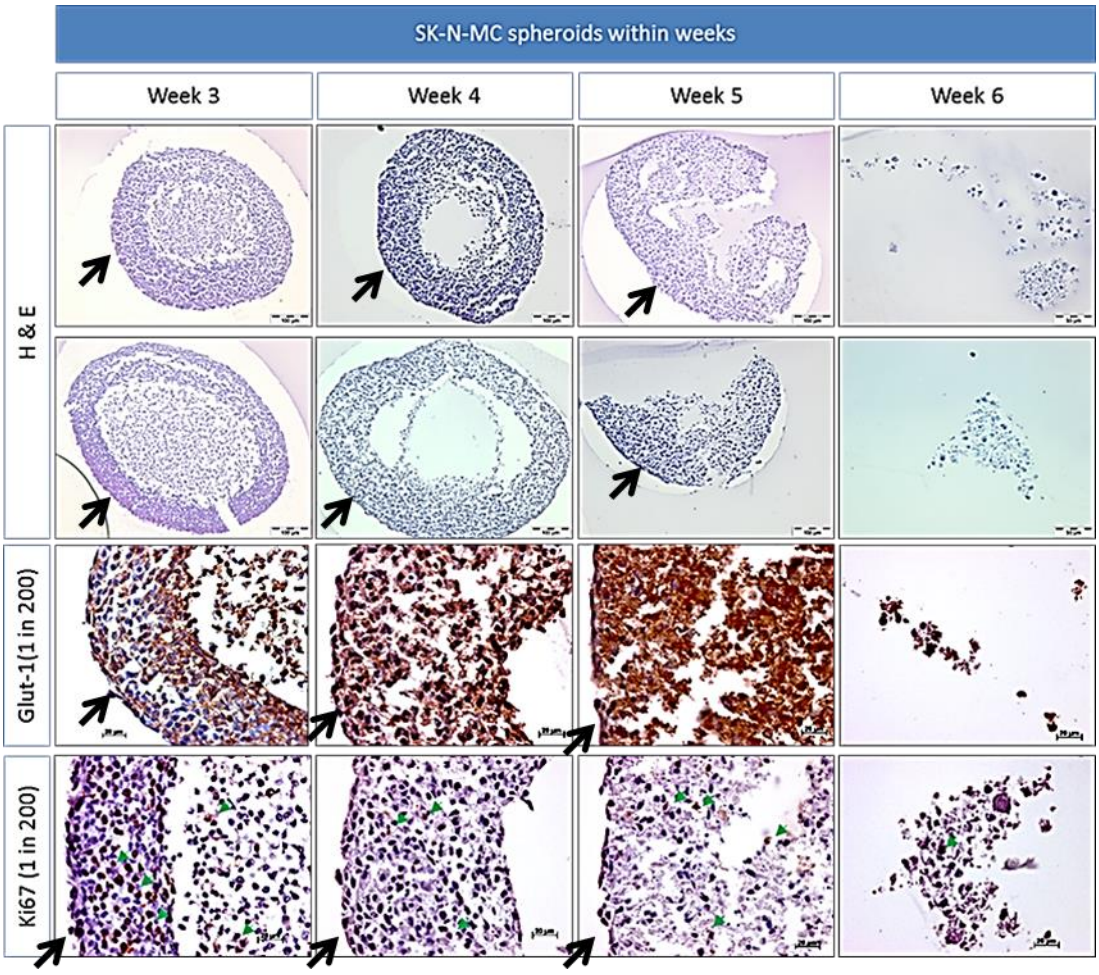

Figure 2.34 Expression of hypoxic and proliferation markers in SK-N-MC spheroids. SK-N-MC spheroids, generated from a single cell using low-adherence plates, stained with H&E, Glut-1, and Ki-67 at week three up to week six. The green arrows demonstrated Ki-67-positive cells. The black arrows demonstrated the edge of spheroids.

2.3.4.3 The migration capacity of 3-w-spheroids and dissociated spheroids

In this section, the multicellular spheroids that formed using parental cell line were termed as SK-N-MC cell line (Red box in Figure 2.35). ES spheroids collected at week 3 (Blue box in Figure 2.35) and termed as 3-w-old spheroids. The other multicellular spheroids were generated using the dissociated spheroids (Yellow box in Figure 2.35), which were grown as substrate adherent cells and collected at passage number two (3-w-dissociated spheroids P2). All spheroids were transferred to coated wells and imaged at different time point to access their migration ability.

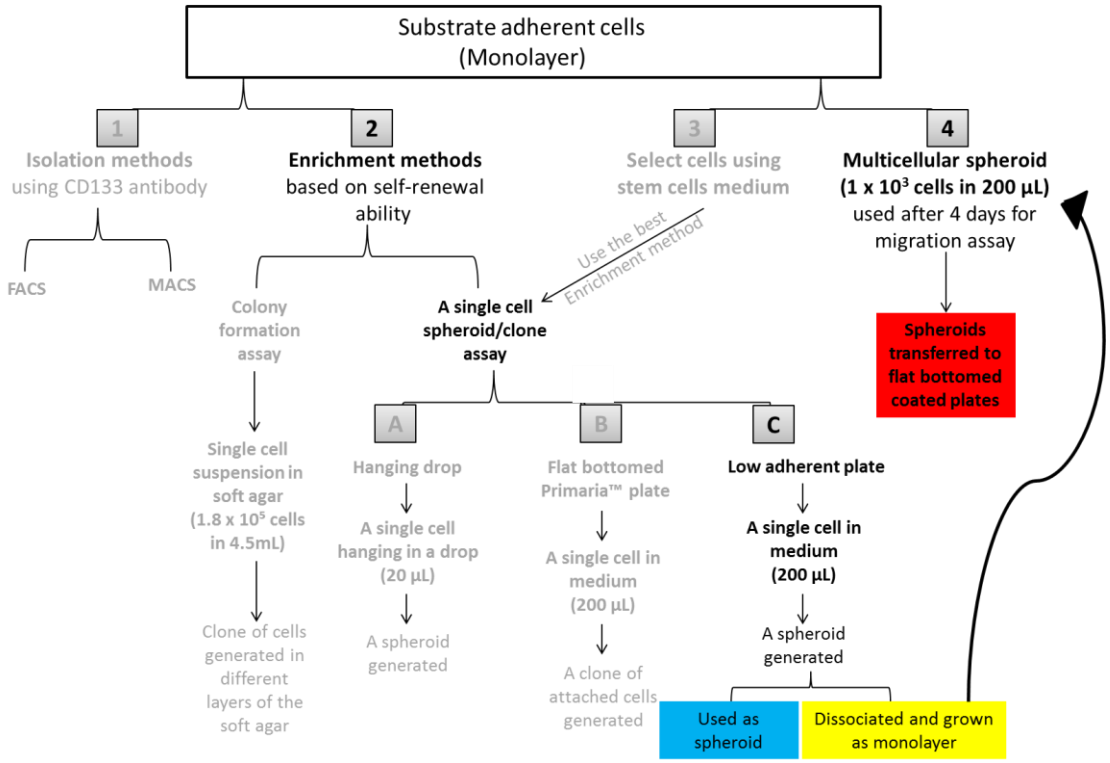

Figure 2.35 Clarification of the original cells that used to form spheroids used in migration experiments. Red box= spheroids from parental cell line grown as monolayer. Blue box= whole spheroids at week 3. Yellow box= dissociated spheroids that grown as monolayer and passaged twice then used to form spheroids.

The MI of SK-N-MC cell lines were compared with the dissociated spheroids at passage two (P2) and with the three-week-old spheroids at 72 h. The difference of the mean of the MI between SK-N-MC and P2 was significant

(MI = 22.2 ± 0.61 and 17.8 ± 0.62, respectively; p=0.0005); there was also a significant difference between the mean MI of SK-N-MC and the three-week-old spheroids (p<0.0001). Furthermore, the three-week-old spheroids migrated less than P2 at 72 h (MI=2.5 ± 0.83; p<0.0001; Figure 2.36).

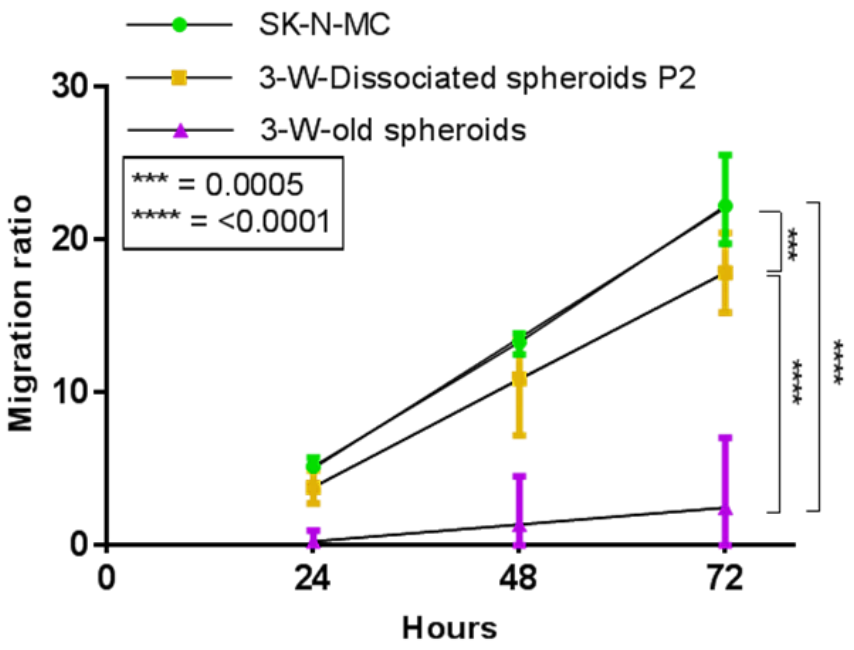

Figure 2.36 Evaluation of migration results using three different clones of SK-N-MC cells. Cells from SK-N-MC cell lines, dissociated three-week-old spheroids at P2 and transferred whole spheroids at week three were used to setup this experiment. Independent experiments (n= three experiments, with three replicates in each experiment) were combined and grouped into three different time points. Data were analysed by ANOVA with Tukey's multiple comparisons *post hoc* tests.

Although there were substantial differences in the maximum migration of SK-N-MC and P2 cells there were no considerable differences in the migration phenotypes. Both SK-N-MC and P2 maintained a distinct spheroid core, while most of the cells had migrated as a sheet with a defined edge (Figure 3.35). On the other hand, few individual cells or a very narrow sheet of cells seemed to migrate from the spheroid core in three-week-old whole spheroids, which increased in size by 72 h (Figure 2.37).

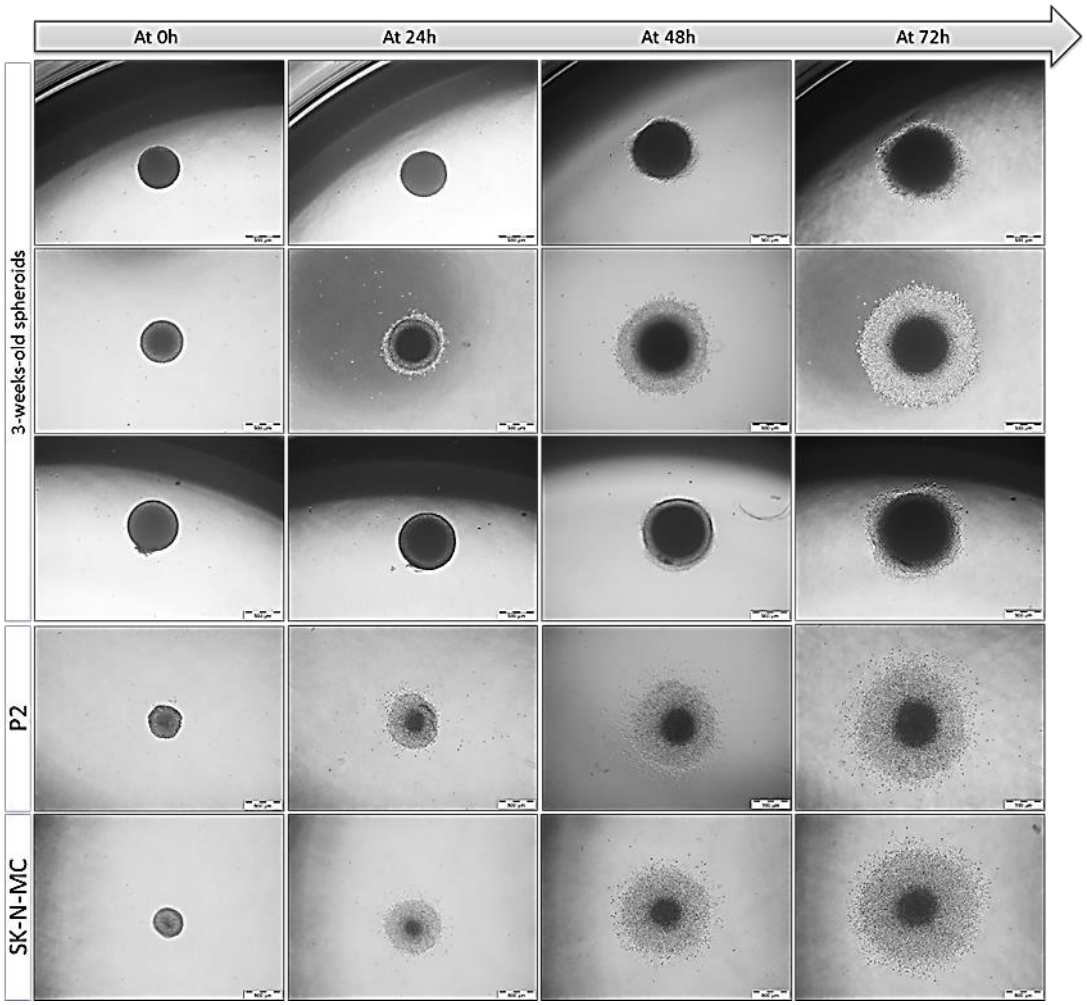

Figure 2.37 Migration phenotype of the three SK-N-MC clones. SK-N-MC cell lines, dissociated P2, and three-week-old spheroid were used. SK-N-MC cell lines and dissociated P2 grew as spheroids for four days and were then plated onto gelatin (0.1%)-coated plastic. The three-week-old spheroids were transferred as a whole spheroid onto gelatin (0.1%)-coated plastic and imaged at 0 h to 72h.

2.3.4.4 The proliferative capacity of dissociated spheroids

A number of three-week-old spheroids (n=40) were pooled and dissociated physically and then seeded in a T75 plate. To quantify the rate of growth for the dissociated spheroids in different passages, cells were counted at 0, 24, 48, and 72 h using Vi-CELL™ XR. Due to the positive correlation between the growth rate and the viable cell number at 72 h (Figure 2.38), the cells were compared at 72 h.

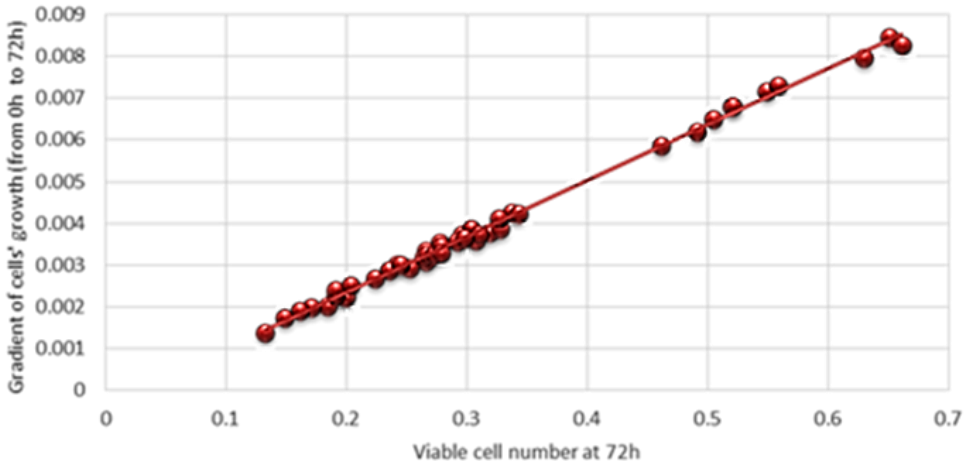

Figure 2.38 Correlation between the growth rate and the viable cell number at 72 h for all dissociated spheroids in different passages.

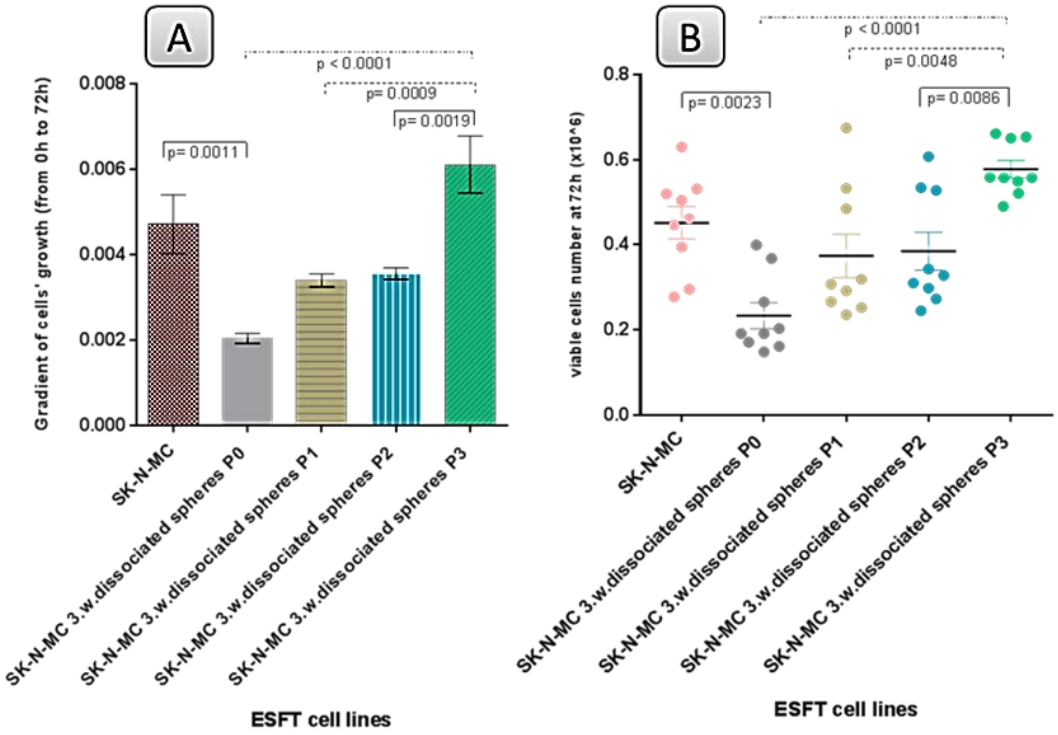

Figure 2.39 Comparison of cell viability between the dissociated spheroids in different passage and the SK-N-MC cell line. A) Represents the gradient of cells' growth (slope). B) Shows the viable cell number at 72 h. Data was analysed using one-way ANOVA with Tukey's multiple comparison *post hoc* tests.

Overall, the growth rate showed a slight increase from dissociated spheroids at passage zero (P0) to passage one (P1). This increase plateaued between P1 and P2 and was then rapidly raised towards passage three (P3). The growth rate of SK-N-MC was greater than P0, P1, and P2. Furthermore, P3 demonstrated a minor difference in the growth rate compared with SK-N-MC (Figure 2.39 A). The difference in the number of viable cells at 72 h was in a similar pattern as the growth rate. There was a significant difference between P0 and the parental cells (SK-N-MC; p=0.0023) and also P3 (p<0.0001). There was no difference in the number of viable cells of P0, P1, and P2. Cells at P3 showed a higher number of viable cells than at P1 and P2 (p-value=0.0048 and 0.0086, respectively; Figure 2.39 B).

2.3.4.5 Self-renewing capacity of dissociated spheroids in soft agar, 2D and 3D culture

In the agar-based colony formation assay, the percentage of spheroid formation was 8.21% (± 0.33, n=3) in the SK-N-MC cell line and 10.54% (± 0.11, n=3) in the P2 cells. The difference between these cells was significant (Figure 2.40). Furthermore, seeding a single cell of P2 into flat Primaria™ plates presented a high frequency of spheroid formation compared with low-adherence plates (52.60% ± 1.7 and 15.83% ± 4.8, n=10, respectively), (p<0.0001) (Figure 2.41).

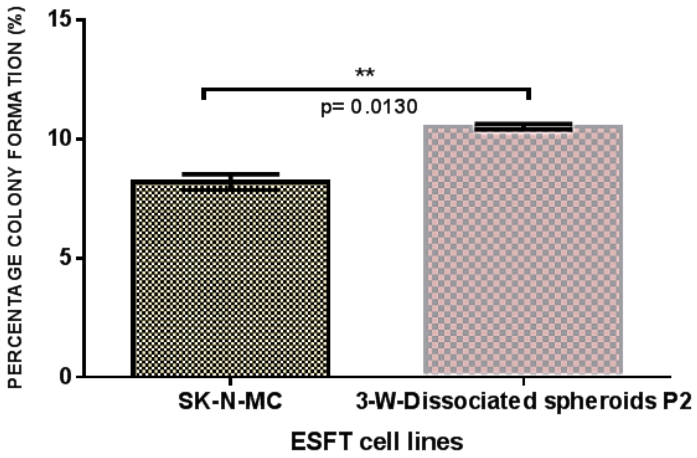

Figure 2.40 Comparison of colony formation between SK-N-MC cell line and the dissociated spheroids at P2. A two-tailed unpaired t test with Welch's correction was used to assess the difference.

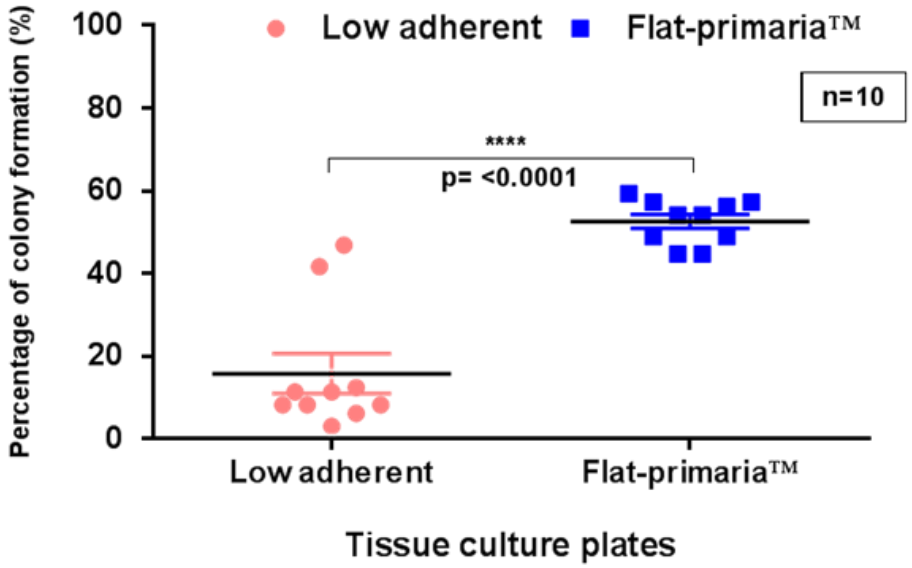

Figure 2.41 Spheroid formation from a single cell of dissociated spheroids at P2. Twenty 96-well plates (10 low-adherent plates and 10 flat Primaria™ plates) were used to grow a single cell in each well. The difference between cell lines was assessed using a two-tailed unpaired t test with Welch's correction.

2.3.4.6 Expression of CD133 in 3-w-spheroids and monolayer

The expression of CD133 in a human colon epithelial cancer cell line (Caco2) was reported and it has been found that Caco2 highly express the glycoslyated form of CD133 (AC133) (Jaksch et al., 2008). Caco2 is therefore a good positive control for CD133 that could be used instead of human stem cells (hSC) because it is much easier and cheaper to culture compared with hSC. It is very difficult to check the CD133 expression in spheroid by FACS because a single spheroid has a very small cell number that includes necrotic cells which can give false positive results. Pooling a large number of spheroids might increase the false positivity rate. Therefore, the protein level of CD133 and structural protein (GRP75) were detected using immunoblotting using cell lysates (50 µg) from cells that were grown as a monolayer, the 3-w-sphereoids and the positive control (Caco2). The blot showed a very clear band of CD133 in Caco2 and a very faint band for CD133 in SK-N-MC cells and nothing detected in SK-N-MC spheroids as well as TTC-466 and its spheroids (Figure 2.42).

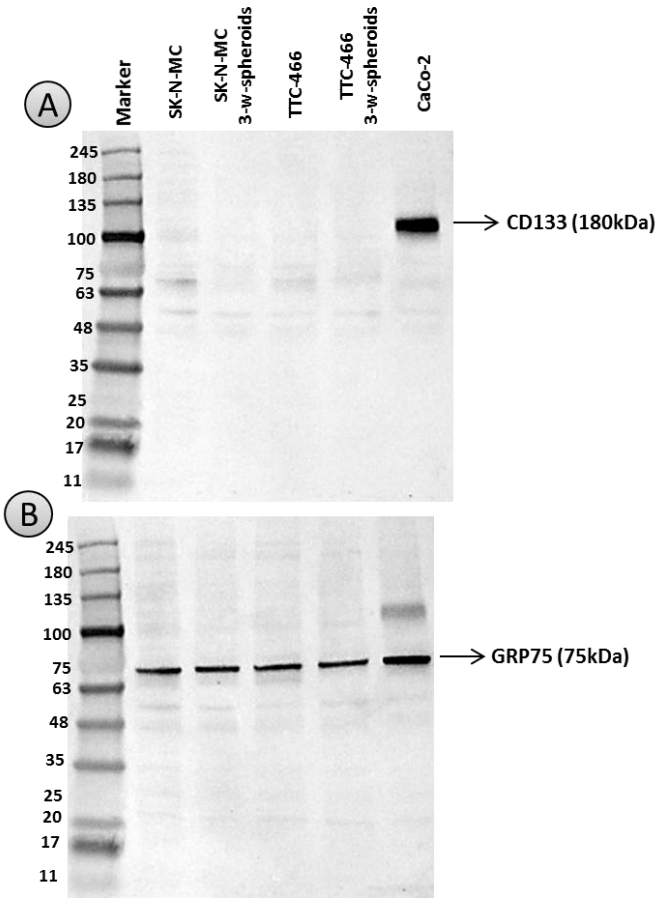

Figure 2.42 Protein expression of CD133 in ES cell lines and spheroids. A) ES cell lines that grew as monolayer (SK-N-MC and TTC-466), 50 pooled 3-w-spheroids and CaCo-2 (as positive control for CD133) lysates were blotted with CD133 antibody. B) GRP75 used as loading control.

2.3.4.7 Expression of MYC-C in CD133+ve/-ve, 3-w-spheroids and dissociated spheroids

ES cell lines (TC-32 and A-673) were sorted depending on the expression of CD133, which is expressed in cancer stem cells. MYC-C and Beta-actin were detected using immunoblotting using cell lysates (25 µg) from ES cell populations (CD133+ve and CD133-ve). The MYC-C expression was higher in CD133-enriched sarcoma cell lines compared with the embryonic stem cell (positive control: SHEF-4) and CD133-ve population (Figure 2.43). However, when compared to the SK-N-MC, the expression of MYC-C was reduced twofold in the three-week-old spheroids and the dissociated spheroids at P0. The expression increased again with the passaging the dissociated spheroids at P2 and then dropped again at P3 (Figure 2.44).

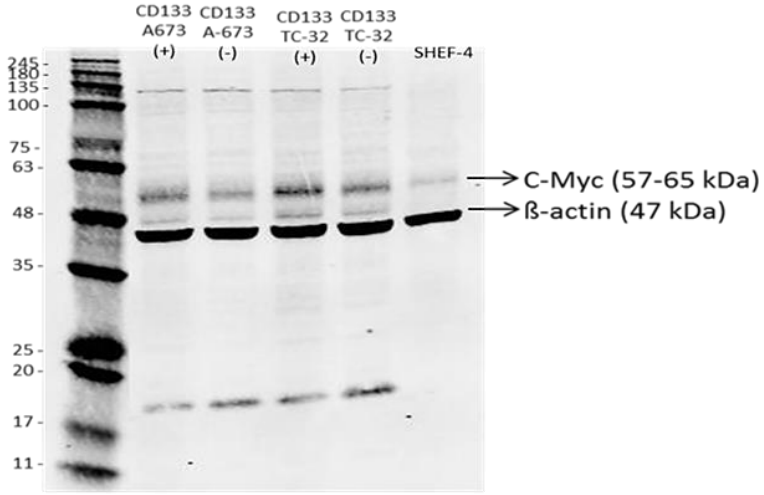

Figure 2.43 Protein expression of MYC-C in ES and other cell lines. ES cell lines (TC-32, TTC-466, SK-N-MC, SKES-1, A-673, and RD-ES) and embryonic stem cells (SHEF-4) expressed MYC-C normally (upper band), as well as Beta-actin (loading control: lower band).

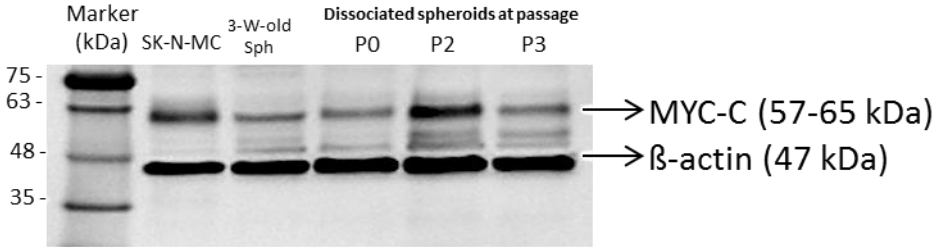

Figure 2.44 Protein expression of MYC-C in whole or dissociated spheroids comparing with substrate adherent cells. SK-N-MC, three-week-old spheroids, and dissociated spheroids at P0, P2, and P3 expressed MYC-C in different intensities (upper band), as well as Beta-actin (loading control: lower band).

2.4 Discussion

In this chapter, the most reliable method to enrich for putative ES-CSCs was by identification of cells with self-renewing ability and the capability of cells to generate spheroids from a single cell in 3D cultures was also evaluated. Seeding single cells in low adherent plates was a useful tool to enrich the possible ES-CS-like cells. These cells showed an ability to divide from a single cell in medium containing 10% FCS. On the other hand, the commercially available stem cell media, which used for culturing stem cells and expected to enhance the growth of ES-CS-like cells, induced cell death of the majority of the ES cells. However, a small population, which might be the putative CS-like cells, remain viable and might enter quiescence status in the stem cell media. The enriched putative ES-CS-likes (3D spheroids) maintained the ability to self-renew for two passages, but they did not have the capacity to migrate. The expression of CD133 protein was not detected in the spheroids and there was a reduction in the expression of MYC-C protein.

The cell sorting method (antigenic method) using a single marker (CD133), which is not specific for ES-CS and its expression may be down-regulated by the cellular microenvironment, is not an ideal method to study ES-CS. The colony formation assay can access the self-renewal capacity in a semi-sold environment but the generated clones are difficult to be isolated and used in further experiments. On the other hand, a single cell sphere/clone formation using a single cell characterized to be able to form a floating 3D spheroid or a clone of attached cells in 2D monolayer culture is promising to be the golden standard to characterize CS-like cells potential. Single cell used leads to the lack of autocrine and/or paracrine signals that are released into the medium by co-cultured cells (Pastrana et al., 2011). The low adherent condition (3D culture: hanging drops or using low adherent plates), unlike the traditional 2D monolayer culture (flat Primaria™ plates), can more closely mimic the *in vivo* tumour microenvironment since it contains areas of necrosis and hypoxia in addition to viable cells. Also, it is very important to consider two important points when performing the 3D culture: firstly, the inability to distinguish the spheroids from aggregates at higher cell densities;

secondly, the difficulty to detect quintessential CSCs in aggregated cells (Pastrana et al., 2011). Seeding a single cell and assessing the ability of this cell to form primary and secondary spheroids are the logical ways to overcome these points (Tirino et al. 2013). In contrast to hanging drops, the low adherent plates were easy to maintain, score and give reproducible results. Using ES cell lines it was possible to identify spheroids from a single cell, which have normal stem cells properties, such as self-renewal in SK-N-MC and TTC-466 lines, but not in TC-32 cells. In addition, compared to hanging drops and flat bottom plates, the spheroids formation efficiency was very high in low adherent plates. The low adherent plate was reproducible and beneficial to enrich possible CS-like cells from ES cell lines.

Similar to solid tumours, cells in 3D spheroids are exposed to different levels of nutrients, oxygen and other stresses that might affect the cells consistent with an inhibitory effect on the cell cycle. Cells from the spheroids were less proliferative than the parental cells and cells from dissociated spheroids that were cultured through two passages. This may be due to a slow rate of division of the cells that form spheroids, or reflect the impact of cells being in the spheroid (i.e. areas of necrosis, hypoxia affecting oxygen and nutrient gradients). More investigations are needed to determine the cell cycle status of the cells that produce spheroids and of the cells in the spheroids. The cell cycle analysis for the proliferative cells could be done using flow cytometry.

It was also found that the majority of cells in the three-week-old spheroids were unable to migrate, whereas cells from the dissociated spheroid regained the ability to migrate. The reason for the lack of migration after three weeks may be that the hypoxic environment affects the proliferated cells. Furthermore, the dissociated spheroids showed a lower efficiency to generate second colonies from a single cell in low adherent plates compared to parental, whereas the flat bottom plates showed a greater efficiency compared to parental. The percentage of colony formation in soft agar for the passaged cells was significantly higher compared with the parental cell line. These observations suggest that the proportion of self-renewing cells within the ES cell line culture is maintained, even after being generated from a single self-renewing cell selection. These spheroids were able to self-

renew from a single cell, adopt the 2D conditions and a small population maintains the capacity to generate spheroids in 3D conditions. This may be due to changes in the epigenetic profile of these cells.

SK-N-MC spheroids at three weeks showed the typical zones that were previously described in other studies (Lin, R. and Chang, 2008). These zones are affected by the diffusion of oxygen and nutrients in a 3D model. The outer rim 'zone' of approximately 200µm (Groebe and Mueller-Klieser, 1996; Grimes et al., 2014), represents the proliferating zone followed by the quiescent viable cell zone (hypoxic rim) and in the middle of the spheroid is the necrotic core. It has been found in glioblastoma that the hypoxic environment promotes self-renewing ability and inhibits differentiation (Li, Z. et al., 2009). The reduction in the oxygen level in the 3D spheroids increases the expression level of CD133 and up-regulates other stem cell-like markers such as Oct4, Sox2 and Nestin (McCord et al., 2009). Furthermore, the hypoxia-inducible-factor (HIF), especially HIF-2α, is assumed to have a unique expression pattern and a role in CSC maintenance, whereas HIF-1α is expressed in CSC and non-CSC in hypoxic conditions (Li, Z. et al., 2009; Myszczyszyn et al., 2015). Future studies might look at HIF-1α, HIF-2α and HIF-1β in spheroids.

MYC-C plays an important role in stem cell maintenance and nuclear reprogramming and is highly expressed in ES cell lines (Sollazzo, M.R. et al., 1998). It has been suggested that the activation of the MYC-C promoter occurs through an indirect mechanism by the EWS-FLI1 gene (Bailly et al., 1994). Like the Suva group, it was shown that the majority of CD133-ve cells are highly positive for MYC-C. Although the percentage of ES cells that express CD133 was low, all these cells were positive for MYC-C.

However, western blotting showed CD133 enriched ES cell lines express MYC-C at higher levels than the embryonic stem cell (SHEF-4) and CD133-ve population. Also, the expression of MYC-C was reduced two-fold in the 3D spheroids and the dissociated spheroids at P0 compared with the SK-N-MC cell line. However, the MYC-C protein expression increased again when cells from the spheroids were disaggregated and passaged consistent with the hypothesis that the increase in MYC-C expression was due to the 3D

culture environment.

The decrease in the expression of the MYC-C protein in 3D spheroids and dissociated spheroids at P0 might be attributed to the hypoxic environment and changes in expression of the HIF genes, which interact with MYC-C. HIF-1α decreased MYC-C driver pathways leading to inhibition of proliferation (cell cycle arrest) in clear-cell renal cell carcinoma (Gordan et al., 2007) as well as colon carcinoma (Koshiji et al., 2004). On the other hand, HIF-2α is reported to stimulate MYC-C activity and increase the proliferation rate (Gordan et al., 2008). In ES cell lines (Leuchte et al., 2014) and glioblastoma cells (Kelly, J.J.P. et al., 2009), cells showed the ability to aggregate in serum-free medium. Like other cancer cells, brain tumour stem cells (BTSCs) have the ability to grow in serum-free medium in the absence of bFGF (Kelly, J.J.P. et al., 2009). Also, the lung epithelial cancer cell line successfully aggregated and expanded without the addition of exogenous mitogenic stimulation (Yakisich et al., 2016).

The serum-free medium containing 10ng/mL EGF and bFGF has been used to investigate the sphere formation ability in sarcoma cells such as osteosarcoma cells (Fujii et al., 2009), ES cell lines (Cornaz-Buros et al., 2014) and freshly dissociated ES tumour samples that formed spheroids from single cells sorted in a number of 96-well plates (Suvà et al., 2009). In this chapter, ES cell lines were cultured in two different commercial serum-free stem cell media to enrich for putative CSCs. The possibility of using AggreWell™ and mTeSR™1 medium was investigated, both of which are designed to culture stem cells. AggreWell™ medium contains a lower level of bFGF compared with mTeSR™1 medium. After 48 h, in both media, the majority of ES cells were non-viable and the cells that survived were not able to self-renew and generate a spheroid from a single cell.

The concentration of bFGF is not stated clearly in the manufacturer information sheet because the final medium formulations are company proprietary. However, Ludwig's group modified the first serum-free medium, known as TeSR1, and established the mTeSR1, which includes BSA and cloned zebra fish basic fibroblast growth factor (zbFGF) at a final concentration of 100µg/mL (Ludwig, T.E. et al., 2006). The reason behind

the use of the high concentrations of bFGF in mTeSR1 is the instability of bFGF in serum-free medium (Levenstein et al., 2006; Ludwig, T.E. et al., 2006). The currently available mTeSR1 medium contains components based on Ludwig's group published formulation and human bFGF was used instead of zebrafish bFGF. In previous studies, 20ng/mL bFGF has been shown to induce cell death of ES cell lines, including the SK-N-MC and TC-32 cells which were studied in this thesis (Sturla et al., 2000). This may explain why the ES cells did not survive in the mTeSR1 media.

Many research groups used the terminology of spheroids to refer to cells which have the ability to aggregate. The resultant spheroids formed from aggregating unknown numbers of cells have the ability to generate secondary spheroids in low adherent condition (Cornaz-Buros et al., 2014). Fujii group managed to aggregate cells ($1x10^5$cells/well) with very low spheroid formation frequencies; 1/400 for MG63, 1/128 for HT1080 and 1/180 for HTB166. Addition of a fresh mitogenic factor such as bFGF and EGF both at 10ng/mL every other day to the serum-free medium in a spheroid formation assay was confirmed to upregulate the expression of stem cell markers on human sarcoma cell lines (Fujii et al., 2009). Others have used serum-free medium supplemented with a higher concentration of bFGF and EGF (20ng/mL) to assess the efficiency of the spheroid formation in lung cancer cells (5 cells/µL) (Chung et al., 2015) as well as glioblastoma (≤20,000 cells/mL) (Kelly, J.J.P. et al., 2009). In this study, none of the ES cell lines were able to generate spheroids from a single cell; 0/96 in each cell line, possibly due to the high concentration of bFGF in medium. ES cell lines were shown to have the ability to generate spheroids from a single cell in the standard medium that contains 10% serum, the presence of serum might not affect the self-renewing capability of the possible CSCs. It has been reported that FACS sorting ES cell lines into wells containing 10% serum medium or serum-free medium had no effect in self-renewing ability (Jiang et al., 2010).Prominin-1 also known as CD133, is a pentaspan transmembrane glycoprotein, which has been described as a CSC surface marker in several cancer types including ES (Suvà et al., 2009; Jiang et al., 2010). CD133+ve population was capable of recapitulating tumours when cells were injected into immunodeficient mice (Suvà et al., 2009). CD133 was used first the first

time as a marker to isolate the stem-like cells of brain tumours (Singh et al., 2004), and subsequently, for other solid tumours such as colon (O'Brien, C. A. et al., 2007), melanoma (Monzani et al., 2007) and prostate (Collins et al., 2005). In future studies, it will be important to confirm the ability of putative ES-CSCs to produce tumours in mice.

The frequency of the CD133+ve population in ES is reported to be 4%–8% (Suvà et al., 2009) and 2.3% to 98.7% (Jiang et al., 2010). However, in this chapter, 1.7% to 14.5% of ES cell lines expressed CD133.

Several tools have been manufactured to isolate putative CSCs exploring cell surface expression of CD133. One of the most popular methods is the immunomagnetic cell separator known as MACS® cell separator enriching for CD133+ve and CD133–ve cell populations. Using ES cells the laboratory have successfully isolating CD133+ve populations that are 95% positive and the CD133–ve populations that are less than 5% positive (Berry, personal communication). Others have found that the purity of CD133+ve cells enriched from ES tumour samples to be 82% (Suvà et al., 2009). However, the purity of CD133 populations isolated from brain tumour samples using MACS® separator was reported to range from 70 to 91% for CD133+ve cells (Singh et al., 2004). CD133-ve cells were also found to contain 0.5% to 12.5% of CD133+ve cells (Singh et al., 2004).

Three different ES cell lines were used in this study and the separation was carried out once for each cell line. Despite following the manufacturers' protocol, the purity of the separated populations were 60% for CD133+ve cells and 12% for CD133-ve cells. In an attempt to increase the separation efficiency, more antibody was used; however, it was impossible to run a purity check on the flow cytometer due to the very small number of cells recovered from the separation. The difficulty of isolating pure CD133+ve cells from cord blood using the MACS separator have been previously reported (Pelagiadis et al., 2012). This group compared the purity of cells separated using the CD34 and CD133 markers. The purity of CD133+ve cells varied between samples (10–85%), whereas CD34+ve cells were consistent (~93%). To increase the purity of CD133+ve population, researchers tried different labelling methods such as direct labelling, extra

labelling with CD133 microbeads, erythrocyte removal and indirect additional binding of CD133 antigen. None of these methods improved the purity of CD133+ve cells. They concluded that the reproducibility of a pure CD133+ve cells was not achievable. Also, they stated that the commercially available CD133 clones do not cross-block the antigen and this cannot be the reason for the difference in the purity of the CD133+ve cells. Glycosylation could also perhaps affect the purity of the CD133 population (Pelagiadis et al., 2012). The use of flow cytometry as an alternative method to separate the CD133 population was then investigated. The isolated CD133 population from the ES cell lines was pure (97–99%) and the purity of cytospun isolated cells was confirmed using IF. Jiang groups used the MACS separator to enrich the CD133 population in ES cell lines with less than 20% CD133+ve cells and thus improved the FACS sorter efficiency, and the sorted cells were cultured in medium containing antibiotics (Jiang et al., 2010). FACS cells should be grown in medium containing antibiotics to minimise the risk of contamination, but since the addition of antibiotics affects the gene expression profile (Roundhill, personal communication), this is not an ideal method to enrich cells that require expression profile analysis (Chapter 3).

However, unlike CD133-ve, the purified CD133+ve displayed spheroid formation capacity in adherent plates from a single cell isolated from fresh tumours as well as a high proliferation rate in medium containing 20 % knockout serum replacement and 10 ng/mL of bFGF and EGF (Suvà et al., 2009). Unlike ES cell lines, the majority of CD133+ve cells that were isolated from tumours have shown a higher ability (5-fold) to generate spheroids in low adherent plates than CD133-ve cells (Jiang et al. 2010). In contrast, flat bottom primaria adherent plates were used to culture the sorted CD133 from ES cell lines in this study. It was found that CD133-ve cells have a higher ability to grow as clones (1.1%–17.1%) than CD133+ve cells (0.3%–10.2%).

Furthermore, the spheroids, derived from a single CD133+ve cell, expressed CD133 (6.9%), the same as the expression level in the parental tumours and xenografts (Suvà et al., 2009). Moreover, the expression of CD133 in spheroids generated from a single primary ES cells in low adherent plates ranged from 2.7% to 40% at 2–3 weeks (Cornaz-Buros et al., 2014). This

proves that CD133+ve cells give rise to +ve and –ve populations, which dilutes the expression level of CD133. Additionally, the 2D cells and the 3D spheroids that resulted from aggregating 2,000–10,000 cells per well in a low adherent plate shared almost the same percentage of CD133. Also, there was no difference in the expression of neural crest stem cell marker (CD57, also known as HNK-1), which has previously been reported to increase in cells that are growing as spheroids and with increased tumorigenicity *in vivo* (Leuchte et al., 2014). In this chapter, expression of CD133 in the clone derived from the sorted ES cell lines needs to be further investigated.

In conclusion, there is no specific marker or culture method to accurately identify CSCs. The majority of spheroid studies in the literature are generated from cell aggregation. The aggregated spheroids represent cell-cell interaction and not true CSCs because of the lack of evidence of self-renewal capacity. In this current study, isolation of possible CSCs that have the ability to self-renew from a single cell have been achieved. Whereas, the ES spheroids need to be investigated in depth to confirm that these are indeed CSCs.

The key finding:

1- The putative ES-CS-like cells grown better in 3D, whereas stem cell medium led to cell death.
2- The putative ES-CS-like cells do not have the ability to migrate.
3- The putative ES-CS-like cells have low expression level of MYC-C and probably not expressing CD133.

Chapter 3
Transcriptional drivers of the CSC phenotype

3.1 Introduction

ES cells are poorly differentiated and highly express stem cell markers (Enrique and William, 2000; Ludwig, J.A., 2008). The phenotypic characteristics of other cancer types that are poorly differentiated have been found to be fairly similar to stem cells (Curry et al., 2015; Tang et al., 2015). The CSC phenotype characterised by self-renewal and resistance to treatment is considered to be critical for ES progression and relapse (Suvà et al., 2009; Jiang et al., 2010). Understanding the drivers of transformation and gain of the cancer stem-like cells phenotypes is therefore essential to improve outcomes and design new treatments (Garvalov and Acker, 2011), yet the fundamental molecular mechanisms for the functional differences between CSC and non-CSC remain unclear recent studies suggest that miRNAs play a role in the regulation of gene expression to maintain stem cell features. miRNAs are short noncoding RNAs capable of negatively and/or positively regulating gene expression post transcriptionally (Bartel, 2009). The downregulation of a wide number of miRNA in tumours seems to be responsible for their malignancy and stemness (Ventura and Jacks, 2009; Melo and Esteller, 2011). Furthermore, several studies indicate miRNA involvement in cancer especially in CSC establishment (De Vito et al., 2012; Takahashi, R. et al., 2013; Garofalo and Croce, 2015). In 2011, it was determined that TARBP2-dependent miRNA expression enhanced CSC self-renewal ability and improved tumour maintenance (De Vito et al., 2012).

Having enriched for putative ES-CS-like (Chapter 2), in this chapter, the hypothesis was that ES-SC-like express driver pathways which may be used to select patients for more personalised medicine to improve outcome.

The aim of this chapter was to identify pathways by comparing the expression of stem cells markers, ABC and miRNA of ES-CS-like with substrate adherent cells. The following specific objectives were needed to help us test this hypothesis: To help us test this hypothesis we need to

1- Characterise the RNA and miRNA profiles of spheroids and substrate adherent cells using Taqman gene expression arrays (TLDA) for stem cells and ABC transporter mRNA and selective miRNAs.
2- Validate selected targets from arrays using RTqPCR and western blot.
3- Find interactions between the highly expressed genes and investigate miRNA involvement in pathway.

3.2 Methodology

3.2.1 Samples details

In this chapter, substrate adherent cells, a pool of three week spheroids (3-w-spheroids) and passaged 3-w-SK-N-MC spheroids, which were grown as substrate adherent cells, at passage number 2 were used. Also, frozen cell pellets including MCF7, HEK-293, n2012, SHEF4, U206, K562 and Caco-2, were used as positive controls. Moreover, RNA was extracted from a collection of ES family tumour derived spheroids (n=8) at different time points in addition to substrate adherent cells. Extracted RNAs were assessed using three different methods to ensure accurate representation of gene expression in subsequent experiments. All arrays and RTqPCR reagents were purchased from Life Technologies unless otherwise stated.

3.2.2 Extraction and assessment of RNA

3.2.2.1 Total RNA extraction

Total RNA was extracted as described previously in (Section 2.2.5.3.1).

3.2.2.2 NanoDrop® Spectrocytometry

The concentration of RNAs was measured as described previously in (section 2.2.5.3.2).

3.2.2.3 Bioanalyzer (Agilent 2100)

The Agilent RNA 6000 Pico Kit was used to determine the quality of RNA, quantity as well as the size of samples such as nucleic acid, proteins and cells. This system is microfluidics based and is essentially a tiny version of acrylamide and agarose gels that are commonly used to separate nucleic acids and proteins by size. Briefly, all reagents and the entire procedure must be at room temperature. At the beginning, RNA gel matrix (550 µL) was pipetted into a spin filter and then centrifuged for 10 min at 4000 rpm. The filtered gel was aliquot into 65 µl and RNA dye concentrate (1 µL) was added to the filtered gel and tube was spin for 10 min at 14000 rpm. An RNA chip was placed on the chip priming station (Figure 3.1). The mixture of RNA

gel-dye (9 µl) was pipetted into three wells, as shown in the diagram. The plunger of the chip priming station was positioned at 1 mL and then the chip priming station was closed. The plunger was pressed until it held by the clip and then released after 30 s. The chip priming station was opened and the RNA conditioning solution (9 µL) and RNA marker (5 µL) were loaded into the wells, as labelled in the diagram. The diluted ladder and denatured (70 °C, 2 min) RNA samples from substrate adherent cells and spheroids (1 µL; 5ng/µL) were loaded into the chip and then the chip was centrifuged for 1 min at 2400 rpm. The chip was run in the Agilent 2100 Bioanalyzer instrument within 5 min. The quality of samples is displayed as a RNA Integrity Number (RIN). This number is calculated by the instrument software using an algorithm method, which takes into account the ratio of 28S and 18S rRNAs as well as the entire electrophoretic trace of the RNA (Wieczorek et al., 2012).

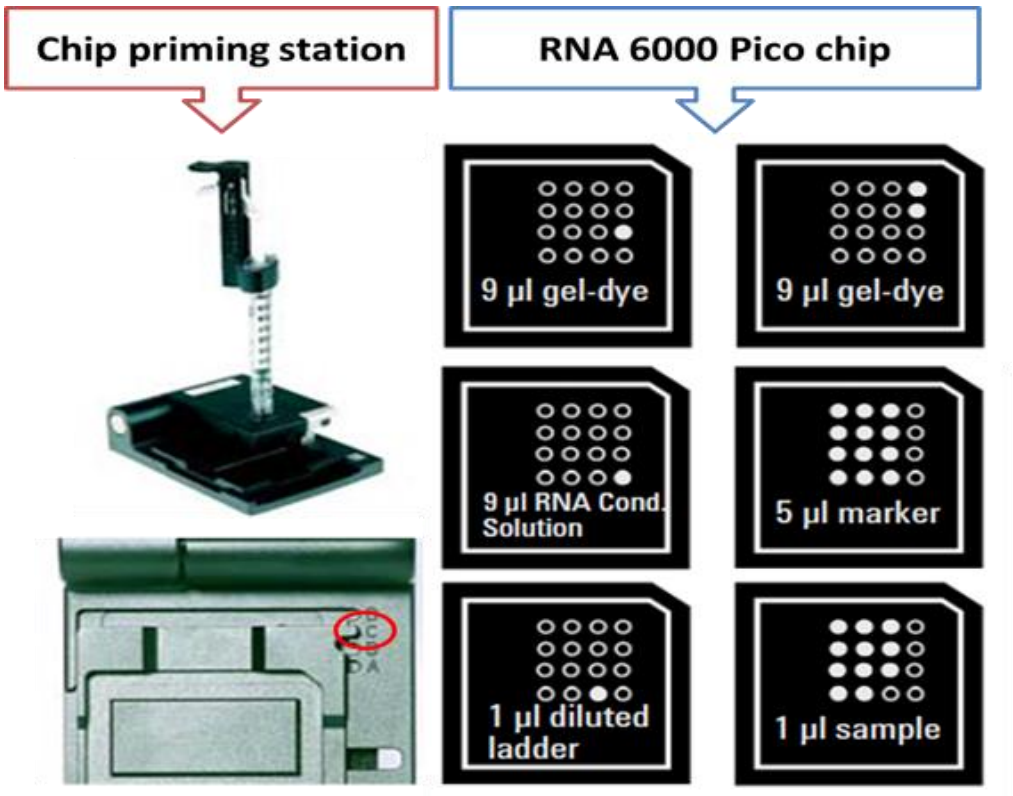

Figure 3.1 Agilent RNA chip that used to check RNA quality. The Agilent station (left) was used to load the RNA on the chip. RNA pico chip used to determine the quality of the extracted RNA (right) (Adapted from Agilent website http://www.genomics.agilent.com/literature.jsp?crumbAction=push&tabId=AG-PR-1172&contentType=User+Manual)

3.2.3 RNA profiles using TaqMan® Low-Density Array (TLDA)

3.2.3.1 mRNA TLDA

The total RNA (concentration; 1000 ng/µL) from substrate adherent cells and also spheroids was used to prepare cDNA as previously described in (Section 2.2.5.3.3) and loaded into two different TLDA platforms that wereused to explore gene expression. TLDA is a RTqPCR assay that measures the expression level of each listed gene in duplicate (Human Stem Cell Pluripotency array; HSCPA; 4385225) or triplicate (ABC transporter array; ABCTA; 4378700). Each cDNA sample (40µL) was added to 220µL of TaqMan® Universal PCR Master Mix and the volume adjusted to 440µL with RNase-free water. The mixture was loaded into the ports of the TLDA plate.

3.2.3.1.1 Loading and processing TLDA

TLDA plate was centrifuged for 1 min x 2 at 1000 rpm, then run in the 7900HT Fast real-time PCR System, under the following thermal conditions were: 50°C for two min, 95°C for 10 min and then 40 cycles of 95°C for 15 sec and 60°C for 1 min. Results were exported to RQ Manager 1.2.1 and a manual threshold was set above the background signal, which indicates a single Ct for each gene, at 0.2 for ABC arrays and 0.25 for SC arrays.

3.2.3.2 miRNA TLDA

3.2.3.2.1 cDNA preparation

The total RNA (concentration; 400 ng/µL in a total volume of 3.2µL) from substrate adherent cells and also spheroids was used to prepare cDNAs using the TaqMan MicroRNA Reverse Transcription Kit and MegaPlex Primers Pool A v2.1. Volumes in (Table 4.1) and RT was performed on a TC500 thermal cycler TC500 under the following conditions (40 cycles); 16°C 2 min; 42°C 1 min; 50°C 1 sec followed by hold 85°C 5 min and finally holding at 4°C. The cDNA was stored at -80°C until used.

Reagent	Volume (µL)	Final concentration
MegaPlex RT Primers (10x)	0.8	1.06x
dNTPs with dTTP (100mM)	0.2	2.6mM
MultiScribe Reverse Transcriptase (50U/µL)	1.5	75U
10X RT Buffer	0.8	1.06x
$MgCl_2$ (25mM)	0.9	3mM
RNase Inhibitor (20U/µL)	0.1	2U
Total RNA in RNase free water	3.2	-
Total volume	7.5	-

Table 3.1 List of reagents used to convert total RNAs to cDNA to be analysied by TLDA. Reagents used to convert total RNA to cDNA using TaqMan MicroRNA Reverse Transcription Kit. The resulted product analysed using TLDA array

3.2.3.2.2 loading and processing miRNA TLDA

The microRNA card (TLDA; 4398965) contains 377 microRNA. The prepared cDNA sample (section 4.2.4.2.1; 6 µL) was added to 450µL of TaqMan® 2× Universal PCR Master Mix, No AmpErase® UNG; the total was adjusted to 444µL with the RNase-free water. After that, samples were processed as described in (Section 3.2.3.1.1). The threshold was set at 0.2 as suggested in (Viprey et al., 2012).

3.2.4 Validation of significant targets from TLDA

3.2.4.1 Primers and probe design for EBAF

UCSC genome browser (http://genome.ucsc.edu/) was used to identify EBAF isoforms. RNA sequences were obtained using NCBI (National Centre for Biotechnology Information) RefSeq accession numbers and aligned using Clustal Omega (The European Bioinformatics Institute website (www.EBI.ac.uk)). Forward and reverse primers of 19-23 nucleotides in length were selected to span Exon 3 and 4 (Figure 3.2). The predicted specificity of each primer to the EBAF sequence was checked using the Basic Local Alignment Search Tool (www.ncbi.nlm.nih.gov/BLAST) and In silico PCR program in the UCSC website (www.genome.ucsc.edu/). The GC

content of the primers was 57-68% and melting temperature (Tm) was 68% (as calculated by Primer express, ThermoFisher software). The primers were designed to minimize dimer or hairpin formation.

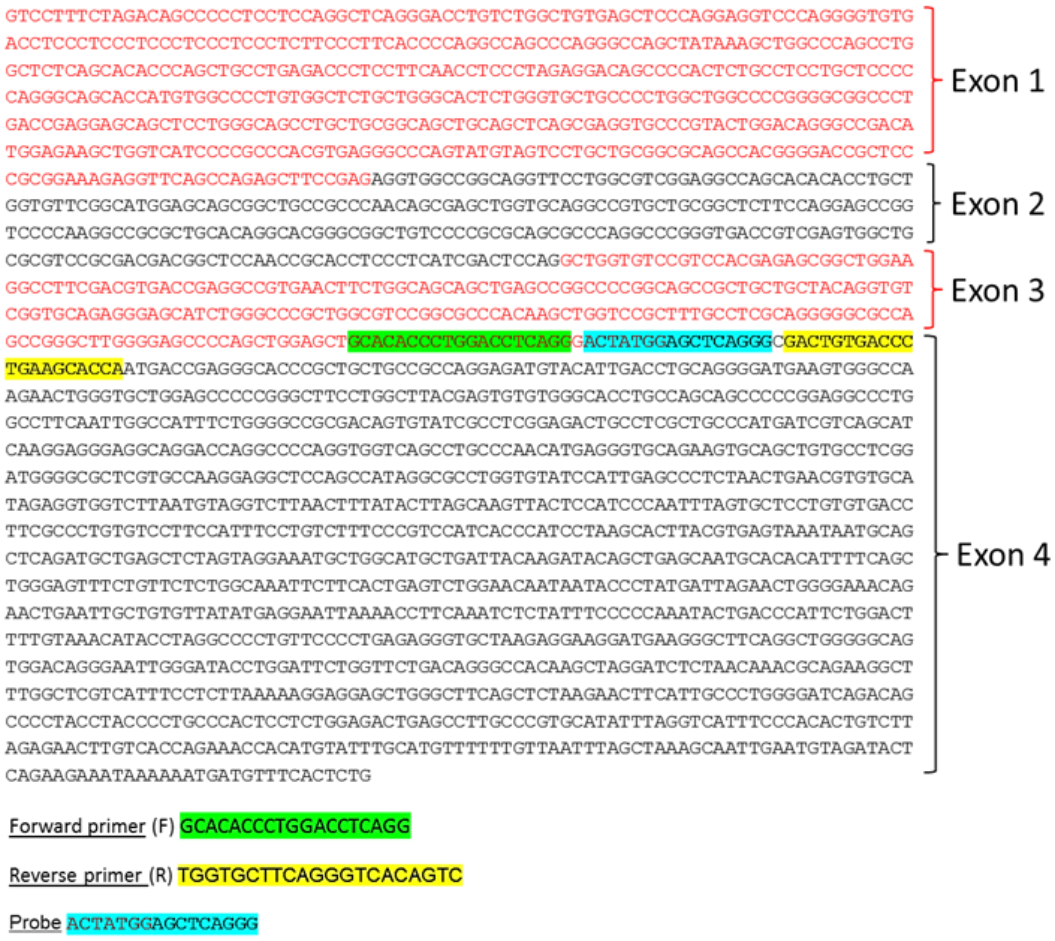

Figure 3.2 RNA sequence of the full length EBAF gene (variant 1). Exons were highlighted in red/black and primers located between exon 3 and 4

3.2.4.2 RTqPCR

The cDNA was prepared as described in (section 2.2.5.3.3). EBAF volume in (Table **3.2**) and RTqPCR was performed as described in (section 2.2.5.3.4). The housekeeping gene selected to normalise results was PPIA and Assay-on-Demand™ primer/probe were listed in (Appendix D.1.1).

	Reagents	Volume (µL, per sample)	Final concentration
EBAF Mix	TaqMan Universal PCR Master Mix	50	1X
	Forward primer (10µM) 5'-GCACACCCTGGACCTCAGG-3'	1	100 nM
	Reverse primer (10µM) 5'-TGGTGCTTCAGGGTCACAGTC-3'	1	100 nM
	Probe (20µM) 5'-ACTATGGAGCTCAGGG-3'	0.5	100 nM
	RNase free H2O	25	-

Table 3.2 List of reagents used to amplify EBAF using RTqPCR

3.2.4.3 RTqPCR for miRNA

RNA was diluted with RNase-free water to contain 10ng total RNA in a volume of 5µl. TaqMan MicroRNA Reverse Transcription Kit and RT Primers were added in quantities listed in Table 3.3. Tubes were processed as described in (section 3.2.4.2). The cDNA (4.8 µL) then was added to 36µL of TaqMan® Universal PCR Master Mix II, no UNG; 3.6µL of primers (TaqMan® Small RNA Assay (20×)) and finally the total was adjusted to 72.01µL with RNase-free water. Primers used are listed in Appendix D.1.2. The samples were analysed in triplicate in 96 well plates. The plates were covered, processed and analysed as described in (Section 2.2.5.3.4)

Reagent	For each sample Volume (µL)	Final concentration
dNTPs with dTTP (100mM)	0.15	1 mM
MultiScribe Reverse Transcriptase (50U/ul)	1	3.3U
10X RT Buffer	1.5	1x
Rnase Inhibitor (20U/ul)	0.19	0.25U
Nuclease -free water	4.16	-
5 X RT primer	3	1x
Diluted total RNA	5	-
Total	15	

Table 3.3 List of components for conversion of RNA to cDNA to be analysed by Taqman RTqPCR. miRNA analysed using Taqman RTqPCR

3.2.4.4 Protein extraction and western blot

The protein extraction, calculation of concentration and western blot were performed as described in (Section 2.2.5.2). Details of antibodies used are described below (Appendix A.1.1).

3.2.5 Analysis of TLDA

3.2.5.1 Identification of optimal normalization method for TLDA arrays and reference RNAs for validation experiments

After removing all Ct values ≥35 within each array. The Ct values from the TLDA array analysis were normalised against the global mean, each individual reference control on the array, all possible combination of reference controls and against the average of the reference controls to give the delta Ct (ΔCt). Normalised values were presented as logRQ values, which were plotted in GraphPad prism 7 software as box plots.

$$\Delta Ct = Ct \text{ (of mRNA or miRNA)} - Ct \text{ (normalisation method)}$$

$$logRQ = \log_{10} 2^{-\Delta Ct}$$

Moreover, the miRNA values were sorted into normalised against the global mean group or un-normalised group. The variation of each miRNA in both groups across all arrays was determined (Standard deviation; SD) using Microsoft excel. The miRNA then were sorted from lowest SD to high. The top 10 miRNA from each group and the common miRNA in both top 10 list were applied to NormFinder software.

3.2.5.2 Clustering analysis

Normalised array data were visualised as a heat map using Cluster 3.0 and Tree views 3.0 (Saldanha, 2004). The samples were clustered hierarchically for all arrays (mRNA and miRNA) according to expression (D'Haeseleer, 2005).

3.2.5.3 Linear Models for Microarray (LIMMA)

LIMMA is a Bioconductor package for differential expression analysis of microarray data as well as any experiments involving comparisons between several genes at the same time. LIMMA fits a linear model to the expression data for each gene and uses shrinkage methods, which keeps all the variables in data and shrinks the numbers towards zero. In LIMMA, Empirical Bayes (eBayes) was used as shrinkage method to stabilise the analyses and improve power in small sample size. The main idea of the eBayes function is to get reasonable multiple t-tests and to borrow information between genes. With guidance and support from Dr Helene Thygesen (Lancaster University), the normalized data generated from arrays uploaded into R software (version 3.3.1; https://www.r-project.org/) and then analysed using LIMMA software (http://www.bioconductor.org/biocLite.R). Two models were used to analysis data. The first model (Model A) was comparing two samples: spheroids with substrate adherent cells. Model B compares four samples: two spheroids with two substrate adherent cells from two different ES family tumours cell lines. The command for Model A and B is as described in (Appendix E.1.1 and E.1.2). Differences were considered significant when the adjusted p value ($q<0.2$).

3.2.6 Analysis of validation experiments

All analyses were undertaken using GraphPad prism 7 software. When comparing spheroids with substrate adherent cells in the validation experiments, data were analysed by ANOVA with Tukey post hoc test.

3.3 Results

In this chapter, the parental cell line that was grown as a monolayer (Red box in Figure 3.3) is termed as substrate adherent cells, a pool of ES spheroids collected at different time points (Blue box in Figure 3.3) is termed as week number-name of cell line-spheroids (e.g. 3-w-SK-N-MC spheroids) and the dissociated spheroids (Yellow box in Figure 3.3) is a terminology used for the passaged 3-w-SK-N-MC spheroids, which were grown as substrate adherent cells and collected at passage number two. All spheroids analysed by TLDA arrays were collected at week 3 (3-w-spheroids).

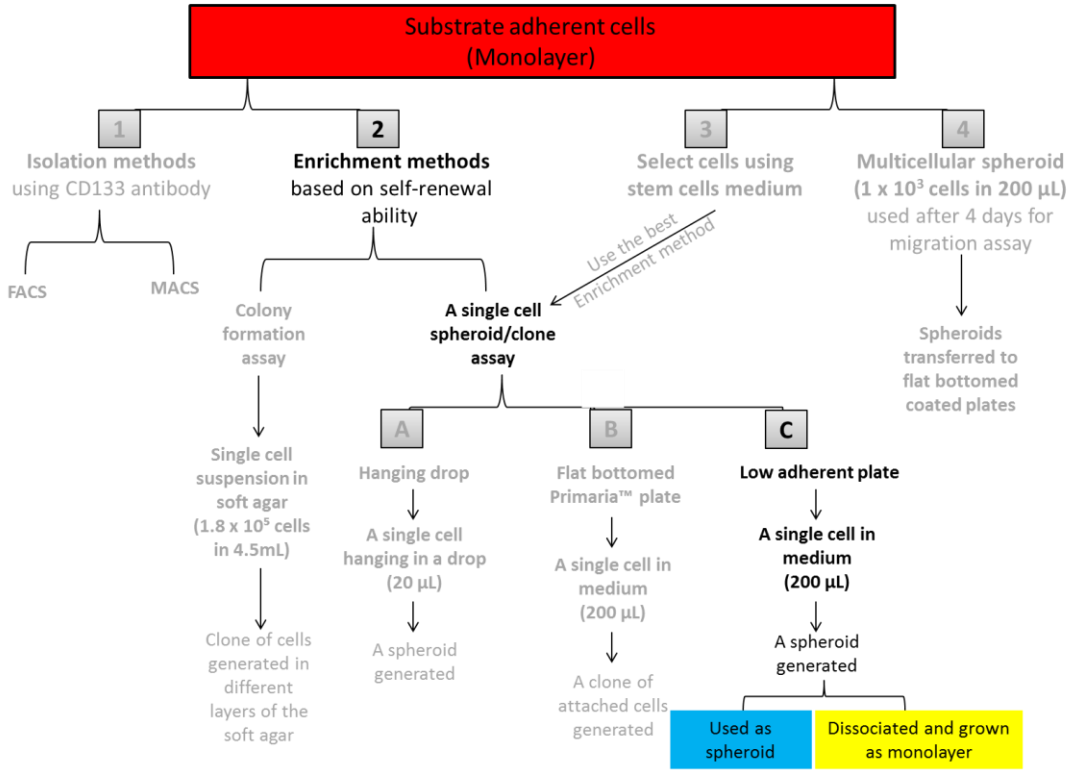

Figure 3.3 Clarification of reference to cells that used in experiments. Red box= parental cell line grown as monolayer. Blue box= whole spheroids. Yellow box= dissociated spheroids that grown as monolayer.

3.3.1 RNA quality and yield extracted from ES spheroids and substrate adherent cells

The A260/A280 ratio of all extracted RNA samples (1.9- 2.0) was consistent with high quality (Wilfinger et al., 1997) (Table 3.4). The difference in cell number between substrate adherent cells and ES spheroids in part explains

the variations in the RNA yield, and differences in the spheroid size may explain the variance between repeats.

In ES spheroids, the average RNA yields (ng) were 6004.4, 5777.8, 2701.8 and 3505.8 at week 3, 4, 5 and 6 respectively. Yields are reduced at week 5 and 6 compared to week 3 and 4. The difference between the RNA yield at week 3 and 4 is only 226.6ng, yet there is a huge reduction (14.6 fold) when comparing the difference between the yield of week 3 and week 5 (3302.6ng) with the difference between the yield of week 3 and week 4 (226.6ng). Also, there is an 11-fold change between the difference in yield between week 3 and week 6 (2498.6ng) compare with the difference in yield between week 3 and week 4 (226.6ng). This reduction most likely reflects the loss of viable cell number on spheroids, increase in size and the hypoxic/necrotic core increases at late time points (Section 2.3.4.2.1, Figure 2.34 in Chapter 2).

	Substrate adherent cells	SK-N-MC spheroids derived from a single cell in low adherent plates (mean ± SEM; n=2)			
	SK-N-MC adherent cells	Week 3	Week 4	Week 5	Week 6
RNA concentration (ng/µL)	2600± 258	500 ± 97	482 ± 91	225 ± 52	292 ± 41
RNA yield (ng)	77988±7743	6004±1158	5778±1089	2702± 625	3506± 489
A260/ A280	2.03± 0.02	2.03 ± 0.03	1.99 ± 0.03	2.02 ± 0.07	1.90 ± 0.00
RIN (n=1)	9.9	8.6	7.7	3.8	2.9

Table 3.4 RNA yield, concentration and quantity from substrate adherent cells and ES spheroids. RNA concentrations (ng/µL), yield (ng) and purity (A260/280 ratio) have been measured by spectrophotometer. RIN= RNA Integrity Number. Results are presented as a mean± standard error of the mean for two different biological repeats (mean± SEM; n=2).

High-quality RNA was extracted from SK-N-MC cells and spheroids at week 3 with distinct 18S and 28S peaks with RIN values between 8.3 and 9.8. Also, TTC-466 cells and spheroids have RIN 10 and 9.7 respectively (Table **3.5**). The SK-N-MC spheroids from week 4 exhibited distinct 18S and 28S peaks and has RIN > 7, indicating that the integrity of the RNA extracted was acceptable (Viljoen and Blackburn, 2013). However, week 5 and week 6

samples showed a sharp decrease in RIN number (2.60 – 3.80) and smaller peaks of 18S and 28S RNA (Figure **3.4** A).

To determine the level of degradation, Agilent 2100 showed gel electrophoresis images for each sample (Figure **3.4** B). The 28S and 18S fragment should be very clear when the RNA is good quality as is evident in the substrate adherent cells and ES spheroids at weeks 3 and 4. The appearance of shorter fragment sizes can be observed with progressing degradation as it appears in ES spheroids at weeks 5 and 6. These results are constant with the histology of spheroids (Section 2.3.4.2.1, Figure 2.34 in Chapter 2). The small decrease in RIN number of spheroids at weeks 3 and 4 weeks could be due to the hypoxia, whereas the huge drop could be due to increased necrosis, the death of cells and destruction of spheroids at weeks 5 and 6.

	SK-N-MC adherent cells (n=4)	3-w-SK-N-MC spheroids (8 pooled spheroids; n=5)	TTC-466 adherent cells (n=4)	3-w-TTC-466 spheroids (8 pooled spheroids; n=14)
RIN	9.8± 0.2	8.3± 0.2	10± 0.0	9.7± 0.1
Yield (ng)	86817± 9765	6413± 1191	45552± 8293	1567± 178

Table 3.5 RIN values and RNA yields of different biological RNA extracts from substrate adherent cells and ES spheroids. Two cell lines have been used (SK-N-MC and TTC-466) to generate spheroids. ES spheroids collected at week three (mean ± SEM).

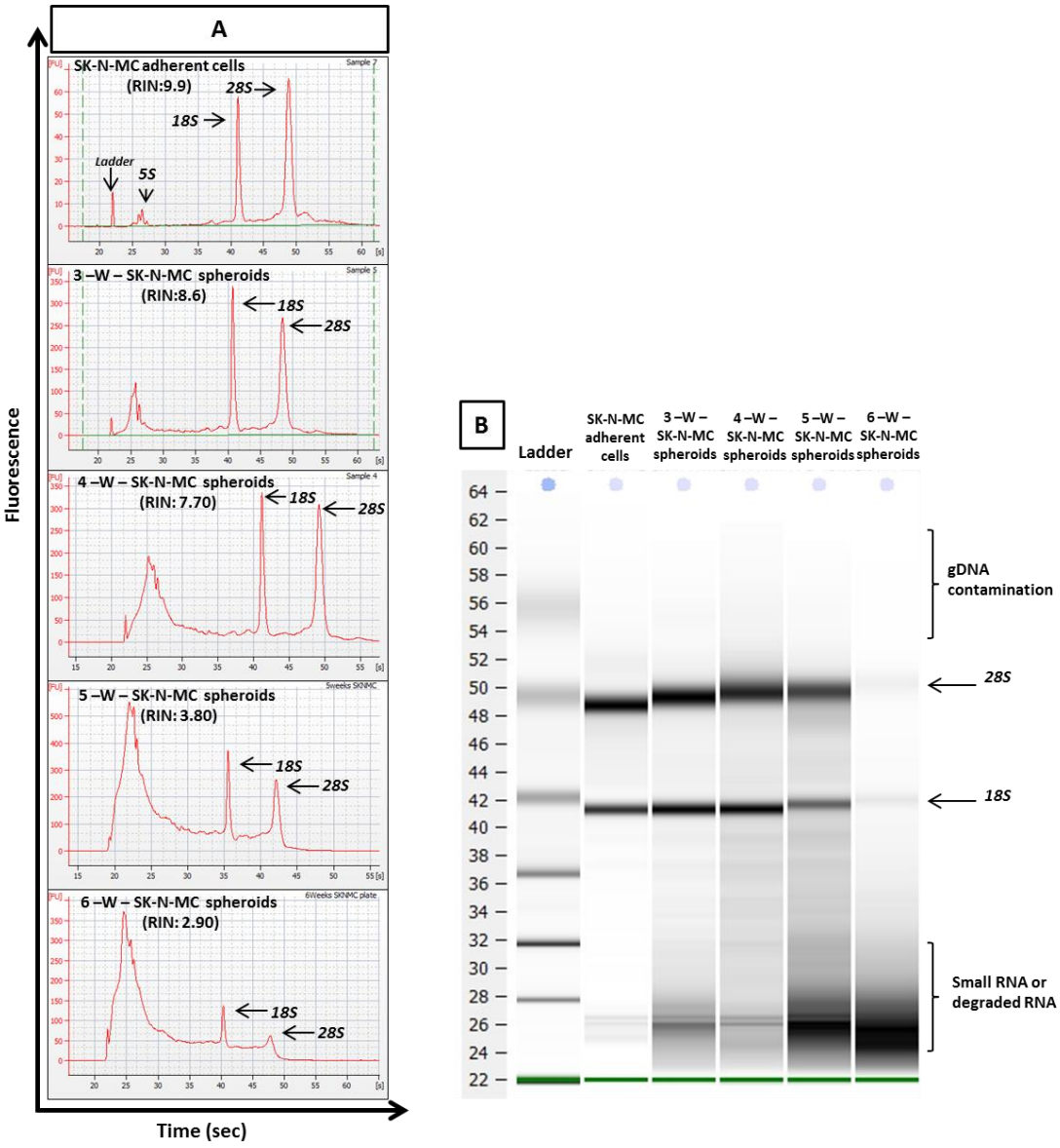

Figure 3.4 Quality of RNAs extracted from ES spheroids collected at 4-time points and substrate adherent cells . RNA analysed by the Bioanalyzer Agilent 2100. A) Electropherograms of RNA extracted from spheroids and adherent cell RNA. There are four peaks in the electropherograms: 28S and 18S are ribosomal RNA whereas, 5S illustrate small or degraded RNA and also a small peak for the marker (ladder), which is a molecular weight used to the size the RNA products. B) Densitometry plot producing an electrophoresis of the extracted RNA samples that separate depending on size and show a specific band for 18S and 28S as well as gDNA contamination and small or degraded RNA. W= week, gDNA= genomic DNA.

Furthermore, the quality of RNA for analysis was evaluated by performing RTqPCR for the housekeeping gene, PPIA. Ct values of PPIA (n = 6; from 2 independent experiments), all SK-N-MC spheroids from the different time points expressed PPIA at similar levels when compared with SK-N-MC substrate adhere cells (Figure 3.5). This is inconsistent with the results from the Bioanalyzer, which demonstrated loss of total RNA quality in week 5 and 6 spheroids. PPIA showed a high stability in low quality RNAs extracted from formalin-fixed, paraffin-embedded samples from sarcoma patients (Aggerholm-Pedersen et al., 2014). Also, PPIA recommended to be used as reference genes when comparing the expression between cancer stem-like cell (CSC) and parental cells (Lemma et al., 2016).

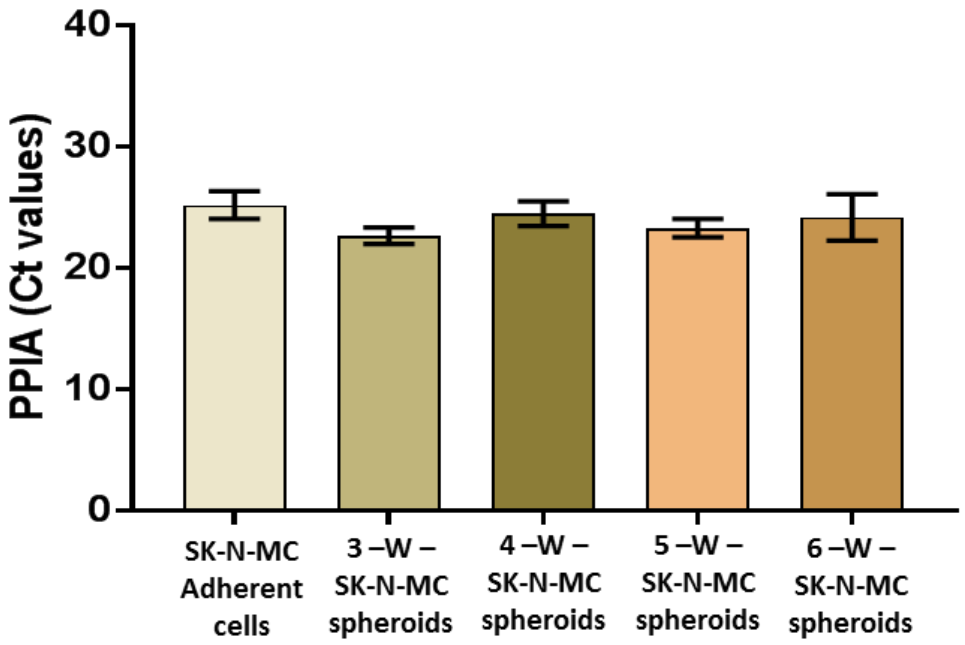

Figure 3.5 The expression level (Ct values) of a housekeeping gene (PPIA) in SK-N-MC adherent cells and spheroids. PPIA mRNA expression was determined by RTqPCR. RNA was extracted from SK-N-MC substrate adherent cells and ES spheroids, RT performed and expression of PPIA determined by RTqPCR using PPIA. Data presented as cycle threshold (Ct) values of the mean of triplicate wells in four experiments.

3.3.2 Analysis of TLDA results

3.3.2.1 Normalisations

The SC array contained 90 target mRNAs and six reference genes included; *18S, CTNNB1, GAPDH, RAF1, β-actin* and *EEF1A1* whilst the ABC array contained 50 target mRNAs and 13 reference genes included: *18S, β-actin, β2M, TBP, GUBS, GAPDH, HMBS, HPRT1, PGK1, YWHAZ, POLR2A, PPIA* and *RPLPO.* Reference genes common to both TLDA were *18S, β-actin* and *GAPDH*. It was essential to first define the optimal way to normalise the expression of SC and ABC components in substrate adherent cells and ES spheroids. In subsequent analyses the most suitable single reference gene against which to normalise the expression of SC and ABC components in substrate adherent cells and ES spheroids was sought. This was investigated by normalised to an individual reference gene as well as to the average of these reference genes and the global mean of all targets including or excluding reference genes. The standard deviation (SD) was calculated to examine the stability of expression across the replicates and results presented as box plots (Figure **3.6** and Figure **3.7**). Furthermore, the TaqMan Human MicroRNA card A consist of 377 miRNAs, three snRNA controls (U6, RNU44 and RNU48) and one negative control that is not expressed in human tissues (ath-miR159a). Total RNA (400 ng) extracted from substrate adherent cells and spheroids (n=3 from each sample) was analysed as described in (Section 3.2.5). Defining the best method to normalise miRNA data is essential in addition to selecting the most suitable reference miRNA to normalise against when performing the validation using RTqPCR.

3.3.2.1.1 mRNA TLDA

Taking into consideration the SD across the replicates, the smallest variation was observed when data was normalised using the global mean (Figure **3.6** and Figure **3.7**). In the SC array, the SD of data normalised to the global mean including or excluding reference genes were 1.62E-15 and 1.84E-15, respectively. The SD of normalising ABC data using the global mean including and excluding reference genes was 1.65E-15 and and 2.05E-15,

respectively. The excuser or inclusion of the reference genes had no significant effect on normalisation of either arrays (ABC and SC). Consequently, we decided to normalise the array data using the global mean including reference genes.

To identify the most suitable single or multiple reference genes, in both arrays (ABC and SC), the smallest SD was observed when data was normalised to the average of 13 reference genes in the ABC array. However, using 13 genes as references in each RTqPCR validation experiment would be prohibitively expensive and time consuming. It is standard practice to validate array data using RTqPCR with a single reference gene to which genes of interest can be normalised. It is essential that great care is taken when selecting the most appropriate gene as a reference gene as it can impact upon the results obtained. The array data indicated that PPIA (SD: 0.09) was the best single reference gene that included as a reference gene in mRNA arrays.

Out of 90 genes, SK-N-MC spheroids and substrate adherent cells expressed 55% (±0.3) of SC genes. In the other cell line, 58% (±2.1) of SC genes were expressed in TTC-466 spheroids and 59% (±1.2) in TTC-466 cells grown as monolayers. ABC genes were expressed in SK-N-MC (out of 50 genes; 75%±1.1) and TTC-466 (67%±1.1) spheroids, monolayer SK-N-MC and TTC-466 cells expressed 76%±0.9 and 67%±0.5 of ABC genes, respectively. Two-way hierarchical clustering of SC and ABC expression demonstrate that the SK-N-MC and TTC-466 cells cluster together regardless of whether they were grown as monolayers or spheroids (Figure **3.8**).

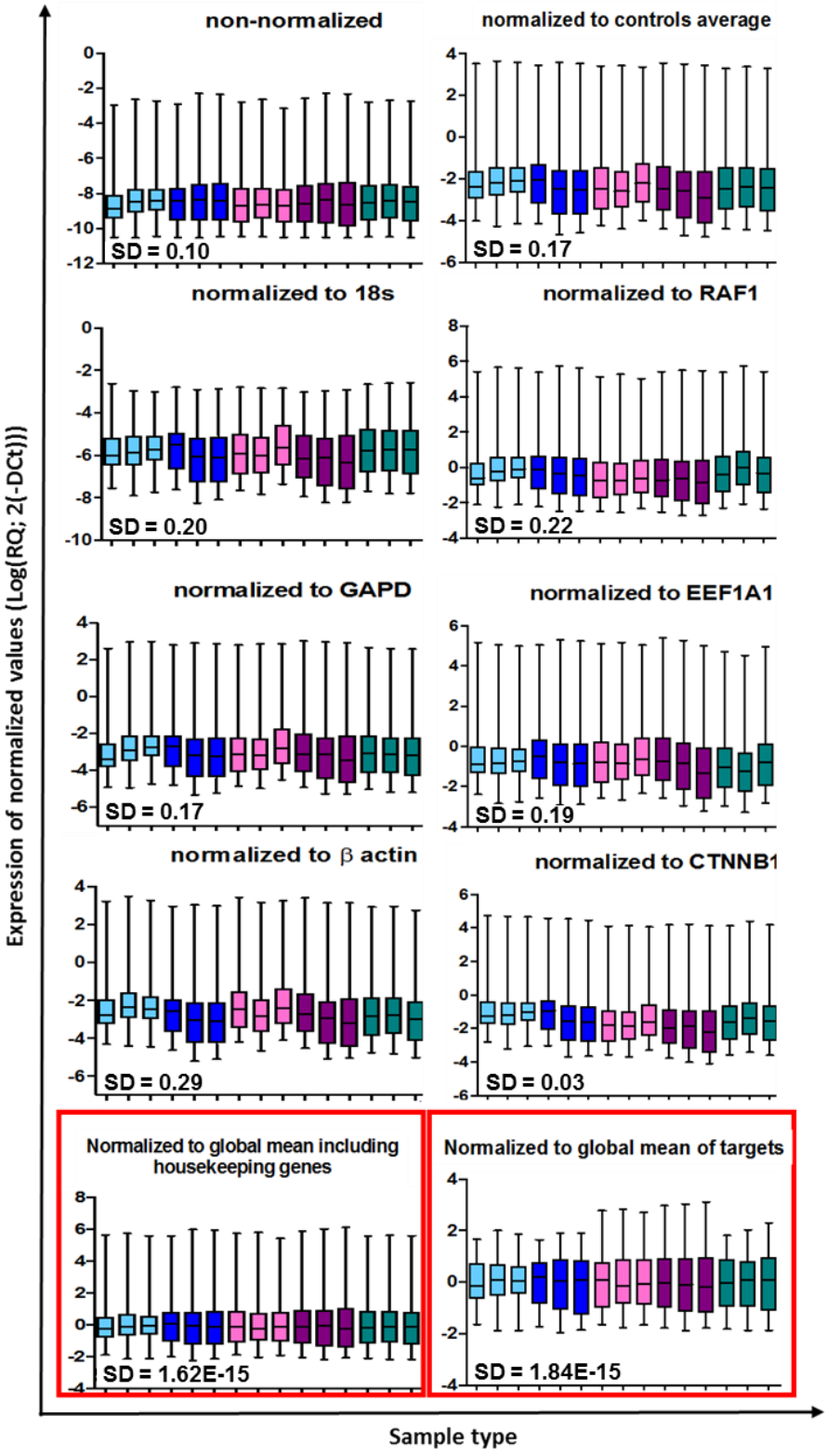

Figure 3.6 Finding the best way to normalise SC array data. Data when normalised to an individual reference gene, an average of reference genes, global mean including or excluding reference genes. Each boxplot represents a single sample; each sample has been analysed 3 times on 3 separate arrays. Light blue= SK-N-MC 3-w-spheroids. Dark blue= SK-N-MC substrate adherent cells. Light pink = TTC-466 3-w-spheroids. Dark pink = TTC-466 substrate adherent cells. Green= dissociated SK-N-MC spheroids. SD= standard deviation. Red boxes= the best normalization target/way with lowest SD value.

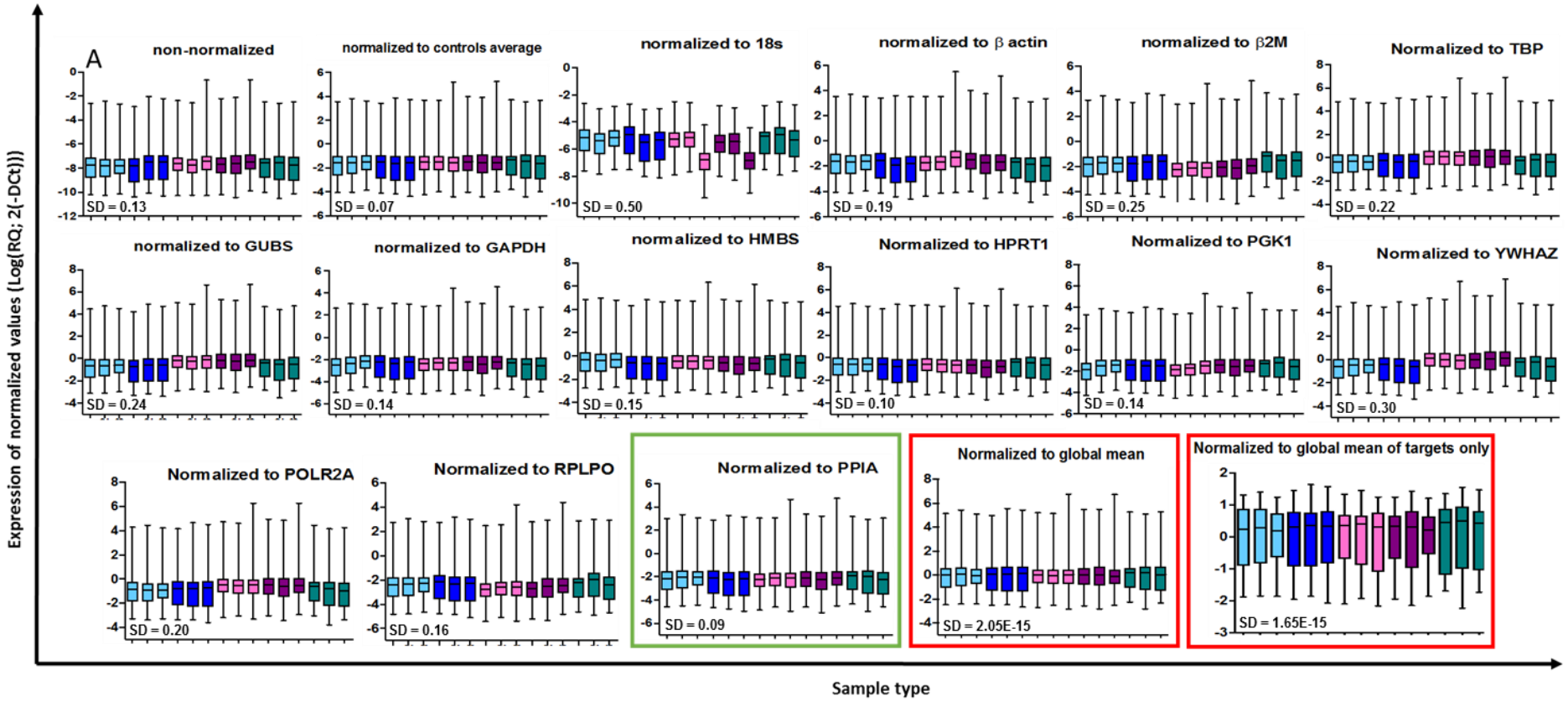

Figure 3.7 Finding the best way to normalise ABC array data. Data when normalised to an individual reference gene, an average of reference genes, global mean including or excluding reference genes. Each box plot represents a single sample; each sample has been analysed 3 times on 3 separate arrays. Light blue= SK-N-MC 3-w-spheroids. Dark blue= SK-N-MC substrate adherent cells. Light pink = TTC-466 3-w-spheroids. Dark pink = TTC-466 substrate adherent cells. Green= dissociated SK-N-MC spheroids. SD = standard deviation. Red boxes= the best normalization targets/way that showed the lowest SD value. The green box= the best housekeeping gene to be used in validation experiments.

-124 -

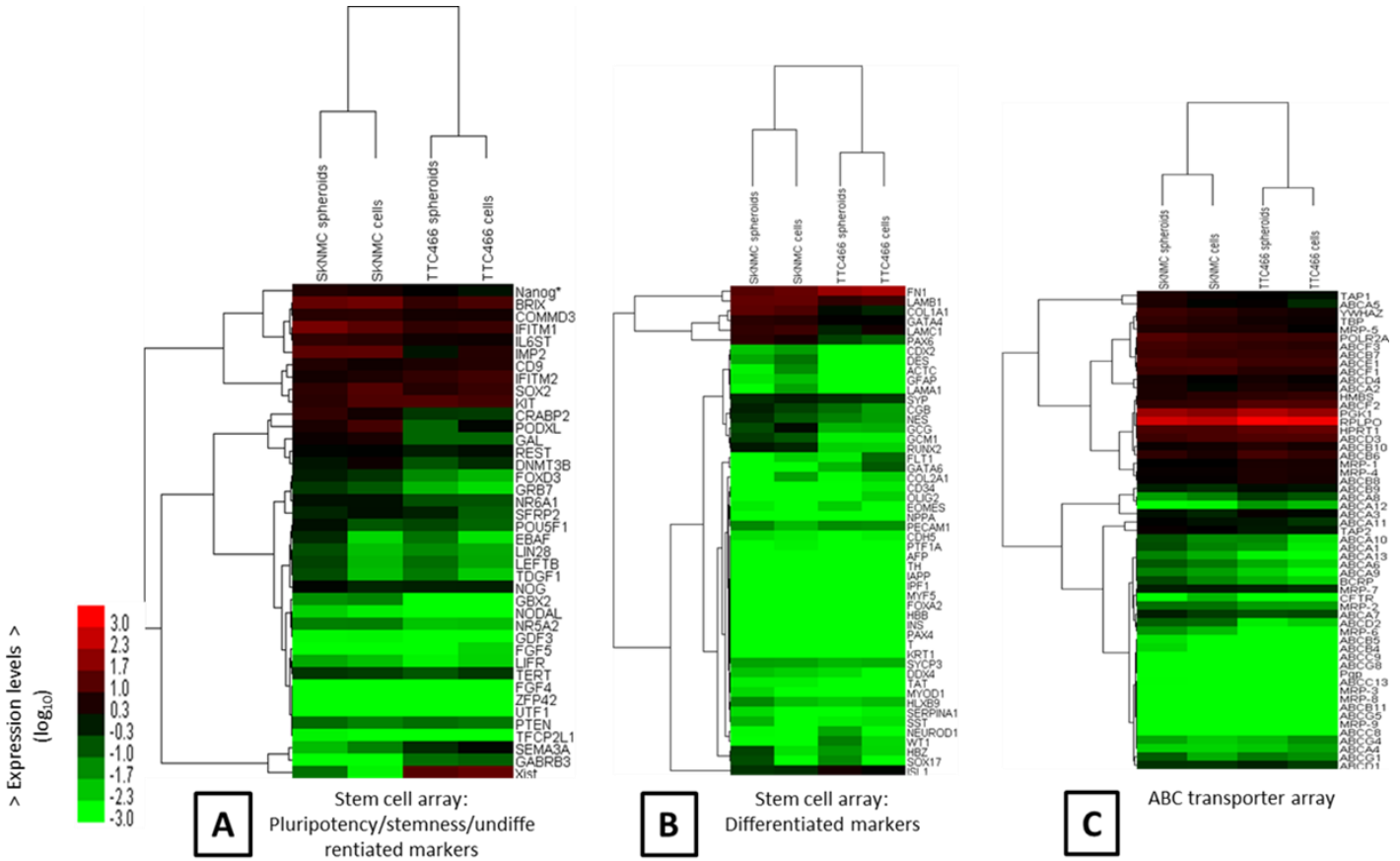

Figure 3.8 Heat map of expression of SC and ABC genes in ES cell lines and spheroids. The dendrograms of cell types using complete linkage were carried out according to expression of all target genes only as determined by the Taqman® SC and ABC array. Data are presented as Log scale of mRNA expression relative to the global mean. Red shows high relative expression and green demonstrations low relative expression. Heatmap shown are representative of 3 independent experiments.

3.3.2.1.2 miRNA TLDA

Data were normalised against individual snRNA controls (U6, RNU44 and RNU48), average of the three controls, different combinations of controls and the global mean of all expressed miRNAs on the array. The stability of expression across the replicates was examined by taking in consideration SD values after normalisation; results are presented as box plots (Figure **3.9**). The optimal normalisation was accomplished using the global mean, with a SD of the median values 3.0E-15. Un-normalized data illustrated a smaller variation (SD; 0.10) compared with normalisation to individual proposed snRNA controls with SD's that vary from 0.21 to 0.28. When normalised to different combinations or the average of snRNAs, the variation of the data was 0.19-22 (Figure **3.9**). The global mean was found to be the optimal method for normalisation of miRNA expression profiles.

Out of 377 miRNA, SK-N-MC spheroids and substrate adherent cells expressed 37% (± 0.3) and 46% (± 1.8) of miRNA respectively. In the other cell line, 46% (± 2.5) of miRNA were expressed in TTC-466 spheroids and 44% (± 0.9) in TTC-466 cells grown as monolayers. Two-way hierarchical clustering of miRNA expression demonstrate that the SK-N-MC and TTC-466 cells cluster together regardless of whether they were grown as monolayers or spheroids (Section 2.2.4.2.2)).

To identify the optimal reference miRNA that is expressed in ES cell lines regardless of the culture methods (substrate adherent cells or spheroids), all miRNA that had Ct values <35 were sorted according to the selecting criteria presented in Figure **3.11**. Three groups (A, B and C) were identified (Figure **3.11**). Group A represent a list of top 10 reference miRNA with smallest SD between Ct values. Group B include top 10 reference miRNA with smallest SD between normalised values. However, group C takes in the common miRNA from the top 10 list of the smallest SD between Ct values and normalised values. Two miRNA (miR-130 and miR-20a) were identified as possible references from group A with SD of 0.18. In group C, miR-30b appears to be the most stable miRNA (SD; 0.12) and in group B, miR-30c with a SD of 0.14 (Figure **3.12**). These miRNA are also appeared to be stable miRNAs on NormFinder software (stability value; miR-30c = 0.17 and

miR-30b = 0.21) when group B and group D were applied to the software (Figure **3.13** A). Furthermore, from NormFinder, miR-16 from group C and miR-454 from group A were suggested as references (stability value; 0.20 and 0.26 respectively). Taking into consideration the stability values that resulted from NormFinder, miR-454 was excluded because it has the highest value, which represents less stability, compared with the rest of the miRNA (miR-16, miR-30b and miR-30c). These three miRNAs were examined in more detail. Though it looks as though any of these miRNA would be good (SD; 0.10 to 0.13). However, a combination of miR-16 + miR-30b (SD; 0.10) was used as a reference in the validation experiments (Figure **3.13** B).

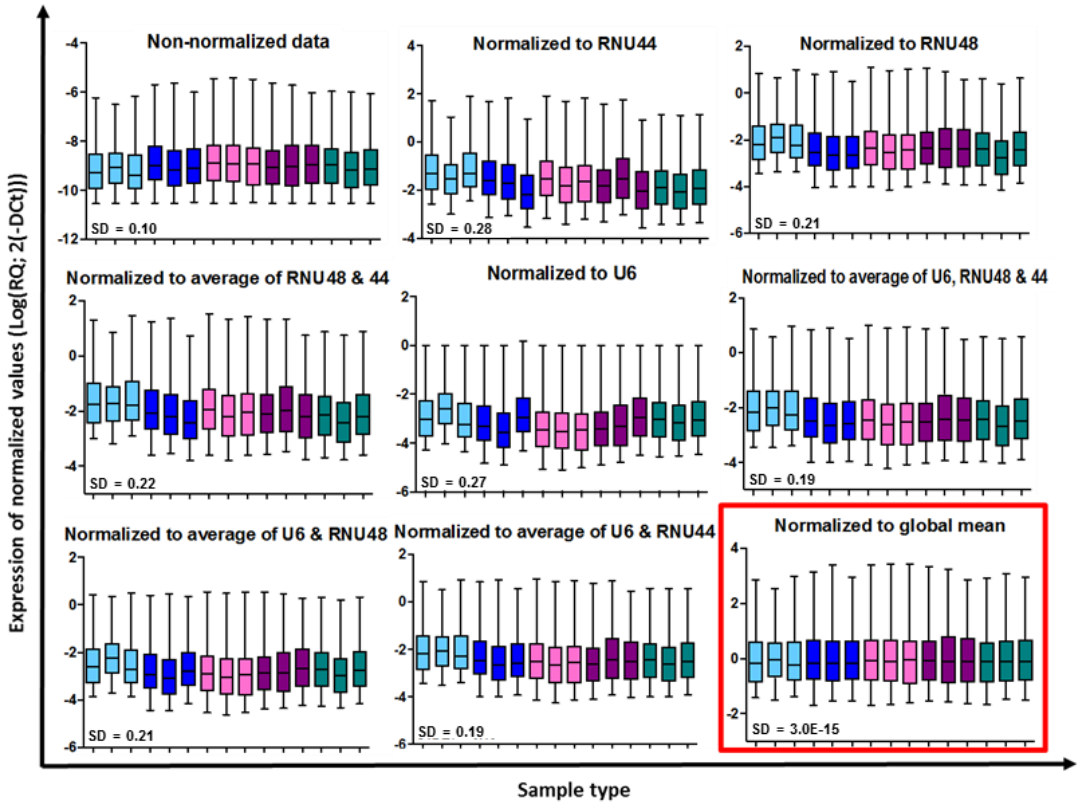

Figure 3.9 Finding the best way to normalise Human miRNA array data. Data when normalised to an individual proposed reference miRNA, an average of reference miRNAs, all possible combination of reference miRNA and the global mean of all miRNA that are expressed with <35 Ct. Each boxplot represents a single sample; each sample type has been analysed thre times. Light blue= SK-N-MC 3-w-spheroids. Dark blue= SK-N-MC substrate adherent cells. Light pink = TTC-466 3-w-spheroids. Dark pink = TTC-466 substrate adherent cells. Green= dissociated SK-N-MC spheroids. SD = standard deviation. Red box= the best normalization targets/way that showed the lowest SD value.

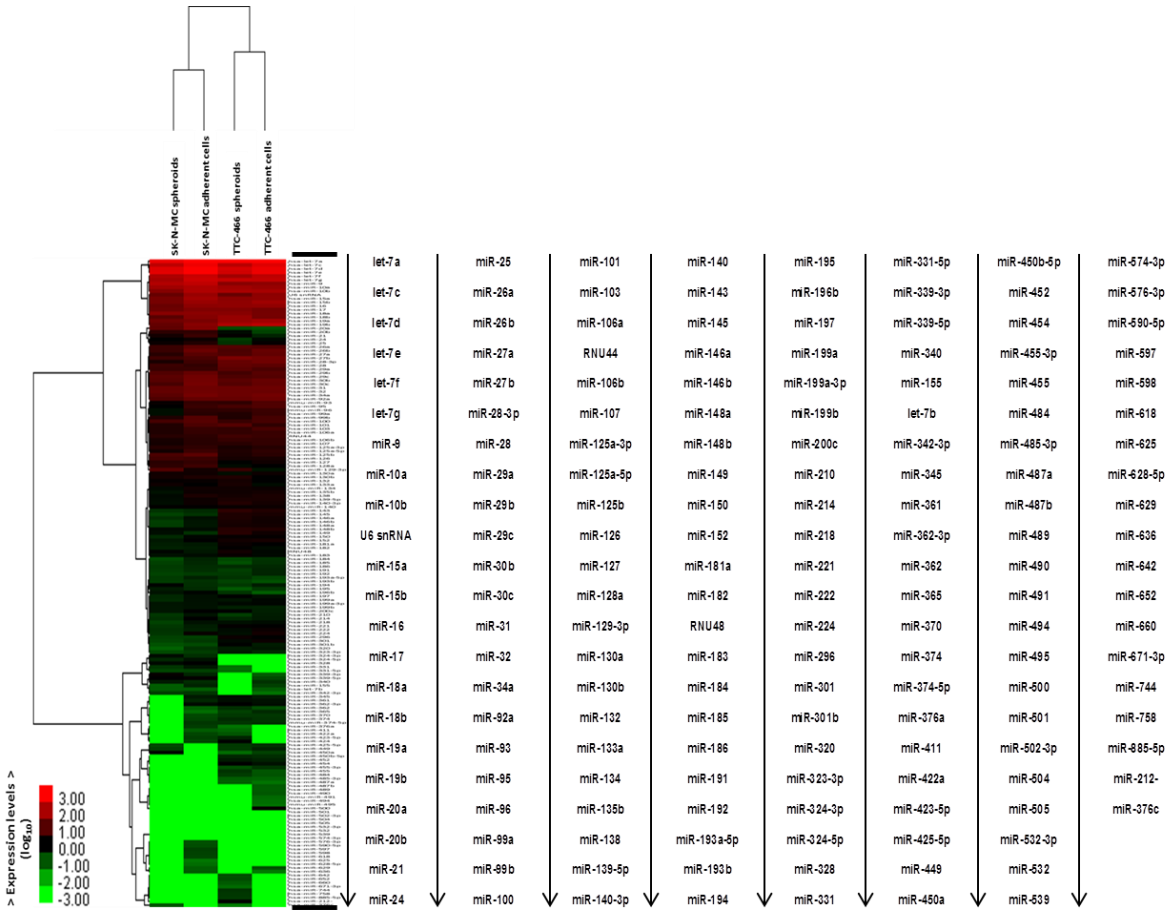

Figure 3.10 Heat map of expression of miRNA in ES cell lines and spheroids. The dendrograms of cell types using complete linkage were carried out according to expression as determined by the Taqman® miRNA array. Data are presented as Log scale of miRNA expression relative to the global mean. Red shows high relative expression and green demonstrations low relative expression. Heatmap is representation of three independent experiments and miRNA names are expanded next to the heatmap.

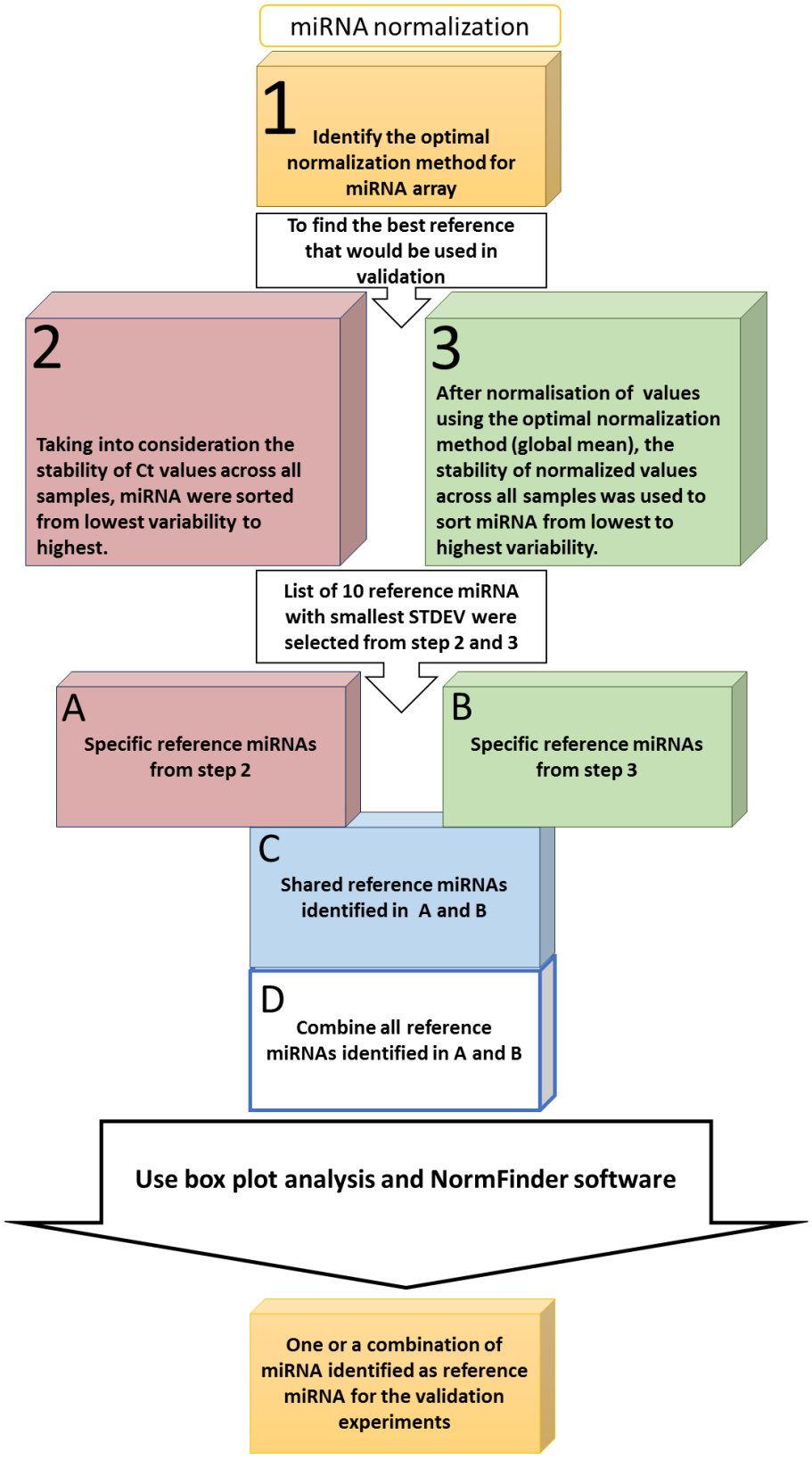

Figure 3.11 Strategy for selecting the best reference miRNA to be used in downstream validation using RTqPCR. Two different steps were used to sort miRNA (Box 2 and Box 3). After sorting miRNAs, four lists (Box A, B, C and D) were used for boxplot analysis and applied to NormFinder software.

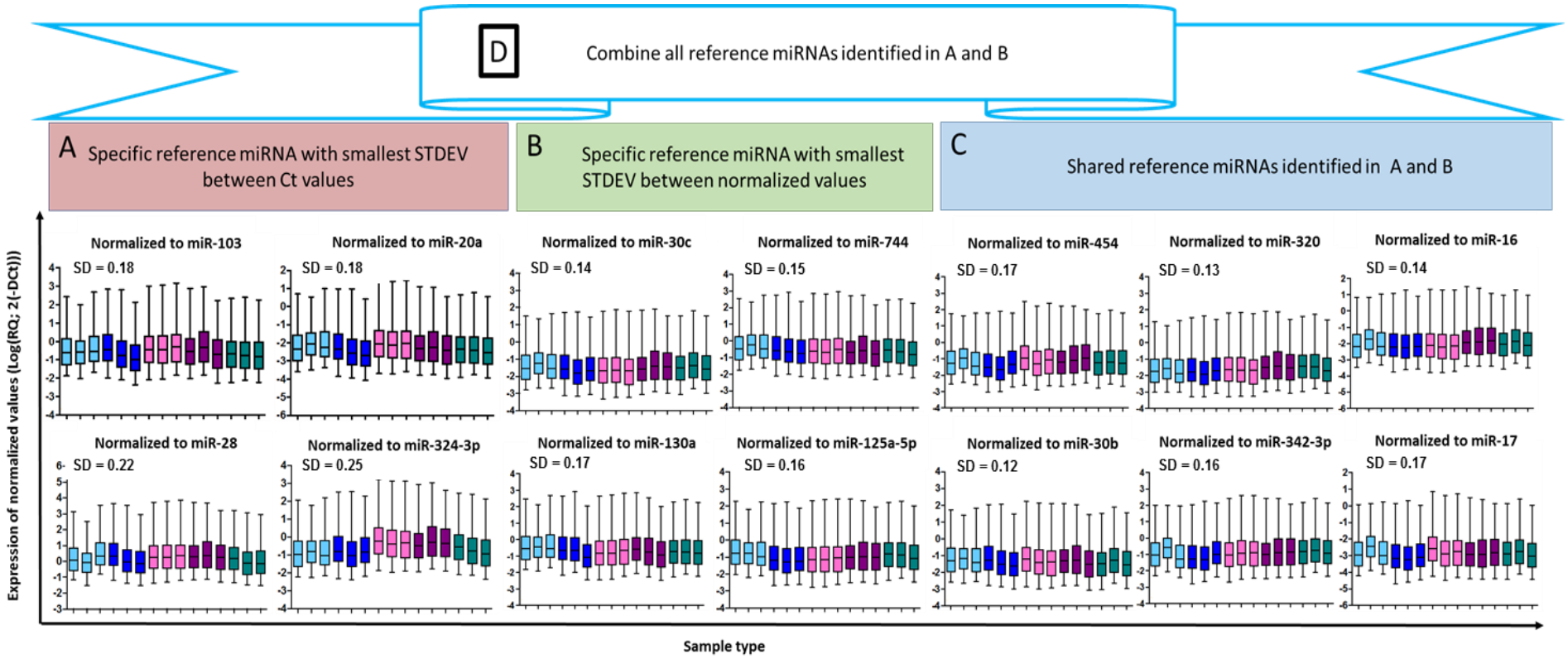

Figure 3.12 Normalisation of Human miRNA array data using potential optimal miRNA identified by selection strategies shown in (Figure 4.10). Light blue= SK-N-MC 3-w-spheroids. Dark blue= SK-N-MC substrate adherent cells. Light pink = TTC-466 3-w-spheroids. Dark pink = TTC-466 substrate adherent cells. Green= dissociated SK-N-MC spheroids. Each sample type has been profiled 3 times using TLDAs.

A

	Group A		Group B		Group C		Group D	
	Top 10 reference miRNA with smallest STDEV between Ct values		The common miRNA from the top 10 list of the smallest STDEV between Ct values and normalized values		Shared reference miRNAs identified in A and B		Combine all reference miRNAs identified in A and B	
	miRNA	Stability value	miRNA	Stability value	miRNA	Stability value	miRNA	Stability value
1	miR-454	0.26	miR-30c	0.17	miR-16	0.20	miR-30b	0.21
2	miR-30b	0.27	miR-16	0.21	miR-320	0.23	miR-30c	0.26
3	miR-17	0.28	miR-125a-5p	0.24	miR-342-3p	0.24	miR-16	0.28
4	miR-320	0.28	miR-30b	0.26	miR-17	0.24	miR-17	0.28
5	miR-20a	0.29	miR-17	0.28	miR-454	0.24	miR-320	0.28
6	miR-16	0.32	miR-320	0.28	miR-30b	0.36	miR-20a	0.29
7	miR-103	0.35	miR-342-3p	0.3			miR-744	0.3
8	miR-342-3p	0.38	miR-744	0.3			miR-125a-5p	0.31
9	miR-28	0.44	miR-454	0.33			miR-454	0.31
10	miR-324-3p	0.5	miR-130a	0.4			miR-103	0.35
11							miR-342-3p	0.36
12							miR-130a	0.39
13							miR-28	0.44
14							miR-324-3p	0.58

B

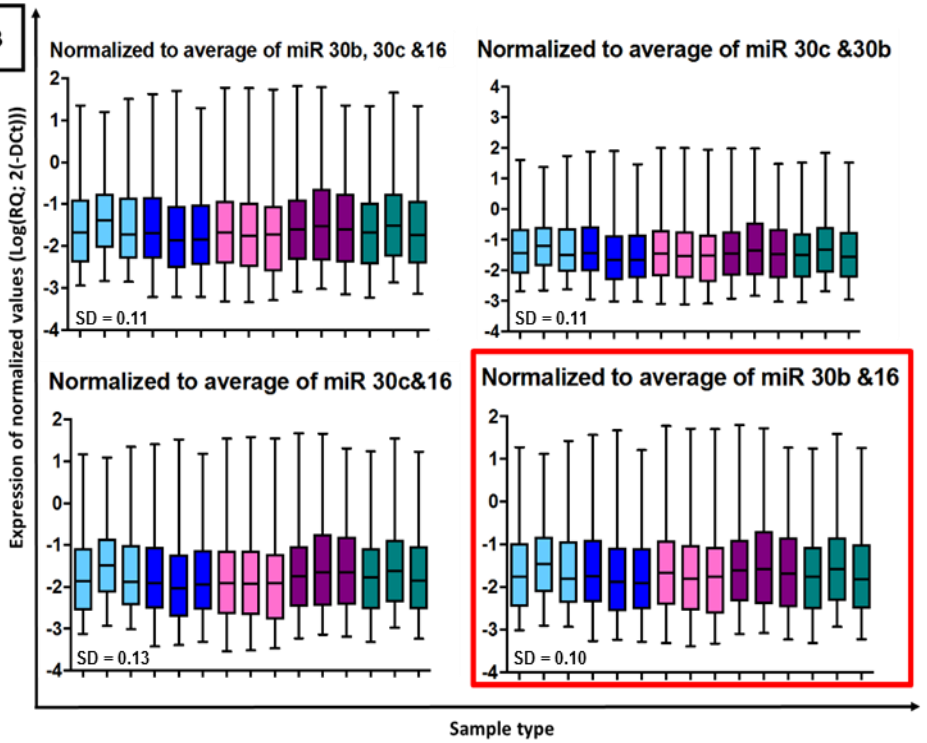

Figure 3.13 Identification of the optimal reference miRNA to be used in validation studies. Sorted miRNA were applied to NormFinder software. A) Summary of miRNAs selected on different criteria. miRNA that has lower stability value was suggested to be a reference (highlighted in yellow). B) Box plot analysis using three stable miRNA. Data normalised to individual, average and all possible combination of miRNA. Light blue= SK-N-MC 3-w-spheroids. Dark blue= SK-N-MC substrate adherent cells. Light pink = TTC-466 3-w-spheroids. Dark pink = TTC-466 substrate adherent cells. Green= dissociated SK-N-MC spheroids. Each sample type was profiled 3 times using the TLDAs. Red boxes= the best combination of miRNA to be used in validation experiments.

3.3.2.2 Expression of stem cells and differentiation genes

3.3.2.2.1 TLDA

TLDA results have been analysed using two models (Section 3.2.5.3). Model A is focused on the identification of mRNA associated with self-renewal independent of cell type; two variables included are growth as spheroids compared to growth as substrate adherent cell lines. Model B takes into consideration the self-renewal feature (as in model A) plus differences due to the cell phenotype; four variables are included in the model, growth as spheroids, growth as substrate adherent cell lines, SK-N-MC phenotype and TTC-466 phenotype.

Taking into consideration results from model A, the expression of Podocalyxin Like (PODXL) was decreased in SK-N-MC spheroids (n=3, q-value; 0.02) with a 2.1 DCt difference, this was marginal (Appendix F). PODXL is not reflecting the self-renewal feature because it also appears as significant (n=3, q-value; 0.07 and DCt difference; 4.0) in model B in TTC-466 spheroids. Other significant genes are common in both models (A and B) such as the decrease of the expression of Semaphorin 3A (SEMA3A; n=3, DCt = 2.8) in spheroids. Regarding pluripotency, stemness and undifferentiated markers, in SK-N-MC spheroids, the majority of the significant genes in both models are increased with expression including endometrial bleeding associated factor (EBAF) known as Left-right determination factor 2 (LEFTY2), teratocarcinoma-derived growth factor 1 (TDGF1), Left-right determination factor B (LEFTB) known as Left-right determination factor 1 (LEFTY1), X-inactive specific transcript (Xist), Lin-28 homolog A (LIN28) and POU domain, class 5, transcription factor 1 (POU5F1) also known as octamer-binding transcription factor 4 (Oct-4) (Appendix F).

On the other hand, TTC-466 spheroids increased the expression of EBAF, TDGF1, LEFTB and Sentrin-specific protease 2 (SERP2) (n=3, DCt; 4.2, 3.0, 2.0 and 2.3 respectively) and decreased the expression of Septation protein imp2 (IMP2) (n=3, Dct; 2.4) in both models. In model B, Fibroblast growth factor 5 (FGF5) and PODXL are significantly decreased in TTC-466 spheroids (n=3, q-value; 0.11 and 0.07 respectively) (Figure 3.14).

No differentiated gene was significantly associated with the self-renewal feature in both cell lines (SK-N-MC and TTC-466). The majority of differentiated genes were common in both models and were significantly decreased expression in SK-N-MC spheroids. However, Haemoglobin subunit zeta (HBZ) and Transcription factor SOX-17 (SOX17) were increased in SK-N-MC spheroids (n=3, DCt; 5.7 and 7.4 respectively). TTC-466 spheroids also upregulated HBZ and SOX17 (n=3, DCt; 2.3 and 4.9 respectively) as well as Wilms tumour protein (WT1; n=3, DCt; 3.4). Laminin Subunit Gamma 1 (LAMC1), GATA-binding factor 6 (GATA6), and Fms-like tyrosine kinase 1 (FLT1) were common in both models and their expressions were decreased in TTC-466 spheroids (n=3, DCt; 2.2, 3.9 and 5.5 respectively). In model B, expression of Oligodendrocyte transcription factor 2 (OLIG2: n=3, q-value: 0.13 and DCt: 2.9) was decreased in TTC-466 spheroids compared to cells grown as substrate adherent monolayers (Figure 3.14).

3.3.2.2.1 Validation of SC genes by RTqPCR and western blot

To select targets for validation, targets with more than 2DCt difference and q-value <2 were sorted by the following criteria (Figure **3.11**). Firstly, the expression of targets must be detectable at Ct <35 in substrate adherent cells and/or spheroids. Secondly, the difference in target expression between substrate adherent cells and spheroids must be ≥ 2 Ct. Some targets highlighted with asterisk (Ct difference < 2 in one cell line only; Figure 3.15) were included in the next sorting step. Finally, targets that were not differentially expression in SK-N-MC and TTC-466 cell lines and some targets with asterisk were excluded from validation. Targets for validation are summarized (Table **3.6**).

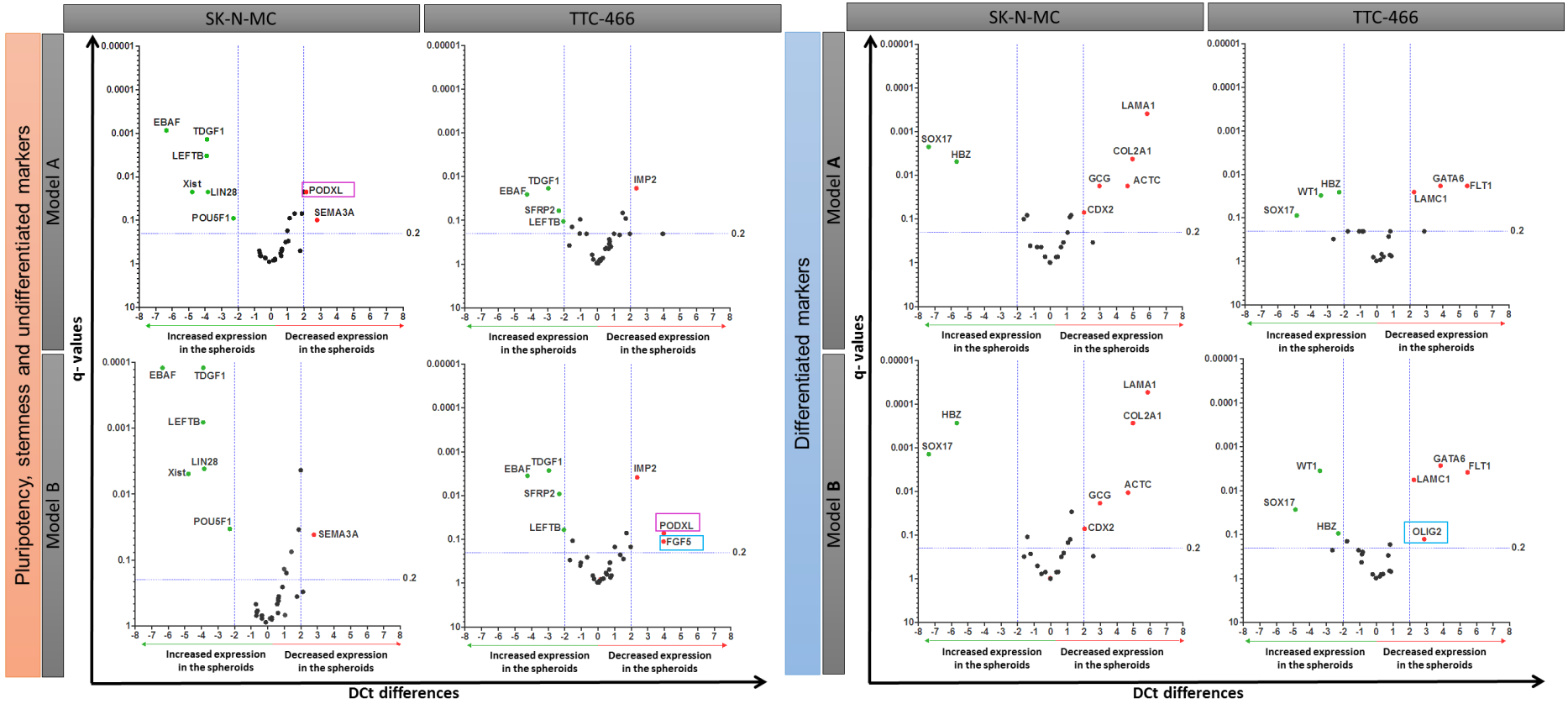

Figure 3.14 Volcano plot of analysed SC array data. Model A represents the self-renewal feature, whereas model B consider the self-renewal feature and the differences between cell lines when compared to the substrate adherent cells with 3-week-spheroids derived from a single cell. The data for all genes are plotted as Delta Ct differences versus the adjusted p-value (q-value). Thresholds are shown as blue dashed lines; for DCt = 2 and q-value = 0.2. Targets selected as significantly increased expression in the spheroids are highlighted as green dots, whereas red dots represent the significant decreased expression of targets in the spheroids. Targets not significantly increased or decreased expressions were represented as black dots. The light blue boxes represented specific significant targets in model B and the pink boxes represented significant targets appear in model A of one cell line and in model B of the other cell line.

	Do the validation techniques work?		Do array results validate?
Genes	**A)** RTqPCR	**B)** Western blot	
EBAF	Yes	Yes	Yes by A and B
SOX17	No	Yes	No by A and Yes by B
TDGF1	-	-	Excluded
LEFTB	-	-	Excluded
HBZ	Yes	Yes	No by A and B

Table 3.6 Summary of validation result of the significant SC genes. Two different techniques were used to validate array results. Some of the techniques used for validation worked nicely but did not validate the array results. Yes and no used in this table to illustrate the status of the validation. In the table, A referred to the RTqPCR, whereas B referred to western blot.

From pluripotency, stemness and undifferentiated markers three genes: TDGF1, LEFTYB and EBAF passed the criteria for validation (Figure 3.15). Both LEFTYB and EBAF belong to the transforming growth factor beta (TGF-beta) family (Ulloa et al., 2001). Taking into considerations Ct and DCt difference, EBAF has the highest difference and was selected for validation. However, RTqPCR for TDGF1 mRNA was not performed as this is encoded by a single exon gene and multiple pseudogenes on chromosomes 2, 3, 6, 8, 19 and X have been described limiting the specificity of RTqPCR assays for this mRNA (Hentschke et al., 2006). Furthermore, it has not been possible to confirm changes in TDGF1 at the protein level, as a suitable control has not been found. From the differentiated makers, two genes were selected for validation; SOX-17 and HBZ.

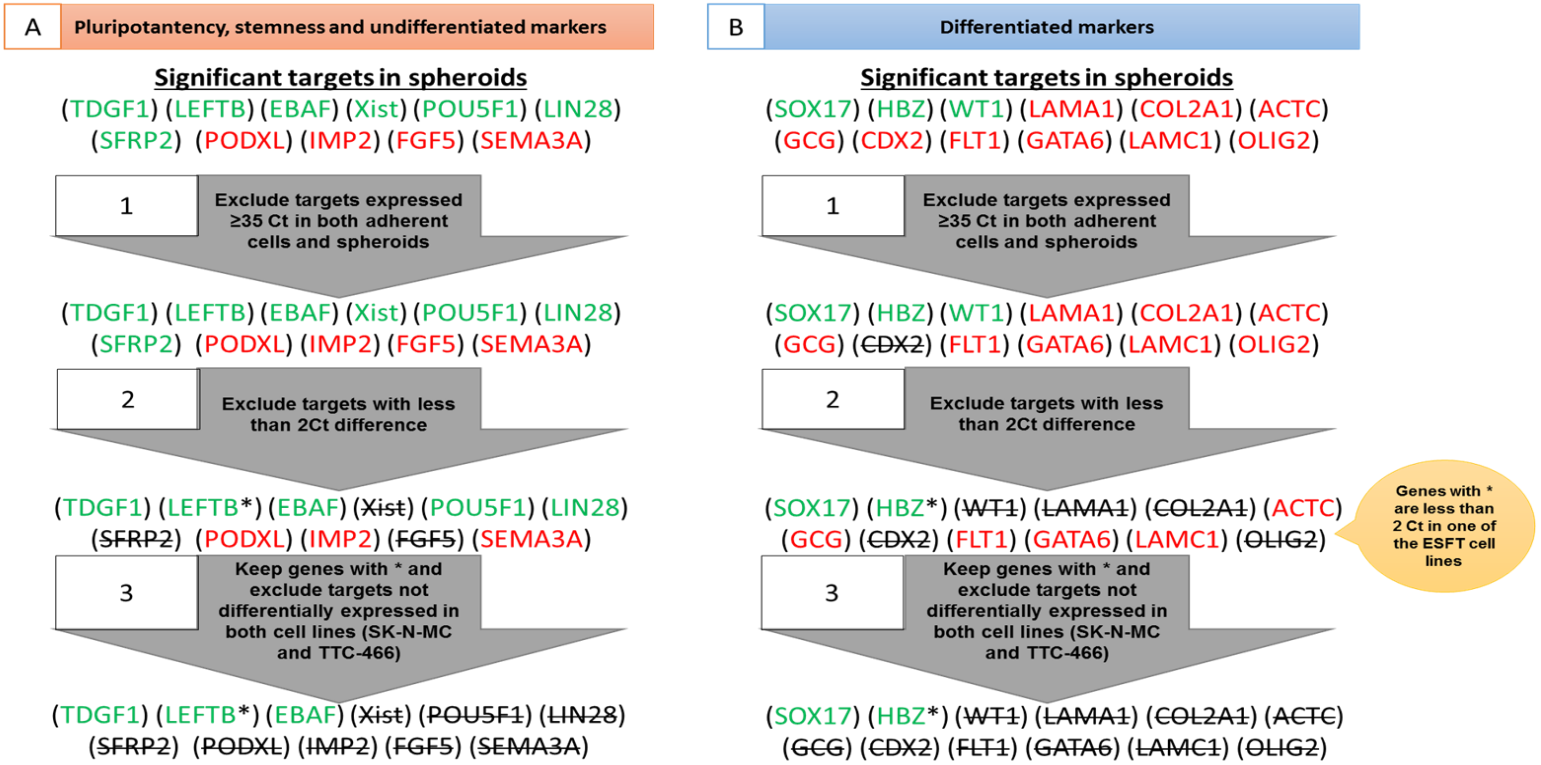

C

Targets	SK-N-MC (Spheroids – substrate adherent cells) Ct difference	DCt difference	q values (Model A)	q values (Model B)	TTC-466 (Spheroids – substrate adherent cells) Ct difference	DCt difference	q values (Model A)	q values (Model B)	Expression in SK-N-MC spheroids	Expression in TTC-466 spheroids
EBAF	-5.3	-6.3	0.0009	0.0001	-3.8	-4.2	0.0255	0.0035	▲	▲
TDGF1	-3.2	-3.9	0.0014	0.0001	-2.6	-3.0	0.0182	0.0027	▲	▲
LEFTB	-3.6	-3.9	0.0033	0.0008	-1.7	-2.0	0.1046	0.0604	▲	▲

Targets	SK-N-MC (Spheroids – substrate adherent cells) Ct difference	DCt difference	q values (Model A)	q values (Model B)	TTC-466 (Spheroids – substrate adherent cells) Ct difference	DCt difference	q values (Model A)	q values (Model B)	Expression in SK-N-MC spheroids	Expression in TTC-466 spheroids
SOX17	-3.9	-7.4	0.0022	0.0014	-2.7	-4.9	0.0875	0.0267	▲	▲
HBZ	-4.3	-5.7	0.0048	0.0003	-1.9	-2.3	0.0255	0.0937	▲	▲

Figure 3.15 Selecting genes for validation. The expression of targets were increased (Green) or decreased (Red) in spheroids compared to the expression in substrate adherent cells. Targets that did not match the criteria were (~~Black~~) crossed out. Targets which passed the selected criteria in one cell line only are identified with black asterisk (*). A) Pluripotency, stemness and undifferentiated targets. B) Differentiated targets. Targets, which appear as significant, were sorted by three steps and ones that passed the three steps (1-3) were selected for validation. C) Summary of Ct, DCt and adjusted p-values generated using LIMMA model A and B. ▲= increased expression in spheroids compared to the expression in substrate adherent cells.

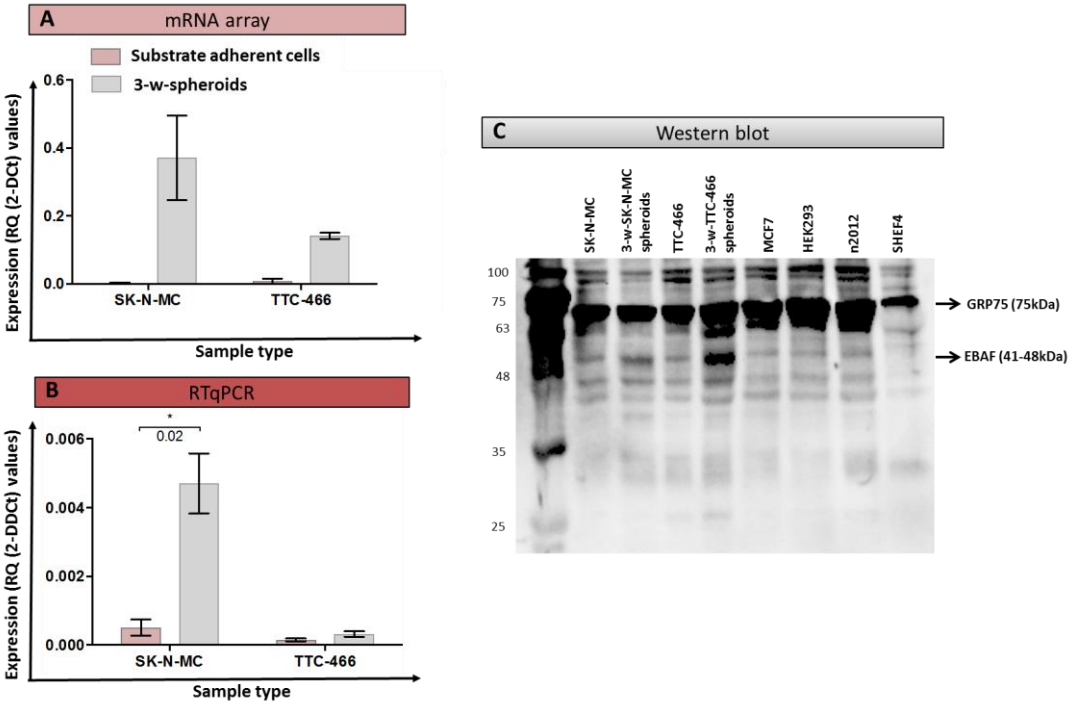

Figure 3.16 Validation of the increased expression of EBAF in spheroids comparing with substrate adherent cells. A) The expression level of EBAF that resulted from the TLDA. B) Validation of EBAF using RTqPCR. PPIA used as reference gene and the significant difference demonstrated by p-value. C) Representative western blot demonstrating elevated EBAF protein expression in TTC-446 and SK-N-MC spheroids compared to the substrate adherent cells. GRP75 was used as a protein loading control. MCF7, HEK293, n2012 and SHEF4 cells extract were used as controls.

The increased of expression of EBAF in SK-N-MC spheroids compared to substrate adherent cells was confirmed at the mRNA level by RTqPCR (n=3, each repeat in triplicate, p value: 0.02). The difference between TTC-466 spheroids and adherent cells was very small and not significant at the RNA level (Figure **3.16** B). Despite, the multiple proteins detected by antibody on the membrane, EBAF protein was increased in the ES spheroids compared to adherent cells in both cell lines (Figure **3.16** C). Surprisingly, the protein difference is much more obvious in TTC-466 spheroids compared to SK-N-MC spheroids.

Despite using a gradient concentration of RNA from 10ng to 1000ng, cell lines; SHEF4 and OSCK3 used to validate array result were negative for SOX-17. At the end of this project a positive control for SOX-17 had been found and western blots were run by Mrs Berry. There was an increase

expression in ES spheroids comparing with substrate adherent cell lines. Expression of β-actin was examined to check the amount of protein on the membrane (Figure **3.17**). However, the expected size of SOX-17 protein is 44kDa. SOX-17 protein was detected in the control cell as a band higher than the expected that might be due to the co-operative binding of SOX-17 and Oct4 (30-38kDa) (Chang, K. et al., 2017).

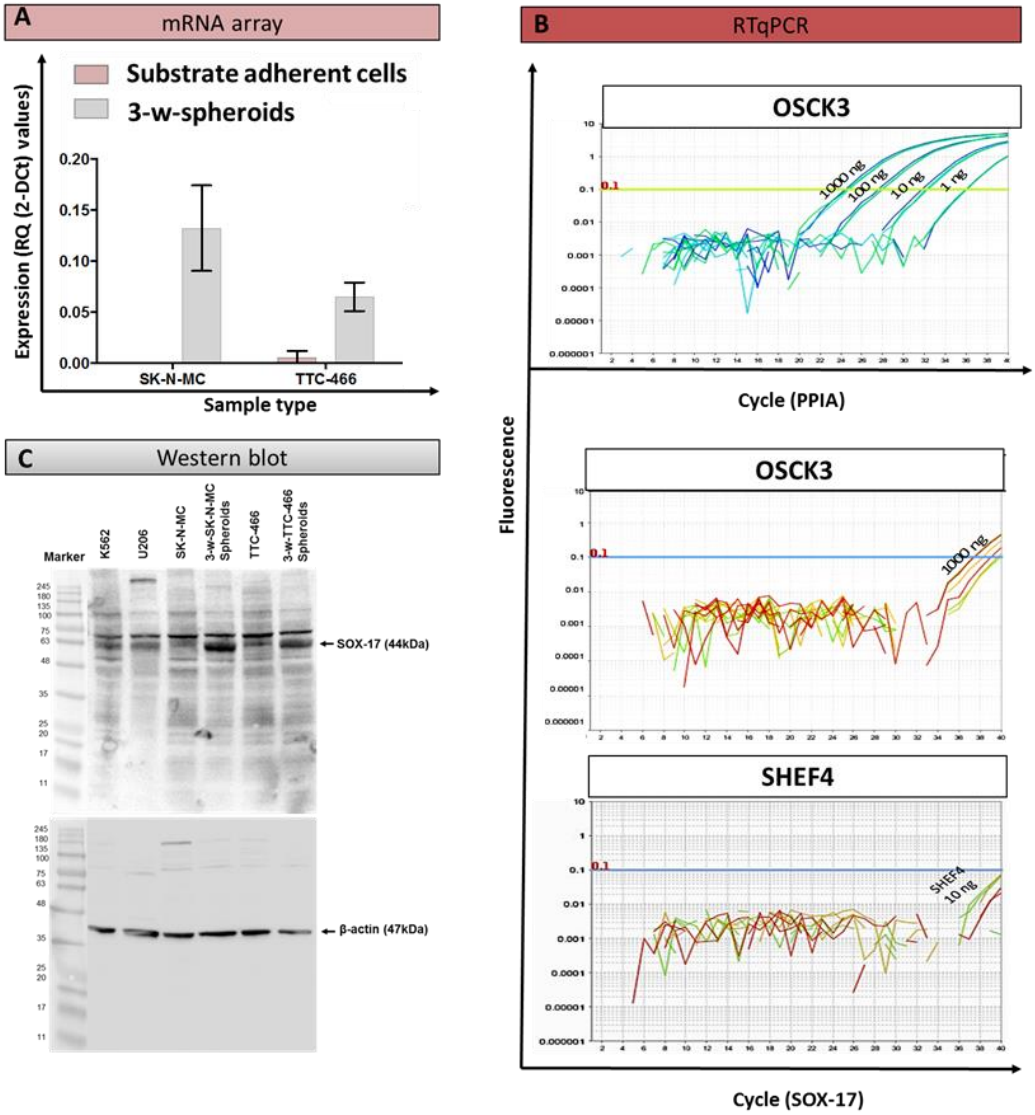

Figure 3.17 Validation of the increased expression of SOX-17 in spheroids comparing with substrate adherent cells. A) The expression level of SOX-17 that resulted from the TLDA. B) Fluorescence detection of SOX-17 using RTqPCR. PPIA used as reference gene. C) Representative western blot demonstrating elevated SOX-17 protein expression in TTC-446 and SK-N-MC spheroids compared to the substrate adherent cells. β-actin was used as a protein loading control. K562 and U206 cells extract were used as controls. ng= nano-gram

At the protein level, the HBZ antibody was optimised using serial dilution (0.02 -0.2 µg) (Figure 3.14). The K-562 cell line was used as a positive control. The size of the protein is very small (14 kDa). So, to avoid losing the protein, the gel was electrophoresed to 50% down the gel and the band identity is confirmed by the reduced intensity of signal as the antibody is dilution. The optimal concentration was 0.1 µg (Figure **3.18**). HBZ protein was detected as a band with a lower molecular weight than that expected from the literature and was not expressed in ES cell lines and spheroids protein extracts. Expression of β-actin was used to check the amount of protein on the membrane (Figure **3.19** C). On the other hand, 3-week-SK-N-MC spheroids illustrated a significant increase in the RNA level by RTqPCR. However, in TTC-466, there was no difference between the RNA expression of HBZ in substrate adherent cells and spheroids (Figure **3.19** B).

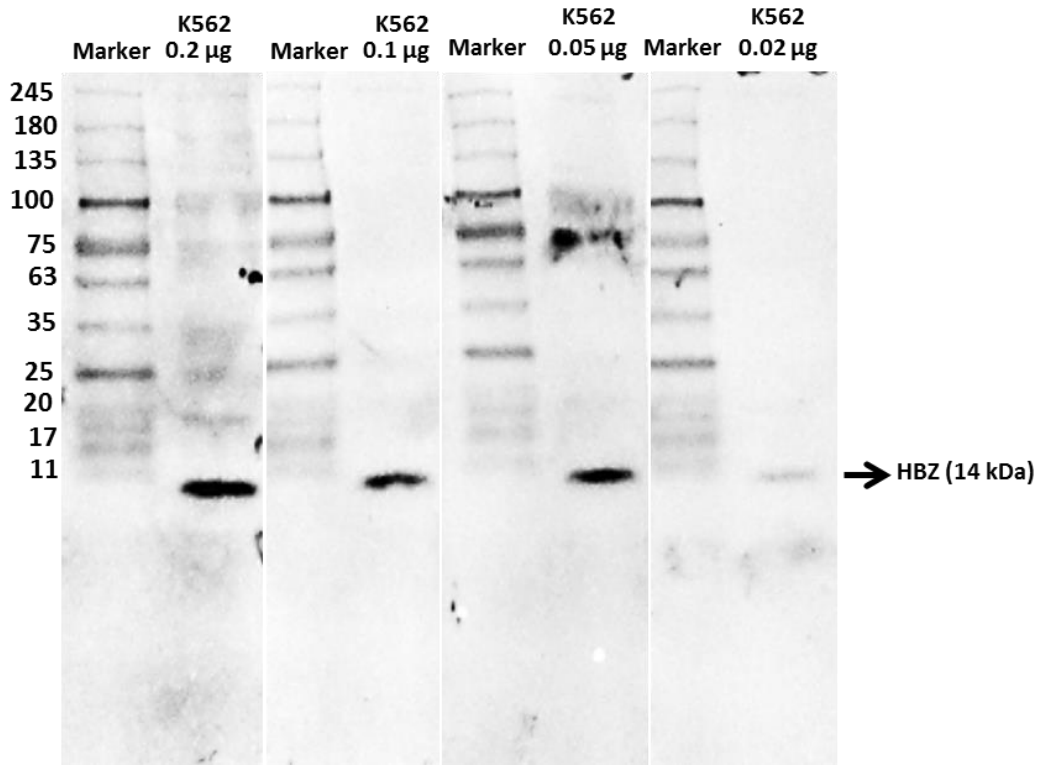

Figure 3.18 Optimisation of HBZ antibody. Total protein a control cell line (K-562) were prepared with DTT and expression of HBZ in 50 µg extract determined by western blot using serial dilution from 0.02 µg to 0.2 µg.

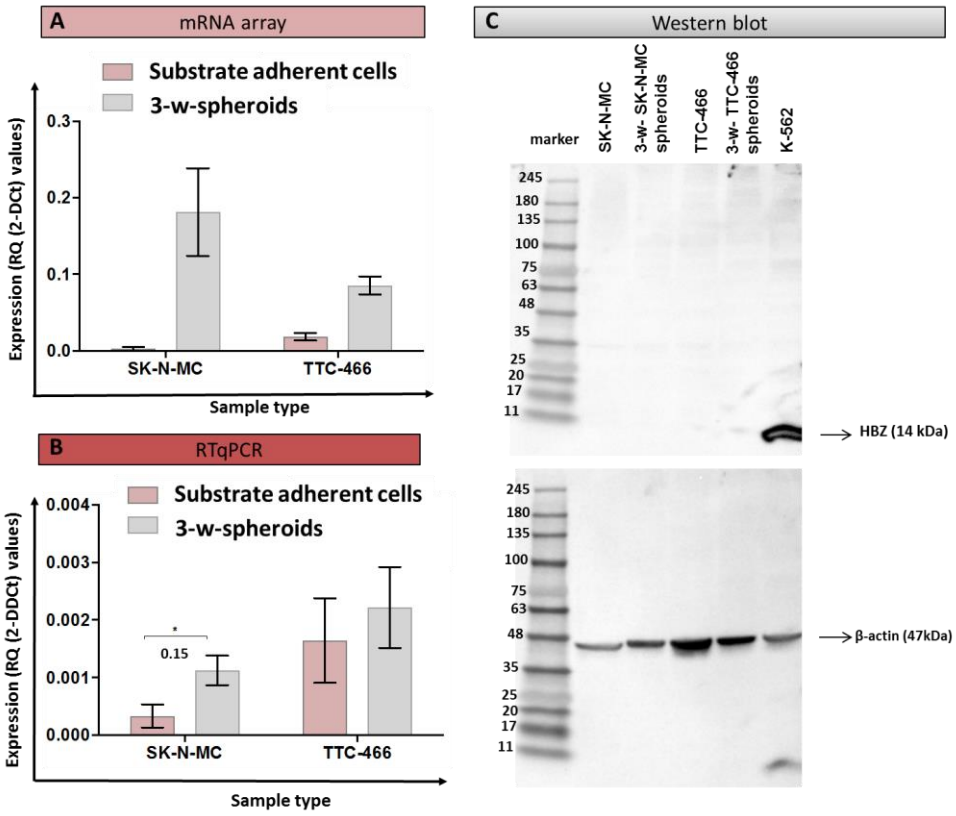

Figure 3.19 Validation of the increased expression of HBZ in spheroids comparing with substrate adherent cells. A) The expression level of HBZ that resulted from the TLDA. B) Validation of HBZ using RTqPCR. PPIA was used as reference gene and the significant difference demonstrated by q-value. C) Representative western blot demonstrating HBZ protein expression only in the positive control K-562. β-actin confirmed proteins were loaded in all the wells.

3.3.2.3 Expression of ABC transporter proteins

3.3.2.3.1 TLDA

The same method as described in Section 3.3.2.2 above was used to identify significant differentially expressed targets for validation (Table **3.7**).

	Do the validation techniques work?		Do array results validate?
Genes	**A)** RTqPCR	**B)** Western blot	
ABCG1	Yes	Yes	Yes by A and B
CFTR	Yes	Yes	No by A and Yes by B

Table 3.7 Summary of validation result of the significant ABC transporter proteins. Two different techniques were used to validate array results. Some of the techniques used for validation worked nicely but did not validate the array results. Yes and no used in this table to illustrate the status of the validation. In the table, A referred to the RT qPCR, whereas B referred to western blot.

There were no significantly increased or decreased ABC transporter mRNA in TTC-466 cells and spheroids. However, two targets appear statically significant in model A and B when analysing SK-N-MC substrate adherent cells and spheroids (Figure **3.20**). The first target is ATP Binding Cassette Subfamily G Member 1 (ABCG1) that was increased in SK-N-MC spheroids. The Ct difference between SK-N-MC and SK-N-MC spheroids is 2.3 (n=3, DCt; 2.6), whereas the difference is very small between TTC-466 and TTC-466 spheroids (n=3, Ct: 0.6 and DCt: 0.5). The other target is Cystic Fibrosis Transmembrane Conductance Regulator (CFTR). This gene is downregulated in SK-N-MC spheroids (DCt: 4.6), with Ct difference lower than two (Table **3.10**). CFTR expression was very low, below the level of detection of the array (> 35 original Ct; 39.5 and 39.6) in TTC-466 and TTC-466 spheroids, respectively. Also, Ct difference was zero (Table **3.8**)

	SK-N-MC (Spheroids – substrate adherent cells)				TTC-466 (Spheroids – substrate adherent cells)				Expression in SK-N-MC spheroids	Expression in TTC-466 spheroids
Targets	Ct difference	DCt difference	q values (Model A)	q values (Model B)	Ct difference	DCt difference	q values (Model A)	q values (Model B)		
CFTR	1.5	4.6	0.03	0.05	0	-	-	-	▼	-
ABCG1	-2.3	-2.6	0.09	0.14	-0.6	0.5	0.76	0.79	▲	-

Table 3.8 Summary of ABC transpoter mRNA that passed the sorting criteria (Step 1-3 in Figure 4.14).. The differences between Ct, DCt and adjusted q-values that resulted from model A and B are illustrated. Each gene showed an increase (▲) or decrease (▼) in the expression in the spheroids compared to the matched substrate adherent cell.

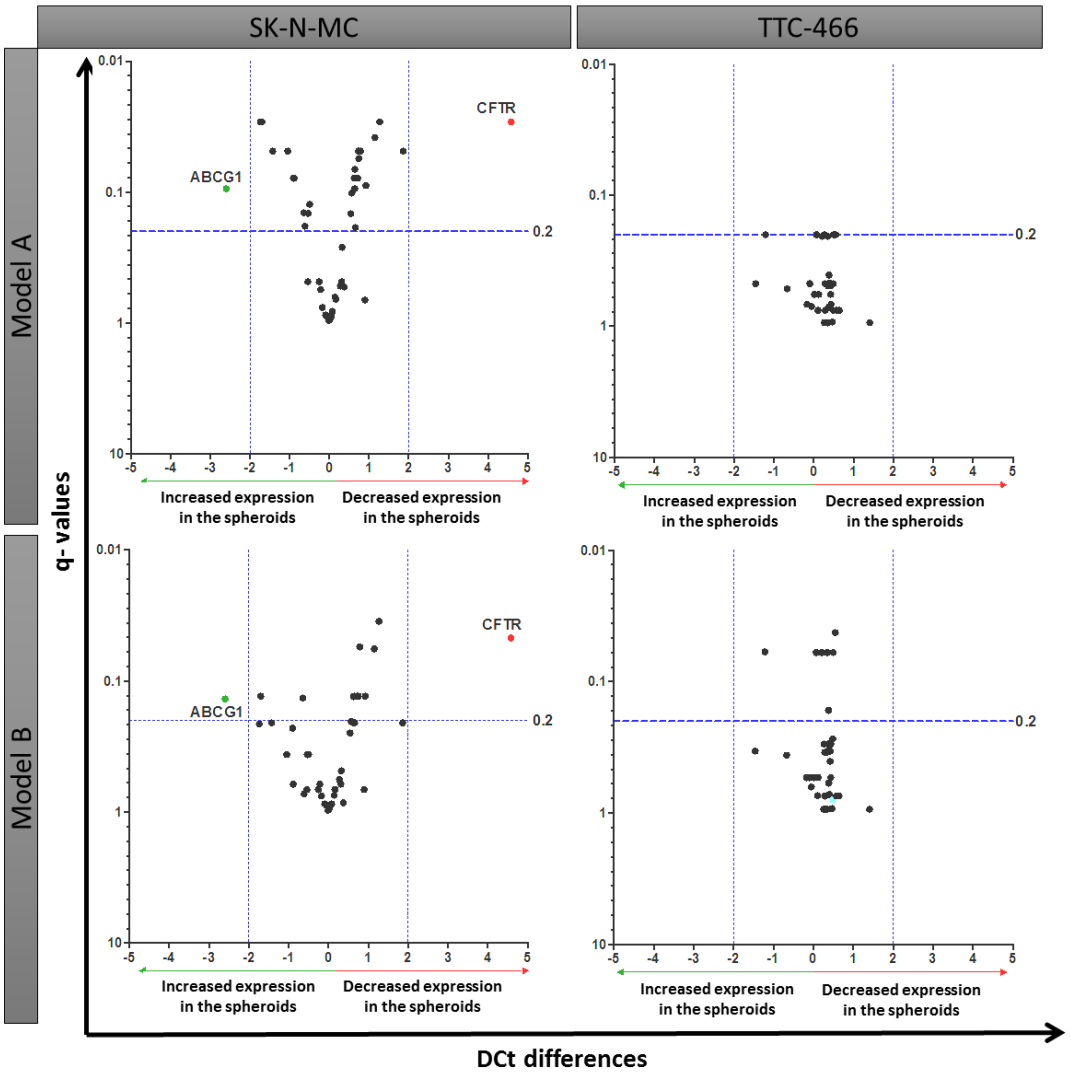

Figure 3.20 Volcano plots of analysed ABC transporter data. Plots represent significance versus DCt differences on the x-axes and adjusted p-values (q-values) on the y-axes, respectively. The cut-off of the DCt values is 2 and genes with q values less than 0.2 were considered as significant, these thresholds are shown as blue dashed lines. Targets selected as significantly increased in the spheroids are shown as green dots, whereas red dots shown mRNA with decreased expression in the spheroids. Targets not significantly increased or decreased are presented as black dots.

3.3.2.3.2 Validation of ABC transporter proteins by RTqPCR and western blot

There were two targets that showed a significant difference in SK-N-MC only. Unlike CFTR, ABCG1 passed all criteria for validation. RTqPCR and western blot confirmed expression of ABCG1. The increased expression of ABCG1 in spheroids was clear but not statistically significant using RTqPCR (n=3; each repeat in triplicate). This most likely reflects the heterogeneity of

spheroid size (Figure **3.21** B). Conversely, the increased expression of ABCG1 protein was evident in the 3-w-SK-N-MC spheroids (the number of pooled spheroids (n=149-150)) compared to substrate adherent cells (Figure **3.21** C).

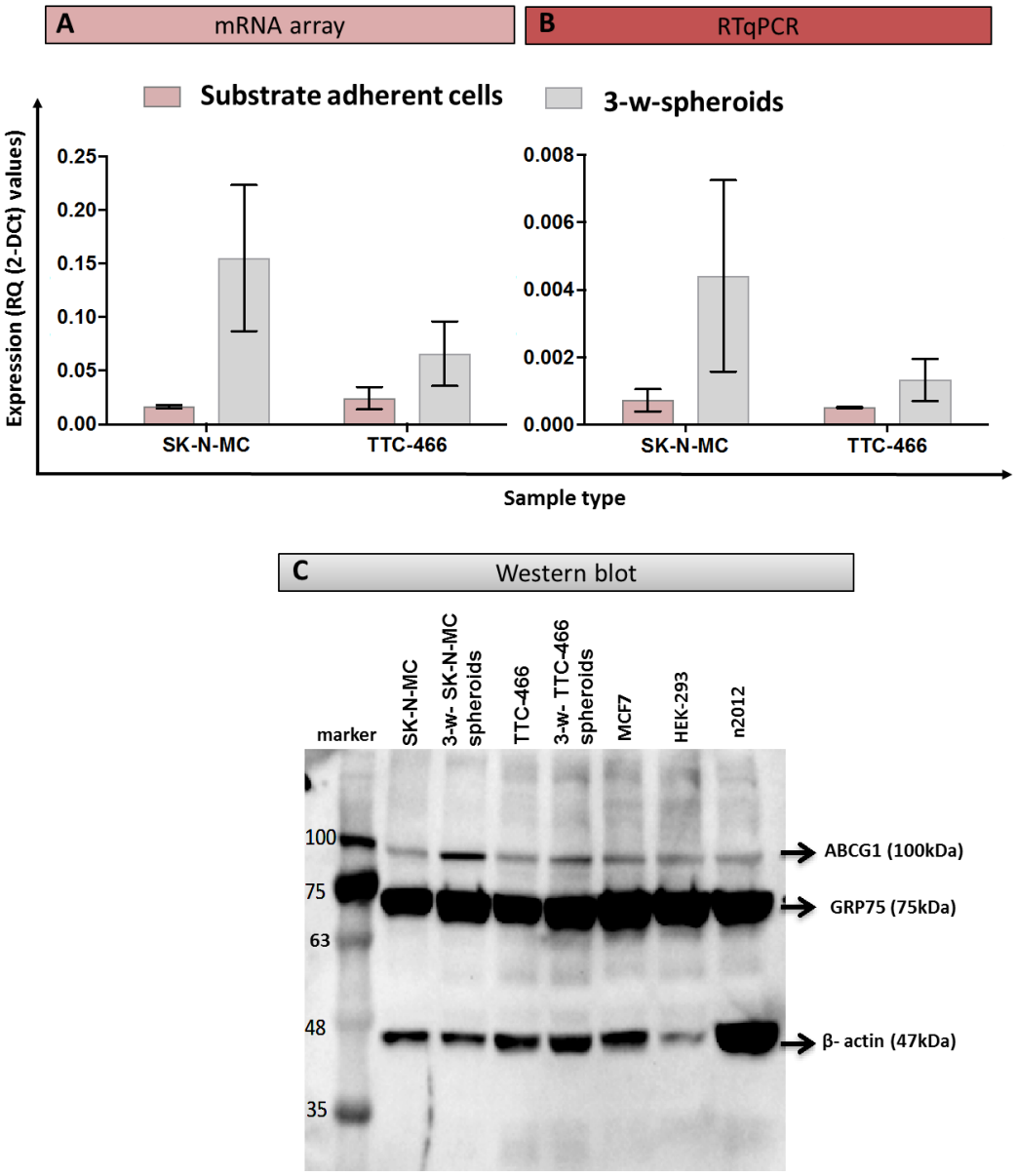

Figure 3.21 Validation of the increased expression of ABCG1 in spheroids comparing with substrate adherent cells. A) The expression level of ABCG1 that resulted from the TLDA. B) Validation of ABCG1 using RTqPCR with PPIA used as a reference gene. C) Validation of ABCG1 using western blotting. MCF7, HEK293 and n2012 were used as controls. β-actin and GRP75 were used to control for the amount of proteins on the blot.

At the protein level, I attempted to optimize the western blot conditions to examine CFTR expression. CFTR antibody was evaluated using a dilution of 0.25 -2µg (Figure **3.22**). The CaCo-2 cell line was used as a positive control. Multiple bands appear on the membrane which represents the full-length and cleaved forms of the CFTR protein (Tosoni et al., 2013). The optimal antibody concentration was 1 µg (Figure **3.22**). The full length and cleaved forms of CFTR protein were both detected in the control cell lysates; however, ES cells did not express the full length isoform of CFTR. There was a clear reduction in both spheroids in the expression of the cleaved form of CFTR resulting from bearing different N- and C- terminal domains. Expression of β-actin was examined to check the amount of protein on the membrane (Figure **3.23** C). On the other hand, there was no difference between the RNA expression levels of CFTR by RT qPCR in both ES cell lines (Figure **3.23** B).

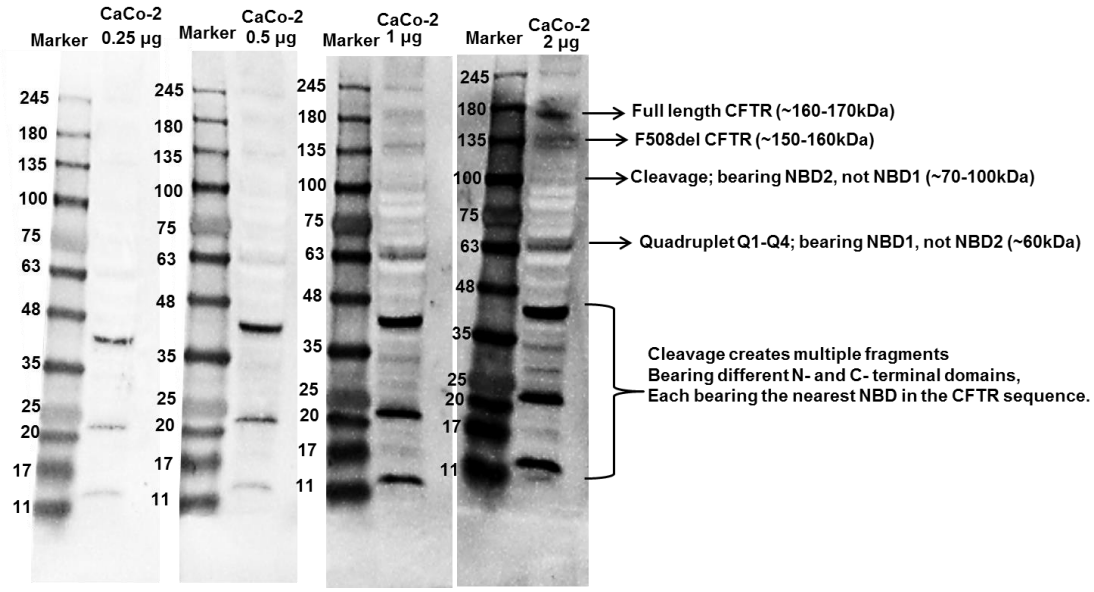

Figure 3.22 Optimisation of CFTR antibody. Protein extract from control cell line (CaCo-2; 50 µg) was used to optimize the concentration of CFTR using western blot using serial dilution of the antibody.

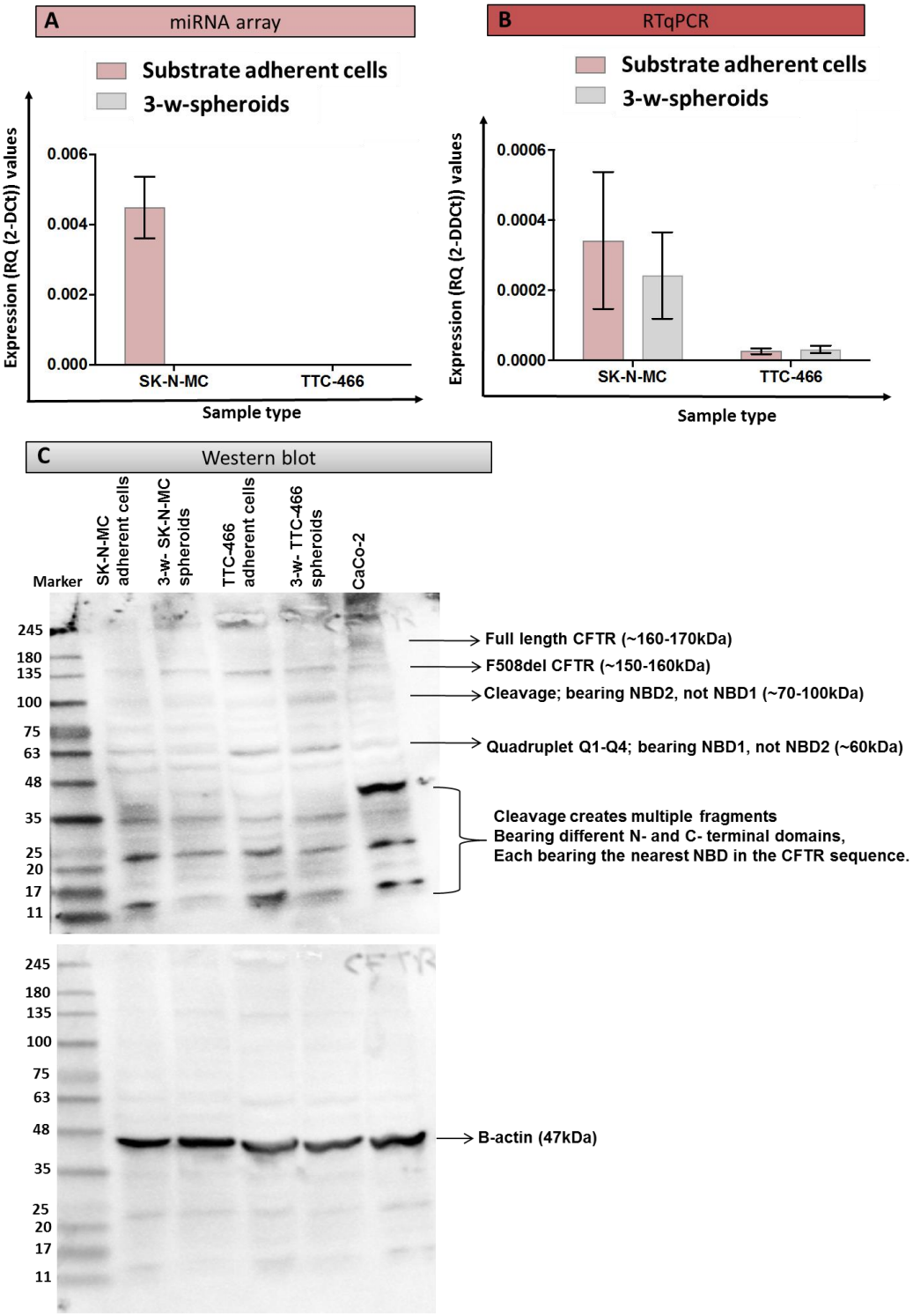

Figure 3.23 Validation of the increased expression of CFTR in spheroids comparing with substrate adherent cells. A) The expression level of CFTR that resulted from the TLDA. B) Validation of CFTR using RTqPCR with PPIA used as reference gene. C) Validation of CFTR using WB.

3.3.2.4 Expression of miRNA

3.3.2.4.1 TLDA

Unlike SK-N-MC, in 3-w-TTC-466 spheroids differentially expressed miRNA were all increased in expression. In contrast the majority of significant miRNAs that were differentially expressed in 3-w-SK-N-MC spheroids were decreased, with the exception of miR-210 which was increased in SK-N-MC and TTC-466 spheroids. In contrast to SK-N-MC, TTC-466 revealed significant miRNAs using Model A that emphasis the self-renewal characteristic (DCt; between 2.4 and 4.8). These miRNAs (miR-133b, miR-376a and miR-411) were increased in 3-w-TTC-466 spheroids (n=3; q value: 0.02, 0.12 and 0.04 respectively). In model B, TTC-466 spheroids increased expression of miR-363 (DCt: 4.5, q value; 0.16) whereas SK-N-MC spheroids decreased expression of miR-495 (DCt; 4.5, q value; 0.17). Taking into consideration the common miRNAs resulted from Model A and B, TTC-466 spheroids increased expression of miR-31 and miR-376c, whereas SK-N-MC spheroids decreased expression of 13 miRNAs (Table 3.9).

For the purpose of my studies potentally the most intresting miRNAs are those which are common in both models (A and B) and both ES cell lines; were miR-210, miR-323-3p, miR-138 and miR-134. One of the miRNA (miR-210) was statistically increased in SK-N-MC and TTC-466 spheroids, whereas the Ct difference between SK-N-MC substrate adherent cells and spheroids was less that two (Ct; 1.8, DCt; 2.4). On the other hand, miR-323-3p was regulated differently (upregulated in TTC-466 spheroids and downregulated in SK-N-MC spheroids). Like miR-323-3p, miR-138 and miR-134 are regulated differently as they appear significant in the different model when looking at TTC-466 spheroids (Table 3.9). These three miRNAs are differentially changing, so unlikely to be related to growth as spheroid as significantly as miR-210. So, miR-210 was chosen for validation based on the DCt difference and the expression (increased in SK-N-MC and TTC-466 spheroids). Furthermore, miR-138 and miR-134 were selected for validation because of the inconsistency changes in TTC-466 spheroids.

	SK-N-MC (Spheroids – substrate adherent cells)					TTC-466 (Spheroids – substrate adherent cells)					Expression in SK-N-MC spheroids	Expression in TTC-466 spheroids
	miRNA	Ct difference	DCt difference	q values (A)	q values (B)	miRNA	Ct difference	DCt difference	q values (A)	q values (B)		
Specific for Model A	-	-	-	-	-	miR-133b	-2.6	-2.4	0.02	-	-	▲
	-	-	-	-	-	miR-376a	-4.6	-4.3	0.12	-	-	▲
	-	-	-	-	-	miR-411	-5.0	-4.8	0.04	-	-	▲
Specific for Model B	-	-	-	-	-	miR-363	-2.6	-4.5	-	0.16	-	▲
	miR-495	2.6	4.1	-	0.17	-	-	-	-	-	▼	-
Common between model A and B	miR-597	2.5	6.9	0.07	0.01	-	-	-	-	-	▼	-
	miR-15a	4.3	6.6	0.19	0.04	-	-	-	-	-	▼	-
	miR-107	1.9	6.3	0.11	0.004	-	-	-	-	-	▼	-
	miR-133a	2.0	6.0	0.01	0.02	-	-	-	-	-	▼	-
	miR-135b	4.8	5.9	0.19	0.03	-	-	-	-	-	▼	-
	miR-339-5p	3.8	5.3	0.19	0.03	-	-	-	-	-	▼	-
	miR-127	2.8	4.1	0.19	0.06	-	-	-	-	-	▼	-
	miR-340	3.0	2.5	0.19	0.04	-	-	-	-	-	▼	-
	miR-140	2.9	2.3	0.02	0.0004	-	-	-	-	-	▼	-
	miR-214	2.8	2.3	0.07	0.002	-	-	-	-	-	▼	-
	miR-29b	2.8	2.2	0.19	0.06	-	-	-	-	-	▼	-
	miR-374	2.7	2.2	0.19	0.06	-	-	-	-	-	▼	-
	miR-18a	2.6	2.0	0.19	0.05	-	-	-	-	-	▼	-
	-	-	-	-	-	miR-31	-3.1	-2.9	0.14	0.06	-	▲
	-	-	-	-	-	miR-376c	-4.0	-3.7	0.001	0.03	-	▲
	miR-210*	-1.8	-2.4	0.12	0.01	miR-210	-4.2	-3.9	0.001	0.0007	▲	▲
	miR-323-3p	2.5	2.0	0.19	0.06	miR-323-3p	-2.8	-2.5	0.02	0.04	▼	▲
	miR-138	2.0	1.4	0.19	0.17	miR-138	-2.5	-2.3	-	0.19	▼	▲
	miR-134*	1.7	1.9	0.19	0.07	miR-134*	-1.9	-1.6	0.17	-	▼	▲

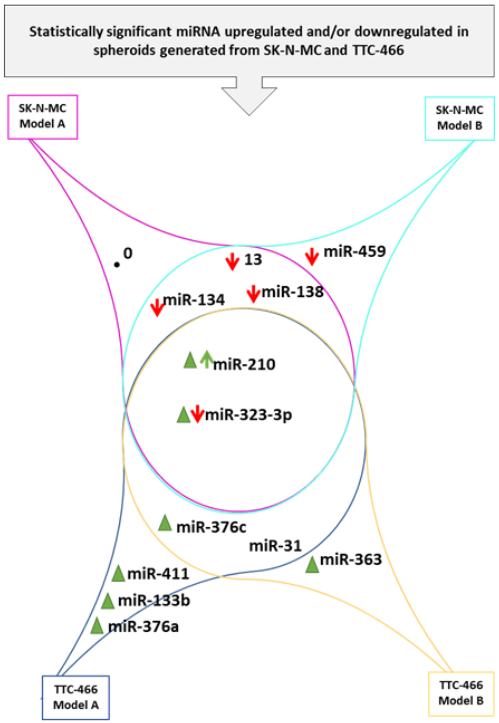

Table 3.9 Summary of miRNA expression in sheroids compared to cells grown as substrate adherent monolayers. RNAs from three biological repeats were profiled using Human miRNA A TLDA array. LIMMA analysis was performed using two models after normalising the data to the global mean to examine the differences between substrate adherent cells and 3-w-spheroids. The increased and decreased expression of miRNAs (miR) in 3-w-spheroids were presented as solid triangle SK-N-MC and TTC-466 presented (increased; ▲ and decreased; ▼). Common miR between SK-N-MC and TTC-466 appear significant when used model A and B were highlighted in Pink and Ct differences that were less than 2 were highlighted in Yellow. In the right, venn diagram summarized the information from the table in the left. The expression of TTC-466 presented as (increased; ▲ and decreased; ▼).In SK-N-MC, increase expression in spheroids presented as an arrows (increased; ↑ and decreased; ↓).

3.3.2.4.2 Validation of miRNA by RTqPCR

To confirm the results from TLDA, total RNA was extracted from substrate adherent cells and 3-w-spheroids (Section 2.2.5.3.1; n=3). The RTqPCR was performed in triplicate using 10ng total RNA and a combination of two miRNA (miR-16 and miR-30b) was used for normalisation. In Figure 3.24, the expression of miR-210 in SK-N-MC and TTC-466 was increased significantly in 3-w-spheroids and validated the array result (p value; 0.003 and 0.04 respectively). RTqPCR showed a lower expression of miR-138 in 3-w-TTC-466 spheroids compared with the array. The expression of miR-138 was validated in 3-w-SK-N-MC spheroids only with significant decreased (p value: 0.07). However, there were no significant differences in the expression level of miR-134 in substrate adherent cells and spheroids. This miRNA was not validated by RTqPCR. Overall, the expression pattern of miR-210, miR-134 and miR-138 in the array and RTqPCR was almost identical except the expression of miR-138 (Figure 3.24).

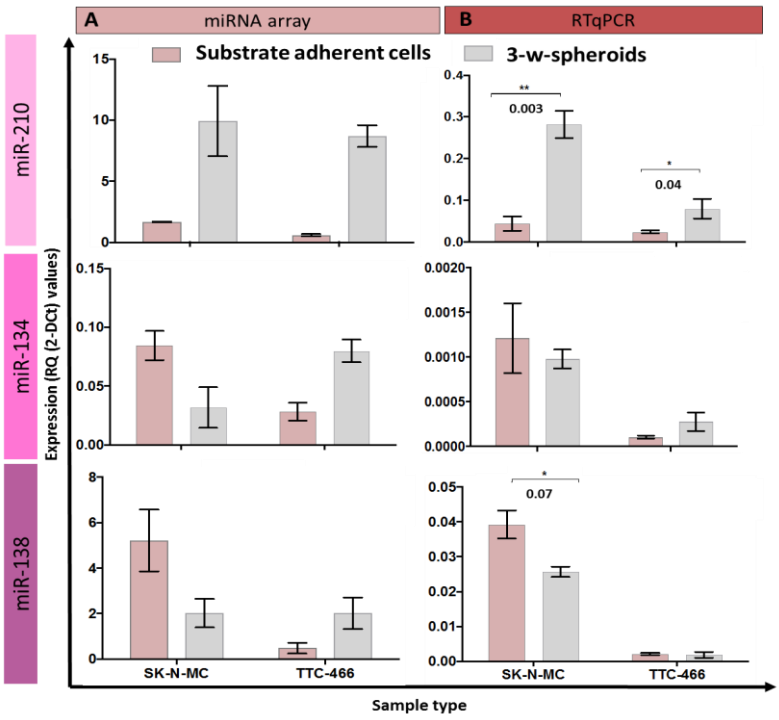

Figure 3.24 Validation of selected miRNAs. Total RNA were extracted from substrate adherent cells and 3-w-spheroids. After LIMMA analysis three miRNA: miR-210, miR-134 and miR-138 were selected for validation. A) The TLDA expression level of the selected miRNA presented the expression pattern (n=3; biological repeats). B) Validation of miRNA using RTqPCR that performed in triplicate from three biological repeats. Two reference miRNAs (miR-16 and miR-30b) were used as references for normalisation and the significant difference demonstrated by p-value.

3.3.3 Investigating if differentially expressed mRNA are induced by growth as spheroids or if cells with increased/decreased expression of mRNAs produce spheroids

The 3-w-SK-N-MC spheroids were dissociated and cultured as a monolayer. The attached cells of dissociated spheroids were passaged and at passage two were profiled using all TLDAs. In SC and ABC, SK-N-MC substrate adherent cells clustered with SK-N-MC dissociated spheroids, whereas SK-N-MC spheroids clustered alone (Figure 3.25 A, B and C). Out of 90 genes, dissociated SK-N-MC spheroids expressed 54% (±0.5) of SC genes and ABC genes were expressed in dissociated SK-N-MC spheroids (out of 50 genes; 75%±0.4). Unlike SC and ABC, in the miRNA TLDA, SK-N-MC adherent cells clustered separately than SK-N-MC spheroids and dissociated spheroids and 44% (±1.6) of miRNA targets were expressed in SK-N-MC dissociated spheroids (Figure 3.26).

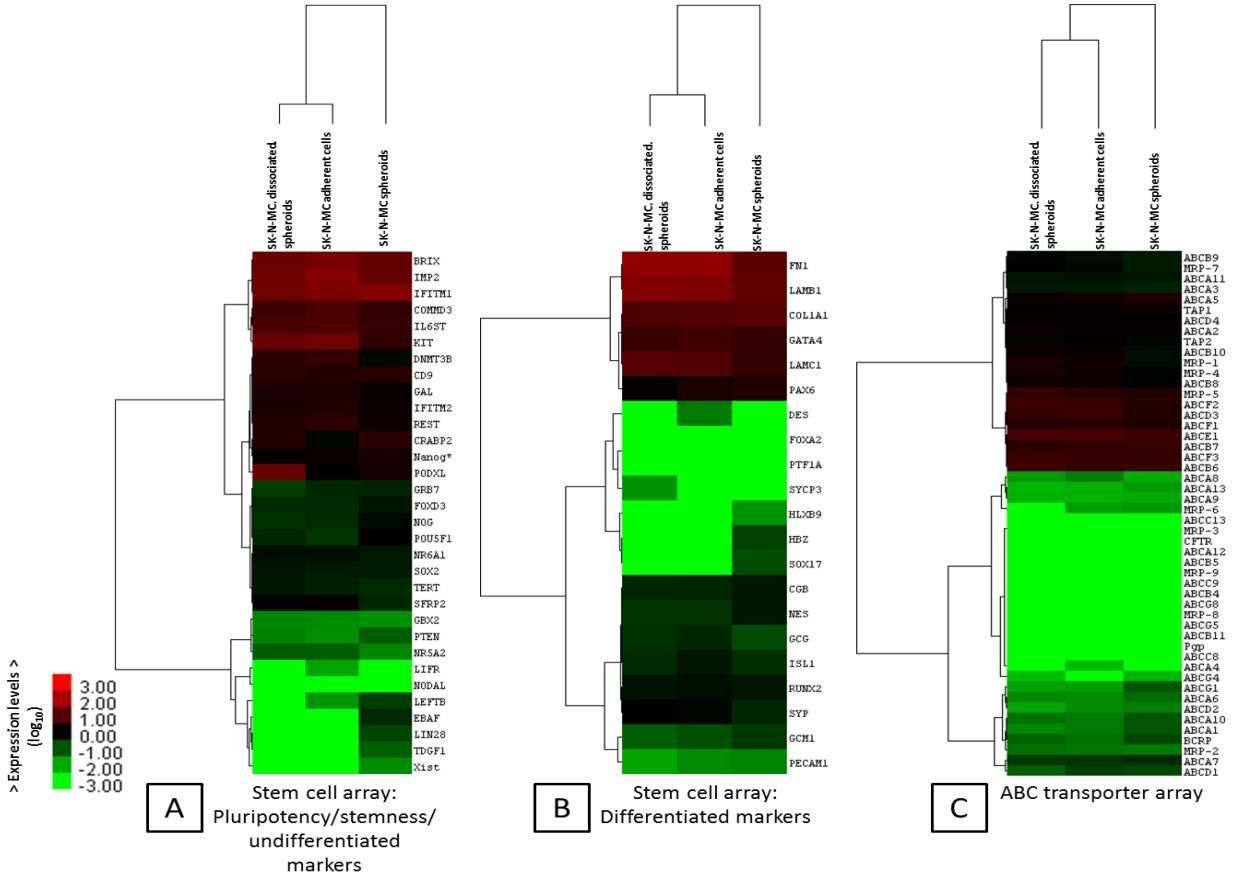

Figure 3.25 Heat map of expression of SC and ABC genes in dissociated SK-N-MC spheroids, substrate adherent cells and spheroids. The dendrograms of cell types using complete linkage were carried out according to expression of all target genes only as determined by the Taqman® SC and ABC array. Data are presented as Log scale of mRNA expression relative to the global mean. Red shows high relative expression and green demonstrations low relative expression. Heatmap shown are representative of 3 independent experiments

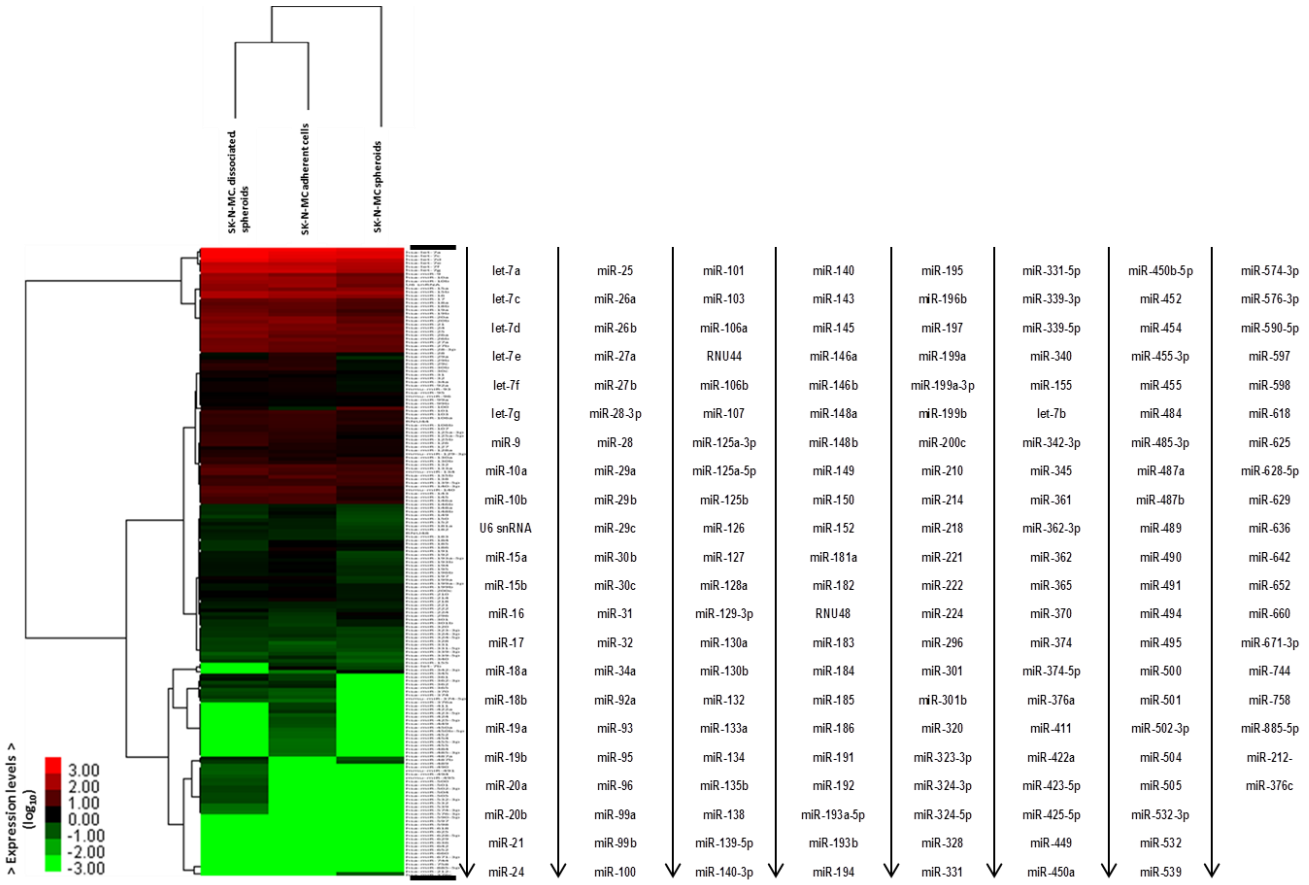

Figure 3.26 Heat map of expression of miRNA genes in dissociated SK-N-MC spheroids, substrate adherent cells and spheroids. The dendrograms of cell types using complete linkage were carried out according to expression of all target genes only as determined by the Taqman® miRNA array (TLDA). Data are presented as Log scale of miRNA expression relative to the global mean. Red shows high relative expression and green demonstrations low relative expression. Heatmap shown are representative of three independent experiments and miRNA names are expanded next to the heatmap.

Taking into consideration results from model A, like SC marker, the expression of ABC markers in dissociated spheroids and substrate adherent cells were identical (Figure **3.27**). The expression of PODXL, Mast/stem cell growth factor receptor Kit (Kit) and DNA (cytosine-5)-methyltransferase 3 (DNMT3B) were increased in dissociated SK-N-MC spheroids (n=3, q-value; 0.1432, 0.0168 and 0.0075 respectively). The expression of other pluripotency, stemness and undifferentiated targets including EBAF, TDGF1, LEFTB and LIN28 were significantly decreased in dissociated SK-N-MC spheroids comparing with 3w-SK-N-MC spheroids (Table **3.10**). On the other hand, one of the differentiated targets, LAMA1, was increased expression, whereas SOX-17 and HBZ were significantly decreased in dissociated SK-N-MC spheroids. Also, ABCG1 was decreased significantly in dissociated SK-N-MC spheroids comparing with non-dissociated spheroids (q-value= 0.12) (Table **3.10**).

	SK-N-MC (Dissociated spheroids - 3-w-pheroids)				Expression in dissociated SK-N-MC spheroids
	Target	Ct difference	DCt difference	q values (A)	
Pluripotantency, stemness and undifferentiated markers	PODXL	-3.5	-3.2	0.143	▲
	KIT	-2.5	-2.2	0.017	▲
	DNMT3B	-2.5	-2.1	0.007	▲
	EBAF	5.3	8.5	0.001	▼
	TDGF1	3.2	4.2	0.002	▼
	LEFTB	3.3	3.6	0.101	▼
	LIN28	4.2	4.8	0.107	▼
Differentiated markers	LAMA1	-1.4	-6.1	0.088	▲
	SOX17	3.9	8.8	0.001	▼
	HBZ	4.3	8.1	0.007	▼
ABC transporter proteins	ABCG1	2.9	3.1	0.115	▼

Table 3.10 Summary of mRNA expression in dissociated SK-N-MC spheroids compare to non-dissociated spheroids. mRNAs from three biological repeats were profiled using SC and ABC TLDA array. LIMMA analysis was performed using models A only after normalising the data to the global mean to examine the differences between dissociate spheroids and non-dissociate (3-w-spheroids). The increased and decreased mRNAs in dissociated spheroids were presented as solid triangle (increased; ▲ and decreased; ▼). Q-values less that 0.2 considered as significant.

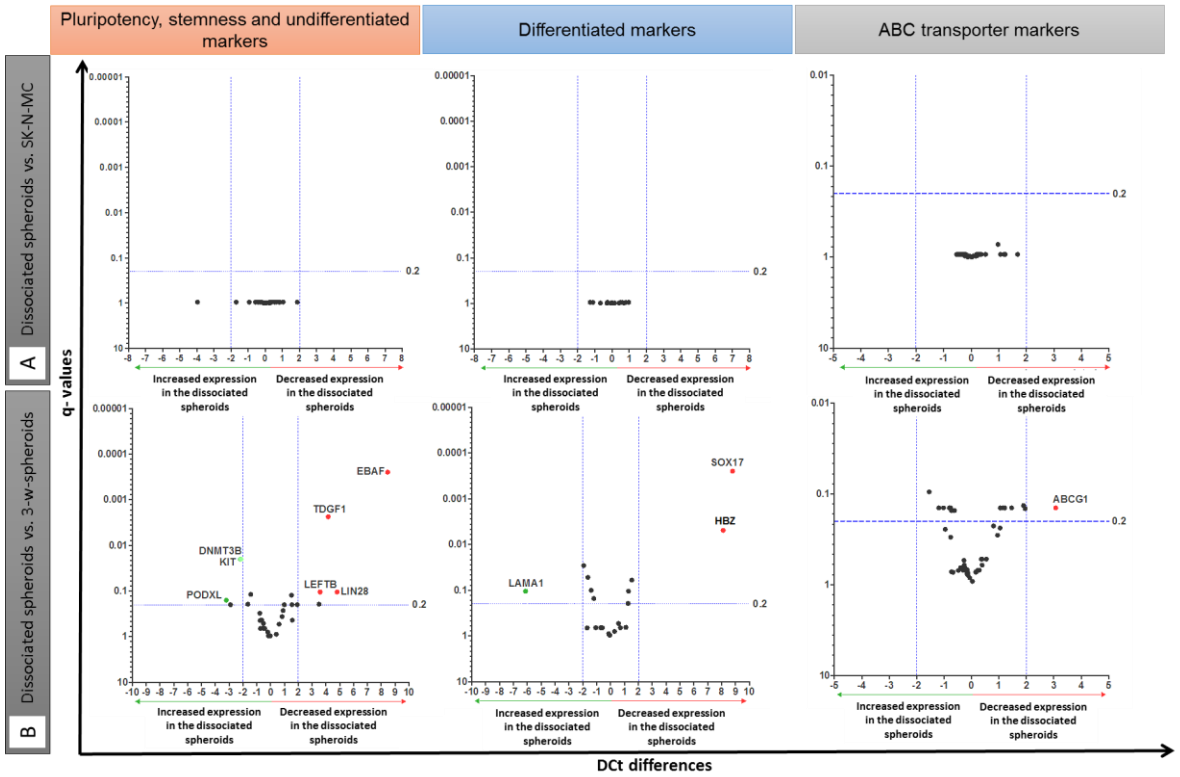

Figure 3.27 Profile of mRNAs in the dissociated spheroids compared to non-dissociated spheroids and substrate adherent cells. Total RNA was extracted from the dissociated spheroids and substrate adherent cells (n=3) and profiled using SC and ABC TLDA. Plots presented significance versus DCt differences on the x-axes and adjusted p-values (q-values) on the y-axes. A) The three graphs compare the expression level of genes of the dissociated spheroids with the adherent cells (SK-N-MC). B) The three graphs in the bottom illustrate the comparison between the dissociated spheroids with 3-w-spheroids. The cut-off of the DCt values is two and genes with q values less than 0.2 were considered as significant.

	SK-N-MC (Dissociated SK-N-MC spheroids – 3-w-SK-N-MC spheroids)									
	miRNA	Ct difference	DCt difference	q values (A)	Expression in Dissociated SK-N-MC spheroids	miRNA	Ct difference	DCt difference	q values (A)	Expression in Dissociated SK-N-MC spheroids
Specific for Model A	miR-210	4.1	4.8	0.056	▼	miR-199a-3p	-2.3	-1.6	0.117	▲
	miR-155	4.0	4.7	0.117	▼	miR-140	-2.4	-1.7	0.117	▲
	miR-212	2.1	3.4	0.151	▼	miR-422a	-2.4	-1.7	0.117	▲
	miR-107	-1.8	-6.0	0.004	▲	miR-455-3p	-2.5	-1.8	0.117	▲
	miR-200c	-2.1	-1.3	0.117	▲	let-7a	-2.5	-1.8	0.174	▲
	miR-128a	-2.1	-1.3	0.149	▲	miR-18a	-2.6	-1.8	0.032	▲
	miR-214	-2.1	-1.4	0.117	▲	miR-296	-2.7	-2.0	0.117	▲
	miR-101	-2.1	-1.4	0.117	▲	miR-15a	-2.8	-4.9	0.117	▲
	miR-221	-2.1	-1.4	0.158	▲	miR-374	-2.8	-2.0	0.117	▲
	miR-597	-2.2	-6.5	0.004	▲	miR-135b	-2.8	-3.8	0.118	▲
	miR-92a	-2.2	-1.5	0.158	▲	miR-340	-2.8	-2.1	0.117	▲
	miR-29c	-2.2	-1.5	0.117	▲	miR-99a	-3.1	-2.4	0.118	▲
	miR-361	-2.2	-1.5	0.158	▲	miR-18b	-3.2	-2.5	0.046	▲
	miR-99b	-2.3	-1.5	0.145	▲	miR-21	-3.4	-2.6	0.117	▲
	miR-100	-2.3	-1.5	0.152	▲	miR-339-5p	-4.0	-5.3	0.117	▲

Table 3.11 Summary of miRNA expression in dissociated SK-N-MC spheroids compare to non-dissociated spheroids. miRNAs from three biological repeats were profiled using miRNA TLDA array. LIMMA analysis was performed using models A only after normalising the data to the global mean to examine the differences between dissociate spheroids and non-dissociate (3-w-spheroids). The increased and decreased miRNAs in dissociated spheroids were presented as solid triangle (increased; ▲ and decreased; ▼). Q-values less than 0.2 considered as significant.

-154 -

3.4 Discussion

Identification of the pathways which drive the self-renewal capacity of the ES cells that are responsible for disease progression and relapse remain to be elucidated. In this chapter, results revealed that ES spheroids are enriched for the ABC transporter protein, ABCG1, which is a protein associated with drug resistance (Bielicki et al., 1999; Gelissen et al., 2006). Interestingly, expression of miR-210-3p “miR-210”, which is associated with low oxygen concentrations, proliferation and survival (Chan, Y.C. et al., 2012), was also increased in ES spheroids compared to cells in 2D. Furthermore, increased expression of one of the stem cell targets EBAF was greater in the SK-N-MC spheroids that had a greater propensity to produce spheroids than the TTC-466 cells. Importantly, after dissociating the spheroids and culturing them as a monolayer for two passages, the mRNA expression profile of the cells was reversed such that it more closely resembled that of the parental cells grown as a monolayer. According to the hierarchical or CSC model that was previously described in (Section 1.2, Figure **1.2**), the putative CSCs might have given rise to non-CSCs, which divide faster and therefore dilute the expression levels of the identified targets in the putative CSCs.

There is a paucity of data that links ABCG1 expression with cancer, although recently elevated expression of ABCG1 was reported in murine and human low-grade glioma cancer stem cells (LG-GSCs) (Chen, Y. et al., 2016). Moreover, knockdown of ABCG1 in glioblastoma cells leads to increased ER stress and cell death *in vitro* and also increased mouse survival *in vivo* (Chen, Y. et al., 2016). Interestingly, in this chapter, ABCG1 was increased in cells grown as spheroids compared to cells grown as monolayers; this was confirmed at both the mRNA and protein level. The phenotypic relevance of ABCG1 will be investigated in the next chapter (Chapter 4).

The profile analysis of 3-w-SK-N-MC spheroids showed a significant increase of EBAF at the mRNA level whereas this increase was not apparent at the protein level. On the other hand, the increased expression of EBAF in TTC-466 spheroids was observed at the protein level only; and there was no difference at the mRNA level. The LEFTY family includes

LEFTY1 and EBAF proteins, which can negatively regulate the Nodal signalling pathway. It has been reported that LEFTY1 and EBAF form heterodimers that interact directly with the Nodal ligand and prevent binding to the TGF-β receptor complex (Chen, C. and Shen, 2004). Also, the LEFTY1/EBAF heterodimer binds to the EGF-CFC Nodal co-receptors, such as Cripto and Cryptic and inhibit their interaction with the TGF-β receptor complex (Chen, C. and Shen, 2004; Schier, 2009). In 2008, human embryonic stem cells (hESCs), like cancer cells were also shown to express Nodal and secrete Nodal inhibitors, whereas only hESCs up regulated LEFTY. In addition, the expression of LEFTY was not detected in other cell types such as, trophoblasts, other stem cell types or normal cells for instance myoepithelial cells (Hs 578 Bst) and primary human mammary epithelial cells (HMEpC) (Postovit et al., 2008). Perhaps, LEFTY stimulates reprogramming and suppression of the malignant cancer cell phenotype. However, this phenomena has been reported in hESC only (Postovit et al., 2008). The lack of functional studies for LEFTY in human cells and unclear reason for the apparent inconsistency between the mRNA and protein level in ES spheroids in the present study warrants further investigation. Unfortunately, time limitations precluded further investigation into the functional significance of this gene in the current studies.

Consistent with the development of a hypoxic rim in 3-w-spheroids of ES confirmed in the previous chapter (Chapter 2) there was an increase in miR-210 expression in 3-w-spheroids compared to substrate adherent cells. To date a broad number of confirmed gene targets of miR-210 have been identified, whilst this miRNA is best known as a regulator of the hypoxic response (Chan, S.Y. and Loscalzo, 2010). This miRNA is also linked to proliferation of hypoxic cells (Huang, X. et al., 2009; Chan, S.Y. and Loscalzo, 2010). Overexpressing miR-210 leads to significant delay at the G1/S transition in hepatocellular carcinoma cells (Tan et al., 2015). Furthermore, decreased proliferation has been shown to correlate with cell cycle arrest at the G1/S transition in hypoxia (Goda et al., 2003; Gordan et al., 2007; Hammer et al., 2007). On the other hand, it has been reported that miR-210 induces, rather than supresses, the G1/S transition leading to a reduction in proliferation (Zhang, Z. et al., 2009). It therefore remains unclear

as to whether miR-210 controls cell cycle and proliferation positively or negatively in ES spheroids. The role of miR-210 could be cell type and microenvironment dependent (Huang, X. and Zuo, 2014; Suzuki et al., 2015). In addition to miR-210 role in hypoxia, it has been shown to predict poor outcome in some cancers including osteosarcoma (Cai et al., 2013). Also, miR-210 has been described as having a role in differentiation of osteosarcoma CSCs induced by TGF-β1 and hypoxia (Zhang, H. et al., 2017).

Several targets of miR-210 are reported to have a profound effect on cell cycle and proliferation (Zhang, Z. et al., 2009; Huang, X. et al., 2009). Fibroblast growth factor receptor-like 1 (FGFRL1) and Homeobox protein Hox-A3 (HOXA3) are both downregulated by miR-210 (Huang, X et al., 2009). This decrease in the expression of FGFRL1 and HOXA3 appears to reduce tumour initiation and growth (Huang, X. et al., 2009). Max-binding protein MNT (MNT) is a known antagonist to MYC-C and a confirmed target of miR-210. The increase of miR-210 expression is reported to downregulate MNT, which in turn leads to activation of the G1/S transition and increases cell cycle and tumour proliferation (Zhang, Z. et al., 2009). This is particularly interesting as ES cells have high levels of MYC-C which may be regulated by miR-210. It could be that miR-210 is a primary driver event in ES.

Moreover, the transcription factor E2F3, which controls cell cycle progression and generates two isoforms (E2F3a and E2F3b) that share the same 3'UTR sequence recognized by miR-210, is confirmed as a target of miR-210 (Leone et al., 2000). E2F3a drives cells in G0 phase through the cell cycle to divide, whereas E2F3b maintains G0 cells in quiescence. Under hypoxia, the predicted effects of miR-210 on E2F3a and E2F3b are still under investigation (Chan, S.Y. and Loscalzo, 2010). Activin receptor type-1B (ACVR1b) was also confirmed as a miR-210 target in primary osteoblasts. ACVR1b can influence proliferation and differentiation and is a member of the transforming growth factor-β (TGFβ) receptor superfamily (Mizuno et al., 2009). Mizuno and colleagues reported that miR-210 acts as a differentiation inducer as a result of inhibiting ACVR1b and leading to downstream TGF/activin signalling in osteoblasts (Mizuno et al., 2009). The

inverse correlation between proliferation and differentiation is likely important although further studies are required to conclude how these targets interact and affect proliferation of the hypoxic cell (Chan, S.Y. and Loscalzo, 2010).

During hypoxic stress, miR-210 appears to be an important regulator of cellular survival during hypoxic-induced cellular adaption (Chan, S.Y. and Loscalzo, 2010). Therefore, miR-210 has been reported as an inhibitor of apoptosis in different cell types including nasopharyngeal carcinoma cell lines (Hua et al., 2006), breast and colon cancer (Kulshreshtha et al., 2007; Camps et al., 2008). It is also a regulator of the angiogenic response to ischemia (Fasanaro et al., 2008). The mechanism by which miR-210 controls cell survival is still not fully understood, although validated targets of miR-210 which likely influence the apoptotic machinery have been identified. For example, miR-210 directly suppress the iron-sulfur cluster proteins 1 and 2 (ISCU1/2), which control mitochondrial respiration and electron transport. This appears to enhance ATP levels in the hypoxic cell and decreases creation of reactive oxygen species (ROS) as well as reducing cellular apoptosis (Semenza, 2007; Chan, S.Y. et al., 2009; Chan, S.Y. and Loscalzo, 2010). Furthermore, Kim and colleagues have reported another direct target of miR-210 that influence cell survival. This target, caspase-8 associated protein-2 (CASP8AP2), is a FLICE-associated protein (FLASH) that interacts with the death-effector domain (DED) of caspase-8 and leads to apoptosis (Kim, H.W. et al., 2009). The activation of caspase-8 results in activation of effector caspases, such as caspases-3, 6 and 7 (Imai et al., 1999). Unlike ISCU1/2 and CASP8AP2, other identified miR-210 direct targets, which are involved in survival pathways, remain to be fully characterized (Chan, S.Y. and Loscalzo, 2010). The interaction between miR-210 and the genes mentioned earlier is summarized in Figure **3.28**.

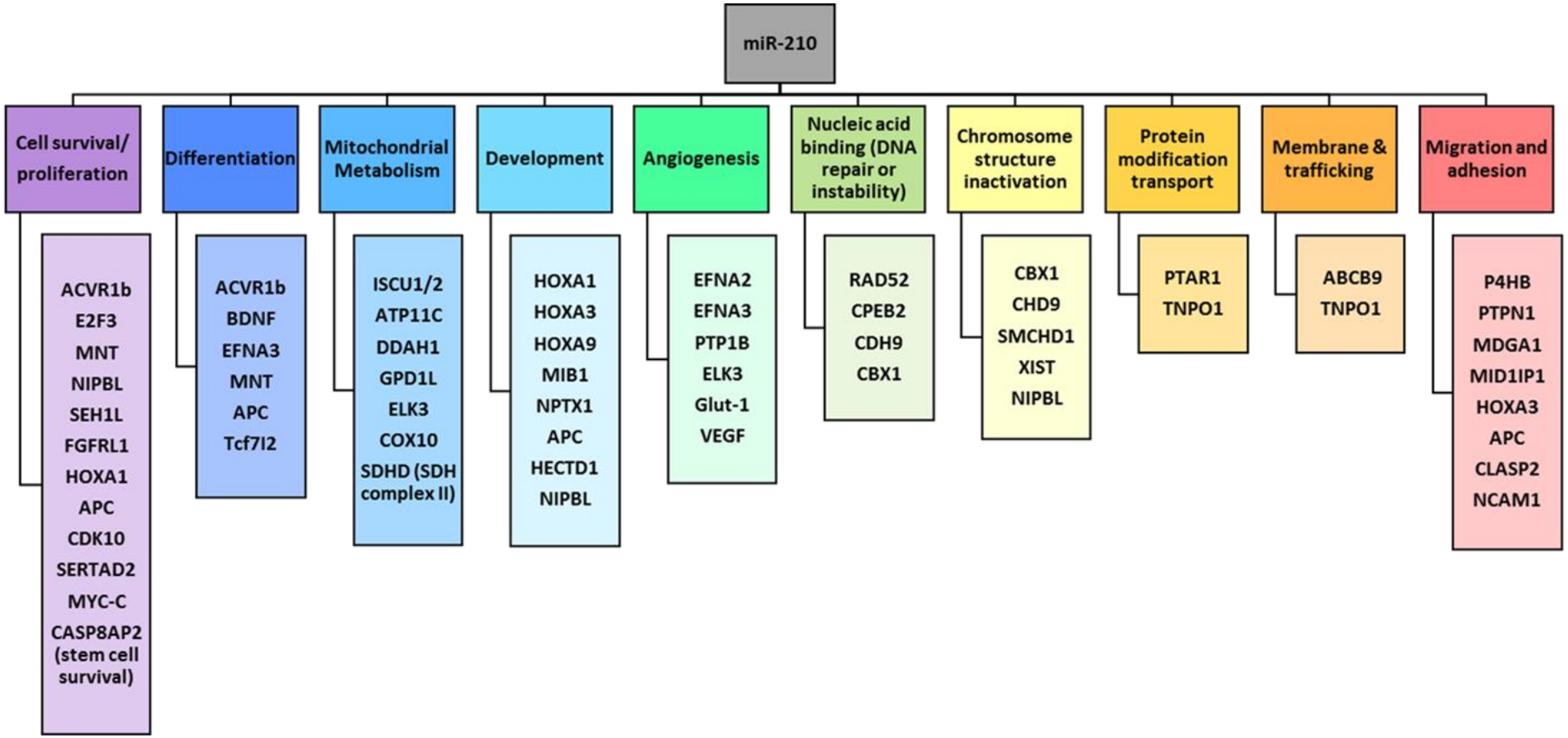

Figure 3.28 Summary of the both directly and indirectly cellular processes affected by miR-210, possible targets involved in each event are shown

The link between miR-210 and hypoxia inducible factor 1-alpha (HIF-1α) is well studied. The increase of miR-210 leads to increased HIF-1α and results in inhibition of cell apoptosis (Greijer and van der Wall, 2004; Kilic et al., 2007). In normoxia, glycerol-3-phosphate dehydrogenase 1-like (GPD1L) enzyme stimulates prolyl hydroxylase (PHD) activity that leads to HIF-1α degradation. Whilst, during hypoxia, the increase of miR-210, associated with a reduction in PHD through downregulation of GPD1L enzyme and thereby prevented HIF-1α degradation (Kelly, T.J. et al., 2011; Grosso et al., 2013).

Since hypoxia is important in maintaining some aspects of the cancer cell phenotypes including invasion and metastasis, miR-210 dependant regulation of HIFs has been exploited therapeutically and a small molecule inhibitor known as Targapremir-210 has been developed in breast cancer (Costales et al., 2017). This small molecule inhibits the production of mature miR-210 by binding to the Dicer site of the miR-210 hairpin precursor, which activates GPD1L, leading to a deceased HIF-1α to induce apoptosis under hypoxic conditions. To date, Targapremir-210 is reported to specifically inhibit mature miR-210 and showed a reduction in tumour size. A single injection of the component was capable of reaching the tumour and was sustained for 21 days (Costales et al., 2017).

The techniques used to analyse gene expression in this chapter only require a small amount of RNA, but the quality of the initial RNA used in this type of analysis is extremely important. Techniques have been developed to evaluate the quantity and quality of DNA and RNA, such as the spectrophotometer (Evans, 1990). However, some have suggested that spectrophotometry that relies on the absorbance at a particular wavelength lacks specificity and sensitivity (Wieczorek et al., 2012). For example, reagents such as phenol, which are commonly used to isolate DNA affect the absorbance measurement. A ratio of 1.8 to 2.0 is generally accepted as a pure sample of nucleic acids. Outside this range nucleic acid is contaminated with phenol or proteins etc. Furthermore, the spectrophotometry does not distinguish between RNA and DNA. This may be a particular problem when analysing small amounts of RNA without using

DNase treatment and removal reagents. Furthermore, the quality of the RNA is not reflected in the spectrophotometer measurement (Wieczorek et al., 2012). Regardless of these disadvantages the spectrophotometer is still useful as it has a wide detection range (dsDNA; 2-15,000 ng/µL) and it is useful to estimate the quantity of RNA in samples before loading into the Bioanalyzer, which has a much smaller quantitative range (dsDNA; 0.05-5ng/µL). However, the advantage of the Bioanalyzer is that it has the ability to distinguish between total RNAs and small RNAs and calculate the RNA integrity number (RIN) based on the quality of the total RNA, not isolated miRNA. Some authors believe this is a good method to assess the quality of miRNA (Nolan et al., 2006; Wieczorek et al., 2012).

The decrease in RIN number is associated with the degradation of RNA and visibility of rRNA. The RNA extracted from substrate adherent cells showed the highest RIN number compared to that from spheroids and the time point at which the spheroids were collected had a strong impact upon the quality and quantity of RNA. This decrease in RNA quality was reflected in the gross appearance of the spheroids which deteriorated over time. The observed RIN suggested that 3-w-spheroids were less intact or more degraded compared to the substrate adherent cells. Perhaps the slight reduction in RIN number of 3-w-spheroids compared to week 1 or 2 spheroids was due to the appearance of necrotic core and hypoxic rim in 3-w-spheroids.

RTqPCR, is one of the most robust methods used today for the analysis of gene expression due to its high sensitivity, efficiency and good reproducibility (Wang, T. and Brown, 1999; Bar et al., 2003). RTqPCR is frequently used to validate data obtained from microarrays which are at best considered to deliver semi-quantitative data (Pfaffl, 2001) and can be used to analyse samples where the RNA is partially degraded (Schoor et al., 2003; Fleige et al., 2006). The value of RTqPCR data is largely determined by the suitability of the normalisation method used. Software such as NormFinder and GeNorm have been used to identify the most stable reference gene to use for normalisation results obtained from RTqPCR (Lemma et al., 2016). Normalisation to a gene which is stably expressed

across cell types and experimental treatments is crucial to obtain meaningful results. Although, there are fifteen commonly used reference genes they are not all suitable across all cell types (Lemma et al., 2016). Identifying a stable reference gene in respect to the cancer type to correct sample-to-sample variation is necessary (Pfaffl, 2001; Lemma et al., 2016).

The geometric mean of PPIA and TATA-box-binding protein (TBP) has been suggested as the optimal normalisation method for substrate adherent cells isolated from human rhabdomyosarcoma (RS), osteosarcoma (OS), Ewing's sarcoma (ES), breast carcinoma (BC) and renal carcinoma (RC) (Lemma et al., 2016). After deep analysis for sarcoma cells only, the Lemma group found that GAPDH and YWHAZ were the most stable reference genes for the parental cells and CSC that aggregate and form floating spheroids (Lemma et al., 2016). GAPDH is not useful as it has lots of pseudogenes (Sun et al., 2012). On the other hand, YWHAZ is on chromosome 8 which is often multiplied (i.e. several copies of chromosome 8) in ES (Tarkkanen et al., 1999; Hattinger et al., 2002). So, it is unlikely to be universally useful. In this chapter, the optimal method to normalise mRNA/miRNA arrays was to use the global mean; in agreement with others (Murray et al., 2015). Furthermore, PPIA displayed the least variation of a single RNA across the different arrays. Also, the stability of PPIA mRNA has been reported to be one of the most stable mRNAs, even when RNAs are of low quality extracted from formalin-fixed, paraffin-embedded samples (Aggerholm-Pedersen et al., 2014). Likewise, in this study, the expression of PPIA across all SK-N-MC spheroids that were collected at different time points (3, 4, 5, and 6 weeks) was homogeneous. PPIA, which had been suggested as a stably expressed transcript (Brownhill, personal communication), showed a very high stability and less variation between cells grown as spheroids or substrate adherent cells. Across a panel of different cancer types, PPIA has been reported as one of the four most stable reference genes and its use recommended when comparing the expression between cancer stem-like cell (CSC) and parental cells (Lemma et al., 2016). Therefore, PPIA was used as reference mRNA reporting the expression of selected targets mRNAs for validation.

In conclusion, the results in this chapter support the proposed hypothesis that ES spheroids derived from a single cell are useful tools to identify putative drivers of the CSC phenotype. Since miR-210 is increased in putative ES-CSCs it would be interesting to investigate the role of miR-210 in ES-CSCs using overexpression and knockdown studies. It would also be very interesting to evaluate the small molecule inhibitor of miR-210, Targapremir-210, on ES cells. Since this has interesting preclinical activity and selectivity in several cancer type (Costales et al., 2017). Functional studies are needed to validate the drivers of ES self-renewing ability to create a more informative biomarker panel to identify ES-CSCs.

The limitation and key finding:

Unlike RNA sequence, TLDA arrays consist of a limited number of PCR probes (Targets) and it is not possible to choose or change the targets which are included because it is pre-made commercial array. The key finding:

1- The expression of EBAF, ABCG1, miR-210 were confirmed in the putative ES-CS-like cells using RTqPCR and WB.

Chapter 4

The expression and role of ATP-Binding Cassette, Sub-Family G (WHITE), Member 1 (ABCG1) in ES family tumours

4.1 Introduction

ABCG1 also known as ABC8 or WHITE 1, controls cellular cholesterol homeostasis, which is essential for cellular functioning and survival (Ikonen, 2008; Tarr et al., 2009). The size of the full length of ABCG1 protein is 75-110 kDa (678 amino acids) (Tarr and Edwards, 2008). ABCG1 forms a homodimer to function (Gelissen et al., 2006; Kerr et al., 2011). However, ABCG1 can also form heterodimers with ABCG4 as these proteins sharing 72% of amino acids (Cserepes et al., 2004; Hegyi and Homolya, 2016).

ABCG1 is expressed in many different cell types, such as endothelial cells, lymphocytes and myeloid cells (Tarr et al., 2009). It is localized in the endoplasmic reticulum (ER) and Golgi (Wang, F. et al., 2013) and also predominantly in the plasma membranes in macrophages and other cell types (Vaughan and Oram, 2005). Moreover, ABCG1 is expressed at the cell surface where it regulates efflux of cholesterol from the cells (Wang, N. et al., 2006) and within intracellular vesicles that control cholesterol distribution inside the cell (Tarr and Edwards, 2008). More recently, ABCG1 has been identified in the cortical filaments (Pandzic et al., 2017).

In the human body, ABCG1 is involved in reverse cholesterol transport from tissues to the liver via the plasma. ABCG1 also effluxes the additional unneeded cholesterol from cells to high-density lipoprotein (HDL) particles (Wang, N. et al., 2004; Kennedy et al., 2005). Additionally, it can promote efflux of the excess cholesterol to low-density lipoprotein (LDL) and also to cyclodextrin (Wang, N. et al., 2004). ABCG1 is crucial for intracellular cholesterol transport (Sturek et al., 2010; Tarling and Edwards, 2011).

On other hand, ATP Binding Cassette Subfamily A Member 1 (ABCA1) and ABCG1 co-operate synergistically in the cellular efflux of cholesterol. According to the literature, it has been proposed that ABCA1 helps loading of lipid-poor apoA-I with cholesterol, as a result forming HDL, which is

removed by the ABCG1-dependent cholesterol efflux (Vaughan and Oram, 2006; Gelissen et al., 2006; Jessup et al., 2006; Oram and Vaughan, 2006).

In ABCG1 deficient mice, subcutaneous growth of B16-melanoma and MB49-bladder carcinoma cells are repressed and survival time was prolonged (Sag et al., 2015). Others studies have confirmed, in ABCG1-/- mice, that pulmonary macrophages store high levels of cholesterol and sterol esters as result of losing the function of ABCG1 (Kennedy et al., 2005; Out et al., 2006; Baldan et al., 2006; Baldan et al., 2008). The accumulation of cholesterol possibly produced a toxic effect that promoted apoptosis in lung cancer cells (Wojcik et al., 2008).

In addition to its role in regulating cellular lipid homeostasis, ABCG1 is reported to have several additional biological effects. For example, it was shown to be a migration and invasion promoter in lung cancer (Tian et al., 2017) and induces apoptosis in macrophages and other cell types (Seres et al., 2008). It is also known that ABCG1 controls the function of immune cells such as macrophages and it acts as a mediator of tumour immunity (Sag et al., 2015). In lung cancer ABCG1 is reported to play a role in lung cancer stem cells since it upregulated CD133 and ALDH1 expression (Tian et al., 2017). Also, overexpressing ABCG1 in HKULC4 lung cancer cells stimulated proliferation and upregulated the anti-apoptotic proteins such as BCL2 and MCL1 (Tian et al., 2017). Moreover, ABCG1 has been reported as a modulator of proliferation, migration, invasion, apoptosis and microRNA regulation in lung cancer (Tian et al., 2017). However, to the extent of our knowledge, the role of ABCG1 has not previously been studied in ES. The hypothesis of this chapter is ABCG1 promotes the self-renewal ability of ES-CS-like. It is expected to see decrease in self-renewal and CS-like phenotype when knock down ABCG1 or vice versa.

To help us test this hypothesis we need to:

1- Examine the expression level of ABCG1 protein in ES cell lines and other cell types.
2- Determine the biological effect of ABCG1 using knock-down and knock-in experiment.
3- Examine the consequence of hypoxia on the expression of ABCG1 protein.

4.2 Methodology

4.2.1 Cell lines and tissue culture

In this chapter, unless otherwise state all plastic ware were purchased from Corning®. ES family tumours cell lines including SK-N-MC, TTC-466 and were cultured, harvested and counted as described in (Section 2.2.1, 2.2.2 and 2.2.3 respectively). HEK-293 cell line (Gift from Professor M Knowles, LICAP, University of Leeds) cultured as substrate adherent cells in DMEM supplemented with 10% FCS and 2mM glutamine. Also, after thawing, HEK-293 were passaged at least twice before being used for the knockdown procedure. Hypoxic cells were prepared by incubation for 6 h in a hypoxic incubator (1.0% O_2; RS Biotech Galaxy R, UK). The starting time which equivalent to 0h was 6h length of incubation then cells were collected in different time points (24, 48, 72 and 96 h). Spheroids were formed as described in (Section 2.2.4.2.2).

4.2.2 Western blot

Proteins were extracted from cell lines and measured as described in (Section 2.2.5.2). Western blots were performed for ABCG1, HIF1, Glut1, β-actin and GRP-75 as described in (Section 2.2.5.2.3). For full details of antibody concentrations and suppliers see Appendix B.2.

4.2.3 RTqPCR

RNA was extracted from a panel of frozen cells pellets, substrate adherent cells and spheroids and then measured as described in (Section 2.2.5.3.1 and 2.2.5.3.2, respectively). The extracted RNAs were converted to cDNA and RTqPCR were performed as described in (Section 2.2.5.3.3 and 2.2.5.3.4, respectively) using ABCG1 as target gene and PPIA as housekeeping gene.

4.2.4 Flow cytometry

Mrs. Andrea Berry (senior research technician, LICAP, The University of Leeds) performed this experiment. She used the following protocol:

Cells were seeded at 2 x10^5 per well in 6 well plates. Following 48 h in culture, cells were harvested via trypsinisation as described in (Section 3.3.2). Antibody labelling was carried out using the BD Cytofix/Cytoperm™ Fixation/Permeabilisation Solution Kit (BD biosciences, UK). The cell pellet was re-suspended in 250µL of permeabilisation solution and incubated at 4°C for 20 min. Following incubation, cells were centrifuged at 405*g* for 5 min. Cells were then re-suspended in 1mL BD Perm/Wash™ Buffer and centrifuged at 405*g* for 5 min. The wash step was repeated then the cells were re-suspended in 100µL of normal goat serum (Sigma) diluted 1:10 in BD Perm/Wash™ Buffer and incubated at 4°C for 30 min. Following incubation, cells were centrifuged at 405*g* for 5 min. Cells were then re-suspended in 1mL BD Perm/Wash™ Buffer and centrifuged at 405*g* for 5 min. The wash step was repeated once then the cells were re-suspended in 50µL ABCG1 rabbit polyclonal antibody (Cat number PA5-13462, Thermo-Fisher Scientific), serial diluted from 100µg/mL to 400µg/mL were used for optimisation. The optimal concentration (400µg/mL) was used for analysis in BD Perm/Wash™ Buffer. Cells were incubated at 4°C for 1 h in the dark. Following incubation, cells were centrifuged at 405*g* for 5 min. Cells were then re-suspended in 1mL BD Perm/Wash™ Buffer and centrifuged at 405*g* for 5 min. The wash step was repeated once then the cells were re-suspended in 50µL of secondary antibody diluted in BD Perm/Wash™ Buffer (Goat anti-Rabbit IgG (H+L) Highly Cross-Adsorbed Secondary Antibody, Alexa Fluor 488 diluted to 4µg/mL, Cat number A11034 for optimisation and Goat anti-Rabbit IgG (H+L) Secondary Antibody, Alexa Fluor 405 Cat number A31556 diluted to 2µg/mL for analysis, Thermo-Fisher Scientific). The cells were incubated with secondary antibody at 4°C for 30 min in the dark. Following incubation, cells were centrifuged at 405*g* for 5 min. Cells were then re-suspended in 1mL BD Perm/Wash™ Buffer and centrifuged at 405*g* for 5 min. The wash step was repeated once then the cells were re-suspended in 1mL FACS buffer and analysed on the Attune®cytometer.

4.2.5 Examine the existence or absence of the internal 12 amino-acids (12aa) of ABCG1 in panel of cell lines

4.2.5.1 Reverse transcribed Polymerase chain reaction (RT-PCR)

Total RNA (1 µg) was reverse transcribed (RT) as previously described in (Section 2.2.5.3.3). The cDNA was combined with the reagents listed in (Table **4.1**) below and analysed by RT-PCR. Published primers were used to span the internal 12 amino-acids (12aa) variable region as previously described (Gelissen et al., 2010; Burns et al., 2013) (Figure 4.1). The AmpliTaq gold was activated by one cycle at 95 °C for 10 min and cDNA amplified for 35 cycles of 95 °C for 30 sec, 60 °C for 30 sec and extension at 72 °C for 1 min. This was followed by a further final extension at 72 °C for 7 min. PCR products were separated by size (Table 4.2) using 2% agarose gel electrophoresis as described in (Section 4.2.5.2).

	Reagent	Volume (µL)	Final concentration
ABCG1 mix	AmpliTaq Gold DNA polymerase (1U)	5	0.1U
	AmpliTaq Reaction Buffer II (1x)	0.25	0.005x
	F-primer (10µM)	1	200nM
	R-primer (10µM)	1	200nM
	RNase-free water	32.75	-
	Product from RT reaction	10	-
β_2-microglobulin mix	AmpliTaq Gold DNA polymerase (1U)	5	0.1U
	AmpliTaq Reaction Buffer II (1x)	0.25	0.005x
	F-primer (40µM) 5'- CTCGCGCTACTCTCTCTTTCT -3'	1	800nM
	R-primer (40µM) 5'- TGTCGGATTGATGAAACCCAG -3'	1	800nM
	RNase-free water	32.75	-
	Product from RT reaction	10	-

Table 4.1 List of components for amplifying ABCG1 (±12aa) using RT-PCR. F= Forward primer, R= Reverse primer and reverse transcription (RT).

Figure 4.1 Sequence Alignment of ABCG1 isoforms and primer location for amplification of the medial region (±12aa). 8F= forward primer on exon 8, 9F= forward primer on exon 9, 9/10F= forward primer spike exon 9 and 10, 11R= reverse primer on exon 11 (Gelissen et al 2010), 10R= reverse primer on exon 10 (Burns et al 2013), Isoforms numbers between bracket: isoform (1) = full length of ABCG1 and other numbers refer to other isoforms.

Primers	Sequence	Size of PCR products Base pair (bp)	
		Full length (+12aa)	All isoforms (-12aa)
8F 10R	5'- GAGGGATTTGGGTCTGAAC -3' 5'-AGGCAGCTGGCAGAGAAGC -3'	278bp	242bp
9F 11R	5'- AGACAAAACGATTAAAGGG -3' 5'-TGTCAGAACAGTAGGCATGAG -3'	300bp	No
9/10F 11R	5'- CTCTGAAGAGGACTCCTC -3' 5'-TGTCAGAACAGTAGGCATGAG -3'	No	279bp

Table 4.2 Size of the amplify ABCG1 isoforms using RT-PCR

4.2.5.2 Gel electrophoresis

Unless otherwise stated all reagents were purchased from Sigma. PCR products were separated by agarose gel electrophoresis. One hundred and fifty mL of 1x Tris-Borate-EDTA (TBE) (90 mM Tris, 90 mM Orthoboric acid, 2 mM EDTA, pH 8) were used to dissolve agarose (2%, w/v, Sigma-Aldrich). The mix was heated in a microwave and allowed to cool to 60°C before adding a DNA gel stain known as Nancy-520 (30µL of 5mg/mL). The agarose gel was mixed by swirling the flask gently and poured into a sealed ended tray (Horizon 20•25TM; Invitrogen). Combs were inserted into the gel and then the gel was allowed to set for 20-30 min at room temperature.

Before loading, 15 µL of sample was diluted in gel loading solution (6:1; 5.6 mM Orange G, 17.3 mM SDS, 0.4 mM Ficoll (Type 400), 0.4 mM Bromophenol blue). The tapes and combs were removed and the tray inserted into a Horizon 20•25TM agarose gel electrophoresis tank (Invitrogen). The PCR products (20µL) were mixed with loading buffer (10µL of Bromophenol blue) and then loaded into the wells and the gel was run in 1 x TBE at 80 V for approximately 2-3 h until the Bromophenol blue had migrated sufficiently through the gel. The gel was exposed to ultra-violet (UV) light on a Gel DOC XR (TM) Imaging System (Bio-rad; Hemel Hempstead, Hertfordshire) to visualise the PCR products.

4.2.6 Knockdown of ABCG1 experiments

4.2.6.1 Using short hairpin RNA (shRNA)

All infected cells were cultured in GM class II conditions for 10 days. Virus stock contains 1.0 x 10^6 infectious units of virus (IFU) of 3 ABCG1-specific constructs that encode 19-25 nucleotides (nt) (plus hairpin) in Dulbecco's Modified Eagle's Medium with 25 mM HEPES pH 7.3. Whereas, Control shRNA Lentiviral contains a construct encoding a scrambled nucleotide sequence. All Lentiviral Particles were from Santa Cruz Biotechnology, Inc. This method was optimized previously by Dr. Elizabeth Roundhill (Research follow, LICAP, University of Leeds). Uninfected cells were used as a second control.

4.2.6.1.1 Infection of cells with shRNA

In 25 cm^2 flasks, cells (SK-N-MC, TTC-466 and HEK-293) at 50% confluency were infected with 0.1 IFU of ABCG1 shRNA viral supernatant (20 µl; sc-41138V) or 0.05 IFU of control shRNA Lentiviral Particles (10 µl; sc-108080) in growth media containing 1 µg/mL hexadimethrine bromide (Polybrene®, Sigma-Aldrich). After 6h, the viral supernatant was discarded and replaced with normal growth medium. After overnight incubation in normal growth medium, the medium was replaced with medium containing puromycin (0.3µg/mL for SK-N-MC cells and 0.5µg/mL for HEK-293 and TTC-466 cells; Sigma-Aldrich) to select for cells transduced with the shRNA

vector. Cells were maintained in selection medium for at least a week. Cells were harvested for protein and RNA extraction after a minimum period of 72h post selection to check for an early knockdown and also at week 1, 2, and 3 after selection. Western blot and/or RTqPCR were performed to check the level of ABCG1.

4.2.6.2 Small interfering RNA (siRNA)

All reagents were purchased from Dharmacon unless otherwise stated. Cells were harvested and counted as described in (Section 2.2.2 and 2.2.3 respectively) and $5x10^3$ cells seeded in normal growth media into wells of a 96 well plate). A 100 µM siRNA solution was prepared in 1x siRNA Buffer by diluting 5x buffer using RNase-free water. The siRNA was supplied in lyophilised form and re-suspended according to the manufacturer's instructions using 1x siRNA Buffer. Seeded cells were incubated overnight to allow them to adhere to the bottom of the flask. In order to determine the optimal concentration to be used, wells were treated with different conditions following removal of the ES medium:

1) Cells grown in a normal ES medium

2) Cells grown in Accell medium

3) Cells infected with Accell Non-targeting Pool (1.5 µM each well in Accell media; D-001910-10-20) control.

4) Cells infected with different concentrations (0.5-1.5 µM) of 1x SMARTpool ABCG1 siRNA (E-008615-00-0005) in Accell media.

Cells were incubated at 37ºC in 5% CO_2; 95% air for 72 h. To evaluate the level of cell death, cells were harvested and counted using trypan blue exclusion assay as described in (Section 2.2.3). To evaluate the RNA reduction, 3x wells for each condition were combined and then RNA extracted and RTqPCR performed for ABCG1 and PPIA as housekeeping control. Following optimisation of the concentration of ABCG1 siRNA to achieve maximum knockdown of ABCG1 with minimal cell death, 96 well plate were prepared as above using the optimal concentration (1 µM) of

ABCG1 siRNA. Cells were collected at different time points (48-96h) and the level of cell death was evaluated in addition to expression of ABCG1 RNA level as described above.

4.2.7 Overexpression of ABCG1 (Knock-in cells)

Cells overexpressing ABCG1 were generated by Dr. Roundhill. The details of the protocol used are described below (Section 4.2.7.1 – 4.2.7.4).

4.2.7.1 Synthesis of the ABCG1.Lenti7.3/V5-DEST™ and Lenti7.3/V5-DEST™ control plasmid.

ABCG1.Lenti7.3/V5-DEST™ was generated by GeneArt™ Services (Thermo Fisher). Briefly, ABCG1 cDNA was synthesised and was surrounded upstream 5'-3' by the attB1 site, the SalI restriction enzyme site and the Kozak consensus sequence (CCACC; immediately preceding the ATG start codon), and downstream by the XhoI restriction enzyme site and finally the attB2 site. The ABCG1 cDNA was cloned into the Gateway®-adapted ViraPower™ HiPerform™ lentiviral expression vector, pLenti7.3/V5-DEST™ (Thermo Fisher) at the corresponding gateway 5' attL1 and 3' attL2 sites. Successful sub-cloning of the ABCG1 sequence into pLenti7.3/V5-DEST™ was confirmed by sequencing (GeneArt™ Services) (Figure **4.2**).

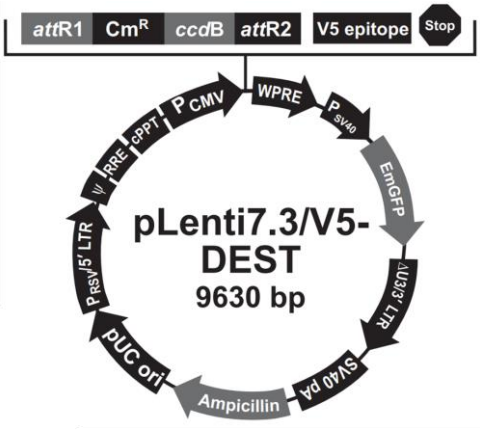

Figure 4.2 The vector map illustrates the elements of pLenti7.3/V5–DEST Gateway® vector that used to knock-in ABCG1 gene

To produce the Lenti7.3/V5-DEST™ plasmid only control, ABCG1 was released from the plasmid backbone by restriction enzyme digest at the SalI and XhoI sites (New England Biolabs Inc., MA, USA). The sticky ends of the plasmid were then blunted using DNA Polymerase I, Large (Klenow) Fragment (1µg of DNA dissolved in 1x NE Buffer supplemented with 33µM dNTPs and 1 unit of Klenow for 15min at 30^{o}C; New England Biolabs Inc.) and the reaction terminated by adding EDTA (10mM for 20min at 75^{o}C; Fisher Scientific). The plasmid was self-ligated using T4 DNA Ligase (50ng of DNA dissolved in 1x T4 DNA Ligase Buffer and 1µL of T4 DNA Ligase and DNase and RNase free water added to a total volume of 20µL; New England Biolabs Inc.). XL-1 Blue Competent Cells (Stratagene, CA, USA) were transformed with 1µg of vector DNA and plated onto Luria Bertani (LB) Agar Medium (MP-Biomedical) containing ampicillin (100µg/mL; Sigma-Aldrich) overnight at 37^{o}C to allow the growth of plasmid containing XL-1 Blue Competent Cells. Colonies were picked by sterile plastic loop and individually incubated overnight at 37^{o}C in LB Medium containing ampicillin (100µg/mL). To determine which colonies contained the Lenti7.3/V5-DEST™ ligated plasmid, DNA was isolated from cell colonies (QIAprep Spin Miniprep Kit, Qiagen), digested using the restriction enzyme NcoI (New England Biolabs Inc.), and the size of the resulting DNA products examined by agarose gel electrophoresis (section 5.2.5.3). As predicted, DNA extracted from cell colonies containing the Lenti7.3/V5-DEST™ digested with the NcoI enzyme generated DNA products of 5221bp, 1463bp, 894bp and 409 bp. Colonies identified as containing the plasmid in LB agar medium (100µL) were then incubated with 200mL of LB agar medium containing ampicillin (100µg/mL) overnight at 37^{o}C and the DNA purified (HighSpeed Plasmid Maxi Kit, Qiagen) to generate a working stock of Lenti7.3/V5-DEST™ DNA. To confirm the complete Lenti7.3/V5-DEST™ plasmid sequence was retained following the removal of ABCG1, sequencing of the DNA was performed by Source Bioscience (analysing 500ng of DNA with Lenti7.3/V5-DEST™ 5’ -3’ forward (AGTGTGGTGGAATTCTGCAG) and reverse primers (TAGGGATAGGCTTACCTTCG); Sigma-Aldrich).

4.2.7.2 Production of lentiviral particles

All GM Class II work described in this thesis are carried out as described in the activity notification GM559/11.2. HEK293T cells were harvested (Section 3.3.2), seeded at a density of 1.5 x10^6 cells per 75cm^2 flask and incubated overnight to allow the cells to adhere. Following this, a transfection mix containing 1mL of serum free DMEM, 3µg of the target plasmid, 3µg of the lentiviral packaging plasmid pCMV-dR8.2dvpr and 600ng of the envelope plasmid pCMV-VSV-G (both a gift from Professor M Knowles) was prepared and mixed by gentle pipetting. TransIT®-293 (24µL; Mirus Bio, supplied by Fisher Scientific) was then added to the transfection mix and incubated at room temperature for 30 min. The transfection mix was then added dropwise to the HEK293T cells (at 50-70% confluency) and the cells incubated overnight (16 h). The medium was replaced with complete DMEM (13 mL) and the cells incubated for 24 h to allow lentiviral production. Following this, the medium containing lentiviruses was collected and replaced with a second 13 mL of complete DMEM for 24 h and the lentivirus collected once again. The lentiviral supernatants were then pooled (26 mL), filtered (0.45µm; Pall Corporation supplied by SLS), aliquoted (1.5mL) and stored in polypropylene 1.5mL tubes (Starstedt, Numbrecht, Germany) at -80^{o}C under GM Class II conditions.

4.2.7.3 Infection of SK-N-MC cells with ABCG1.Lenti7.3/V5-DEST™ or Lenti7.3/V5-DEST™ lentiviral particles

SK-N-MC cells at 50% confluency were infected with lentiviral supernatant as previously described (Tomlinson, D.C. et al., 2005; Roundhill and Burchill, 2012). Infected cells were cultured in GM class II conditions for 10 days. To confirm the uptake of ABCG1.Lenti7.3/V5-DEST™ or Lenti7.3/V5-DEST™, EmGFP expression was determined in infected SK-N-MC cells by flow cytometry using the Attune® Acoustic Focusing Cytometer (Applied Biosystems).

4.2.7.4 Cell sorting of ABCG1.Lenti7.3/V5-DEST™ and Lenti7.3/V5-DEST™ infected SK-N-MC cells

The positivity of EmGFP was assessed using flow cytometry as described in (Section 2.2.5.4) then sorted using FACS as described in (Section 2.2.4.3.2). The cells were sorted based on EmGFP expression and the observed number of cells was 1.5 x10^5 ABCG1 cells and 5 x 10^5 Lenti control cells.

4.2.8 Immunohistochemistry (IHC)

The generated spheres were processed and sectioned as described (Section 2.2.5.5.1). Sections were stained with ABCG1 antibody (detail Appendix C.1.3) at 1:50 dilution using three-stage peroxidase method described (Section 2.2.5.5.3). Slides were scanned using the Aperio AT2 (Lieca biosystem, UK) which is one of the whole slide imaging (WSI) systems, which scan the glass slides in order to produce digital high resolution slides. The analysis step was carried out using the Aperio ImageScope™ viewer, which includes the positive pixel count algorithm. In Aperio ImageScope™ viewer, scanned slides were viewed and some spheroids were selected for analysis based on the shape of spheroids and the existing of the necrotic core which indicate that the selected spheroid was showing the middle section of the spheroid. The size of spheroids was measured by drawing a number of diameters (n=6) using ruler tool and then average them for accuracy. Regions were designated for analysis using the pen tool. The positive pixel count v9 was used for analysis. The analysis results were confirmed and exported as excel file. The diagram below illustrated the analysis steps (Figure 4.3).

4.2.9 Statistics

Analyses were undertaken using the GraphPad Prism 7 software. Data were analysed by ANOVA when comparing 3 or more conditions or cell lines. Variation between means of all conditions or cell lines were compared using Bonferroni's post hoc multiple comparison test and differences were considered significant at $p<0.05$.

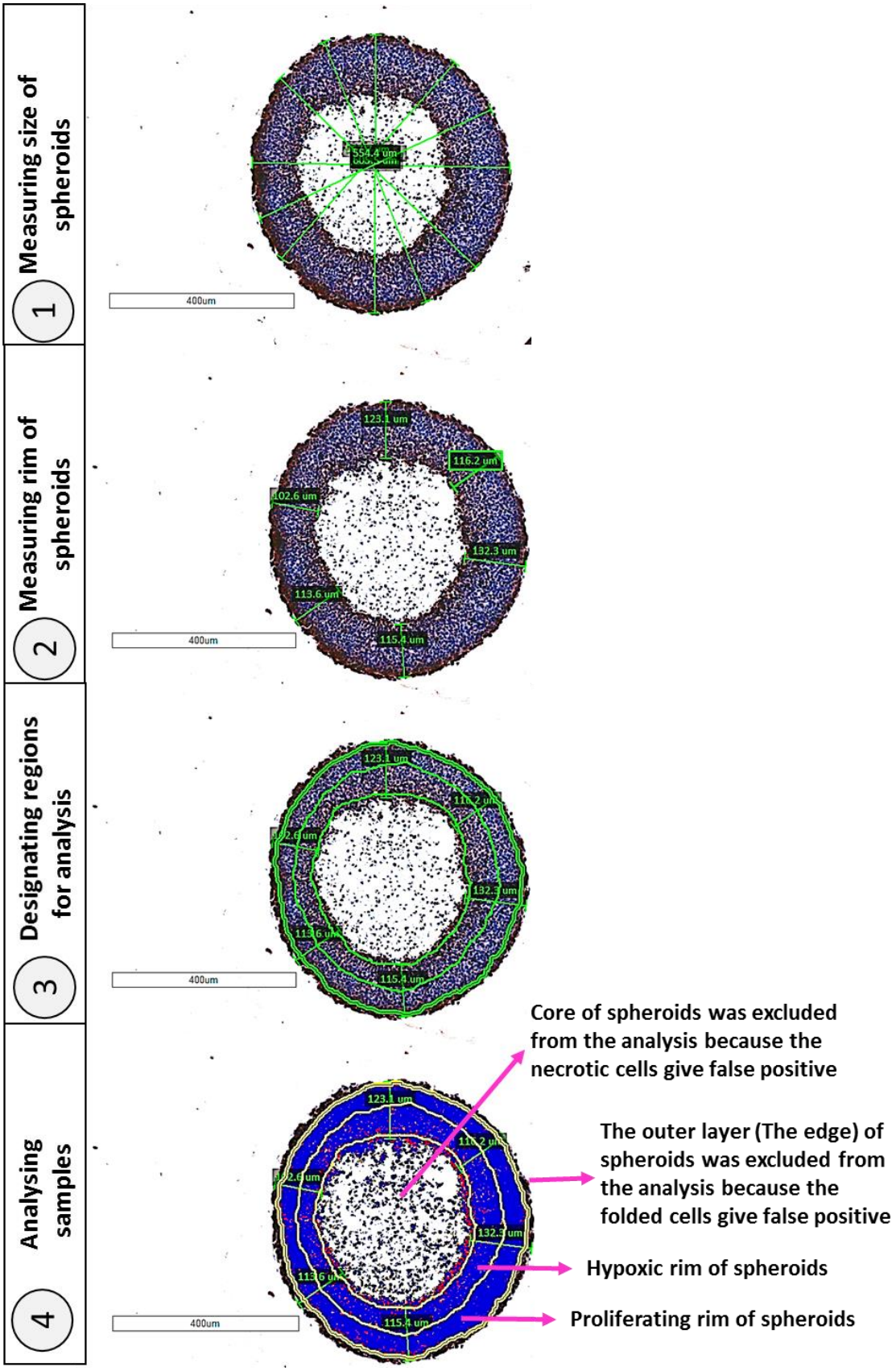

Figure 4.3 Method of IHC analysis of spheroids. Spheroids were analysis using Aperio ImageScope™ viewer following the steps as described from step 1-4.

4.3 Results

4.3.1 Expression profile of ABCG1

4.3.1.1 Expression of ABCG1 mRNA by RTqPCR

The expression of ABCG1 mRNA was determined in three cell lines; SK-N-MC, TTC-466 and SHEF4 (Figure **4.4**). There was significant difference between expression in the TTC-466 cells and the other two cell lines ($p<0.01$). SK-N-MC cells expressed ABCG1 to approximately the same level as the positive control cells SHEF4.

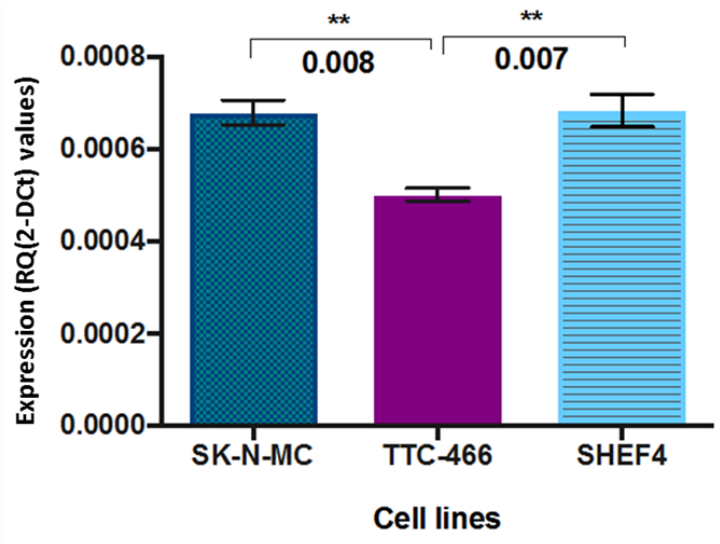

Figure 4.4 The expression of ABCG1 at mRNA level using RTqPCR. SK-N-MC and TTC-466, ES cell lines. SHEF4, neural crest cells (positive control). PPIA used as reference gene and the significant difference demonstrated by p-value. Data were analysed by ANOVA and error bars were stander deviation (SD).

4.3.1.2 Identification of ABCG1 isoforms in ES cell line and other tumour and normal cell lines

Two isoform of ABCG1 have been identified and confirmed at the RNA level. The main difference between the two isoforms is the length of exon 9. The isoform missing 12 amino-acids (12aa) at the end of exon 9, whereas the full length has the 12aa (Burns et al., 2013). Furthermore, five additional ABCG1

isoforms have been described and were freely available database at the NCBI.

Three different primer sets (Section 4.2.5.1) have been used in SK-N-MC, TTC-466 and BE(2)C (Figure **4.5**; one primer set is presented other not shown). Then these primer sets have been used to confirm the presence or absence of the 12aa in a panel of cell lines (Figure **4.6**). All ES cells express the full length and the 12aa missing isoforms which would be isoform 2, 3, 4, 5 or 6. The expression of the full length of ABCG1 and its isoforms were detected at low level in RD-ES and SK-ES1 comparing to other ES cell lines. Like ES cell line, all NB cell lines expressing ±12aa isoforms higher than the expression in SK-N-SH cell line. Moreover, human rhabdomyosarcoma (RH30) and human promyelocytic leukemia cells (HL60) showed a low level of ABCG1 ±12aa isoforms isoforms comparing to the expression level in OST cell lines, MCF7 and HEK-293 cell lines (Figure **4.6**).

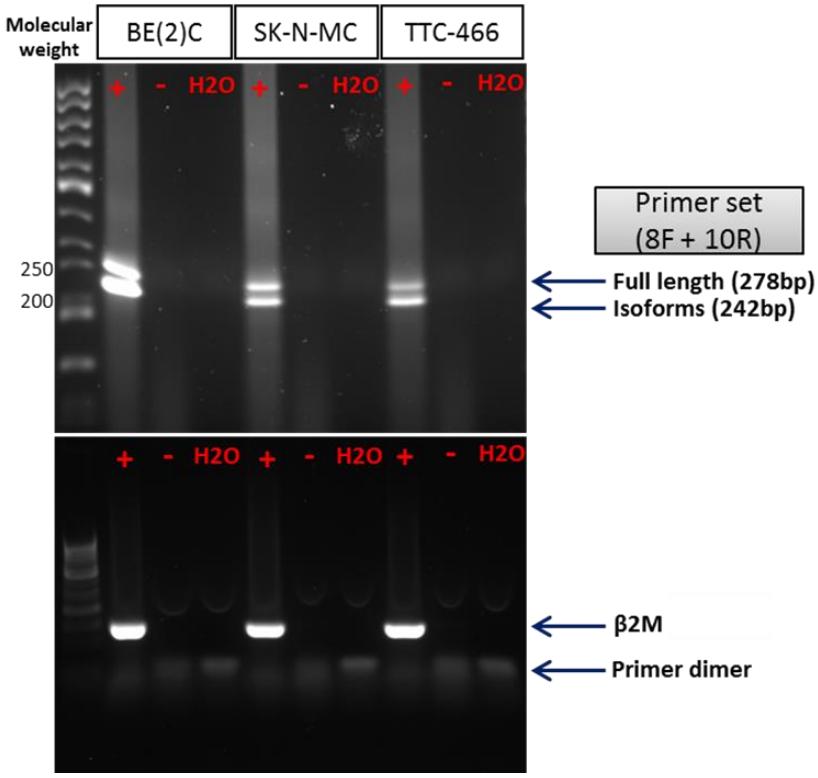

Figure 4.5 The existing and/or missing of 12aa using primer set (8F+10R). Contrasting to the full length, all ABCG1 isoforms missing the 12aa on exon 9. This primers set spike the end of exon 8 to exon 9 to show the presence or absence of both or either full length and/or isoforms. + = RT reaction that resulted in RT-PCR product. Two negative control used (-) and water (H2O). β2M= β_2-microglobulin used as positive control for RT-PCR reaction. bp= base pairs.

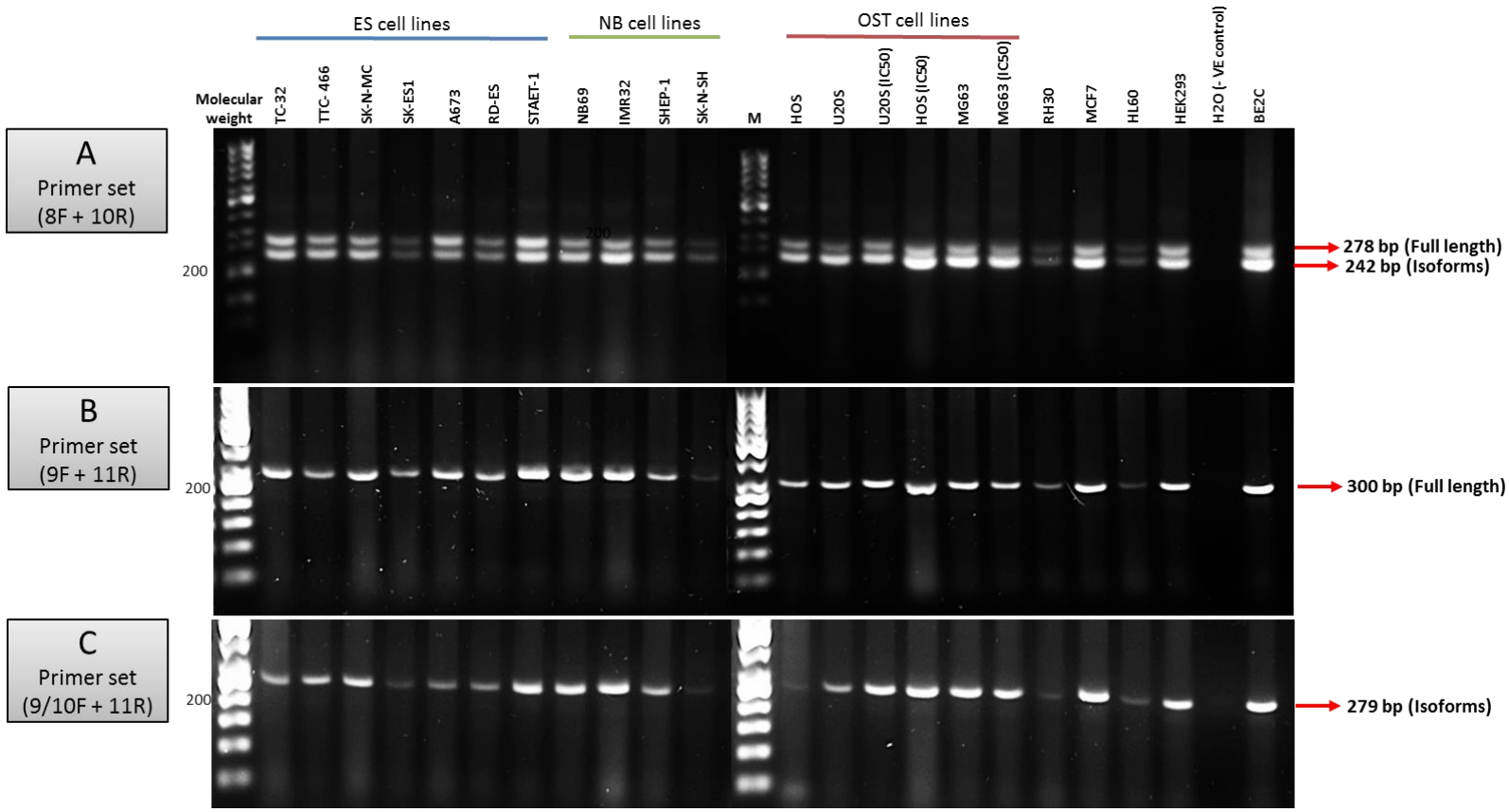

Figure 4.6 Confirm the existing and/or missing of 12aa using three different primer sets.. The key important way to distinguish between the full length and ABCG1 splice variant is checking the middle part of the gene. Unlike the full length, all ABCG1 isoforms missing the 12aa. Three specific primers set have been used (Section 5.3.5.1; Table 5.2) to spike the end of exon 9 to show the presence or absence of both or either full length and/or isoforms. A) Specific primers (8F +10R) were used to confirm the full length and isoforms. B) To confirm the existence of the full length only 9F+11R were used. C) Isoforms were detected using 9/10F +11R primers. bp= base pairs.

- 179 -

4.3.1.3 Expression of ABCG1 protein by western blot

Expression of ABCG1 protein has not previously been described in ES. A band of 100 kDa corresponding to the predicted size of the ABCG1 protein was detected in all ES cell lines, osteosarcoma and a number of other cell lines such as MCF7, HEK-293 and Human embryonal carcinoma (N2102EP) (Figure **4.7**). Expression of β-actin and GRP75 were used to confirm equal loading of protein. The level of ABCG1 in MCF7, HEK-293 and N2102EP was low. In the ES cell lines, TTC-466, A673 and RD-ES ABCG1 was highly expressed compared with the other ES cell lines. ABCG1 expression was low in HOS comparing with U20S and MG63 in the osteosarcoma cell lines.

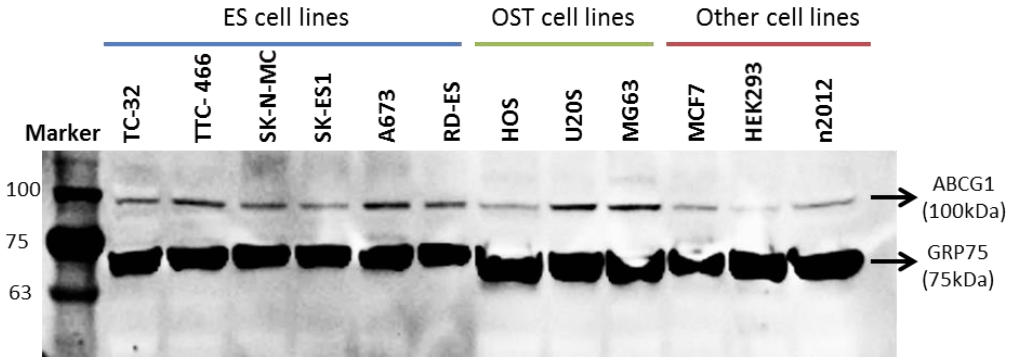

Figure 4.7 ABCG1protein expression determined by western blot inES and other cell lines.. Total protein was extracted from ES, osteosarcoma (OST) and other cell lines. The figure shows expression of ABCG1 in 50ng of protein extract determined by western blot. GRP75 and β-actin were used to check for equal amounts of protein (control).

4.3.1.4 Analysis of ABCG1 protein expression by flow cytometry

Antibody dilution optimisation for flow cytometry was carried out on the positive control cell line HEK293. The ABCG1 antibody was serially diluted from 50 to 400µg/mL and labelled using the protocol above (section 5.3.4). The level of fluorescence observed increased with increasing concentration of primary antibody. Minimal fluorescence was observed when the primary antibody was omitted. Dilution of antibody at 400µg/mL was chosen as the optimal dilution (Figure **4.8**).

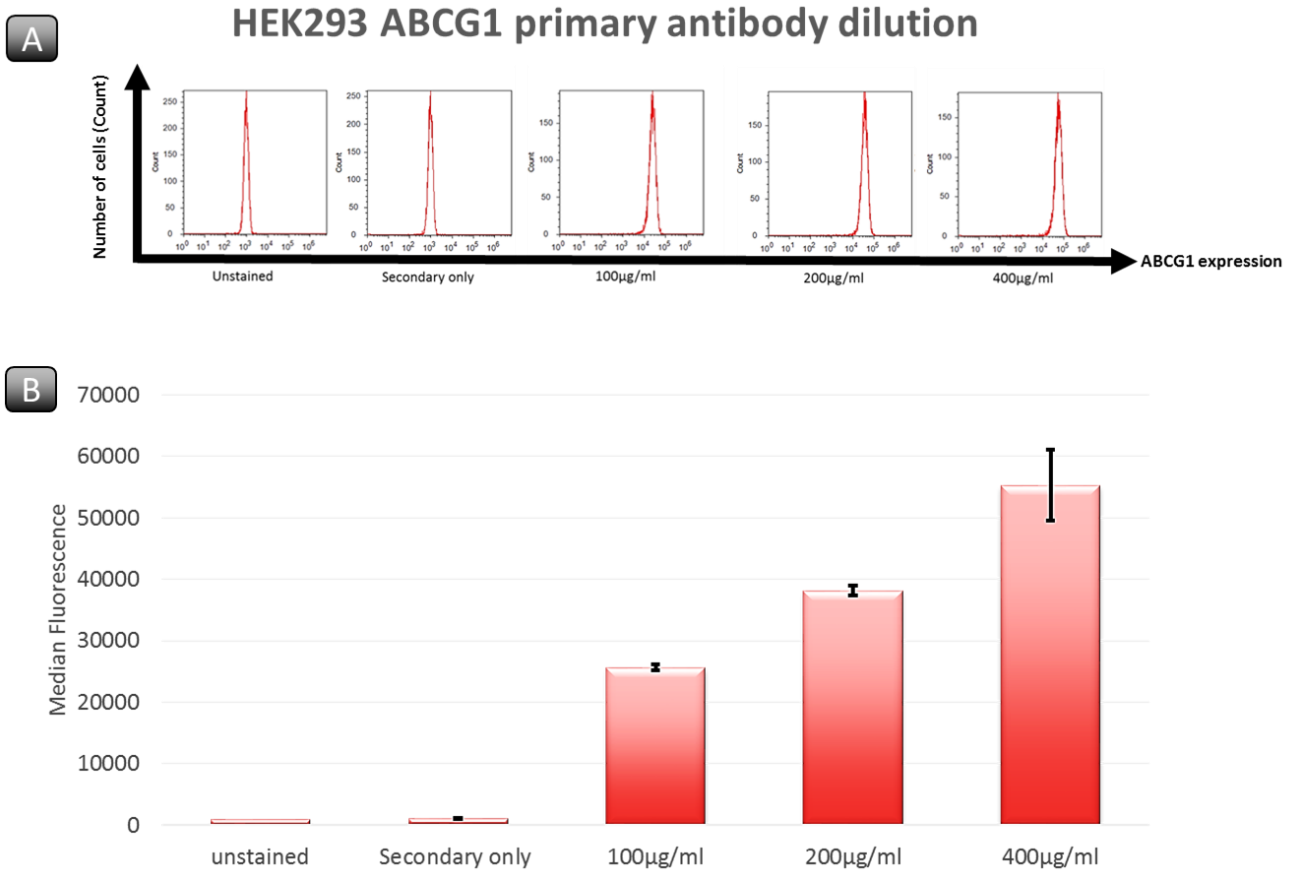

Figure 4.8 Titration of ABCG1 antibody in HEK-293 cell lines determined by flow cytometry. A) Representative fluorescence plots of unstained cells and cells stained with secondary only as well as serial dilutions of ABCG1 antibody (100-400µg/mL). B) Median fluorescence of cells in different conditions (as shown in A). Results are presented as the mean of three independent replicates. Error bars were stander deviation (SD).

-181-

The concentration of ABCG1 that was required for flow cytometry was optimized Mrs Andrea Berry (Figure **4.8**). HEK-293 cells were used as a positive control and the expression of ABCG1 was examined on SK-N-MC cell lines because SK-N-MC spheroids showed an increase in ABCG1 protein and RNA comparing with substrate adherent cells (Chapter 3; section 3.3.2.4). In agreement with results observed by western blot, flow cytometry result confirms that SK-N-MC cells express higher levels of ABCG1 protein than HEK-293 (Figure **4.9**).

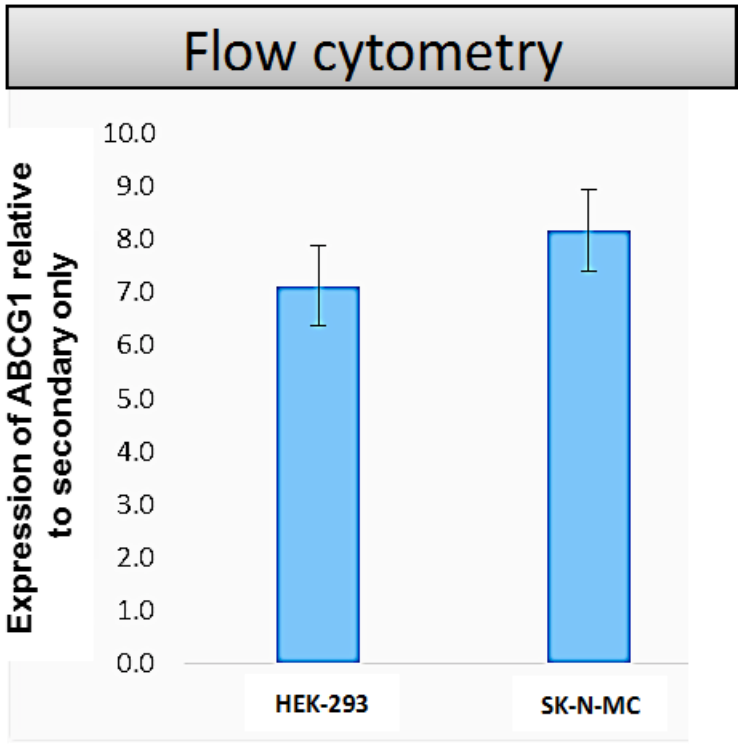

Figure 4.9 ABCG1 expression in SK-N-MC and HEK293 cell lines determined by flow cytometry. The expression level of ABCG1 was calculated relative to the secondary only in ES cell lines. t-test was performed. Results are presented as the mean ± standard deviation of three independent replicates.

4.3.2 Knock-down of ABCG1 using two different approaches

The shRNA is a siRNA sequence expressed from plasmid DNA or from virus-derived constructs and delivered to the nucleus of cells. In 2002, the effectiveness of shRNA was reported for the first time (Paddison and Hannon, 2002). The beneficial effect of siRNAs is transient (few weeks

maximum), whereas, shRNAs expression is more sustained (months) (Tsujiuchi et al., 2014). The two approaches, shRNA and siRNA were used to knock-down ABCG1 protein. The knock-down using siRNA was used in SK-N-MC only. On the other hand, shRNA was performed in three different cell lines (2xTTC-466, 1xSK-N-MC and 1xHEK293)

4.3.2.1 Optimization and effect of ABCG1 knock down by siRNA

The SMARTpool siRNA against ABCG1 is provided with 4 individual molecules. The specificity of which were checked using BLAST database and location within ABCG1 protein of each siRNA was identified (Figure **4.10**).

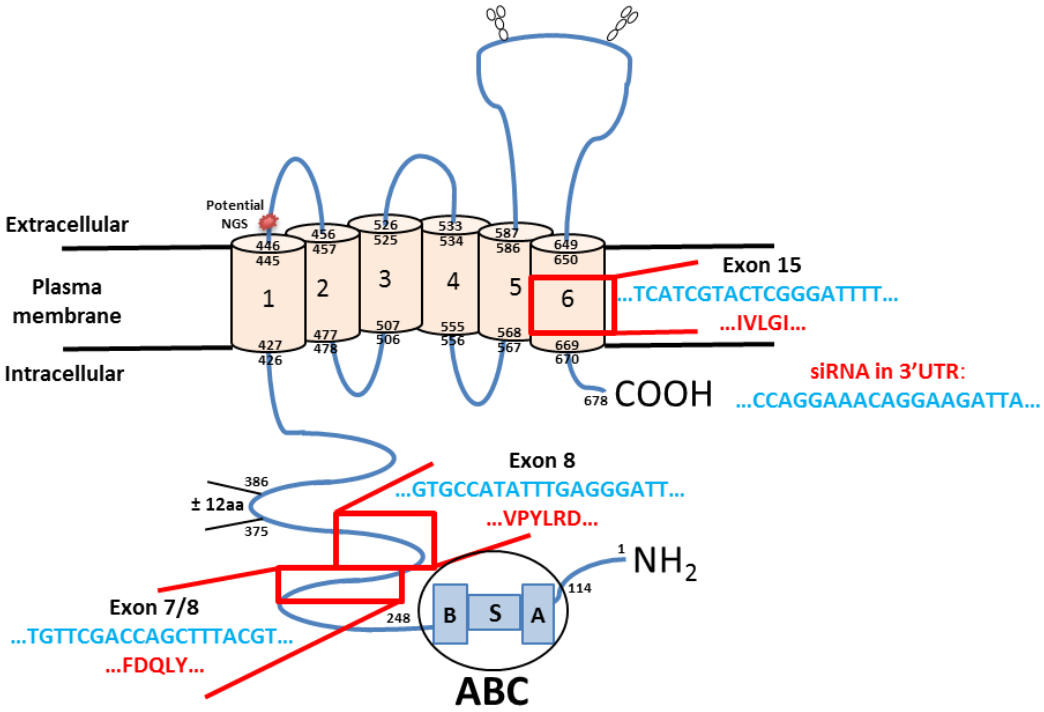

Figure 4.10 The region of ABCG1 in which the four ABCG1 siRNA sequences bind. Each siRNA sequence, the blue and red text showing mRNA and protein sequence respectively in exon 7/8, 8 and exon 15. One of the shRNA bind against the 3' UTR of ABCG1.

Incubation with increasing concentrations of siRNA (24-72h; 0.5-1.5µM) was not toxic for the cells (Figure **4.11**). The number of dead cells was not high;

however, there was a reduction in cell proliferation (Figure **4.12**). At 72 h, there was no significant different between the viable cell number that grow in ES media, which contains 10% serum and cells which grew in Accell medium, which is serum free. There was, however a significant reduction in viable cell number between cells infected with scrambled siRNA (-ve control) and cells incubated with 1μm of ABCG1 siRNA for 72h (p value = 0.02).

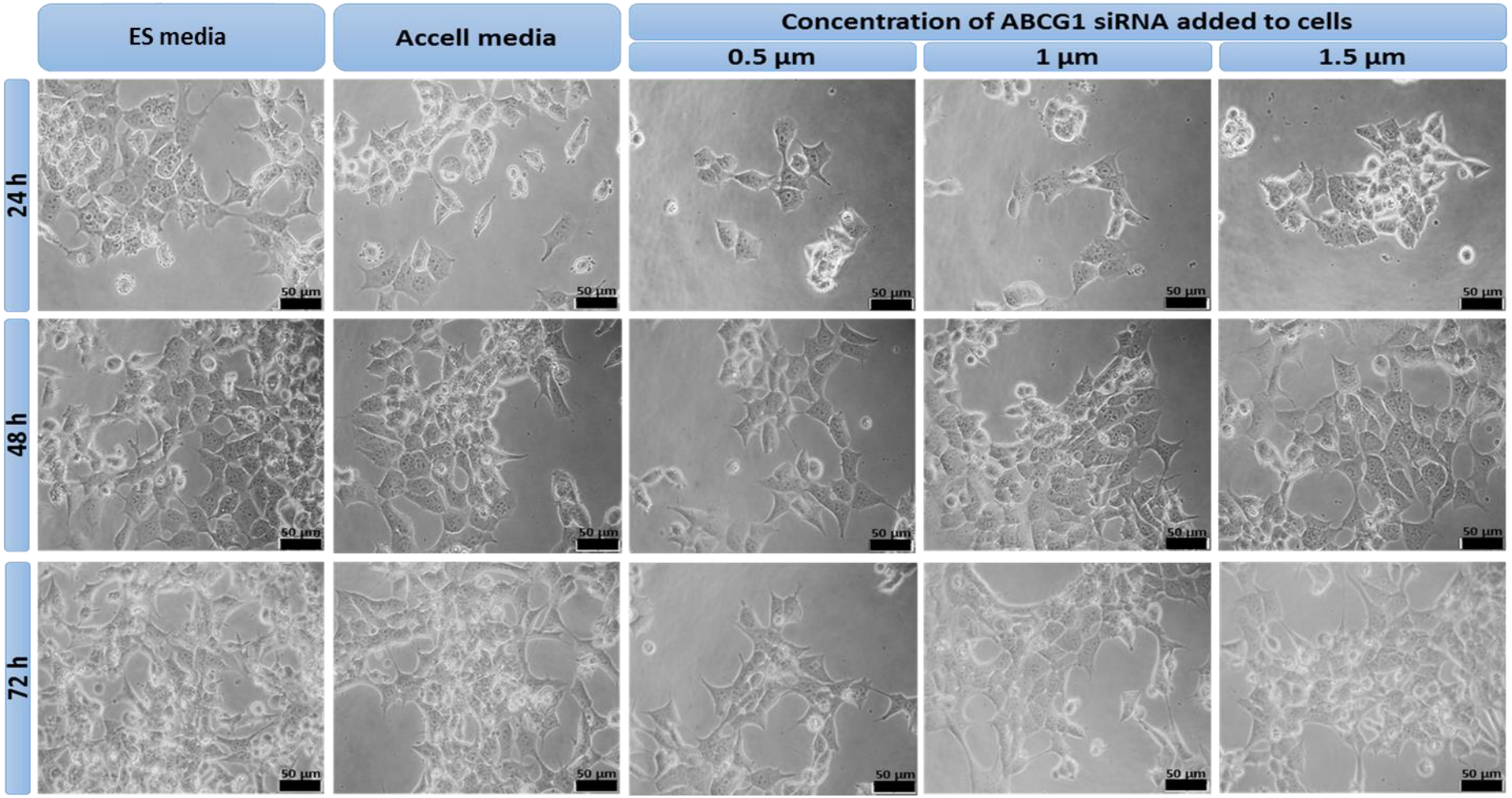

Figure 4.11 Morphology of SK-N-MC in ES medium and Accell conditions. Like cells in ES media, cells in Accell medium and cells infected with different concentrations (0.5-1.5 µM of siRNA ABCG1) maintained a similar morphological appearance. The scale bar is 50 µm.

-185 -

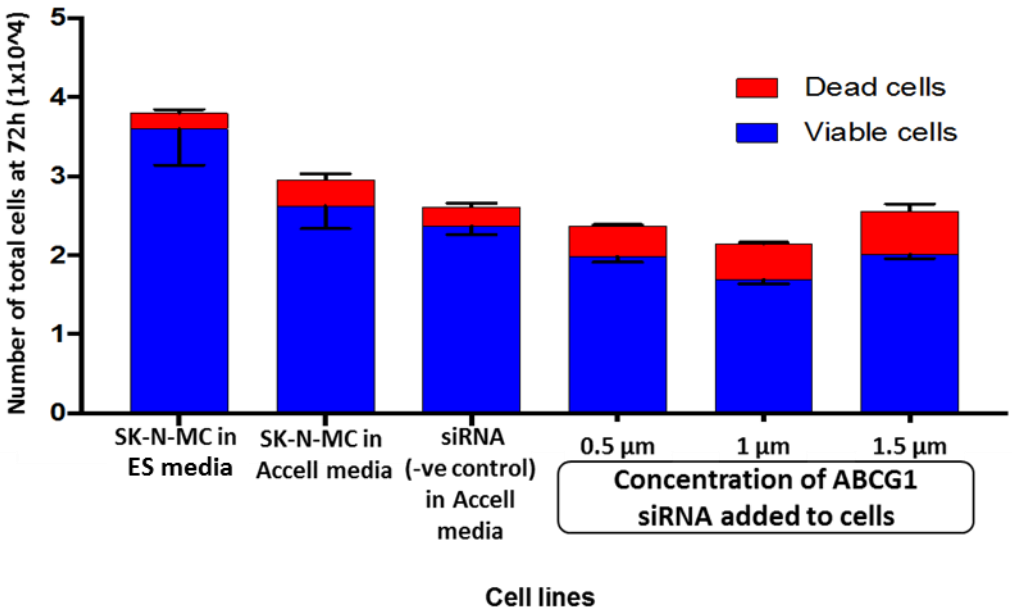

Figure 4.12 The total cell number after 72h incubations with siRNA. Cells were either gown in ES media or grown in Accell media (serum free media) or in the presence of siRNA control (1.5 µM) or siABCG1 at 0.5 µM, 1 µM and 1.5 µM. infected with –ve siRNA control and 3 different doses of siRNA ABCG1. Cells counted by haemocytometer. ANOVA was performed. Results are presented as the mean ± standard deviation of three wells.

At 72h, the level of ABCG1 mRNA was checked (Figure **4.13**). There was a reduction of ABCG1 mRNA in most conditions relative to –ve control. For example, incubating cells with –ve control led to an increase in ABCG1 expression and the expression level of ABCG1 in SK-N-MC that grow in normal condition in ES media appear as reduced. There was a reduction in ABCG1 expression level in cells incubated in Accell media. This might have resulted from switching off ABCG1 because cells are growing in serum free media, that have low/zero level of lipid, and don't need to efflux lipid from inside cells to the medium. The decrease of ABCG1 expression was similar when cells were incubated with 0.5 µM or 1.5 µM siRNA, although the greatest reduction was observed when the 1µm concentration was used for 72h. This siRNA is not showing a concentration dependent effect.

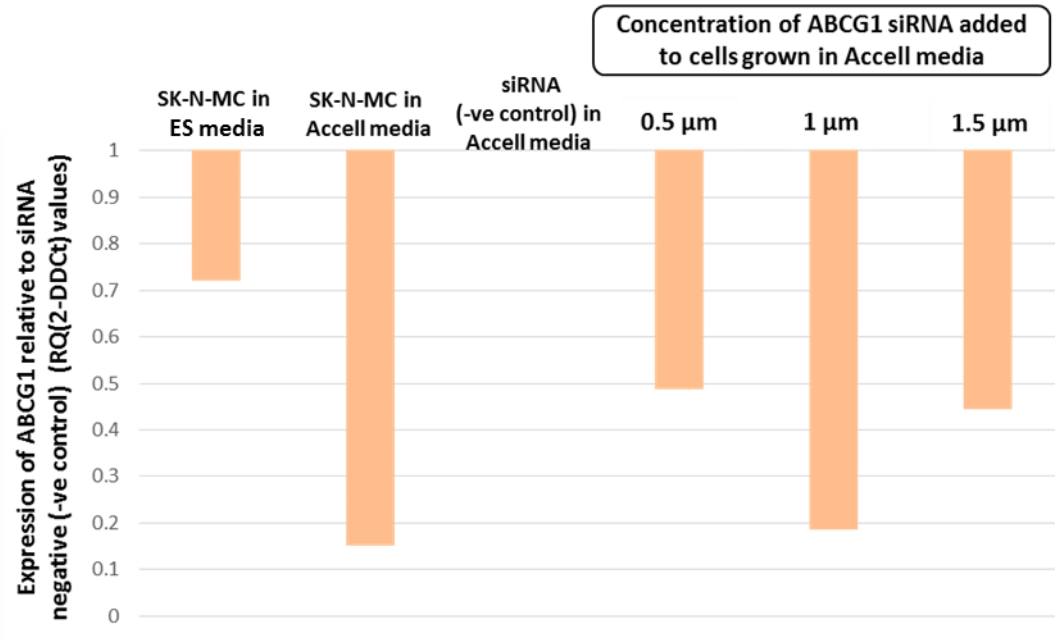

Figure 4.13 RNA expression level of ABCG1 following transfecting cells with siRNA. Cells were grown in ES media, in Accell media, infected with –ve siRNA control in Accell medium and 3 different concentrations of siRNA ABCG1 in Accell medium. Cells incubated for 72h and then RNA extracted to perform RTqPCR using ABCG1 assay on demand. (n=1; each condition 3 wells).

The optimal concentration (1 µM) was used and the effect of this concentration on the viable cell number was determined over time (Figure **4.14**). Between 48-72h, there was a gradual increase in viable cell number in cells grown in ES media and the well was full of cells at 72h. At 96h, cells were growth inhibited as they had reached confluency. This led to cell death and a decreased in viable cell number. When cells were maintained in Accell medium, the viable cell number remained almost the same at 48h and 72h, whereas the majority of cells died at 96h. Cells death at 96h might resulted from starvation as cells were grown in serum free media. The viable number of cells incubated with the –ve siRNA control followed a similar trend as cells cultured in Accell medium with a reduction in viable cell number and cell debris which was not count as dead cells at 96h. However, cells incubated with 1 µM of siRNA-ABCG1 displayed almost same viable cell number at 48h and 72h.

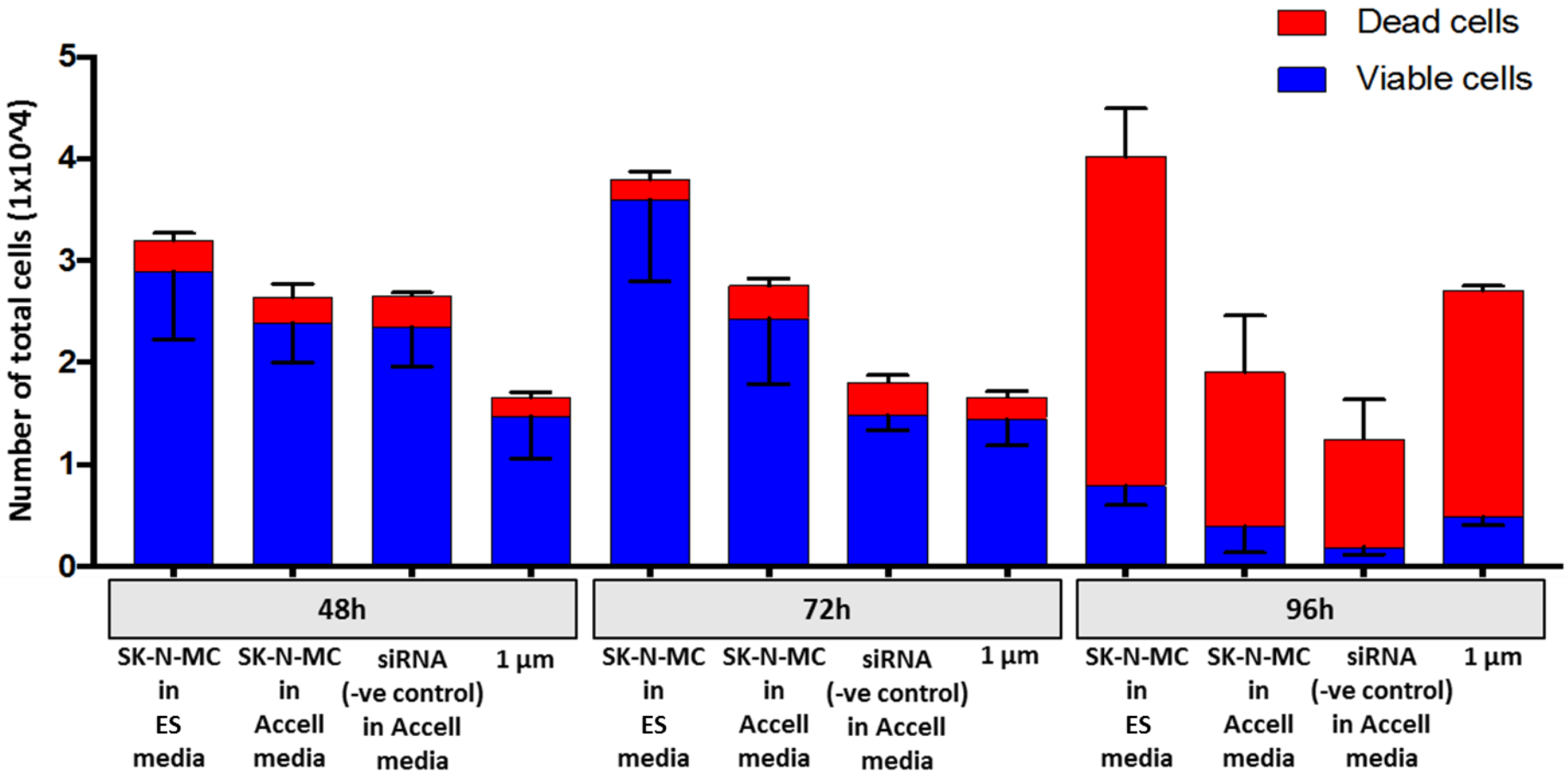

Figure 4.14 The total cell number of 48h to 96h post transfection. Cells were grown in ES media, in Accell media, infected with –ve siRNA control in Accell media and the optimal concentration of siRNA ABCG1 (1 µm) in Accell media. Viable cell number was counted using the trypan blue exclusion assay and neubauer haemocytometer. Results are presented as the mean ± standard deviation of three wells for each time point.

-188 -

4.3.2.2 Permanent knockdown using shRNA constructs

Three target specific shRNA constructs were used. The sequence of each of the 3 constructs was checked for specificity and location within the ABCG1 protein (Figure **4.15**). When checking against the blast database, two of shRNA sequences were confirmed to be specific and to target ABCG1 only, however, the third shRNA, which was located in exon 6, targeted both ABCG1 and ABCG4. ABCG1 and ABCG4 in the region of siRNA in exon 6 were 100% identical and the expected value (E-value) equal 0.28.

In all cell lines tested (TTC-466, SK-N-MC and HEK293), there was no reduction in the level of ABCG1 protein after treatment with shABCG1 (TTC-466; Figure **4.16** B). However, there was a reduction in ABCG1 mRNA at week 1 and 2 and then an increase of ABCG1 mRNA at week 3 (TTC-466; Figure **4.16** A). SK-N-MC that collected at week 3 as well as HEK-293 at week 1 illustrated a reduction in the expression of ABCG1 mRNA comparing to shControl (Figure **4.16** C).

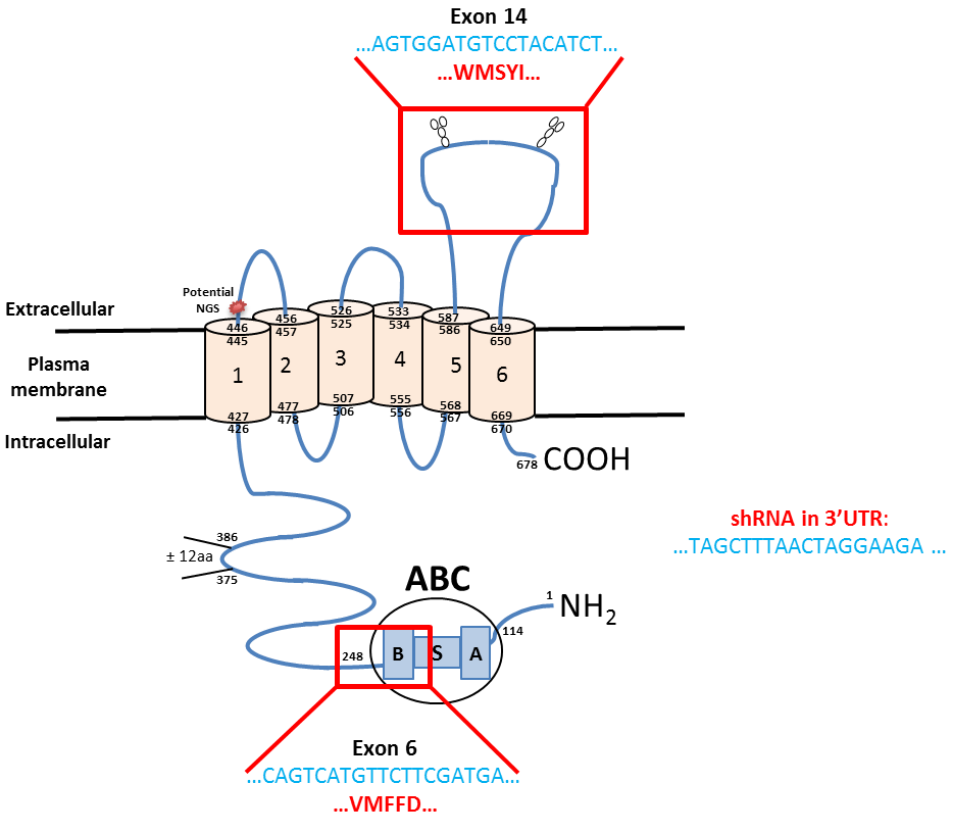

Figure 4.15 The region of ABCG1 in which the three ABCG1 shRNA sequences bind. Each shRNA sequence, the blue and red text showing mRNA and protein sequence respectively in exon 6 and exon 14. One of the shRNA bind against the 3' UTR of ABCG1.

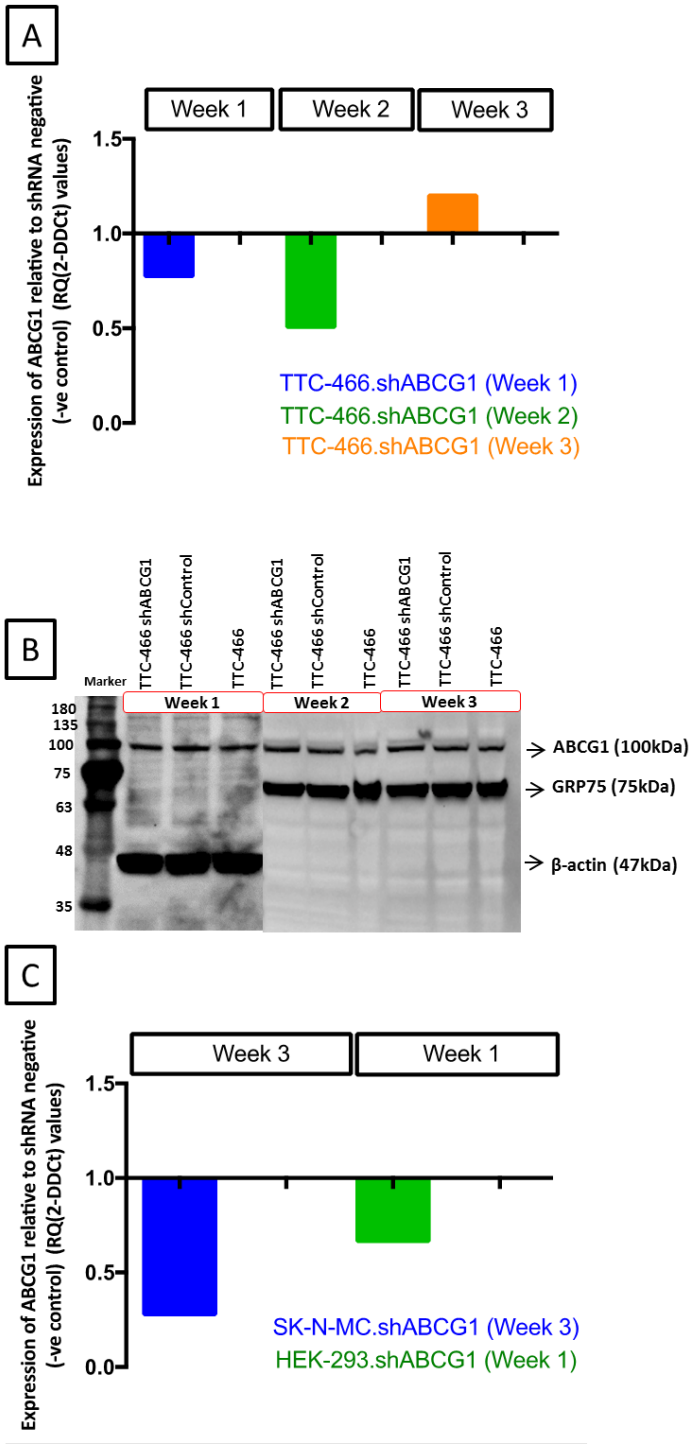

Figure 4.16 The effect of shRNA on the expression level of ABCG1 in the TTC-466 cell line. Cells were transduced with shRNA targeting ABCG1 as well as a negative control (shControl). Cells collected at different time points, after selection with puromycin antibiotic, at week 2 and then week 3 after selection. A) RTqPCR for ABCG1 in TTC-466 cells transduced with shABCG1 or shControl siRNA at 1, 2 and 3 weeks. Results are shown as RQ(2^{-DDCt}), were ABCG1 expression is normalized to the house keeping control β actin. B) Western blot for ABCG1 expression in TTC-466 cells transduced with shABCG1 or shControl siRNA at 1-3 weeks. β actin and GRP75 were used to confirm equal loading of protein. C) RTqPCR for ABCG1 in SK-N-MC at week 3 and HEK293 at week 1. Results are shown as RQ(2^{-DDCt}), were ABCG1 expression is normalized to the house keeping control PPIA.

4.3.3 ABCG1 knock-in study using SK-N-MC cell line

The expression of ABCG1 was quantified at the RNA and protein level using WB, flow cytometry and RTqPCR that included no-RT-enzyme control in all experiments to exclude the amplification of DNA.

4.3.3.1 Expression of ABCG1 at RNA

The fold increase of exogenous ABCG1 (p value = 0.0007) in SK-N-MC.pLenti.ABCG1 cells was higher than the parental SK-N-MC and SK-N-MC.pLenti.control. The RTqPCR primers for ABCG1 were designed to detected the full length ABCG1 mRNA that was endogenous (derived from the cells) and produced following infection with pLenti.ABCG1 (n=3 biological repeats). The level of endogenous ABCG1 was detected in parental SK-N-MC and SK-N-MC.pLenti.control cells was the same; there was no significant difference between them (Figure **4.17**).

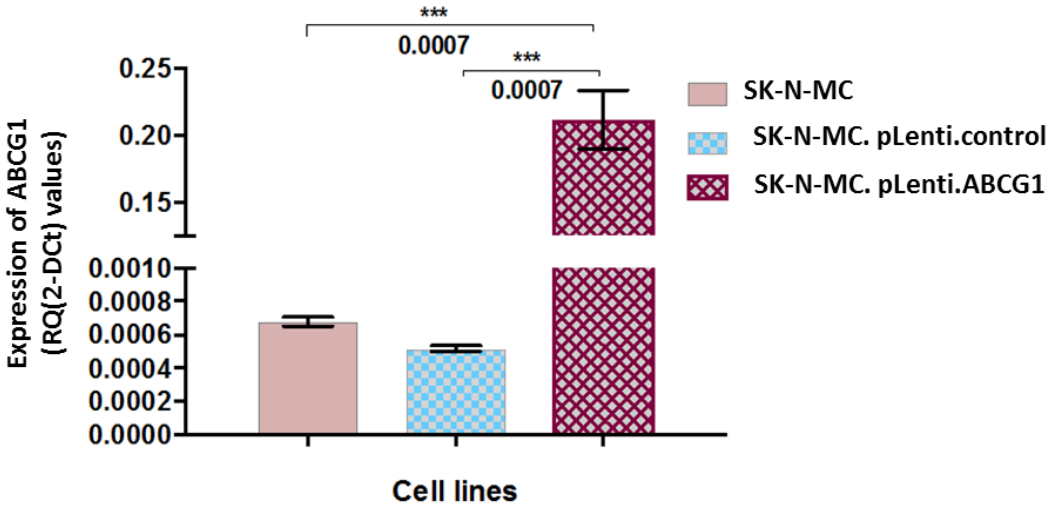

Figure 4.17 Expression of ABCG1 mRNA in knock-in cell lines compared to parental SK-N-MC and control cells. RNA was extracted from the generated knock-in cell lines to evaluate the overexpression and compare it with the parental SK-N-MC (n=3 biological repeats). ANOVA was performed. Results are presented as the mean ± standard deviation of three independent replicates.

4.3.3.2 Stability of ABCG1 in cells after sorting

The level of ABCG1 was determined by flow cytometry in SK-N-MC parental cells, and SK-N-MC cells infected with either the pLenti.control or pLenti.ABCG1 plasmid. The percent of cells containing the plasmid was

determined using flow cytometry to detect the GFP tag. The expression of ABCG1 protein has been lost as the vector has been lost with time (Figure **4.18**).

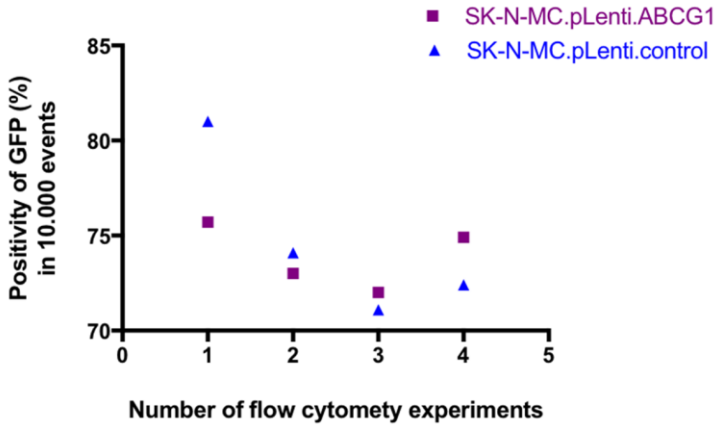

Figure 4.18 The expression of GFP.pLenti plasmid in transfected knock-in cell lines. Flow cytometry experiments were carried out 4 times to check the stability of ABCG1 plasmid in knock in cell lines.

After freeze thaw cells, HEK293 and SK-N-MC cells were used as a negative control for GFP. The proportions of cells expressing the pLenti plasmid were 8.3% and 13.6% in SK-N-MC.pLenti.control and SK-N-MC.pLenti.ABCG1 respectively (Figure **4.19**).

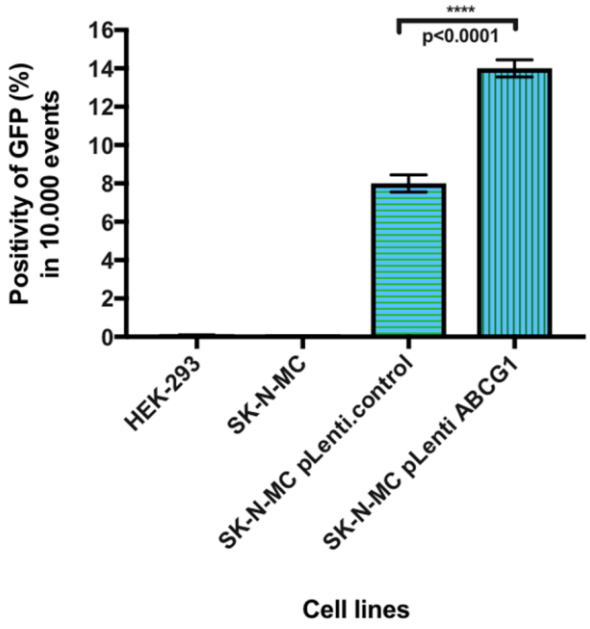

Figure 4.19 The percentage of GFP positive cells to confirm the percentage of cells that have been injected with plasmid using flow cytometry). ANOVA was performed. Results are presented as the mean ± standard deviation of three independent replicates.

4.3.3.3 Expression of ABCG1 at protein level

Using early passaged cells after FACS sorting, there was no increase in ABCG1 protein in SK-N-MC.pLenti.ABCG1 comparing to SK-N-MC.pLenti.control and parental SK-N-MC (Figure **4.20**). This experiment was performed three times using different biological repeats from different passages. None of the blots showed an increase in ABCG1 protein in SK-N-MC.pLenti.ABCG1 and the detected band was the same in all cells.

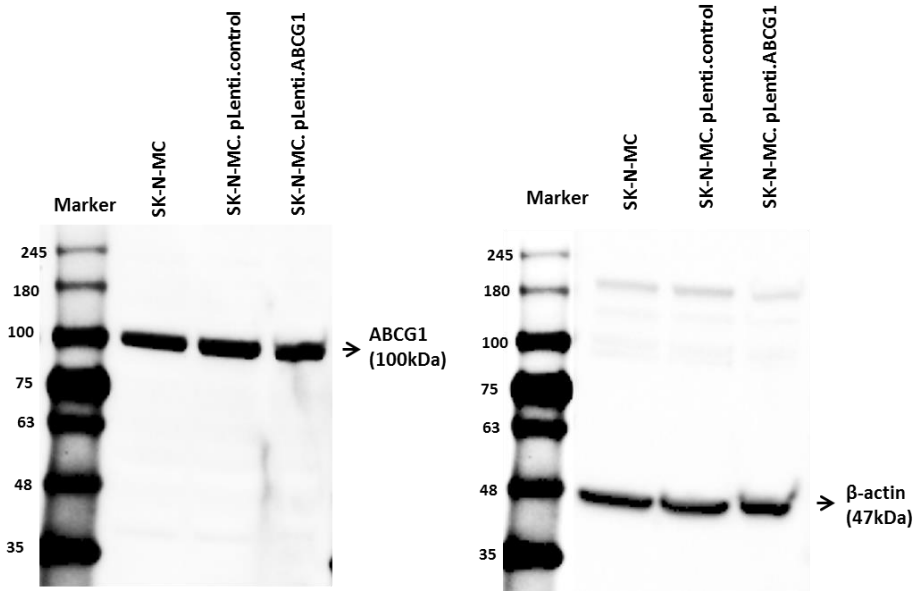

Figure 4.20 Expression of ABCG1 protein in SK-N-MC and cells infected with pLenti.control and pLenti.ABCG1. ABCG1 determined by WB. β-actin used as loading control.

The median expression level of ABCG1 expressed relative to secondary antibody only in HEK293 cells was 7.1%, ABCG1 was expressed in 95.6%of cells (Figure **4.21** A and B). The median expression level of ABCG1 expressed relative to secondary only in SK-N-MC, SK-N-MC plenti and SK-N-MC plenti.ABCG1 was 8.2, 9.2 and 8.6 respectively (Figure **4.21** B). The percent of SK-N-MC, SK-N-MC plenti and SK-N-MC plenti.ABCG1 cells expressing ABCG1 was 98.4%, 99.1% and 98.9%, respectively (Figure **4.21**

A). Although the level of plasmid expression was low, ABCG1 was not overexpressed in the SK-N-MC cells transfected with plenti.ABCG1. in both SK-N-MC.pLenti.control and SK-N-MC.pLenti.ABCG1, there was no difference in the expression of ABCG1 in cells positive and cells negative to GFP (Figure **4.22**).

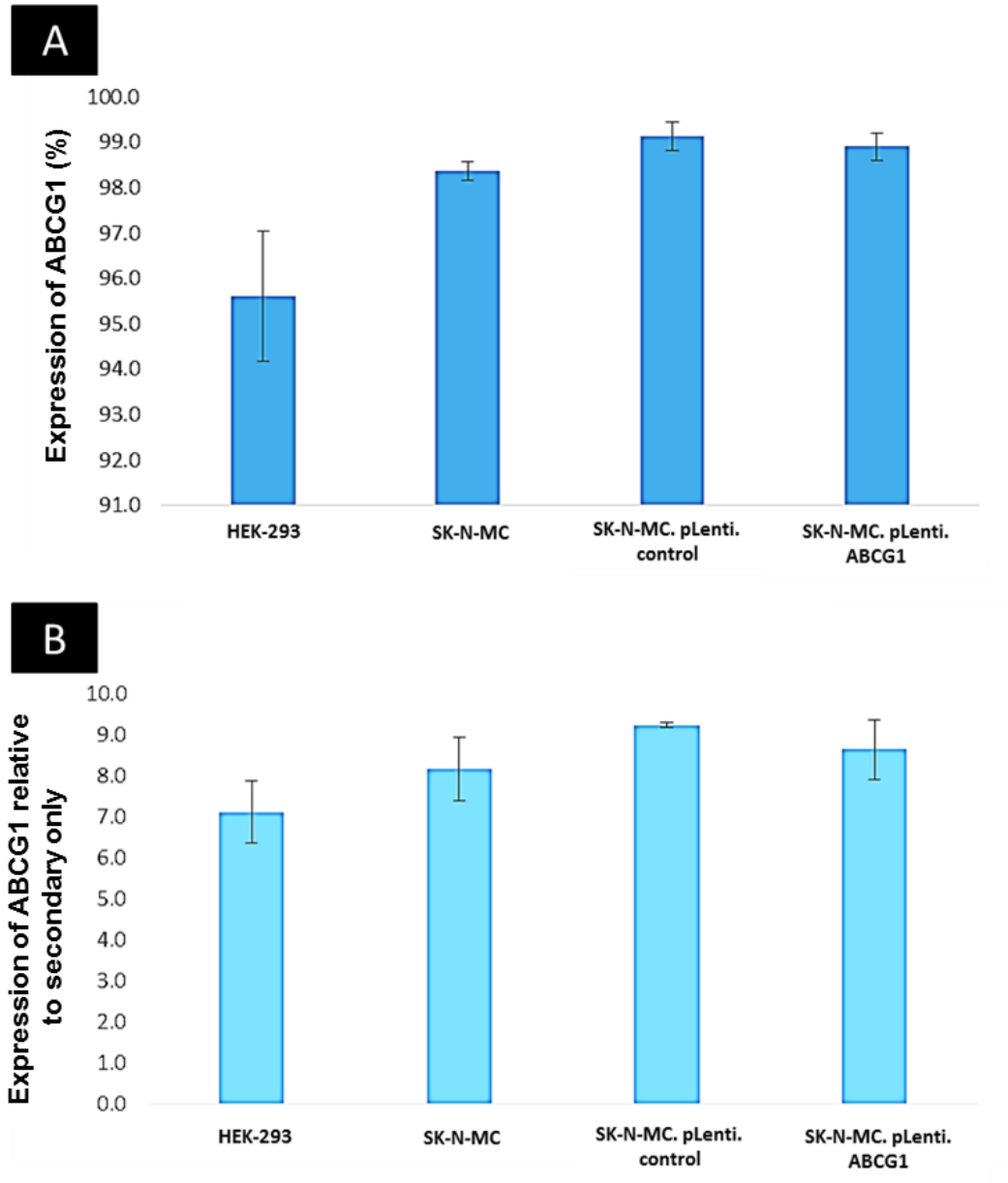

Figure 4.21 ABCG1 expression in SK-N-MC, HEK293 and knock-in cell lines determined by flow cytometry. A) The percentage of cells that express the endogenous ABCG1 in the selected area for analysis B) The expression level of the endogenous ABCG1 was calculated relative to the secondary only in ES cell lines. Results are presented as the mean ± standard deviation of three independent replicates.

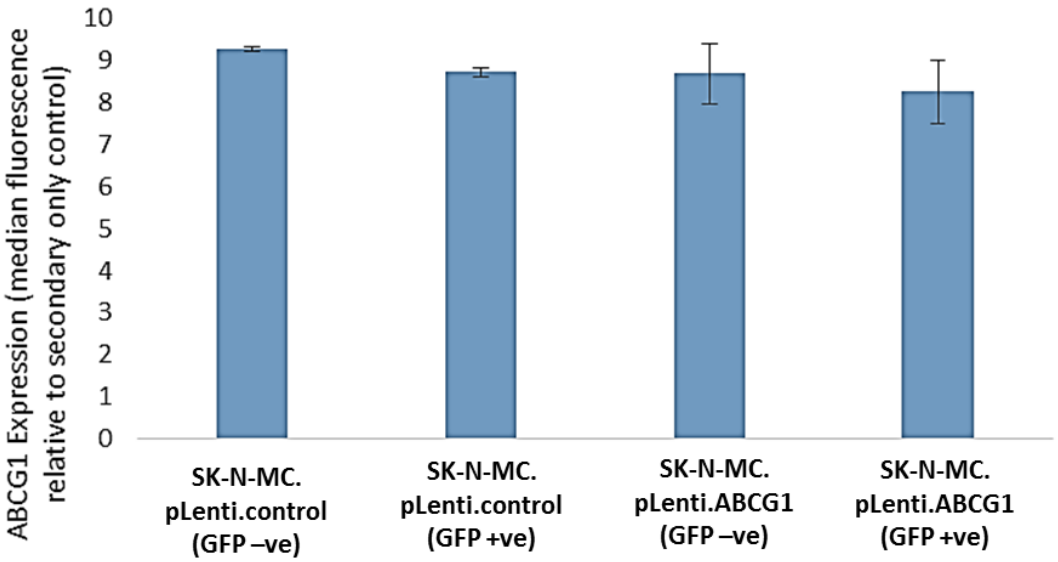

Figure 4.22 ABCG1 expression in SK-N-MC.pLenti.control and SK-N-MC.pLenti.ABCG1 determined by flow cytometry. The expression level of the ABCG1 was calculated relative to the secondary only. Results are presented as the mean ± standard deviation of three independent replicates. Cells holding GFP constructs (GFP +ve) and cells without GFP construct (GFP –ve).

4.3.3.4 Self-renewal ability of knock-in cell lines with high level of ABCG1 mRNA

4.3.3.4.1 Spheroids formation from a single cell

Regardless of the low protein level of ABCG1 in the knock-in model, the self-renewal capability was checked using low adherent plates (n=10 plates for each cell line) to examine the effect of high ABCG1 mRNA on self-renewal ability. There was a significant increase of spheroids number in SK-N-MC.pLenti.ABCG1 (50% ± 1.293, n=10) comparing to SK-N-MC.pLenti.control (36% ± 1.306, n=10) (Figure 4.23).

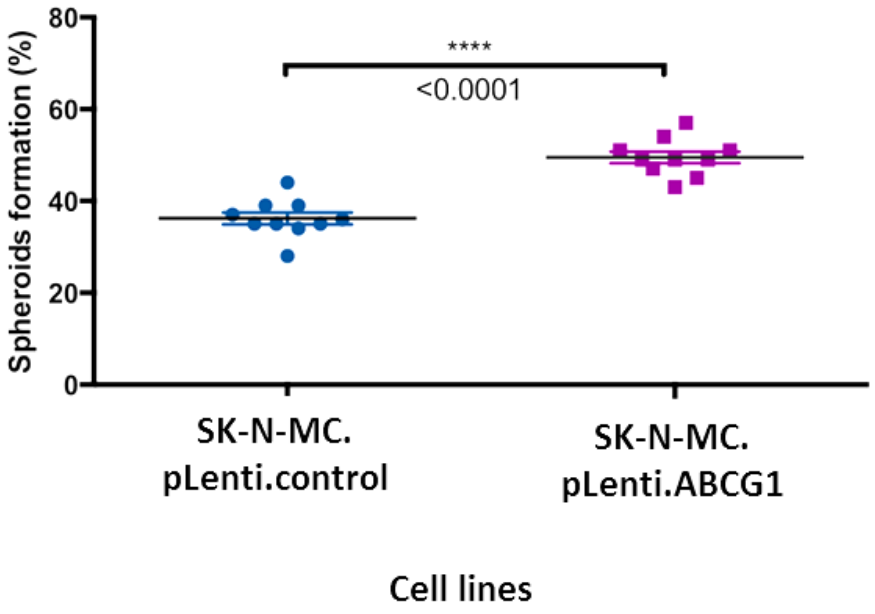

Figure 4.23 Spheroid formation from a single cell of knock-in cell lines. Low adherent 96-well plates (10 plates for each cell line) were used to grow a single cell in each well using SK-N-MC.pLenti.control and SK-N-MC.pLenti.ABCG1 cells. The difference between cell lines was assessed using t-test. Significantly different (P value < 0.05)

Distinguishing between the endogenous and exogenous ABCG1 mRNA was impossible using RTqPCR. Also, the existence of pLenti plasmid in the single cell that form spheroid was not confirmed. However, the expression of ABCG1 mRNA in SK-N-MC.pLenti.ABCG1 spheroids was reduced significantly compared with the SK-N-MC.pLenti.ABCG1 monolayer ($p<0.0001$, $n=3$), maybe because the expression level of ABCG1 as so high in SK-N-MC.pLenti.ABCG1 cells so can't get the expression of ABCG1 to increase any more. However, SK-N-MC.pLenti.control spheroids illustrated an increase of ABCG1 mRNA compared with SK-N-MC.pLenti.control grown as substrate adherent ($p<0.0001$, $n=3$) (Figure 4.24). There was no difference in ABCG1 mRNA expression between spheroids generated from SK-N-MC.pLenti.control and SK-N-MC.pLenti.ABCG1. The freeze thaw has an effect on pLenti cells (Section 4.3.3.2). Also, the 3D culture has an effect on the expression of ABCG1 protein, data showed increased ABCG1 in spheroids compared to substrate adherent cells. In contrast with previous results, SK-N-MC.pLenti.control substrate adherent cells increased the

expression of ABCG1 protein as same level as SK-N-MC.pLenti.control spheroids. Also, in substrate adherent cells, there was a decrease in ABCG1 protein in SK-N-MC.pLenti.ABCG1 comparing to SK-N-MC.pLenti.control. On other hand, there was an increase in ABCG1 protein, which might be the endogenous and/or exogenous ABCG1, in SK-N-MC.pLenti.ABCG1 spheroids compared with substrate adherent SK-N-MC.pLenti.ABCG1 cells (Figure 4.25).

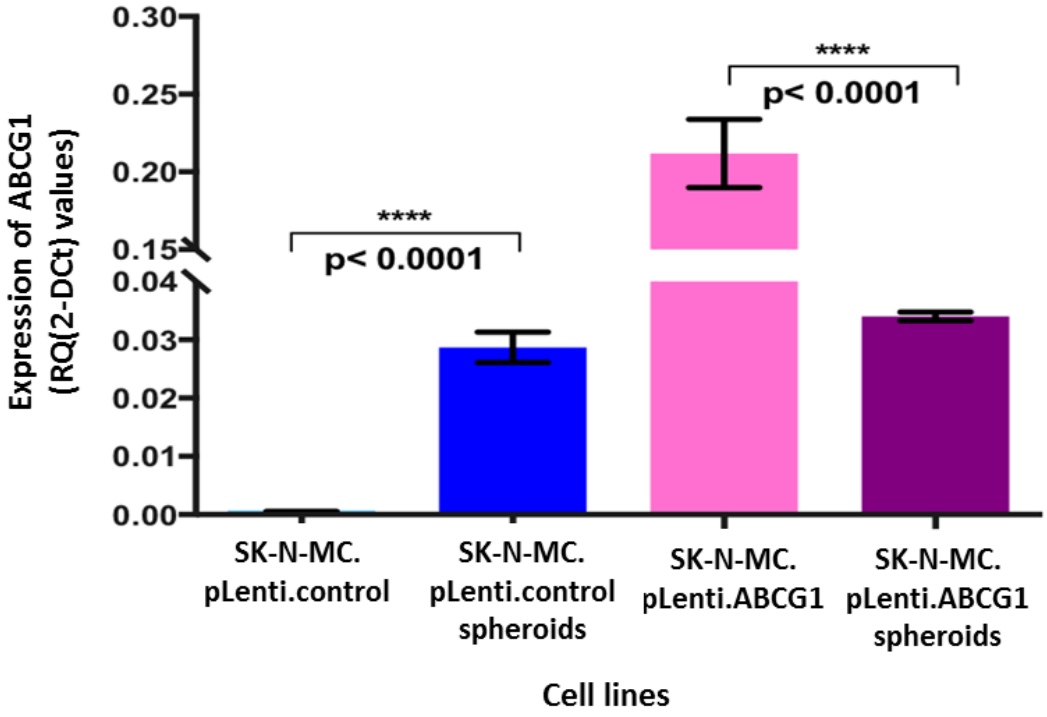

Figure 4.24 ABCG1 RNA expression in knock in cell lines grown as substrate adherent cells and spheroids measured using RTqPCR. Cells were grown as substrate adherent cells and spheroids derived from a single cell in low adherent plates. Experiments performed in triplicate using different biological repeats (n=3). ANOVA was performed. Results are presented as the mean ± standard deviation of three independent replicates.

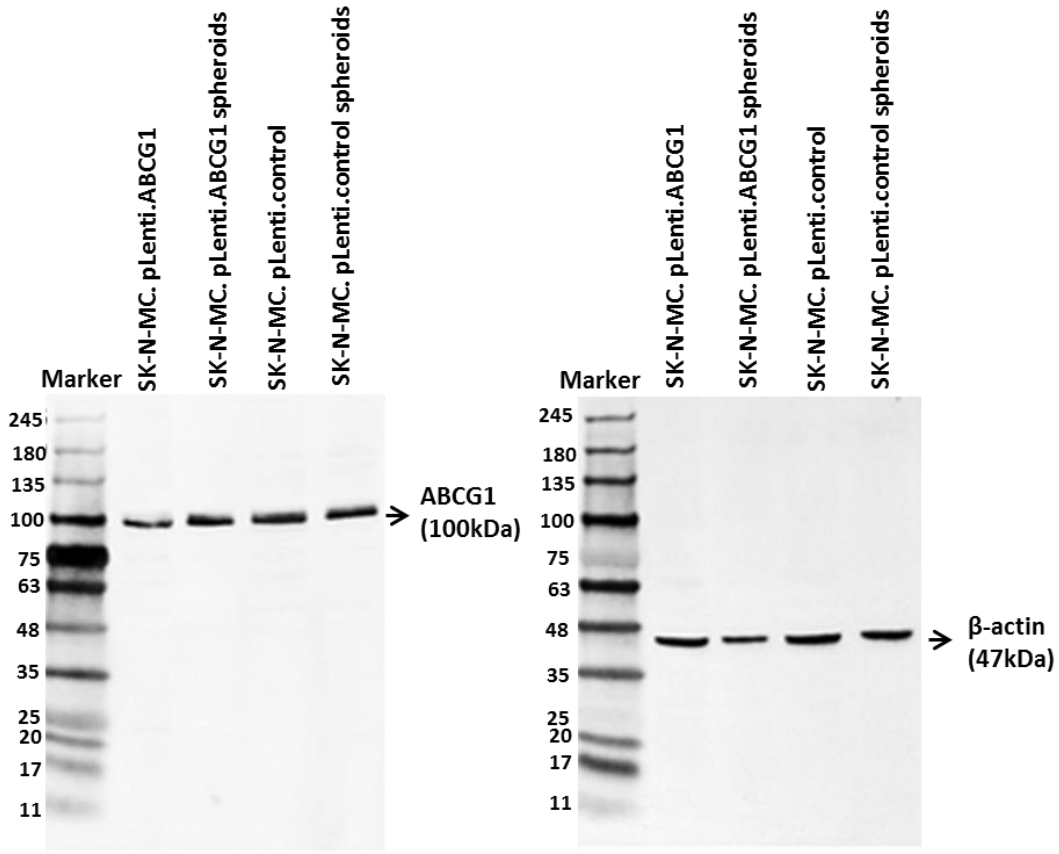

Figure 4.25 Expression of ABCG1 in knock in substrate adherent and spheroids. SK-N-MC.pLenti.control and SK-N-MC.pLenti.ABCG1 substrate adherent cells and spheroids collected at 3 week from SK-N-MC.pLenti.control and SK-N-MC.pLenti.ABCG1 cells were used. β-actin was used to confirm equal protein loading.

4.3.3.4.2 The effect of 3D culture on E3-ubiquitin ligases

In 2015, it has been confirmed that E3 ligases have an effect on ABCG1 protein expression (Aleidi et al., 2015). knock-down of these ligases; NEDD4-1 and HUWE1 led to increased and stabilized the expression of ABCG1 protein in knock in cell line (Aleidi et al., 2015). So, NEDD4-1 and HUWE1 were optimized for western blot assay. HUWE1 optimization does not give meaningful result on western blot, whereas NEDD4-1 worked at concentration (1:40.000). SK-N-MC parental, SK-N-MC.pLenti.control and SK-N-MC.pLenti.ABCG1 highly express NEDD4-1 (Figure **4.26**).

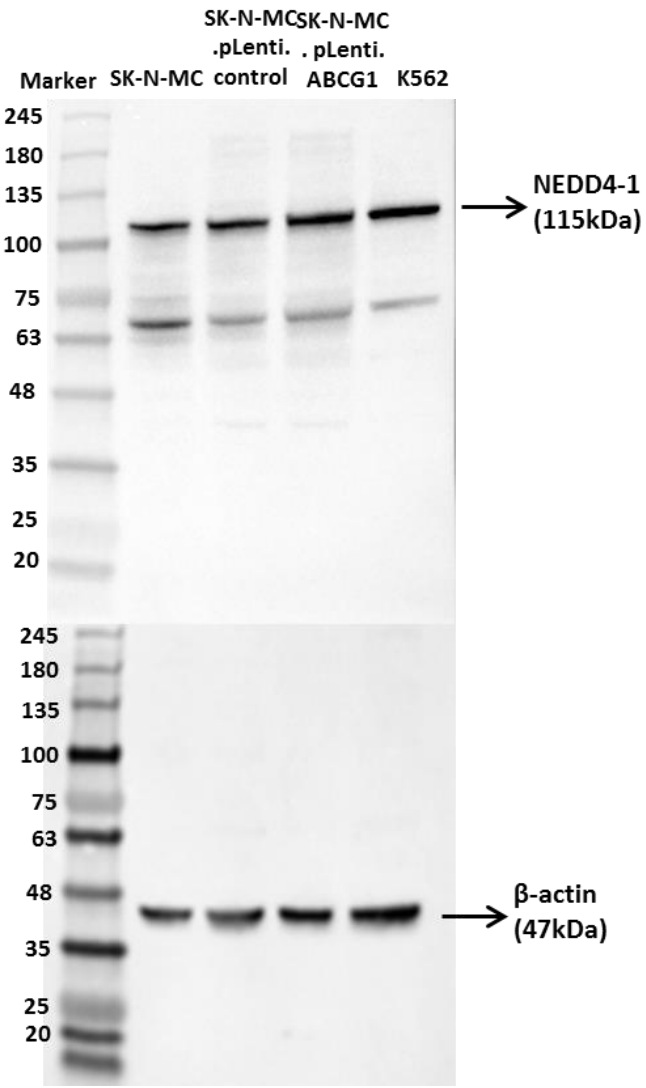

Figure 4.26 Expression of NEDD4-1 in knock in substrate adherent cell lines and SK-N-MC parental. NEDD4-1 expression in SK-N-MC parental, SK-N-MC.pLenti.control and SK-N-MC.pLenti.ABCG1 substrate adherent cells was illustrated using western blot. K562 cell line used as positive control for NEDD4-1 and β-actin was used to confirm equal protein loading.

The expression of NEDD4-1 was low in 3-w-SK-N-MC spheroids, whereas the spheroids generated from a single cell from knock in cell lines illustrated a higher expression of NEDD4-1 protein comparing to 3-w-spheroids. NEDD4-1 expression was lower in knock in spheroids comparing to knock in cells grown as monolayer (Figure **4.27**).

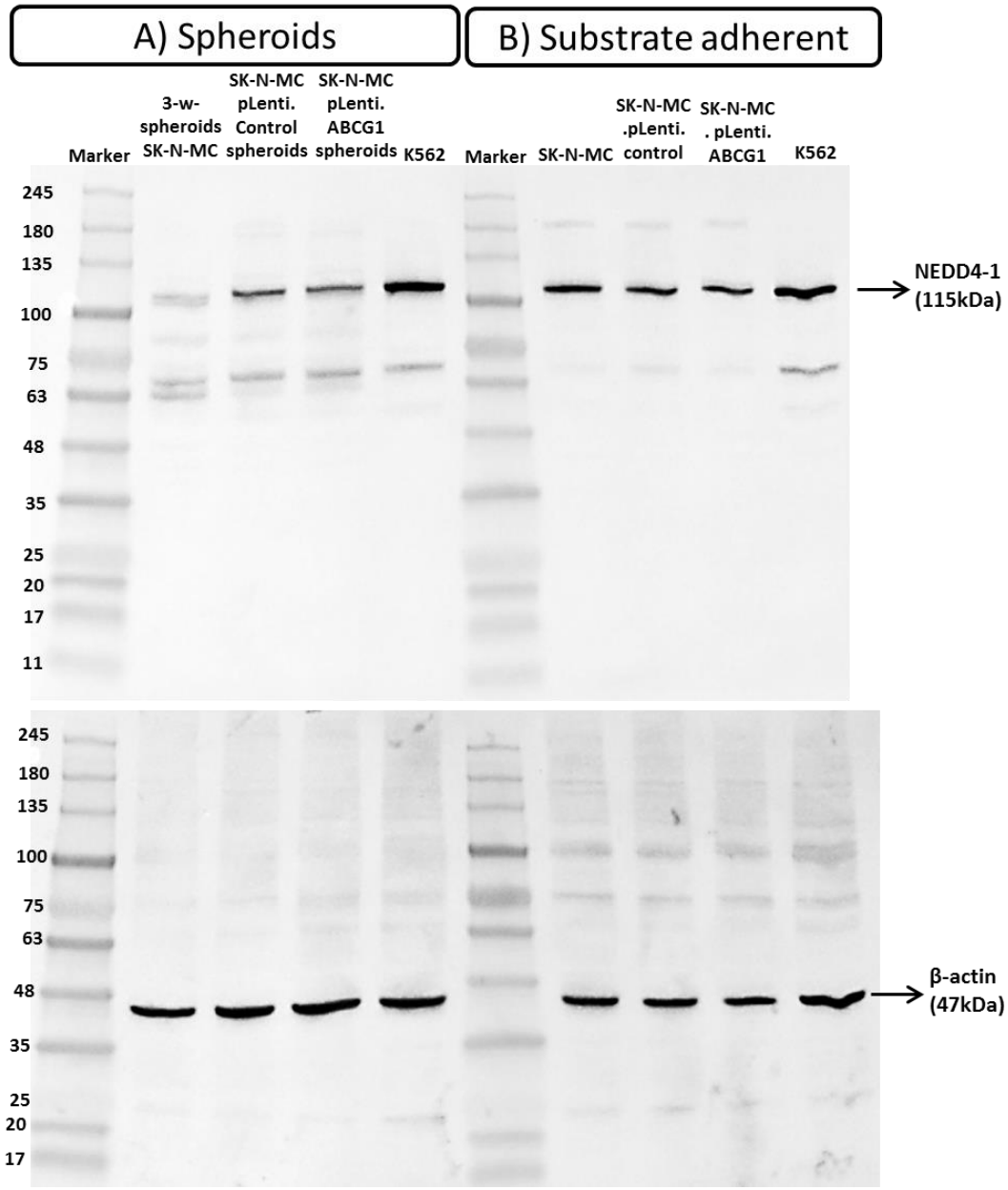

Figure 4.27 Expression of NEDD4-1 in knock in substrate adherent and spheroids. A) NEDD4-1 expression in spheroids collected at 3 week from SK-N-MC parental, SK-N-MC.pLenti.control and SK-N-MC.pLenti.ABCG1 cells. B) SK-N-MC parental, SK-N-MC.pLenti.control and SK-N-MC.pLenti.ABCG1 substrate adherent cells used to investigate expression of NEDD4-1. K562 cell line used as positive control for NEDD4-1 and β-actin was used to confirm equal protein loading.

4.3.3.5 The expression of ABCG1 protein using IHC

IHC using ABCG1 antibody was optimized on 3-w-spheroids that were generated from SK-N-MC cells. The optimal concentration (1:50) was then used to stain the SK-N-MC.pLenti.control and SK-N-MC.pLenti.ABCG1s and the expression of ABCG1 was measured in the proliferating and hypoxic rim of 3-w-spheroids. The size of spheroids derived from SK-N-MC, SK-N-MC.pLenti.control and SK-N-MC.pLenti.ABCG1 was 577± 34 µm, 503 ± 16 µm and 580.3 ± 3.1 µm respectively (n=3; results are given as mean±SEM). The positivity of ABCG1 in SK-N-MC and SK-N-MC.pLenti.ABCG1 spheroids was higher in proliferating rim in some spheroids or in hypoxic rim in others. The expression of ABCG1 was 6% ± 0.7 and 7%± 2.3 in the hypoxic and proliferating rim in SK-N-MC spheroids, respectively. In SK-N-MC.pLenti.ABCG1 spheroids, the expression of ABCG1 was 13%± 2 in both proliferating and hypoxic rim. In SK-N-MC.pLenti.control, the majority of cells that express ABCG1 were in the hypoxic rim and some cells in the proliferating rim (Figure **4.28**, A and B). The expression of ABCG1 in the hypoxic rim was 15% ± 3.8 and 9%± 2.6 in proliferating rim of SK-N-MC.pLenti.control.

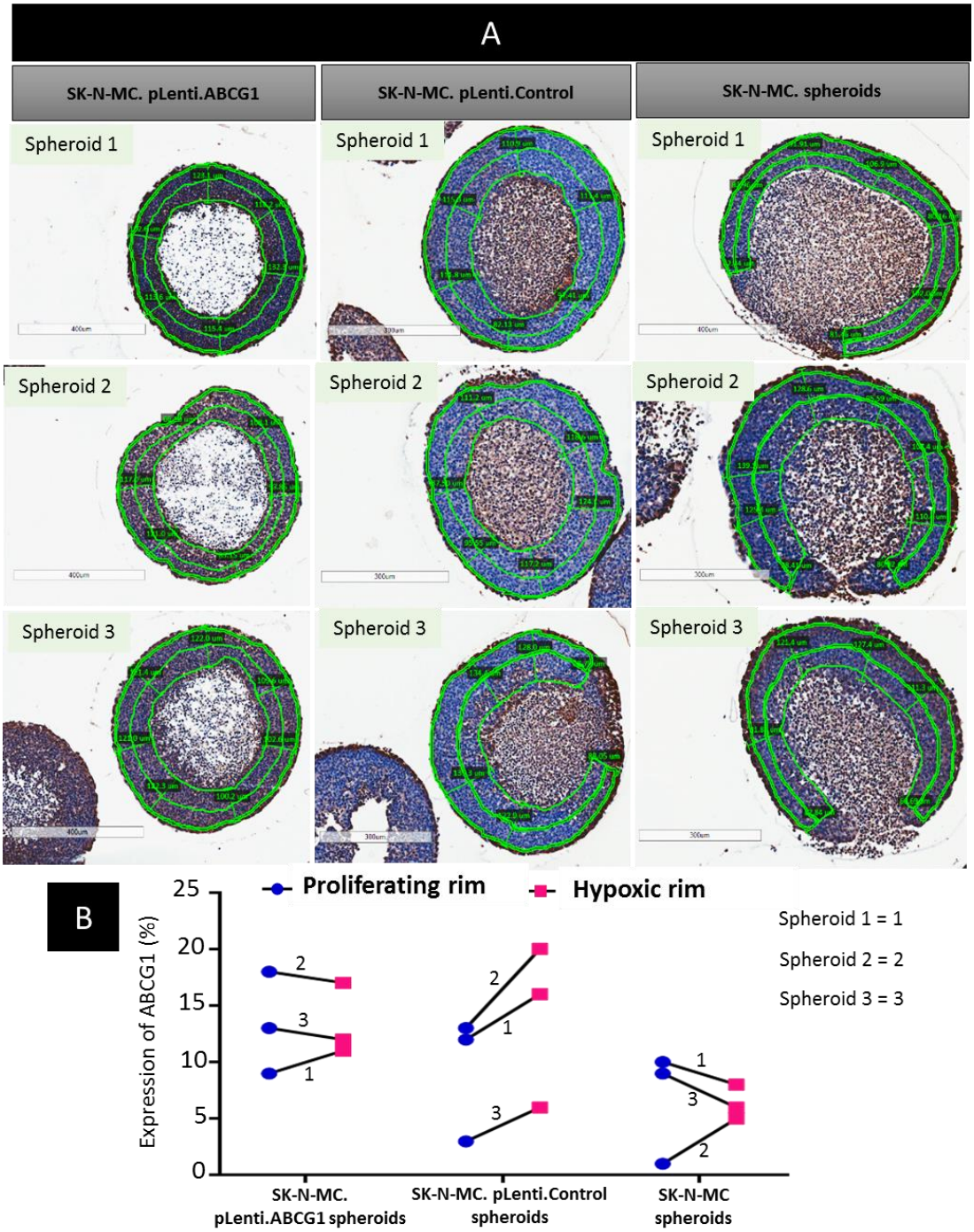

Figure 4.28 ABCG1 expression in spheroids analysed by IHC. Aperio Algorithms was used to measure the size of spheroids and the expression level of ABCG1 in 3-w-spheroids that were generated from SK-N-MC and knock-in cell lines.A) the three selected spheroids for analysis from each cell lines and in green regions were designated for analysis using the pen tool. B) The percentage of ABCG1 expression (%) in the proliferating or hypoxic rim for each cell line (n=3).

4.3.4 The effect of hypoxia on the expression of ABCG1 protein

From the histology of spheroids (Section 2.3.4.1), spheroids have a clear necrotic core, hypoxic rim and outer proliferating rim. Furthermore, IHC of spheroids suggested that hypoxia might have an effect on ABCG1 expression at protein level. To investigating the possibility that ABCG1 may be regulated by hypoxia, cells were incubated in a Hypoxic incubator (5% CO_2 and 1% O_2) (Section 4.2.1). The protein level of ABCG1 in these cells was analysed by western blot. Glucose transporter 1 (Glut-1) and Hypoxia-inducible factor 1-alpha (HIF-1α) antibodies were used to confirm the hypoxic conditions (Figure **4.29** C and D). The protein level of endogenous ABCG1 increased after 24h in hypoxia (Figure **4.29** A). Unlike ABCG1, HIF-1α decreased gradually with time, whereas Glut-1 expressed at high level in the first time points (6h-48h) and then a small reduction occur at 72h and 96h (Figure **4.29** C and D).

Similarly, ABCG1 protein expression increased gradually with time in SK-N-MC.pLenti.ABCG1 and SK-N-MC.pLenti.control cells (Figure **4.30** A). There was no difference in ABCG1 expression between SK-N-MC.pLenti.ABCG1 and SK-N-MC.pLenti.control cells. The increase over time might have resulted from the endogenous ABCG1 whilst the exogenous ABCG1 might remain as untranslated RNA. On the other hand, HIF-1α decreased gradually with time in both cell lines SK-N-MC.ABCG1 and SK-N-MC.control and Glut-1 expressed at high level through the all-time points (6h-96h) (Figure **4.30** C and D).

The slope of trend line of cells growth within time was higher in normoxia comparing with hypoxia. It was expected to see a reduction in cell growth in hypoxia comparing with normal oxygen level. However, all cell lines had the ability to continue growing in the hypoxic environment for 96h (Figure 4.31). In normoxia, the slope of trend line of cells growth within time showed no difference between SK-N-MC, SK-N-MC.control and SK-N-MC.ABCG1. Also there was no difference between cell lines grown in hypoxic environment (Figure **4.32**). SK-N-MC.pLenti.ABCG1 only illustrated a significant difference between cell grown in normoxia and hypoxia (Figure **4.32** B).

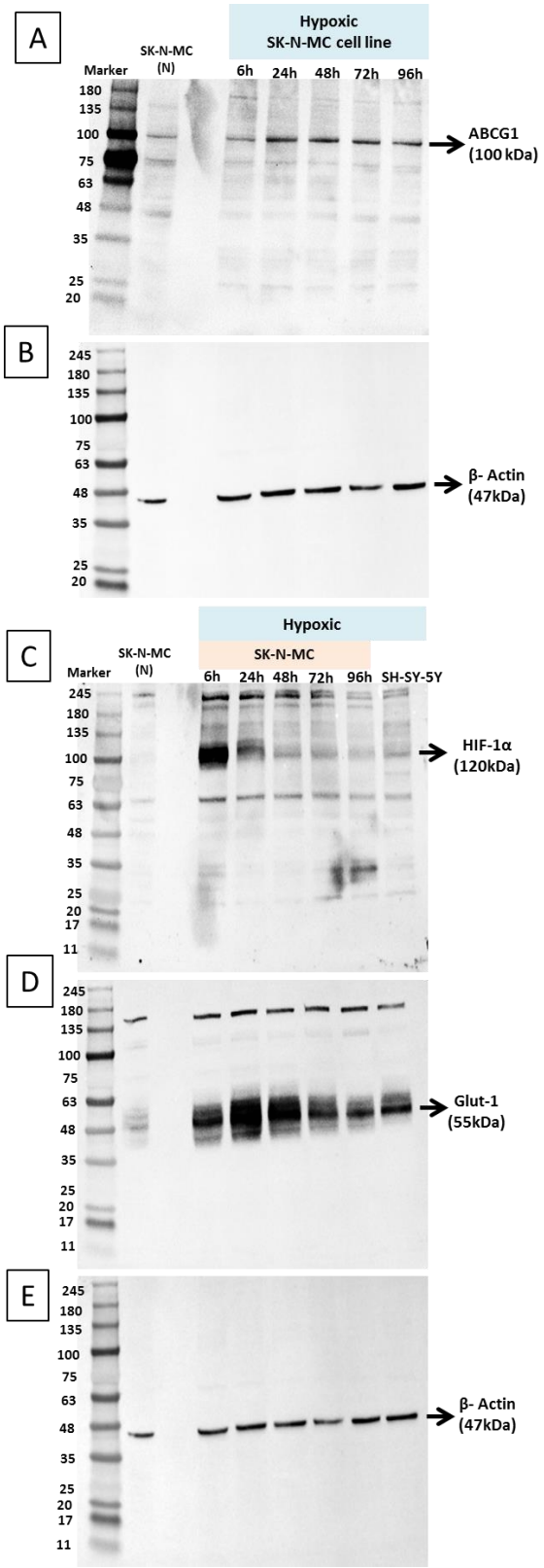

Figure 4.29 Protein expression of ABCG1, HIF1a and Glut-1 in SK-N-MC cells grown under hypoxic conditions. Cells collected for protein extraction at different time points. SK-N-MC cells extracted from cells incubated in normoxia (5% Co2 in 95% air|) were used as a negative control. SK-N-MC (N) = SK-N-MC cells extracted from cells in normoxia. A) The expression of ABCG1 in normoxic and hypoxic cells. B and E) loading control β-actin. C) The expression of HIF-1α. D) Expression of Glut-1. SH-SY-5Y was used as positive control for HIF-1α and Glut-1

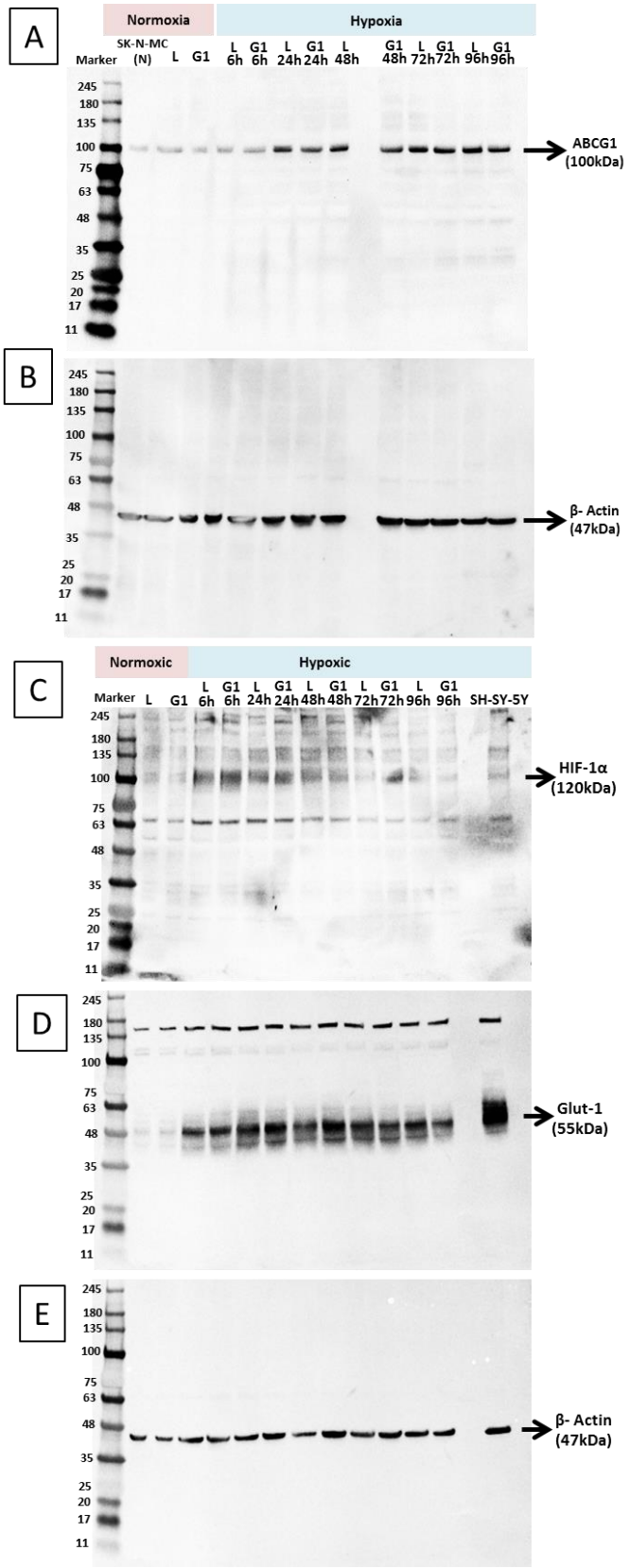

Figure 4.30 Protein expression of ABCG1, HIF1a and Glut-1 in knock-in cells grown under hypoxic conditions. SK-K-MC.pLenti.control (L) and SK-N-MC.pLenti.ABCG1 (G1) collected for protein extraction at different time points.Normoxic SK-N-MC were used as a control. SK-N-MC (N) = SK-N-MC cells extracted from cells in normoxia. A) The expression of ABCG1 in normoxic and hypoxic cells. B and E) loading control β-actin. C) The expression of HIF1a D) the expression of Glut-1.

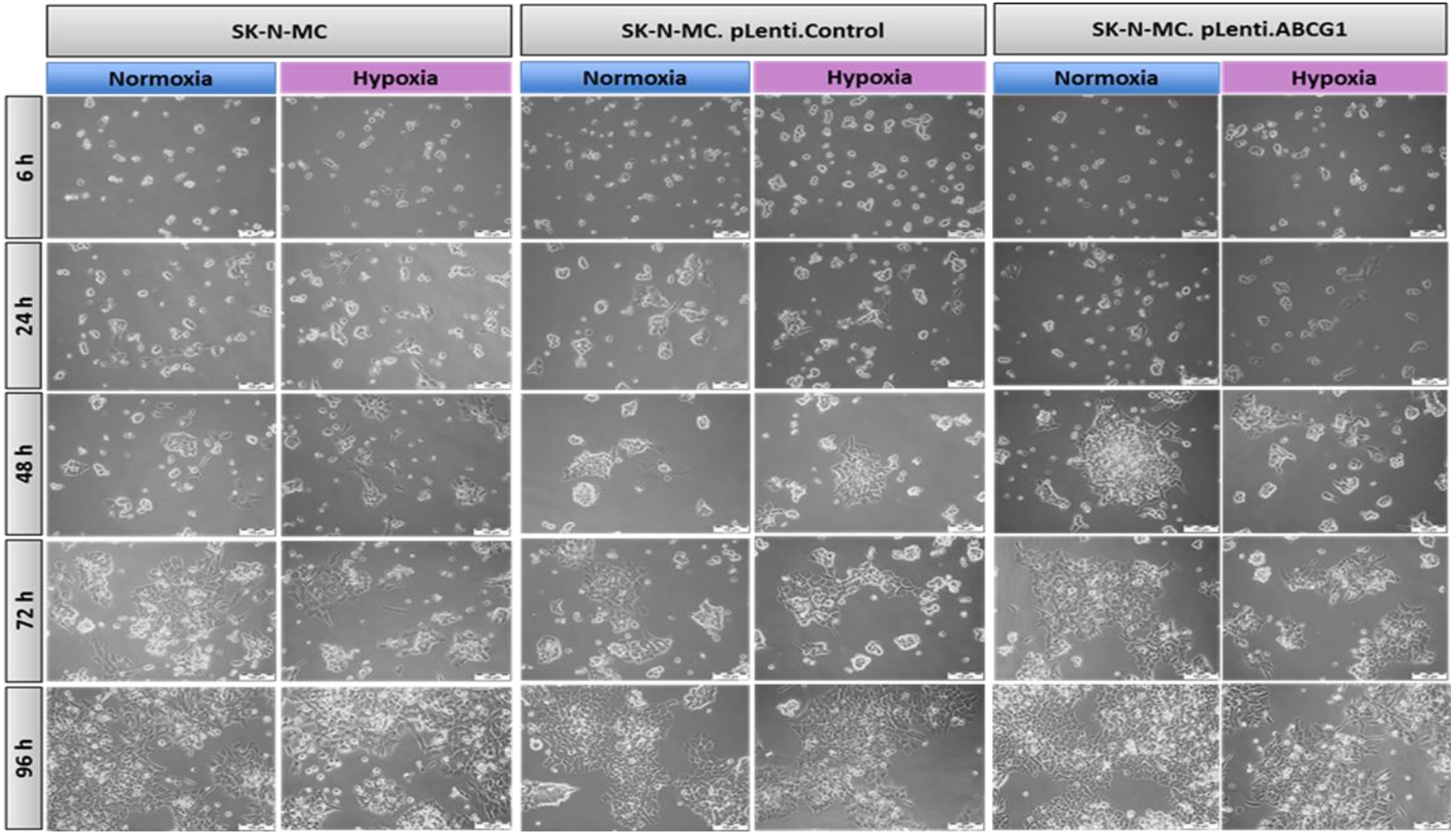

Figure 4.31 Morphology of cell growth in normoxia and hypoxia. SK-N-MC, SK-N-MC.pLenti.control and SK-N-MC.pLenti.ABCG1 were imaged by light microscope in different time point (6-96h).

- 206 -

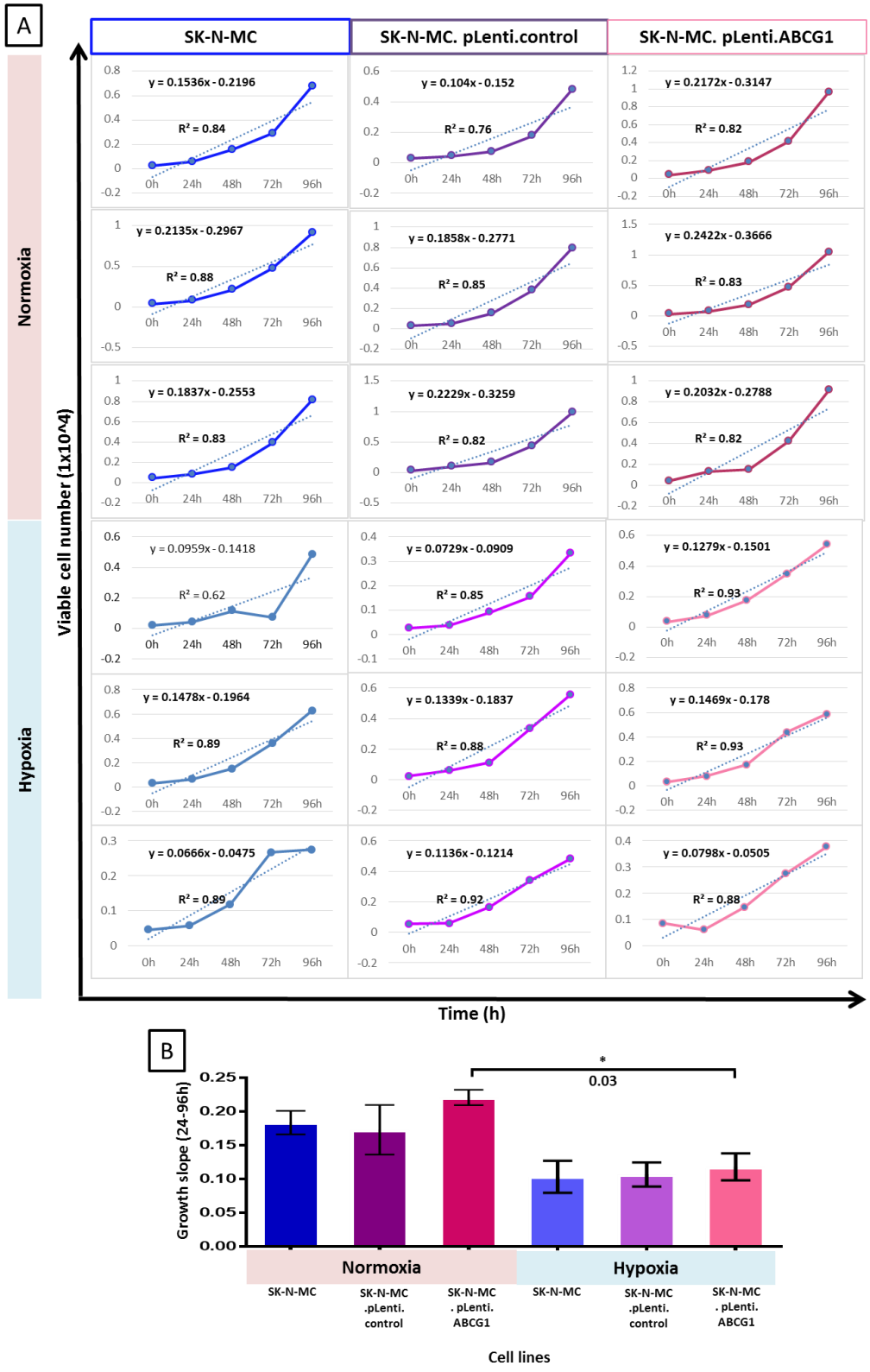

Figure 4.32 The viable cell number and slope of cells growth in normoxia and hypoxia environment for 24-96h. Viable cells number was counted using automated trypan blue exclusion assay. A) Viable cells number for each cell line from 24h to 96h in normoxia and hypoxia. B) The growth slope for each cell line was calculated using excel and then plot using Prism. ANOVA was performed. Results are presented as the mean ± standard deviation of three independent replicates.

4.4 Discussion

For the first time ES cell lines were examined for the expression of ABCG1 protein. The expression level was variable between cell lines. In Chapter 3, 3-w- SK-N-MC spheroids showed an increase of ABCG1 expression level at protein and RNA level. Like ES, this finding was confirmed in osteosarcoma stem cell-like (OSC). The expression of ABCG1 was high in OSC and in the sarcospheres derived from TGF-β1-stimulated residual adherent cells (iOSCs) compared with cells grown as a monolayer (Zhang, H. et al., 2013). In this chapter, the effect of knocking-out ABCG1 mRNA might lead to senescence. The SK-N-MC.pLenti.ABCG1 cell lines had increased the expression of ABCG1 mRNA compared to that in SK-N-MC.pLenti.control. However, this increase at RNA level did not result in an increased expression of ABCG1 protein; suggesting there is a posttranscriptional block of expression since expression of ABCG1 is regulated by the E3 ligases NEDD4-1 and HUWE1 (Aleidi et al., 2015). Knocking-down one or both of these ligases may lead to stabilized and increase the expression of ABCG1 protein, as it has been confirmed in CHO-K1 cells (Aleidi et al., 2015). From western blot analysis in this chapter, NEDD4-1 is expressed in ES cell lines and may be an important regulator for ABCG1. In future studies, the expression level of HUWE1 will be assessed and whether knock-down of these ligases in ES cell lines resulted in increased expression of ABCG1. It has been reported that the high expression of human ABCG1 in macrophages, HEK-293 and HepG2 results in ER stress that leads to apoptosis. This finding assumes that increasing ABCG1 activity surpasses the cholesterol capacity of the cell, which leads to an increase in the free cholesterol in the ER (Seres et al., 2008). However, in mouse and human low-grade glioma stem cells (LG-GSCs), it has been proven that the high levels of ABCG1 expression is essential for protecting against ER-stress-induced mouse LG-GSC apoptosis (Chen, Y. et al., 2015).

Furthermore, It has been confirmed that overexpressing the short (isoform 4) and the full length variants of the human ABCG1 stimulated cholesterol efflux from cells (Gelissen et al., 2010) and also the apoptotic effect of ABCG1 was only confirmed by using the full length of the ABCG1

transporter (Seres et al., 2008). Moreover, it has been confirmed that the inactive mutant form of isoform 4 and the full length were able to functionally co-operate with one another. The reduction of apoptosis by the inactive isoform 4 was promoted by the full length isoform and inversely (Hegyi and Homolya, 2016). Examination of the expression of ABCG1 isoforms in ES cell lines and spheroids is a considerable undertaking which would be very interesting to be done in the future.

Several studies proposed that abolition of ABCG1 expression either by generation of knockout mice models or by RNAi knockdown decreased cholesterol efflux to HDL (Wang, N. et al., 2006; Kennedy et al., 2005; Wang, N. et al., 2004; Wang, X. et al., 2007). However, in this chapter, knocking-down ABCG1 protein in ES cell lines, SK-N-MC and TTC-466 as well as HEK-293 cells was not successful suggesting that the construct is being silenced. It would be interesting to investigate the methylation status of ABCG1 in knock-out cell lines. Also, an alternative siRNA could be investigated such as the specific siRNA targeting ABCG1 (s18482) that has been used by Crouchet group. This group successfully knocked-down ABCG1 in hepatic cells to prove the role of ABCA1 and ABCG1 in inhibiting the replication of hepatitis C virus (HCV) (Crouchet et al., 2016).

The decrease in HIF1-α protein may have resulted from increasing the expression of the hypoxia-associated factor (HAF) (Koh et al., 2008) and/or E3 ubiquitin-protein ligase (Hsp70/CHIP complex) (Luo, W. et al., 2010), which cause HIF-1α ubiquitination and degradation. However, under prolonged hypoxia (>24h) HAF and/ or Hsp70/CHIP complex have been reported to be a promoter for HIF-2α transactivation (Koh and Powis, 2012).

Recently, a connection between activation of Liver X receptor alpha (LXRα) and induction of apoptosis was described, LXR agonists lead to increased pro-apoptotic gene expression and reactive oxygen species (ROS) production in neuroblastoma cells (Raina and Kaul, 2010). Therefore, ABCG1 and ABCG4, which are LXR-inducible gene products, might be linked with ROS production that leads to cell damage. However, this proposed explanation has yet to be proven (Hegyi and Homolya, 2016).

Under normoxia, it has been reported that the HIF pathway remains functional and this oxygen-resistant function is critical in cancer biology and

immunology (Finlay et al., 2012; Doedens et al., 2013). In solid tumours, it has been confirmed that expression of HIF-1α and HIF-2α is regulated by the E3 ligases HAF and Hsp70/CHIP complex. The increase of these ligases in normoxia leads to decrease or degrade HIF1 family (Figure **4.33** A). The switch from HIF-1α to HIF-2α has been confirmed during chronic hypoxia (Koh and Powis, 2012). Acute hypoxia (< 24h, Figure **4.33** B) promotes induction of both HIF-1α and -2α; however, HIF-1α, which is the major driver of the acute response, promotes angiogenesis and/or reperfusion, or cell death (Kotch et al., 1999; Bento et al., 2010). Alternatively, chronic hypoxia (> 24h, Figure **4.33** C) is reported to increase expression of HAF and HIF-2α and also mediate a switch from HIF-1α to HIF-2α, which promotes tumour adaptation, proliferation and progression (Li, Z. et al., 2009; Wang, Y. et al., 2011; Wang, Y. et al., 2014).

High expression of miR-210 in spheroids compared to substrate adherent cells was confirmed previously (Chapter 3, section 3.3.2.4.2). It has been confirmed that miRNA transport from cell-to-cell by different transporters such as exosomes, microvesicles, apoptosis bodies, and RNA-binding proteins including high-density lipoproteins (HDL) (Vickers et al., 2011), which normally efflux via ABCG1 and influx via scavenger receptor B1 (SR-B1). Currently, there is no more evidence supporting HDL as a miRNA transporter and many questions about the HDL–miRNA complex formation still remain unanswered and recent research focus on exosomes has still not been fully explored (Valadi et al., 2007; Vickers and Remaley, 2012; Boon and Vickers, 2013; Mathiyalagan and Sahoo, 2017). A possible link for the observations from Chapter 3 and Chapter 4 are summarized in a schematic diagram (Figure **4.33**).

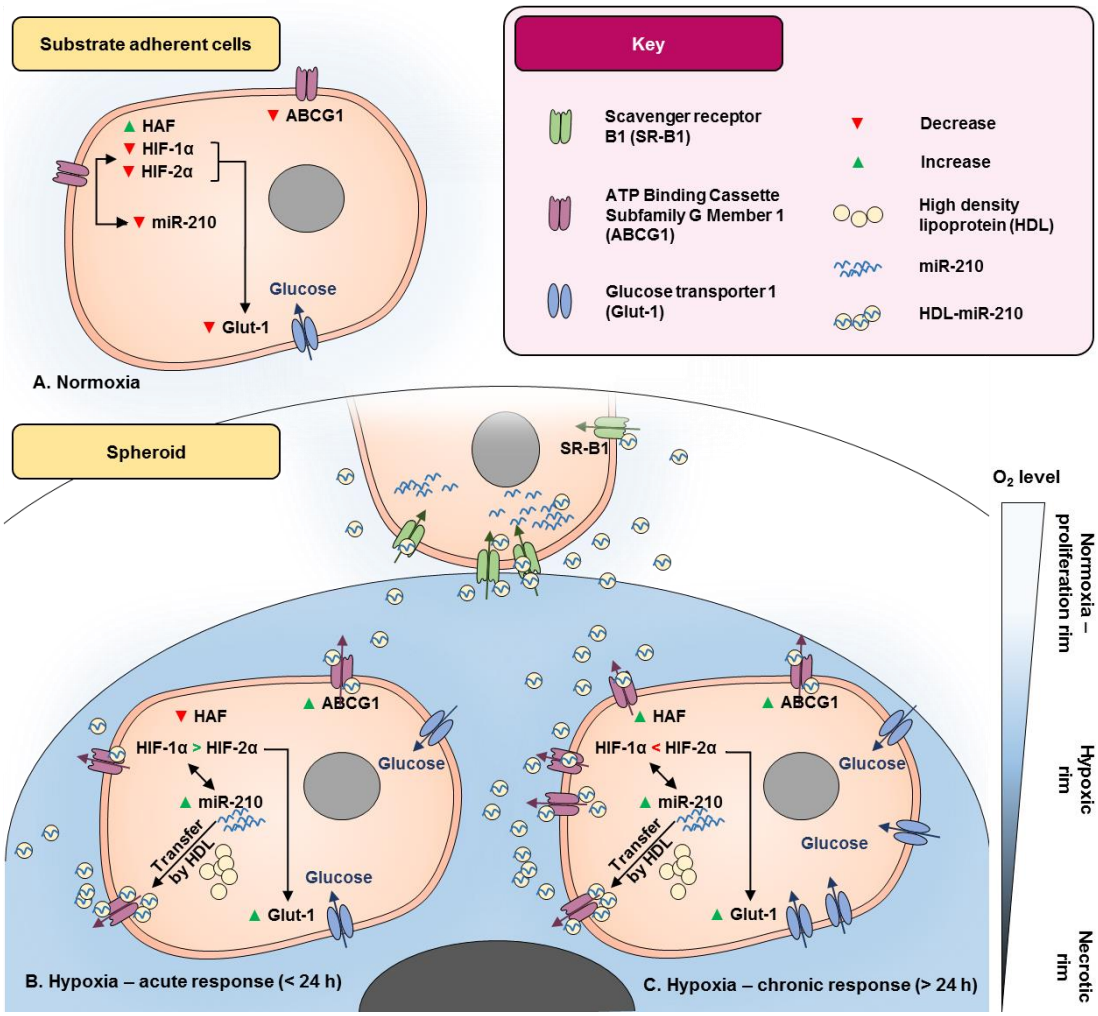

Figure 4.33 Schematic diagram showing the association of different genes in substrate adherent cells and spheroids (oxygen diffusion rims; O_2 levels). A) Normoxia; substrate adherent cells attempt to decrease the expression level of ABCG1, Glut-1, HIF family and miR-210. This also occurs in the outer layer of proliferative rim in spheroids. Cells in the inner layer of the proliferative rim in spheroids (cells very close to the hypoxic rim), might influx HDL-miR-210 that is transported from hypoxic cells. In the hypoxic rim, two different responses to low oxygen level appear (B and C). In general, cells attempt to increase the expression level of ABCG1, Glut-1, HIF family and miR-210. However, in B) the expression level of HIF-1a is higher than HIF-2a due to a decreased expression level of HAF and vice versa in C. In the hypoxic rim, the increase of glucose uptake helps with increasing the energy level (ATP) needed by ABCG1 for HDL-miR-210 efflux. Cell death occurs in the necrotic rim of spheroids.

The key finding:

1- Increase ABCG1 mRNA increase spheroid formation in SK-N-MC.
2- Knock down ABCG1 using transient methods (siRNA) led to cell death, whereas permanent methods (shRNA) led to stabilized ABCG1 protein

Chapter 5

Characterize mouse model null Cdkn1A Interacting Zinc finger protein 1 (CIZ1)

5.1 Introduction

CIZ1 interacts directly with the cdk inhibitor p21 (Mitsui et al., 1999), CDK2 (den Hollander and Kumar, 2006), cyclin E and cyclin A (Copeland et al., 2010). In early S-phase, CIZ1 inhabits sub-nuclear foci coincident with DNA replication foci and promotes initiation of S-phase in a p21 independent manner (Ainscough et al., 2007; Coverley et al., 2005). Furthermore, it has been reported that DNA replication activity is driven through N-terminal regions of CIZ1 protein, while the C-terminus interact with the dynamic sub-nuclear scaffold (nuclear matrix) (Section 1.6.2). The CIZ1-matrix interaction is strong in differentiated cells, but relatively weak in stem cells (Figure 5.1).

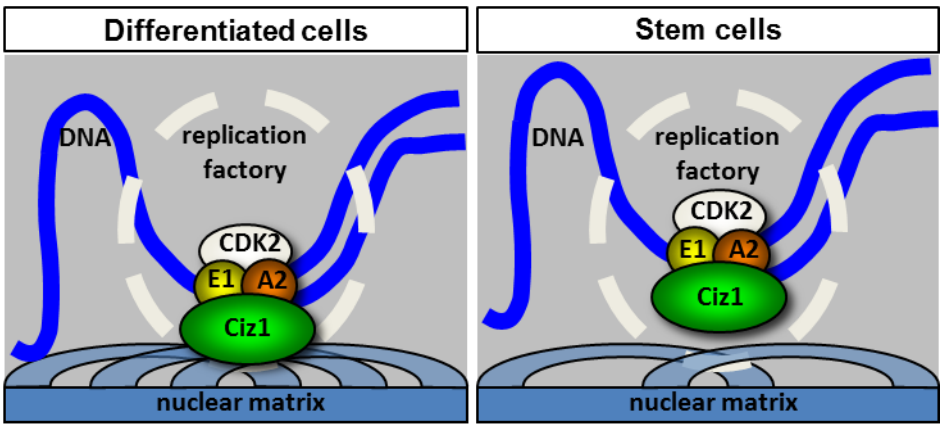

Figure 5.1 Interaction of CIZ1-matrix with cell cycle factors. The replication factory, which include CIZ1, CDK2 and cyclin E (E1) and cyclin A (A2), interact with the nuclear matrix in differentiated cells. This interaction is weak in stem cells.

To begin to understand the potential role CIZ1 might play in regulation of pluripotentiality and differentiation two existing mouse models will be utilized. These have both been developed in the Ainscough laboratory at Leeds, with one that enables upregulation of CIZ1 expression (CIZ24 mouse), and the other loss of CIZ1 expression (CIZKO mouse).

The CIZ 24 mouse allows for conditional up-regulation of full length CIZ1 expression as described in (Bageghni et al., 2017). This is a double transgenic model system that requires expression of a tetracycline regulatable transactivator molecule (tTA) to facilitate tissue and temporal specific expression. Bidirectional conditional promoters (mini CMV promoters flanking a tetracycline response element - TRE) are used to promote expression of mouse CIZ1 tagged with EGFP and a LacZ reporter gene (Figure 5.2).

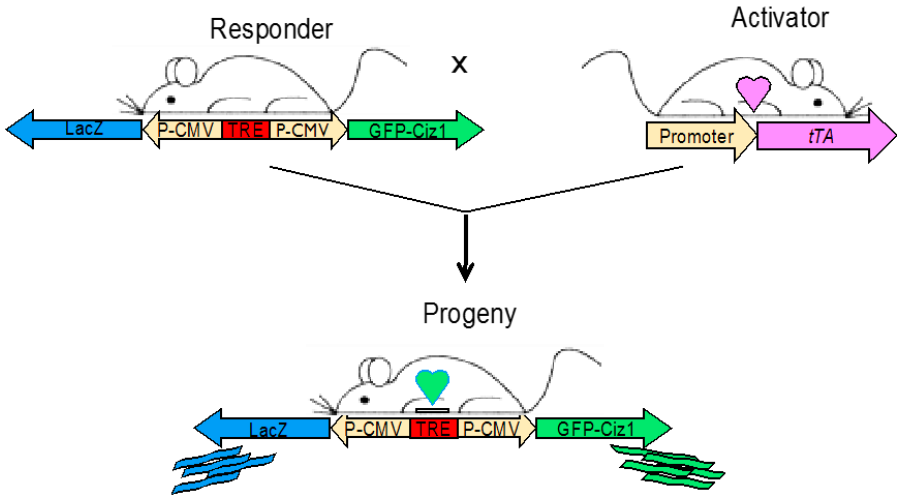

Figure 5.2 Breeding strategy used to obtain conditional double transgenic mouse model (CIZ 24) overexpressing CIZ1. Tetracycline transactivator (tTA), mouse *CIZ1* tagged with EGFP (EGFP-Ciz1), tetracycline response element (TRE), reporter gene (LacZ) and minimal Cytomegalovirus promoter (P-CMV).

In previous experiments a cardiomyocyte specific transactivator mouse was used to limit expression to this cell type only (Bageghni et al., 2017). In this chapter, the activities of three ubiquitous promoters are going to be quantified and compared in mouse tissues. The first promoter is a viral promoter (cytomegalovirus; CMV). The second promoter is an artificial compound (The CMV enhancer fused to the chicken β-actin promoter/rabbit β-globin intron composite promoter; CAG) and ROSA26 locus (Gt(ROSA)26Sor), which became the preferred docking site for the ubiquitous expression of transgenes (Chen, C. et al., 2011). These promoters can be used to drive expression in all cell types. In addition, any

promoter can be used to drive tTA enabling expression in any cell type of interest.

The CIZKO mouse does not express any CIZ1, in the homozygous state. In the heterozygous state expression is reduced to approximately 50%. This mouse was generated using a promoter trap mutational insertion of a NEO selectable marker, by the Texas Institute for Genomic Medicine (TIGM - ES cell clone IST13830B6). The mouse is fully viable and fertile, and develops normally during early life.

By combining these two models to generate a triple transgenic mouse it should be possible to produce mice (and derived cultured cells) that are ROSA-rtTA and EGFP-CIZ1 positive on a CIZ1 deficient background. Thus these mice would not express CIZ1, but using tetracycline (or more commonly the analogue doxycycline) could be induced to express CIZ1 at levels far above normal. This mouse would provide an important source of cells in which the level of CIZ1 can be regulated (Figure 5.3), for generation of induced pluripotent stem (iPS) cells and their subsequent differentiation into any differentiated cell types.

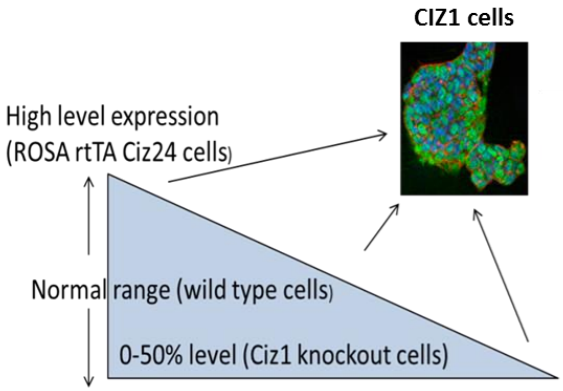

Figure 5.3 Isolate cells from two transgenic mouse lines (Ciz1 knockout and overexpression) and wild type mouse. Also, isolated cells from triple transgenic mouse will be studied before and/or after adding doxycycline (dox). Using dox will increase CIZ1 expression level in those cells from 0-50% to over 100%.

Several lines of research led to the first report of iPS cells in 2006. In 1962, Sir John Gurdon provided the first indisputable evidence that somatic amphibian cells retain all the necessary information for generation of all cell types in the adult body (Gurdon, 1962). It took a further 35 years for Gurdons observations to be confirmed in a mammalian system, when Sir Ian

Wilmut reported the birth of Dolly the sheep, created by somatic cloning from mammary epithelial cells (Wilmut et al., 1997). These successes confirmed that differentiated cells contain all of the necessary genetic information required for the generation of a whole organism, and the oocytes provided the necessary environment to reprogram nuclei of somatic cells. In 2001, Takashi Tada and colleagues demonstrated that pluripotent ES cells could similarly provide the necessary factors for reprogramming somatic nuclei (Tada et al., 2001). In 2006 Shinya Yamanaka reported that as few as 4 factors were sufficient for inducing pluripotency in differentiated mammalian somatic cells, which they named iPS cells (Takahashi, K. and Yamanaka, 2006; Yamanaka, 2012; Graf, 2011).

Yamanaka demonstrated that a cocktail of Oct4, Sox2, c-Myc, and Klf4 transcription factors, introduced by retroviral transduction, could induce mouse fibroblasts to achieve pluripotency under ES cell culture conditions (Takahashi, K. and Yamanaka, 2006). The morphology, growth properties and marker gene expression profile of the reprogrammed (iPS) fibroblasts were similar to ES cells (Takahashi, K. and Yamanaka, 2006). Oct4 and Sox2 work together to co-regulate target genes involved in the management of pluripotency (Avilion et al., 2003). C-myc is an oncogene that regulates cell proliferation, differentiation, growth and apoptosis. In 2008, Werning group has shown that c-Myc is dispensable for reprogramming. However, its involvement does highly increase reprogramming efficiency (Wernig et al., 2008). Klf4, which is highly expressed in undifferentiated ES cells, adult gut, lung, and testis functions to maintain proliferation, cell survival, prevent ES differentiation (Zhang, P. et al., 2010) and are involved in epithelial cell differentiation (Foster et al., 2005).

When iPS cells are injected into mouse blastocysts, they contribute to development of all embryonic lineages (Takahashi, K. and Yamanaka, 2006). However, a key problem associated with the use of viral vectors, and c-Myc in particular, is genetic mutations which can lead to tumour formation. To circumvent this Nakagawa reported a modified iPS cells protocol that reprogrammed mouse and human fibroblasts without c-Myc. However, efficiency of iPS cell induction was severely compromised (Nakagawa et al., 2008). A further methodology that has been tested uses multi-protein plasmid based vectors to introduce the reprogramming factors by non-viral means, removing potential problems associated with viral integration into the mouse genome (Kaji et al., 2009).

Since many cell types can be generated from iPS cells, successful reprogramming of somatic cells from human patients, by whatever means, offer exciting possibilities for use in regenerative medicine, screening of drugs and the generation of novel disease models. Development of robust protocols for accurate cell differentiation from the iPS state would provide a significant hope of tissue regeneration to replace or repair the degenerated tissue (Zhang, F. et al., 2011). However, at this time the mechanisms that regulate induction of pluripotency, and methods for efficient differentiation into mature cell types that might be usefully applied to regenerative medicine remain poorly understood.

The immediate goal of this project is to induce pluripotentiality in cells derived from mice lacking CIZ1 and mice with excess production of CIZ1. Transfection and transduction procedures will be developed further using Ds-Red reporter vectors available in the laboratory, until robust methodology has been established. If required an alternative plasmid based approach is available that eliminates the need for generation of virus. This approach has been successfully used by another group in LIGHT (Adam Odell, personal communication) and the techniques can be adapted to this project. It is possible that different levels of CIZ1 will have a fundamental impact on capacity for cells to reprogram. Indeed, this is a key point to be tested in this project. Based on our current understanding of CIZ1 and its role in regulating the cell cycle we are working towards testing the hypothesis that low levels of CIZ1 (as seen in stem cells) may have a positive impact on the cells ability to reprogram.

The aim of this chapter, testing the hypothesis that low levels or loss of CIZ1 may have a positive impact on the cells ability to reprogram or cancer development, without introduction of additional oncogenic stimuli. To help us test this hypothesis we need to:

1. Generate a triple transgenic mouse model
2. Phenotypic characterisation of CIZ24 and CIZKO mouse models
3. Generate iPS cells from this mouse model and Test these cells directly for changes in their cell activity, DNA replication and proliferation.

5.2 Methodology

All reagents in this chapter were purchased from Sigma-Aldrich Ltd unless otherwise stated.

5.2.1 Breeding strategy

To generate triple transgenic mice, the ROSA-rtTA transgene was transferred onto the CIZ1 knockout (CIZKO) homozygous (Ciz1-/-) background (Ciz1-/-, ROSA+). At the same time, the Ciz24 transgene was also transfer onto the Ciz1-/- background. Selected CIZ1 knockout heterozygous (Ciz1+/-), Ciz24+ progeny was mate with Ciz1-/-, ROSA+ progeny. As a result, progeny were a mix of Ciz1-/- and Ciz1+/-, with or without ROSA and/or Ciz24. Finally, a breeding colony of ROSA+; Ciz24+; Ciz1-/- was establish and maintained.

5.2.2 Genotyping

5.2.2.1 DNA extraction

Mouse ear biopsies were incubated in 0.5 mL of tail lysis buffer (TLB) with 3µL proteinase K (10mg/mL) at 37°C overnight. The following morning, 0.4 mL of 1 Phenol: 1 (Chloroform (24): iso-amyl alcohol (1)) was added and the samples were shaken vigorously at 10 minute intervals for one hour, and then centrifuged at 13,000*g* for 15 min. After centrifugation, 0.4 mL of the supernatant was transferred into a sterile 1.5mL Eppendorf tube, 40ul of 3M NaCl and 0.44mL of isopropanol were added and mixed gently. Samples were left at room temperature for one hour to allow for complete preceipitation of the DNA. Following centrifugation at 13,000*g* for 30 min the supernatant was discarded, the DNA pellet washed with 70% ethanol, and residual ethanol removed by brief centrifugation. The pellet was re-suspended in 50µL Tris/EDTA (TE) buffer, vortexed briefly and left at 4°C for 24 h before complete resuspension by pipette.

5.2.2.2 Genotyping PCR

Location and sequence of specific primers were illustrated in (Table 5.1 and Figure 5.4). A master mix was prepared containing 2.5µL 10x buffer, 0.5µL 0.2mM dNTPs, 0.5µL forward sequence specific primers, 0.5µL reverse sequence specific primers, 0.25µL Taq DNA polymerase and water to make up the reaction volume to 24.7µL, followed by addition of 0.3µl DNA. DNA amplification was performed using an initial denaturation step of 94°C for 5 min followed by 29 cycles of 94°C for 30 sec, 60°C for 30 sec and 72°C for 45 sec. A final extension step of 72°C for 7 min ensured completion of products. PCR products were analysed by electrophoresis through 1% agarose gel.

Primers	Direction	Sequence	Size
LacZ 4	Forward	5´ AATGGTCTGCTGCTGCTGAACG 3´	(225 bp)
LacZ 5	Reverse	5´ GGCTTCATCCACCACATACAGG 3´	
tTA 1	Forward	5´ CGCTGGGGGGCATTTTACTTTAG 3´	(450bp)
tTA 2	Reverse	5´ CATGTCCAGATCGAAATCGTC 3´	
Downstream reverse (VR)	Reverse	5' CCAATAAACCCTCTTGCAGTTGC 3'	Wild type (Ciz1+/+) (515bp)
IST13830B6-F (IF)	Forward	5' GTGGCGTTGGCTATATCTGC 3'	
IST13830B6-R (IR)	Reverse	5' GTTGAACATGGTGGCTGAAG 3'	Ciz1-/- (360bp) Ciz1+/- (515bp & 360bp)

Table 5.1 Primers sequences used for genotyping mice and size of RT-PCR products.

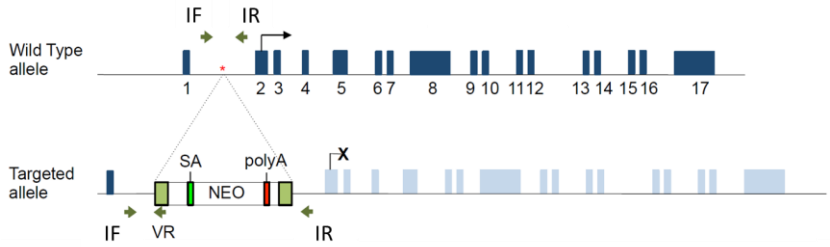

Figure 5.4 Location of Ciz1 primers that used for genotyping PCR. Three primers; one forward (IF) and two reverse (VR and IR) used to distinguish between Ciz1-/-, Ciz1+/- and Ciz1+/+ mice.

5.2.3 LacZ staining

The method used was adapted from (Ainscough et al., 1997). Briefly, cells and/or tissues were fixed for 5min at room temperature in 5% formaldehyde, 0.8% glutaraldehyde, 0.02% detergent, 1mM $MgCl_2$, 0.1mg/mL deoxycholate in PBS, then washed twice with PBS and incubated for 24 h in X-Gal staining solution (1 mg/mL X-Gal, 4 mM potassium ferrocyanide, 4 mM potassium ferricyanide, 2 mM $MgCl_2$ in PBS). Samples were then fixed in 4% formaldehyde overnight.

5.2.4 RTqPCR

5.2.4.1 RNA extraction

Mouse tissue samples and/or cells were homogenized and lysed in a 1.5mL tube by adding 1mL of TRI-reagent (Invitrogen) and gentle grinding. Homogenates were incubated at room temperature for 5 min to dissociate nucleoprotein complexes. Then 0.2mL chloroform was added and samples were incubated at room temperature for 5 min. The samples were centrifuged for 15 min at 12,000*g*. The upper aqueous RNA containing phase was transferred to a 1.5mL microfuge tube. Following addition of 0.5mL isopropanol and gentle mixing, the solution was incubated at room temperature for 10 min. RNA was pelleted by centrifugation for 10 min at 12,000*g*. The pellet was washed with 1mL 70% ethanol which had been prepared using DEPC treated water (Invitrogen). Residual ethanol was removed from the tubes after centrifugation. The RNA was re-suspended in 30-50µL RNase-free water, incubated for 10 min at 55°C, and then stored at -80°C until required.

5.2.4.2 cDNA preparation

DNase–free RNA was reverse transcribed into first-strand cDNA using reverse transcriptase SuperScript™ III. A 20µl reaction was prepared, containing the following: 5µl DNase-free RNA (0.25µg-1µg), 1µl random

hexamers, 1µl (10mM) dNTPs and 6µl DNase-RNase-free water. The reaction was heated to 65°C for 5 min, and then placed on ice while adding the following: 4µl 5x first strand buffer, 1µl (0.1M) DTT, 1µl RNaseOUT™ (40U/µl) and 1µl (200U/µl) SuperScript™ III. The reaction was then incubated at 50°C for 60 min and deactivated by heating up to 70°C for 15 min. The cDNA was stored at -80°C until required.

5.2.4.3 RTqPCR

To determine *Ciz1* expression levels relative to GAPDH, TaqMan® Gene Expression Assays (Applied Biosystems), were used. The assay reaction, which contained 1µL cDNA, 10µL TaqMan Universal MasterMix, 1µL specific primers (*GAPDH* (Mm99999915-g1) or *Ciz1* (N-terminal exon 10, Mm00503766-m1)), 1µL of TaqMan® probe and 6µL RNase free water, were loaded in triplicate in 96 well plates. The plates were covered and centrifuged for 5 min, then analysed using a 7500 Real Time PCR System under the following conditions: 50°C for 2 min, 95°C for 10 min and then 50 cycles of 95ºC for 15 sec and 60°C for 1 min. Results were analysed using 7500 System SDS software version 1.2.3. The formula: % Relative to GAPDH = $2^{-\Delta Ct}$ x 100 was used to calculate expression level of *Ciz1* normalized against an endogenous control (*GAPDH*).

5.2.5 Histology

5.2.5.1 Tissue processing

Following dissection, tissues were transferred immediately into histological grade formalin for 24h, then placed in histological cassettes and kept in 70% ethanol before processing. Cassettes were processed on a Leica ASP200 tissue processor (Leica Microsystems (UK) Ltd, UK) using a routine protocol. Briefly, cassettes were dehydrated in a series of ethanol solutions, starting with 70% and completing with 100%. Cassettes were cleared from ethanol by using multiple changes of xylene, and finally infused with paraffin wax (The protocol details; Appendix C.1.1). Agar embedded cells pellet and

spheroids were embedded in paraffin wax (CellPath Ltd, UK) and the paraffin blocks were stored at 4˚C until sectioning.

5.2.5.2 Sectioning

The paraffin blocks were sectioned at 4µm using microtome (AS325 retraction Thermo Shandon; Thermo Scientific, UK). Sections were placed in a water bath (Leica HI1210; Leica Microsystems (UK) Ltd, UK) at 45˚C and, carefully, one section was placed onto superfrost® plus glass slides (Thermo Scientific, UK). The slides were dried overnight in an oven (Galaxy B; Scientific Laboratory Supplies Ltd (SLS), UK) at 37˚C. Prior to staining, the slides were heated for 20 min at 60˚C on a hot plate (SH3, Stuart Scientific, Bibby Scientific Limited (Group HQ), UK).

5.2.5.3 Staining

5.2.5.3.1 Haematoxylin and Eosin (H&E) Staining

The slides were dewaxed and stained, as described in Section 2.2.5.5.2.

5.2.5.3.2 Immunostaining

Immunostaining for CD antigens was performed by Mr Michael Shires (senior technician, LICAP, University of Leeds) using rabbit anti-CD3 for T cells (Abcam, ab16669) at 1:200 and goat anti-CD20 for B cells (Santa Cruz Biotechnology, sc7735) at 1:500.

5.2.5.3.3 Histological assessment

The histological assessment was performed by Dr Jo-an Roulson (Urological Pathology, LIMM, University of Leeds).

5.3 Results

5.3.1 Transgenic mice and breeding strategy

In the Ainscough laboratory at Leeds, there are two transgenic mouse models that are relevant to this project, as described in the Introduction. CIZ24 mice provide potential for expressing CIZ1 at high levels under doxycycline control (Bageghni et al., 2017). Homozygous CIZ1 knockout (Ciz-/-) mice do not express CIZ1, while heterozygous animals express CIZ1 at approximately 50% of wild type level (Ridings-Figueroa et al., 2017). A key objective of this project is to generate triple transgenic mice in which expression of CIZ1 can be upregulated from 0% to very high using doxycycline. The homozygous Ciz-/- mice have been mated with ubiquitously expressing ROSA-rtTA mice. Progeny from the first generation have been genotyped and confirmed as CIZKO heterozygous (Ciz1+/-) and ROSA-rtTA positive. These progeny are currently being interbred to generate Ciz1-/-; ROSA-rtTA progeny. Breedings have also been established between Ciz1-/- mice and CIZ24 positive mice. Once Ciz1+/-; CIZ24 progeny are confirmed they will be bred with Ciz1-/-; ROSA-rtTA mice to generate a mix of Ciz1-/- and Ciz1+/- mice, with or without ROSA-rtTA and/or CIZ24. Finally, a ROSA-rtTA; CIZ24; Ciz1-/- breeding colony were established for continued use in this project (Figure 5.5).

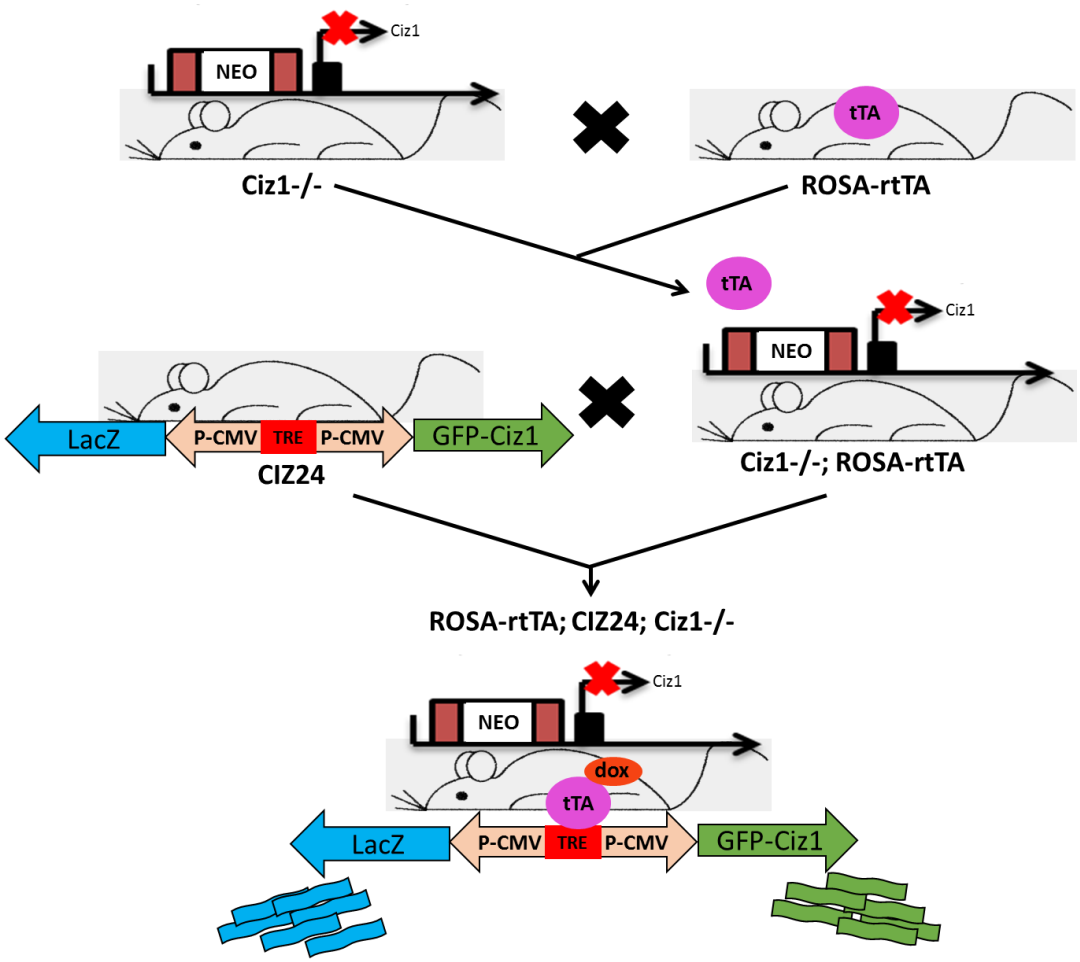

Figure 5.5 Breeding strategy used to obtain conditional triple transgenic mouse model expressing CIZ1 in the presence of doxycycline. tetracycline transactivator (tTA) Ciz1 gene trap IST13830B6 (NEO), mouse *CIZ1* tagged with EGFP (EGFP-Ciz1), tetracycline response element (TRE), reporter gene (LacZ), Minimal Cytomegalovirus promoter (P-CMV) and doxycycline (dox).

5.3.2 Progeny characterisation

To identify appropriate progeny, a reliable genotyping PCR strategy was used that had been developed previously. DNA was extracted (Methodology; section 5.2.2.1); from mouse ear biopsies taken for identification purposes and PCR amplification performed with forward and reverse primers (Section 5.2.2.2). Knockout line specific primer set (IF, IR and VR) can be used to distinguish between homozygous (-/-), heterozygous (+/-), and wild type (+/+) mice. The LacZ primers set verify the presence of CIZ24 transgene, and the tTA primers set verify the presence of the transactivator transgene. Band size and gel electrophoresis pattern were used to confirm

identity of each mouse (**Figure 5.6**). Mice of all expected genotype combinations have been produced with no evidence of lethality.

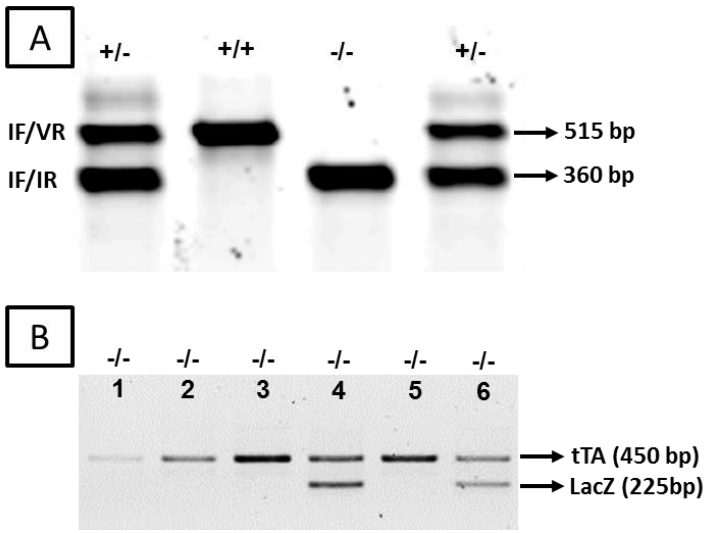

Figure 5.6 Genotyping of Ciz1-/- mice. A) IF, IV, VR primers were used. Lanes 1 & 4 heterozygous (+/-), Lane 2 wild type (+/+) and lane 3 homozygous (-/-) progeny. B) tTA and LacZ primers were used to identify single transgenic (Lane 1-3 & 5) and double transgenic (Lanes 4&6) mice.

5.3.3 Evaluation of CIZ1 and LacZ expression

Following confirmation of the presence of the CIZ24 and ROSA-rtTA transgenes in the same animal it is possible to evaluate tissue specificity of CIZ1 activation using the LacZ reporter gene as a marker. To test this system, cells and/or tissues were fixed in a mild fixative and then incubated in staining solution overnight in the dark. Figure 5.7 shows that within a single tissue type, such as the kidney, different transactivator lines will drive transgene expression in entirely different sub-sets of cells. The ROSA-tTA transgene provides reasonably widespread expression in kidney (and other tissues – data not shown), but not equally in all cell types. Compared to the endothelial expression observed through using the Tie1 promoter, expression in endothelium appears weak from the ROSA promoter (**Figure 5.7**). The CMV promoter appears to drive less stable expression and is therefore less suitable for use as a ‘ubiquitously’ expressing line. Clearly these issues can have a significant impact on phenotypic differences between animals, associated with gene overexpression. Examination of

LacZ expression provides an excellent means of assessing this. Transgenes are also often susceptible to inactivation by epigenetic mechanisms, sometimes throughout the tissue, but often in a more unstable mosaic fashion. LacZ monitoring at regular intervals also enables potential shut down to be identified in a transgenic line at a very early stage. At this time the CIZ24 line shows good activity that is controllable with Doxycycline and thus suitable for further use in this project.

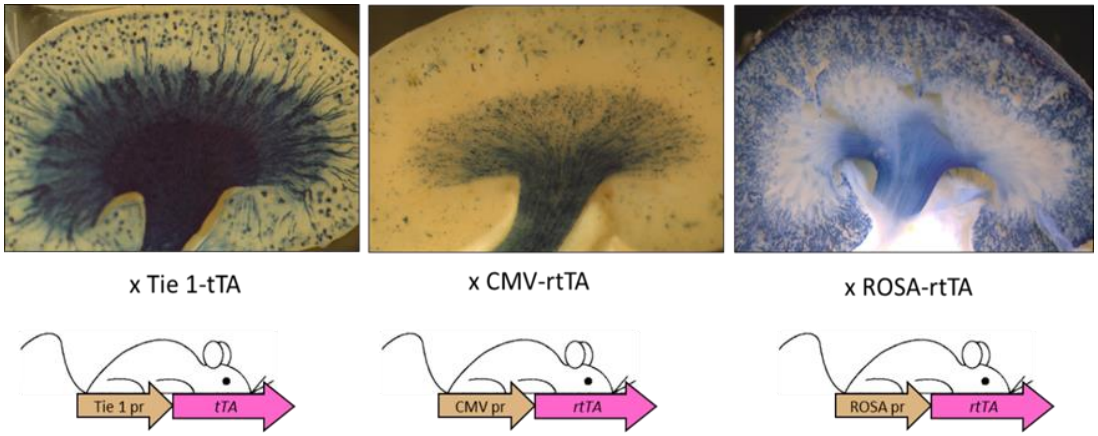

Figure 5.7 LacZ staining of kidney tissues from different transgenic lines. Tie1-tTA is specific for endothelial cells, CMV-rtTA and ROSA-rtTA are reported to be expressed in most cell types but clearly show a high degree of variability, visualised by the broad range of LacZ activity.

5.3.4 CIZ1 expression level in transgenic mice

In addition to monitoring LacZ expression it is extremely important to confirm that the CIZ1 transgene is also expressed. A range of tissues (including kidneys) from ROSA-rtTA; CIZ24 and control mice were homogenized and lysed for RNA extraction. The controls were rtTA negative and therefore should express CIZ1 at normal levels. All mice received doxycycline in their drinking water for 2 weeks prior to tissue isolation. Dox activation and tissue extraction were performed previously by J Ainscough, and the tissue samples stored at -80°C. CIZ1 expression was examined by quantitative RTqPCR (Figure 5.8).

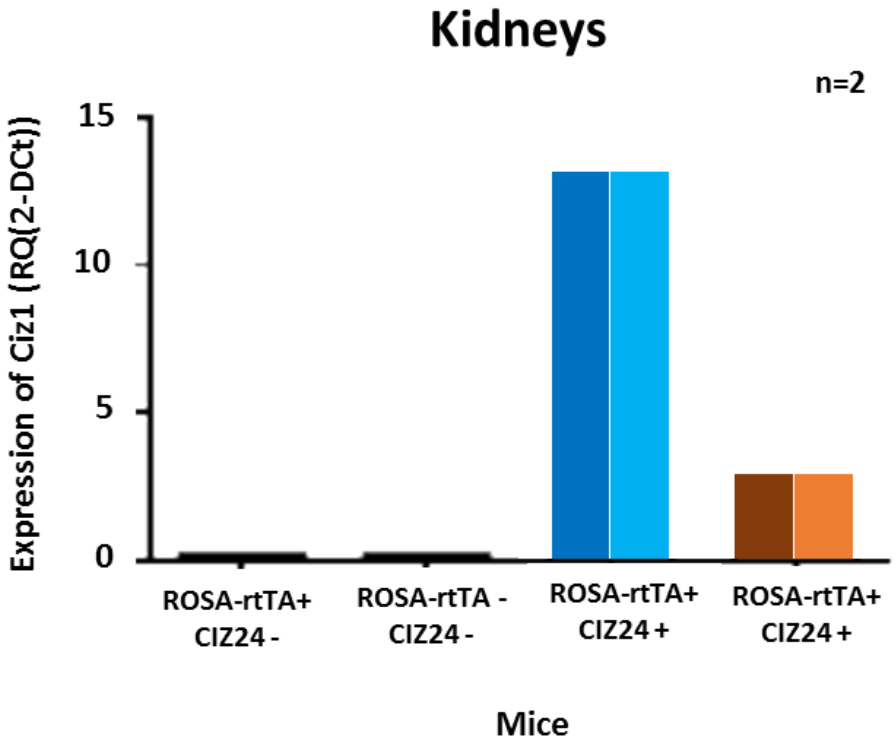

Figure 5.8 Expression of *Ciz1* in kidneys from ROSA-rtTA;CIZ24 mice using RTqPCR. Values were normalized relative to the housekeeping gene (*GAPDH*). ROSA-rtTA + ;CIZ24 - and ROSA-rtTA - ;CIZ24 - are negative controls, two ROSA-rtTA + ;CIZ24 + are overexpressing *Ciz1*.

The experiment was repeated twice and gave the same results, indicating that individual experimental mice express Ciz1 at different levels within the same tissue. This might be because their level of exposure to doxycycline cannot be accurately controlled resulting in different levels of activation. More likely is the genetic status i.e. zygosity for transactivator and Ciz1 transgenes affecting expression. Mice homozygous for both might be expected to express 2x heterozygous for Ciz1, (even if homozygous for tTA), and heterozygous for both could be lower. All depends on relative dynamics of number of TA molecules available, for which no data is available. Alternatively, the tissue samples contain different proportions of individual cell types of the kidney, some of which are ROSA promoter active and others not. These issues must again be considered throughout this project.

However, at this stage I have confirmed the suitability of the CIZ24 and ROSA-rtTA transgenes for this project.

5.3.5 Phenotypic characterisation of Ciz1-/- mouse models

Viable Ciz1-/- mice showed no difference in growth rate up to 160 days (Figure 5.9 A) and had no significant differences body weight defects (Figure 5.9 B). This is demonstrating that CIZ1 is not essential for embryogenesis, early post-natal development, or cell viability ex vivo. Notably, in all Ciz1-/- adult females, there were some enlarged organs such as spleen, liver and lungs, in comparison to wild type (Ciz1+/+), whereas kidneys and heart were not affected (Figure 5.10). Lungs have thickened vessels and liver has nodular outgrowths (Figure 5.11). Also, lymph nodes in the body cavity were enlarged, whereas brain was normal (Figure 5.11).

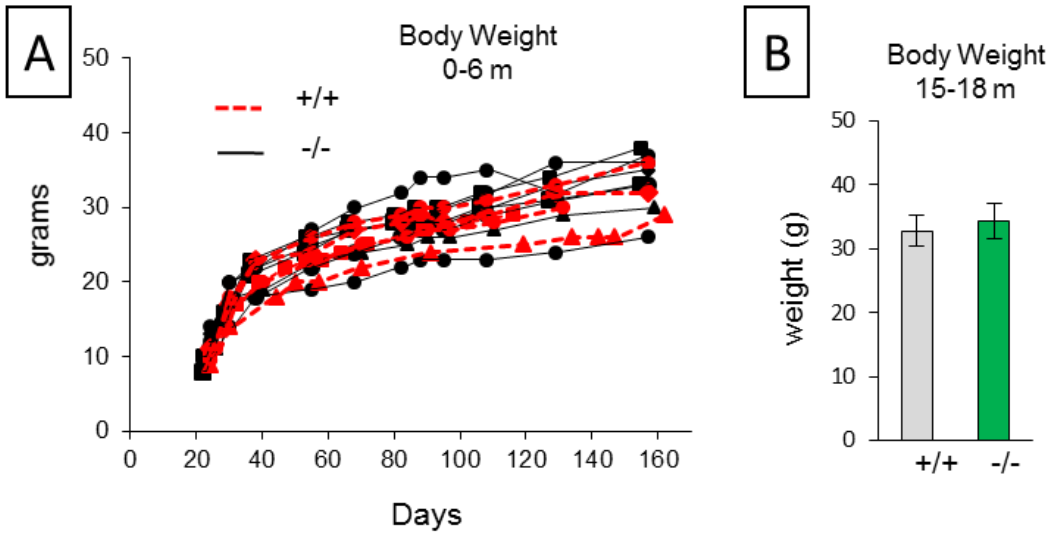

Figure 5.9 Growth profiles of knockout (-/-) compared to wild type (+/+) mice. A) Growth of Ciz1+/+ (n = 5) and Ciz1−/− (n = 8) mice between 20 and 160 days after birth. B) Compare the body weight at 15–18 month old in Ciz1+/+ (n = 8) and Ciz1−/− (n = 7) females. Adapted from (Ridings-Figueroa et al., 2017).

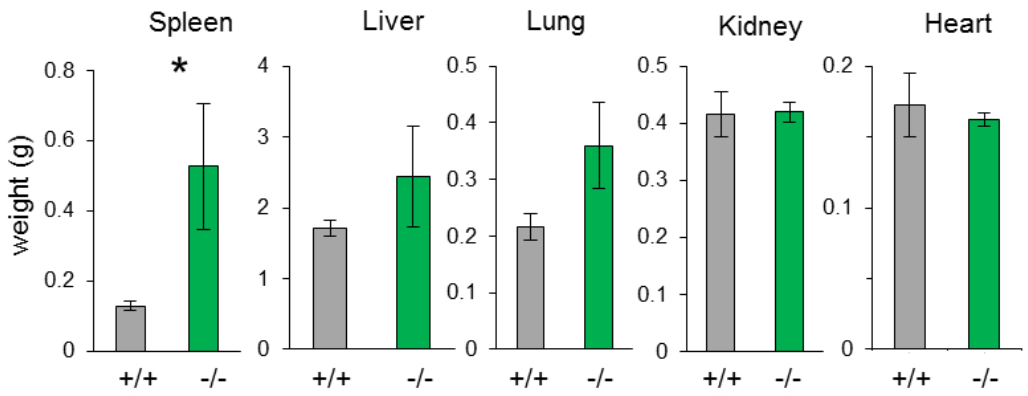

Figure 5.10 Organs weight of Ciz1−/− females. Weight in grams (g) of spleens (n = 8 Ciz1+/+; n = 6 Ciz1−/−), livers (n = 6 Ciz1+/+; n = 4 Ciz1−/−), and lungs (n = 5 Ciz1+/+; n = 5 Ciz1−/−). Other organs, including the kidney and heart. Adapted from (Ridings-Figueroa et al., 2017).

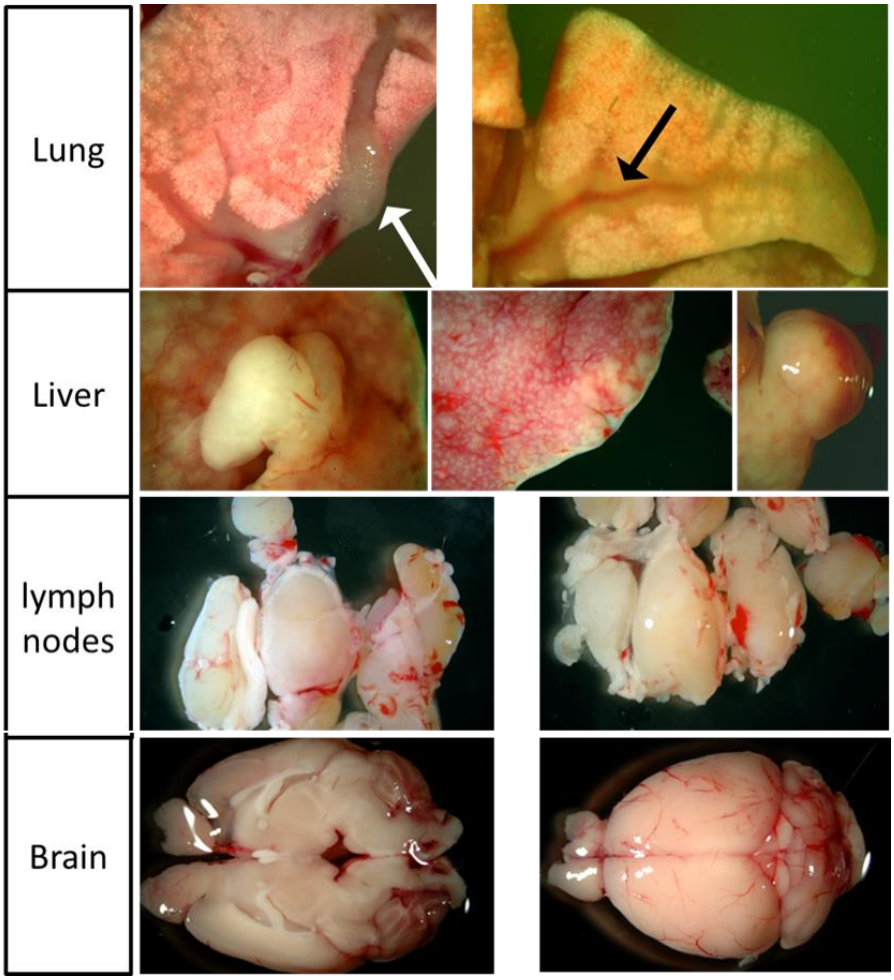

Figure 5.11 Gross anatomy of Ciz1-/- mice, Enlarged organs such as lung, liver and lymph nodes and other normal tissues such as brain were imaged by Nikon D70S, attached to Zeiss SV6 binocular scope.

Secondary lymphoid tissues such as spleen, enlarged in Ciz1−/− (fivefold; 181–3679 mg) comparing to Ciz1+/+ (88–167 mg) mice (Figure 5.12 A). In the secondary lymphoid sites, B and T lymphocytes interact with each other and non-lymphoid cells in search of antigens. The lymph node and spleen architecture were abnormal (Figure 5.12 A and C), with abnormal B (CD20 +ve) and reactive T (CD3 +ve) lymphocytes in all affected tissues (Figure 5.12 B and C).

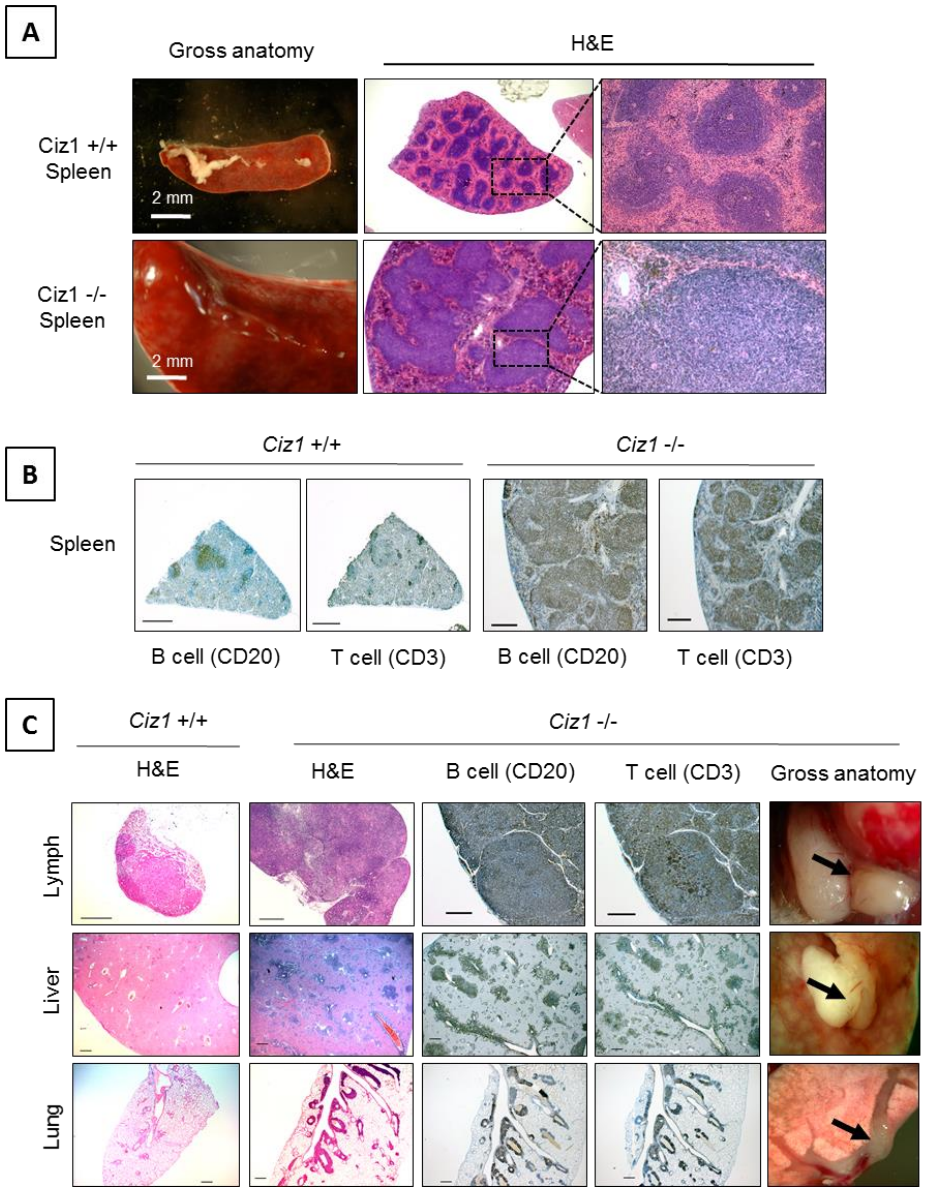

Figure 5.12 Spleen histology in Ciz1+/+ and Ciz1-/- mice, A) represent the gross anatomy and H&E staining. B) immunostaining of spleen using T cell marker (CD3) and B cell marker (CD20). C) Lymph node, liver, and lung histology. In the left, H&E staining of Ciz1+/+ organs, followed by H&E of Ciz1-/- organs then immunostaining using CD3 and CD20. At the far end to the right, gross anatomy for the organs. Bar, 200 µm. Adapted from (Ridings-Figueroa et al., 2017).

5.4 Discussion

In mouse model (Ciz1-/-), the histology indicated that lack of CIZ1 lead to tumour formation though deregulated proliferation within lymphoid lineages in females. In aging mice, it has been found at the cellular level 100% (8/8) of female mice developed non-Hodgkin follicular type lymphomas. Three out of eight mice resembled high-grade transformation with large B cell lymphoma (Ward, 2006). Currently, this mouse model was used to prove that CIZ1 localize with Xist long non-coding RNA that coats the inactive X chromosome in female cells ((Ridings-Figueroa et al., 2017); see Appendix G). Due to circumstances beyond my control, I was unable to continue this line of research and commenced a new project with a different supervisor, focussing on Ewing sarcoma.

Chapter 6
Conclusion and future directions

The main hypothesis of the ES family tumour project was to prove the existence of ES-CSCs and to identify the key molecular signature. The objectives were: firstly to validate the currently available CSCs surface marker ‘CD133’. Secondly, to determine whether 3D spheroids formed from a single cell could be utilised as a beneficial *in vitro* tool to enrich for cells with CSCs properties as well as to aid in the identification of factors that contribute to tumour development and progression. Additionally, it was important to testify the preliminary data and to optimize and validate methods using established ES cell lines.

ABCG1 and miR-210 were identified as drivers of putative ES-CSCs. The advantage of using the functional self-renewing spheroid assay over cell surface markers such as CD133 is to identify a key molecular signature based on self-renewal ability. MYC-C and EBAF were also identified and validated and were shown to increase in ES spheroids compared to cells grown as substrate adherent cell lines; MYC-C is known to be expressed at high levels in ES (regulated by EWS-FLI1) whereas EBAF was a novel observation. The key findings are summarised in Figure 6.1.

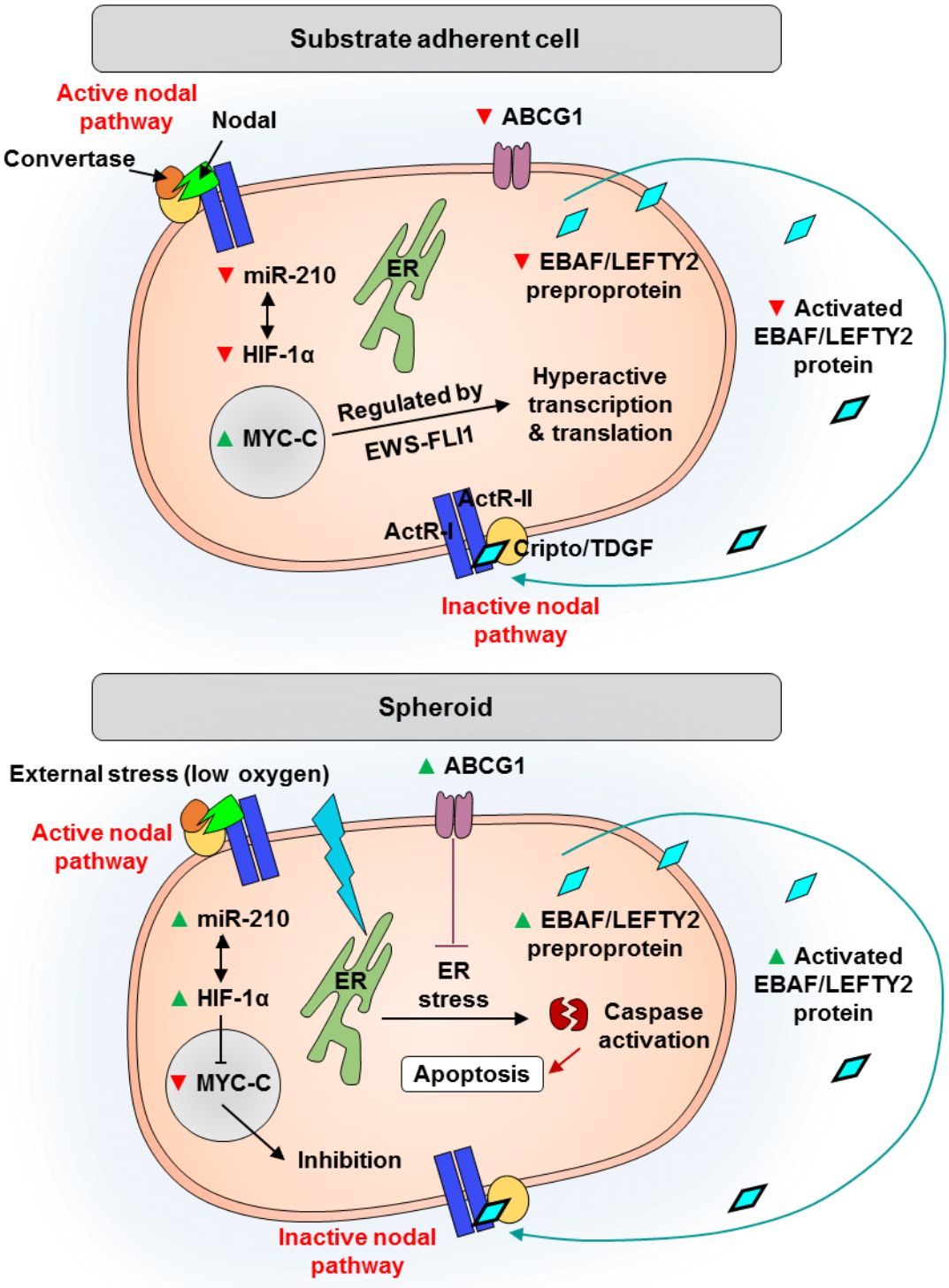

Figure 6.1 Summary of key finding of this project. The expression level of MYC-C is high in substrate adherent cells compared to spheroids, whereas other genes including HIF-1a, ABCG1 and EBAF as well as miR-210 are lower than in spheroids. The EBAF is secreted from the cell and then activated allowing its binding to the complex of activin receptors type I and II (ActR-I and ActR-II) combined with cripto to inactivate the nodal pathway. The increased expression of ABCG1 in spheroids inhibits the apoptosis through the inhibition of the ER stress. In addition, the increase in miR-210 and HIF-1a due to low oxygen levels results in inhibition of MYC-C expression.

6.1 Isolation of ES-CSCs

Similar to normal SC, CSCs have the capacity to self-renew and differentiate to different cancer phenotypes. However, they are not capable of developing truly multi-lineage progeny. Although it has been reported that CSCs are resistant to the current cancer treatments and express proposed SC markers, there is heterogeneity in the expression of these markers and no specific maker has been described is reliable on multiple cancer types. Therefore, there remains a real need for the identification of a new molecular factor that could serve as a biomarker for the self-renewing CSC population. Focusing on SC genes only and the extracellular markers to discover novel markers are not beneficial because ES is poorly differentiated and highly express the majority of SC markers (Berry, personal communication). One of the general limitations of the approach I used was that the antigenic profile would be affected by many factors such as media condition.

The CSCs surface marker 'CD133' which is frequently used to isolate the putative ES-CSCs (Suvà et al., 2009; Jiang et al., 2010) was used in this study. The enrichment isolation of a pure CD133+ve cell population using FACS (97-99%) was more reproducible, however cells sorted by FACS have to be maintained in culture medium which contains antibiotics to minimise the risk of contamination. Since antibiotics are known to have an effect on the gene expression profile, the isolated cells were not used for more experiments. On other hand, the purity of isolated CD133+ve cell population using magnetic cell isolation technology (MACS®) (purity 60%) was not extremely high, and might have been due to protein glycosylation (Pelagiadis et al., 2012). Cells sorted by MACS® were also not used since the high purity was required for more accurate results. To overcome this issue, a functional method '3D spheroids assay' was used to enrich putative ES-CS-like cells. Even then, it was very difficult to measure the expression level of CD133 in putative ES-CS-like cells, which were enriched using functional methods '3D spheroid assay' or using FACS, however WB analysis showed no CD133 expression in spheroids, which means that the population expressing the CD133 marker was very small or non existent.

Therefore, further methods needed to be explored such as in situ, immunocytology, localization and/or IHC in spheroids.

Based on the 3D spheroid assay, two out of three ES family tumours cell lines reproducibly contained a self-renewing CSCs population and were capable of generating 3D spheroids in low adherent culture without a requirement for a specific stem cell medium frequently used to maintain stemness. The non-stem cell media was used to compare the monolayer cells with spheroids for two reasons. Firstly, it was used to reduce the variation and to standardize the culture conditions that might have an effect on the expression of cell markers. Secondly, the currently available commercial stem cell media contains a high level of bFGF that as the undesired effect of inducing ES cells to quiescence.

In other reports the spheroids are aggregates of cells grown in 3D culture methods (Fujii et al., 2009; Kelly, J.J.P. et al., 2009; Cornaz-Buros et al., 2014). These ‘3D spheroids’ are commonly used for studies of drug screening, proliferation of tumours and immune interactions, whereas spheroids embedded in a matrix are used for studies of invasion and angiogenesis (Mueller-Klieser, 1987; Gottfried et al., 2006; Hirschhaeuser et al., 2010; LaBarbera et al., 2012). Spheroids are a more physiological research tool than adherent cell lines as they are able to recapitulate interactions between cells, multicellular spheroids and the microenvironment (Fennema et al., 2013) in addition to enabling the study of transport properties of drugs, oxygen and nutrients (Mehta et al., 2012). Like poorly vascularized tumours with intra-tumoral hypoxia, large spheroids form proliferation zones including an intra-spheroids hypoxia ‘necrotic core’ which result from developing gradients of oxygen and nutrients (Mueller-Klieser, 1987; Hirschhaeuser et al., 2010).

The size of the spheroids will impact on their suitability for different investigations; including cell function besides drug penetration and transport. It has been proposed that the most acceptable spheroid size for the study of drug testing is 200 µm whereas larger spheroids between 200 and 500 µm are sufficient to study cell functions including recapitulate cell–cell interactions (Friedrich et al., 2009). In this project, the 3-week spheroids that were generated from ES cell lines were an ideal model based on the size of

spheroids of between 400 and 700 µm. The spheroids at 3 weeks were also intact and so the quality of RNA and protein extracted was good for downstream analyses. Furthermore, tumour vascularization may be assessed by the migration of endothelial cells into spheroids or the formation of small vasculature within spheroids (Timmins et al., 2004). This is achievable *in vitro* by formation of spheroids from a mixture of tumours cells and endothelial cells (Timmins et al., 2004; Ghosh, S. et al., 2007; Upreti et al., 2011). The 3D spheroids in this project were generated from ES cells only and they seemed to alleviation of hypoxia through generating a sheet/tube of cells which looked like tails (Section 2.3.2.2.1, Figure 2.25).

6.2 Expression of significant drivers in ES-CSCs

EBAF was significantly increased in ES-CSCs compared with substrate adherent cells. The high expression of EBAF mRNA and protein were confirmed in this thesis. The activated EBAF protein, which is normally secreted outside the cells as preprotein, was reported to function as an inhibitor of the Nodal-signalling pathway in metastatic cancer cells and may abrogate cell tumorigenicity (Postovit et al., 2008). However, many cancer cells reactivate the Nodal pathway as a result of the absence of its negative regulator EBAF (Postovit et al., 2008; Lawrence et al., 2011). Like embryonic stem cells (ESC), in this project EBAF was highly expressed at protein and RNA level in putative ES-CSCs spheroids compared with adherent cells. The un-methylated status of the EBAF gene leads to high-level expression of EBAF in ESC. However, in melanoma cells, the existence of methylated status of EBAF could explain their inability to produce this inhibitor (Costa et al., 2009). Moreover, it has been reported that miR-302 targets EBAF directly resulting in a negative variation of its expression in ESC. In contrast, in this project miR-302 was not expressed in substrate adherent cells or spheroids, which highly expressed EBAF. This phenomenon may be critical for the stability of EBAF in pluripotency and germ layer (Barroso-delJesus et al., 2011; Cavallari et al., 2013). The methylation status as well as the effect of EBAF on Nodal-signalling pathway has not been assessed in this project

and it would be interesting to do a functional study such as knock-in and knock-out on EBAF in ES family tumours.

The comparison between the substrate adherent cells and 3-w-spheroids identified three statistically significant intracellular drivers: MYC-C, miR-210 and ABCG1. The expression of miR-210 and ABCG1 was highly upregulated, whereas MYC-C expression was decreased in the putative CSCs population of the 3D spheroids. Overexpressing miR-210, which regulate expression of HIF-1α and HIF-2α, leads to bypass cell cycle 'G1' arrest in hypoxic condition and changes the hypoxic gene expression signature (Zhang, Z. et al., 2009). High expression of miR-210 has also been correlated with tumour metastases (Zhang, Z. et al., 2009). This finding supports a possible oncogenic role for miR-210, which may facilitate adaptation of cancer cells to the hypoxic microenvironment, as well as target the MYC-C antagonist known as Max-binding protein MNT (MNT) (Zhang, Z. et al., 2009). It is known that antagonizing MYC-C transcriptional activity inhibits canonical Wnt signalling through miR-210 and its regulator HIF-1α leads to reduced tumour cell proliferation; arguably it has been proven that this phenomenon helps tumour cell survival under hypoxic stress (Koshiji et al., 2004; Kaidi et al., 2007). It has been suggested that increased miR-210 expression promotes tumour initiation which could be responsible for the opportunity of tumour cells to overcome the stressful microenvironment (Huang, Xin et al., 2009). Also, HIF-2α regulates miR-210 expression to promote cell proliferation (Gordan et al., 2007).

The generation of the necrotic area is due to size of spheroids. As size exceeded 100um then O_2 and nutrients cannot pass into spheroids and so areas of hypoxia arise and then cells die giving raise to necrosis. With the existence of intra-spheroids hypoxia and increased miR-210 as well as decreased MYC-C, cells in the 3-w-spheroids survive and continue growing for a week then the majority of the cells start the apoptotic process. Elucidation of this would clarify whether cells with self-renewal capacity are more likely to keep their self-renewal ability for a long period or are merely trying to survive under the hypoxic stress.

Moreover, it has been noticed in this project that some of the 3-w-spheroids started to form a tube which resembles a tail and it is possibly a sheet of cells. This phenomenon occurred in almost all spheroids from week 4 onwards. Possibly, the intra-spheroids hypoxia stress might stimulate the tubule formation to oxygenate cells and provide nutrients. In tumours, cells induce angiogenesis to deliver nutrients and oxygen as well as clear metabolic waste and carbon dioxide to sustain the tumour cells. Also, this phenomenon facilitates metastasis (Hanahan and Weinberg, 2011). Many miRNAs have been reported to be involved in angiogenesis including miR-210 (Donnem et al., 2012). Overexpression of miR-210 prompted the formation of capillary-like structures and migration and it is also essential for the endothelial cell response to hypoxia (Fasanaro et al., 2008). It has been reported that hypoxia can increase the expression of Ephrin-A3 (EFNA3) mRNA and miR-210 can suppress EFNA3 mRNA directly which allows angiogenesis to occur (Fasanaro et al., 2008; Hu et al., 2010). Although the involvement of EFNA3 in the inhibition of angiogenesis is reported through the inhibition of the formation of new blood vessels, its specific role and the unpredictable effects of miR-210 on its expression is still unidentified (Fasanaro et al., 2008; Pulkkinen et al., 2008).

According to the data in this thesis, ABCG1 was highly expressed at the RNA and protein level in putative ES-CSCs. However, little is known about ABCG1 function in ES and other cancers. Like ABCG2, ABCG1 is known as director for lipid transport (Klucken et al., 2000; Kennedy et al., 2005). Furthermore, it has been reported that ABCG1 (666) known as isoform 4 is located in the plasma membrane of HeLa cells and also encodes a functional variant (Engel et al., 2006). To functionally validate the role of ABCG1 in ES-CSCs, I have tried to knock down and overexpress the full length of this protein, however, these approaches were unsuccessful suggesting that the cells somehow managed to stabilize the protein level of ABCG1, even when there was a decrease in RNA level. The viable cell number was reduced in knock down cells compared to negative control at 48h. In this regard, cancer cells grow and survive using adaptive pathways to avoid the cellular stress situations such as hypoxia, low glucose levels, or chemo-drug exposure (Luo, B. and Lee, 2013). However, other studies

proposed that downregulation of ABCG1 can encourage apoptosis (Tarling et al., 2010; Yvan-Charvet et al., 2010). This phenomena occurs as a response to intracellular lipid mass and subsequent endoplasmic reticulum (ER) stress (Tarling and Edwards, 2011; Xue et al., 2013; Chen, Y. et al., 2015). So far, ABCG1-dependent mechanisms for inducing ER stress still remain unclear.

The overexpressing ABCG1 cell line generated for this project expressed high level of ABCG1 at the RNA level only. Currently, the molecular mechanism that regulates ABCG1 expression is known, it has been reported in CHO cells that E3-ubiquitin ligases (HUWE1 and NEDD4-1) is involved in the post-translational regulation of ABCG1 protein, stability and also cholesterol export (Aleidi et al., 2015). Interestingly, NEDD4-1 protein was expressed at the same level in overexpressing ABCG1 cell line, control and parental cells which normally express a low level of ABCG1 compared to spheroids. However, the expression level of HUWE1 remained untested in this project. Possibly HUWE1 and NEDD4 regulated the expression of ABCG1 in ES and ES-CSCs. It would be interesting to determine whether knockdown of one or both E3-ubiquitin ligases in the overexpressing ABCG1 cell line could regulate ABCG1 protein expression. In HKULC4 lung cancer cells, overexpressing ABCG1 promotes cell proliferation and also upregulates the anti-apoptotic proteins; BCL2 and MCL1 (Tian et al., 2017). Furthermore, it has been indicated that ABCG1 is a regulator of CD133 and ALDH1 in lung cancer stem cells lung cancer cell lines with ABCG1 overexpression (Tian et al., 2017). The possible involvement of ABCG1 in transporting HDL-miR-210 between cells has been described in Section 4.4, Figure **4.33**.

6.3 Future directions

In conclusion, the results in this thesis have provided interesting data to designate that the putative ES-CSCs have a molecular signatures that could possibly serve as important biomarkers. These data could provide further understanding of how to target ES-CSCs as well as develop new treatments

6.3.1 Future directions:

6.3.1.1 The effect of 3D spheroids in expression of CIZ1

The initial aim of CIZ1 project was to understand the potential role of CIZ1 in cancer development and regulation of pluripotency and differentiation. The main objective was the generation and characterization of a CIZ1-null mouse. Interestingly, it has been confirmed that the loss of CIZ1 lead to dispersal of X-inactive specific transcript (Xist) in somatic cells, which results in the loss of the ability to reactivate inactive X chromosome (Xi), which can give rise to female-specific lymphoma (Ridings-Figueroa et al., 2017). It was unfortunate that for reasons beyond my control I was unable to continue this work for the duration of my PhD but the outcome from my work has been published (Ridings-Figueroa et al., 2017). However, in ES family tumours, it is worth to mention that one of the substrate adherent cells, TTC-466, was highly expressing Xist at RNA level. There was no statistical difference between TTC-466 and 3-w-TTC-466 spheroids. On the other hand, there was no expression detected in SK-N-MC substrate adherent cells and the expression of Xist was increasing in 3-w-SK-N-MC spheroids. This gene ‘Xist’ does not match the proposed criteria to be selected as a target for validation. So, the current result needs to be validated using RTqPCR. Moreover, the expression of CIZ1 and its isoforms has not been investigated yet in the putative ES-CSCs. So, the effect of 3D model on CIZ1 role in cancer development remains to be explored.

6.3.1.2 Enriching CS-like cells from patient-derived cells

Identify the ideal functional methods to enrich CS-like cells based on their self-renewal capacity. Then generate spheroids from a single cell.

6.3.1.3 Establishing an ideal matched control for patient-derived cells

Compare patient-derived spheroids from ES family tumours with tumour-associated normal bone tissue, which supports the testing of a variety of therapeutic combinations in a patient-relevant model.

6.3.1.4 Transplant ES-CSCs into mouse model

Examine the ability of putative ES-CS-like cells enriched from ES family tumour cell lines and also patient-derived cells to generate tumours by transplant spheroids to severe combined immune deficient (SCID) mice.

6.3.1.5 Examine the effect of Targapremir-210 on ES family tumour cell lines and also patient-derived cells

Targapremir-210 has the ability to minimize tumour size (Costales et al., 2017). The outcome of this component on self-renewal ability as well as the expression level of ABCG1 has not yet been investigated.

6.3.1.6 Investigate the N-terminus region of ABCG1

Relying on the freely available database at the NCBI for designing specific primers that detect and distinguish between ABCG1 isoforms is not accurate. Also, finding a positive control for each isoform was essential to optimize the PCR condition and then screen a panel of cancer cell lines. The only tool that could help in identifying controls for each isoform was RNA sequence (RNAseq). A high quality of ES RNA samples were prepared and then sent to RNAseq, which was performed by Mrs. Sally Harrison (Senior Technical Specialist, Sequencing Facility, University of Leeds). RNAseq data was analysis by Dr. Alastair Droop (Visiting Research Fellow, School of Molecular and Cellular Biology, University of Leeds) and Dr. Roundhill. Briefly, looking back over the RNAseq data we didn't identify a single cell line that expressed all the published ABCG1 isoforms. BE(2)C cells express high levels of a couple of isoforms (1 and 6). RDES express high levels of 4 and 10, SK-N-MC high levels of 7 and 9 (unpublished observations).

To optimise and complete qPCR for the different ABCG1 isoforms, examine expression in ES cell lines and tumours is a considerable undertaking which would be very interesting to be done in the future. Also, identification of the ABCG1 isoforms that are highly expressed in 3-w-spheroids would be very important to know which isoform is linked to the self-renewal capability or survival in ES cell lines. It would be interesting to dissect 3-w-spheroids to

isolate cells from each rim (proliferating and hypoxic) and determine whether each rim expresses a different ABCG1 isoform. Thus we would be able to classify isoforms to two groups; proliferating and survival group of ABCG1 isoforms.

6.3.1.7 Knockdown E3-ubiquitin ligases in overexpressing ABCG1 cell line

The protein level of HUWE1 needs to be determined in overexpressing ABCG1 cell lines to know wither NEDD4-1 or HUWE1 or both block the post-translation of ABCG1. Also, knockdown one or both E3-ubiquitin ligases in overexpressing ABCG1 cell line is needed to regulate ABCG1 protein and then determine if the high expression of ABCG1 protein would enhance the self-renewal ability.

List of suppliers

Abcam	Abcam Plc. Cambridge Science Park Cambridge, CB4 0FL, UK www.abcam.com
Agilent Technologies	Agilent Technologies 5500 Lakeside, Cheadle SK8 3GR, UK www.agilent.com/home
Applied Biosystems®	Part of Life Technologies Ltd
ASAHI Techno Glass	Supplied by Sigma-Aldrich
BD Biosciences	BD Biosciences Edmund Halley Road, Oxford Science Park Oxford, OX4 4DQ, UK www.bdbiosciences.com/eu
Beckman Coulter	Beckman Coulter UK Inc. Oakley Court, Kingsmead Business Park, London Road, High Wycombe, HP11 1JU, UK www.beckmancoulter.com
Bibby Scientific	Bibby Scientific UK Beacon Road, Stone, Staffordshire, ST15 OS, UK www.bibby-scientific.com
Bio-Rad	Bio-Rad Laboratories Ltd. Bio-Rad House, Hemel Hempstead, Hertfordshire, HP2 7DX, UK www.bio-rad.com
BioSera	BioSera, Labtech International Ltd, East Sussex, UK www.biosera.com
CellPath	Cell Path Ltd 80 Mochdre Enterprise Park, Newtown, Powys, SY16 4LE, UK www.cellpath.com
Corning®	Supplied by Fisher Scientific UK and SLS
Dako	Part of Agilent Technologies Cambridge House, St Thomas Place Ely, Cambridgeshire, CB7 4EX, UK http://www.agilent.com/en-gb/dako-products
Envair Limited	Envair Limited York Avenue, Haslingden, Rossendale, Lancashire, BB4 4HX, UK. www.envair.co.uk

Eppendorf UK	Eppendorf UK Ltd Arlington Business Park, Stevenage, SG1 2FP, UK www.eppendorf.co.uk
Fisher Scientific	Fisher Scientific UK Ltd Bishop Meadow Road, Loughborough, LE11 5RG, UK www.fisher.co.uk
GE Healthcare	GE Healthcare UK Pollards Wood, Chalfont St Giles, Buckinghamshire, HP8 4SP, UK www.gehealthcare.com/uken
Geneflow	Geneflow Ltd Fradley Business Centre Wood End Lane, Fradley Staffordshire WS13 8NF www.geneflow.co.uk
Hawksley	Hawksley Marlborough Road, Lancing Business Park, Lancing, Sussex, BN15 8TN, UK www.hawksley.co.uk
Hettich	Hettich UK ltd 200 Broadway, Salford M50 2U, UK www.hettich.com
Invitrogen™ Labtech	Part of Life Technologies Ltd Labtech International Ltd. Acorn House, The Broyle Ringmer, East Sussex, BN8 5NN, UK www.labtech.co.uk
Leica Microsystems	Leica Microsystems UK Ltd Lothbury House, Newmarket Rd, Cambridge CB5 8PB, UK www.leica-microsystems.com/
LI-COR Biosciences	Supplied by VWR
Life Technologies	Life Technologies Ltd Inchinnan Business Park Paisley, PA4 9RF, UK www.lifetechnologies.com/uk
Miltenyi Biotech Ltd	Miltenyi Biotech Ltd Almac House, Bisley, Woking GU24 9DR, UK www.miltenyibiotec.com
Nikon Instruments	Division of Nikon Corporation www.nikoninstruments.com

Olympus	Olympus Microscopy KeyMed House, Southend-on-Sea Essex, SS2 5QH,UK www.olympus.co.uk
PerkinElmer	PerkinElmer Saxon Way, Cambridge, Cambridgeshire, CB23 8SL, UK www.perkinelmer.co.uk
Qiagen	QIAGEN Ltd. QIAGEN House, Fleming Way Crawley, West Sussex, RH10 9NQ, UK www.qiagen.com
R&D Systems	R&D Systems Europe, Ltd. Abingdon Science Park Abingdon, OX14 3NB, UK www.rndsystems.com
Sanyo Gallenkamp	Sanyo Gallenkamp Plc. The Office Village , Loughborough Leicestershire, LE11 1QJ, UK www.sanyo-biomedical.co.uk
Sigma-Aldrich	Sigma-Aldrich Company Ltd. Fancy Road, Poole Dorset, BH12 4QH, UK www.sigma-aldrich.com
SLS	Scientific Laboratory Supplies (SLS) Ltd Orchard House, Hessle, East Riding of Yorkshire, HU13 0AE, UK www.scientificlabs.co.uk
Starlab UK	Starlab UK 5 Tanners Dr, Blakelands, Milton Keynes MK14 5BU, UK www.starlabgroup.com/GB-en
STEMCELL Technologies	STEMCELL Technologies Inc Rue des Berges, Miniparc Polytec, Bâtiment Sirocco, 38000 Grenoble, France www.stemcell.com
Techne	Supplied by SLS

Thermo Fisher Scientific	Thermo Fisher Scientific UK Altrincham Business Park, 1 St George's Ct, Altrincham WA14 5TP, UK www.thermofisher.com/uk/en/home.html
Titertek-Berthold Instruments	Geneflow Ltd Fradley Business Centre Wood End Lane, Fradley Staffordshire WS13 8NF www.geneflow.co.uk
Vi-CELL™ XR Cell Counter	Beckman Coulter United Kingdom Ltd. Oakley Court, Kingsmead Business Park, London Road, Buckinghamshire HP, 11 1JU, High Wycombe, UK www.uk.beckman.com
VWR	VWR International Ltd. Hunter Boulevard, Magna Park, Lutterworth, Leicestershire, LE17 4XN, UK www.uk.vwr.com
Zeiss	Carl Zeiss Microscopy Ltd Coldhams Lane, Cambridge, CB1 3JS, UK www.zeiss.co.uk

Appendix A

A.1 Western blotting

A.1.1 Antibodies

Antibody concentrations were determined empirically. All primary antibodies were incubated overnight at 4°C, secondary antibodies were incubated for 1 h at RT unless a statement to the contrary is made. N/A = not applicable.

Antibody	Antibody species	Dilution (Optimised concentration)	Positive control	Supplier code and name
EBAF (LEFTY)	Rabbit monoclonal	1:2000	Panel of cells	Ab88088; Abcam
HBZ	Mouse monoclonal	0.2µg/mL	K562	MAB7708; R&D systems
ABCG1	Rabbit monoclonal	1:2500 (191µg/mL)	HEK-293	Ab52617; Abcam
CFTR	Mouse monoclonal	5:1000 (1µg/mL)	CaCo-2	MAB25031; R&D systems
CD133	Mouse monoclonal	1:100	CaCo-2	W6B3C1, Miltenyi, (130-092-395)
SOX17	Mouse monoclonal	1: 200	K562	Ab84990; Abcam
NEDD4-1		1:40.000	K562	
Myc-c	Rabbit monoclonal	1:2000	TC-32	D84C12; Cell Signaling Technology
ABCG1	Rabbit monoclonal	1:1000 (191µg/mL)	HEK-293	Ab52617; Abcam
HIF1	Mouse monoclonal	1:500	SK-SY-5Y	610958; BD Transduction Laboratories™
Glut1	Rabbit polyclonal	1:400	SK-SY-5Y	Ab15309; Abcam
GRP-75	Mouse monoclonal	1:10000	N/A	Ab2799; Abcam
ß- actin	Rabbit Polyclonal	1:1000	N/A	ab8227; Abcam
Secondary antibodies; anti-mouse	N/A	1:1000	N/A	170-6516; BioRad
Secondary antibodies; anti-rabbit	N/A	1:1000	N/A	4010-05; SouthernBiotech

A.1.2 Bradford assay

Dilution series of Bovine Serum Albumin in 10% RIPA buffer used to measure protein concentration

	concentration	BSA (2mg/mL)	10% RIPA buffer
1	0.1 µg/µL	5 µL	95 µL
2	0.25 µg/µL	12.5 µL	87.5 µL
3	0.5 µg/µL	25 µL	75 µL
4	0.8 µg/µL	40 µL	60 µL
5	1 µg/µL	50 µL	50 µL
6	1.5 µg/µL	75 µL	25 µL
7	2 µg/µL	100 µL	0 µL

Appendix B

B.1 Columns and microbeads for Magnetic MACS® Separator from Miltenyi

Items	Supplier code
CD133 microbeads	(Cat# 130-050-801)
LS columns	(Cat # 130-042-401)
LD column	(Cat # 130-042-901)

B.2 Antibodies for Flow cytometry

Antibodies	Catalogue number	Supplier
CD133-PE; clone 293C	130-090-853	Miltenyi
IgG2b-PE;	130-098-875	Miltenyi
c-Myc (D84C12)	5605	Cell Signaling Technology
Rabbit (DA1E) mAb IgG XP® Isotype Control	3900	Cell Signaling Technology
ABCG1	PA5-13462	Thermo-Fisher Scientific
Secondary antibody (Goat anti-Rabbit IgG (H+L)	Alexa Fluor 488, A11034	Thermo-Fisher Scientific
	Alexa Fluor 405, A31556	Thermo-Fisher Scientific

Appendix C

C.1 Histology

C.1.1 Leica ASP200 Tissue Processor: routine processing protocol

Reagents	Duration (Time)	Temperature (°C)
70% ethanol	30 min	37°C
80% ethanol	30 min	37°C
90% ethanol	30 min	37°C
95% ethanol	30 min	37°C
100% ethanol	1:00h	37°C
100% ethanol	1:00h	37°C
100% ethanol	1:30h	37°C
xylene	1:00h	37°C
xylene	1:30h	37°C
xylene	1:30h	37°C
paraffin wax	1:00h	65°C
paraffin wax	1:00h	65°C
paraffin wax	1:00h	65°C

C.1.2 Meyer's haematoxylin

To prepare a litre of Meyer's haematoxylin, 3g of haematoxylin (0.3%; w/v) was dissolved in 20mL of ethanol (2%; v/v), then mixed with 0.3g of sodium iodate (0.03%; w/v), 1g of citric acid (0.1%; w/v), 50g of choral hydrate (5%; w/v), 50g of aluminium potassium sulphate (5%; w/v) and 120mL of glycerol (12%; v/v) in distilled water (dH_2O; 850mL). All the chemicals from Sigma and the dye were filtered and stored at room temperature.

C.1.3 Antibodies used to detect antigens using three-stage peroxidase method

Antibody name	Stock concentration	Optimised working condition	Species	Supplier and catalogue number
Ki67	0.046 mg/mL	1:200	Monoclonal mouse IgG1	Dako Cat # IS626
Isotype	0.5 mg/mL	1:2173.9	Mouse IgG1	Abcam Cat # ab18443
Secondary Antibody	0.73 mg/mL	1:200	Polyclonal Rabbit Anti-Mouse	Dako, E0413
Glut-1	0.2 mg/mL = 200 µg/mL	1:200	Polyclonal Rabbit IgG	Abcam Cat # ab15309
Isotype	0.5µg/mL	Neat	Rabbit Ig Mix	Invitrogen Cat # 086199
Secondary Antibody	0.82 mg/mL	1:200	Polyclonal Goat Anti-Rabbit	Dako, E0432

C.1.4 Immunofluorescent antibodies

Antibodies	Catalogue number	Supplier
CD133-PE; clone 293C	130-090-853	Miltenyi
Nestin	.6994	Cell Signaling Technology
DAPI	0.2µg/mL	Sigma-Aldrich

Appendix D

D.1 Assay-on-Demand™ primer/probe

D.1.1 mRMA primers

Primer/ Probe	catalogue number of Assay-on-Demand™
MYC-C	Hs00153408_ml
SOX17	Hs00751752_s1
HBZ	Hs00744391_s1
ABCG1	Hs00245154_m1
CFTR	Hs00357011_m1

D.1.2 miRNA primers

Assay ID	Assay Name	Assay Target Sequence	miRBase ID (v21) or NCBI Name (for Controls)	miRBase Alias	Used as
000391	hsa-miR-16	UAGCAGCACGUAAAUAUUGGCG	hsa-miR-16-5p,	hsa-miR-16(17),	R
000602	hsa-miR-30b	UGUAAACAUCCUACACUCAGCU	hsa-miR-30b-5p,	hsa-miR-30b(17),	R
001186	hsa-miR-134	UGUGACUGGUUGACCAGAGGGG	hsa-miR-134-5p,	hsa-miR-134(19),	T
002284	hsa-miR-138	AGCUGGUGUUGUGAAUCAGGCCG	hsa-miR-138-5p,	hsa-miR-138(17),	T
000512	hsa-miR-210	CUGUGCGUGUGACAGCGGCUGA	hsa-miR-210-3p,	hsa-miR-210(19),	T

Appendix E

E.1 LIMMA command

E.1.1 Model A

```
source("http://www.bioconductor.org/biocLite.R")
biocLite('limma')
library(limma)
design<-model.matrix(~0+factor(rep(1:2,each=3)))
colnames(design)<-c("Sample A","Sample B")
fit <- lmFit(data[,2:7], design)
contrast.matrix<-makeContrasts(Sample A - Sample B,( Sample A - Sample B),levels=design)
fit2<-contrasts.fit(fit,contrast.matrix)
fit2<- eBayes(fit2)
data$limma. Sample A.vs. Sample B.p =data$limma.Sample A.vs. Sample B.q = rep(NA,nrow(data))
data$limma.Sample A.vs.Sample B.p=fit2$p.value[,1]
data$limma. Sample A.vs.Sample B.q =p.adjust(data$limma. Sample A.vs.Sample B.p,method="BH")
write.csv(data,c("TLDA-Sample A .vs. Sample B-results.csv"))
```

E.1.2 Model B

```
source("http://www.bioconductor.org/biocLite.R")
biocLite('limma')
library(limma)
design<-model.matrix(~0+factor(rep(1:4,each=3)))
colnames(design)<-c("Sample A"," Sample B"," Sample C"," Sample D")
fit <- lmFit(data[,2:13], design)
contrast.matrix<-makeContrasts(Sample A- Sample B, Sample C- Sample D,( Sample A- Sample B)-( Sample C- Sample D),levels=design)
fit2<-contrasts.fit(fit,contrast.matrix)
fit2 <- eBayes(fit2)
data$limma. Sample A.vs. Sample B.p =data$limma. Sample A.vs. Sample B.q = rep(NA,nrow(data))
data$limma. Sample C.vs. Sample D.p =data$limma. Sample C.vs. Sample D.q = rep(NA,nrow(data))
data$limma.combined.p =data$limma.combined.q = rep(NA,nrow(data))
data$limma. Sample A.vs. Sample B.p=fit2$p.value[,1]
data$limma. Sample C.vs. Sample D.p=fit2$p.value[,2]
data$limma.combined.p=fit2$p.value[,3]
data$limma. Sample A.vs. Sample B.q =p.adjust(data$limma. Sample A.vs. Sample B.p,method="BH")
data$limma. Sample C.vs. Sample D.q =p.adjust(data$limma. Sample C.vs. Sample D.p,method="BH")
data$limma.combined.q =p.adjust(data$limma.combined.p,method="BH")
write.csv(data,c("name-file-results.csv"))
```

Appendix F

	SK-N-MC (Spheroids – substrate adherent cells)					TTC-466 (Spheroids – substrate adherent cells)					Expression in SK-N-MC spheroids	Expression in TTC-466 spheroids
	Target	Ct difference	DCt difference	q values (A)	q values (B)	Target	Ct difference	DCt difference	q values (A)	q values (B)		
Specific for Model A	-	-	-	-	-	-	-	-	-	-	-	-
Specific for Model B	-	-	-	-	-	FGF5	1.2	3.9	-	0.1118	-	▼
	-	-	-	-	-	OLIG2	0.7	2.9	-	0.1268	-	▼
Common between model A and B	PODXL	2.4	2.1	0.0223	-	PODXL	4.3	4.0	-	0.0719	▼	▼
	EBAF	-5.3	-6.3	0.0009	0.0001	EBAF	-3.8	-4.2	0.0255	0.0035	▲	▲
	TDGF1	-3.2	-3.9	0.0014	0.0001	TDGF1	-2.6	-3.0	0.0182	0.0027	▲	▲
	LEFTB	-3.6	-3.9	0.0033	0.0008	LEFTB	-1.7	-2.0	0.1046	0.0604	▲	▲
	POU5F1	-2.0	-2.3	8.9E-02	3.4E-02	-	-	-	-	-	▲	-
	LIN28	-3.6	-3.8	2.2E-02	4.1E-03	-	-	-	-	-	▲	-
	Xist	-1.4	-4.8	2.2E-02	4.9E-03	-	-	-	-	-	▲	-
	-	-	-	-	-	SERP2	-1.9	-2.3	0.0598	0.0092	-	▲
	SOX17	-3.9	-7.4	0.0022	0.0014	SOX17	-2.7	-4.9	0.0875	0.0267	▲	▲
	HBZ	-4.3	-5.7	0.0048	0.0003	HBZ	-1.9	-2.3	0.0255	0.0937	▲	▲
	-	-	-	-	-	WT1	-3.0	-3.4	0.0303	0.0035	-	▲
	SEMA3A	1.8	2.8	9.8E-02	4.1E-02	-	-	-	-	-	▼	-
	-	-	-	-	-	IMP2	2.7	2.4	0.0182	0.0038	-	▼
	LAMA1	1.1	5.9	3.9E-04	5.4E-05	-	-	-	-	-	▼	-
	COL2A1	1.1	5.0	4.2E-03	2.7E-04	-	-	-	-	-	▼	-
	ACTC	2.0	4.7	1.7E-02	1.1E-02	-	-	-	-	-	▼	-
	GCG	3.2	3.0	1.7E-02	1.8E-02	-	-	-	-	-	▼	-
	CDX2	0	2.0	7.0E-02	7.1E-02	-	-	-	-	-	▼	-
	-	-	-	-	-	GATA6	4.2	3.9	0.0182	0.0027	-	▼
	-	-	-	-	-	LAMC1	2.6	2.2	0.0255	0.0056	-	▼
	-	-	-	-	-	FLT1	5.8	5.5	0.0182	0.0038	-	▼

Appendix G

The nuclear matrix protein CIZ1 facilitates localization of Xist RNA to the inactive X-chromosome territory

Rebeca Ridings-Figueroa,[1,7] Emma R. Stewart,[1] Tatyana B. Nesterova,[2] Heather Coker,[2] Greta Pintacuda,[2] Jonathan Godwin,[2] Rose Wilson,[1,8] Aidan Haslam,[1] Fred Lilley,[1] Renate Ruigrok,[3] Sumia A. Bageghni,[3] Ghadeer Albadrani,[3,4] William Mansfield,[5] Jo-An Roulson,[6] Neil Brockdorff,[2] Justin F.X. Ainscough,[1,3] and Dawn Coverley[1]

[1]Department of Biology, University of York, York YO10 5DD, United Kingdom; [2]Department of Biochemistry, University of Oxford, Oxford OX1 3QU, United Kingdom; [3]Leeds Institute of Cardiovascular and Metabolic Medicine (LICAMM), University of Leeds, Leeds LS2 9JT, United Kingdom; [4]Princess Nourah Bint Abdulrahman University (PNU), Riyadh, Kingdom of Saudi Arabia; [5]Stem Cell Institute, University of Cambridge, Cambridge CB2 1QR, United Kingdom; [6]Leeds Institute of Molecular Medicine (LIMM), University of Leeds, Leeds LS9 7TF, United Kingdom

The nuclear matrix protein Cip1-interacting zinc finger protein 1 (CIZ1) promotes DNA replication in association with cyclins and has been linked to adult and pediatric cancers. Here we show that CIZ1 is highly enriched on the inactive X chromosome (Xi) in mouse and human female cells and is retained by interaction with the RNA-dependent nuclear matrix. CIZ1 is recruited to Xi in response to expression of X inactive-specific transcript (Xist) RNA during the earliest stages of X inactivation in embryonic stem cells and is dependent on the C-terminal nuclear matrix anchor domain of CIZ1 and the E repeats of *Xist*. CIZ1-null mice, although viable, display fully penetrant female-specific lymphoproliferative disorder. Interestingly, in mouse embryonic fibroblast cells derived from CIZ1-null embryos, Xist RNA localization is disrupted, being highly dispersed through the nucleoplasm rather than focal. Focal localization is reinstated following re-expression of CIZ1. Focal localization of Xist RNA is also disrupted in activated B and T cells isolated from CIZ1-null animals, suggesting a possible explanation for female-specific lymphoproliferative disorder. Together, these findings suggest that CIZ1 has an essential role in anchoring *Xist* to the nuclear matrix in specific somatic lineages.

[*Keywords*: CIZ1; *Xist*; X-chromosome inactivation; nuclear matrix; lymphoproliferative disorder]

Supplemental material is available for this article.

Received January 5, 2017; revised version accepted April 20, 2017.

In mammals, dosage compensation for X-linked transcripts is achieved by the developmentally regulated inactivation of one of the two X chromosomes in female cells. X-chromosome inactivation (XCI) is initiated by X inactive-specific transcript (*Xist*), a noncoding RNA ~17 kb in length (Brockdorff et al. 1992; Brown et al. 1992; Lee et al. 1996; Penny et al. 1996). Xist RNA is expressed from the inactive X chromosome (Xi) elect and accumulates in *cis* to form a domain over the entire chromosome, serving as a trigger for a cascade of chromatin modifications that results in the progressive transition toward a stable, heritable, repressed state (for review, see Heard and Disteche 2006).

Analysis of *Xist* transgenes has revealed that *Xist*-mediated chromosome silencing and Xist RNA localization are conferred by distinct elements (Wutz et al. 2002). Silencing activity maps in large part to the A repeat, a short tandemly repeated region located at the 5′ end of *Xist*. In contrast, localization maps to several redundantly acting elements, including the tandem repeat regions C, E, and F (Wutz et al. 2002; Jeon and Lee 2011; Makhlouf et al. 2014; Yamada et al. 2015).

Xist spreading occurs through a sequence of events dictated by the architecture of the X chromosome. Xist RNA searches for binding sites in three dimensions, leading to modification of chromosome structure, before spreading to newly accessible locations (Engreitz et al. 2013; Simon et al. 2013). While the nature of Xist RNA-binding sites is poorly defined, it is known that Xist RNA localizes to the perichromatin compartment that corresponds to the nuclear matrix (NM) (Clemson et al. 1996; Smeets et al. 2014). Accordingly, the NM proteins scaffold attachment

Present addresses: [7]Department of Genetics, University of Cambridge, Cambridge CB2 3EH, UK; [8]Wellcome Trust Centre for Human Genetics, Oxford OX3 7BN, UK.
Corresponding author: dawn.coverley@york.ac.uk
Article published online ahead of print. Article and publication date are online at http://www.genesdev.org/cgi/doi/10.1101/gad.295907.117. Freely available online through the *Genes & Development* Open Access option.

factor A (SAF-A; hnRNPU) and hnRNP UL1 are involved in anchoring Xist RNA within Xi (Helbig and Fackelmayer 2003; Hasegawa et al. 2010; Sakaguchi et al. 2016). Additionally, NM protein 1 (NMP1; YY1) (Guo et al. 1995) has been implicated in tethering Xist RNA to chromatin (Jeon and Lee 2011; Makhlouf et al. 2014). In naïve B and T cells, Xist RNA is dispersed in the nucleoplasm but is recruited to Xi upon lymphocyte activation in a process that involves YY1 and SAF-A (Wang et al. 2016).

Recent proteomic and genetic screens have identified several novel *Xist*-interacting factors, some of which now have confirmed roles in *Xist*-mediated silencing (Chu et al. 2015; McHugh et al. 2015; Moindrot et al. 2015; Monfort et al. 2015). With the exception of SAF-A identified previously (Hasegawa et al. 2010), none of the factors investigated in detail was found to affect *Xist* localization (Chu et al. 2015; McHugh et al. 2015).

Random XCI of the paternal or maternal chromosome occurs around embryonic day 5.5 (E5.5) and is propagated through subsequent cell divisions. This can be recapitulated in XX mouse embryonic stem cells (mESCs), allowing fine-tuned analysis of the timing and the earliest events in the initiation process. Examples include deposition of histone 3 Lys27 trimethylation (H3K27me3) and hypoacetylation of H4, which occur rapidly at the onset of Xist RNA expression, and DNA methylation of promoters of X-linked genes and association of the variant histone macroH2A, which occur at later stages of the XCI process (Pollex and Heard 2012). *Xist*-dependent silencing occurs within a developmental window of opportunity corresponding to early stages of differentiation in the XX ESC model (Wutz and Jaenisch 2000). Beyond this time, XCI enters a maintenance phase in which *Xist* is largely dispensable (Brown and Willard 1994; Csankovszki et al. 1999) despite continued expression.

Here we define a novel *Xist* localization factor, the NM protein Cip1-interacting zinc finger protein 1 (CIZ1). CIZ1 was characterized previously as a factor with roles in initiation of DNA replication (Coverley et al. 2005), interacting directly with CDK2, p21/CIP1 (Mitsui et al. 1999), and cyclins (Copeland et al. 2010) and supporting cyclin recruitment to the NM (Copeland et al. 2015). The NM anchor domain in the C-terminal third of CIZ1 (Ainscough et al. 2007) mediates immobilization of CIZ1 and its interaction partners but retains the ability to become incorporated into the NM in the absence of cyclin cargo. CIZ1 has also been linked with post-replicative functions in male germ cell differentiation (Greaves et al. 2012). *CIZ1* transcripts are alternatively spliced to yield at least 22 variants (Rahman et al. 2010), most of which are not characterized. Aberrant alternative splicing underlies its links with a range of pathologies, including pediatric tumors and common adult-onset cancers of the breast (den Hollander et al. 2006) and lung (Higgins et al. 2012) as well as neurological abnormalities (Xiao et al. 2016). Here we describe *Xist*-dependent recruitment of CIZ1 to Xi and a requirement for CIZ1 to maintain Xist RNA localization at Xi in fibroblasts and splenocytes.

Results

CIZ1 accumulates at Xi in female cells

Immunolocalization of endogenous CIZ1 via epitopes in its N-terminal DNA replication domain (Coverley et al. 2005; Copeland et al. 2010) or C-terminal NM anchor domain (Fig. 1A; Ainscough et al. 2007) reveal one or two high-intensity domains within the nucleus of female human or mouse cultured fibroblasts plus smaller nucleus-wide foci in both male and female cells (Fig. 1B; Supplemental Fig. S1A). In immortalized or primary embryonic fibroblasts (PEFs), CIZ1 domains are discrete, while, in cancer-derived cell lines, they are more irregular (shown for MCF7 breast cancer cells in Supplemental Fig. S1A). We hypothesized that the high-intensity domains present only in female cells correspond to Xi. Consistent with this, immunostaining of H3K27me3, a marker for Xi, colocalizes with CIZ1 in PEFs (Fig. 1B) and a range of other female cell types (Supplemental Fig. S1A). CIZ1 did not colocalize with the active chromatin mark H3K4me3 or constitutive heterochromatin mark H3K9me3 (Supplemental Fig. S1B). Identification of the CIZ1 domains observed in female PEFs as the silenced X chromosome was confirmed by immuno-FISH for CIZ1 and Xist RNA (Fig. 1C), which revealed localization within the same chromosome territory.

To determine at which stage of the XCI process CIZ1 is recruited, we analyzed CIZ1 localization in PGK12.1 XX mESCs at time points following the initiation of differentiation. CIZ1 localization to Xi was observed from day 1 and persisted throughout the time course (Fig. 1D, Supplemental Fig. S1C). This closely correlates with the dynamics of Xist RNA expression reported previously (Sheardown et al. 1997). As in PEFs, CIZ1 domains colocalized with H3K27me3, identifying their location as Xi. CIZ1 is lost from Xi in late metaphase in both ESCs (Fig. 1E) and PEFs (Supplemental Fig. S1D), indicating a cycle of recruitment and loss that is similar to Xist RNA (Duthie et al. 1999). The smaller nucleus-wide foci remain qualitatively similar throughout ESC differentiation but are excluded from chromosomes in late metaphase (Supplemental Fig. S1D; Greaves et al. 2012).

Superresolution three-dimensional structured illumination microscopy (SR 3D-SIM) of endogenous CIZ1 together with endogenous Xist RNA in diploid female somatic C127I cells confirmed their adjacent localization, similar to that for SAF-A (Fig. 2A; Supplemental Fig. S2B; Smeets et al. 2014).

NM association of CIZ1 at Xi

The NM is a biochemically defined fraction that resists extraction from the nucleus and is thought to anchor and spatially organize nuclear processes, including DNA replication and repair, transcription, and pre-mRNA splicing (Wilson and Coverley 2013). Serial extraction (Wilson et al. 2016) to reveal the fraction of CIZ1 that remains in cells after solubilization with (1) low-level detergent under physiological salt concentrations, (2) 0.5 M salt, or

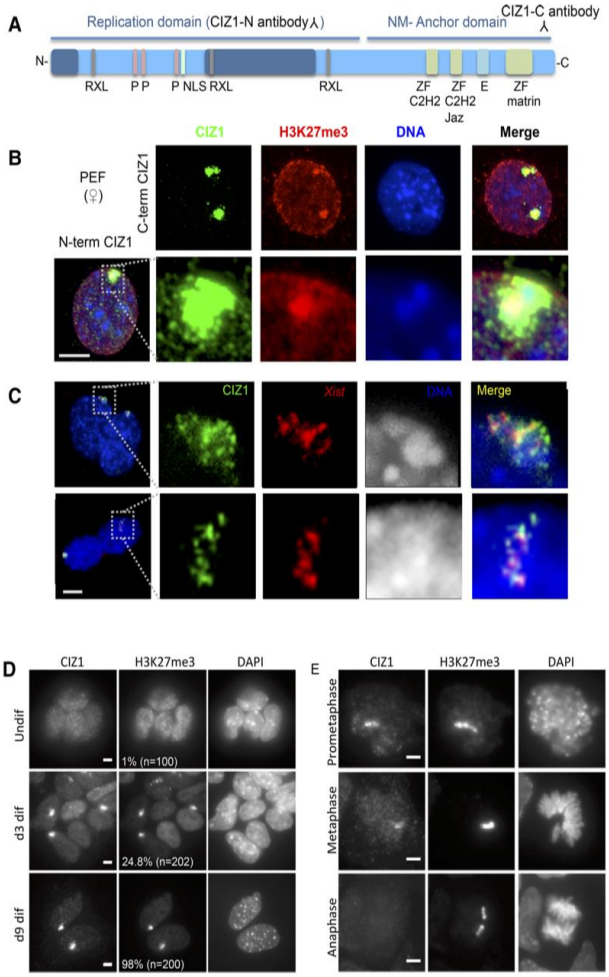

Figure 1. CIZ1 is enriched at Xi. (*A*) Schematic of CIZ1 indicating the replication domain (Copeland et al. 2015) with the nuclear localization signal (NLS, green), functional CDK phosphorylation sites (pink), and RXL cyclin-binding motifs (gray) and the NM anchor domain (Ainscough et al. 2007) with the locations of C2H2-type zinc fingers (green), the Matrin3-type RNA-binding zinc finger (Prosite PS50171), and the acidic domain (labeled E). The locations of epitopes recognized by N-terminal and C-terminal antibodies are indicated. (*B*) Immunodetection of CIZ1 (green) in female PEFs from wild-type mice using N-terminal and C-terminal antibodies. Colocalization of CIZ1 and histone H3K27me3 (red) was observed as a discrete domain in all cells with H3K27me3 staining. $n > 100$. DNA was stained with DAPI (blue). Additional cell lines are shown in Supplemental Figure S1; some have two domains, indicative of chromosomal duplication. (*C*) RNA-FISH for *Xist* (red) in female PEFs showing colocalization with CIZ1 protein (green) and the Barr body (gray). Bar, 5 µM. (*D*) CIZ1 recruitment to Xi in differentiating XX ESCs correlates with *Xist*-mediated deposition of H3K27me3. d3 and d9 are days of differentiation after withdrawal of LIF. Additional time points are shown in Supplemental Figure S1C. (*E*) CIZ1 and H3K27me3 in differentiated XX ESCs during mitosis showing a reduction of CIZ1 in late metaphase and complete loss in anaphase but retention of H3K27me3. Bar, 5 µm.

(3) nuclease (DNase or RNase) (Fig. 2B) revealed distinct populations in female 3T3 cells (Fig. 2C) and PEFs (Supplemental Fig. S2C). While the small nucleus-wide foci remained under all conditions (part of the core protein NM), the high-intensity domain at Xi was released by digestion with RNase but not DNase. This resistance to high salt and DNase defines CIZ1 at Xi as part of the NM, but release by RNase shows this to be the RNA fraction of the NM and is consistent with its close association with Xist RNA.

When 3T3 cells were treated with the protein–protein cross-linker DTSP prior to extraction (Fig. 2D), the CIZ1 domain at Xi was rendered resistant to digestion with RNase. This suggests that it is in close proximity to proteins in the core NM, possibly the resistant fraction of CIZ1. Thus, two qualitatively different populations of NM-anchored CIZ1 are present in the nucleus, but most of the CIZ1 at Xi is anchored by association with RNA (Fig. 2E).

Similar analysis of the NM proteins SAF-A and YY1 in 3T3 cells showed that they are not enriched at Xi, that a NM-associated population can be revealed by removal of chromatin, and that both proteins are completely extracted by digestion of RNA (Supplemental Fig. S3). All three of these features are consistent with the published literature but distinguish SAF-A and YY1 from CIZ1.

Recruitment to Xi requires the CIZ1 C-terminal NM anchor domain

To ask whether recruitment of CIZ1 to Xi is mediated by the sequences that support attachment to the NM (Ainscough et al. 2007), the C-terminal anchor domain (GFP-C275, which includes C2H2-type zinc fingers and Matrin3-type RNA-binding zinc finger domains) and the N-terminal DNA replication domain (GFP-N572, which includes CDK phosphorylation sites and cyclin-binding motifs) were transiently transfected separately into 3T3 cells, and the frequency of accumulation at the Xi territory was scored after one cell cycle. N572 completely failed to accumulate at Xi, while C275 accumulated in large foci

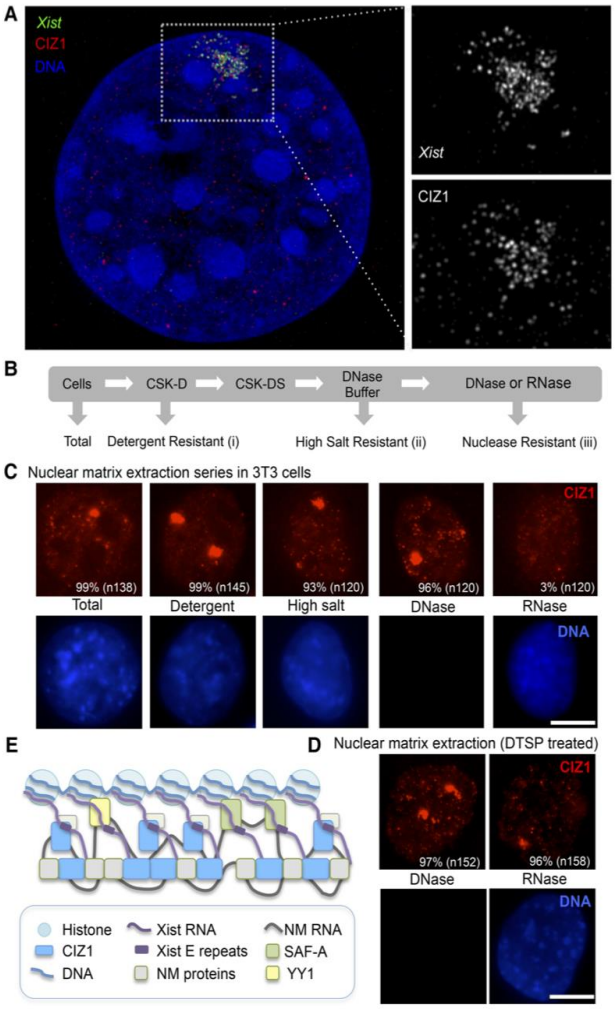

Figure 2. CIZ1 is part of the RNA-dependent NM at Xi. (*A*) Maximum intensity projection SR 3D-SIM image of a single C127I cell nucleus showing adjacent localization of *Xist* foci (green) with CIZ1 foci (red) at Xi. Examples of individual *Z* sections from several cells are shown in Supplemental Figure S2. (*B*) Schematic showing the protocol for serial extraction with detergent, high salt, DNase, or RNase to reveal the protein–RNA NM fraction or the RNA-independent NM fraction (protein only). (*C*) Images show CIZ1 (red) after serial extraction of 3T3 cells. The proportion of cells with discrete CIZ1-Xi domains is indicated ($n > 100$ for each condition), some with two domains, indicating that a proportion of cells is tetraploids with two Xis. Similar results were obtained with PEFs (Supplemental Figure S2C). DNA (blue) shows the extent of nuclease treatment. Images were equally modified to allow direct comparison of fluorescence intensity across the different extraction conditions. Bar, 5 µm. (*D*) As in *C* but with prior protein–protein cross-linking with DTSP. (*E*) Model showing two populations of CIZ1 in the NM (blue); RNA-dependent CIZ1 interacts with *Xist*, and RNA-independent CIZ1 is part of the core NM. SAF-A (Hasegawa et al. 2010) is also shown interacting with *Xist* E repeats and is depicted with YY1 in the RNA-dependent NM.

that colocalized with endogenous CIZ1 at Xi (Fig. 3A). However, compared with GFP-full-length CIZ1, the frequency of C275-marked X chromosomes was significantly reduced despite their presence in the nucleus. Thus, while sequences encoded in N572 are not sufficient to specify recruitment to Xi on their own, they do increase the efficiency of targeting. Live-cell imaging of a stably transfected P4D7F4 XY mESC line, which carries an mCherry-tagged inducible *Xist* transgene (Moindrot et al. 2015), revealed colocalization between C275 and Xist RNA domains, whereas N572 showed no *Xist* colocalization (Fig. 3B). Together, these findings support a key role for the C terminus of CIZ1 in binding at Xi.

Recruitment of CIZ1 by Xist *requires the* Xist *E repeat region*

In undifferentiated male MG-3E (XY) ESCs carrying an inducible *Xist* transgene, CIZ1 is recruited to the *Xist* domain and shows an adjacent localization to *Xist* similar to that in female ESCs (Supplemental Fig. S4A). To define elements in Xist RNA required for CIZ1 recruitment, we analyzed a series of inducible transgenic *Xist* deletion constructs in XY ESCs (Fig. 3C; Supplemental Fig. S5) and a deletion of *Xist* exon IV from the endogenous *Xist* locus in female mouse embryonic fibroblasts (MEFs) (Supplemental Fig. S4B; Caparros et al. 2002). The deletions encompassed key elements, including six short tandem repeat regions (A–F) (Brockdorff et al. 1992; Brown et al. 1992; Nesterova et al. 2001), which are conserved and, in some cases, have been shown to be functionally important. CIZ1 recruitment was found to be independent of the A repeat region, which is required for *Xist*-mediated silencing (Wutz et al. 2002), and the XN region (repeats B and F), which is involved in the recruitment of PRC2 to Xi (Fig. 3C; da Rocha et al. 2014). However, a truncated Xist construct, which corresponds to the first 3 kb of *Xist*, does not recruit CIZ1, implicating regions further

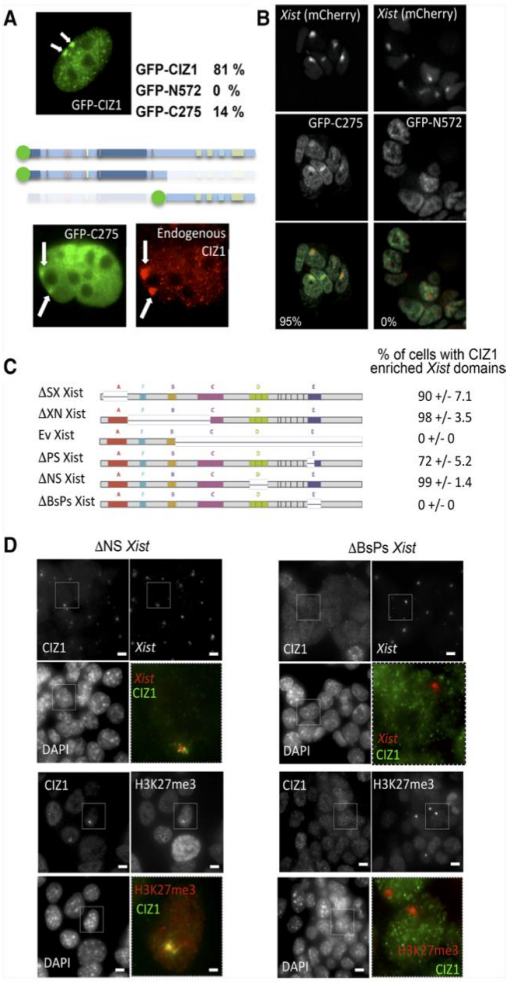

Figure 3. Delineation of the *Xist* and CIZ1 domains. (*A*) Recruitment of the indicated GFP-tagged CIZ1 constructs (Coverley et al. 2005) 24 h after transient transfection into cycling wild-type PEFs. The proportion of transfected cells with nuclear GFP, in which accumulation at Xi was observed ($n > 100$ for each construct), is indicated with representative images. For GFP-C275, endogenous CIZ1 (red) is also shown, detected via epitopes in the N-terminal end. (*B*) Accumulation of GFP-C275 but not GFP-N572 at Xi in stably expressing ESC lines that also carry inducible Xist RNA tagged with Bgl stem–loops that bind a BglG-mCherry fusion protein (Moindrot et al. 2015). Almost all (58 out of 61) *Xist*-mCherry-expressing cells were positive for GFP-C275, while none ($n = 47$) was positive for GFP-N572. (*C*) Schematic of inducible *Xist* constructs transfected into XY ESCs to study CIZ1 recruitment. The result of CIZ1 localization studies in the transgenic cell lines is summarized. (*D*) Example images showing the lack of CIZ1 colocalization with H3K27me3 domains (*bottom* panels) or *Xist* (*top* panels) in a ΔBsPs *Xist* construct missing the E repeat. The absence of the *Xist* D repeat (ΔNS) does not affect recruitment of CIZ1. Data for all transgenes are shown in Supplemental Figure S5.

3′. Accordingly, deletion of the E repeats, encompassing a 1.5-kb span of *Xist* exon 7, entirely abolished CIZ1 recruitment by Xist RNA (Fig. 3D). Deletion of other 3′ regions, the D repeats, or the highly conserved *Xist* exon 4 had no effect (Fig. 3C,D; Supplemental Fig. S4B). These findings demonstrate a requirement for *Xist* E repeats for recruitment of CIZ1 and together raise the possibility that the C terminus of CIZ1 might functionally interact with Xist RNA via the E repeat region.

Functional analysis of CIZ1 in XCI

Loss-of-function mutations affecting factors critical for XCI, including Xist RNA, result in female-specific lethality, usually during early or mid-stages of embryogenesis. To determine whether this is the case for CIZ1, targeted C57BL/6 ESCs generated using a gene trap strategy were used to produce heterozygous knockout mice (Supplemental Fig. S6A,B). Viable *ciz1*$^{-/-}$ male and female F1 progeny were born at the expected ratio (Supplemental Table S1), showed no difference in growth rate, and had no overt developmental defects. Loss of *ciz1* transcript was confirmed in embryos (E12) and fibroblasts from 3-wk postnatal tail tip dermal tissue (tail tip fibroblasts [TTFs]) (Supplemental Fig. S6C). Loss of protein expression was confirmed in TTFs, lymphocytes (Supplemental Fig. S6D,E), and differentiating male germ cells, which normally express high levels of CIZ1 (Supplemental Fig. S6F; Greaves et al. 2012). Thus, the gene trap insertion abrogates expression from the CIZ1 locus in vivo and in vitro, demonstrating that CIZ1 is not essential for embryogenesis, early postnatal development, or cell viability ex vivo.

The absence of an embryonic phenotype suggests that CIZ1 is not required for the establishment of a transcriptionally quiescent, inactivated X chromosome despite recruitment during *Xist*-dependent initiation of X inactivation (Fig. 1D). Consistent with this, the transcriptome of CIZ1-null-derived female PEFs did not reveal widespread reactivation of Xi compared with wild-type controls (Fig. 4A; Supplemental Data Set S1). As expected, the *Ciz1* gene was silenced in null cells ($P = 5.00 \times 10^{-05}$; $q = 0.005$) (Supplemental Data Set S2), but comparison of all transcripts that map to the X chromosome of the *Mus musculus* C57BL/6 primary assembly GRCm38 (downloaded from http://www.ensembl.org on May 4, 2016) showed that most were not significantly altered and revealed little change in genes associated with the X inactivation center (XIC) (Fig. 4B). The lack of widespread reactivation is in line with similar analyses and the understanding that loss of Xist RNA or other factors does not significantly compromise the maintenance of XCI (Csankovszki et al. 1999).

However, deregulation at the single-gene level was significant ($P < 0.05$) for 62 X-linked transcription units dispersed across the X. This is 3.6% of those that are expressed in PEFs and includes a similar number of up-regulated and down-regulated genes and six where $q < 0.05$ (*Agtr2*, *Fhl1*, *Tmem164*, *Gpm6b*, XLOC3750, and XLOC830) (Supplemental Data Set S2). Induction of the

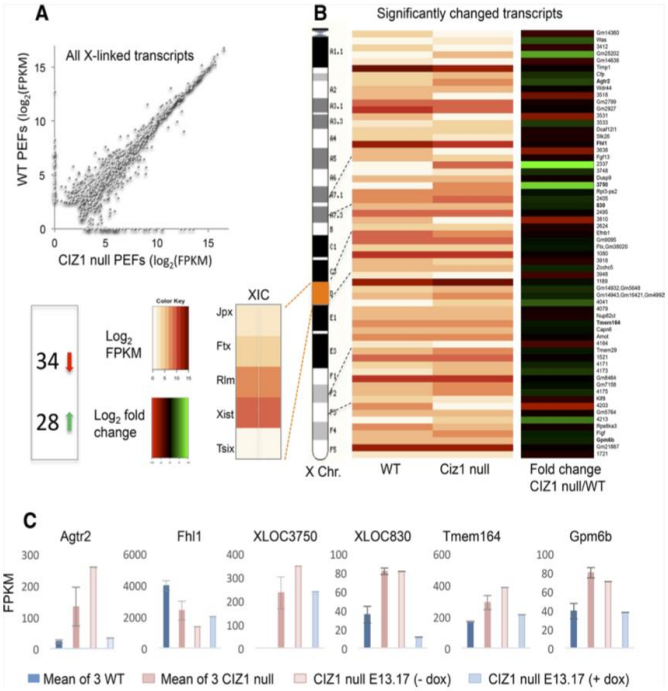

Figure 4. Expression of X-linked genes. (*A*) Scatter plot showing mean expression in three wild-type and three CIZ1-null PEF lines (log_2 FPKM [fragments per kilobase per million mapped fragments]) for all expressed X-linked transcription units. FPKM <0.99 were rounded to 1. The mean expression for all X-linked transcription units is in Supplemental Data Set S1. (*B*) Heat map showing (white to brown) expression levels in log_2 FPKM for 62 X-linked genes that are significantly changed in CIZ1-null PEFs. $P < 0.05$. Genes are listed in order against a schematic of the X chromosome. Unannotated transcripts are indicated by XLOC gene ID number (Supplemental Data Set S1), and predicted genes are indicated by the prefix Gm. A list of significantly changed transcription units is in Supplemental Data Set S2, of which 35 are annotated, and 23 have known functions. (*Right*) Fold change showing the 34 down-regulated (red) and 28 up-regulated (green) transcription units distributed across the chromosome. (*Left* of the X-chromosome schematic) Also shown are results for genes at the XIC. (*C*) Expression of six X-linked transcription units where $q < 0.05$, showing mean FPKM for three wild-type and three CIZ1-null cell lines as well as the effect of reinduction of CIZ1 in null-derived transgenic primary PEF line e13.17.

full-length GFP-CIZ1 transgene in PEFs derived from CIZ1-null line e13.17 harboring an inducible CIZ1 transgene and doxycycline-regulatable transactivator (see the Supplemental Material) rebalanced the expression of all six genes, modulating four of them back to wild-type levels (Fig. 4C). Thus, expression of full-length CIZ1 compensates for genetic ablation and presumptive loss of the full repertoire of *Ciz1* variant transcripts in the regulation of these genes.

Lymphoproliferative disorder in adult female mice

Although we observed no overt defects in embryogenesis or early postnatal development (Fig. 5), progressive infirmity was observed in female CIZ1-null mice from 9 mo onward. Eight females and an equivalent number of males were therefore evaluated for abnormalities between 9 and 19 mo. This revealed lymphoproliferative disorder in all eight females and none of the males. Detailed histological assessment was undertaken for six of the females and compared with six wild-type females. A summary assessment of abnormalities in the spleens, livers, lungs, and lymph nodes for individual CIZ1-null and wild-type females is in Supplemental Table S2, and pathology notes describing histological assessments are in Supplemental Tables S3 and S4. Notably, primary and secondary lymphoid tissues (spleen, lymph node, lung, and liver) were enlarged in all $Ciz1^{-/-}$ adult females (Fig. 5C). Secondary lymphoid tissues are sites where B and T lymphocytes are directed in search of antigen, leading to the regulated turnover or amplification of subsets of cells within germinal centers. This process is deregulated most notably in the spleen (Fig. 5C,D), which displayed a fivefold enlargement in $Ciz1^{-/-}$ (181–3679 mg) compared with $Ciz1^{+/+}$ (88–167 mg) mice. Histologically, lymph node and spleen architectures were abnormal, with effacement of normal follicles and significant infiltration of abnormal B (CD20 +ve) and reactive T (CD3 +ve) lymphocytes in all affected tissues (Fig. 5D,E). At the cellular level, the disorder resembled non-Hodgkin follicular-type lymphoma, with three showing evidence of high-grade transformation consistent with diffuse large B-cell lymphoma (Ward 2006). These data point to compromised XCI in lymphoid lineages and suggest that CIZ1 normally protects against tumor formation.

CIZ1 is required for Xist RNA localization in fibroblasts and splenocytes

While the viability of CIZ1-null embryos suggests that CIZ1 is not critical for the establishment of XCI, female-specific lymphoid hyperproliferation nevertheless implies an important lineage-restricted function. To further investigate this, we performed RNA-FISH to analyze *Xist* domains in PEFs and splenocytes derived from CIZ1-null mice. In independently derived CIZ1-null fibroblast cell lines, we observed a strikingly dispersed *Xist* signal that occupies 40% of the nuclear area compared with <5% in wild-type cells as well as loss of H3K27me3 (Fig. 6A). Dispersal cannot be attributed to increased *Xist* levels, as none of the three CIZ1-null PEFs showed any change in *Xist* transcript (Supplemental data set S1). X-chromosome

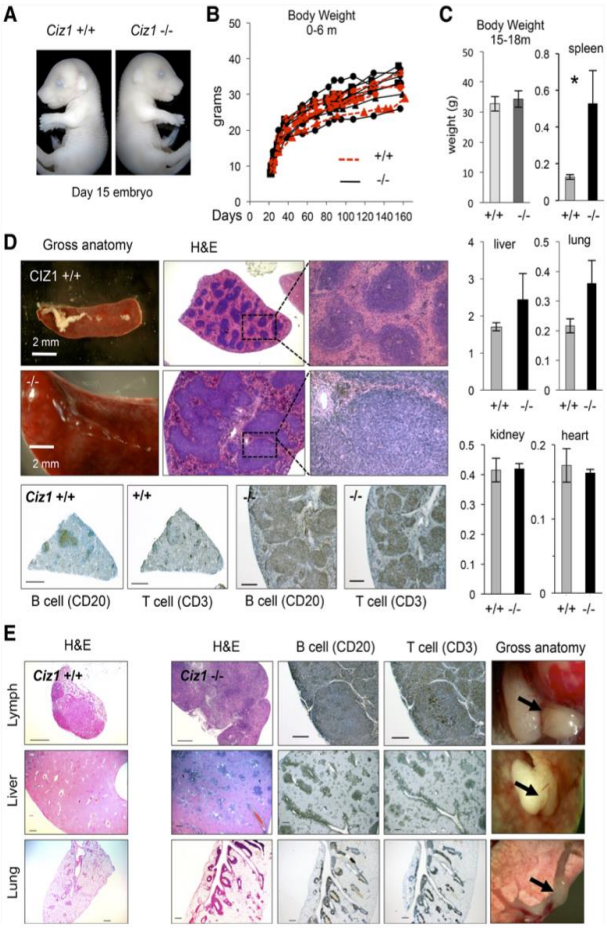

Figure 5. CIZ1-null mice develop normally but show gross lymphoid abnormalities in adult females. (*A*) *Ciz1*$^{-/-}$ embryos are indistinguishable from wild-type littermates at E15. (*B*,*C*) Growth profiles of *Ciz1*$^{+/+}$ ($n = 5$) and *Ciz1*$^{-/-}$ ($n = 8$) mice between days 20 and 160 after birth (*B*) and at 15–18 mo old in *Ciz1*$^{+/+}$ ($n = 8$) and *Ciz1*$^{-/-}$ ($n = 7$) females (*C*). No significant differences were detected. However, *Ciz1*$^{-/-}$ females had enlarged spleens ($n = 8$ *Ciz1*$^{+/+}$; $n = 6$ *Ciz1*$^{-/-}$), livers ($n = 6$ *Ciz1*$^{+/+}$; $n = 4$ *Ciz1*$^{-/-}$), and lungs ($n = 5$ *Ciz1*$^{+/+}$; $n = 5$ *Ciz1*$^{-/-}$). Other organs, including the kidney and heart, were not affected. (*D*) Representative image of gross spleen enlargement in *Ciz1*$^{-/-}$ females, with histological sections stained with hematoxylin and eosin (H&E). Lymphoid cell nuclei (stain darkly) are highly organized into foci in *Ciz1*$^{+/+}$ spleens but not *Ciz1*$^{-/-}$ spleens. (*Right*) High-magnification images show morphology consistent with lymphoproliferative disorder in *Ciz1*$^{-/-}$ mice. (*Below*) Immunohistochemical detection of CD20 and CD3 (B-cell-specific and T-cell-specific, respectively) suggests B-cell lymphoma with T-cell infiltration. Positive cells are stained dark gray and show overlapping distribution. Bar, 200 µm. (*E*) Representative H&E staining of *Ciz1*$^{+/+}$ and *Ciz1*$^{-/-}$ female lymph nodes, livers, and lungs. Enlargement of secondary lymphoid tissues in *Ciz1*$^{-/-}$ females correlates with excess proliferation of lymphoid cells, as in *D*. (*Right*) Examples of gross tissue anatomy in *Ciz1*$^{-/-}$ females showing areas of lymphoproliferative disorder as pale outgrowths. Bar, 200 µm.

paints showed no significant difference between wild-type and CIZ1-null PEFs (Fig. 6B), suggesting that there is a deficit in Xist RNA localization rather than Xi organization.

Further substantiating the conclusion that CIZ1 plays a role in Xist RNA localization, induction of the full-length GFP-CIZ1 transgene (Fig. 6C–E) fully reinstated the localization of Xist RNA over Xi domains (Fig. 6F,G). Prior to induction of CIZ1, *Xist* was dispersed in >80% of CIZ1-null e13.17 PEFs but became relocalized to discrete domains that overlap with GFP-CIZ1 domains within 20 h (Fig. 6H). Together, these observations demonstrate that CIZ1 plays a key role in Xist RNA localization in PEFs.

In light of the female-specific lymphoproliferative disorder observed in CIZ1-null animals, we went on to investigate the role of CIZ1 in X inactivation in hematopoetic lineages. We evaluated the impact of CIZ1 deletion in splenocytes from 6-wk-old females after stimulation of mixed populations of naïve B/T cells with either the B-cell activator lipopolysaccharide (LPS) or T-cell activator αCD3 antibody (αCD3). Consistent with a previous report (Wang et al. 2016), activation of both cell types from wild-type mice induced dramatic focal localization of *Xist* to Xi within 24 h, and this was mirrored by accumulation of CIZ1 (Fig. 7). However, activated B and T lymphocytes from CIZ1-null mice failed to efficiently localize Xist RNA to the Xi territory (Fig. 7B). This finding identifies a transition point in the affected lineages that is compromised in CIZ1-null animals. To ask whether aberrant *Xist* localization leads to relaxed control over X-linked genes, we compared the transcriptomes of wild-type spleens (containing mostly naïve cells) and CIZ1-null spleens (containing hyperproliferative cell populations likely expanded from rare activated precursors) from adult mice. Overall, from the 2209 X-linked genes that returned test data (Supplemental Fig. S7A; Supplemental data set S2), 16.4% were up-regulated and 8.7% were down-regulated by greater than twofold (Supplemental Fig. S7B). As expected, whole-genome gene set enrichment analysis returned highly significant overlap with immunological processes and cell division gene ontology terms (Supplemental Fig. S7C; Supplemental data set S3). Comparison of the X-linked genes with the gene list reported to be up-regulated in blood cells of *Xist* mutant mice (Yildirim et al. 2013) showed that many of the same genes are

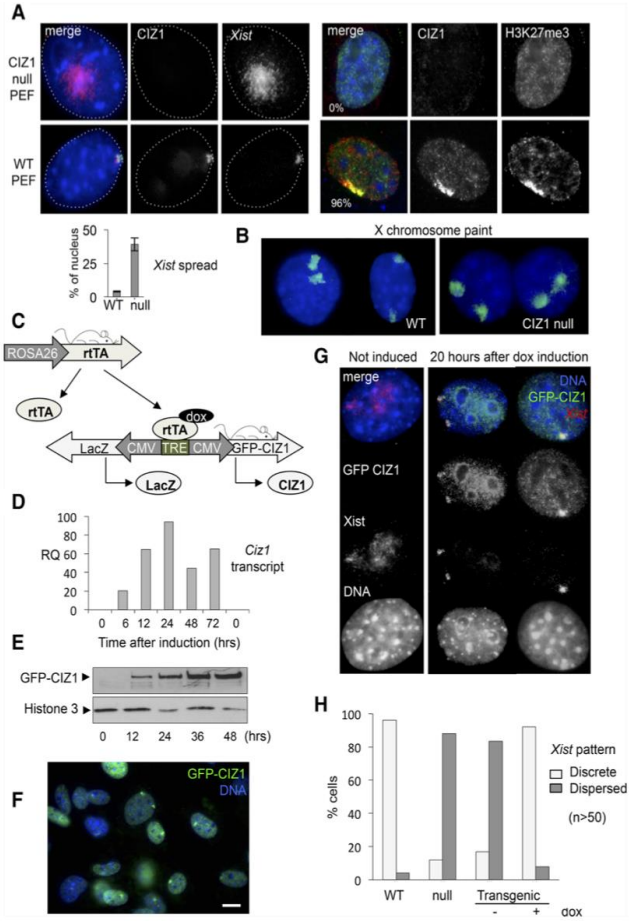

Figure 6. Loss and reinstatement of *Xist* localization at Xi is dependent on CIZ1. (*A*, *left*) Immuno-FISH showing CIZ1 and Xist RNA, which is delocalized in CIZ1-null (*ciz1*$^{-/-}$) PEFs. DNA was stained with DAPI (blue). (*Below*) Quantitation of the area of *Xist* FISH signal showing mean distribution over ~40% of the nucleus in CIZ1-null PEFs compared with <5% in wild-type cells. (*Right*) CIZ1 and H3K27me3 in wild-type and CIZ1-null cells showing the proportion of cells with marked Xis. $n = 100$. (*B*) X-chromosome paint shows similar X-chromosome territories in CIZ1-null and wild-type PEFs. (*C*) Double-transgenic female PEFs were derived from embryos harboring a tetracycline-responsive *Ciz1* responder transgene and reverse transactivator transgene on the CIZ1-null background. (*D*,*E*) *Ciz1* transcript (primers Mm00503766_m1) (*D*) and protein (N-terminal antibody in whole-cell lysates) (*E*) were detected after doxycycline induction. (*F*) Representative field view of GFP-CIZ1 expressed from the transgene on a CIZ1-null background 24 h after induction with doxycycline. Note the presence of two domains in some cells, indicating two Xis in tetraploid cells. Bar, 10 µm. (*G*) Expression of full-length CIZ1 in *ciz1*$^{-/-}$ PEFs leads to relocalization of *Xist* to the Xi territory. (*H*) Quantitation of the proportion of cells with *Xist* FISH signal that is "dispersed" (defined as occupation of >10% of the nuclear area). CIZ1 transgene induction reverts CIZ1-null cells to apparent normality for this criterium by 20 h.

affected (Supplemental Fig. S7D; Supplemental data set S4); however, a similar proportion of genes was affected genome-wide (Supplemental Fig. S7B). Together, the data demonstrate that CIZ1 plays a key role in stabilizing *Xist* association with Xi in lymphoid lineages but that its effects are not limited to the X chromosome.

Discussion

Here we demonstrate that the NM protein CIZ1 is strongly enriched over the Xi territory. Although CIZ1 was not previously linked to XCI, one of four recent screens identified CIZ1 among 81 candidate *Xist* interactors (Chu et al. 2015). Based on our findings, a relationship between CIZ1 and *Xist* is clear, although whether localization of CIZ1 to Xi domains is attributable to a direct interaction with Xist RNA or an interaction with other *Xist* or Xi-bound factors remains to be seen. Several observations support a functional interaction. First, loss of CIZ1 results in the dispersal of *Xist* in somatic cells. Second, CIZ1 enrichment occurs rapidly at the onset of Xist RNA expression and is present in all observed cases in which Xist RNA domains are observed. Third, SR 3D-SIM analyses demonstrate that CIZ1 and Xist RNA lie in very close proximity and that CIZ1 is localized to the RNA-dependent NM compartment at Xi. Finally, the C terminus of CIZ1, which anchors it at Xi, encompasses known RNA-binding domains, notably the Matrin3-type zinc finger, suggesting a possible direct interaction. Interestingly, Matrin3 has also been identified as a candidate *Xist* interactor (Chu et al. 2015; Moindrot et al. 2015). Further studies are nevertheless required to determine whether there is a direct interaction between CIZ1 and Xist RNA, specifically the E repeat region, and, at this stage, we cannot rule out that CIZ1 recognizes other *Xist*-interacting protein; for example, PTBP1 and PTBP2, recently shown to bind the E repeat region (Chen et al. 2016).

Several studies have pointed to a role for the NM in anchoring Xist RNA within the Xi territory, and a number of other proteins that interact with the NM or with DNA sequences that interact with the NM (S/MARs) have been implicated in XCI, including SAF-A, YY1, and SATB1. SAF-A and CIZ1 are similar in that their ability to support

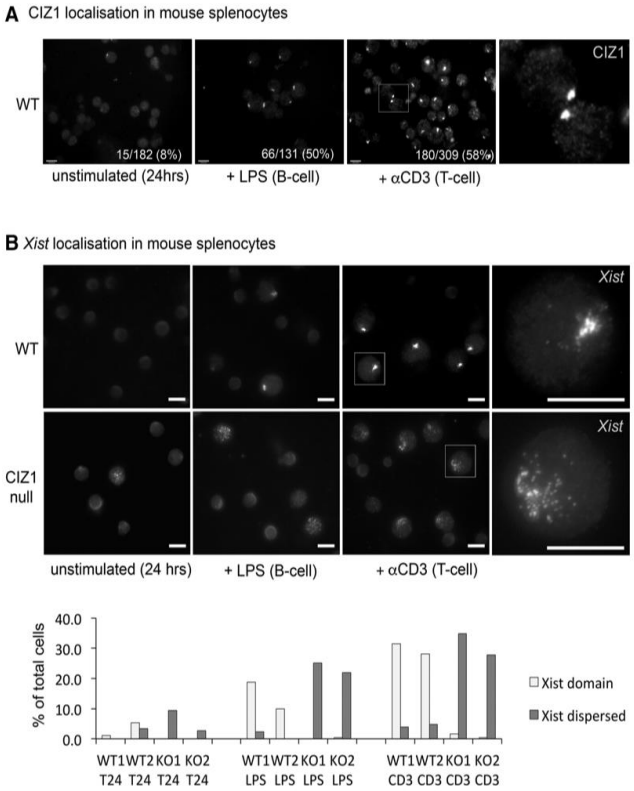

Figure 7. CIZ1 modulates *Xist* localization in splenocytes (*A*) CIZ1 localization in wild-type splenocytes before and after activation with LPS or αCD3. Stimulation causes the accumulation of CIZ1 at Xi in both B and T lymphocytes within 24 h. Bar, 10 µm. (*B*) Xist RNA localization in splenocytes before and after activation with LPS or αCD3. Similar to CIZ1, stimulation causes accumulation of *Xist* at Xi of wild-type B and T lymphocytes within 24 h, whereas Xist RNA is not properly localized in CIZ1-null cells. Bar, 10 µm. $n = 200–300$ per group.

Xist-mediated gene silencing and recruitment of *Xist* to Xi, respectively, is dependent on *Xist* E repeats (Hasegawa et al. 2010), possibly identifying a common mechanism. Moreover, deletion of the E repeats was shown recently to result in dispersed localization of Xist RNA (Yamada et al. 2015). These findings were attributed to SAF-A; however, our results suggest that loss of interaction with CIZ1 might contribute to the observed phenotype. Notably, the sensitivity of both SAF-A and YY1 to digestion of the RNA component of the NM distinguish them from CIZ1, which is part of the core protein matrix throughout the nucleus, suggesting important differences in their roles.

Scaffolding the structural reorganization of Xi during XCI or the maintenance of the compacted structure are possible functions for the NM to which CIZ1 might contribute. Another possibility, suggested by the function of CIZ1 in DNA replication, is the regulatable recruitment of factors into or away from the Xi territory. During late G1 phase, CIZ1 supports the recruitment of cyclin A to the NM. Cyclin docking on CIZ1, but not CIZ1 recruitment to the NM, is switched off at S phase (Copeland et al. 2015). Thus, in the context of DNA replication, CIZ1 appears to be a cargo carrier or mediator that is sensitive to cell cycle stage, raising the possibility of a relationship with cell cycle regulators implicated in *Xist* retention (Hall et al. 2009).

Although our observations in PEFs and lymphocytes implicate CIZ1 in anchoring *Xist* to the NM, the fact that CIZ1-null females are viable implies that the same relationship might not apply during early embryogenesis. Based on this, we hypothesize that CIZ1 functions redundantly with other anchoring factors (for example, SAF-A) and that these are sufficient during embryogenesis but insufficient in PEFs or lymphocytes. A recent report suggested that SAF-A is not essential for *Xist* localization in all lineages and that other factors may compensate for its loss (Kolpa et al. 2016). However, this is in contrast to genetic depletion of SAF-A in MEFs, which showed a requirement for SAF-A (Sakaguchi et al. 2016). Thus, the relationship between CIZ1 and SAF-A is not known, and there may be more factors capable of anchoring *Xist* at Xi.

Here we show that the compact localization of *Xist* upon the stimulation of lymphoid lineages (Wang et al. 2016) is dependent on CIZ1, describing a role for CIZ1 in a lineage-restricted transition that occurs throughout the lifetime of mice. An *Xist*-dependent silencing pathway was reported previously to be transiently activated during hematopoetic differentiation (Savarese et al. 2006), with pre-B and pre-T cells the most dependent. This aligns closely with our observation of B-cell and T-cell hyperplasia in CIZ1-null mice and is consistent with independent analysis that described a susceptibility to oncogene-induced transformation leading to leukemias in the absence of CIZ1, although no sex bias was reported in this study (Nishibe et al. 2013).

We observed widespread deregulation of gene expression in the absence of CIZ1 in affected lineages, although this was not specific to the X chromosome. However, we cannot rule out that low-level reactivation of multiple X-linked genes together, considered collectively, confers the female-specific lymphoproliferation phenotype. Thus, it remains an open question whether the disorder observed in CIZ1-null mice is a consequence of compromised XCI. Proliferative disorders of the hematopoetic system have been associated with deletion or suppression of factors linked with XCI (Leong et al. 2013; Yildirim et al. 2013), and abnormalities of XCI are reported frequently in cancers, including duplication of the active X (Xa) in breast and ovarian cancers and leukemias (Spatz et al. 2004; Lee and Bartolomei 2013). However, X chromosomes carry proportionally more immune-related genes than the rest of the genome (Bianchi et al. 2012), which means that a more general failure of the control of gene expression might manifest preferentially in females. Transcriptome analysis in PEFs identified candidate X-linked drivers of hematopoetic malignancies; *Gpm6b* overexpression is linked with B-cell lymphoma (Charfi et al. 2014), and *Figf* (VEGF-D) is implicated in the metastatic spread of tumors via lymph nodes (Bardelli et al. 2007; Pazgal et al. 2007). However, we interpret this with caution because changes elsewhere in the genome, initiated directly or indirectly as a consequence of the loss of CIZ1, are also likely to play a role.

In conclusion, we defined a novel component of the X inactivation pathway: the NM protein CIZ1. Our results indicate that CIZ1 functionally interacts with Xist RNA via the E repeat region and, moreover, that CIZ1 facilitates in *cis*-localization of Xist RNA, functioning as an anchor to the NM in somatic cell lineages.

Materials and methods

Further details are available in the Supplemental Material.

Animals and genotyping

All animal work was carried out under a UK Home Office license. CIZ1-null mice were generated from C57BL/6 ES clone IST13830B6 (TIGM) harboring a neomycin resistance gene trap inserted downstream from exon 1. The absence of *Ciz1*/CIZ1 in homozygous progeny was confirmed by quantitative PCR, immunofluorescence, and immunoblot with CIZ1 N-terminal antibody. Inducible *GFPCiz1*-Tg mice, generated by pronuclear injection of a GFP full-length *Ciz1* construct into CBA/C57BL6 fertilized eggs, were crossed with ROSA26-rtTA mice (Jackson Laboratories). All primers used for the characterization of *Ciz1* targeting and the detection of transactivator and responder transgenes and sex are in the Supplemental Material.

Cell lines

All stable cell lines were grown following standard procedures. Mouse PEFs were derived from individual embryos at days 13–14 of gestation. Primary TTFs were generated from individual 3-wk-old mice. Genotype and sex were confirmed after explant culture using primers listed in the Supplemental Material. For inducible cells harboring ROSA26-rtTA and *GFPCiz1*-Tg transgenes, the addition of 5 µg/mL doxycycline to medium was used to induce detectable GFP-CIZ1 within 6 h. ESCs were grown on feeders with the addition of LIF. Where applicable, *Xist* expression was induced with doxycycline at 1.5 µg/mL. Male XY P4D7 ESCs, derived from the cross between *Mus castaneous* and 129+*Ter*/SvJcl and containing an rtTA cassette in the Gt(ROSA)26Sor locus (Moindrot et al. 2015) were used to generate stable autosomal integrants of *Xist*-inducible deletion variants.

Splenocyte isolation and activation

Spleens isolated from 6-wk-old wild-type and *Ciz1*-null females were pressed through 70-µm nylon filters to dissociate naïve B and T lymphocytes into medium (RPMI 1640; Invitrogen) supplemented with 10% fetal calf serum, 100 µ/mL penicillin, 10 µg/mL streptomycin, and 2 mM L-glutamine. The cells were pelleted at 450 g for 5 min and then resuspended in red blood cell lysis solution (Sigma) for 3 min before being pelleted and resuspended in 2 mL of medium. The cell suspensions were counted with Trypan blue to determine viability and adjusted to 10×10^6 cells per milliliter. One-hundred microliters (1×10^6 cells) was transferred into individual wells of a 96-well plate and supplemented with 100 µL of (1) medium for unactivated control, (2) 1 µg/mL LPS (Sigma) for B-cell activation, or (3) 1 µg/mL αCD3 (BioLegend) for T-cell activation. After 24–48 h, the cells were processed for RNA-FISH, immunofluorescence, and protein isolation.

Whole-genome RNA sequencing and bioinformatics

In brief, cell lines (detailed in the Supplemental Material) were grown to 80% density before RNA extraction and DNase I treatment. Libraries, optimized for 250- to 400-base-pair inserts, were prepared using NEBNext Ultra (Illumina), enriched for mRNA using NEBNext poly(A) mRNA magnetic isolation module, and sequenced to generate $\sim 5 \times 10^7$ reads per sample. STAR software was used to align reads to the C57BL/6 X chromosome. Transcriptome assembly and expression quantification were performed using Cufflinks and Cuffdiff. Of 85 differentially expressed X-linked transcription units ($P < 0.05$), 23 were excluded due to differential expression between biological replicates. Heat maps and gene enrichment analysis were carried out as described in the Supplemental Material.

Histology

Following dissection, tissues were transferred immediately into histological grade formalin and processed after 24–48 h. Immunostaining for CD antigens was performed using rabbit anti-CD3 for T cells (Abcam, ab16669) at 1:200 and goat anti-CD20 for B cells (Santa Cruz Biotechnology, sc7735) at 1:500.

ESC differentiation

Female PGK12.1 ESCs were grown in ES medium with LIF on gelatin without feeders. To induce differentiation, 1×10^6 cells were plated onto nongelatinized dishes without LIF. On day 3, differentiating colonies were replated onto bacterial dishes to stimulate embryoid body formation. On day 7, embryoid bodies were transferred to nongelatinized dishes to reattach. Fibroblast outgrowths were passaged as required.

NM extraction

Cells were serially extracted with (1) detergent to reveal soluble factors, (2) salt to reveal loosely bound chromatin-associated factors, (3) DNase I to reveal tightly attached chromatin-associated factors, and (4) RNase to reveal RNA-associated factors, as described (Wilson et al. 2016), with improvements detailed in the Supplemental Material. Coverslips were then fixed and processed for immunofluorescence.

Immunofluorescence

Cells were washed in PBS and either (1) fixed in 4% PFA to reveal total protein or (2) treated with detergent prior to fixing to reveal chromatin- and NM-associated factors prior to incubation with primary antibody for 2 h, and then secondary antibody for 1 h. For the ESC differentiation course, PGK12.1 cells were fixed in 2% formaldehyde for 15 min prior to permeabilization. The antibodies used were α-H3K27me3 mAb (Abcam, ab6002; Active Motif, ab61017), α-CIZ1 N-terminal (1794), α-CIZ1 C-terminal (Novus, NB100-74624), SAFA anti-HNRNP-U (Abcam, ab10297), and anti-YY1 (SC7341). Coverslips were costained with limiting concentrations of Hoechst 33258 (10 ng/mL; Sigma) for quantitative detection of chromatin.

RNA-FISH

Female cultured cells were processed for the detection of *Xist* transcript (red) by RNA-FISH followed by immuno-FISH for CIZ1 (green) using N-terminal antibody 1794. An 11-kb Spe1–Sal1 mouse *Xist* fragment was fluorescently tagged with Cy3-dUTP (GE Healthcare) using BioPrime labeling kit (Invitrogen). Samples were incubated with probe overnight at 37°C. For subsequent detection of CIZ1, antibody 1794 was applied for 1 h followed by secondary anti-rabbit FITC (Sigma) for 1 h. Cells were imaged and processed using Adobe Photoshop CS4 to enhance signal definition. Prior RNA-FISH processing resulted in reduced CIZ1 signal intensity throughout the nucleus. For SR 3D-SIM and RNA-FISH on splenocyte *Xist*, cDNA was labeled with Spectrum green-dUTP or Spectrum red-dUTP by nick translation (Abbott Molecular). Following fixation and permeabilization, cells were incubated with primary antibody for 1 h and then with Alexa fluor goat anti-rabbit 594 for 30 min and then washed and post-fixed before detection of *Xist* overnight. After extensive washing, the cells were incubated with 2 µg/mL DAPI and mounted with VectorShield.

Chromosome paints

FITC-conjugated X-chromosome paint (AMP 0XG) was used as instructed (Cytocell Ltd.). Labeled cells were mounted in VectorShield with DAPI and imaged.

Microscopy

Images were collected using a Zeiss Axiovert 200M and Axiocam and Openlab image acquisition software and quantified using ImageJ (National Institutes of Health) using raw images acquired under identical conditions. Images for publication were enhanced using Adobe Photoshop or Affinity Photo 1.4 by applying identical manipulations to test and control samples so that image intensities reflect actual relationships. Live images were collected on a PE Ultraview spinning-disk confocal microscope. SR 3D-SIM was performed on a DeltaVision OMX V3 Blaze system (GE Healthcare) equipped with a 60×/1.42 NA plan apo oil immersion objective (Olympus), sCMOS cameras (PCO), and 405-, 488-, and 593-nm lasers. 3D-SIM image stacks were acquired as described in the Supplemental Material.

Acknowledgments

X-chromosome paints were a kind gift from Cytocell. We are grateful to James Hewitson, Dimitris Lagos, Mike Shires, and Matthew Wiseman for advice or assistance, and Sally James, Richard Randle-Boggis, Katherine Newling, and Peter Ashton of York Technology Facility Genomics laboratory. This work was supported by a Radhika Sreedhar Scholarship to R.R.-F., University of York priming funds, Biotechnology and Biological Sciences Research Council PhD training scholarships to E.R.S. and R.W., Genetics Society training funds to R.R., Wellcome Trust grants to N.B. (081385,091911), and the Micron Advance Imaging Initiative (Wellcome Trust 103768).

References

Ainscough JF, Rahman FA, Sercombe H, Sedo A, Gerlach B, Coverley D. 2007. C-terminal domains deliver the DNA replication factor Ciz1 to the nuclear matrix. *J Cell Sci* **120:** 115–124.

Bardelli M, Leucci E, Schurfeld K, Bellan C, Passiatore G, Rocchigiani M, Bartolommei S, Orlandini M, Zagursky J, Lazzi S, et al. 2007. VEGF-D is expressed in activated lymphoid cells and in tumors of hematopoietic and lymphoid tissues. *Leuk Lymphoma* **48:** 2014–2021.

Bianchi I, Lleo A, Gershwin ME, Invernizzi P. 2012. The X chromosome and immune associated genes. *J Autoimmun* **38:** J187–J192.

Brockdorff N, Ashworth A, Kay GF, McCabe VM, Norris DP, Cooper PJ, Swift S, Rastan S. 1992. The product of the mouse Xist gene is a 15 kb inactive X-specific transcript containing no conserved ORF and located in the nucleus. *Cell* **71:** 515–526.

Brown CJ, Willard HF. 1994. The human X-inactivation centre is not required for maintenance of X-chromosome inactivation. *Nature* **368:** 154–156.

Brown CJ, Hendrich BD, Rupert JL, Lafreniere RG, Xing Y, Lawrence J, Willard HF. 1992. The human XIST gene: analysis of a 17 kb inactive X-specific RNA that contains conserved repeats and is highly localized within the nucleus. *Cell* **71:** 527–542.

Caparros ML, Alexiou M, Webster Z, Brockdorff N. 2002. Functional analysis of the highly conserved exon IV of XIST RNA. *Cytogenet Genome Res* **99:** 99–105.

Charfi C, Edouard E, Rassart E. 2014. Identification of GPM6A and GPM6B as potential new human lymphoid leukemia-associated oncogenes. *Cell Oncol (Dordr)* **37:** 179–191.

Chen CK, Blanco M, Jackson C, Aznauryan E, Ollikainen N, Surka C, Chow A, Cerase A, McDonel P, Guttman M. 2016. Xist recruits the X chromosome to the nuclear lamina to enable chromosome-wide silencing. *Science* **354:** 468–472.

Chu C, Zhang QC, da Rocha ST, Flynn RA, Bharadwaj M, Calabrese JM, Magnuson T, Heard E, Chang HY. 2015. Systematic discovery of Xist RNA binding proteins. *Cell* **161:** 404–416.

Clemson CM, McNeil JA, Willard HF, Lawrence JB. 1996. XIST RNA paints the inactive X chromosome at interphase: evidence for a novel RNA involved in nuclear/chromosome structure. *J Cell Biol* **132:** 259–275.

Copeland NA, Sercombe HE, Ainscough JF, Coverley D. 2010. Ciz1 cooperates with cyclin-A–CDK2 to activate mammalian DNA replication in vitro. *J Cell Sci* **123:** 1108–1115.

Copeland NA, Sercombe HE, Wilson RH, Coverley D. 2015. Cyclin-A–CDK2-mediated phosphorylation of CIZ1 blocks replisome formation and initiation of mammalian DNA replication. *J Cell Sci* **128:** 1518–1527.

Coverley D, Marr J, Ainscough J. 2005. Ciz1 promotes mammalian DNA replication. *J Cell Sci* **118:** 101–112.

Csankovszki G, Panning B, Bates B, Pehrson JR, Jaenisch R. 1999. Conditional deletion of Xist disrupts histone macroH2A localization but not maintenance of X inactivation. *Nat Genet* **22:** 323–324.

da Rocha ST, Boeva V, Escamilla-Del-Arenal M, Ancelin K, Granier C, Matias NR, Sanulli S, Chow J, Schulz E, Picard C, et al. 2014. Jarid2 is implicated in the initial Xist-induced targeting of PRC2 to the inactive X chromosome. *Mol Cell* **53:** 301–316.

den Hollander P, Rayala SK, Coverley D, Kumar R. 2006. Ciz1, a novel DNA-binding coactivator of the estrogen receptor α, confers hypersensitivity to estrogen action. *Cancer Res* **66:** 11021–11030.

Duthie SM, Nesterova TB, Formstone EJ, Keohane AM, Turner BM, Zakian SM, Brockdorff N. 1999. Xist RNA exhibits a banded localization on the inactive X chromosome and is excluded from autosomal material in *cis*. *Hum Mol Genet* **8:** 195–204.

Engreitz JM, Pandya-Jones A, McDonel P, Shishkin A, Sirokman K, Surka C, Kadri S, Xing J, Goren A, Lander ES, et al. 2013. The Xist lncRNA exploits three-dimensional genome architecture to spread across the X chromosome. *Science* **341:** 1237973.

Greaves EA, Copeland NA, Coverley D, Ainscough JF. 2012. Cancer-associated variant expression and interaction of CIZ1 with cyclin A1 in differentiating male germ cells. *J Cell Sci* **125:** 2466–2477.

Guo B, Odgren PR, van Wijnen AJ, Last TJ, Nickerson J, Penman S, Lian JB, Stein JL, Stein GS. 1995. The nuclear matrix protein NMP-1 is the transcription factor YY1. *Proc Natl Acad Sci* **92:** 10526–10530.

Hall LL, Byron M, Pageau G, Lawrence JB. 2009. AURKB-mediated effects on chromatin regulate binding versus release of XIST RNA to the inactive chromosome. *J Cell Biol* **186:** 491–507.

Hasegawa Y, Brockdorff N, Kawano S, Tsutui K, Tsutui K, Nakagawa S. 2010. The matrix protein hnRNP U is required for chromosomal localization of Xist RNA. *Dev Cell* **19:** 469–476.

Heard E, Disteche CM. 2006. Dosage compensation in mammals: fine-tuning the expression of the X chromosome. *Genes Dev* **20:** 1848–1867.

Helbig R, Fackelmayer FO. 2003. Scaffold attachment factor A (SAF-A) is concentrated in inactive X chromosome territories through its RGG domain. *Chromosoma* **112:** 173–182.

Higgins G, Roper KM, Watson IJ, Blackhall FH, Rom WN, Pass HI, Ainscough JF, Coverley D. 2012. Variant Ciz1 is a circulating biomarker for early-stage lung cancer. *Proc Natl Acad Sci* **109:** E3128–E3135.

Jeon Y, Lee JT. 2011. YY1 tethers Xist RNA to the inactive X nucleation center. *Cell* **146:** 119–133.

Kolpa HJ, Fackelmayer FO, Lawrence JB. 2016. SAF-A requirement in anchoring XIST RNA to chromatin varies in transformed and primary cells. *Dev Cell* **39:** 9–10.

Lee JT, Bartolomei MS. 2013. X-inactivation, imprinting, and long noncoding RNAs in health and disease. *Cell* **152:** 1308–1323.

Lee JT, Strauss WM, Dausman JA, Jaenisch R. 1996. A 450 kb transgene displays properties of the mammalian X-inactivation center. *Cell* **86:** 83–94.

Leong HS, Chen K, Hu Y, Lee S, Corbin J, Pakusch M, Murphy JM, Majewski IJ, Smyth GK, Alexander WS, et al. 2013. Epigenetic regulator Smchd1 functions as a tumor suppressor. *Cancer Res* **73:** 1591–1599.

Makhlouf M, Ouimette JF, Oldfield A, Navarro P, Neuillet D, Rougeulle C. 2014. A prominent and conserved role for YY1 in Xist transcriptional activation. *Nat Commun* **5:** 4878.

McHugh CA, Chen CK, Chow A, Surka CF, Tran C, McDonel P, Pandya-Jones A, Blanco M, Burghard C, Moradian A, et al. 2015. The Xist lncRNA interacts directly with SHARP to silence transcription through HDAC3. *Nature* **521:** 232–236.

Mitsui K, Matsumoto A, Ohtsuka S, Ohtsubo M, Yoshimura A. 1999. Cloning and characterization of a novel p21{Cip1/Waf1}-interacting zinc finger protein, ciz1. *Biochem Biophys Res Commun* **264:** 457–464.

Moindrot B, Cerase A, Coker H, Masui O, Grijzenhout A, Pintacuda G, Schermelleh L, Nesterova TB, Brockdorff N. 2015. A pooled shRNA screen identifies Rbm15, Spen, and Wtap as factors required for Xist RNA-mediated silencing. *Cell Rep* **12:** 562–572.

Monfort A, Di Minin G, Postlmayr A, Freimann R, Arieti F, Thore S, Wutz A. 2015. Identification of *Spen* as a crucial factor for Xist function through forward genetic screening in haploid embryonic stem cells. *Cell Rep* **12:** 554–561.

Nesterova TB, Slobodyanyuk SY, Elisaphenko EA, Shevchenko AI, Johnston C, Pavlova ME, Rogozin IB, Kolesnikov NN, Brockdorff N, Zakian SM. 2001. Characterization of the genomic Xist locus in rodents reveals conservation of overall gene structure and tandem repeats but rapid evolution of unique sequence. *Genome Res* **11:** 833–849.

Nishibe R, Watanabe W, Ueda T, Yamasaki N, Koller R, Wolff L, Honda Z, Ohtsubo M, Honda H. 2013. CIZ1, a p21Cip1/Waf1-interacting protein, functions as a tumor suppressor in vivo. *FEBS Lett* **587:** 1529–1535.

Pazgal I, Boycov O, Shpilberg O, Okon E, Bairey O. 2007. Expression of VEGF-C, VEGF-D and their receptor VEGFR-3 in diffuse large B-cell lymphomas. *Leuk Lymphoma* **48:** 2213–2220.

Penny GD, Kay GF, Sheardown SA, Rastan S, Brockdorff N. 1996. Requirement for Xist in X chromosome inactivation. *Nature* **379:** 131–137.

Pollex T, Heard E. 2012. Recent advances in X-chromosome inactivation research. *Curr Opin Cell Biol* **24:** 825–832.

Rahman FA, Aziz N, Coverley D. 2010. Differential detection of alternatively spliced variants of Ciz1 in normal and cancer cells using a custom exon-junction microarray. *BMC Cancer* **10:** 482.

Sakaguchi T, Hasegawa Y, Brockdorff N, Tsutsui K, Tsutsui KM, Sado T, Nakagawa S. 2016. Control of chromosomal localization of Xist by hnRNP U family molecules. *Dev Cell* **39:** 11–12.

Savarese F, Flahndorfer K, Jaenisch R, Busslinger M, Wutz A. 2006. Hematopoietic precursor cells transiently reestablish permissiveness for X inactivation. *Mol Cell Biol* **26:** 7167–7177.

Sheardown SA, Duthie SM, Johnston CM, Newall AE, Formstone EJ, Arkell RM, Nesterova TB, Alghisi GC, Rastan S, Brockdorff N. 1997. Stabilization of Xist RNA mediates initiation of X chromosome inactivation. *Cell* **91:** 99–107.

Simon MD, Pinter SF, Fang R, Sarma K, Rutenberg-Schoenberg M, Bowman SK, Kesner BA, Maier VK, Kingston RE, Lee JT. 2013. High-resolution Xist binding maps reveal two-step spreading during X-chromosome inactivation. *Nature* **504:** 465–469.

Smeets D, Markaki Y, Schmid VJ, Kraus F, Tattermusch A, Cerase A, Sterr M, Fiedler S, Demmerle J, Popken J, et al.

2014. Three-dimensional super-resolution microscopy of the inactive X chromosome territory reveals a collapse of its active nuclear compartment harboring distinct Xist RNA foci. *Epigenetics Chromatin* **7:** 8.

Spatz A, Borg C, Feunteun J. 2004. X-chromosome genetics and human cancer. *Nat Rev Cancer* **4:** 617–629.

Wang J, Syrett CM, Kramer MC, Basu A, Atchison ML, Anguera MC. 2016. Unusual maintenance of X chromosome inactivation predisposes female lymphocytes for increased expression from the inactive X. *Proc Natl Acad Sci* **113:** E2029–E2038.

Ward JM. 2006. Lymphomas and leukemias in mice. *Exp Toxicol Pathol* **57:** 377–381.

Wilson RH, Coverley D. 2013. Relationship between DNA replication and the nuclear matrix. *Genes Cells* **18:** 17–31.

Wilson RH, Hesketh EL, Coverley D. 2016. Preparation of the nuclear matrix for parallel microscopy and biochemical analyses. *Cold Spring Harb Protoc* doi: 10.1101/pdb.prot083758.

Wutz A, Jaenisch R. 2000. A shift from reversible to irreversible X inactivation is triggered during ES cell differentiation. *Mol Cell* **5:** 695–705.

Wutz A, Rasmussen TP, Jaenisch R. 2002. Chromosomal silencing and localization are mediated by different domains of Xist RNA. *Nat Genet* **30:** 167–174.

Xiao J, Vemula SR, Xue Y, Khan MM, Kuruvilla KP, Marquez-Lona EM, Cobb MR, LeDoux MS. 2016. Motor phenotypes and molecular networks associated with germline deficiency of Ciz1. *Exp Neurol* **283:** 110–120.

Yamada N, Hasegawa Y, Yue M, Hamada T, Nakagawa S, Ogawa Y. 2015. Xist exon 7 contributes to the stable localization of Xist RNA on the inactive X-chromosome. *PLoS Genet* **11:** e1005430.

Yildirim E, Kirby JE, Brown DE, Mercier FE, Sadreyev RI, Scadden DT, Lee JT. 2013. Xist RNA is a potent suppressor of hematologic cancer in mice. *Cell* **152:** 727–742.

List of References

Aggerholm-Pedersen, N., Safwat, A., Bærentzen, S., Nordsmark, M., Nielsen, O., Alsner, J. and Sørensen, B.S. 2014. The Importance of Reference Gene Analysis of Formalin-Fixed, Paraffin-Embedded Samples from Sarcoma Patients — An Often Underestimated Problem. *Translational Oncology.* **7**(6), pp.687-693.

Ainscough, J.F.X., Koide, T., Tada, M., Barton, S. and Surani, M.A. 1997. Imprinting of Igf2 and H19 from a 130 kb YAC transgene. *Development.* **124**(18), pp.3621-3632.

Ainscough, J.F.X., Rahman, F., Sercombe, H., Sedo, A., Gerlach, B. and Coverley, D. 2007. C-terminal domains deliver the DNA replication factor Ciz1 to the nuclear matrix. *Journal of Cell Science.* **120**(1), pp.115-124.

Al-Hajj, M., Wicha, M.S., Benito-Hernandez, A., Morrison, S.J. and Clarke, M.F. 2003. Prospective identification of tumorigenic breast cancer cells. *Proceedings of the National Academy of Sciences of the United States of America.* **100**(7), pp.3983-3988.

Aleidi, S.M., Howe, V., Sharpe, L.J., Yang, A., Rao, G., Brown, A.J. and Gelissen, I.C. 2015. The E3 Ubiquitin Ligases, HUWE1 and NEDD4-1, Are Involved in the Post-translational Regulation of the ABCG1 and ABCG4 Lipid Transporters. *The Journal of Biological Chemistry.* **290**(40), pp.24604-24613.

Ambros, I.M., Ambros, P.F., Strehl, S., Kovar, H., Gadner, H. and Salzer-Kuntschik, M. 1991. Mic2 is a specific marker for ewing's sarcoma and peripheral primitive neuroectodermal tumors. Evidence for a common histogenesis of ewing's sarcoma and peripheral primitive neuroectodermal tumors from mic2 expression and specific chromosome aberration. *Cancer.* **67**(7), pp.1886-1893.

Angervall, L. and Enzinger, F.M. 1975. Extraskeletal neoplasm resembling Ewing's sarcoma. *Cancer.* **36**, pp.240-251.

Armbruster, C., Huber, M., Prosch, H., Dworan, N. and Attems, J. 2008. Ewing's Sarcoma and Peripheral Primitive Neuroectodermal Tumor in Adults: Different Features of a Rare Neoplasm. *Oncology Research and Treatment.* **31**(4), pp.179-184.

Askin, F.B., Rosai, J., Sibley, R.K., Dehner, L.P. and McAlister, W.H. 1979. Malignant small cell tumor of the thoracopulmonary region in childhood. A distinctive clinicopathologic entity of uncertain histogenesis. *Cancer.* **43**, pp.2438–2451.

Aubin, J.E. 1979. Autofluorescence of viable cultured mammalian cells. *Journal of Histochemistry & Cytochemistry.* **27**(1), pp.36-43.

Avilion, A.A., Nicolis, S.K., Pevny, L.H., Perez, L., Vivian, N. and Lovell-Badge, R. 2003. Multipotent cell lineages in early mouse development depend on SOX2 function. *Genes Dev.* **17**(1), pp.126-140.

Avnet, S., Di Pompo, G., Lemma, S., Salerno, M., Perut, F., Bonuccelli, G., Granchi, D., Zini, N. and Baldini, N. 2013. V-ATPase is a candidate therapeutic target for Ewing sarcoma. *Biochimica et Biophysica Acta (BBA) - Molecular Basis of Disease.* **1832**(8), pp.1105-1116.

Bageghni, S.A., Frentzou, G.A., Drinkhill, M.J., Mansfield, W., Coverley, D. and Ainscough, J.F.X. 2017. Cardiomyocyte-specific expression of the nuclear matrix protein, CIZ1, stimulates production of mono-nucleated cells

with an extended window of proliferation in the postnatal mouse heart. *Biology Open.* **6**(1), pp.92-99.
Bailly, R.A., Bosselut, R., Zucman, J., Cormier, F., Delattre, O., Roussel, M., Thomas, G. and Ghysdael, J. 1994. DNA-binding and transcriptional activation properties of the EWS-FLI-1 fusion protein resulting from the t(11;22) translocation in Ewing sarcoma. *Molecular and Cellular Biology.* **14**(5), pp.3230-3241.
Baldan, A., Gomes, A.V., Ping, P. and Edwards, P.A. 2008. Loss of ABCG1 Results in Chronic Pulmonary Inflammation. *The Journal of Immunology.* **180**(5), pp.3560-3568.
Baldan, A., Tarr, P., Vales, C.S., Frank, J., Shimotake, T.K., Hawgood, S. and Edwards, P.A. 2006. Deletion of the transmembrane transporter ABCG1 results in progressive pulmonary lipidosis. *J Biol Chem.* **281**(39), pp.29401-29410.
Bao, S., Wu, Q., McLendon, R.E., Hao, Y., Shi, Q., Hjelmeland, A.B., Dewhirst, M.W., Bigner, D.D. and Rich, J.N. 2006. Glioma stem cells promote radioresistance by preferential activation of the DNA damage response. *Nature.* **444**(7120), pp.756-760.
Bar, T., Ståhlberg, A., Muszta, A. and Kubista, M. 2003. Kinetic Outlier Detection (KOD) in real-time PCR. *Nucleic Acids Research.* **31**(17), pp.e105-e105.
Barroso-delJesus, A., Lucena-Aguilar, G., Sanchez, L., Ligero, G., Gutierrez-Aranda, I. and Menendez, P. 2011. The Nodal inhibitor Lefty is negatively modulated by the microRNA miR-302 in human embryonic stem cells. *FASEB J.* **25**(5), pp.1497-1508.
Bartel, D.P. 2009. MicroRNA Target Recognition and Regulatory Functions. *Cell.* **136**(2), pp.215-233.
Bennani-Baiti, I.M., Cooper, A., Lawlor, E.R., Kauer, M., Ban, J., Aryee, D.N. and Kovar, H. 2010. Intercohort gene expression co-analysis reveals chemokine receptors as prognostic indicators in Ewing's sarcoma. *Clinical cancer research.* **16**(14), pp.3769-3778.
Bento, C., Fernandes, R., Ramalho, J., Marques, C., Shang, F., Taylor, A. and Pereira, P. 2010. The Chaperone-Dependent Ubiquitin Ligase CHIP Targets HIF-1α for Degradation in the Presence of Methylglyoxal. *PLoS ONE.* **5**(11), pe15062.
Bernstein, E., Caudy, A.A., Hammond, S.M. and Hannon, G.J. 2001. Role for a bidentate ribonuclease in the initiation step of RNA interference. *Nature.* **409**(6818), pp.363-366.
Bernstein, m., Hovar, H., Paulussen, M., Randall, R.I., Schuck, A., Teot, I.A. and Juergensg, h. 2006. Ewing's sarcoma family of tumors: Current management. *The Oncologist.* **11**(5), pp.503-519.
Bhatia, M., Wang, J.C.Y., Kapp, U., Bonnet, D. and Dick, J.E. 1997. Purification of primitive human hematopoietic cells capable of repopulating immune-deficient mice. *Proceedings of the National Academy of Sciences.* **94**(10), pp.5320-5325.
Bielicki, J.K., McCall, M.R. and Forte, T.M. 1999. Apolipoprotein A-I promotes cholesterol release and apolipoprotein E recruitment from THP-1 macrophage-like foam cells. *J Lipid Res.* (40), pp.85-92.
Bohnsack, M.T., Czaplinski, K. and GÖRlich, D. 2004. Exportin 5 is a RanGTP-dependent dsRNA-binding protein that mediates nuclear export of pre-miRNAs. *RNA.* **10**(2), pp.185-191.

Bonnet, D. and Dick, J.E. 1997. Human acute myeloid leukemia is organized as a hierarchy that originates from a primitive hematopoietic cell. *Nat Med.* **3**(7), pp.730-737.
Boon, R.A. and Vickers, K.C. 2013. Intercellular Transport of MicroRNAs. *Arteriosclerosis, thrombosis, and vascular biology.* **33**(2), pp.186-192.
Borchert, G.M., Lanier, W. and Davidson, B.L. 2006. RNA polymerase III transcribes human microRNAs. *Nat Struct Mol Biol.* **13**(12), pp.1097-1101.
Bossen, C., Ingold, K., Tardivel, A., Bodmer, J.L., Gaide, O., Hertig, S., Ambrose, C., Tschopp, J. and Schneider, P. 2006. Interactions of tumor necrosis factor (TNF) and TNF receptor family members in the mouse and human. *J Biol Chem.* **281**(20), pp.13964-13971.
Boutonnat, J., Barbier, M., Muirhead, K., Mousseau, M., Grunwald, D., Ronot, X. and Seigneurin, D. 2000. Response of chemosensitive and chemoresistant leukemic cell lines to drug therapy: simultaneous assessment of proliferation, apoptosis, and necrosis. *Cytometry.* **42**(1), pp.50-60.
Brasme, J., Chalumeau, M., Oberlin, O., Valteau-Couanet, D. and Gaspar, N. 2014. Time to Diagnosis of Ewing Tumors in Children and Adolescents Is Not Associated With Metastasis or Survival: A Prospective Multicenter Study of 436 Patients. *Journal of Clinical Oncology.* **32**(18), pp.1935-1940.
Brownhill, S.C., Taylor, C. and Burchill, S.A. 2007. Chromosome 9p21 gene copy number and prognostic significance of p16 in ESFT. *British Journal of Cancer.* **96**(12), pp.1914-1923.
Buczacki, S.J.A., Zecchini, H., Nicholson, A.M., Russell, R., Vermeulen, L., Kemp, R. and Winton, D.J. 2013. Intestinal label-retaining cells are secretory precursors expressing Lgr5. *Nature.* **495**(7439), pp.65-69.
Burchill, S.A. 2003. Ewing's sarcoma: diagnostic, prognostic, and therapeutic implications of molecular abnormalities. *Journal of Clinical Pathology.* **56**(2), pp.96-102.
Burchill, S.A. 2008. Molecular abnormalities in Ewing's sarcoma. *Expert Review of Anticancer Therapy.* **8**(10), pp.1675-1687.
Burkert, J., Otto, W.R. and Wright, N.A. 2008. Side populations of gastrointestinal cancers are not enriched in stem cells. *The Journal of Pathology.* **214**(5), pp.564-573.
Burns, V., Sharpe, L.J., Gelissen, I.C. and Brown, A.J. 2013. Species variation in ABCG1 isoform expression: implications for the use of animal models in elucidating ABCG1 function. *Atherosclerosis.* **226**(2), pp.408-411.
Cai, H., Lin, L., Cai, H., Tang, M. and Wang, Z. 2013. Prognostic evaluation of microRNA-210 expression in pediatric osteosarcoma. *Medical Oncology.* **30**(2), p499.
Calabrese, C., Poppleton, H., Kocak, M., Hogg, T.L., Fuller, C., Hamner, B., Oh, E., Gaber, M.W., Finklestein, D., Allen, M., Frank, A., Bayazitov, I.T., Zakharenko, S.S., Gajjar, A., Davidoff, A. and Gilbertson, R.J. 2007. A Perivascular Niche for Brain Tumor Stem Cells. *Cancer Cell.* **11**(1), pp.69-82.
Calvet, C.Y., André, F.M. and Mir, L.M. 2014. The Culture of Cancer Cell Lines as Tumorspheres Does Not Systematically Result in Cancer Stem Cell Enrichment. *PLoS ONE.* **9**(2), pe89644.
Camps, C., Buffa, F.M., Colella, S., Moore, J., Sotiriou, C., Sheldon, H., Harris, A.L., Gleadle, J.M. and Ragoussis, J. 2008. hsa-miR-210 Is Induced

by Hypoxia and Is an Independent Prognostic Factor in Breast Cancer. *Clinical Cancer Research.* **14**(5), p1340.
Casey, D.A., Wexler, L.H., Merchant, M.S., Chou, A.J., Merola, P.R., Price, A.P. and Meyers, P.A. 2009. Irinotecan and temozolomide for Ewing sarcoma: The Memorial Sloan-Kettering experience. *Pediatric Blood & Cancer.* **53**(6), pp.1029-1034.
Cavallari, C., Fonsato, V., Herrera, M.B., Bruno, S., Tetta, C. and Camussi, G. 2013. Role of Lefty in the anti tumor activity of human adult liver stem cells. *Oncogene.* **32**(7), pp.819-826.
Ceder, J., Aalders, T. and Schalken, J. 2017. Label retention and stem cell marker expression in the developing and adult prostate identifies basal and luminal epithelial stem cell subpopulations. *Stem Cell Research & Therapy.* **8**, p95.
Chan, S.Y. and Loscalzo, J. 2010. MicroRNA-210: a unique and pleiotropic hypoxamir. *Cell Cycle.* **9**(6), pp.1072-1083.
Chan, S.Y., Zhang, Y.Y., Hemann, C., Mahoney, C.E., Zweier, J.L. and Loscalzo, J. 2009. MicroRNA-210 controls mitochondrial metabolism during hypoxia by repressing the iron-sulfur cluster assembly proteins ISCU1/2. *Cell Metab.* **10**(4), pp.273-284.
Chan, Y.C., Banerjee, J., Choi, S. and Sen, C.K. 2012. miR-210: the master hypoxamir. *Microcirculation (New York, N.Y. : 1994).* **19**(3), pp.215-223.
Chang, E.H., Gonda, M.A., Ellis, R.W., Scolnick, E.M. and Lowy, D.R. 1982. Human genome contains four genes homologous to transforming genes of Harvey and Kirsten murine sarcoma viruses. *Proceedings of the National Academy of Sciences of the United States of America.* **79**(16), pp.4848-4852.
Chang, J.C. 2016. Cancer stem cells: Role in tumor growth, recurrence, metastasis, and treatment resistance. *Medicine (Baltimore).* **95**(1 Suppl 1), pp.S20-25.
Chang, K., Srivastava, Y., Hu, C., Joyce, A., Yang, X., Zuo, Z., Havranek, J., Stormo, G.D. and Jauch, R. 2017. Quantitative profiling of selective Sox/POU pairing on hundreds of sequences in parallel by Coop-seq. *Nucleic Acids Research.* **45**(2), pp.832-845.
Chen, C., Krohn, J., Bhattacharya, S. and Davies, B. 2011. A Comparison of Exogenous Promoter Activity at the ROSA26 Locus Using a PhiC31 Integrase Mediated Cassette Exchange Approach in Mouse ES Cells. *PLoS ONE.* **6**(8), pe23376.
Chen, C. and Shen, M.M. 2004. Two modes by which Lefty proteins inhibit nodal signaling. *Curr Biol.* **14**(7), pp.618-624.
Chen, Y., Cimino, P.J., Luo, J., Dahiya, S. and Gutmann, D.H. 2016. ABCG1 maintains high-grade glioma survival in vitro and in vivo. *Oncotarget.* **7**(17), pp.23416-23424.
Chen, Y., McGowan, L., Cimino, P.J., Dahiya, S., Leonard, J.R., Lee, D. and Gutmann, D.H. 2015. Mouse Low-Grade Gliomas Contain Cancer Stem Cells with Unique Molecular and Functional Properties. *Cell Reports.* **10**(11), pp.1899-1912.
Chiba, T., Kita, K., Zheng, Y., Yokosuka, O., Saisho, H., Iwama, A., Nakauchi, H. and Taniguchi, H. 2006. Side population purified from hepatocellular carcinoma cells harbors cancer stem cell–like properties. *Hepatology.* **44**(1), pp.240-251.

Choi, Y., Yi, E., Lee, J., Yoo, K., Sung, K. and Koo, H. 2016. High-Dose Chemotherapy and Autologous Stem Cell Transplantation in Children with High-Risk or Recurrent Bone and Soft Tissue Sarcomas. *Journal of Korean Medical Science.* **31**(7), pp.1055-1062.
Chu, P., Clanton, D.J., Snipas, T.S., Lee, J., Mitchell, E., Nguyen, M., Hare, E. and Peach, R.J. 2009. Characterization of a subpopulation of colon cancer cells with stem cell-like properties. *International Journal of Cancer.* **124**(6), pp.1312-1321.
Chu, W.C., Reznikov, B., Lee, E.Y., Grant, R.M., Cheng, F.W. and Babyn, P. 2008. Primitive neuroectodermal tumour (PNET) of the kidney: a rare renal tumour in adolescents with seemingly characteristic radiological features. *Pediatr Radiol.* **38**(10), pp.1089-1094.
Chung, L., Tang, S., Wu, Y., Sun, G., Liu, H. and Sun, K. 2015. Galectin-3 augments tumor initiating property and tumorigenicity of lung cancer through interaction with β-catenin. *Oncotarget.* **6**(7), pp.4936-4952.
Cicalese, A., Bonizzi, G., Pasi, C.E., Faretta, M., Ronzoni, S., Giulini, B., Brisken, C., Minucci, S., Di Fiore, P. and Pelicci, P. 2009. The Tumor Suppressor p53 Regulates Polarity of Self-Renewing Divisions in Mammary Stem Cells. *Cell.* **138**(6), pp.1083-1095.
Cironi, L., Riggi, N., Provero, P., Wolf, N., Suvà, M., Suvà, D., Kindler, V. and Stamenkovic, I. 2008. IGF1 is a common target gene of Ewing's sarcoma fusion proteins in mesenchymal progenitor cells. *PloS one.* **3**(7), pe2634.
Civin, C.I., Almeida-Porada, G., Lee, M.J., Olweus, J., Terstappen, L.W. and Zanjani, E.D. 1996. Sustained, retransplantable, multilineage engraftment of highly purified adult human bone marrow stem cells in vivo. *Blood.* **88**(11), pp.4102-4109.
Clarke, M.F., Dick, J.E., Dirks, P.B., Eaves, C.J., Jamieson, C.H.M., Jones, D.L., Visvader, J., Weissman, I.L. and Wahl, G.M. 2006. Cancer Stem Cells—Perspectives on Current Status and Future Directions: AACR Workshop on Cancer Stem Cells. *Cancer Research.* **66**(19), pp.9339-9344.
Cleaver, A.L., Beesley, A.H., Firth, M.J., Sturges, N.C., O'Leary, R.A., Hunger, S.P., Baker, D.L. and Kees, U.R. 2010. Gene-based outcome prediction in multiple cohorts of pediatric T-cell acute lymphoblastic leukemia: a Children's Oncology Group study. *Molecular cancer.* **9**(1), p105.
Collins, A.T., Berry, P.A., Hyde, C., Stower, M.J. and Maitland, N.J. 2005. Prospective Identification of Tumorigenic Prostate Cancer Stem Cells. *Cancer Research.* **65**(23), pp.10946-10951.
Collura, A., Marisa, L., Trojan, D., Buhard, O., Lagrange, A., Saget, A., Bombled, M., Méchighel, P., Ayadi, M., Muleris, M., de Reynies, A., Svrcek, M., Fléjou, J., Florent, J., Mahuteau-Betzer, F., Faussat, A. and Duval, A. 2013. Extensive characterization of sphere models established from colorectal cancer cell lines. *Cellular and Molecular Life Sciences.* **70**(4), pp.729-742.
Colovic, R.B., Grubor, N.M., Micev, M.T., Matic, S.V., Atkinson, H. and Latincic, S.M. 2009. Perigastric extraskeletal Ewing's sarcoma: A case report. *World Journal of Gastroenterology : WJG.* **15**(2), pp.245-247.
Copeland, N.A., Sercombe, H.E., Ainscough, J.F.X. and Coverley, D. 2010. Ciz1 cooperates with cyclin-A-CDK2 to activate mammalian DNA replication in vitro. *Journal of Cell Science.* **123**(7), pp.1108-1115.

Copeland, N.A., Sercombe, H.E., Wilson, R.H.C. and Coverley, D. 2015. Cyclin-A–CDK2-mediated phosphorylation of CIZ1 blocks replisome formation and initiation of mammalian DNA replication. *Journal of Cell Science.* **128**(8), pp.1518-1527.
Cornaz-Buros, S., Riggi, N., DeVito, C., Sarre, A., Letovanec, I., Provero, P. and Stamenkovic, I. 2014. Targeting cancer stem-like cells as an approach to defeating cellular heterogeneity in Ewing sarcoma. *Cancer Res.* **74**(22), pp.6610-6622.
Costa, F.F., Seftor, E.A., Bischof, J.M., Kirschmann, D.A., Strizzi, L., Arndt, K., de Fatima Bonaldo, M., Soares, M.B. and Hendrix, M.J.C. 2009. Epigenetically reprogramming metastatic tumor cells with an embryonic microenvironment. *Epigenomics.* **1**(2), pp.387-398.
Costales, M.G., Haga, C.L., Velagapudi, S.P., Childs-Disney, J.L., Phinney, D.G. and Disney, M.D. 2017. Small Molecule Inhibition of microRNA-210 Reprograms an Oncogenic Hypoxic Circuit. *J Am Chem Soc.* **139**(9), pp.3446-3455.
Cotterill, S.J., Parker, L., Malcolm, A.J., Reid, M., More, L. and Craft, A.W. 2000. Incidence and survival for cancer in children and young adults in the North of England, 1968–1995: a report from the Northern Region Young Persons' Malignant Disease Registry. *British Journal of Cancer.* **83**(3), pp.397-403.
Coverley, D., Marr, J. and Ainscough, J. 2005. Ciz1 promotes mammalian DNA replication. *Journal of Cell Science.* **118**(1), pp.101-112.
Crouchet, E., Lefèvre, M., Verrier, E.R., Oudot, M.A., Baumert, T.F. and Schuster, C. 2016. Extracellular lipid-free apolipoprotein E inhibits HCV replication and induces ABCG1-dependent cholesterol efflux. *Gut.*
Cserepes, J., Szentpetery, Z., Seres, L., Ozvegy-Laczka, C., Langmann, T., Schmitz, G., Glavinas, H., Klein, I., Homolya, L., Varadi, A., Sarkadi, B. and Elkind, N.B. 2004. Functional expression and characterization of the human ABCG1 and ABCG4 proteins: indications for heterodimerization. *Biochem Biophys Res Commun.* **320**(3), pp.860-867.
Curry, E.L., Moad, M., Robson, C.N. and Heer, R. 2015. Using induced pluripotent stem cells as a tool for modelling carcinogenesis. *World Journal of Stem Cells.* **7**(2), pp.461-469.
D'Haeseleer, P. 2005. How does gene expression clustering work? *Nat Biotech.* **23**(12), pp.1499-1501.
Dahmcke, C.M., Buchmann-Moller, S., Jensen, N.A. and Mitchelmore, C. 2008. Altered splicing in exon 8 of the DNA replication factor CIZ1 affects subnuclear distribution and is associated with Alzheimer's disease. *Mol Cell Neurosci.* **38**(4), pp.589-594.
Dauphinot, L., De Oliveira, C., Melot, T., Sevenet, N., Thomas, V., Weissman, B.E. and Delattre, O. 2001. Analysis of the expression of cell cycle regulators in Ewing cell lines: EWS-FLI-1 modulates p57^ K^ I^ P^ 2 and c-Myc expression. *Oncogene.* **20**(25), pp.3258-3265.
De Vito, C., Riggi, N., Cornaz, S., Suvà, M., Baumer, K., Provero, P. and Stamenkovic, I. 2012. A TARBP2-Dependent miRNA Expression Profile Underlies Cancer Stem Cell Properties and Provides Candidate Therapeutic Reagents in Ewing Sarcoma. *Cancer Cell.* **21**(6), pp.807-821.
Dean, M. 2009. ABC Transporters, Drug Resistance, and Cancer Stem Cells. *Journal of Mammary Gland Biology and Neoplasia.* **14**(1), pp.3-9.

Delattre, O., Zucman, J., Plougastel, B., Desmaze, C., Melot, T., Peter, M., Kovar, H., Joubert, I., de Jong, P., Rouleau, G., Aurias, A. and Thomas, G. 1992. Gene fusion with an ETS DNA-binding domain caused by chromosome translocation in human tumours. *Nature.* **359**(6391), pp.162-165.

den Hollander, P. and Kumar, R. 2006. Dynein Light Chain 1 Contributes to Cell Cycle Progression by Increasing Cyclin-Dependent Kinase 2 Activity in Estrogen-Stimulated Cells. *Cancer Research.* **66**(11), pp.5941-5949.

den Hollander, P., Rayala, S.K., Coverley, D. and Kumar, R. 2006. Ciz1, a Novel DNA-binding coactivator of the estrogen receptor alpha, confers hypersensitivity to estrogen action. *Cancer Res.* **66**(22), pp.11021-11029.

Deng, X., Qiu, R., Wu, Y., Li, Z., Xie, P., Zhang, J., Zhou, J., Zeng, L., Tang, J., Maharjan, A. and Deng, J. 2014. Overexpression of miR-122 promotes the hepatic differentiation and maturation of mouse ESCs through a miR-122/FoxA1/HNF4a-positive feedback loop. *Liver International.* **34**(2), pp.281-295.

Denoyelle, C., Lambert, B., Meryet-Figuière, M., Vigneron, N., Brotin, E., Lecerf, C., Abeilard, E., Giffard, F., Louis, M.H., Gauduchon, P., Juin, P. and Poulain, L. 2014. miR-491-5p-induced apoptosis in ovarian carcinoma depends on the direct inhibition of both BCL-X(L) and EGFR leading to BIM activation. *Cell Death & Disease.* **5**(10), pe1445.

Di Cristofano, A., De Acetis, M., Koff, A., Cordon-Cardo, C. and P Pandolfi, P. 2001. Pten and p27KIP1 cooperate in prostate cancer tumor suppression in the mouse. *Nat Genet.* **27**(2), pp.222-224.

Dick, J.E. 2008. Stem cell concepts renew cancer research. *Blood.* **112**(13), pp.4793-4807.

Diehn, M., Cho, R.W., Lobo, N.A., Kalisky, T., Dorie, M., Kulp, A.N., Qian, D., Lam, J.S., Ailles, L.E., Wong, M., Joshua, B., Kaplan, M.J., Wapnir, I., Dirbas, F., Somlo, G., Garberoglio, C., Paz, B., Shen, J., Lau, S.K., Quake, S.R., Brown, J.M., Weissman, I.L. and Clarke, M.F. 2009. Association of Reactive Oxygen Species Levels and Radioresistance in Cancer Stem Cells. *Nature.* **458**(7239), pp.780-783.

Doedens, A.L., Phan, A.T., Stradner, M.H., Fujimoto, J.K., Nguyen, J.V., Yang, E., Johnson, R.S. and Goldrath, A.W. 2013. Hypoxia-inducible factors enhance the effector responses of CD8(+) T cells to persistent antigen. *Nature immunology.* **14**(11), pp.1173-1182.

Donnem, T., Fenton, C.G., Lonvik, K., Berg, T., Eklo, K., Andersen, S., Stenvold, H., Al-Shibli, K., Al-Saad, S., Bremnes, R.M. and Busund, L. 2012. MicroRNA Signatures in Tumor Tissue Related to Angiogenesis in Non-Small Cell Lung Cancer. *PLoS ONE.* **7**(1), pe29671.

Dontu, G., Abdallah, W.M., Foley, J.M., Jackson, K.W., Clarke, M.F., Kawamura, M.J. and Wicha, M.S. 2003. In vitro propagation and transcriptional profiling of human mammary stem/progenitor cells. *Genes & Development.* **17**(10), pp.1253-1270.

Dubash, T.D., Hoffmann, C.M., Oppel, F., Giessler, K.M., Weber, S., Dieter, S.M., Hüllein, J., Zenz, T., Herbst, F., Scholl, C., Weichert, W., Werft, W., Benner, A., Schmidt, M., Schneider, M., Glimm, H. and Ball, C.R. 2016. Phenotypic differentiation does not affect tumorigenicity of primary human colon cancer initiating cells. *Cancer Letters.* **371**(2), pp.326-333.

Duchman, R., Gao, Y. and Miller, J. 2015. Prognostic factors for survival in patients with Ewing's sarcoma using the surveillance, epidemiology, and end results (SEER) program database. *Cancer Epidemiology.* **39**(2), pp.189-195.
Engel, T., Bode, G., Lueken, A., Knop, M., Kannenberg, F., Nofer, J.R., Assmann, G. and Seedorf, U. 2006. Expression and functional characterization of ABCG1 splice variant ABCG1(666). *FEBS Lett.* **580**(18), pp.4551-4559.
Enrique, D.A. and William, L.G. 2000. Molecular Biology of the Ewing's Sarcoma/Primitive Neuroectodermal Tumor Family. *Journal of Clinical Oncology.* **18**(1), pp.204-204.
Eramo, A., Lotti, F., Sette, G., Pilozzi, E., Biffoni, M., Di Virgilio, A., Conticello, C., Ruco, L., Peschle, C. and De Maria, R. 2007. Identification and expansion of the tumorigenic lung cancer stem cell population. *Cell Death Differ.* **15**(3), pp.504-514.
Erho, N., Crisan, A., Vergara, A., Mitra, A.P., Ghadessi, M., Buerki, C., Bergstralh, E.J., Kollmeyer, T., Fink, S., Haddad, Z., Zimmermann, B., Sierocinski, T., Ballman, K.V., Triche, T.J., Black, P.C., Karnes, R.J., Klee, G., Davicioni, E. and Jenkins, R.B. 2013. Discovery and Validation of a Prostate Cancer Genomic Classifier that Predicts Early Metastasis Following Radical Prostatectomy. *PLoS ONE.* **8**(6), pe66855.
Esteller, M. 2000. Epigenetic lesions causing genetic lesions in human cancer. *European Journal of Cancer.* **36**(18), pp.2294-2300.
Evans, G.A. 1990. Molecular cloning: A laboratory manual. Second edition. Volumes 1, 2, and 3. Current protocols in molecular biology. Volumes 1 and 2. *Cell.* **61**(1), pp.17-18.
Evola, F.R., Costarella, L., Pavone, V., Caff, G., Cannavo, L., Sessa, A., Avondo, S. and Sessa, G. 2017. Biomarkers of Osteosarcoma, Chondrosarcoma, and Ewing Sarcoma. *Front Pharmacol.* **8**, p150.
Ewing, J. 1921. Diffuse endothelioma of bone. *Proc N Y Pathol Soc.* **21**, pp.17-24.
Fang, D., Nguyen, T.K., Leishear, K., Finko, R., Kulp, A.N., Hotz, S., Van Belle, P.A., Xu, X.T., Elder, D.E. and Herlyn, M. 2005. A Tumorigenic Subpopulation with Stem Cell Properties in Melanomas. *Cancer Research.* **65**(20), pp.9328-9337.
Fasanaro, P., D'Alessandra, Y., Di Stefano, V., Melchionna, R., Romani, S., Pompilio, G., Capogrossi, M.C. and Martelli, F. 2008. MicroRNA-210 modulates endothelial cell response to hypoxia and inhibits the receptor tyrosine kinase ligand Ephrin-A3. *J Biol Chem.* **283**(23), pp.15878-15883.
Feng, M., Li, Z., Aau, M., Wong, C., Yang, X. and Yu, Q. 2011. Myc/miR-378/TOB2/cyclin D1 functional module regulates oncogenic transformation. *Oncogene.* **30**(19), p2242.
Fenger, J.M., Roberts, R.D., Iwenofu, O.H., Bear, M.D., Zhang, X., Couto, J.I., Modiano, J.F., Kisseberth, W.C. and London, C.A. 2016. MiR-9 is overexpressed in spontaneous canine osteosarcoma and promotes a metastatic phenotype including invasion and migration in osteoblasts and osteosarcoma cell lines. *BMC Cancer.* **16**, p784.
Fennema, E., Rivron, N., Rouwkema, J., van Blitterswijk, C. and de Boer, J. 2013. Spheroid culture as a tool for creating 3D complex tissues. *Trends in Biotechnology.* **31**(2), pp.108-115.
Ferrari, S., del Prever, A.B., Palmerini, E., Staals, E., Berta, M., Balladelli, A., Picci, P., Fagioli, F., Bacci, G. and Vanel, D. 2009. Response to high-

dose ifosfamide in patients with advanced/recurrent Ewing sarcoma. *Pediatric Blood & Cancer.* **52**(5), pp.581-584.
Fillmore, C.M. and Kuperwasser, C. 2008. Human breast cancer cell lines contain stem-like cells that self-renew, give rise to phenotypically diverse progeny and survive chemotherapy. *Breast Cancer Research.* **10**(2), pR25.
Finlay, D.K., Rosenzweig, E., Sinclair, L.V., Feijoo-Carnero, C., Hukelmann, J.L., Rolf, J., Panteleyev, A.A., Okkenhaug, K. and Cantrell, D.A. 2012. PDK1 regulation of mTOR and hypoxia-inducible factor 1 integrate metabolism and migration of CD8(+) T cells. *The Journal of Experimental Medicine.* **209**(13), pp.2441-2453.
Fleige, S., Walf, V., Huch, S., Prgomet, C., Sehm, J. and Pfaffl, M.W. 2006. Comparison of relative mRNA quantification models and the impact of RNA integrity in quantitative real-time RT-PCR. *Biotechnol Lett.* **28**(19), pp.1601-1613.
Fonseca, N.A., He, Y., Greger, L., Brazma, A. and Zhang, Z. 2017. Comprehensive genome and transcriptome analysis reveals genetic basis for gene fusions in cancer. *bioRxiv.*
Foster, K.W., Liu, Z., Nail, C.D., Li, X., Fitzgerald, T.J., Bailey, S.K., Frost, A.R., Louro, I.D., Townes, T.M., Paterson, A.J., Kudlow, J.E., Lobo-Ruppert, S.M. and Ruppert, J.M. 2005. Induction of KLF4 in basal keratinocytes blocks the proliferation-differentiation switch and initiates squamous epithelial dysplasia. *Oncogene.* **24**(9), pp.1491-1500.
Fox, E., Patel, S., Wathen, J.K., Schuetze, S., Chawla, S., Harmon, D., Reinke, D., Chugh, R., Benjamin, R.S. and Helman, L.J. 2012. Phase II Study of Sequential Gemcitabine Followed by Docetaxel for Recurrent Ewing Sarcoma, Osteosarcoma, or Unresectable or Locally Recurrent Chondrosarcoma: Results of Sarcoma Alliance for Research Through Collaboration Study 003. *The Oncologist.* **17**(3), pp.321-321.
Francis, M., Dennis, N., Charman, J., Lawrence, G. and Grimer, R. 2013. Bone and Soft Tissue Sarcomas: Changes to Pathology Codes in the 4th Edition of the World Health Organisation Classification of Bone and Soft Tissue Sarcomas *NCIN.* pp.2-17.
Friedman, R.C., Farh, K.K., Burge, C.B. and Bartel, D.P. 2009. Most mammalian mRNAs are conserved targets of microRNAs. *Genome research.* **19**(1), pp.92-105.
Friedrich, J., Seidel, C., Ebner, R. and Kunz-Schughart, L.A. 2009. Spheroid-based drug screen: considerations and practical approach. *Nat. Protocols.* **4**(3), pp.309-324.
Friend, S.H., Horowitz, J.M., Gerber, M.R., Wang, X.F., Bogenmann, E., Li, F.P. and Weinberg, R.A. 1987. Deletions of a DNA sequence in retinoblastomas and mesenchymal tumors: organization of the sequence and its encoded protein. *Proceedings of the National Academy of Sciences.* **84**(24), pp.9059-9063.
Fuchs, B., Valenzuela, R.G., Petersen, I.A., Arndt, C.A. and Sim, F.H. 2003. Ewing's sarcoma and the development of secondary malignancies. *Clinical orthopaedics and related research.* **415**, pp.82-89.
Fujii, H., Honoki, K., Tsujiuchi, T., Kido1, A., Yoshitani, K. and Takakura, Y. 2009. Sphere-forming stem-like cell populations with drug resistance in human sarcoma cell lines. *International Journal of Oncology.*

Fukuma, M., Okita, H., Hata, J. and Umezawa, A. 2003. Upregulation of Id2, an oncogenic helix-loop-helix protein, is mediated by the chimeric EWS/ets protein in Ewing sarcoma. *Oncogene.* **22**(1), pp.1-9.
Funes, J.M., Quintero, M., Henderson, S., Martinez, D., Qureshi, U., Westwood, C., Clements, M.O., Bourboulia, D., Pedley, R.B., Moncada, S. and Boshoff, C. 2007. Transformation of human mesenchymal stem cells increases their dependency on oxidative phosphorylation for energy production. *Proceedings of the National Academy of Sciences.* **104**(15), pp.6223-6228.
Garcia-Aragoncillo, E., Carrillo, J., Lalli, E., Agra, N., Gomez-Lopez, G., Pestana, A. and Alonso, J. 2008. DAX1, a direct target of EWS/FLI1 oncoprotein, is a principal regulator of cell-cycle progression in Ewing's tumor cells. *Oncogene.* **27**(46), pp.6034-6043.
Garofalo, M. and Croce, C.M. 2015. Role of microRNAs in maintaining cancer stem cells. *Advanced drug delivery reviews.* **81**, pp.53-61.
Garvalov, B.K. and Acker, T. 2011. Cancer stem cells: a new framework for the design of tumor therapies. *Journal of Molecular Medicine.* **89**(2), pp.95-107.
Gaspar, N., Hawkins, D.S., Dirksen, U., Lewis, I.J., Ferrari, S., Le Deley, M., Kovar, H., Grimer, R., Whelan, J., Claude, L., Delattre, O., Paulussen, M., Picci, P., Sundby Hall, K., van den Berg, H., Ladenstein, R., Michon, J., Hjorth, L., Judson, I., Luksch, R., Bernstein, M.L., Marec-Bérard, P., Brennan, B., Craft, A.W., Womer, R.B., Juergens, H. and Oberlin, O. 2015. Ewing Sarcoma: Current Management and Future Approaches Through Collaboration. *Journal of Clinical Oncology.* **33**(27), pp.3036-3046.
Gelissen, I.C., Cartland, S., Brown, A.J., Sandoval, C., Kim, M., Dinnes, D.L., Lee, Y., Hsieh, V., Gaus, K., Kritharides, L. and Jessup, W. 2010. Expression and stability of two isoforms of ABCG1 in human vascular cells. *Atherosclerosis.* **208**(1), pp.75-82.
Gelissen, I.C., Harris, M., Rye, K.A., Quinn, C., Brown, A.J., Kockx, M., Cartland, S., Packianathan, M., Kritharides, L. and Jessup, W. 2006. ABCA1 and ABCG1 synergize to mediate cholesterol export to apoA-I. *Arterioscler Thromb Vasc Biol.* **26**(3), pp.534-540.
Ghosh, G., Subramanian, I.V., Adhikari, N., Zhang, X., Joshi, H.P., Basi, D., Chandrashekhar, Y.S., Hall, J.L., Roy, S., Zeng, Y. and Ramakrishnan, S. 2010. Hypoxia-induced microRNA-424 expression in human endothelial cells regulates HIF-α isoforms and promotes angiogenesis. *The Journal of Clinical Investigation.* **120**(11), pp.4141-4154.
Ghosh, S., Joshi, M.B., Ivanov, D., Feder-Mengus, C., Spagnoli, G.C., Martin, I., Erne, P. and Resink, T.J. 2007. Use of multicellular tumor spheroids to dissect endothelial cell–tumor cell interactions: A role for T-cadherin in tumor angiogenesis. *FEBS Letters.* **581**(23), pp.4523-4528.
Goda, N., Ryan, H.E., Khadivi, B., McNulty, W., Rickert, R.C. and Johnson, R.S. 2003. Hypoxia-Inducible Factor 1 Is Essential for Cell Cycle Arrest during Hypoxia. *Molecular and Cellular Biology.* **23**(1), pp.359-369.
Goldsby, R., Burke, C., Nagarajan, R., Zhou, T., Chen, Z., Marina, N., Friedman, D., Neglia, J., Chuba, P. and Bhatia, S. 2008. Second solid malignancies among children, adolescents, and young adults diagnosed with malignant bone tumors after 1976. *Cancer.* **113**(9), pp.2597-2604.

Golebiewska, A., Brons, N.H.C., Bjerkvig, R. and Niclou, S.P. 2011. Critical Appraisal of the Side Population Assay in Stem Cell and Cancer Stem Cell Research. *Cell Stem Cell.* **8**(2), pp.136-147.
Gordan, J.D., Bertovrt, J.A., Hu, C., Diehl, J.A. and Simon, M.C. 2007. HIF-2α promotes hypoxic cell proliferation by enhancing c-Myc transcriptional activity. *Cancer cell.* **11**(4), pp.335-347.
Gordan, J.D., Lal, P., Dondeti, V.R., Letrero, R., Parekh, K.N., Oquendo, C.E., Greenberg, R.A., Flaherty, K.T., Rathmell, W.K., Keith, B., Simon, M.C. and Nathanson, K.L. 2008. HIF-α effects on c-Myc distinguish two subtypes of sporadic VHL-deficient clear cell renal carcinoma. *Cancer cell.* **14**(6), pp.435-446.
Gottfried, E., Kunz-Schughart, L.A., Andreesen, R. and Kreutz, M. 2006. Brave Little World: Spheroids as an in vitro Model to Study Tumor-Immune-Cell Interactions. *Cell Cycle.* **5**(7), pp.691-695.
Graf, T. 2011. Historical origins of transdifferentiation and reprogramming. *Cell Stem Cell.* **9**(6), pp.504-516.
Greaves, E.A., Copeland, N.A., Coverley, D. and Ainscough, J.F. 2012. Cancer associated variant expression and interaction of CIZ1 with cyclin A1 in differentiating male germ cells. *J. Cell Sci.*, pp.1-24.
Greer Card, D.A., Hebbar, P.B., Li, L., Trotter, K.W., Komatsu, Y., Mishina, Y. and Archer, T.K. 2008. Oct4/Sox2-Regulated miR-302 Targets Cyclin D1 in Human Embryonic Stem Cells. *Molecular and Cellular Biology.* **28**(20), pp.6426-6438.
Greijer, A.E. and van der Wall, E. 2004. The role of hypoxia inducible factor 1 (HIF-1) in hypoxia induced apoptosis. *Journal of Clinical Pathology.* **57**(10), p1009.
Grier, H.E. 1997. The ewing family of tumors: Ewing's Sarcoma and Primitive Neuroectodermal Tumors. *Pediatric Clinics of North America.* **44**(4), pp.991-1004.
Grimes, D., Kelly, C., Bloch, K. and Partridge, M. 2014. A method for estimating the oxygen consumption rate in multicellular tumour spheroids. *Journal of the Royal Society Interface.* **11**(92), p20131124.
Groebe, K. and Mueller-Klieser, W. 1996. On the relation between size of necrosis and diameter of tumor spheroids. *International Journal of Radiation Oncology*Biology*Physics.* **34**(2), pp.395-401.
Grosso, S., Doyen, J., Parks, S.K., Bertero, T., Paye, A., Cardinaud, B., Gounon, P., Lacas-Gervais, S., Noël, A., Pouysségur, J., Barbry, P., Mazure, N.M. and Mari, B. 2013. MiR-210 promotes a hypoxic phenotype and increases radioresistance in human lung cancer cell lines. *Cell Death & Disease.* **4**(3), pe544.
Gurdon, J.B. 1962. DEVELOPMENTAL CAPACITY OF NUCLEI TAKEN FROM INTESTINAL EPITHELIUM CELLS OF FEEDING TADPOLES. *Journal of Embryology and Experimental Morphology.* **10**(4), pp.622-&.
Hahm, K., Cho, K., Lee, C., Im, Y., Chang, J., Choi, S., Sorensen, P.H., Thiele, C.J. and Kim, S. 1999. Repression of the gene encoding the TGF-β type II receptor is a major target of the EWS-FLI1 oncoprotein. *Nature genetics.* **23**(2), pp.222-227.
Hamburger, A. and Salmon, S.E. 1977. Primary Bioassay of Human Myeloma Stem Cells. *Journal of Clinical Investigation.* **60**(4), pp.846-854.

Hammer, S., To, K.K., Yoo, Y.G., Koshiji, M. and Huang, L.E. 2007. Hypoxic suppression of the cell cycle gene CDC25A in tumor cells. *Cell Cycle.* **6**(15), pp.1919-1926.
Han, H., Sun, D., Li, W., Shen, H., Zhu, Y., Li, C., Chen, Y., Lu, L., Li, W. and Zhang, J. 2013. A c-Myc-MicroRNA functional feedback loop affects hepatocarcinogenesis. *Hepatology.* **57**(6), pp.2378-2389.
Hanahan, D. and Coussens, L.M. 2012. Accessories to the Crime: Functions of Cells Recruited to the Tumor Microenvironment. *Cancer Cell.* **21**(3), pp.309-322.
Hanahan, D. and Weinberg, R.A. 2000. The Hallmarks of Cancer. *Cell.* **100**(1), pp.57-70.
Hanahan, D. and Weinberg, R.A. 2011. Hallmarks of Cancer: The Next Generation. *Cell.* **144**(5), pp.646-674.
Haraguchi, N., Utsunomiya, T., Inoue, H., Tanaka, F., Mimori, K., Barnard, G.F. and Mori, M. 2006. Characterization of a Side Population of Cancer Cells from Human Gastrointestinal System. *STEM CELLS.* **24**(3), pp.506-513.
Hashimoto, N., Tsunedomi, R., Yoshimura, K., Watanabe, Y., Hazama, S. and Oka, M. 2014. Cancer stem-like sphere cells induced from de-differentiated hepatocellular carcinoma-derived cell lines possess the resistance to anti-cancer drugs. *BMC Cancer.* **14**, p722.
Hatfield, S.D., Shcherbata, H.R., Fischer, K.A., Nakahara, K., Carthew, R.W. and Ruohola-Baker, H. 2005. Stem cell division is regulated by the microRNA pathway. *Nature.* **435**(7044), pp.974-978.
Hattinger, C.M., Pötschger, U., Tarkkanen, M., Squire, J., Zielenska, M., Kiuru-Kuhlefelt, S., Kager, L., Thorner, P., Knuutila, S., Niggli, F.K., Ambros, P.F., Gadner, H. and Betts, D.R. 2002. Prognostic impact of chromosomal aberrations in Ewing tumours. *British Journal of Cancer.* **86**(11), pp.1763-1769.
He, L., Thomson, J.M., Hemann, M.T., Hernando-Monge, E., Mu, D., Goodson, S., Powers, S., Cordon-Cardo, C., Lowe, S.W. and Hannon, G.J. 2005. A microRNA polycistron as a potential human oncogene. *nature.* **435**(7043), p828.
Hegyi, Z. and Homolya, L. 2016. Functional Cooperativity between ABCG4 and ABCG1 Isoforms. *PLoS ONE.* **11**(5), pe0156516.
Hentschke, M., Kurth, I., Borgmeyer, U. and Hubner, C.A. 2006. Germ cell nuclear factor is a repressor of CRIPTO-1 and CRIPTO-3. *J Biol Chem.* **281**(44), pp.33497-33504.
Hermann, P.C., Huber, S.L., Herrler, T., Aicher, A., Ellwart, J.W., Guba, M., Bruns, C.J. and Heeschen, C. 2007. Distinct Populations of Cancer Stem Cells Determine Tumor Growth and Metastatic Activity in Human Pancreatic Cancer. *Cell Stem Cell.* **1**(3), pp.313-323.
Hermeking, H. 2012. MicroRNAs in the p53 network: micromanagement of tumour suppression. *Nature Reviews Cancer.* **12**(9), p613.
Herrero-Martin, D., Osuna, D., Ordonez, J., Sevillano, V., Martins, A., Mackintosh, C., Campos, M., Madoz-Gurpide, J., Otero-Motta, A. and Caballero, G. 2009. Stable interference of EWS–FLI1 in an Ewing sarcoma cell line impairs IGF-1/IGF-1R signalling and reveals TOPK as a new target. *British journal of cancer.* **101**(1), pp.80-90.
Higgins, G., Roper, K.M., Watson, I.J., Blackhall, F.H., Rom, W.N., Pass, H.I., Ainscough, J.F.X. and Coverley, D. 2012. Variant Ciz1 is a circulating

biomarker for early-stage lung cancer. *Proceedings of the National Academy of Sciences of the United States of America.* **109**(45), pp.E3128-E3135.
Hirschhaeuser, F., Menne, H., Dittfeld, C., West, J., Mueller-Klieser, W. and Kunz-Schughart, L.A. 2010. Multicellular tumor spheroids: An underestimated tool is catching up again. *Journal of Biotechnology.* **148**(1), pp.3-15.
Hirschmann-Jax, C., Foster, A.E., Wulf, G.G., Nuchtern, J.G., Jax, T.W., Gobel, U., Goodell, M.A. and Brenner, M.K. 2004. A distinct “side population” of cells with high drug efflux capacity in human tumor cells. *Proceedings of the National Academy of Sciences of the United States of America.* **101**(39), pp.14228-14233.
Ho, M.M., Ng, A.V., Lam, S. and Hung, J.Y. 2007. Side Population in Human Lung Cancer Cell Lines and Tumors Is Enriched with Stem-like Cancer Cells. *Cancer Research.* **67**(10), pp.4827-4833.
Hogan, C.J., Shpall, E.J. and Keller, G. 2002. Differential long-term and multilineage engraftment potential from subfractions of human CD34+ cord blood cells transplanted into NOD/SCID mice. *Proceedings of the National Academy of Sciences.* **99**(1), pp.413-418.
Hu, S., Huang, M., Li, Z., Jia, F., Ghosh, Z., Lijkwan, M.A., Fasanaro, P., Sun, N., Wang, X., Martelli, F., Robbins, R.C. and Wu, J.C. 2010. MicroRNA-210 as a Novel Therapy for Treatment of Ischemic Heart Disease. *Circulation.* **122**(11 Suppl), pp.S124-S131.
Hua, Z., Lv, Q., Ye, W., Wong, C.A., Cai, G., Gu, D., Ji, Y., Zhao, C., Wang, J., Yang, B.B. and Zhang, Y. 2006. MiRNA-Directed Regulation of VEGF and Other Angiogenic Factors under Hypoxia. *PLoS ONE.* **1**(1), pe116.
Huang, H., Illei, P.B., Zhao, Z., Mazumdar, M., Huvos, A.G., Healey, J.H., Wexler, L.H., Gorlick, R., Meyers, P. and Ladanyi, M. 2005. Ewing sarcomas with p53 mutation or p16/p14ARF homozygous deletion: a highly lethal subset associated with poor chemoresponse. *Journal of Clinical Oncology.* **23**(3), pp.548-558.
Huang, S., Chiang, J., Jan, H., Chou, S., Chen, T. and Chen, T. 2011. Intra-abdomen Ewing's sarcoma. *ANZ Journal of Surgery.* **81**(5), pp.377-378.
Huang, X., Ding, L., Bennewith, K., Tong, R., Ang, K.K., Story, M., Le, Q.-T. and Giaccia, A.J. 2009. Hypoxia inducible mir-210 regulates normoxic gene expression involved in tumor initiation. *Molecular cell.* **35**(6), pp.856-867.
Huang, X., Ding, L., Bennewith, K.L., Tong, R.T., Welford, S.M., Ang, K.K., Story, M., Le, Q.T. and Giaccia, A.J. 2009. Hypoxia-inducible mir-210 regulates normoxic gene expression involved in tumor initiation. *Mol Cell.* **35**(6), pp.856-867.
Huang, X. and Zuo, J. 2014. Emerging roles of miR-210 and other non-coding RNAs in the hypoxic response. *Acta Biochimica et Biophysica Sinica.* **46**(3), pp.220-232.
Huertas-Martínez, J., Court, F., Rello-Varona, S., Herrero-Martín, D., Almacellas-Rabaiget, O., Sáinz-Jaspeado, M., Garcia-Monclús, S., Lagares-Tena, L., Buj, R., Hontecillas-Prieto, L., Sastre, A., Azorin, D., Sanjuan, X., López-Alemany, R., Moran, S., Roma, J., Gallego, S., Mora, J., García del Muro, X., Giangrande, P.H., Peinado, M.A., Alonso, J., E., d.A., Monk, D., Esteller, M. and Tirado, O.M. 2017. DNA methylation profiling identifies PTRF/Cavin-1 as a novel tumor suppressor in Ewing sarcoma when co-expressed with caveolin-1. *Cancer Letters.* **386**(Supplement C), pp.196-207.

Hunold, A., Weddeling, N., Paulussen, M., Ranft, A., Liebscher, C. and Jürgens, H. 2006. Topotecan and cyclophosphamide in patients with refractory or relapsed Ewing tumors. *Pediatric Blood & Cancer.* **47**(6), pp.795-800.
Ikonen, E. 2008. Cellular cholesterol trafficking and compartmentalization. *Nat Rev Mol Cell Biol.* **9**(2), pp.125-138.
Imai, Y., Kimura, T., Murakami, A., Yajima, N., Sakamaki, K. and Yonehara, S. 1999. TheCED-4-homologous protein FLASH is involved in Fas-mediated activation of caspase-8 during apoptosis. *Nature.* **400**(6739), pp.89-89.
Inch, W.R., McCredie, J.A. and Sutherland, R.M. 1970. Growth of nodular carcinomas in rodents compared with multi-cell spheroids in tissue culture. *Growth, Development and Aging.* **34**(3), pp.271-282.
Jackstadt, R. and Hermeking, H. 2015. MicroRNAs as regulators and mediators of c-MYC function. *Biochimica et Biophysica Acta (BBA)-Gene Regulatory Mechanisms.* **1849**(5), pp.544-553.
Jacques, C., Calleja, L., Baud'huin, M., Quillard, T., Heymann, D., Lamoureux, F. and Ory, B. 2016. miRNA-193a-5p repression of p73 controls Cisplatin chemoresistance in primary bone tumors. *Oncotarget.* **7**(34), pp.54503-54514.
Jaksch, M., Múnera, J., Bajpai, R., Terskikh, A. and Oshima, R.G. 2008. Cell cycle dependent variation of a CD133 epitope in human embryonic stem cell, colon cancer and melanoma cell lines. *Cancer research.* **68**(19), pp.7882-7886.
Jessup, W., Gelissen, I.C., Gaus, K. and Kritharides, L. 2006. Roles of ATP binding cassette transporters A1 and G1, scavenger receptor BI and membrane lipid domains in cholesterol export from macrophages. *Curr. Opin. Lipidol.* **17** pp.247-257.
Ji, J., Yamashita, T., Budhu, A., Forgues, M., Jia, H., Li, C., Deng, C., Wauthier, E., Reid, L.M., Ye, Q., Qin, L., Yang, W., Wang, H., Tang, Z., Croce, C.M. and Wang, X. 2009. Identification of microRNA-181 by genome-wide screening as a critical player in EpCAM-positive hepatic cancer stem cells. *Hepatology (Baltimore, Md.).* **50**(2), pp.472-480.
Jiang, X., Gwye, Y., Russell, D., Cao, C., Douglas, D., Hung, L., Kovar, H., Triche, T.J. and Lawlor, E.R. 2010. CD133 expression in chemo-resistant Ewing sarcoma cells. *BMC Cancer.* **10**, pp.116-116.
Judex, M., Neumann, E., Lechner, S., Dietmaier, W., Ballhorn, W., Grifka, J., Gay, S., Scholmerich, J., Kullmann, F. and Muller-Ladner, U. 2003. Laser-mediated microdissection facilitates analysis of area-specific gene expression in rheumatoid synovium. *Arthritis Rheum.* **48**(1), pp.97-102.
Kaidi, A., Williams, A.C. and Paraskeva, C. 2007. Interaction between [beta]-catenin and HIF-1 promotes cellular adaptation to hypoxia. *Nat Cell Biol.* **9**(2), pp.210-217.
Kaji, K., Norrby, K., Paca, A., Mileikovsky, M., Mohseni, P. and Woltjen, K. 2009. Virus-free induction of pluripotency and subsequent excision of reprogramming factors. *Nature.* **458**(7239), pp.771-U112.
Kanellopoulou, C., Muljo, S.A., Kung, A.L., Ganesan, S., Drapkin, R., Jenuwein, T., Livingston, D.M. and Rajewsky, K. 2005. Dicer-deficient mouse embryonic stem cells are defective in differentiation and centromeric silencing. *Genes & Development.* **19**(4), pp.489-501.
Kang, H., Chen, I., Wilson, C.S., Bedrick, E.J., Harvey, R.C., Atlas, S.R., Devidas, M., Mullighan, C.G., Wang, X. and Murphy, M. 2010. Gene

expression classifiers for relapse-free survival and minimal residual disease improve risk classification and outcome prediction in pediatric B-precursor acute lymphoblastic leukemia. *Blood.* **115**(7), pp.1394-1405.
Kawano, M., Tanaka, K., Itonaga, I., Iwasaki, T. and Tsumura, H. 2016. MicroRNA-301a promotes cell proliferation via PTEN targeting in Ewing's sarcoma cells. *Int J Oncol.* **48**(4), pp.1531-1540.
Kelly, J.J.P., Stechishin, O., Chojnacki, A., Lun, X., Sun, B., Senger, D.L., Forsyth, P., Auer, R.N., Dunn, J.F., Cairncross, J.G., Parney, I.F. and Weiss, S. 2009. Proliferation of Human Glioblastoma Stem Cells Occurs Independently of Exogenous Mitogens. *STEM CELLS.* **27**(8), pp.1722-1733.
Kelly, T.J., Souza, A.L., Clish, C.B. and Puigserver, P. 2011. A Hypoxia-Induced Positive Feedback Loop Promotes Hypoxia-Inducible Factor 1α Stability through miR-210 Suppression of Glycerol-3-Phosphate Dehydrogenase 1-Like. *Molecular and Cellular Biology.* **31**(13), pp.2696-2706.
Kennedy, M.A., Barrera, G.C., Nakamura, K., Baldán, Á., Tarr, P., Fishbein, M.C., Frank, J., Francone, O.L. and Edwards, P.A. 2005. ABCG1 has a critical role in mediating cholesterol efflux to HDL and preventing cellular lipid accumulation. *Cell Metabolism.* **1**(2), pp.121-131.
Kerr, I.D., Haider, A.J. and Gelissen, I.C. 2011. The ABCG family of membrane-associated transporters: you don't have to be big to be mighty. *British Journal of Pharmacology.* **164**(7), pp.1767-1779.
Kidd, S., Spaeth, E., Dembinski, J.L., Dietrich, M., Watson, K., Klopp, A., Battula, L., Weil, M., Andreeff, M. and Marini, F.C. 2009. Direct Evidence of Mesenchymal Stem Cell Tropism for Tumor and Wounding Microenvironments using In Vivo Bioluminescence Imaging. *Stem cells (Dayton, Ohio).* **27**(10), pp.2614-2623.
Kikuchi, R., Murakami, M., Sobue, S., Iwasaki, T., Hagiwara, K., Takagi, A., Kojima, T., Asano, H., Suzuki, M. and Banno, Y. 2007. Ewing's sarcoma fusion protein, EWS/Fli-1 and Fli-1 protein induce PLD2 but not PLD1 gene expression by binding to an ETS domain of 5′ promoter. *Oncogene.* **26**(12), pp.1802-1810.
Kilic, M., Kasperczyk, H., Fulda, S. and Debatin, K.M. 2007. Role of hypoxia inducible factor-1 alpha in modulation of apoptosis resistance. *Oncogene.* **26**(14), pp.2027-2038.
Kim, H.S., Kim, S., Min, Y.D., Kee, K.H. and Hong, R. 2012. Ewing's Sarcoma of the Stomach; Rare Case of Ewing's Sarcoma and Suggestion of New Treatment Strategy. *J Gastric Cancer.* **12**(4), pp.258-261.
Kim, H.W., Haider, H.K., Jiang, S. and Ashraf, M. 2009. Ischemic preconditioning augments survival of stem cells via miR-210 expression by targeting caspase-8-associated protein 2. *J Biol Chem.* **284**(48), pp.33161-33168.
Kim, Y., Kang, Y., Lee, N., Kim, K., Hwang, Y., Kim, H., Rhyu, I., Her, S., Jung, M., Kim, S., Lee, C., Ko, S., Kowall, N.W., Lee, S., Lee, J. and Ryu, H. 2015. Uvrag targeting by Mir125a and Mir351 modulates autophagy associated with Ewsr1 deficiency. *Autophagy.* **11**(5), pp.796-811.
Klein, W.M., Wu, B.P., Zhao, S., Wu, H., Klein-Szanto, A.J.P. and Tahan, S.R. 2006. Increased expression of stem cell markers in malignant melanoma. *Mod Pathol.* **20**(1), pp.102-107.
Kloosterman, W.P., Coebergh van den Braak, R.R.J., Pieterse, M., van Roosmalen, M.J., Sieuwerts, A.M., Stangl, C., Brunekreef, R., Lalmahomed,

Z.S., Ooft, S., van Galen, A., Smid, M., Lefebvre, A., Zwartkruis, F., Martens, J.W.M., Foekens, J.A., Biermann, K., Koudijs, M.J., Ijzermans, J.N.M. and Voest, E.E. 2017. A Systematic Analysis of Oncogenic Gene Fusions in Primary Colon Cancer. *Cancer Research.*

Klucken, J., Büchler, C., Orsó, E., Kaminski, W.E., Porsch-Özcürümez, M., Liebisch, G., Kapinsky, M., Diederich, W., Drobnik, W., Dean, M., Allikmets, R. and Schmitz, G. 2000. ABCG1 (ABC8), the human homolog of the Drosophila white gene, is a regulator of macrophage cholesterol and phospholipid transport. *Proceedings of the National Academy of Sciences of the United States of America.* **97**(2), pp.817-822.

Knight, S.W. and Bass, B.L. 2001. A Role for the RNase III Enzyme DCR-1 in RNA Interference and Germ Line Development in Caenorhabditis elegans. *Science (New York, N.Y.).* **293**(5538), pp.2269-2271.

Knudson, A.G. 1971. Mutation and Cancer: Statistical Study of Retinoblastoma. *Proceedings of the National Academy of Sciences of the United States of America.* **68**(4), pp.820-823.

Koh, M., Darnay, B.G. and Powis, G. 2008. Hypoxia-Associated Factor, a Novel E3-Ubiquitin Ligase, Binds and Ubiquitinates Hypoxia-Inducible Factor 1α, Leading to Its Oxygen-Independent Degradation. *Molecular and Cellular Biology.* **28**(23), pp.7081-7095.

Koh, M. and Powis, G. 2012. Passing the baton: The HIF switch. *Trends in biochemical sciences.* **37**(9), pp.364-372.

Kong, W., Yang, H., He, L., Zhao, J., Coppola, D., Dalton, W.S. and Cheng, J.Q. 2008. MicroRNA-155 Is Regulated by the Transforming Growth Factor β/Smad Pathway and Contributes to Epithelial Cell Plasticity by Targeting RhoA. *Molecular and Cellular Biology.* **28**(22), pp.6773-6784.

Koren, E. and Fuchs, Y. 2016. *The Bad Seed: Cancer Stem Cells in Tumor Development and Resistance.*

Koshiji, M., Kageyama, Y., Pete, E.A., Horikawa, I., Barrett, J.C. and Huang, L.E. 2004. HIF-1α induces cell cycle arrest by functionally counteracting Myc. *The EMBO Journal.* **23**(9), pp.1949-1956.

Kotch, L.E., Iyer, N.V., Laughner, E. and Semenza, G.L. 1999. Defective Vascularization of HIF-1α-Null Embryos Is Not Associated with VEGF Deficiency but with Mesenchymal Cell Death. *Developmental Biology.* **209**(2), pp.254-267.

Kreso, A. and Dick, J.E. 2014. Evolution of the Cancer Stem Cell Model. *Cell Stem Cell.* **14**(3), pp.275-291.

Kress, T.R., Cannell, I.G., Brenkman, A.B., Samans, B., Gaestel, M., Roepman, P., Burgering, B.M., Bushell, M., Rosenwald, A. and Eilers, M. 2011. The MK5/PRAK kinase and Myc form a negative feedback loop that is disrupted during colorectal tumorigenesis. *Molecular cell.* **41**(4), pp.445-457.

Kulshreshtha, R., Ferracin, M., Wojcik, S.E., Garzon, R., Alder, H., Agosto-Perez, F.J., Davuluri, R., Liu, C.G., Croce, C.M., Negrini, M., Calin, G.A. and Ivan, M. 2007. A microRNA signature of hypoxia. *Mol Cell Biol.* **27**(5), pp.1859-1867.

Kumar, P., Luo, Y., Tudela, C., Alexander, J.M. and Mendelson, C.R. 2013. The c-Myc-regulated microRNA-17~ 92 (miR-17~ 92) and miR-106a~ 363 clusters target hCYP19A1 and hGCM1 to inhibit human trophoblast differentiation. *Molecular and cellular biology.* **33**(9), pp.1782-1796.

LaBarbera, D.V., Reid, B.G. and Yoo, B. 2012. The multicellular tumor spheroid model for high-throughput cancer drug discovery. *Expert Opinion on Drug Discovery.* **7**(9), pp.819-830.
Lagos-Quintana, M., Rauhut, R., Lendeckel, W. and Tuschl, T. 2001. Identification of Novel Genes Coding for Small Expressed RNAs. *Science.* **294**(5543), pp.853-858.
Lal, A., Navarro, F., Maher, C.A., Maliszewski, L.E., Yan, N., O'Day, E., Chowdhury, D., Dykxhoorn, D.M., Tsai, P. and Hofmann, O. 2009. miR-24 Inhibits cell proliferation by targeting E2F2, MYC, and other cell-cycle genes via binding to "seedless" 3′ UTR microRNA recognition elements. *Molecular cell.* **35**(5), pp.610-625.
Lane, D.P. and Crawford, L.V. 1979. T antigen is bound to a host protein in sv40-transformed cells. *Nature.* **278**(5701), pp.261-263.
Lansdorp, P.M. 1993. In vitro properties of purified human stem cell candidates. *Journal of Hematotherapy.* **2**(3), pp.329-332.
Lapidot, T., Sirard, C., Vormoor, J., Murdoch, B., Hoang, T., Caceres-Cortes, J., Minden, M., Paterson, B., Caligiuri, M.A. and Dick, J.E. 1994. A cell initiating human acute myeloid leukaemia after transplantation into SCID mice. *Nature.* **367**(6464), pp.645-648.
Lawlor, E.R., Scheel, C., Irving, J. and Sorensen, P.H. 2002. Anchorage-independent multi-cellular spheroids as an in vitro model of growth signaling in ewing tumors. *Oncogene.* **21**(2), pp.307-318.
Lawrence, M.G., Margaryan, N.V., Loessner, D., Collins, A., Kerr, K.M., Turner, M., Seftor, E.A., Stephens, C.R., Lai, J., BioResource, A.P.C., Postovit, L., Clements, J.A. and Hendrix, M.J.C. 2011. Reactivation of Embryonic Nodal Signaling is Associated with Tumor Progression and Promotes the Growth of Prostate Cancer Cells. *The Prostate.* **71**(11), pp.1198-1209.
Lee, C., Feinbaum, R.L. and Ambros, V. 1993. The C. elegans heterochronic gene lin-4 encodes small RNAs with antisense complementarity to lin-14. *Cell.* **75**(5), pp.843-854.
Lee, J., Kotliarova, S., Kotliarov, Y., Li, A., Su, Q., Donin, N.M., Pastorino, S., Purow, B.W., Christopher, N., Zhang, W., Park, J.K. and Fine, H.A. 2006. Tumor stem cells derived from glioblastomas cultured in bFGF and EGF more closely mirror the phenotype and genotype of primary tumors than do serum-cultured cell lines. *Cancer Cell.* **9**(5), pp.391-403.
Lee, S., Hong, J., Park, H., Park, J., Kim, B., Lee, J., Jeong, J., Yoon, G., Inoue, M., Choi, G. and Lee, I. 2015. Colorectal cancer-derived tumor spheroids retain the characteristics of original tumors. *Cancer Letters.* **367**(1), pp.34-42.
Lee, Y., Ahn, C., Han, J., Choi, H., Kim, J., Yim, J., Lee, J., Provost, P., Radmark, O., Kim, S. and Kim, V.N. 2003. The nuclear RNase III Drosha initiates microRNA processing. *Nature.* **425**(6956), pp.415-419.
Lee, Y., Kim, M., Han, J., Yeom, K., Lee, S., Baek, S.H. and Kim, V.N. 2004. MicroRNA genes are transcribed by RNA polymerase II. *The EMBO Journal.* **23**(20), pp.4051-4060.
Lee, Y.S. and Dutta, A. 2007. The tumor suppressor microRNA let-7 represses the HMGA2 oncogene. *Genes & development.* **21**(9), pp.1025-1030.

Lei, L., Wu, J., Gu, D., Liu, H. and Wang, S. 2016. CIZ1 interacts with YAP and activates its transcriptional activity in hepatocellular carcinoma cells. *Tumor Biology.* **37**(8), pp.11073-11079.
Lemma, S., Avnet, S., Salerno, M., Chano, T. and Baldini, N. 2016. Identification and Validation of Housekeeping Genes for Gene Expression Analysis of Cancer Stem Cells. *PLoS One.* **11**(2), pe0149481.
Leone, G., Nuckolls, F., Ishida, S., Adams, M., Sears, R. and Jakoi, L. 2000. Identification of a novel E2F3 product suggests a mechanism for determining specificity of repression by Rb proteins. *Mol Cell Biol.* **20**, pp.3626–3632.
Leuchte, K., Altvater, B., Hoffschlag, S., Potratz, J., Meltzer, J., Clemens, D., Luecke, A., Hardes, J., Dirksen, U., Juergens, H., Kailayangiri, S. and Rossig, C. 2014. Anchorage-independent growth of Ewing sarcoma cells under serum-free conditions is not associated with stem-cell like phenotype and function. *Oncol Rep.* **32**(2), pp.845-852.
Levenstein, M.E., Ludwig, T.E., Xu, R., Llanas, R.A., VanDenHeuvel-Kramer, K., Manning, D. and Thomson, J.A. 2006. Basic FGF Support of Human Embryonic Stem Cell Self-Renewal. *Stem cells (Dayton, Ohio).* **24**(3), pp.568-574.
Li, C., Heidt, D.G., Dalerba, P., Burant, C.F., Zhang, L., Adsay, V., Wicha, M., Clarke, M.F. and Simeone, D.M. 2007. Identification of pancreatic cancer stem cells. *Cancer Res.* **67**(3), pp.1030-1037.
Li, J., Yen, C., Liaw, D., Podsypanina, K., Bose, S., Wang, S.I., Puc, J., Miliaresis, C., Rodgers, L., McCombie, R., Bigner, S.H., Giovanella, B.C., Ittmann, M., Tycko, B., Hibshoosh, H., Wigler, M.H. and Parsons, R. 1997. PTEN, a Putative Protein Tyrosine Phosphatase Gene Mutated in Human Brain, Breast, and Prostate Cancer. *Science.* **275**(5308), pp.1943-1947.
Li, P., Zhang, R., Sun, H., Chen, L., Liu, F., Yao, C., Du, M. and Jiang, X. 2013. PKH26 Can Transfer to Host Cells In Vitro and Vivo. *Stem Cells and Development.* **22**(2), pp.340-344.
Li, W., Li, Y., Guo, J., Pan, H., Zhang, Y. and Wang, X. 2015. Overexpression of miR-199b-5p inhibits Ewing's sarcoma cell lines by targeting CCNL1. *Molecular Medicine Reports.* **12**(3), pp.3359-3364.
Li, X., Zhang, J., Gao, L., McClellan, S., Finan, M.A., Butler, T.W., Owen, L.B., Piazza, G.A. and Xi, Y. 2012. MiR-181 mediates cell differentiation by interrupting the Lin28 and let-7 feedback circuit. *Cell Death and Differentiation.* **19**(3), pp.378-386.
Li, Z., Bao, S., Wu, Q., Wang, H., Eyler, C., Sathornsumetee, S., Shi, Q., Cao, Y., Lathia, J., McLendon, R.E., Hjelmeland, A.B. and Rich, J.N. 2009. Hypoxia-Inducible Factors Regulate Tumorigenic Capacity of Glioma Stem Cells. *Cancer cell.* **15**(6), pp.501-513.
Liao, J. and Lu, H. 2011. Autoregulatory suppression of c-Myc by miR-185-3p. *Journal of Biological Chemistry.* **286**(39), pp.33901-33909.
Lin, C., Jackson, A.L., Guo, J., Linsley, P.S. and Eisenman, R.N. 2009. Myc-regulated microRNAs attenuate embryonic stem cell differentiation. *The EMBO Journal.* **28**(20), pp.3157-3170.
Lin, P., Wang, Y. and Lozano, G. 2011. Mesenchymal Stem Cells and the Origin of Ewing's Sarcoma. *Sarcoma.* **2011**.
Lin, R. and Chang, H. 2008. Recent advances in three-dimensional multicellular spheroid culture for biomedical research. *Biotechnology Journal.* **3**(9-10), pp.1172-1184.

Liu, C., Teng, Z., Santistevan, N.J., Szulwach, K.E., Guo, W., Jin, P. and Zhao, X. 2010. Epigenetic regulation of miR-184 by MBD1 governs neural stem cell proliferation and differentiation. *Cell stem cell.* **6**(5), pp.433-444.
Liu, L., Li, C., Chen, Q., Jing, Y., Carpenter, R., Jiang, Y., Kung, H., Lai, L. and Jiang, B. 2011. MiR-21 Induced Angiogenesis through AKT and ERK Activation and HIF-1α Expression. *PLoS ONE.* **6**(4), pe19139.
Liu, S., Ginestier, C., Ou, S.J., Clouthier, S.G., Patel, S.H., Monville, F., Korkaya, H., Heath, A., Dutcher, J., Kleer, C.G., Jung, Y., Dontu, G., Taichman, R. and Wicha, M.S. 2011. Breast Cancer Stem Cells Are Regulated by Mesenchymal Stem Cells through Cytokine Networks. *Cancer Research.* **71**(2), pp.614-624.
Liu, T., Ren, X., Li, L., Yin, L., Liang, K., Yu, H., Ren, H., Zhou, W., Jing, H. and Kong, C. 2015. Ciz1 promotes tumorigenicity of prostate carcinoma cells. *Front Biosci (Landmark Ed).* **1**(20), pp.705-715.
Lou, Y., Guo, F., Liu, F., Gao, F., Zhang, P., Niu, X., Guo, S., Yin, J., Wang, Y. and Deng, Z. 2012. miR-210 activates notch signaling pathway in angiogenesis induced by cerebral ischemia. *Molecular and Cellular Biochemistry.* **370**(1), pp.45-51.
Ludwig, J.A. 2008. Ewing sarcoma: historical perspectives, current state-of-the-art, and opportunities for targeted therapy in the future. *Current Opinion in Oncology.* **20**(4), pp.412-418.
Ludwig, T.E., Bergendahl, V., Levenstein, M.E., Yu, J., Probasco, M.D. and Thomson, J.A. 2006. Feeder-independent culture of human embryonic stem cells. *Nat Meth.* **3**(8), pp.637-646.
Luo, B. and Lee, A.S. 2013. The critical roles of endoplasmic reticulum chaperones and unfolded protein response in tumorigenesis and anti-cancer therapies. *Oncogene.* **32**(7), p10.1038/onc.2012.1130.
Luo, W., Zhong, J., Chang, R., Hu, H., Pandey, A. and Semenza, G.L. 2010. Hsp70 and CHIP Selectively Mediate Ubiquitination and Degradation of Hypoxia-inducible Factor (HIF)-1α but Not HIF-2α. *The Journal of Biological Chemistry.* **285**(6), pp.3651-3663.
Ma, F., Zhang, J., Zhong, L., Wang, L., Liu, Y., Wang, Y., Peng, L. and Guo, B. 2014. Upregulated microRNA-301a in breast cancer promotes tumor metastasis by targeting PTEN and activating Wnt/β-catenin signaling. *Gene.* **535**(2), pp.191-197.
Ma, L., Young, J., Prabhala, H., Pan, E., Mestdagh, P., Muth, D., Teruya-Feldstein, J., Reinhardt, F., Onder, T.T. and Valastyan, S. 2010. miR-9, a MYC/MYCN-activated microRNA, regulates E-cadherin and cancer metastasis. *Nature cell biology.* **12**(3), p247.
Maeda, M., Tsuda, A., Yamanishi, S., Uchikoba, Y., Fukunaga, Y., Okita, H. and Hata, J. 2008. Ewing sarcoma/primitive neuroectodermal tumor of the kidney in a child. *Pediatric Blood & Cancer.* **50**(1), pp.180-183.
Magee, J.A., Piskounova, E. and Morrison, S.J. 2012. Cancer stem cells: impact, heterogeneity, and uncertainty. *Cancer cell.* **21**(3), pp.283-296.
Mahmoudi, E. and Cairns, M.J. 2017. MiR-137: an important player in neural development and neoplastic transformation. *Mol Psychiatry.* **22**(1), pp.44-55.
Marino, M.T., Grilli, A., Baricordi, C., Manara, M., Ventura, S., Pinca, R., Bellenghi, M., Calvaruso, M., Mattia, G., Donati, D., Tripodo, C., Picci, P., Ferrari, S. and Scotlandi, K. 2014. *Prognostic significance of miR-34a in Ewing Sarcoma is associated with cyclin D1 and ki-67 expression.*

Martínez-Serrano, M.J., Caballero-Baños, M., Vilella, R., Vidal, L., Pahisa, J. and Martínez-Roman, S. 2015. Is Sphere Assay Useful for the Identification of Cancer Initiating Cells of the Ovary? *International Journal of Gynecological Cancer.* **25**(1), pp.12-17.
Mathiyalagan, P. and Sahoo, S. 2017. Exosomes-Based Gene Therapy for MicroRNA Delivery. *Methods in molecular biology (Clifton, N.J.).* **1521**, pp.139-152.
Matsui, W., Wang, Q., Barber, J.P., Brennan, S., Smith, B.D., Borrello, I., McNiece, I., Lin, L., Ambinder, R.F., Peacock, C., Watkins, D.N., Huff, C. and Jones, R.J. 2008. Clonogenic Multiple Myeloma Progenitors, Stem Cell Properties, and Drug Resistance. *Cancer research.* **68**(1), pp.190-197.
Maurici, D., Perez-Atayde, A., Grier, H.E., Baldini, N., Serra, M. and Fletcher, J.A. 1998. Frequency and Implications of Chromosome 8 and 12 Gains in Ewing Sarcoma. *Cancer Genetics and Cytogenetics.* **100**(2), pp.106-110.
Mayer, U., Wagenaar, E., Beijnen, J.H., Smit, J.W., Meijer, D.K., van Asperen, J., Borst, P. and Schinkel, A.H. 1996. Substantial excretion of digoxin via the intestinal mucosa and prevention of long-term digoxin accumulation in the brain by the mdr 1a P-glycoprotein. *British Journal of Pharmacology.* **119**(5), pp.1038-1044.
McCord, A.M., Jamal, M., Shankavarum, U.T., Lang, F.F., Camphausen, K. and Tofilon, P.J. 2009. Physiologic Oxygen Concentration Enhances the Stem-Like Properties of CD133+ Human Glioblastoma Cells In vitro. *American Association for Cancer Research.* **7**(4), pp.489-497.
McNally, R.J.Q., Blakey, K., Parslow, R.C., James, P.W., Pozo, B., Stiller, C., Vincent, T.J., Norman, P., McKinney, P.A., Murphy, M.F., Craft, A.W. and Feltbower, R.G. 2012. Small-area analyses of bone cancer diagnosed in Great Britain provide clues to aetiology. *BMC Cancer.* **12**(1), p270.
Meacham, C.E. and Morrison, S.J. 2013. Tumor heterogeneity and cancer cell plasticity. *Nature.* **501**(7467), pp.328-337.
Mehta, G., Hsiao, A.Y., Ingram, M., Luker, G.D. and Takayama, S. 2012. Opportunities and Challenges for use of Tumor Spheroids as Models to Test Drug Delivery and Efficacy. *Journal of controlled release : official journal of the Controlled Release Society.* **164**(2), pp.192-204.
Melo, S.A. and Esteller, M. 2011. Dysregulation of microRNAs in cancer: Playing with fire. *FEBS Letters.* **585**(13), pp.2087-2099.
Mendoza-Naranjo, A., El-Naggar, A., Wai, D.H., Mistry, P., Lazic, N., Ayala, F., da Cunha, I., Rodriguez-Viciana, P., Cheng, H., Tavares Guerreiro Fregnani, J.H., Reynolds, P., Arceci, R.J., Nicholson, A., Triche, T.J., Soares, F.A., Flanagan, A.M., Wang, Y.Z., Strauss, S.J. and Sorensen, P.H. 2013. ERBB4 confers metastatic capacity in Ewing sarcoma. *EMBO Molecular Medicine.* **5**(7), pp.1019-1034.
Mestas, J. and Hughes, C.C.W. 2004. Of Mice and Not Men: Differences between Mouse and Human Immunology. *The Journal of Immunology.* **172**(5), p2731.
Mestdagh, P., Fredlund, E., Pattyn, F., Schulte, J., Muth, D., Vermeulen, J., Kumps, C., Schlierf, S., De Preter, K. and Van Roy, N. 2010. MYCN/c-MYC-induced microRNAs repress coding gene networks associated with poor outcome in MYCN/c-MYC-activated tumors. *Oncogene.* **29**(9), p1394.
Miranda-Lorenzo, I., Dorado, J., Lonardo, E., Alcala, S., Serrano, A.G., Clausell-Tormos, J., Cioffi, M., Megias, D., Zagorac, S., Balic, A., Hidalgo,

M., Erkan, M., Kleeff, J., Scarpa, A., Sainz Jr, B. and Heeschen, C. 2014. Intracellular autofluorescence: a biomarker for epithelial cancer stem cells. *Nat Meth.* **11**(11), pp.1161-1169.
Missiaglia, E., Williamson, D., Chisholm, J., Wirapati, P., Pierron, G., Petel, F., Concordet, J., Thway, K., Oberlin, O. and Pritchard-Jones, K. 2012. PAX3/FOXO1 fusion gene status is the key prognostic molecular marker in rhabdomyosarcoma and significantly improves current risk stratification. *Journal of Clinical Oncology.* **30**(14), pp.1670-1677.
Mitsui, K., Matsumoto, A., Ohtsuka, S., Ohtsubo, M. and Yoshimura, A. 1999. Cloning and characterization of a novel p21(Cip1/Waf1)-interacting zinc finger protein, ciz1. *Biochem. Biophys. Res. Commun.* **264**, pp.457-464.
Mizrak, D., Brittan, M. and Alison, M.R. 2008. CD133: molecule of the moment. *The Journal of Pathology.* **214**(1), pp.3-9.
Mizuno, Y., Tokuzawa, Y., Ninomiya, Y., Yagi, K., Yatsuka-Kanesaki, Y., Suda, T., Fukuda, T., Katagiri, T., Kondoh, Y., Amemiya, T., Tashiro, H. and Okazaki, Y. 2009. miR-210 promotes osteoblastic differentiation through inhibition of AcvR1b. *FEBS Lett.* **583**(13), pp.2263-2268.
Monzani, E., Facchetti, F., Galmozzi, E., Corsini, E., Benetti, A., Cavazzin, C., Gritti, A., Piccinini, A., Porro, D. and Santinami, M. 2007. Melanoma contains CD133 and ABCG2 positive cells with enhanced tumourigenic potential. *Eur J Cancer.* **43**.
Moore, C., Parrish, J.K. and Jedlicka, P. 2017. MiR-193b, downregulated in Ewing Sarcoma, targets the ErbB4 oncogene to inhibit anchorage-independent growth. *PLOS ONE.* **12**(5), pe0178028.
Mori, S., Chang, J.T., Andrechek, E.R., Matsumura, N., Baba, T., Yao, G., Kim, J., Gatza, M., Murphy, S. and Nevins, J.R. 2009. An Anchorage-Independent Cell Growth Signature Identifies Tumors with Metastatic Potential. *Oncogene.* **28**(31), pp.2796-2805.
Mott, J.L., Kurita, S., Cazanave, S.C., Bronk, S.F., Werneburg, N.W. and Fernandez-Zapico, M.E. 2010. Transcriptional suppression of mir-29b-1/mir-29a promoter by c-Myc, hedgehog, and NF-kappaB. *Journal of cellular biochemistry.* **110**(5), pp.1155-1164.
Mourelatos, Z., Dostie, J., Paushkin, S., Sharma, A., Charroux, B., Abel, L., Rappsilber, J., Mann, M. and Dreyfuss, G. 2002. miRNPs: a novel class of ribonucleoproteins containing numerous microRNAs. *Genes & Development.* **16**(6), pp.720-728.
Mueller-Klieser, W. 1987. Multicellular spheroids. A review on cellular aggregates in cancer research. *J. Cancer Res . Clin. Oncol.* **113**, pp.101-122.
Murray, M.J., Raby, K.L., Saini, H.K., Bailey, S., Wool, S.V., Tunnacliffe, J.M., Enright, A.J., Nicholson, J.C. and Coleman, N. 2015. Solid tumors of childhood display specific serum microRNA profiles. *Cancer epidemiology, biomarkers & prevention : a publication of the American Association for Cancer Research, cosponsored by the American Society of Preventive Oncology.* **24**(2), pp.350-360.
Myszczyszyn, A., Czarnecka, A.M., Matak, D., Szymanski, L., Lian, F., Kornakiewicz, A., Bartnik, E., Kukwa, W., Kieda, C. and Szczylik, C. 2015. The Role of Hypoxia and Cancer Stem Cells in Renal Cell Carcinoma Pathogenesis. *Stem Cell Reviews.* **11**, pp.919-943.
Nakagawa, M., Koyanagi, M., Tanabe, K., Takahashi, K., Ichisaka, T., Aoi, T., Okita, K., Mochiduki, Y., Takizawa, N. and Yamanaka, S. 2008.

Generation of induced pluripotent stem cells without Myc from mouse and human fibroblasts. *Nat Biotechnol.* **26**(1), pp.101-106.
Nakatani, F., Ferracin, M., Manara, M., Ventura, S., del Monaco, V., Ferrari, S., Alberghini, M., Grilli, A., Knuutila, S., Schaefer, K., Mattia, G., Negrini, M., Picci, P., Serra, M. and Scotlandi, K. 2012. miR-34a predicts survival of Ewing's sarcoma patients and directly influences cell chemo-sensitivity and malignancy. *The Journal of Pathology.* **226**(5), pp.796-805.
Nakatani, F., Tanaka, K., Sakimura, R., Matsumoto, Y., Matsunobu, T., Li, X., Hanada, M., Okada, T. and Iwamoto, Y. 2003. Identification of p21 WAF1/CIP1 as a direct target of EWS-Fli1 oncogenic fusion protein. *Journal of Biological Chemistry.* **278**(17), pp.15105-15115.
Navid, F., Billups, C., Liu, T., Krasin, M.J. and Rodriguez-Galindo, C. 2008. Second cancers in patients with the Ewing sarcoma family of tumours. *European Journal of Cancer.* **44**(7), pp.983-991.
Nie, J., Liu, L., Zheng, W., Chen, L., Wu, X., Xu, Y., Du, X. and Han, W. 2012. microRNA-365, down-regulated in colon cancer, inhibits cell cycle progression and promotes apoptosis of colon cancer cells by probably targeting Cyclin D1 and Bcl-2. *Carcinogenesis.* **33**(1), pp.220-225.
Nishibe, R., Watanabe, W., Ueda, T., Yamasaki, N., Koller, R., Wolff, L., Honda, Z., Ohtsubo, M. and Honda, H. 2013. CIZ1, a p21Cip1/Waf1-interacting protein, functions as a tumor suppressor in vivo. *FEBS Letters.* **587**(10), pp.1529-1535.
Njoroge, J.M., Mitchell, L.B., Centola, M., Kastner, D., Raffeld, M. and Miller, J.L. 2001. Characterization of viable autofluorescent macrophages among cultured peripheral blood mononuclear cells. *Cytometry.* **44**(1), pp.38-44.
Nolan, T., Hands, R.E. and Bustin, S.A. 2006. Quantification of mRNA using real-time RT-PCR. *Nat. Protocols.* **1**(3), pp.1559-1582.
Nowell, P.C. 1976. The clonal evolution of tumor cell populations. *Science.* **194**(4260), pp.23-28.
O'Brien, C.A., Kreso, A., Ryan, P., Hermans, K.G., Gibson, L., Wang, Y., Tsatsanis, A., Gallinger, S. and Dick, J.E. 2012. ID1 and ID3 Regulate the Self-Renewal Capacity of Human Colon Cancer-Initiating Cells through p21. *Cancer Cell.* **21**(6), pp.777-792.
O'Brien, C.A., Pollett, A., Gallinger, S. and Dick, J.E. 2007. A human colon cancer cell capable of initiating tumour growth in immunodeficient mice. *Nature.* **445**(7123), pp.106-110.
O'donnell, K.A., Wentzel, E.A., Zeller, K.I., Dang, C.V. and Mendell, J.T. 2005. c-Myc-regulated microRNAs modulate E2F1 expression. *Nature.* **435**(7043), p839.
Ogden, A.T., Waziri, A.E., Lochhead, R.A., Fusco, D., Lopez, K., Ellis, J.A., Kang, J., Assanah, M., McKhann, G.M., Sisti, M.B., McCormick, P.C., Canoll, P. and Bruce, J.N. 2008. Identification of A2B5+CD133− Tumor-Initiating Cells in adult human gliomas. *Neurosurgery.* **62**(2), pp.505-515.
Ohali, A., Avigad, S., Zaizov, R., Ophir, R., Horn-Saban, S., Cohen, I.J., Meller, I., Kollender, Y., Issakov, J. and Yaniv, I. 2004. Prediction of high risk Ewing's sarcoma by gene expression profiling. *Oncogene.* **23**(55), pp.8997-9006.
Oram, J.F. and Vaughan, A.M. 2006. ATP-Binding Cassette Cholesterol Transporters and Cardiovascular Disease. *Circulation Research.* **99**(10), p1031.

Out, R., Hoekstra, M., Hildebrand, R.B., Kruit, J.K., Meurs, I., Li, Z., Kuipers, F., Van Berkel, T.J.C. and Van Eck, M. 2006. Macrophage ABCG1 Deletion Disrupts Lipid Homeostasis in Alveolar Macrophages and Moderately Influences Atherosclerotic Lesion Development in LDL Receptor-Deficient Mice. *Arteriosclerosis, Thrombosis, and Vascular Biology.* **26**(10), p2295.
Paddison, P.J. and Hannon, G.J. 2002. RNA interference: the new somatic cell genetics? *Cancer Cell.* **2**(1), pp.17-23.
Pandzic, E., Gelissen, I.C., Whan, R., Barter, P.J., Sviridov, D., Gaus, K., Rye, K.A. and Cochran, B.J. 2017. The ATP binding cassette transporter, ABCG1, localizes to cortical actin filaments. *Sci Rep.* **7**, p42025.
Park, J., Lee, S., Kang, H., Kim, H. and Park, S. 2007. Primary Ewing's sarcoma-primitive neuroectodermal tumor of the uterus: A case report and literature review. *Gynecologic Oncology.* **106**(2), pp.427-432.
Pastò, A., Marchesi, M., Diamantini, A., Frasson, C., Curtarello, M., Lago, C., Pilotto, G., Parenti, A., Esposito, G., Agostini, M., Nitti, D. and Amadori, A. 2012. PKH26 Staining Defines Distinct Subsets of Normal Human Colon Epithelial Cells at Different Maturation Stages. *PLOS ONE.* **7**(8), pe43379.
Pastrana, E., Silva-Vargas, V. and Doetsch, F. 2011. Eyes Wide Open: A Critical Review of Sphere-Formation as an Assay For Stem Cells. *Cell stem cell.* **8**(5), pp.486-498.
Patrawala, L., Calhoun, T., Schneider-Broussard, R., Zhou, J., Claypool, K. and Tang, D.G. 2005. Side Population Is Enriched in Tumorigenic, Stem-Like Cancer Cells, whereas ABCG2⁺ and ABCG2[−] Cancer Cells Are Similarly Tumorigenic. *Cancer Research.* **65**(14), pp.6207-6219.
Pauzaite, T., Thacker, U., Tollitt, J. and Copeland, N.A. 2017. Emerging Roles for Ciz1 in Cell Cycle Regulation and as a Driver of Tumorigenesis. *Biomolecules.* **7**(1), p1.
Payne, G.S., Bishop, J.M. and Varmus, H.E. 1982. Multiple arrangements of viral DNA and an activated host oncogene in bursal lymphomas. *Nature.* **295**(5846), pp.209-214.
Pece, S., Tosoni, D., Confalonieri, S., Mazzarol, G., Vecchi, M., Ronzoni, S., Bernard, L., Viale, G., Pelicci, P. and Di Fiore, P. 2010. Biological and Molecular Heterogeneity of Breast Cancers Correlates with Their Cancer Stem Cell Content. *Cell.* **140**(1), pp.62-73.
Pelagiadis, I., Relakis, K., Kalmanti, L. and Dimitriou, H. 2012. CD133 immunomagnetic separation: effectiveness of the method for CD133+ isolation from umbilical cord blood. *Cytotherapy.* **14**(6), pp.701-706.
Peng, J., Marshall, N.F. and Price, D.H. 1998. Identification of a Cyclin Subunit Required for the Function of Drosophila P-TEFb. *THE JOURNAL OF BIOLOGICAL CHEMISTRY.* **273**(22), pp.13855-13860.
Peng, L., Yang, L., Wu, N.A.N. and Wu, B.O. 2015. Primary primitive neuroectodermal tumor arising in the mesentery and ileocecum: A report of three cases and review of the literature. *Experimental and Therapeutic Medicine.* **9**(4), pp.1299-1303.
Peng, Y. and Croce, C.M. 2016. The role of MicroRNAs in human cancer. *Signal Transduction and Targeted Therapy.* **1**, p15004.
Peng, Y., Dai, Y., Hitchcock, C., Yang, X., Kassis, E.S., Liu, L., Luo, Z., Sun, H., Cui, R., Wei, H., Kim, T., Lee, T., Jeon, Y., Nuovo, G.J., Volinia, S., He, Q., Yu, J., Nana-Sinkam, P. and Croce, C.M. 2013. Insulin growth factor signaling is regulated by microRNA-486, an underexpressed microRNA in

lung cancer. *Proceedings of the National Academy of Sciences of the United States of America.* **110**(37), pp.15043-15048.
Peter, M.E. 2009. Let-7 and miR-200 microRNAs: Guardians against pluripotency and cancer progression. *Cell cycle (Georgetown, Tex.).* **8**(6), pp.843-852.
Pfaffl, M.W. 2001. A new mathematical model for relative quantification in real-time RT–PCR. *Nucleic Acids Research.* **29**(9), pp.e45-e45.
Pichiorri, F., Suh, S., Rocci, A., De Luca, L., Taccioli, C., Santhanam, R., Wenchao, Z., Benson, D.M., Hofmainster, C., Alder, H., Garofalo, M., Di Leva, G., Volinia, S., Lin, H., Perrotti, D., Kuehl, M., Aqeilan, R.I., Palumbo, A. and Croce, C.M. 2010. Down-regulation of p53-inducible microRNAs 192, 194 and 215 impairs the p53/MDM2 auto-regulatory loop in multiple myeloma development. *Cancer cell.* **18**(4), pp.367-381.
Platet, N., Liu, S., Atifi, M., Oliver, L., Vallette, F.M., Berger, F. and Wion, D. 2007. Influence of oxygen tension on CD133 phenotype in human glioma cell cultures. *Cancer Letters.* **258**(2), pp.286-290.
Podsypanina, K., Ellenson, L.H., Nemes, A., Gu, J., Tamura, M., Yamada, K.M., Cordon-Cardo, C., Catoretti, G., Fisher, P.E. and Parsons, R. 1999. Mutation of Pten/Mmac1 in mice causes neoplasia in multiple organ systems. *Proceedings of the National Academy of Sciences of the United States of America.* **96**(4), pp.1563-1568.
Ponti, D., Costa, A., Zaffaroni, N., Pratesi, G., Petrangolini, G., Coradini, D., Pilotti, S., Pierotti, M.A. and Daidone, M.G. 2005. Isolation and *In vitro* Propagation of Tumorigenic Breast Cancer Cells with Stem/Progenitor Cell Properties. *Cancer Research.* **65**(13), pp.5506-5511.
Postovit, L.M., Margaryan, N.V., Seftor, E.A., Kirschmann, D.A., Lipavsky, A., Wheaton, W.W., Abbott, D.E., Seftor, R.E. and Hendrix, M.J. 2008. Human embryonic stem cell microenvironment suppresses the tumorigenic phenotype of aggressive cancer cells. *Proc Natl Acad Sci U S A.* **105**(11), pp.4329-4334.
Prieur, A., Tirode, F., Cohen, P. and Delattre, O. 2004. EWS/FLI-1 silencing and gene profiling of Ewing cells reveal downstream oncogenic pathways and a crucial role for repression of insulin-like growth factor binding protein 3. *Molecular and cellular biology.* **24**(16), pp.7275-7283.
Psaila, B. and Lyden, D. 2009. The Metastatic Niche: Adapting the Foreign Soil. *Nature reviews. Cancer.* **9**(4), pp.285-293.
Pulkkinen, K., Malm, T., Turunen, M., Koistinaho, J. and Ylä-Herttuala, S. 2008. Hypoxia induces microRNA miR-210 in vitro and in vivo. *FEBS Letters.* **582**(16), pp.2397-2401.
Quintana, E., Shackleton, M., Foster, H.R., Fullen, D.R., Sabel, M.S., Johnson, T.M. and Morrison, S.J. 2010. Phenotypic heterogeneity among tumorigenic melanoma cells from patients that is reversible and not hierarchically organized. *Cancer cell.* **18**(5), pp.510-523.
Quintana, E., Shackleton, M., Sabel, M.S., Fullen, D.R., Johnson, T.M. and Morrison, S.J. 2008. Efficient tumor formation by single human melanoma cells. *Nature.* **456**(7222), pp.593-598.
Qureshi-Baig, K., Ullmann, P., Rodriguez, F., Frasquilho, S., Nazarov, P.V., Haan, S. and Letellier, E. 2016. What Do We Learn from Spheroid Culture Systems? Insights from Tumorspheres Derived from Primary Colon Cancer Tissue. *PLOS ONE.* **11**(1), pe0146052.

Rafiee, M., Malekzadeh Shafaroudi, A., Rohban, S., Khayatzadeh, H., Kalhor, H. and Mowla, S. 2015. Enrichment of A Rare Subpopulation of miR-302-Expressing Glioma Cells by Serum Deprivation. *Cell Journal (Yakhteh).* **16**(4), pp.494-505.
Rahman, F.A., Ainscough, J.F., Copeland, N. and Coverley, D. 2007. Cancer-associated missplicing of exon 4 influences the subnuclear distribution of the DNA replication factor CIZ1. *Hum Mutat.* **28**(10), pp.993-1004.
Rahman, F.A., Aziz, N. and Coverley, D. 2010. Differential detection of alternatively spliced variants of Ciz1 in normal and cancer cells using a custom exon-junction microarray. *BMC Cancer.* **10**(1), p482.
Raina, A. and Kaul, D. 2010. LXR-α genomics programmes neuronal death observed in Alzheimer's disease. *Apoptosis.* **15**(12), pp.1461-1469.
Rappa, G., Fodstad, O. and Lorico, A. 2008. The Stem Cell-Associated Antigen CD133 (Prominin-1) Is a Molecular Therapeutic Target for Metastatic Melanoma. *Stem cells (Dayton, Ohio).* **26**(12), pp.3008-3017.
Redon, R., Hussenet, T., Bour, G., Caulee, K., Jost, B., Muller, D., Abecassis, J. and Manoir, S. 2002. Amplicon Mapping and Transcriptional Analysis Pinpoint Cyclin L as a Candidate Oncogene in Head and Neck Cancer. *Cancer Research.* **62**(21), p6211.
Ricci-Vitiani, L., Lombardi, D.G., Pilozzi, E., Biffoni, M., Todaro, M., Peschle, C. and De Maria, R. 2007. Identification and expansion of human colon-cancer-initiating cells. *Nature.* **445**(7123), pp.111-115.
Richter, G.H., Plehm, S., Fasan, A., Rössler, S., Unland, R., Bennani-Baiti, I.M., Hotfilder, M., Löwel, D., von Luettichau, I. and Mossbrugger, I. 2009. EZH2 is a mediator of EWS/FLI1 driven tumor growth and metastasis blocking endothelial and neuro-ectodermal differentiation. *Proceedings of the National Academy of Sciences.* **106**(13), pp.5324-5329.
Ridings-Figueroa, R., Stewart, E.R., Nesterova, T.B., Coker, H., Pintacuda, G., Godwin, J., Wilson, R., Haslam, A., Lilley, F., Ruigrok, R., Bageghni, S.A., Albadrani, G., Mansfield, W., Roulson, J.A., Brockdorff, N., Ainscough, J.F.X. and Coverley, D. 2017. The nuclear matrix protein CIZ1 facilitates localization of Xist RNA to the inactive X-chromosome territory. *Genes Dev.* **31**(9), pp.876-888.
Riggi, N., Suvà, M., De Vito, C., Provero, P., Stehle, J., Baumer, K., Cironi, L., Janiszewska, M., Petricevic, T. and Suvà, D. 2010. EWS-FLI-1 modulates miRNA145 and SOX2 expression to initiate mesenchymal stem cell reprogramming toward Ewing sarcoma cancer stem cells. *Genes & development.* **24**(9), pp.916-932.
Roberts, P., Burchill, S.A., Brownhill, S., Cullinane, C.J., Johnston, C., Griffiths, M.J., McMullan, D.J., Bown, N.P., Morris, S.P. and Lewis, I.J. 2008. Ploidy and karyotype complexity are powerful prognostic indicators in the Ewing's sarcoma family of tumors: A study by the United Kingdom Cancer Cytogenetics and the Children's Cancer and Leukaemia Group. *Genes, Chromosomes and Cancer.* **47**(3), pp.207-220.
Rongvaux, A., Takizawa, H., Strowig, T., Willinger, T., Eynon, E.E., Flavell, R.A. and Manz, M.G. 2013. Human Hemato-Lymphoid System Mice: Current Use and Future Potential for Medicine. *Annual review of immunology.* **31**, pp.635-674.

Rosen, J.M. and Jordan, C.T. 2009. The Increasing Complexity of the Cancer Stem Cell Paradigm. *Science (New York, N.Y.).* **324**(5935), pp.1670-1673.
Roundhill, E.A. and Burchill, S.A. 2012. Detection and characterisation of multi-drug resistance protein 1 (MRP-1) in human mitochondria. *British Journal of Cancer.* **106**(6), pp.1224-1233.
Rowley, J.D. 1973. A New Consistent Chromosomal Abnormality in Chronic Myelogenous Leukaemia identified by Quinacrine Fluorescence and Giemsa Staining. *Nature.* **243**(5405), pp.290-293.
Sachdeva, M., Zhu, S., Wu, F., Wu, H., Walia, V., Kumar, S., Elble, R., Watabe, K. and Mo, Y.-Y. 2009. p53 represses c-Myc through induction of the tumor suppressor miR-145. *Proceedings of the National Academy of Sciences.* **106**(9), pp.3207-3212.
Sag, D., Cekic, C., Wu, R., Linden, J. and Hedrick, C.C. 2015. The Cholesterol Transporter ABCG1 Links Cholesterol Homeostasis and Tumor Immunity. *Nature communications.* **6**, pp.6354-6354.
Sainz, B., Miranda-Lorenzo, I. and Heeschen, C. 2015. The Fuss Over Lipo“fuss”cin: Not All Autofluorescence is the Same. *European Journal of Histochemistry : EJH.* **59**(1), p2512.
Saldanha, A.J. 2004. Java Treeview—extensible visualization of microarray data. *Bioinformatics.* **20**(17), pp.3246-3248.
Sampson, V.B., Rong, N.H., Han, J., Yang, Q., Aris, V., Soteropoulos, P., Petrelli, N.J., Dunn, S.P. and Krueger, L.J. 2007. MicroRNA let-7a down-regulates MYC and reverts MYC-induced growth in Burkitt lymphoma cells. *Cancer research.* **67**(20), pp.9762-9770.
Sander, S., Bullinger, L., Klapproth, K., Fiedler, K., Kestler, H.A., Barth, T.F., Möller, P., Stilgenbauer, S., Pollack, J.R. and Wirth, T. 2008. MYC stimulates EZH2 expression by repression of its negative regulator miR-26a. *Blood.* **112**(10), pp.4202-4212.
Schaefer, K., Eisenacher, M., Braun, Y., Brachwitz, K., Wai, D.H., Dirksen, U., Lanvers-Kaminsky, C., Juergens, H., Herrero, D. and Stegmaier, S. 2008. Microarray analysis of Ewing’s sarcoma family of tumours reveals characteristic gene expression signatures associated with metastasis and resistance to chemotherapy. *European journal of cancer.* **44**(5), pp.699-709.
Schaft, D., Hillen, F., Pauwels, P., Kirschmann, D., Castermans, K., oude Egbrink, M., Tran, M., Sciot, R., Hauben, E., Hogendoorn, P., Delattre, O., H Maxwell, P., J C Hendrix, M. and W Griffioen, A. 2006. *Tumor cell plasticity in Ewing Sarcoma, an alternative circulatory system stimulated by hypoxia.*
Scharenberg, C.W., Harkey, M.A. and Torok-Storb, B. 2002. The ABCG2 transporter is an efficient Hoechst 33342 efflux pump and is preferentially expressed by immature human hematopoietic progenitors. *Blood.* **99**(2), p507.
Schier, A.F. 2009. Nodal Morphogens. *Cold Spring Harbor Perspectives in Biology.* **1**(5), pa003459.
Schinkel, A.H. 1999. P-Glycoprotein, a gatekeeper in the blood–brain barrier. *Advanced Drug Delivery Reviews.* **36**(2), pp.179-194.
Schoor, O., Weinschenk, T., Hennenlotter, J., Corvin, S., Stenzl, A., Rammensee, H.-G. and Stevanovic, S. 2003. Moderate degradation does not preclude microarray analysis of small amounts of RNA. *BioTechniques.* **35**, pp.1192–1201.

Schulte, J.H., Horn, S., Otto, T., Samans, B., Heukamp, L.C., Eilers, U.C., Krause, M., Astrahantseff, K., Klein-Hitpass, L. and Buettner, R. 2008. MYCN regulates oncogenic MicroRNAs in neuroblastoma. *International journal of cancer.* **122**(3), pp.699-704.

Schwentner, R., Herrero-Martin, D., Kauer, M.O., Mutz, C.N., Katschnig, A.M., Sienski, G., Alonso, J., Aryee, D.N.T. and Kovar, H. 2017. The role of miR-17-92 in the miRegulatory landscape of Ewing sarcoma. *Oncotarget.* **8**(7), pp.10980-10993.

Scotlandi, K., Remondini, D., Castellani, G., Manara, M., Nardi, F., Cantiani, L., Francesconi, M., Mercuri, M., Caccuri, A. and Serra, M. 2009. Overcoming resistance to conventional drugs in Ewing sarcoma and identification of molecular predictors of outcome. *Journal of clinical oncology.* **27**(13), pp.2209-2216.

Semenza, G.L. 2007. Oxygen-dependent regulation of mitochondrial respiration by hypoxia-inducible factor 1. *Biochem J.* **405**(1), pp.1-9.

Seres, L., Cserepes, J., Elkind, N.B., Törőcsik, D., Nagy, L., Sarkadi, B. and Homolya, L. 2008. Functional ABCG1 expression induces apoptosis in macrophages and other cell types. *Biochimica et Biophysica Acta (BBA) - Biomembranes.* **1778**(10), pp.2378-2387.

Shaffiey, F., Cross, E. and Sathyanarayana, P. 2013. Mir-590 Is a Novel STAT5 Regulated Oncogenic miRNA and Targets FasL In Acute Myeloid Leukemia. *Blood.* **122**(21), pp.3811-3811.

Shek, T.W., Chan, G.C., Khong, P.L., Chung, L.P. and Cheung, A.N. 2001. Ewing sarcoma of the small intestine. *J Pediatr Hematol Oncol.* **1**(23), pp.530-532.

Sherr, C.J. 1994. Gl Phase Progression: Cycling on Cue. *Cell.* **79**, pp.551-555.

Shibuya, S., Takamizawa, S., Hatata, T., Komori, K., Ogiso, Y., Yoshizawa, K. and Yoshizawa, K. 2015. Extraosseous Ewing sarcoma in the mesentery: the first report of cases in children. *Pediatr Surg Int.* **31**(10), pp.995-999.

Shimono, Y., Ugalde, M., Cho, R.W., Lobo, N.A., Dalerba, P., Qian, D., Diehn, M., Liu, H., Panula, S.P., Chiao, E., Dirbas, F.M., Somlo, G., Reijo Pera, R.A., Lao, K. and Clarke, M.F. 2009. Down-regulation of miRNA-200c Links Breast Cancer Stem Cells with Normal Stem Cells. *Cell.* **138**(3), pp.592-603.

Shmelkov, S.V., Butler, J.M., Hooper, A.T., Hormigo, A., Kushner, J., Milde, T., St. Clair, R., Baljevic, M., White, I., Jin, D.K., Chadburn, A., Murphy, A.J., Valenzuela, D.M., Gale, N.W., Thurston, G., Yancopoulos, G.D., D'Angelica, M., Kemeny, N., Lyden, D. and Rafii, S. 2008. CD133 expression is not restricted to stem cells, and both CD133(+) and CD133(–) metastatic colon cancer cells initiate tumors. *The Journal of Clinical Investigation.* **118**(6), pp.2111-2120.

Shukla, N., Schiffman, J.D., Reed, D., Davis, I.J., Womer, R.B., Lessnick, S.L. and Lawlor, E.R. 2013. Biomarkers in Ewing sarcoma: the promise and challenge of personalized medicine. A report from the Children's Oncology Group. *Frontiers in oncology.* **3**.

Siligan, C., Ban, J., Bachmaier, R., Spahn, L., Kreppel, M., Schaefer, K., Poremba, C., Aryee, D.N. and Kovar, H. 2005. EWS-FLI1 target genes recovered from Ewing's sarcoma chromatin. *Oncogene.* **24**(15), pp.2512-2524.

Singh, S.K., Clarke, I.D., Terasaki, M., Bonn, V.E., Hawkins, C., Squire, J. and Dirks, P.B. 2003. Identification of a Cancer Stem Cell in Human Brain Tumors. *Cancer Research.* **63**(18), pp.5821-5828.
Singh, S.K., Hawkins, C., Clarke, I.D., Squire, J.A., Bayani, J., Hide, T., Henkelman, R.M., Cusimano, M.D. and Dirks, P.B. 2004. Identification of human brain tumour initiating cells. *Nature.* **432**(7015), pp.396-401.
Slezak, S. and Horan, P. 1989. Fluorescent in vivo tracking of hematopoietic cells. Part I. Technical considerations. *Blood.* **74**(6), pp.2172-2177.
Smart, C.E., Morrison, B.J., Saunus, J.M., Vargas, A., Keith, P., Reid, L., Wockner, L., Amiri, M., Sarkar, D., Simpson, P.T., Clarke, C., Schmidt, C.W., Reynolds, B.A., Lakhani, S.R. and Lopez, J.A. 2013. In Vitro Analysis of Breast Cancer Cell Line Tumourspheres and Primary Human Breast Epithelia Mammospheres Demonstrates Inter- and Intrasphere Heterogeneity. *PLOS ONE.* **8**(6), pe64388.
Smit, J.W., Schinkel, A.H., Weert, B. and Meijer, D.K.F. 1998. Hepatobiliary and intestinal clearance of amphiphilic cationic drugs in mice in which both mdr1a and mdr1b genes have been disrupted. *British Journal of Pharmacology.* **124**(2), pp.416-424.
Smith, R., Owen, L.A., Trem, D.J., Wong, J.S., Whangbo, J.S., Golub, T.R. and Lessnick, S.L. 2006. Expression profiling of EWS/FLI identifies NKX2. 2 as a critical target gene in Ewing's sarcoma. *Cancer cell.* **9**(5), pp.405-416.
Smrt, R.D., Szulwach, K.E., Pfeiffer, R.L., Li, X., Guo, W., Pathania, M., Teng, Z., Luo, Y., Peng, J., Bordey, A., Jin, P. and Zhao, X. 2010. MicroRNA miR-137 regulates neuronal maturation by targeting ubiquitin ligase Mind Bomb-1. *Stem cells (Dayton, Ohio).* **28**(6), pp.1060-1070.
Sollazzo, M., Benassi, M., Magagnoli, G., Gamberi, G., Molendini, L., Ragazzini, P., Merli, M., Ferrari, C., Balladelli, A. and Picci, P. 1998. Increased c-myc oncogene expression in Ewing's sarcoma: correlation with Ki67 proliferation index. *Tumori.* **85**(3), pp.167-173.
Sollazzo, M.R., Benassi, M.S., Magagnoli, G., Gamberi, G., Molendini, L., Ragazzini, P., Merli, M., Ferrari, C., Balladelli, A. and Picci, P. 1998. Increased c-myc oncogene expression in Ewing's sarcoma: correlation with Ki67 proliferation index. *Tumori.* **85**(3), pp.167-173.
Sticht, C., Hofele, C., Flechtenmacher, C., Bosch, F.X., Freier, K., Lichter, P. and Joos, S. 2005. Amplification of Cyclin L1 is associated with lymph node metastases in head and neck squamous cell carcinoma (HNSCC). *British Journal of Cancer.* **92**(4), pp.770-774.
Stoler, D.L., Chen, N., Basik, M., Kahlenberg, M.S., Rodriguez-Bigas, M.A., Petrelli, N.J. and Anderson, G.R. 1999. The onset and extent of genomic instability in sporadic colorectal tumor progression. *Proceedings of the National Academy of Sciences of the United States of America.* **96**(26), pp.15121-15126.
Stout, A.P. 1918. A tumour of the ulnar nerve. *Proc N Y Pathol Soc.* **12**, pp.2-12.
Stricker, T.P., Morales La Madrid, A., Chlenski, A., Guerrero, L., Salwen, H.R., Gosiengfiao, Y., Perlman, E.J., Furman, W., Bahrami, A. and Shohet, J.M. 2014. Validation of a prognostic multi-gene signature in high-risk neuroblastoma using the high throughput digital NanoString nCounter™ system. *Molecular oncology.* **8**(3), pp.669-678.
Sturek, J.M., Castle, J.D., Trace, A.P., Page, L.C., Castle, A.M., Evans-Molina, C., Parks, J.S., Mirmira, R.G. and Hedrick, C.C. 2010. An

intracellular role for ABCG1-mediated cholesterol transport in the regulated secretory pathway of mouse pancreatic β cells. *The Journal of Clinical Investigation.* **120**(7), pp.2575-2589.
Sturla, L., Westwood, G., Selby, P.J., Lewis, I.J. and Burchill, S.A. 2000. Induction of Cell Death by Basic Fibroblast Growth Factor in Ewing's Sarcoma. *Cancer Research.* **60**(21), p6160.
Suetsugu, A., Nagaki, M., Aoki, H., Motohashi, T., Kunisada, T. and Moriwaki, H. 2006. Characterization of CD133+ hepatocellular carcinoma cells as cancer stem/progenitor cells. *Biochemical and Biophysical Research Communications.* **351**(4), pp.820-824.
Sultan, I., Rihani, R., Hazin, R. and Rodriguez-Galindo, C. 2010. Second malignancies in patients with Ewing Sarcoma Family of Tumors: A population-based study. *Acta Oncologica.* **49**(2), pp.237-244.
Sun, Y., Li, Y., Luo, D. and Liao, D.J. 2012. Pseudogenes as Weaknesses of ACTB (Actb) and GAPDH (Gapdh) Used as Reference Genes in Reverse Transcription and Polymerase Chain Reactions. *PLOS ONE.* **7**(8), pe41659.
Sutherland, R.M., McCredie, J.A. and Inch, W.R. 1971. Growth of multicell spheroids in tissue culture as a model of nodular carcinomas. *Journal of the National Cancer Institute.* **46**(1), pp.113-120.
Suvà, M.L., Riggi, N., Stehle, J.C., Baumer, K., Tercier, S., Joseph, J.M., Suva, D., Clement, V., Provero, P. and Cironi, L. 2009. Identification of Cancer Stem Cells in Ewing's Sarcoma. *Cancer Res.* **69**.
Suzuki, H.I., Katsura, A., Matsuyama, H. and Miyazono, K. 2015. MicroRNA regulons in tumor microenvironment. *Oncogene.* **34**(24), pp.3085-3094.
Suzuki, H.I., Yamagata, K., Sugimoto, K., Iwamoto, T., Kato, S. and Miyazono, K. 2009. Modulation of microRNA processing by p53. *Nature.* **460**(7254), p529.
Szotek, P.P., Pieretti-Vanmarcke, R., Masiakos, P.T., Dinulescu, D.M., Connolly, D., Foster, R., Dombkowski, D., Preffer, F., MacLaughlin, D.T. and Donahoe, P.K. 2006. Ovarian cancer side population defines cells with stem cell-like characteristics and Mullerian Inhibiting Substance responsiveness. *Proceedings of the National Academy of Sciences of the United States of America.* **103**(30), pp.11154-11159.
Tada, M., Takahama, Y., Abe, K., Nakatsuji, N. and Tada, T. 2001. Nuclear reprogramming of somatic cells by in vitro hybridization with ES cells. *Current Biology.* **11**(19), pp.1553-1558.
Takahashi, K. and Yamanaka, S. 2006. Induction of pluripotent stem cells from mouse embryonic and adult fibroblast cultures by defined factors. *Cell.* **126**(4), pp.663-676.
Takahashi, R., Miyazaki, H. and Ochiya, T. 2013. The role of microRNAs in the regulation of cancer stem cells. *Frontiers in Genetics.* **4**, p295.
Tan, W., Lim, S. and Tan, T.M.C. 2015. Up-regulation of microRNA-210 inhibits proliferation of hepatocellular carcinoma cells by targeting YES1. *World Journal of Gastroenterology.* **21**(46), pp.13030-13041.
Tang, B., Raviv, A., Esposito, D., Flanders, K.C., Daniel, C., Nghiem, B., Garfield, S., Lim, L., Mannan, P., Robles, A.I., Smith, W., Zimmerberg, J., Ravin, R. and Wakefield, L. 2015. A Flexible Reporter System for Direct Observation and Isolation of Cancer Stem Cells. *Stem Cell Reports.* **4**(1), pp.155-169.
Tanida, S., Tanioka, F., Inukai, M., Yoshioka, N., Saida, Y., Imai, K., Nakamura, T., Kitamura, H. and Sugimura, H. 2000. Ewing's

sarcoma/peripheral primitive neuroectodermal tumor (pPNET) arising in the omentum as a multilocular cyst with intracystic hemorrhage. *Journal of Gastroenterology.* **35**(12), pp.933-940.
Tanzer, A. and Stadler, P.F. 2004. Molecular evolution of a microRNA cluster. *Journal of molecular biology.* **339**(2), pp.327-335.
Tarkkanen, M., Kiuru-Kuhlefelt, S., Blomqvist, C., Armengol, G., Böhling, T., Ekfors, T., Virolainen, M., Lindholm, P., Monge, O., Picci, P., Knuutila, S. and Elomaa, I. 1999. Clinical Correlations of Genetic Changes by Comparative Genomic Hybridization in Ewing Sarcoma and Related Tumors. *Cancer Genetics and Cytogenetics.* **114**(1), pp.35-41.
Tarling, E.J., Bojanic, D.D., Tangirala, R.K., Wang, X., Lovgren-Sandblom, A., Lusis, A.J., Bjorkhem, I. and Edwards, P.A. 2010. Impaired Development of Atherosclerosis in Abcg1(−/−)Apoe(−/−) Mice; Identification of Specific Oxysterols that both Accumulate in Abcg1(−/−)Apoe(−/−) Tissues and Induce Apoptosis. *Arteriosclerosis, thrombosis, and vascular biology.* **30**(6), pp.1174-1180.
Tarling, E.J. and Edwards, P.A. 2011. ATP binding cassette transporter G1 (ABCG1) is an intracellular sterol transporter. *Proceedings of the National Academy of Sciences of the United States of America.* **108**(49), pp.19719-19724.
Tarr, P.T. and Edwards, P.A. 2008. ABCG1 and ABCG4 are coexpressed in neurons and astrocytes of the CNS and regulate cholesterol homeostasis through SREBP-2. *J Lipid Res.* **49**(1), pp.169-182.
Tarr, P.T., Tarling, E.J., Bojanic, D.D., Edwards, P.A. and Baldán, Á. 2009. Emerging New Paradigms for ABCG Transporters. *Biochimica et biophysica acta.* **1791**(7), pp.584-593.
Taussig, D.C., Miraki-Moud, F., Anjos-Afonso, F., Pearce, D.J., Allen, K., Ridler, C., Lillington, D., Oakervee, H., Cavenagh, J., Agrawal, S.G., Lister, T.A., Gribben, J.G. and Bonnet, D. 2008. Anti-CD38 antibody–mediated clearance of human repopulating cells masks the heterogeneity of leukemia-initiating cells. *Blood.* **112**(3), pp.568-575.
Tay, Y., Zhang, J., Thomson, A.M., Lim, B. and Rigoutsos, I. 2008. MicroRNAs to Nanog, Oct4 and Sox2 coding regions modulate embryonic stem cell differentiation. *Nature.* **455**(7216), pp.1124-1128.
Thorell, B. 1983. Flow-cytometric monitoring of intracellular flavins simultaneously with NAD(P)H levels. *Cytometry.* **4**(1), pp.61-65.
Tian, C., Huang, D., Yu, Y., Zhang, J., Fang, Q. and Xie, C. 2017. ABCG1 as a potential oncogene in lung cancer. *Experimental and Therapeutic Medicine.*
Timmins, N.E., Dietmair, S. and Nielsen, L.K. 2004. Hanging-drop multicellular spheroids as a model of tumour angiogenesis. *Angiogenesis.* **7**, pp.97-103.
Tirino, V., Desiderio, V., d'Aquino, R., De Francesco, F., Pirozzi, G., Galderisi, U., Cavaliere, C., De Rosa, A. and Papaccio, G. 2008. Detection and Characterization of CD133(+) Cancer Stem Cells in Human Solid Tumours. *PLoS ONE.* **3**(10), pe3469.
Tirino, V., Desiderio, V., Paino, F., De Rosa, A., Papaccio, F., La Noce, M., Laino, L., De Francesco, F. and Papaccio, G. 2013. Cancer stem cells in solid tumors: an overview and new approaches for their isolation and characterization. *FASEB J.* **27**(1), pp.13-24.

Tirode, F., Surdez, D., Ma, X., Parker, M., Le Deley, M., Bahrami, A., Zhang, Z., Lapouble, E., Grossetête-Lalami, S., Rusch, M., Reynaud, S., Rio-Frio, T., Hedlund, E., Wu, G., Chen, X., Pierron, G., Oberlin, O., Zaidi, S., Lemmon, G., Gupta, P., Vadodaria, B., Easton, J., Gut, M., Ding, L., Mardis, E.R., Wilson, R.K., Shurtleff, S., Laurence, V., Michon, J., Marec-Bérard, P., Gut, I., Downing, J., Dyer, M., Zhang, J. and Delattre, O. 2014. Genomic landscape of Ewing sarcoma defines an aggressive subtype with co-association of STAG2 and TP53 mutations. *Cancer discovery.* **4**(11), pp.1342-1353.

Tomlinson, D.C., L'Hote, C.G., Kennedy, W., Pitt, E. and Knowles, M.A. 2005. Alternative splicing of fibroblast growth factor receptor 3 produces a secreted isoform that inhibits fibroblast growth factor-induced proliferation and is repressed in urothelial carcinoma cell lines. *Cancer Res.* **65**(22), pp.10441-10449.

Tomlinson, I.P. and Bodmer, W.F. 1995. Failure of programmed cell death and differentiation as causes of tumors: some simple mathematical models. *Proceedings of the National Academy of Sciences of the United States of America.* **92**(24), pp.11130-11134.

Tomlinson, I.P., Sasieni, P. and Bodmer, W.F. 2002. How Many Mutations in a Cancer? *The American Journal of Pathology.* **160**(3), pp.755-758.

Tosoni, K., Stobbart, M., Cassidy, D.M., Venerando, A., Pagano, M.A., Luz, S., Amaral, M.D., Kunzelmann, K., Pinna, L.A., Farinha, C.M. and Mehta, A. 2013. CFTR mutations altering CFTR fragmentation. *Biochemical Journal.* **449**(Pt 1), pp.295-305.

Trinquand, A., Tanguy-Schmidt, A., Ben Abdelali, R., Lambert, J., Beldjord, K., Lengliné, E., De Gunzburg, N., Payet-Bornet, D., Lhermitte, L. and Mossafa, H. 2013. Toward a NOTCH1/FBXW7/RAS/PTEN–Based Oncogenetic Risk Classification of Adult T-Cell Acute Lymphoblastic Leukemia: A Group for Research in Adult Acute Lymphoblastic Leukemia Study. *Journal of Clinical Oncology.* **31**(34), pp.4333-4342.

Tsujiuchi, T., Miller, A.D., Wakabayashi, T. and Natsume, A. 2014. Chapter 27 - RNA Interference Therapeutics for Tumor Therapy: Promising Work in Progress A2 - Lattime, Edmund C. In: Gerson, S.L. ed. *Gene Therapy of Cancer (Third Edition).* San Diego: Academic Press, pp.393-408.

Ulloa, L., Creemers, J.W., Roy, S., Liu, S., Mason, J. and Tabibzadeh, S. 2001. Lefty proteins exhibit unique processing and activate the MAPK pathway. *J Biol Chem.* **276**(24), pp.21387-21396.

Upreti, M., Jamshidi-Parsian, A., Koonce, N.A., Webber, J.S., Sharma, S.K., Asea, A.A.A., Mader, M.J. and Griffin, R.J. 2011. Tumor-Endothelial Cell Three-dimensional Spheroids: New Aspects to Enhance Radiation and Drug Therapeutics. *Translational Oncology.* **4**(6), pp.365-376.

Valadi, H., Ekstrom, K., Bossios, A., Sjostrand, M., Lee, J.J. and Lotvall, J.O. 2007. Exosome-mediated transfer of mRNAs and microRNAs is a novel mechanism of genetic exchange between cells. *Nat Cell Biol.* **9**(6), pp.654-659.

Valencia-Sanchez, M.A., Liu, J., Hannon, G.J. and Parker, R. 2006. Control of translation and mRNA degradation by miRNAs and siRNAs. *Genes Dev.* **20**, pp.515-524.

van den Berg, H., Heinen, R.C., van der Pal, H.J. and Merks, J.H.M. 2009. Extra-osseous Ewing sarcoma. *Pediatric hematology and oncology.* **26**(4), pp.175-185.

van Doorninck, J.A., Ji, L., Schaub, B., Shimada, H., Wing, M.R., Krailo, M.D., Lessnick, S.L., Marina, N., Triche, T.J., Sposto, R., Womer, R.B. and Lawlor, E.R. 2010. Current Treatment Protocols Have Eliminated the Prognostic Advantage of Type 1 Fusions in Ewing Sarcoma: A Report From the Children's Oncology Group. *Journal of Clinical Oncology.* **28**(12), pp.1989-1994.

Vasudevan, S. 2012. Posttranscriptional Upregulation by MicroRNAs. *Wiley Interdisciplinary Reviews: RNA.* **3**(3), pp.311-330.

Vasudevan, S., Tong, Y. and Steitz, J.A. 2007. Switching from Repression to Activation: MicroRNAs Can Up-Regulate Translation. *Science.* **318**(5858), pp.1931-1934.

Vaughan, A.M. and Oram, J.F. 2005. ABCG1 redistributes cell cholesterol to domains removable by high density lipoprotein but not by lipid-depleted apolipoproteins. *J Biol Chem.* **280**(34), pp.30150-30157.

Vaughan, A.M. and Oram, J.F. 2006. ABCA1 and ABCG1 or ABCG4 act sequentially to remove cellular cholesterol and generate cholesterol-rich HDL. *Journal of Lipid Research.* **47**(11), pp.2433-2443.

Ventura, A. and Jacks, T. 2009. MicroRNAs and Cancer: Short RNAs Go a Long Way. *Cell.* **136**(4), pp.586-591.

Ventura, A., Young, A.G., Winslow, M.M., Lintault, L., Meissner, A., Erkeland, S.J., Newman, J., Bronson, R.T., Crowley, D. and Stone, J.R. 2008. Targeted deletion reveals essential and overlapping functions of the miR-17~ 92 family of miRNA clusters. *Cell.* **132**(5), pp.875-886.

Vermeulen, K., Van Bockstaele, D.R. and Berneman, Z.N. 2003. The cell cycle: a review of regulation, deregulation and therapeutic targets in cancer. *Cell Proliferation.* **36**(3), pp.131-149.

Vermeulen, L., Todaro, M., de Sousa Mello, F., Sprick, M.R., Kemper, K., Perez Alea, M., Richel, D.J., Stassi, G. and Medema, J.P. 2008. Single-cell cloning of colon cancer stem cells reveals a multi-lineage differentiation capacity. *Proceedings of the National Academy of Sciences of the United States of America.* **105**(36), pp.13427-13432.

Vickers, K.C., Palmisano, B.T., Shoucri, B.M., Shamburek, R.D. and Remaley, A.T. 2011. MicroRNAs are Transported in Plasma and Delivered to Recipient Cells by High-Density Lipoproteins. *Nature cell biology.* **13**(4), pp.423-433.

Vickers, K.C. and Remaley, A.T. 2012. Lipid-based carriers of microRNAs and intercellular communication. *Current Opinion in Lipidology.* **23**(2), pp.91-97.

Viljoen, K.S. and Blackburn, J.M. 2013. Quality assessment and data handling methods for Affymetrix Gene 1.0 ST arrays with variable RNA integrity. *BMC Genomics.* **14**, pp.14-14.

Vinci, M., Box, C., Zimmermann, M. and Eccles, S.A. 2013. Tumor spheroid-based migration assays for evaluation of therapeutic agents. *Target identification and validation in drug discovery: methods and protocols.* pp.253-266.

Viprey, V.F., Corrias, M.V. and Burchill, S.A. 2012. Identification of reference microRNAs and suitability of archived hemopoietic samples for robust microRNA expression profiling. *Anal Biochem.* **421**(2), pp.566-572.

Visvader, J.E. and Lindeman, G.J. 2012. Cancer Stem Cells: Current Status and Evolving Complexities. *Cell Stem Cell.* **10**(6), pp.717-728.

Vogelstein, B., Papadopoulos, N., Velculescu, V.E., Zhou, S., Diaz, L.A. and Kinzler, K.W. 2013. Cancer Genome Landscapes. *Science (New York, N.Y.).* **339**(6127), pp.1546-1558.
Volchenboum, S.L., Andrade, J., Huang, L., Barkauskas, D.A., Krailo, M., Womer, R.B., Ranft, A., Potratz, J., Dirksen, U., Triche, T.J. and Lawlor, E.R. 2015. Gene expression profiling of Ewing sarcoma tumours reveals the prognostic importance of tumour–stromal interactions: a report from the Children's Oncology Group. *The Journal of Pathology: Clinical Research.* **1**(2), pp.83-94.
Vychytilova-Faltejskova, P., Pesta, M., Radova, L., Liska, V., Daum, O., Kala, Z., Svoboda, M., Kiss, I. and Slaby, O. 2016. Genome-wide microRNA Expression Profiling in Primary Tumors and Matched Liver Metastasis of Patients with Colorectal Cancer. *Cancer Genomics Proteomics.* **13**(4), pp.311-316.
Wang, F., Li, G., Gu, H.M. and Zhang, D.W. 2013. Characterization of the role of a highly conserved sequence in ATP binding cassette transporter G (ABCG) family in ABCG1 stability, oligomerization, and trafficking. *Biochemistry.* **52**(52), pp.9497-9509.
Wang, G., Guo, X., Hong, W., Liu, Q., Wei, T., Lu, C., Gao, L., Ye, D., Zhou, Y., Chen, J., Wang, J., Wu, M., Liu, H. and Kang, J. 2013. Critical regulation of miR-200/ZEB2 pathway in Oct4/Sox2-induced mesenchymal-to-epithelial transition and induced pluripotent stem cell generation. *Proceedings of the National Academy of Sciences of the United States of America.* **110**(8), pp.2858-2863.
Wang, J., Sakariassen, P., Tsinkalovsky, O., Immervoll, H., Bøe, S.O., Svendsen, A., Prestegarden, L., Røsland, G., Thorsen, F., Stuhr, L., Molven, A., Bjerkvig, R. and Enger, P. 2008. CD133 negative glioma cells form tumors in nude rats and give rise to CD133 positive cells. *International Journal of Cancer.* **122**(4), pp.761-768.
Wang, N., Lan, D., Chen, W., Matsuura, F. and Tall, A.R. 2004. ATP-binding cassette transporters G1 and G4 mediate cellular cholesterol efflux to high-density lipoproteins. *Proceedings of the National Academy of Sciences of the United States of America.* **101**(26), pp.9774-9779.
Wang, N., Ranalletta, M., Matsuura, F., Peng, F. and Tall, A.R. 2006. LXR-induced redistribution of ABCG1 to plasma membrane in macrophages enhances cholesterol mass efflux to HDL. *Arterioscler Thromb Vasc Biol.* **26**(6), pp.1310-1316.
Wang, P., Zhuang, L., Zhang, J., Fan, J., Luo, J., Chen, H., Wang, K., Liu, L., Chen, Z. and Meng, Z. 2013. The serum miR-21 level serves as a predictor for the chemosensitivity of advanced pancreatic cancer, and miR-21 expression confers chemoresistance by targeting FasL. *Molecular Oncology.* **7**(3), pp.334-345.
Wang, T. and Brown, M.J. 1999. mRNA Quantification by Real Time TaqMan Polymerase Chain Reaction: Validation and Comparison with RNase Protection. *Analytical Biochemistry.* **269**(1), pp.198-201.
Wang, X., Collins, H.L., Ranalletta, M., Fuki, I.V., Billheimer, J.T., Rothblat, G.H., Tall, A.R. and Rader, D.J. 2007. Macrophage ABCA1 and ABCG1, but not SR-BI, promote macrophage reverse cholesterol transport in vivo. *Journal of Clinical Investigation.* **117**(8), pp.2216-2224.
Wang, Y., Baskerville, S., Shenoy, A., Babiarz, J.E., Baehner, L. and Blelloch, R. 2008. Embryonic Stem Cell Specific MicroRNAs Regulate the

G1/S Transition and Promote Rapid Proliferation. *Nature genetics.* **40**(12), pp.1478-1483.
Wang, Y., Israelsen, W.J., Lee, D., Yu, V.W.C., Jeanson, N.T., Clish, C.B., Cantley, L.C., Heiden, M.G.V. and Scadden, D.T. 2014. Cell state-specific metabolic dependency in hematopoiesis and leukemogenesis. *Cell.* **158**(6), pp.1309-1323.
Wang, Y., Liu, Y., Malek, S.N., Zheng, P. and Liu, Y. 2011. Targeting HIF1α eliminates cancer stem cells in hematological malignancies. *Cell stem cell.* **8**(4), pp.399-411.
Wang, Y., Medvid, R., Melton, C., Jaenisch, R. and Blelloch, R. 2007. DGCR8 is essential for microRNA biogenesis and silencing of embryonic stem cell self-renewal. *Nature genetics.* **39**(3), pp.380-385.
Wang, Z.M., Du, W.J., Piazza, G.A. and Xi, Y. 2013. MicroRNAs are involved in the self-renewal and differentiation of cancer stem cells. *Acta Pharmacol Sin.* **34**(11), pp.1374-1380.
Ward, J.M. 2006. Lymphomas and leukemias in mice. *Experimental and Toxicologic Pathology.* **57**(5), pp.377-381.
Wasilewski-Masker, K., Liu, Q., Yasui, Y., Leisenring, W., Meacham, L.R., Hammond, S., Meadows, A.T., Robison, L.L. and Mertens, A.C. 2009. Late Recurrence in Pediatric Cancer: A Report From the Childhood Cancer Survivor Study. *JNCI Journal of the National Cancer Institute.* **101**(24), pp.1709-1720.
Wee, B., Pietras, A., Ozawa, T., Bazzoli, E., Podlaha, O., Antczak, C., Westermark, B., Nelander, S., Uhrbom, L., Forsberg-Nilsson, K., Djaballah, H., Michor, F. and Holland, E.C. 2016. ABCG2 regulates self-renewal and stem cell marker expression but not tumorigenicity or radiation resistance of glioma cells. *Sci Rep.* **6**, p25956.
Weidner, N. and Tjoe, J. 1994. Immunohistochemical Profile of Monoclonal Antibody 013: Antibody That Recognizes Glycoprotein p30/32MIC2 and is Useful in Diagnosing Ewing's Sarcoma and Peripheral Neuroepithelioma. *The American Journal of Surgical Pathology.* **18**(5), pp.486-494.
Weiswald, L., Bellet, D. and Dangles-Marie, V. 2015. Spherical Cancer Models in Tumor Biology. *Neoplasia (New York, N.Y.).* **17**(1), pp.1-15.
Wernig, M., Meissner, A., Cassady, J.P. and Jaenisch, R. 2008. c-Myc Is Dispensable for Direct Reprogramming of Mouse Fibroblasts. *Cell Stem Cell.* **2**, pp.10-12.
White, J. and Dalton, S. 2005. Cell cycle control of embryonic stem cells. *Stem Cell Reviews.* **1**(2), pp.131-138.
Wieczorek, D., Delauriere, L. and Schagat, T. 2012. Methods of RNA Quality Assessment. *Promega Corporation.* **Web site. http://www.promega.co.uk/resources/pubhub/methods-of-rna-quality-assessment/**(Updated October 2012.), pp.Accessed April 16, 2017.
Wilfinger, W.W., Mackey, K. and Chomczynski, P. 1997. Effect of pH and ionic strength on the spectro-photometric assessment of nucleic acid purity. *Biotechniques.* **22**(3), pp.474-&.
Wilmut, I., Schnieke, A.E., McWhir, J., Kind, A.J. and Campbell, K.H.S. 1997. Viable offspring derived from fetal and adult mammalian cells (vol 385, pg 810, 1997). *Nature.* **386**(6621), pp.200-200.
Wilson, R.A., Teng, L., Bachmeyer, K.M., Bissonnette, M.Z., Husain, A.N., Parham, D.M., Triche, T.J., Wing, M.R., Gastier-Foster, J.M. and Barr, F.G.

2013. A novel algorithm for simplification of complex gene classifiers in cancer. *Cancer research.* **73**(18), pp.5625-5632.
Wojcik, A.J., Skaflen, M.D., Srinivasan, S. and Hedrick, C.C. 2008. A Critical Role for ABCG1 in Macrophage Inflammation and Lung Homeostasis. *The Journal of Immunology.* **180**(6), p4273.
Wu, C., Wei, Q., Utomo, V., Nadesan, P., Whetstone, H., Kandel, R., Wunder, J.S. and Alman, B.A. 2007. Side Population Cells Isolated from Mesenchymal Neoplasms Have Tumor Initiating Potential. *Cancer Research.* **67**(17), p8216.
Wu, J., Lei, L., Gu, D., Liu, H. and Wang, S. 2016. CIZ1 is upregulated in hepatocellular carcinoma and promotes the growth and migration of the cancer cells. *Tumor Biology.* **37**(4), pp.4735-4742.
Wu, Y. and Wu, P.Y. 2009. CD133 as a marker for cancer stem cells: progresses and concerns. *Stem Cells Dev.* **18**(8), pp.1127-1134.
Xu, N., Papagiannakopoulos, T., Pan, G., Thomson, J.A. and Kosik, K.S. 2009. MicroRNA-145 Regulates OCT4, SOX2, and KLF4 and Represses Pluripotency in Human Embryonic Stem Cells. *Cell.* **137**(4), pp.647-658.
Xu, X.T., Xu, Q., Tong, J.L., Zhu, M.M., Nie, F., Chen, X., Xiao, S.D. and Ran, Z.H. 2012. MicroRNA expression profiling identifies miR-328 regulates cancer stem cell-like SP cells in colorectal cancer. *British Journal of Cancer.* **106**(7), pp.1320-1330.
Xue, J., Wei, J., Dong, X., Zhu, C., Li, Y., Song, A. and Liu, Z. 2013. ABCG1 deficiency promotes endothelial apoptosis by endoplasmic reticulum stress-dependent pathway. *The Journal of Physiological Sciences.* **63**(6), pp.435-444.
Yakisich, J., Azad, N., Venkatadri, R., Kulkarni, Y., Wright, C., Kaushik, V. and Iyer, A.V. 2016. Formation of Tumorspheres with Increased Stemness without External Mitogens in a Lung Cancer Model. *Stem Cells International.* **2016**, p5603135.
Yamamura, S., Saini, S., Majid, S., Hirata, H., Ueno, K., Deng, G. and Dahiya, R. 2012. MicroRNA-34a modulates c-Myc transcriptional complexes to suppress malignancy in human prostate cancer cells. *PloS one.* **7**(1), pe29722.
Yamanaka, S. 2012. Induced pluripotent stem cells: past, present, and future. *Cell Stem Cell.* **10**(6), pp.678-684.
Yan, H., Xue, G., Mei, Q., Wang, Y., Ding, F., Liu, M., Lu, M., Tang, Y., Yu, H. and Sun, S. 2009. Repression of the miR-17-92 cluster by p53 has an important function in hypoxia-induced apoptosis. *The EMBO Journal.* **28**(18), pp.2719-2732.
Yang, J.D. and Roberts, L.R. 2010. Hepatocellular carcinoma: a global view. *Nature Reviews Gastroenterology and Hepatology.* **7**(8), p448.
Yang, M., Zhang, R., Yan, M., Ye, Z., Liang, W. and Luo, Z. 2010. Detection and characterization of side population in Ewing's sarcoma SK-ES-1 cells in vitro. *Biochemical and Biophysical Research Communications.* **391**(1), pp.1062-1066.
Yin, A.H., Miraglia, S., Zanjani, E.D., Almeida-Porada, G., Ogawa, M., Leary, A.G., Olweus, J., Kearney, J. and Buck, D.W. 1997. AC133, a Novel Marker for Human Hematopoietic Stem and Progenitor Cells. *Blood.* **90**(12), pp.5002-5012.

Yin, J., Wang, C., Tang, X., Sun, H., Shao, Q., Yang, X. and Qu, X. 2013. CIZ1 regulates the proliferation, cycle distribution and colony formation of RKO human colorectal cancer cells. *Mol Med Rep.* **8**(6), pp.1630-1634.
Yin, S., Li, J., Hu, C., Chen, X., Yao, M., Yan, M., Jiang, G., Ge, C., Xie, H., Wan, D., Yang, S., Zheng, S. and Gu, J. 2007. CD133 positive hepatocellular carcinoma cells possess high capacity for tumorigenicity. *International Journal of Cancer.* **120**(7), pp.1444-1450.
Yu, F., Yao, H., Zhu, P., Zhang, X., Pan, Q., Gong, C., Huang, Y., Hu, X., Su, F., Lieberman, J. and Song, E. 2007. let-7 Regulates Self Renewal and Tumorigenicity of Breast Cancer Cells. *Cell.* **131**(6), pp.1109-1123.
Yvan-Charvet, L., Pagler, T.A., Seimon, T.A., Thorp, E., Welch, C.L., Witztum, J.L., Tabas, I. and Tall, A.R. 2010. ABCA1 and ABCG1 Protect Against Oxidative Stress–Induced Macrophage Apoptosis During Efferocytosis. *Circulation research.* **106**(12), pp.1861-1869.
Zambo, I., Hermanova, M., Adamkova Krakorova, D., Mudry, P., Zitterbart, K., Kyr, M., Vesely, K., Sterba, J. and Veselska, R. 2012. Nestin expression in high-grade osteosarcomas and its clinical significance. *Oncology reports.* **27**(5), pp.1592-1598.
Zeine, R. and Owens, T. 1992. Direct demonstration of the infiltration of murine central nervous system by Pgp-1/CD44high CD45RB(low) CD4+ T cells that induce experimental allergic encephalomyelitis. *Neuroimmunology.* **40**(1), pp.57-69.
Zhang, D., Wang, Y., Dai, Y., Wang, J., Suo, T., Pan, H., Liu, H., Shen, S. and Liu, H. 2015. CIZ1 promoted the growth and migration of gallbladder cancer cells. *Tumor Biology.* **36**(4), pp.2583-2591.
Zhang, F., Citra, F. and Wang, D.A. 2011. Prospects of induced pluripotent stem cell technology in regenerative medicine. *Tissue Eng Part B Rev.* **17**(2), pp.115-124.
Zhang, H., Li, Y., Huang, Q., Ren, X., Hu, H., Sheng, H. and Lai, M. 2011. MiR-148a promotes apoptosis by targeting Bcl-2 in colorectal cancer. *Cell Death and Differentiation.* **18**(11), pp.1702-1710.
Zhang, H., Mai, Q. and Chen, J. 2017. MicroRNA-210 is increased and it is required for dedifferentiation of osteosarcoma cell line. *Cell Biol Int.* **41**(3), pp.267-275.
Zhang, H., Wu, H., Zheng, J., Yu, P., Xu, L., Jiang, P., Gao, J., Wang, H. and Zhang, Y. 2013. Transforming growth factor beta1 signal is crucial for dedifferentiation of cancer cells to cancer stem cells in osteosarcoma. *Stem Cells.* **31**(3), pp.433-446.
Zhang, P., Andrianakos, R., Yang, Y., Liu, C. and Lu, W. 2010. Kruppel-like Factor 4 (Klf4) Prevents Embryonic Stem (ES) Cell Differentiation by Regulating Nanog Gene Expression. *Journal of Biological Chemistry.* **285**(12), pp.9180-9189.
Zhang, X., Chen, X., Lin, J., Lwin, T., Wright, G., Moscinski, L., Dalton, W., Seto, E., Wright, K. and Sotomayor, E. 2012. Myc represses miR-15a/miR-16-1 expression through recruitment of HDAC3 in mantle cell and other non-Hodgkin B-cell lymphomas. *Oncogene.* **31**(24), p3002.
Zhang, Z., Sun, H., Dai, H., Walsh, R., Imakura, M., Schelter, J., Burchard, J., Dai, X., Chang, A.N., Diaz, R.L., Marszalek, J.R., Bartz, S.R., Carleton, M., Cleary, M.A., Linsley, P.S. and Grandori, C. 2009. MicroRNA miR-210 modulates cellular response to hypoxia through the MYC antagonist MNT. *Cell Cycle.* **8**(17), pp.2756-2768.

Zhen, Y., Liu, Z., Yang, H., Yu, X., Wu, Q., Hua, S., Long, X., Jiang, Q., Song, Y. and Cheng, C. 2013. Tumor suppressor PDCD4 modulates miR-184-mediated direct suppression of C-MYC and BCL2 blocking cell growth and survival in nasopharyngeal carcinoma. *Cell death & disease.* **4**(10), pe872.
Zheng, L., Qi, T., Yang, D., Qi, M., Li, D., Xiang, X., Huang, K. and Tong, Q. 2013. microRNA-9 Suppresses the Proliferation, Invasion and Metastasis of Gastric Cancer Cells through Targeting Cyclin D1 and Ets1. *PLoS ONE.* **8**(1), pe55719.
Zhou, S., Schuetz, J.D., Bunting, K.D., Colapietro, A.M., Sampath, J., Morris, J.J., Lagutina, I., Grosveld, G.C., Osawa, M., Nakauchi, H. and Sorrentino, B.P. 2001. The ABC transporter Bcrp1/ABCG2 is expressed in a wide variety of stem cells and is a molecular determinant of the side-population phenotype. *Nat Med.* **7**(9), pp.1028-1034.
Zhu, L., Gibson, P., Currle, D.S., Tong, Y., Richardson, R.J., Bayazitov, I.T., Poppleton, H., Zakharenko, S., Ellison, D.W. and Gilbertson, R.J. 2009. Prominin 1 marks intestinal stem cells that are susceptible to neoplastic transformation. *Nature.* **457**(7229), pp.603-607.
Zwerner, J., Joo, J., Warner, K., Christensen, L., Hu-Lieskovan, S., Triche, T. and May, W. 2008. The EWS/FLI1 oncogenic transcription factor deregulates GLI1. *Oncogene.* **27**(23), pp.3282-3291.